

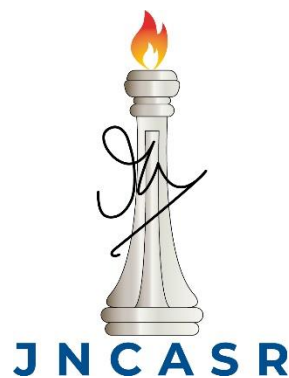
**Elucidating the role of mitochondrial dynamics and
endosomal protein sorting in *Drosophila* blood cell
homeostasis**

A Thesis submitted for the degree of

Doctor of Philosophy

By

Arindam Ray



Molecular Biology and Genetics Unit (MBGU)

Jawaharlal Nehru Centre for Advanced Scientific Research

(JNCASR)

Bangalore-560064, India

December 2021

DEDICATION

I dedicate my PhD thesis to my parents. Their constant support throughout my career has allowed me to carry out my studies and research without any distraction and disturbance. My father is my biggest inspiration.

DECLARATION

I hereby declare that this thesis entitled “**Elucidating the role of mitochondrial dynamics and endosomal protein sorting in *Drosophila* blood cell homeostasis**” is an authentic record of research work carried out by me under the guidance of Prof. Maneesha S. Inamdar at the Laboratory of Stem Cell and Vascular Biology, Molecular Biology and Genetics Unit, Jawaharlal Nehru Centre for Advanced Scientific Research, Bangalore.

In keeping with the norms of scientific observations, due acknowledgement has been made whenever work described here has been based on the findings of other investigators. Any omission owing to oversight or misjudgement is regretted.



Arindam Ray

Place: Bangalore

Date: 22nd December 2021

CERTIFICATE

This is to certify that the work described in this thesis entitled “**Elucidating the role of mitochondrial dynamics and endosomal protein sorting in *Drosophila* blood cell homeostasis**” is the result of investigations carried out by **Mr. Arindam Ray** in the Laboratory of Stem Cell and Vascular Biology, Molecular Biology and Genetics Unit, Jawaharlal Nehru Centre for Advanced Scientific Research, Bangalore, India under my guidance and that the results presented here have previously not formed the basis for the award of any other degree, diploma or fellowship.



Prof. Maneesha S. Inamdar

Place: Bangalore

Date: 22nd December 2021

Acknowledgements

The work presented in this thesis would not have been possible without the support of several people. I take this opportunity to extend my sincere gratitude and appreciation to all those who made my PhD thesis possible.

First and foremost, I would like to gratefully acknowledge the guidance, encouragement and support of my supervisor, Prof. Maneesha S. Inamdar. She has immensely contributed to the development of my professional skills, and I really cannot thank her enough for that. Her support throughout my PhD was instrumental for my development as a professional researcher. Most importantly, she has been the architect of my massive development as a human being altogether during my PhD. Thank you for everything Ma'am!

I would like to thank all the faculty members from MBGU and NSU for their feedback and critical evaluation of my work during annual work presentations and various other discussion forums- Prof. M.R.S. Rao, Prof. Anuranjan Anand, Prof. Ranga Uday Kumar, Prof. Kaustuv Sanyal, Prof. Ravi Manjithaya, Prof. Hemalatha Balaram, Prof. Tapas Kumar Kundu, Prof. Namita Surolia, Prof. Sheeba Vasu, Prof. James P. Clement Chelliah, Dr. Kushagra Bansal. I thank the members of my comprehensive examination committee-Prof. Varadharajan Sundaramurthy, Prof. Ravi Manjithaya, Late Prof. Vijay Kumar Sharma, Prof. Ranga Uday Kumar and the GSAC members Prof. Anuranjan Anand and Prof. Sheeba Vasu for giving valuable inputs. I have really benefited from one-on-one discussions with Prof. Sundaramurthy and Prof. Manjithaya.

I would like to thank the Drosophila research community for sharing reagents. I am thankful to Prof. Utpal Banerjee, Prof. Angela Giangrande, Prof. Lucas Waltzer, Prof. David Bilder and Prof. Andreas Bergmann for providing constructive criticism to my work at various conferences or discussion sessions.

I thank all my teachers who contributed to my learning and the development of my passion for research. My teacher from School days, Mr. Arup Sengupta was the first teacher I encountered who used to push the students towards learning anything with great depth. I am highly obliged to my teachers from college-Dr. Arup Kumar Mitra, Prof. Anirban Siddhanta, Prof. Maitrayee Dasgupta, Prof. Maitree Bhattacharya, Dr. Mahashweta Mitra Ghosh, Dr. Debjani Dutta and Dr. Kasturi Sarkar.

I would like to thank all the lab members-ex- and present. I thank Dr. Ronak, Dr. Deeti, Dr. Rohan, Dr. Simi, Dr. Divyesh, Dr. Saloni, Dr. Sudhir, Diana, Praveen, Rajarshi, Preeti, Kajal,

Alice, Prathamesh, Aishwarya, Yashashwinee, Arghakusum, Aksah, Anudeep, Priyamvada, Bharat, Kaustubh, Chetan, Abarna, Dr. Anand T., Jasper, Tirath, Roja, Rahul, Sumedha, Vanshika, Dr. Ligy and Shruti M.K. I thank Diana and Rohan for their help as seniors in the fly lab. I am also thankful to the summer interns of our lab-Lavanya and Arun for assisting me with the work. I thank Nagaraj, Vijay and Vanitha for managing smooth running of daily lab work.

I thank my batchmates Shrilaxmi, Arun, Raktim, Akash, Jigyasa, Zeenat, Aditi, Neelakshi, Neha and Sarika for a wonderful time at JNCASR. I thank my friends from JNCASR-Priya Jaitly, Arijit, Monoj, Verghese, Utsa, Dr. Arnab, Dr. Aditya Mahadevan, Dr. Payel, Dr. Vijay Akhade, Priya Brahma, Rashi, Sambhavi, Akshaya, Ranabir, Rohit, Ashutosh, Dr. Shubhajit RoyChowdhury, Dr. Manisha Samanta, Dr. Sudip, Dr. Sourav Mondal, Dr. Ranjan, Anaranya. I thank Deeti, Ronak, Divyesh, Diana, Saloni, Abhilash, Alice for a wonderful time in lab and JNCASR. I also acknowledge my friends from outside JNCASR- Sreemantee, Divya, Shiladitya, Sampurna, Krishanu and Pramit.

I would like to acknowledge the JNCASR and NCBS confocal facility. I would like to thank Suma Ma'am who has been very helpful in my imaging-based experiments. I also thank Keerthana, Sunil, Prajjwal, Dr. Krishnamurthy and Dr. Manoj Mathew. I thank Dr. R.G. Prakash from the animal house facility of JNCASR for helping out with raising antibody, NCBS fly facility, JNCASR hostel, mess, utility store, dining Hall, library, complab, gym and housekeeping.

I am grateful to CSIR, JNCASR, DST and DBT, Government of India for providing fellowship, travel grant and funding for my research.

I am thankful to Aditya, Sayantan and Kajal for their friendship and continuous support. I have rarely spent a day of my PhD life without talking to them. Their company has been a big stress buster for me. I love all of them very much.

Lastly, I would like to acknowledge my family for their continuous support. My parents have always given me the freedom to pursue my dream. Every single day of my PhD life at JNCASR, I have missed them and felt guilty of not giving them the time they deserve. My sister has been extremely supportive as a friend and has taken care of my parents while I was away for PhD. All of them have sacrificed a lot for me. I dedicate my PhD thesis to my beloved family.

Contents

	Page No.
List of Figures	xi
Abbreviations	xvi
Synopsis	xix
Chapter 1. Introduction	1
1.1 Hematopoiesis: A model to understand progenitor homeostasis and development	2
1.1.1 Vertebrate hematopoiesis	2
1.1.2 Hematopoiesis in invertebrates	4
1.1.2.1 <i>Drosophila</i> as a model of hematopoiesis	4
1.2 Parallels between vertebrate and invertebrate hematopoiesis	8
1.2.1 Signaling pathways controlling vertebrate hematopoiesis	8
1.2.2 Conserved signaling pathways controlling <i>Drosophila</i> Hematopoiesis	10
1.2.3 <i>Drosophila</i> lymph gland serves as an ideal model for a comprehensive <i>in situ</i> analysis of blood progenitor homeostasis.	11
1.3 Immune functions of the blood lineages.	12
1.4 Role of organelles in cell fate decisions and hematopoiesis	14
1.4.1. Mitochondria as regulators of hematopoiesis	15
1.4.1.1 Link between mitochondrial dynamics and hematopoiesis	16
1.4.2 Role of endosomes in hematopoiesis	20
1.4.2.1 Link between endosomal protein sorting and hematopoiesis	22
1.4.2.2. The ESCRT machinery	23
1.5. Aims of the present study	27

Chapter 2. The endosomal ARF1-Asrij axis modulates cellular and humoral immunity of <i>Drosophila</i> to regulate survival upon infection.	29
2.1 Introduction	29
2.2 Materials and methods	31
2.2.1 Fly stocks and genetics	31
2.2.2 <i>In-vivo</i> adult phagocytosis assay	32
2.2.3 Immunostaining of the circulating hemocyte and fat body	32
2.2.4 Infection and survival assay	33
2.2.5 Statistical analysis	33
2.3 Results	33
2.3.1 Depletion of endosomal proteins ARF1 or Asrij does not affect phagocytosis in hemocytes.	33
2.3.2 The ARF1-Asrij axis suppresses AMP production through the Toll pathway by stabilizing Cactus.	34
2.3.3 ARF1 and Asrij inhibit AMP biosynthesis through the Imd pathway in hemocytes.	38
2.3.4 Asrij and ARF1 depletion reduces survival of flies upon acute bacterial infection.	39
2.4 Discussion	41
2.5 Acknowledgement	44
Chapter 3. Asrij mutant lymph gland proteome analysis reveals potential role of mitochondrial and endosomal proteins in <i>Drosophila</i> blood cell homeostasis.	45
3.1 Introduction	45
3.2 Materials and methods	48
3.2.1 Fly stocks	48
3.2.2 Immunostaining-based analysis	48
3.2.3 Quantification	48
3.3 Results	49
3.3.1 Validation of candidates shows 73% match with the <i>Drosophila</i> lymph gland proteome.	49
3.4 Discussion	59

3.5 Acknowledgement	60
Chapter 4. A conserved role for Asrij/OCIAD1 in progenitor differentiation and lineage specification through functional interaction with mitochondrial dynamics regulators.	61
4.1 Introduction	61
4.2 Materials and methods	62
4.2.1 Fly stocks	62
4.2.2 Immunostaining-based analysis	63
4.2.3 Mitotracker staining	63
4.2.4 Live imaging of mitochondria	64
4.2.5 Quantification	64
4.2.5.1 Mitochondria quantification	64
4.2.5.2 Quantification of hemocytes in the lymph gland	64
4.2.6 Statistical analyses	65
4.3 Results	65
4.3.1 Mitochondrial morphology reflects larval blood progenitor heterogeneity in <i>Drosophila</i>	65
4.3.2 Asrij regulates mitochondrial morphology in <i>Drosophila</i> blood progenitors and hemocytes	67
4.3.3 Anterior progenitors are more sensitive to perturbation of the mitochondrial fission-fusion machinery	75
4.3.4 Asrij/OCIAD1 depletion reduces mitochondrial network dynamics	76
4.3.5 Inhibition of mitochondrial fission prevents crystal cell differentiation.	79
4.3.6 Reduced mitochondrial fusion promotes Notch signaling and crystal cell differentiation.	82
4.3.7 Asrij integrates mitochondrial dynamics with crystal cell differentiation.	86
4.4 Discussion	93

4.5 Acknowledgement	98
Chapter 5. ESCRT components play distinct role in cargo sorting and lineage-specific differentiation of blood progenitors in the <i>Drosophila</i> lymph gland.	99
5.1 Introduction	99
5.2 Materials and methods	101
5.2.1 Fly stocks	101
5.2.2 Fly Genetics	102
5.2.3 Immunofluorescence Microscopy	102
5.2.4 <i>In situ</i> hybridization	103
5.2.5 RT qPCR	104
5.2.6 Quantification	105
5.2.7 Statistical analyses	105
5.3 Results	106
5.3.1 ESCRT components are uniformly expressed across the lymph gland.	106
5.3.2 Conserved endosomal regulator of hematopoiesis, Asrij regulates ESCRT expression in the lymph gland.	108
5.3.3 ESCRT components regulate ubiquitinated cargo sorting in the lymph gland in a distinct manner.	110
5.3.4 ESCRT components play distinct roles in progenitor maintenance and lineage-specific differentiation in the lymph gland.	115
5.3.5 ESCRT cell-autonomously regulates ubiquitinated cargo sorting in blood progenitor.	128
5.3.6 ESCRT regulates blood cell differentiation in cell non-autonomous manner as well.	130
5.3.7 Vps25 is dispensable for lineage-specification of the blood progenitors in the lymph gland	131
5.4 Discussion	135
5.5 Acknowledgement	138

Chapter 6. ESCRT regulates Notch signaling to maintain progenitor homeostasis in the <i>Drosophila</i> lymph gland.	139
6.1 Introduction	139
6.2 Materials and methods	141
6.2.1 Fly stocks	141
6.2.2 Fly Genetics	141
6.2.3 Immunofluorescence Microscopy	142
6.2.4 Proximity ligation assay	142
6.2.5 Quantification	143
6.2.6 Statistical analyses	143
6.3 Results	143
6.3.1 ESCRT components inhibit Notch signaling in a distinct manner across lymph gland progenitors.	143
6.3.2 Depletion of ESCRT components in the blood progenitor causes accumulation of NICD.	147
6.3.3 ESCRT components co-localize with NICD in lymph gland progenitors.	152
6.3.4 ESCRT regulates Notch activation in blood progenitors independent of Deltex and eIF3f1.	143
6.3.5 ESCRT components play distinct roles in regulating mitotic potential across different progenitor subsets of the lymph gland.	155
6.4 Discussion	161
6.5 Acknowledgement	164
Chapter 7. Discussion	165
7.1 Asrij mutant lymph gland proteome serves as a valuable resource for organellar hits with potentially conserved roles in hematopoiesis.	165
7.2 The Asrij-dependent endocytic axis contributes to immune signaling activation in <i>Drosophila</i> .	165
7.3 Endosomes emerge as potential regulatory hubs for signaling during hematopoiesis.	166
7.4 Asrij significantly impacts regulators of metabolism.	167
7.5 Critical regulators of mitochondrial dynamics play an indispensable role in Notch signaling-dependent differentiation of <i>Drosophila</i> blood progenitors.	167

7.6 Asrij/OCIAD1 acts as a conserved modulator of mitochondrial dynamics.	169
7.7 Redundancy, multifunctionality and post-translational regulatory mechanisms may underlie the distinct role of ESCRT components in progenitor homeostasis and lineage choice.	169
7.8 Organelle level contribution to inherent developmental and functional heterogeneity of the blood progenitor subsets in the lymph gland lobes.	173
7.9 Organelle membrane remodelling is critical for the modulation of developmental signaling.	175
7.10 Asrij may potentially mediate inter-organellar crosstalk.	176
7.11 Misexpression of mitochondrial dynamics regulators and ESCRT components may result in hematological disorders.	178
7.12 Concluding remarks	179
References	180
Appendices	197
Appendix 1: Details of the antibodies	197
Appendix 2: Details of the reagents	199
List of publications	200

List of Figures

	Page No.
Chapter 1. Introduction	
Fig 1.1. Models of vertebrate hematopoiesis.	3
Fig 1.2. Hematopoiesis during <i>Drosophila</i> development.	5
Fig 1.3. Schematic of <i>Drosophila</i> larval hematopoiesis.	6
Fig 1.4. Schematic representation of the lymph gland progenitor subsets.	7
Fig 1.5. Signaling pathways regulating vertebrate bone marrow hematopoiesis.	9
Fig 1.6. Signaling pathways operating in the lymph gland.	10
Fig 1.7. Comparison of <i>Drosophila</i> immune system with vertebrates.	14
Fig 1.8. Multiple mitochondrial processes regulate hematopoiesis.	16
Fig 1.9. Regulation of Mitochondrial Fusion and Fission.	17
Fig 1.10. Role of mitochondrial dynamics regulators in HSC maintenance.	19
Fig 1.11. Conserved regulator of stemness and hematopoiesis, OCIAD1 regulates mitochondrial activity in hESC.	19
Fig 1.12. Asrij interacts with the ubiquitous endocytic trafficking protein ARF1 for endosomal regulation of hematopoiesis in <i>Drosophila</i> .	21
Fig 1.13. Asrij regulates endocytic trafficking of Notch in <i>Drosophila</i> hemocytes.	23
Fig 1.14. ESCRT mediates endosomal protein sorting through MVB biogenesis.	24
Figure 1.15. ESCRT plays a multifunctional role through membrane remodelling.	27
Chapter 2. The endosomal ARF1-Asrij axis modulates cellular and humoral immunity of <i>Drosophila</i> to regulate survival upon infection.	
Fig 2.1 <i>In vivo</i> phagocytic uptake assay.	34
Fig 2.2 Cactus ubiquitination in <i>asrij null</i> and <i>arf1</i> KD larval fat body.	35
Fig 2.3 Cactus ubiquitination in <i>asrij null</i> and <i>arf1</i> KD adult fly fat body.	36
Fig 2.4 Toll pathway activation through Dorsal nuclear translocation in <i>asrij null</i> and <i>arf1</i> KD hemocytes.	37
Fig 2.5 Imd pathway activation through Relish nuclear translocation in <i>asrij null</i> and <i>arf1</i> KD larval fat bodies.	39
Fig 2.6 Survival of flies upon blood and trachea-specific depletion of Asrij.	40

Fig 2.7 Survival of flies upon blood and trachea-specific depletion of ARF1.	41
--	----

Chapter 3. Asrij mutant lymph gland proteome analysis reveals potential role of mitochondrial and endosomal proteins in *Drosophila* blood cell homeostasis.

Fig 3.1 Pathway enrichment analysis of Asrij lymph gland proteome.	47
Fig 3.2 Validation of lymph gland proteome for endosomal candidates Rab7, Rab11 and ARF1.	51
Fig 3.3 Immunofluorescence based validation of endosomal candidates identified from the lymph gland proteome.	54
Fig 3.4 Validation of lymph gland proteome for mitochondrial candidates COXIV, ATP5A, NDUFS3 and SDHB.	55
Fig 3.5 Immunofluorescence based validation of mitochondrial candidates identified from the lymph gland proteome.	57

Chapter 4. A conserved role for Asrij/OCIAD1 in progenitor differentiation and lineage specification through functional interaction with mitochondrial dynamics regulators.

Fig 4.1 Mitochondrial morphology across blood progenitors of the <i>Drosophila</i> lymph gland reflects heterogeneity.	66
Fig 4.2 Asrij localizes to mitochondria of the <i>Drosophila</i> lymph gland progenitors and circulatory hemocytes.	68
Fig 4.3 Asrij regulates mitochondrial morphology in blood progenitors of the <i>Drosophila</i> lymph gland.	69
Fig 4.4 Asrij regulates mitochondrial aggregation in the lymph gland progenitors.	70
Fig 4.5. Asrij regulates mitochondrial morphology in <i>Drosophila</i> circulatory hemocytes.	72
Fig 4.6 Asrij overexpression affects mitochondrial network architecture in hemocytes.	74
Fig 4.7 Asrij, Drp1 and Marf regulate mitochondrial morphology in blood progenitors of the <i>Drosophila</i> lymph gland.	76
Fig 4.8 Asrij depletion reduces mitochondrial network dynamics in hemocytes.	77
Fig 4.9. OCIAD1 depletion reduces mitochondrial network dynamics in hESC.	78

Fig 4.10 Drp1 depletion inhibits crystal cell differentiation in the <i>Drosophila</i> lymph gland.	79
Fig 4.11 Drp1 does not regulate differentiation to plasmatocytes or lamellocytes in the <i>Drosophila</i> lymph gland.	81
Fig 4.12 Inhibition of Drp1-dependent mitochondrial fission in blood progenitors selectively inhibits crystal cell differentiation.	82
Fig 4.13 Marf regulates crystal cell differentiation and Notch signaling in the <i>Drosophila</i> lymph gland.	83
Fig 4.14 Marf does not affect differentiation to plasmatocytes or lamellocytes in the <i>Drosophila</i> lymph gland.	84
Fig 4.15 Inhibition of Marf-dependent mitochondrial fusion in blood progenitors selectively promotes crystal cell differentiation.	85
Fig 4.16 Overexpression of Drp1 and Marf differentially affect crystal cell differentiation in the <i>Drosophila</i> lymph gland.	86
Fig 4.17. NRE-GFP expression increases upon <i>asrij</i> knockdown.	87
Fig 4.18 Inhibition of <i>Marf</i> -dependent mitochondrial fusion rescues mitochondrial elongation phenotype of <i>Asrij</i> in the lymph gland progenitors.	88
Fig 4.19 Progenitor-specific genetic interaction of <i>asrij</i> with <i>Drp1</i> and <i>Marf</i> controls crystal cell differentiation in lymph gland.	89
Fig 4.20 Schematic representation of the effect of mitochondrial morphology and dynamics on blood cell differentiation.	90
Fig 4.21 Genetic interaction of <i>asrij</i> with Drp1 and Marf controls mitochondrial network architecture in circulatory hemocytes.	91
Fig 4.22 Pan-hemocyte-specific genetic interaction of <i>asrij</i> with Drp1 and Marf controls crystal cell differentiation in lymph gland.	92

Chapter 5. ESCRT components play distinct role in cargo sorting and lineage-specific differentiation of blood progenitors in the *Drosophila* lymph gland.

Fig 5.1 ESCRT is uniformly expressed in the lymph gland.	107
Fig 5.2 <i>Asrij</i> regulates ESCRT expression in the lymph gland.	108
Fig 5.3 Validation for knockdown of ESCRT genes in the lymph gland.	111
Fig 5.4 ESCRT components regulate ubiquitinated cargo sorting in the lymph gland primary lobe.	113
Fig 5.5 ESCRT components differentially regulate ubiquitinated cargo sorting across the lymph gland.	115

Fig 5.6 ESCRT components regulate progenitor maintenance and plasmacyte differentiation in the lymph gland primary lobe.	117
Fig 5.7 ESCRT components differentially regulate plasmacyte differentiation across the lymph gland.	119
Fig 5.8 ESCRT components differentially regulate crystal cell differentiation in the lymph gland primary lobe.	121
Fig 5.9 ESCRT components regulate crystal cell differentiation across the lymph gland.	122
Fig 5.10 ESCRT components regulate lamellocyte differentiation in the lymph gland primary lobe.	124
Fig 5.11 ESCRT components differentially regulate lamellocyte differentiation across the lymph gland.	125
Fig 5.12 A functional map of ESCRT components in cargo sorting and lineage-specific differentiation in the <i>Drosophila</i> lymph gland.	127
Fig 5.13 Hypothetical model for cell-autonomous function of ESCRT in the lymph gland progenitors.	129
Fig 5.14 ESCRT cell-autonomously regulates ubiquitinated cargo sorting in the lymph gland progenitors.	130
Fig 5.15 ESCRT may regulate progenitor differentiation in both cell-autonomous and cell non-autonomous manner.	131
Figure 5.16. Vps25 knockdown in the blood progenitor does not affect ubiquitination or blood cell differentiation.	132
Figure 5.17. Vps25 homozygous mutant clone does not affect ubiquitination and blood cell differentiation in the lymph gland.	133

Chapter 6. ESCRT regulates Notch signaling to maintain progenitor homeostasis in the *Drosophila* lymph gland.

Fig 6.1 ESCRT components regulate Notch signaling in the lymph gland primary lobe.	145
Fig 6.2 ESCRT regulates Notch activation across the lymph gland.	147
Fig 6.3 Progenitor-specific depletion of ESCRT causes NICD accumulation in the lymph gland primary lobe.	149
Fig 6.4 Progenitor-specific knockdown of ESCRT components causes NICD accumulation across the lymph gland.	151
Fig 6.5 ESCRT components colocalize and interact with NICD across all progenitor subsets of the lymph gland.	153
Fig 6.6 ESCRT does not genetically interact with Deltex and eIF3f1 to regulate Notch signaling in the lymph gland progenitor.	154

Fig 6.7 ESCRT components differentially regulate mitotic potential across the lymph gland.	157
Fig 6.8 Depletion of ESCRT components affects the morphology of the lymph gland lobes.	160
Fig 6.9. Model showing ESCRT-dependent regulation of cargo trafficking and Notch signaling across lymph gland progenitor subsets.	163

Chapter 7. Discussion

Fig 7.1. ESCRT components play a distinct role in lineage choice.	172
Fig 7.2. Asrij integrates critical organellar circuitries to maintain blood progenitor homeostasis in the <i>Drosophila</i> lymph gland.	177

List of abbreviations

AAA:	ATPases Associated with Diverse Cellular Activities
ALL:	Acute Lymphocytic Leukemia
AML:	Acute Myeloid Leukemia
AMP:	Antimicrobial peptide
ANOVA:	Analysis of Variance
ARF1:	ADP-Ribosylation Factor 1
BMP:	Bone Morphogenetic Protein
bp:	base pair
CFU:	Colony Forming Unit
CHMP:	Charged Multivesicular Body protein
CLL:	Chronic Lymphocytic Leukemia
CLP:	Common Lymphoid Progenitors
CML:	Chronic Myeloid Leukemia
CMP:	Common Myeloid Progenitors
CORVET:	Class C Core Vacuole/Endosome Tethering
CZ:	Cortical Zone
DAPI:	4',6-diamidino-2-phenylindole
DIG:	Digoxigenin
DNM1L:	Dynamin 1 Like
DPP:	Decapentaplegic
DRP1:	Dynamin Related Protein 1
DV:	Dorsal Vessel
EA:	Eye-Antennal Disc
EGFP:	Enhanced Green Fluorescent Protein
EGFR:	Epidermal Growth Factor Receptor
ESC:	Embryonic Stem Cell
ESCRT:	Endosomal Sorting Complex Required for Transport
ET:	Essential Thrombocytopenia

ETC:	Electron Transport Chain
FGF:	Fibroblast Growth Factor
FLP:	Flippase
FRT:	Flippase Recombination Target
GATA2:	GATA Binding Protein 2
H3P:	Phosphorylated Histone H3
HD-PTP:	His-Domain Containing Protein Tyrosine Phosphatase
HRS:	Hepatocyte Growth Factor Regulated Tyrosine Kinase Substrate
HS:	Hematopoietic Stem Cell
IF:	Immunofluorescence
Imd:	Immune Deficiency
ISH:	<i>in situ</i> hybridisation
IP:	Intermediate Progenitor
JAK:	Janus Kinase
JNK:	c-Jun N-terminal Kinase
KD:	Knockdown
KO:	Knockout
LG:	Lymph Gland
LT-HSC:	Long Term Hematopoietic Stem Cell
MARF:	Mitochondria Assembly Regulatory Factor
MDV:	Mitochondria-Derived Vesicle
MFF:	Mitochondrial Fission Factor
MFN:	Mitofusin
MitoPLD:	Mitochondrial phospholipase D
MPD:	Myeloproliferative Disease
MVB:	Multivesicular Body
MVE:	Multivesicular endosome
MZ:	Medullary Zone
NDUFS3:	NADH dehydrogenase (Ubiquinone) Iron-Sulfur Protein 3

NECD:	Notch Extracellular Domain
NFAT:	Nuclear Factor of Activated T-cells
NICD:	Notch Intracellular Domain
NimC1:	Nimrod C1
NRE:	Notch Responsive Element
OCIAD1:	Ovarian Carcinoma Immunoreactive Antigen Domain containing 1
Opa1:	Optic Atrophy 1
OV:	Overexpressing
PBS:	Phosphate-Buffered Saline
PLA:	Proximity Ligation Assay
PMF:	Primary Myelofibrosis
ProPO:	Prophenoloxidase
PSC:	Posterior Signaling Centre
ROS:	Reactive Oxygen Species
RT-qPCR:	Reverse Transcription-quantitative Polymerase Chain Reaction
SDHB:	Succinate Dehydrogenase (Ubiquinone) Iron-Sulfur Subunit
SNF7:	Sucrose Non-fermenting protein 7
STAM:	Signal Transducing Adaptor Molecule
STAT:	Signal Transducer and Activator of Transcription
Su(H):	Suppressor of Hairless
TepIV:	Thiolester Containing Protein IV
TLR:	Toll-Like Receptor
TSG:	Tumor Suppressor Gene
UAS:	Upstream Activation Sequence
Ub:	Ubiquitin
VPS:	Vacuolar Protein Sorting
WASH:	Wiscott-Aldrich Syndrome Protein and SCAR Homolog
WT:	Wild Type

Synopsis of the thesis titled

Elucidating the role of mitochondrial dynamics and endosomal protein sorting in *Drosophila* blood cell homeostasis

Arindam Ray

Molecular Biology and Genetics Unit,
Jawaharlal Nehru Centre for Advanced Scientific Research,
Jakkur, Bangalore- 560064, India.

Thesis Advisor: **Prof. Maneesha S. Inamdar**

Blood cell homeostasis depends on the co-ordination of various intracellular and extracellular cues. Sub-cellular organelles play critical roles in post-transcriptional control of signal generation and attenuation. Recently endosomal and mitochondrial proteins have been shown to play active roles in maintaining stem and progenitor cell homeostasis in mouse and *Drosophila*. We aim to understand the role of organelles in progenitor maintenance and cell fate determination in *Drosophila* hematopoiesis. Previous studies showed that *Asrij*/OCIAD1 localizes to endosomes and mitochondria and can maintain stemness in *Drosophila* and mouse hematopoiesis. This thesis contributed to identifying critical immune pathways regulated by *Asrij* and validated candidates from a previous study of the *asrij* mutant hematopoietic proteome. Further using the *Drosophila* genetics and the lymph gland as a model of hematopoiesis, here I explore the role of mitochondria and endosomes in progenitor maintenance and differentiation by imaging-based *in situ* analyses. My studies reveal that the mitochondrial dynamics regulators and the Endosomal Sorting Complex Required for Transport (ESCRT) actively control blood progenitor heterogeneity, homeostasis, and lineage choice.

Vertebrate hematopoiesis takes place in a complex milieu across multiple sites. Hematopoietic stem cells (HSC) in adult vertebrates reside as an impure and scanty population in the bone marrow. Hence, a comprehensive *in situ* analysis of blood cell homeostasis is difficult. The *Drosophila* lymph gland serves as a simple yet powerful model to study hematopoiesis *in situ*. The primary lobe of the lymph gland comprises of three developmentally distinct zones enriched in blood progenitors (prohemocytes), differentiated blood cells (hemocytes) and hematopoietic niche, thus allowing spatial and temporal imaging-based *in situ* analysis of hematopoiesis across the entire hematopoietic organ. Moreover, the signaling pathways regulating blood cell homeostasis in the lymph gland are evolutionarily conserved. Studies so far have primarily focused on the anterior-most primary lobe, ignoring the rest of the progenitor populations in the posterior lobes. As the lymph gland harbors the entire blood progenitor population of *Drosophila*, studying the entire organ allows complete sampling and a comprehensive study of progenitor homeostasis at the organismal level. Blood progenitors of *Drosophila* are linearly arranged across the lymph gland and are characterized by the expression of several markers such as Domeless, TepIV, DE-Cadherin, etc. A recent report highlights that the posterior progenitors are developmentally distinct from the anterior subset and are refractile to immune challenge, possibly due to differential activation of signaling pathways. Using this powerful *in vivo* model, we aim to understand conserved mechanisms underlying blood progenitor homeostasis and heterogeneity.

Membrane-bound dynamic organelles such as mitochondria and endosomes act as critical regulatory stations of signaling. Mitochondria regulate progenitor fate choice such as differentiation, proliferation, and aging through metabolic and signaling homeostasis. Endosomes act as scaffolding platforms for various receptors. Endocytic trafficking maintains signaling homeostasis through receptor trafficking, sorting, and turnover. Hence, modulation of organelle dynamics and function allows rapid post-transcriptional control of cell fate decisions.

Earlier reports showed that the pan-hemocytic conserved endosomal protein Asrij interacts with the ubiquitous trafficking protein ADP Ribosylation Factor 1 (ARF1) to regulate *Drosophila* hematopoiesis. Loss of Asrij leads to precocious differentiation of *Drosophila* blood progenitors. However, its organismal level impact, such as on immunity remained underexplored. The terminally differentiated blood cells (hemocytes) in *Drosophila* are of three different categories: plasmatocytes, crystal cells and lamellocytes which functionally and ontogenetically resemble the vertebrate myeloid lineage and primarily control the cellular arm of *Drosophila* immunity. On the other hand, antimicrobial peptides secreted by the fat body and also partly by the blood cells control the humoral immune response. Infection and survival assays on Asrij and ARF1 depleted flies showed reduced survival of adult flies upon bacterial infection. My work contributed to showing that Asrij or ARF1 depletion led to increased translocation of NF- κ B homolog Dorsal and Rel-like factor Relish to the nucleus of the blood cells and fat body, promoting increased biosynthesis of antimicrobial peptides through activation of Toll and Imd pathways. **This study establishes the essential role of the endosomal ARF1-Asrij axis in *Drosophila* immunity and survival of flies upon infection** (Khadiolkar, Ray, et al., *Sci. Rep.* 2017).

A comparative proteomic analysis of the *Drosophila* lymph gland was performed previously to understand further the role of Asrij in tissue-restricted regulation of conserved organellar pathways and blood cell homeostasis. Mitochondria and endosome-associated proteins emerged as potential candidates. I validated these by immunofluorescence microscopy-based expression analysis and found that 73% match with the proteome, thus assuring the reliability of the proteome data. **This proteomic analysis reveals the potential conserved regulators of hematopoiesis and may find implication in various hematological disease contexts in vertebrate models** (Sinha et al., *Mol. Cell. Proteomics*, 2019).

Apart from the known roles of Asrij in signaling, cellular homeostasis, and immunity, the lymph gland proteome analysis revealed a potential role for Asrij-mediated organelle function in blood cell homeostasis. An earlier report showed that loss of OCIAD1, the human

ortholog of *Asrij*, results in elongation of mitochondria in hESC. However, the *in vivo* relevance of the role of *Asrij*/OCIAD1 in mitochondrial dynamics was missing. Hence one major aim of my thesis was to test whether *Asrij* affects mitochondria for progenitor homeostasis. Immunolocalization-based experiments revealed mitochondrial localization of *Asrij* in *Drosophila* blood progenitors and circulatory hemocytes. *Asrij* depletion resulted in elongation of mitochondria, suggesting a shift of mitochondrial dynamics towards decreased fission or increased fusion. Hence, I undertook a detailed analysis of mitochondrial morphology in wild type lymph gland and found that it varies across progenitor subsets, from anterior to posterior. Tertiary lobe progenitors are less mature and show shorter mitochondria compared to primary and secondary lobes. **This reveals mitochondrial heterogeneity of blood progenitors that was not reported before.** Comparisons to progenitors depleted of *Asrij* showed that while anterior progenitors had elongated mitochondria like in *asrij* null hemocytes, the effect was insignificant in posterior progenitors. Moreover, depletion of canonical regulators of mitochondrial dynamics such as Drp1 or Marf (Mitofusin) that regulate mitochondrial fission and fusion respectively, affected mitochondrial morphology predominantly in the anterior (primary) lobe, further supporting progenitor heterogeneity.

Interestingly, mitochondrial dynamics regulators affected only crystal cell differentiation. Drp1 and Marf had opposite effects on Notch signaling-dependent crystal cell differentiation. The posterior pool of progenitors remained refractile to differentiation upon perturbation of *Asrij*, Drp1 or Marf expression. Moreover, a synergistic interaction of *Asrij* with Drp1 and Marf affected mitochondrial morphology and crystal cell differentiation in distinct ways in the lymph gland. **These results indicate the active role of mitochondrial dynamics regulators in blood cell homeostasis and Notch-dependent crystal cell specification** (Ray et al., *Front. Cell Dev. Biol.*, 2021).

Endosomes regulate multiple signaling pathways associated with hematopoiesis through endocytic trafficking and endosomal protein sorting. However, any active role of endosomal

protein sorting in blood cell homeostasis is underexplored. The conserved ESCRT (Endosomal Sorting Complex Required for Transport) machinery actively regulates endosomal protein sorting for lysosomal degradation. ESCRT consists of four functionally distinct subunits, which sequentially bind to the endomembrane bound ubiquitinated cargoes to allow intraluminal protein sorting. Loss of ESCRT results in dysregulated activation of signaling pathways, leading to tissue hyperproliferation, apoptotic resistance and neoplastic transformation. Previous reports showed that loss of *Asrij* causes entrapment of Notch intracellular domain (NICD) in *Hrs*⁺ sorting endosomes, phenocopying ESCRT mutants. Moreover, bioinformatic analyses showed ESCRT might underlie various hematological malignancies, including myeloproliferative disorders. Hence, ESCRT may potentially play an active role in hematopoiesis.

I assessed the role of all 13 components (constituting 4 subunits) of *Drosophila* ESCRT in lymph gland hematopoiesis by knocking down individual genes using the blood progenitor-specific driver *domeGal4*. Ubiquitination status was evaluated by immunostaining across all *dome*⁺ progenitor subsets for a generic readout of the effect of ESCRT depletion. Further, progenitor status was assessed by reporter expression and immunostaining for plasmacytes, crystal cells, and lamellocytes to assess the extent of differentiation. **This generated a functional map for each ESCRT charting its role in *dome*⁺ progenitor maintenance and lineage specification in the entire lymph gland.** The map indicated that in spite of their ubiquitous expression, only 7 ESCRT components (Vps28, Tsg101, Vps32, Vps20, Vps2 in primary lobe and Vps28, Vps37A, Vps22, Vps20 in posterior lobes) resulted in accumulation of ubiquitinated cargoes, whereas depletion of others had no effect. Further, some ESCRTs were essential to regulate differentiation to a given lineage, where others were dispensable. Interestingly, Vps25 depletion had no effect on lymph gland hematopoiesis. **Distinct phenotypes of co-expressing ESCRT components indicate context-dependent function and additional organelle level regulation of hematopoiesis.**

Despite uniform expression of ESCRT components, progenitor sensitivity decreased from anterior to posterior lobes of the lymph gland as fewer ESCRT components affected progenitor maintenance or blood cell differentiation in the posterior lobes. **This also reaffirms progenitor heterogeneity and the developmentally immature nature of the posterior progenitors.** Also, depletion of Vps36 and Vps2 triggered lamellocyte differentiation in the refractile progenitors of the posterior lobes highlighting the critical role of endosomes and ESCRT in controlling differentiation in progenitors with low potency even without immune challenge.

Depletion of most ESCRT components promotes precocious crystal cell differentiation. Notch signaling regulates crystal cell differentiation. ESCRT depletion caused NICD accumulation and Notch signaling activation in all lymph gland lobes in concordance with crystal cell differentiation. However, Notch activation and crystal cell differentiation in ESCRT knockdown lymph glands correlated only partially to the status of ubiquitinated cargo. Knocking down either of Notch ubiquitin ligase Deltex or deubiquitinase eIF3f1 in the blood progenitors did not rescue Notch activation or crystal cell differentiation phenotype of ESCRT. Hence Notch activation downstream of ESCRT knockdown in blood progenitors may be independent of the status of ubiquitination.

The effect of ESCRT depletion may be cell autonomous or non-autonomous. Mitotic mutant clone analysis revealed that ESCRT regulates ubiquitinated cargo transport and sorting in blood progenitors in a cell-autonomous manner, whereas it may affect blood cell differentiation in a cell non-autonomous manner as well. Also, analysis of mitotic potential suggested a possible role of cell proliferation as an additional contributor to the perturbed blood cell hematopoiesis. **These data show distinct role of ESCRT components in lymph gland hematopoiesis, especially lineage choice and reflect the heterogeneity of progenitor subsets.**

In summary, this thesis shows the active role of conserved organelle machinery in blood progenitor maintenance, lineage choice, and function *in vivo*. *In situ* analyses show an active role of mitochondrial dynamics regulators in the lineage-specific differentiation of progenitors. Further, ESCRT components play distinct roles in lineage choice and signaling activation. These components differentially affect blood lineage choice suggesting complex post-transcriptional regulation of individual ESCRT function. Also, both mitochondrial dynamics regulators and ESCRT contribute to progenitor heterogeneity and control differentiation of the refractile progenitor pools of *Drosophila*. This knowledge can be applied to elucidate mechanisms of conserved organellar regulation of blood progenitor maintenance, heterogeneity, and lineage choice in vertebrate models and would allow screening of candidates to modulate blood regeneration.

Chapter 1. Introduction

Understanding mechanisms that control cell fate decisions remains an outstanding question in biology. A plethora of cell-intrinsic and -extrinsic factors may govern cell fate choice during development. Concerted activation of signaling pathways is pivotal to the maintenance, proliferation and differentiation of stem cells and progenitors that give rise to various cell types within a tissue. Additionally, metabolic status contributes to cell fate and tissue homeostasis. Elucidating the intricate and dynamic molecular networks that dictate developmental signaling and cell fate choice still remains incomplete and has garnered attention as a pressing problem in developmental biology and regenerative medicine.

Membrane-bound organelles act as dynamic regulatory stations for various signaling pathways as well as metabolic flux by integrating extracellular and intracellular cues at a post-transcriptional level. Endocytosis regulates the internalization, transport and degradation of signaling receptors. Endosomal compartments constitute a network of molecular hubs that modulate cellular signaling relays. On the other hand, mitochondria regulate energy metabolism, signal generation and also the epigenome to dictate a number of developmental processes. How these organelles contribute to the precise control of lineage-specific signaling activation and progenitor fate decisions is largely underexplored. Also, how context-dependent regulation of ubiquitously functional organellar machineries fine tunes cell fate choice is an enigma. **A deeper understanding of the organellar framework regulating cell fate choice requires an in-depth analysis of the molecular components to gain conceptual insight into the process.**

Hematopoiesis involves a complex hierarchy of hematopoietic stem cell (HSC) and progenitor differentiation. Signaling pathway activation, bioenergetic profile, marker expression, tissue microenvironment and various other factors may contribute to blood stem and progenitor cell maintenance and their differentiation. Hence, the rudimentary questions of progenitor biology could be addressed through study of the mechanisms of

HSC and progenitor homeostasis. *Drosophila melanogaster* serves as a simple, easily accessible yet powerful and relevant *in vivo* model for studying conserved mechanisms of hematopoietic development. *Drosophila* shows less lineage diversity of blood cells as compared to vertebrates. Further, the *Drosophila* larva harbors the entire blood progenitor population in distinct zones of a specialized hematopoietic organ called the lymph gland. This allows a comprehensive *in situ* analysis of progenitor homeostasis at the whole organismal level. Using *Drosophila* as the experimental model, **we aimed to address the role of conserved and generic organellar machinery (mitochondrial dynamics regulators and endosomal sorting complex) in progenitor homeostasis and fate choice *in vivo* and also to elucidate how the functional output of such a ubiquitous molecular network is regulated in a context-dependent manner.**

1.1 Hematopoiesis: A model to understand progenitor homeostasis and development

The process of hematopoiesis is a suitable model to study stem cell and progenitor homeostasis due to its robust and complex developmental hierarchy with intricate interplay of signaling, gene expression and metabolism. Hematopoietic stem cell (HSC) biology has been studied extensively using several *in vivo* vertebrate models such as zebrafish and mouse (Jing and Zon, 2011; Clements and Traver, 2013; Robertson et al., 2016). Conserved mechanisms of HSC maintenance and differentiation have also been investigated using blood progenitor population of invertebrate models such as *Drosophila* (Jung et al, 2005; Banerjee et al., 2019). The following sub-sections provide a detailed account of hematopoiesis in both vertebrate and *Drosophila* models and their comparison.

1.1.1 Vertebrate hematopoiesis

Hematopoiesis in the adult stage of vertebrates involves a robust developmental and lineage hierarchy. The lineage diversity could be exploited to explore many fundamental aspects of cell fate decisions. Hematopoiesis in adult mouse and human occur in the bone marrow across different bone compartments. However, the lungs have also been shown as an active reservoir of hematopoietic progenitors and platelet biogenesis (LeFrancais et al.,

2017). Extramedullary hematopoiesis, which may also occur during hematological disorders takes place in other sites such as the spleen, liver, lymph nodes, heart, adipose tissue, adrenal gland etc (Yamamoto et al., 2016). Presence of multiple sites for hematopoiesis thus makes it infeasible to analyse the entire HSC and progenitor pool and homeostatic mechanisms at all hematopoietic sites in vertebrates. HSCs residing in the bone marrow generate common lymphoid progenitors (CLP) and common myeloid progenitors (CMP) that eventually give rise to different types of terminally differentiated blood cells (Fig 1.1A). Though the classical model describes hematopoiesis as distinct stepwise events of blood cell differentiation, recent research highlights the continuous Waddington model, which describes it as a continuum of intermediate states varying in their transcriptomic profile and gradually acquiring lineage commitment (Fig 1.1B) (Haas et al., 2018). Regenerative potential of HSCs is assessed through transplantation-based experiments in lethally irradiated mice as well as through *in vitro* colony-forming assays. Several mouse models of hematological disorders show perturbed HSC and multipotent progenitor maintenance (Zhou et al., 2015; Kohnken et al., 2017; Tyagi et al., 2020). These models are amenable to chemical screens and serve as useful tools to study mechanisms of blood cell homeostasis and cell fate decisions.

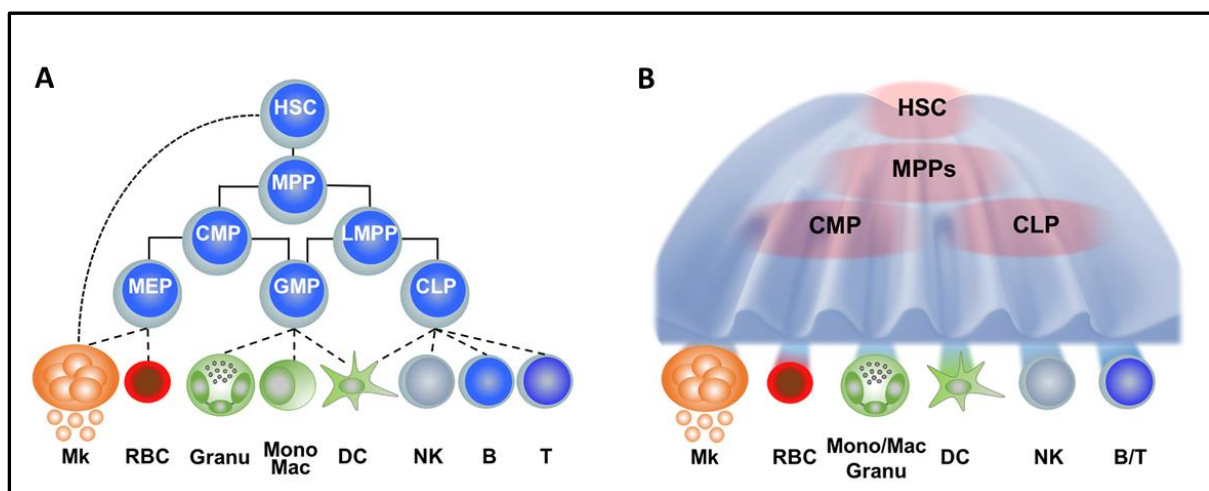


Figure 1.1. Models of vertebrate hematopoiesis. (A) The classical model describes hematopoiesis as discrete stepwise differentiation of hematopoietic stem and progenitor cells [HSPC: HSC and MPP (Multipotent progenitors)] to committed progenitors termed as CMP (common myeloid progenitors) and CLP (common lymphoid progenitors). These

progenitors differentiate to various terminally differentiated blood cells such as Megakaryocytes, RBC, Granulocytes, Monocytes and Macrophages, Dendritic cells, Natural Killer cells, B and T lymphocytes. (B) The continuous Waddington model defines hematopoiesis as a continuum of intermediate states with different gene expression profiles, which eventually differentiate into lineage-committed progenitors and blood cells (Adapted and modified from Haas et al., *Cell Stem Cell*, 2018).

1.1.2 Hematopoiesis in invertebrates

Invertebrate models have been used quite extensively in developmental biology due to evolutionarily conserved mechanisms of development, ease of genetic manipulation and short lifespan. Some blood cell types in metazoans are analogous to vertebrates and develop through similar pathways, suggesting a monophyletic origin for these blood cells, whereas other blood cells might have arisen through dissimilar processes (Millar and Ratcliffe, 1989). For example, phagocytic blood cells are maintained throughout the course of evolution across all phyletic groups. This allows use of certain invertebrate metazoan members such as arthropods as suitable models for studying hematopoiesis and blood cell function.

1.1.2.1 *Drosophila* as a model of hematopoiesis

Hematopoiesis in *Drosophila melanogaster* occurs in two distinct waves- embryonic and larval. Embryonic hematopoiesis occurs from the head mesoderm (Ramond et al, 2015). Mature hemocytes generated from mesoderm disperse throughout the hemocoel and are maintained in the larval stage as well. Larval wave of hematopoiesis takes place in a specialized organ called the lymph gland, which originates from the embryonic thoracic mesoderm (Krzemien et al., 2010; Banerjee et al, 2019). Lymph gland hemocytes do not enter the circulation until the onset of metamorphosis or immune stress. The lymph gland disintegrates during metamorphosis and the hemocytes of both embryonic and larval origin are carried to the adult stage (Tan et al., 2012) (Fig 1.2).

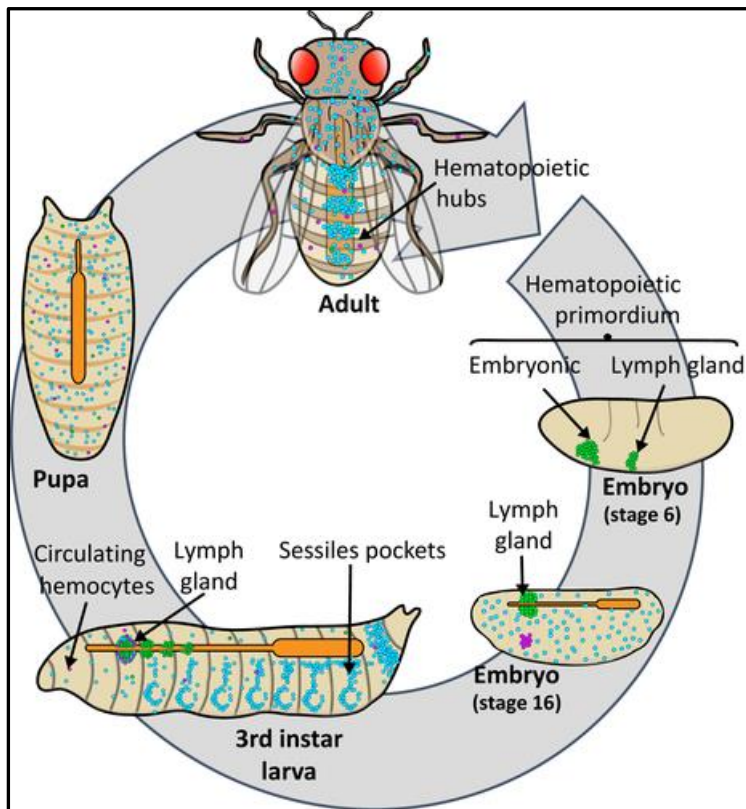


Figure 1.2. Hematopoiesis during *Drosophila* development.

Specification of lymph gland primordium occurs in stage 6 *Drosophila* embryo. At stage 16, the head mesoderm differentiates to plasmatocytes (blue) or crystal cells (pink). At the larval stage, the hemolymph and the cuticular sessile pockets contain embryonic hemocytes. The lymph gland lobes grow till the third instar stage and are aligned along the antero-posterior axis towards the dorsal half, flanking the cardiac tube. At the pupal and adult stage, hemocytes from the sessile

pockets, circulation and the lymph gland are released into the hemolymph. In adults, the hemocytes remain attached to the abdomen as clusters near the dorsal vessel (Adapted from Letourneau et al., *FEBS Letters*, 2016).

As discussed in the previous section, vertebrate hematopoiesis takes place in a complex milieu across multiple shifting sites. HSCs reside as an impure and scanty population in the bone marrow. Hence, a comprehensive *in situ* analysis of blood cell homeostasis is difficult. The *Drosophila* larval lymph gland serves as a simple yet powerful model to study hematopoiesis *in situ*. It is a multilobed organ flanking the cardiac tube (Fig 1.3). The anterior pair of lobes, also known as the primary lobe, is the most well characterized part of the lymph gland. The primary lobe of the lymph gland comprises of three developmentally distinct zones enriched with three different groups of cells: 1) the inner/medial medullary zone (MZ) comprising blood progenitors (prohemocytes), 2) the outer/distal cortical zone (CZ) constituted by differentiated blood cells (hemocytes) and 3) the posterior signaling centre (PSC), thought to serve as a hematopoietic niche. The CZ and MZ flank a thin zone of intermediate progenitors (IP) that express both prohemocyte and hemocyte markers at low levels (Krzemien et al., 2010). The secondary, tertiary and occasionally quaternary lobes,

together known as the posterior lobes harbor progenitor subsets but no differentiated blood cell population. Such distinct zonation of different blood cell types across the tissue is advantageous for imaging-based *in situ* analysis of blood cell status, thus overcoming the limitation of restricted sample access and an impure milieu as observed in the vertebrate hematopoietic compartments.

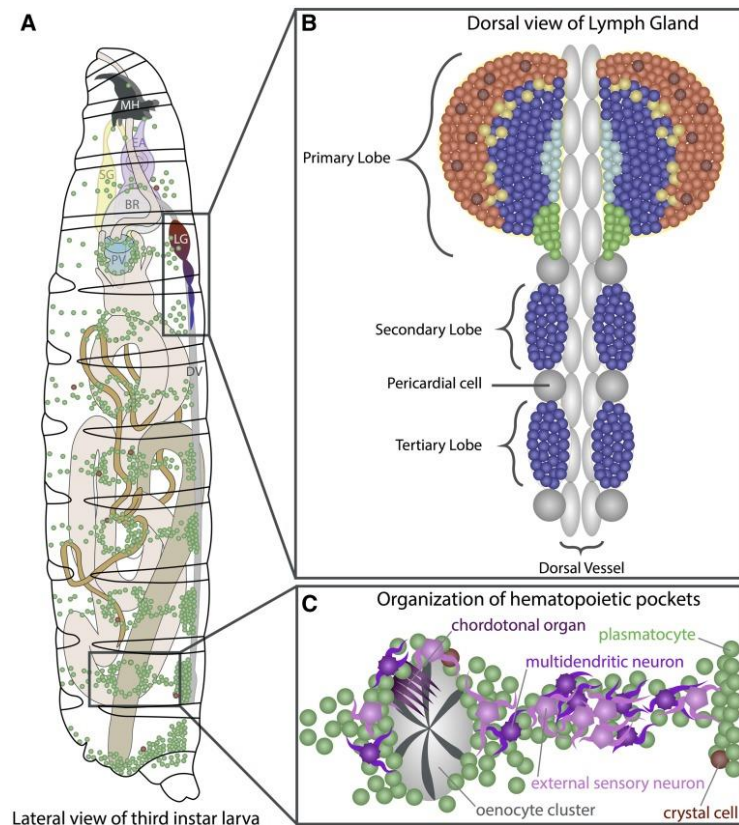


Figure 1.3. Schematic of *Drosophila* larval hematopoiesis.

(A) In the third-instar larva, the lymph gland (LG) flanks the Dorsal vessel (DV) towards the dorsal side of the hemocoel. Differentiated blood cell [Plasmatocytes (green) and crystal cells (red)] are observed in the circulation (hemolymph) as well as in segmentally distributed sessile pockets. (B) The LG flanks the DV from anterior to posterior and consists of at least three pairs of lobes. The anterior lobes, also known as primary lobes, are the largest and consist of three developmentally distinct zones. The inner/medial region of the

primary lobe (blue), also known as the medullary zone (MZ) consists of undifferentiated blood progenitors (prohemocytes). The outer/distal region (red), known as the cortical zone (CZ) contains differentiated blood cells (hemocytes). The posterior signaling centre (PSC), shown in green, act as hematopoietic niche. Pericardial cells (gray sphere) separate the posterior lobes from each other and the primary lobe. The posterior lobes harbor progenitor subsets and remain largely undifferentiated. (C) The sessile hematopoietic pockets reside along the dorsal side of the larval cuticle. External sensory and multidendritic neurons (purple) regulate adherence, proliferation, and maintenance of hemocytes within hematopoietic pockets. Hematopoiesis in sessile pockets involve hemocyte proliferation and transdifferentiation. BR, brain; DV, dorsal vessel; EA, eye-antennal disc; LG, lymph gland; MH, mouth hooks; PV, proventriculus; SG, salivary gland (Adapted from Banerjee et al., *Genetics*, 2019).

Studies so far have primarily focused on the anterior-most primary lobe, ignoring the rest of the progenitor populations in the posterior lobes. As the lymph gland harbors the entire blood progenitor population of *Drosophila*, studying the entire organ allows complete sampling and a comprehensive study of progenitor homeostasis at the organismal level. Blood progenitor subsets of *Drosophila* are linearly arranged across the lymph gland and are characterized by the expression of several markers such as Domeless, TepIV, DE-Cadherin, etc (Figure 1.4). A recent report from our lab highlights that the posterior progenitors are developmentally distinct from the anterior subset and are refractile to immune challenge, possibly due to differential activation of signaling pathways (Rodrigues et al., *eLife*, 2021). Also, previous phenotypic analyses of mutants showing hematopoietic aberrations indicate differential response of primary and posterior lobes to genetic perturbation (Kulkarni, Khadilkar et al., 2011; Khadilkar et al, 2014). We aim to understand conserved mechanisms underlying blood progenitor homeostasis and heterogeneity using the larval lymph gland as a model.

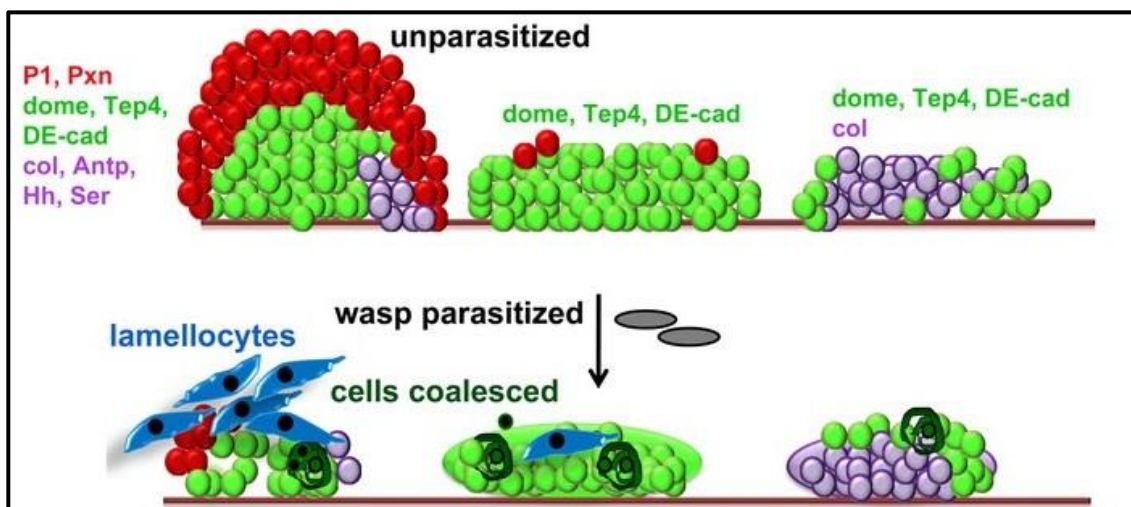


Figure 1.4. Schematic representation of the lymph gland progenitor subsets. Blood progenitor subsets across different lobes express various markers such as domeless, TepIV, DE-cadherin and respond differentially to immune challenge. The anterior lobe progenitors are most sensitive and readily differentiate upon infection with parasitoid wasp, whereas the posterior lobe progenitors are refractile (Adapted from Rodrigues et al., *eLife*, 2021).

Drosophila prohemocytes differentiate into three types of hemocytes. Plasmatocytes constitute the major proportion, accounting for 90-92%. Plasmatocytes are phagocytic in nature and engulf pathogens such as bacteria. Crystal cells constitute 8-10% of the hemocyte population. The primary function of crystal cells is wound healing and destruction of invading pathogens through melanisation. Lamellocytes, the third type of *Drosophila* hemocyte, rarely develop in circulation or lymph gland under normal conditions and are induced upon infestation with parasitoid wasp eggs. Lamellocytes are distinguishable by their larger size and are capable of encapsulating and melanising wasp eggs. *Drosophila* blood cells are analogous to vertebrate myeloid lineage and constitute the cellular arm of *Drosophila* innate immunity. They also play a significant role in development through tissue remodelling.

1.2 Parallels between vertebrate and invertebrate hematopoiesis

1.2.1 Signaling pathways controlling vertebrate hematopoiesis

Hematopoiesis in vertebrates involves several transcription factors and signaling pathways (Fig 1.5). One of the conserved transcription factors for the maintenance of HSC is GATA2. Conditional knockout-based studies reveal the role of GATA2 in both HSC generation and maintenance (de-Pater et al., 2013). A total of 12 transcription factors could establish hematopoietic program *in vivo* (Wilson et al., 2010) or *in vitro* (Goode et al., 2016). Hedgehog signaling is an important regulator of critical downstream signaling cascades required for generation of hemogenic endothelium (Lawson et al., 2002; Gering et al., 2005; Wilkinson et al., 2009). Impairment of hedgehog signaling leads to proliferation of HSCs (Trowbridge et al., 2006). However, contradictory results suggest a dispensable role of Hedgehog signaling in adult hematopoiesis (Hoffmann et al., 2009; Gao et al., 2009). On the other hand, BMP4 (member of Transforming Growth Factor -beta superfamily) signaling promotes biogenesis, homing and survival of HSCs (Durand et al., 2007; Wilkinson et al. 2009). Also, inhibition of BMP signaling leads to expansion of niche and HSC number (Zhang et al., 2003). Canonical Wnt signaling is essential to strike a balance between LT-HSC quiescence and proliferation (Kinder et al., 2010).

JAK-STAT signaling plays an indispensable role in blood cell homeostasis. JAK2 mutation is associated with 95% cases of polycythemia vera (PV) whereas 50% cases of essential thrombocythemia (ET) and primary myelofibrosis (PMF), all of which account for myeloproliferative neoplasms (MPN) (James et al., 2005; Kralovics et al., 2005; Levine et al., 2005; Baxter et al., 2005; Jones et al., 2005; Zhao et al., 2005). JAK2 V617F mutation leads to constitutive activation of STAT3 and STAT5, which are associated with HSC expansion during MPNs (James et al., 2005; Teofili et al., 2007).

Notch signaling plays an essential role for normal hematopoiesis. Analyses of null mutant of Mindbomb-1 (Mib-1), a regulator of Notch endocytosis and activation reveals that defective Notch signaling in the hematopoietic microenvironment leads to myeloproliferative disease (MPD) (Kim et al., 2008). However, all components of Notch signaling may not be essential for hematopoiesis. Inactivation of Notch1 in progenitors and the cognate ligand Jagged-1 in stroma of bone marrow does not affect HSC maintenance or reconstitution potential (Mancini et al., 2005).

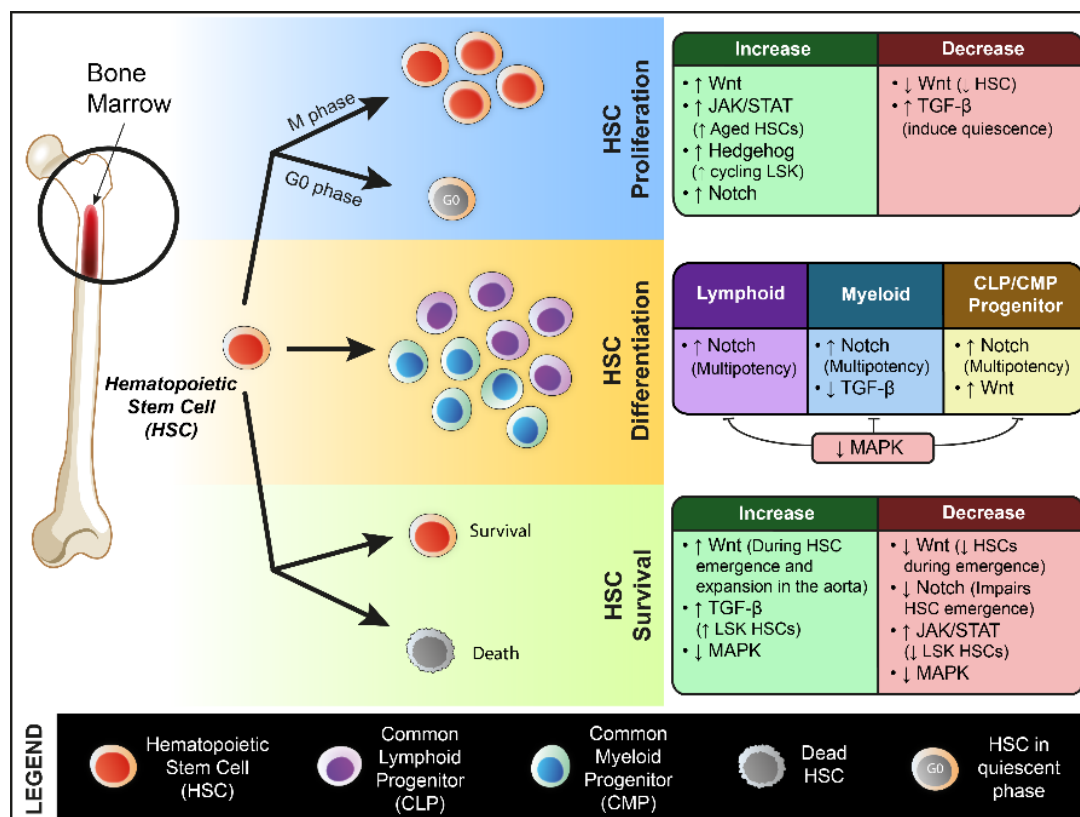


Figure 1.5. Signaling pathways regulating vertebrate bone marrow hematopoiesis. Hematopoietic stem cells (HSC) give rise to all the differentiated blood cells in the bone marrow. Key signaling pathways regulating the proliferation, differentiation, and self-renewal of HSCs are shown (Adapted from Krishnan et al., *Biomolecules*, 2021).

1.2.2 Conserved signaling pathways controlling *Drosophila* hematopoiesis

Blood cells of *Drosophila* are analogous to the myeloid lineage of vertebrates. Specification of the progenitor to each blood cell type requires activation of specific signaling pathways (Fig 1.6). Lineage specification is regulated by combinatorial action of GATA (Serpent), Friend of GATA (U-shaped) and Runx (Lozenge) family of transcription factors. Serpent (Srp) regulates differentiation to both plasmatocytes and crystal cells (Bernardoni et al., 1997; Lebestky et al., 2000; Fossett et al., 2001; Alfonso and Jones, 2002; Waltzer et al., 2002). Ush inhibits uncontrolled hemocyte proliferation and lamellocyte differentiation (Sorrentino et al., 2007). However, concerted action of all three transcription factors regulates crystal cell specification (Fossett et al., 2003).

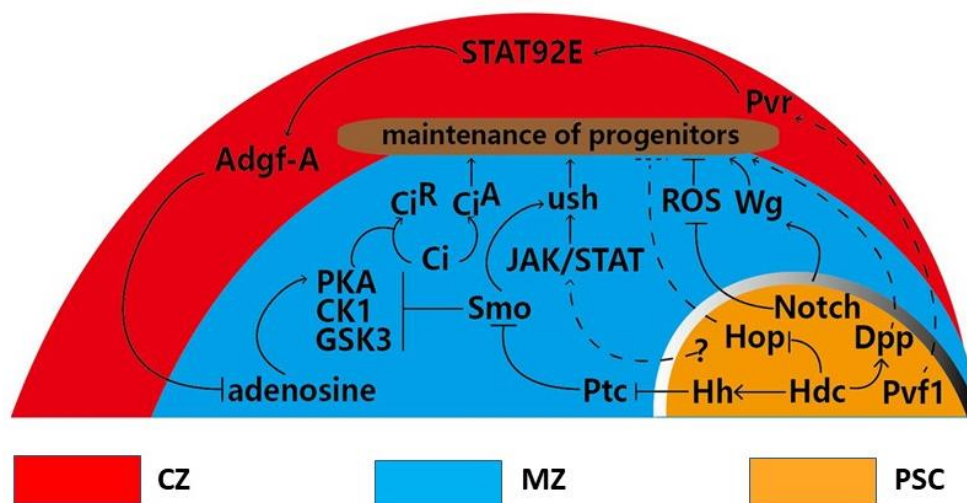


Figure 1.6. Signaling pathways operating in the lymph gland. Several conserved signaling pathways such as JAK/STAT, Notch, Dpp, Hh regulate blood cell homeostasis in the lymph gland. Ligands secreted from the PSC play a crucial role in signaling regulation for maintaining progenitor homeostasis. CZ: Cortical zone, MZ: Medullary zone, PSC: Posterior signaling centre (Adapted from Luo et al., *Front. Cell Dev. Biol.*, 2020).

JAK/STAT signaling actively maintains progenitor populations that express the receptor Domeless. Downregulation of STAT activation causes loss of prohemocyte pool (Jung et al., 2005; Krzemien et al., 2007) and increased lamellocyte differentiation in the primary lobes (Makki et al., 2010). On the other hand, Notch signaling positively regulates crystal cell differentiation (Duvic et al., 2002). Notch signaling also regulates the overall size of the lymph gland lobes by negatively regulating proliferation of the preprogenitors (domeless-ve cells toward the medial region of the primary lobe) at the third instar larval stage (Dey et al., 2016). Notch activation in progenitors require secretion of Notch ligand Serrate from PSC (Lebestky et al., 2003). However, a recent report suggests a context-dependent role of Notch in progenitor maintenance and binary fate decision between plasmatocyte and crystal cell at MZ-CZ boundary (Blanco-Obregon et al., 2019). On the other hand, extracellular growth factor secreted from PSC promotes differentiation of progenitors to lamellocyte (Sinenko et al, 2011). Further, EGFR signaling positively regulates plasmatocyte proliferation in Graf depleted larval hemolymph (Kim et al., 2017). Other signaling pathways such as Hedgehog, Wnt and Dpp signaling are essential for progenitor and niche maintenance and expansion (Sinenko et al., 2009; Pennetier et al., 2012; Dey et al., 2016; Baldeosingh et al, 2018). This suggests active contribution of various conserved signaling pathways toward blood progenitor maintenance and lineage commitment in *Drosophila*.

1.2.3 *Drosophila* lymph gland serves as an ideal model for a comprehensive *in situ* analysis of blood progenitor homeostasis.

Vertebrate HSCs are transcriptionally heterogeneous (Adolfsson et al., 2005; Grover et al., 2016; Guo et al., 2013, Haas et al., 2015, Karamitros et al., 2018; Velten et al., 2017; Haas et al., 2018). However, functional heterogeneity of HSC across different compartments is underexplored. Despite the lack of substantial evidence to claim *Drosophila* prohemocytes as *bona fide* HSCs, genetic similarity has been reported (Cho et al., 2021). Blood progenitors of *Drosophila* remain compartmentalized across the antero-posterior axis of the larval lymph gland. Unlike primary lobe prohemocytes, the progenitor populations in posterior lobes (which include secondary, tertiary and at times, quaternary lobes) are poorly characterized. Prohemocytes of primary lobes are ontogenetically and functionally heterogeneous (Cho et al., 2021). A recent preprint highlights combinatorial gene

expression as the dictating factor for progenitor fate choice in the lymph gland rather than stepwise binary decision of lineage commitment, thus drawing a conceptual parallel with continuous model of vertebrate hematopoiesis which is based on transcriptomic, metabolic and developmental heterogeneity of hematopoietic stem and progenitor cells (Girard et al, bioRxiv, 2021). However, the functional, developmental and genetic identity of the blood progenitor subsets across different lobes of the lymph gland are only recently being explored (Rodrigues et al, *eLife*, 2021) and merit further detailed analysis.

1.3 Immune functions of the blood lineages.

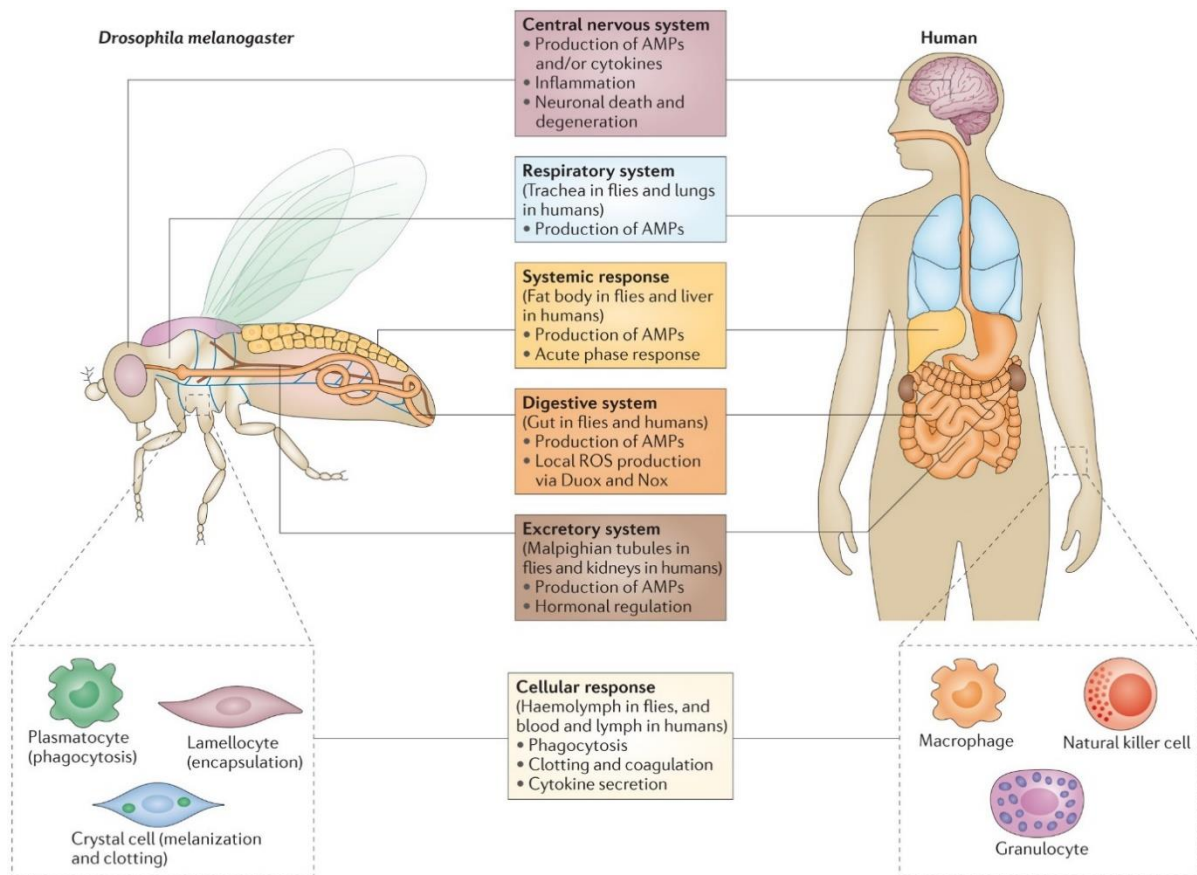
Hematopoiesis is directly linked to vital physiological functions such as immunity. Immune challenge affects blood progenitor homeostasis and triggers differentiation. Organismal immunity not only depends on the function of blood cells but also on the efficiency of blood cell production and generation of various systemic cues. Hence, immune response reflects the impact of hematopoiesis at a whole organismal level.

Drosophila immunity is innate in nature and consists of the cellular and humoral arms, similar to the vertebrate innate immune system (Fig 1.7). While the cellular arm relies majorly on the phagocytic and enzymatic activities of the circulatory hemocytes, the humoral arm acts through integration of several diffusible molecular cues operating at a systemic level. Hence, perturbed blood cell homeostasis can adversely affect the balance of various immune signalling networks and hence the response to pathological situations.

The three terminally differentiated blood cell types in *Drosophila* mediate cellular immunity. The plasmatocyte membrane contains NimC1 and Eater proteins that synergistically aid in phagocytosis of Gram-positive bacteria (Melcarne et al., 2019). Crystal cells destroy pathogens through oxidative stress caused by the production of ROS as a by-product of melanisation reaction. On the other hand, lamellocyte differentiation occurs only at the larval stage upon infestation with parasitoid wasps (e.g. *Leptopilina boulardi*). As mentioned

previously, lamellocytes mediate encapsulation of the wasp eggs (Lanot et al., 2001; Sorrentino et al., 2002).

The humoral arm in *Drosophila* is established through the concerted action of anti-microbial peptides (AMP), secrete primarily from the larval and adult fat bodies and partially from the hemocytes and epithelial tissues such as gut and trachea. Two critical immune signaling pathways, known as Toll and Imd pathway, contribute to AMP production upon immune challenge with bacteria or fungi (described in details in Chapter 2) (Ip et al., 1993; Lemaitre et al., 1995; Stoven et al., 2000; Michel et al., 2001). Previous reports have highlighted hemocyte-dependent regulation of various signaling pathways in the fat body and vice-versa that not only affect the organismal immunity but also the metabolic homeostasis and organismal development (Schmid et al., 2014; Shin et al., 2020). However, the communication of the hematopoietic system with the systemic immune signals remain largely elusive and merits meticulous exploration.



Nature Reviews | Immunology

Figure 1.7. Comparison of *Drosophila* immune system with vertebrates. Innate immunity of *Drosophila* consists of cellular and humoral arms: three different blood cell types—plasmatocytes, crystal cells and lamellocytes constitute the cellular arm which hold functional similarity to mammalian myeloid lineage. The humoral arm depends on the antimicrobial peptides (AMP) secreted majorly from various epithelial tissues such as fat body, gut and trachea and also from the brain. The hemocytes also partly contribute to AMP secretion (Adapted from Buchon et al., *Nat Rev Immunol.*, 2014).

1.4 Role of organelles in cell fate decisions and hematopoiesis

Sub-cellular organelles govern cell fate through co-ordination of signaling and metabolic networks (Julian and Stanford, 2020). Dynamic organelles fine tune cell identity through rapid regulation of various extracellular and intracellular cues at a post-transcriptional level. Homotypic and heterotypic inter-organelle communications allow metabolite exchange and signal transduction. Organelle dynamics establish a spatiotemporal continuum of signal modulatory nodes that orchestrate cell fate in a context-dependent manner (Sigismund et

al., 2021). Several recent reviews have highlighted the role of membrane-bound organelles in vertebrate hematopoietic stem cell fate specification and blood cell homeostasis (Ito and Ito, 2018; Filippi and Ghaffari, 2019; Koschade and Brandts, 2020; Ghafouri-Fard et al., 2021). Mitochondria regulate ATP biosynthesis, metabolic flux and generate signals critical for HSC fate decisions. On the other hand, endomembrane system provides a scaffold for the assembly of several important signaling complexes (Scita and Di Fiore, 2010). Endosomes regulate trafficking of various receptors that play a critical role in lineage-specific signaling activation. We aim to elucidate the role of conserved mitochondrial and endosomal machineries in blood cell homeostasis that involve progenitor maintenance and lineage-specific differentiation.

1.4.1. Mitochondria as regulators of hematopoiesis

Mitochondria act as the active site for ATP biosynthesis via oxidative phosphorylation and contribute significantly to the cellular metabolic flux. However, mitochondria can additionally influence cell fate through regulation of signaling and modulation of epigenome (Ryall et al., 2015; Lisowski et al., 2018; Fu et al., 2019). Mitochondria have emerged in recent times as a critical regulatory node for HSC differentiation, specification and homeostasis (Filippi and Ghaffari, 2019). Though energy metabolism regulated by mitochondria plays a major driving force for HSC maintenance and differentiation, recent discoveries suggest active contribution of mitochondria in HSC fate decision through additional mechanisms (Diebold and Chandel, 2016; Schell and Rutter, 2017; Hinge et al., 2020). HSCs in the quiescent state depend on glycolysis for energy metabolites despite a relatively higher mitochondrial content (de Almeida et al., 2017). An earlier report showed that HSCs and blood progenitors depend on mitochondrial *SdhD* gene, which encodes a subunit of mitochondrial complex II, for survival (Bejarano-Garcia et al., 2016). Also, components of mitochondrial respiration, though dispensable for HSC proliferation, are absolutely indispensable for fetal HSC differentiation and maintenance of adult HSC quiescence (Anso et al., 2017). Loss of function of mitochondrial proteins involved in mitochondrial respiration and mitochondrial gene transcription causes alteration in metabolite generation that can affect the epigenetic landscape (Schell and Rutter, 2017). Regulators of mitochondrial dynamics maintain HSCs with lymphoid potential through

calcium-dependent signaling and also control multiple biosynthetic pathways that regulate HSC regenerative potential (Luchsinger et al., 2016; Hinge et al., 2020). Fatty acid oxidation-dependent, PARKIN-mediated mitophagic flux maintains regenerative potential of Tie2+ primitive HSCs (Ito et al., 2016). All these reports suggest an indispensable role of mitochondria in HSC fate choice despite dependence on anaerobic metabolism (Fig 1.8).

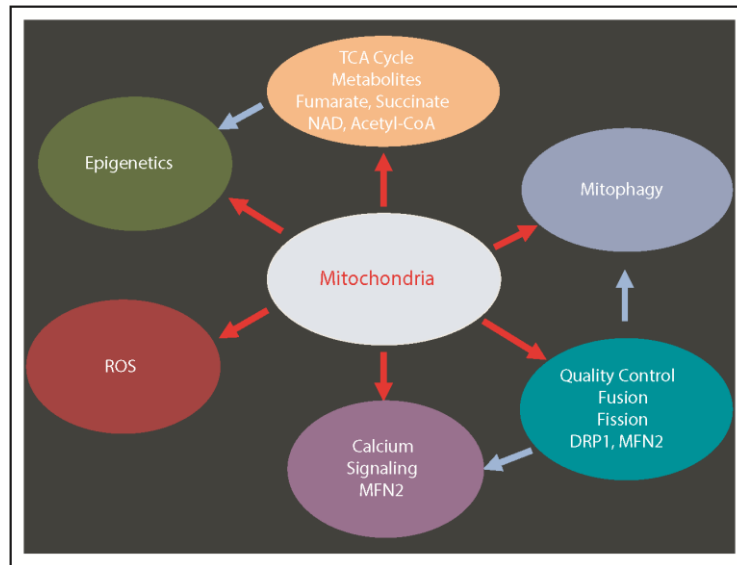


Figure 1.8. Multiple mitochondrial processes regulate hematopoiesis. Mitochondria are associated with various pathways and mechanisms such as energy metabolism, mitophagy, mitochondrial dynamics, Calcium and ROS signaling, epigenetic regulation of the genome, all of which contribute to HSC fate (Adapted from Filippi and Ghaffari, *Blood*, 2019).

1.4.1.1 Link between mitochondrial dynamics and hematopoiesis

Mitochondrial dynamics regulate mitochondrial function and cell fate choice (Wai and Langer, 2017). Mitochondrial fission and fusion segregate damaged mitochondria and allow exchange of components, electrochemical gradients, and metabolites (Twig et al, 2008; van der Bliet et al., 2013; Liu et al, 2020). Mitochondrial morphology and dynamics may vary across cell states, lineages, and tissues (Seo et al., 2018).

Mitochondrial dynamics involve mitochondrial fission, fusion, biogenesis and degradation. Mitochondrial dynamics depends on a number of conserved proteins, initially identified in yeast, that govern mitochondrial fission and fusion (Fig 1.9). Of them, Dynamin-like GTPases are associated with mitochondrial outer and inner membrane and play the most critical role in mitochondrial membrane dynamics. Dynamin related protein (Drp1) mediates mitochondrial outer membrane fission. Fis1, MFF, Mid49/51 recruit Drp1 on the mitochondrial outer membrane and promotes fission (Labbe et al., 2014). On the other hand, Mitofusins (Mfn 1/2) regulate mitochondrial outer membrane fusion and leads to fragmentation of mitochondria upon depletion (Mishra and Chan, 2014). Opa1, mitoPLD and MTP18 also play a critical role in mitochondrial fusion or fission (Tondera et al, 2004; Huang et al, 2011; Watanabe et al., 2011). Opa1 regulates fusion of inner mitochondrial membrane. Opa1 consists of long and short splice variants that differentially contribute to mitochondrial fusion to balance mitochondrial dynamics- while the long isoform promotes mitochondrial fusion, the short isoform promotes fission (Anand et al., 2014).

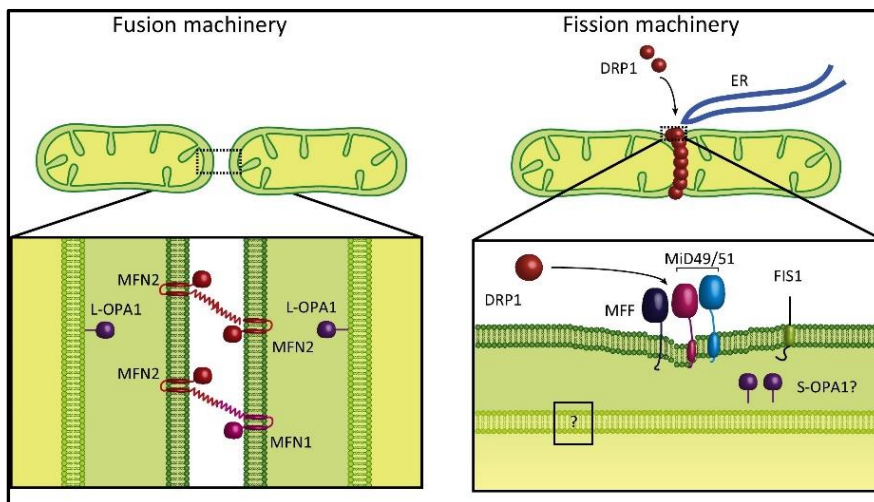


Figure 1.9. Regulation of Mitochondrial Fusion and Fission. Homo- and heterotypic interactions between Mfn1 and Mfn2 (red) promote fusion of the outer mitochondrial membrane (OMM, dark green) and L-OPA1 (purple) mediates fusion of the

inner mitochondrial membrane (IMM, light green). MitoPLD (green) is required for OMM fusion. FIS1, MFF, and MID49/51 recruit Dynamin-related protein 1 (DRP1; red) from the cytosol to the OMM. Contact points between OMM and endoplasmic reticulum (ER, blue) mark the site of mitochondrial fission (Adapted from Wai and Langer, *Trends in Endocrinology and Metabolism*, 2016).

Drp1 and Mfn act as the main regulators of mitochondrial dynamics across various tissues (Seo et al., 2018). Many signaling pathways, including calcium, ROS, and Notch signaling, which are essential for cell fate decisions depend on the fission-fusion machinery. Drp1 can act in a positive feedback loop with Notch signaling in triple-negative breast cancer cells (Chen et al., 2018). Inhibition of Mitofusin2 can upregulate Notch signaling through Calcineurin A in mouse embryonic stem cells (Kasahara et al., 2013). Recent reports highlight the active role of these canonical mitochondrial dynamics regulators in HSC fate decisions. Drp1 imparts regenerative potential to HSCs and its expression regulates the development of divisional memory in HSC (Hinge et al., 2020). Loss of Drp1 leads to functional decline of HSC due to accumulation of damaged mitochondria and dysregulated activation of cell cycle and biosynthetic pathways (Fig 1.10A). On the other hand, Mfn2 maintains HSCs with extensive lymphoid potential through calcium-dependent NFAT (Nuclear Factor of Activated T-cells) signaling (Luchsinger et al., 2016). This could be attributed to the role of Mfn2 in mitochondrial dynamics as well as ER-mitochondria communication (Fig 1.10B). Further, conserved regulator of stem cell fate and hematopoiesis, OCIAD1 regulates mitochondrial oxidative phosphorylation and mitochondrial morphology (Shetty et al., 2018) (Fig 1.11). However, a comprehensive understanding of the role of mitochondrial dynamics in lineage specification of HSC or blood progenitors in an *in vivo* context remains largely unachieved.

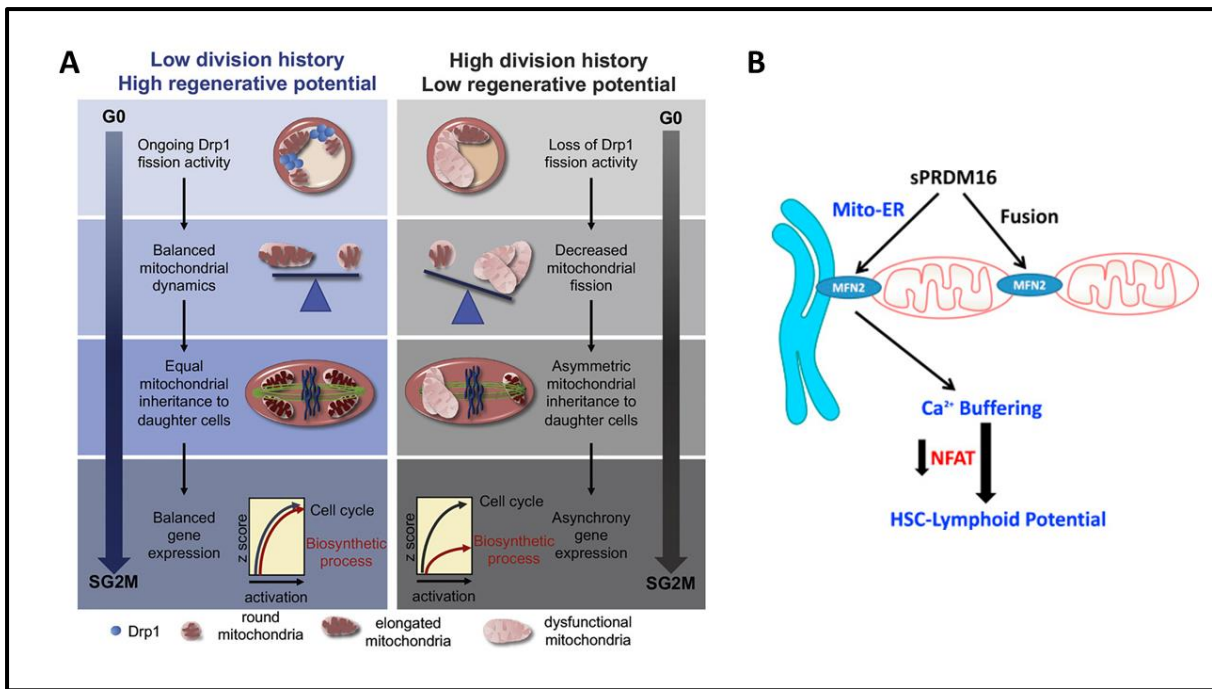


Figure 1.10. Role of mitochondrial dynamics regulators in HSC maintenance. (A) Equal segregation of mitochondria, mediated by Drp1, maintains regenerative potential of HSC through balanced expression of biosynthetic pathway genes. Loss of Drp1 contributes to the divisional memory of HSCs through unequal partition of mitochondrial content, leading to decline in repopulation capacity of HSCs (Adapted from the graphical abstract of Hinge et al., *Cell Stem Cell*, 2020). (B) Mifusin2 (Mfn2), a critical regulator of mitochondrial dynamics and mitochondria-ER tethering maintains HSC with extensive lymphoid potential through calcium-dependent NFAT signaling (Adapted from Diebold and Chandel, *Cell Stem Cell*, 2016).

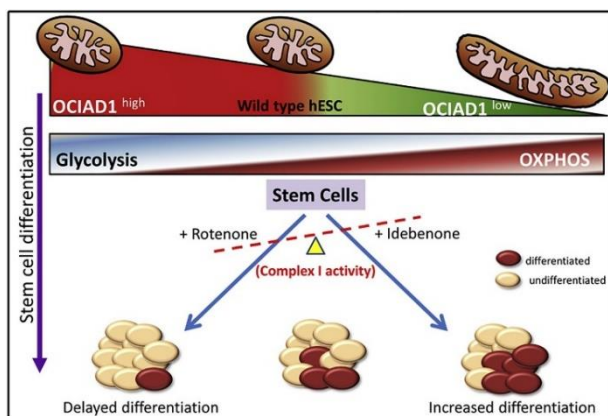


Figure 1.11. Conserved regulator of stemness and hematopoiesis, OCIAD1 regulates mitochondrial activity in hESC. Heatmap shows the correlation of OCIAD1 levels with energy metabolic state (glycolysis and oxidative phosphorylation) of hESCs. The lower panel shows the inhibitory role of OCIAD1 in controlling mitochondrial ETC complex I activity that dictate stem cell differentiation (Adapted

from Shetty et al., *Stem Cell Reports*, 2018).

In this thesis, we tried to address the functional link of mitochondrial dynamics to lineage choice. Asrij acts as a conserved regulator of signaling and blood cell homeostasis (Kulakrni, Khadilkar et al., 2011; Sinha et al., 2013; Khadilkar et al., 2014; Sinha et al., 2019). Though its human ortholog OCIAD1 regulates mitochondrial morphology in hESC (Shetty et al., 2018) (Fig 1.11), the *in vivo* relevance remains unexplored. As Asrij expression is enriched in the *Drosophila* hematopoietic system (Inamdar et al., 2003), its functional link to mitochondrial dynamics may provide insight into context-dependent regulation of generic mitochondrial function to dictate cell fate.

1.4.2 Role of endosomes in hematopoiesis

Endosomes act as critical bridging stations for various intracellular and extracellular cues (Scita and DiFiore, 2010; Sigismund et al, 2021). Endocytosis regulates internalization of plasma membrane bound signaling receptors and their lysosomal degradation. Earlier and recent reports showed the critical role of multiple endosomal proteins in signaling homeostasis during *Drosophila* or vertebrate hematopoiesis. Endosome associated RabGEF, Rabex5 downregulates Ras signaling activation to maintain blood cell homeostasis in the lymph gland (Riemels and Pfelger, 2015). Rab5 and Rab11 suppress JNK and EGFR signaling to control blood cell proliferation and lamellocyte differentiation (Yu et al., 2020). Rab5c also contributes to hematopoietic stem and progenitor cell fate specification and survival of hemogenic endothelium through modulation of Notch trafficking and also Akt signaling (Heng et al., 2020). Graf regulates EGFR trafficking in hemocytes to control EGFR signaling and plasmacyte proliferation (Kim et al., 2017). Moreover, autophagy regulatory protein Atg6 controls endocytosis and vesicular trafficking to maintain blood cell homeostasis in the lymph gland (Shravage et al., 2013). Other endosomal protein such as CORVET tethering complex component Vps8 regulates phagocytosis by hemocytes and also regulates hemocyte number in larval circulation (Lorincz et al., 2016). Further, improper endosomal sorting caused by downregulation of WASH (Wiscott-Aldrich syndrome protein and SCAR Homolog) complex inhibits differentiation of HSCs in mouse bone marrow (Xia et al., 2014).

Though endosomes act as critical regulatory pods of signaling pathways, context-specific regulatory mechanisms significantly contribute to the varying functional output of the endocytic network across tissues (Sigismund et al., 2021). Hematopoiesis involves several post-transcriptional and post-translational regulatory circuits to optimize blood cell production in a rapidly fluctuating environment. Blood cell enriched protein, Asrij interacts with ubiquitous endosomal protein ADP-Ribosylation Factor 1 (ARF1) in its ATP bound form to maintain progenitor homeostasis in the *Drosophila* lymph gland (Kulkarni and Khadilkar et al., 2014; Khadilkar et al., 2014) (Fig 1.12). Asrij plays a conserved role in the maintenance of stemness through endosomal activation of STAT3 (Sinha et al., 2013). Also, loss of Asrij leads to Notch intracellular domain (NICD) accumulation, leading to Notch gain-of-function effect and precocious crystal cell differentiation (Kulkarni, Khadilkar et al., 2011; Khadilkar et al., 2014). Such tissue-enriched conserved endosomal regulators of signaling and blood cell homeostasis could serve as potential therapeutic targets for hematological anomalies.

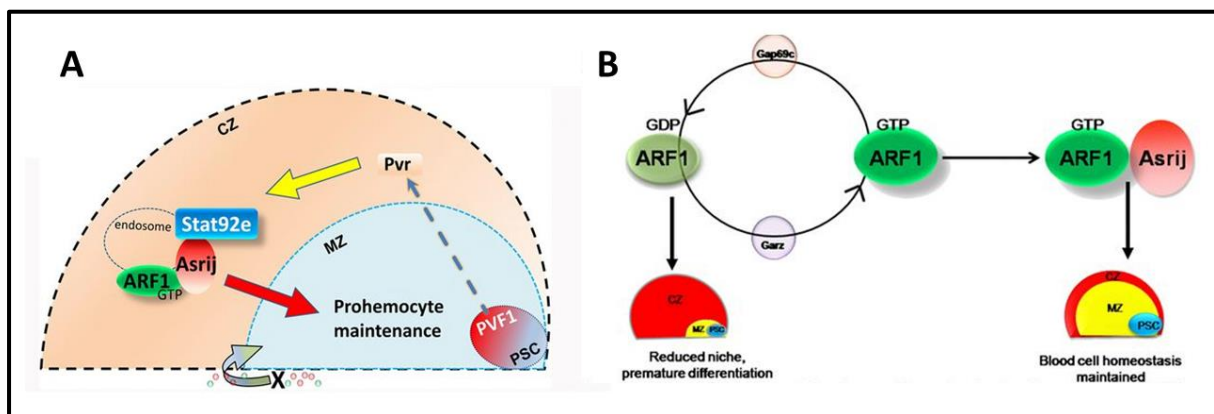


Figure 1.12. Asrij interacts with the ubiquitous endocytic trafficking protein ARF1 for endosomal regulation of hematopoiesis in *Drosophila*. (A) The ARF1-Asrij endosomal axis regulates multiple signaling pathways to maintain homeostasis in *Drosophila* (B) ARF1 cycles through GTP and GDP bound forms by the action of its GEF (Garz) and GAP (Gap69c). Asrij interacts with ARF1-GTP to maintain blood cell homeostasis. In presence of ARF1-GDP Asrij, interaction and stem cell maintenance are lost leading to hyperproliferation and differentiation (red zone) (Adapted from Khadilkar et al., *PNAS*, 2014).

1.4.2.1 Link between endosomal protein sorting and hematopoiesis

Blood progenitor homeostasis and lineage-specific differentiation involve a complex interplay of signaling pathways. The complex endocytic molecular network, also termed as the “endocytic matrix” integrates various intracellular and extracellular cues on the endosomal signaling platforms (Scita and di Fiore, 2010). Protein trafficking and turnover through the endolysosomal route fine-tunes signal transduction. Endosomal protein sorting plays a critical role in endocytic degradation of cargoes and signaling homeostasis. Asrij interacts with ARF1-GTP to maintain stemness of blood progenitors in the *Drosophila* lymph gland (Kulkarni, Khadilkar et al., 2011). Loss of Asrij leads to entrapment of endocytic cargo NICD in the sorting endosomes of hemocytes, mimicking sorting defect (Fig 1.13). This suggests a possible link of endosomal protein sorting with blood cell homeostasis. Depletion of chromatin remodelling and actin nucleating WASH complex, which also mediates endosomal protein sorting through endosomal fission and biogenesis inhibits HSC differentiation in mouse bone marrow in a cell autonomous manner (Xia et al., 2014). An RNAi based screen indicates possible roles of endosomal protein sorting in larval blood cell homeostasis (Avet-Rochex et al., 2010). Also, loss of Chmp5, an auxiliary component of the endosomal protein sorting machinery, inhibits normal reticulocyte formation during the late stage of terminal erythropoiesis in mouse bone marrow (Liu et al., 2021). These reports suggest a potential role of endosomal protein sorting in blood cell homeostasis.

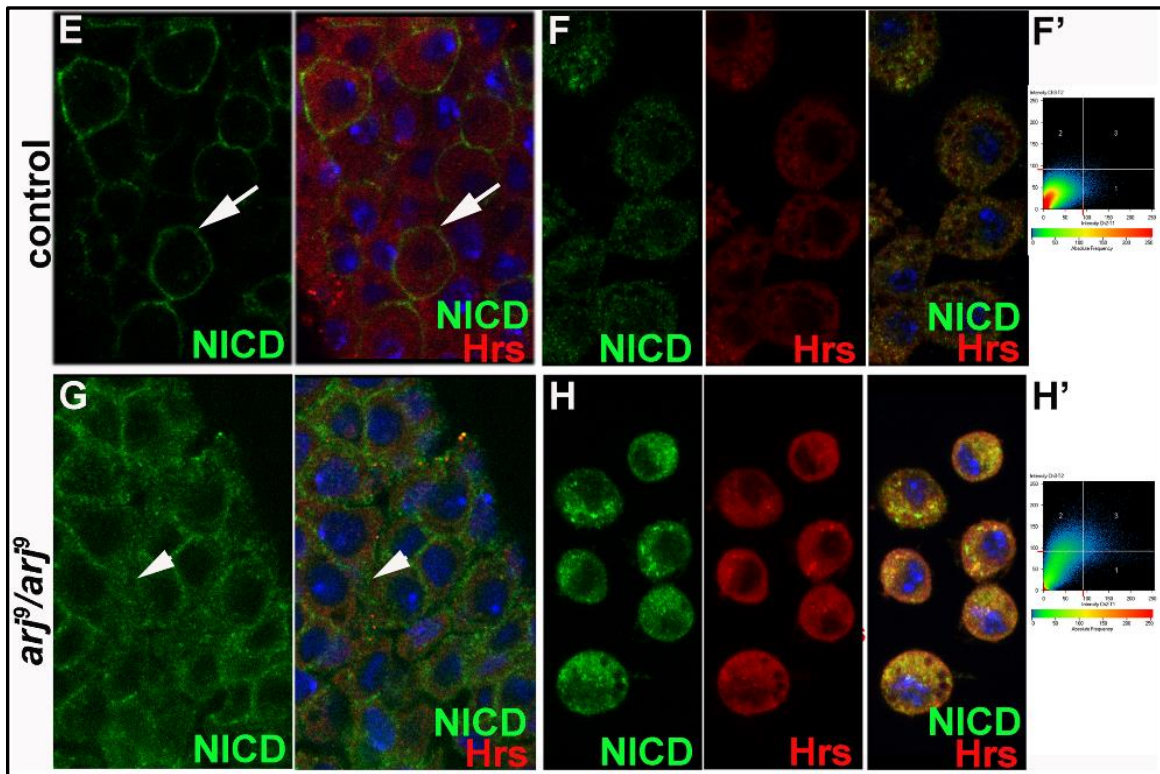


Figure 1.13. Asrij regulates endocytic trafficking of Notch in *Drosophila* hemocytes. Loss of Asrij leads to endocytosis of Notch intracellular domain (NICD) from the plasma membrane and accumulation in Hrs+ve sorting endosomes in *Drosophila* lymph gland and circulatory hemocytes (Adapted from Kulkarni, Khadilkar et al., *PLoS One*, 2011).

1.4.2.2. The ESCRT machinery

The conserved Endosomal Sorting Complex Required for Transport (ESCRT) machinery actively controls protein sorting for lysosomal degradation. ESCRT was discovered in yeast *Saccharomyces cerevisiae* through a screening for mutants that accumulate aberrant vacuolar structures, called class-E compartments, due to disrupted endosomal protein sorting (Bankaitis et al., 1986; Rothman et al., 1989; Horner et al., 2018). It is a multi-component complex that remodels and severs membranes in a reverse-topology (away from the cytoplasm) (Pavlin and Hurley, 2020). ESCRT consists of four subunits (ESCRT-0, I, II and III) each made of multiple proteins that sequentially bind to the endomembrane-bound ubiquitinated cargoes, allowing them to be sequestered in the intraluminal vesicles (ILV) of the multivesicular bodies (MVB) (Fig 1.14).

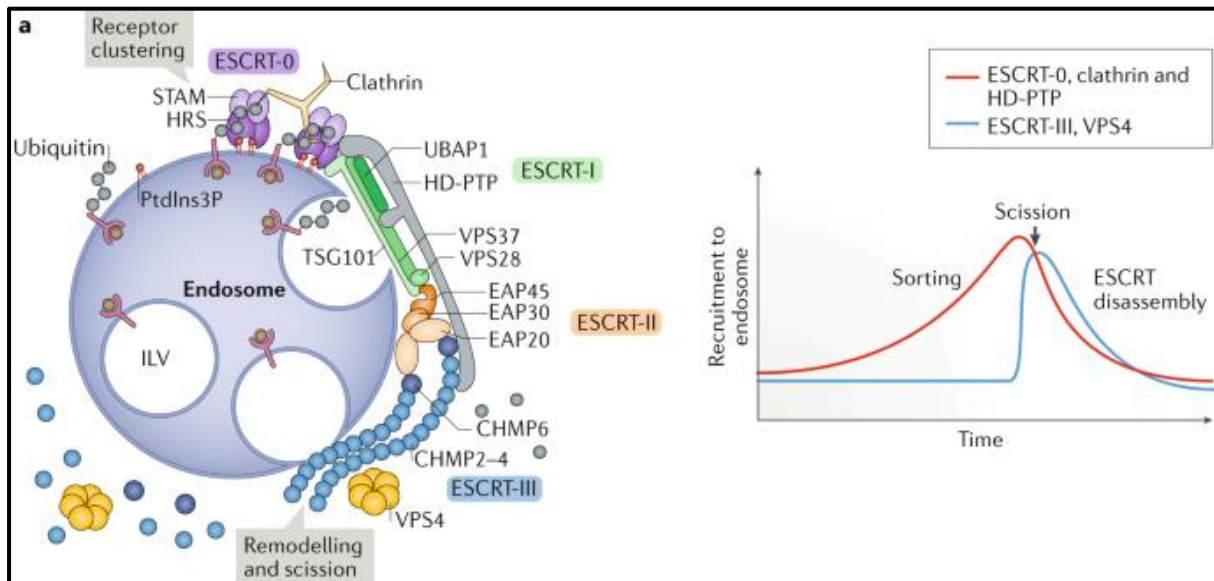


Figure 1.14. ESCRT mediates endosomal protein sorting through MVB biogenesis. ESCRT-0 (Hrs, Stam) recognizes ubiquitinated cargo (receptor) on the endosomal membrane. ESCRT-0 recruits ESCRT-I and transfers ubiquitinated cargo. ESCRT-I recruits ESCRT-II and promotes budding of membrane inside the endosomal lumen to allow sequestration of cargoes in ILV (intraluminal vesicle) for sorting. The two EAP20 (Vps25) subunits of ESCRT-II recruit CHMP6 (Vps20) in ESCRT-III, which nucleates ESCRT-III filaments consisting of CHMP4 (Vps32), CHMP2 (Vps2) and CHMP3 (Vps24). Vps4 remodels the filaments to achieve scission of the ILV neck. ESCRT-III nucleation is accompanied by cargo deubiquitination. HD-PTP acts as a bridging factor between ESCRT-I and ESCRT-III to bypass ESCRT-II-dependent endosomal sorting. Mechanoenzyme complex consisting of Vps4 mediates ESCRT-III disassembly in the final step of endosomal protein sorting. Thus, endosomal protein sorting in ILV, membrane scission and ESCRT disassembly occur in a sequential manner (Adapted from Vietri et al., *Nat Rev Mol Cell Biol.*, 2020).

Drosophila ESCRT consists of 13 core components with distinct molecular properties (Vaccari et al., 2009; Alfred and Vaccari, 2016). ESCRT-0 executes the first step of endosomal sorting by binding to the ubiquitinated cargoes through ubiquitin interacting motif (UIM). Two components, Hrs and Stam interact in 1:1 stoichiometric ratio to constitute ESCRT-0 (Bilodeau et al., 2002; Gao et al., 2017). Despite important role in animals and fungi, ESCRT-0 is absent from plants and protists (Schuh and Audhya, 2014). The C-terminus of Vps27, the yeast homolog of Hrs, contains a P(S/T)AP motif through which it binds to the N-terminus of ESCRT-I component Tsg101 (Katzmann et al, 2001; Ren and Hurley, 2011). *Drosophila* ESCRT-I is a hetero-tetrameric soluble complex that is

composed of Tsg101, Vps28 and Vps37 group of proteins (Vps37A and Vps37B), all of which are present in yeast as well (Kostelansky et al, 2007; Vaccari et al., 2009). Yeast ESCRT-I also contains Mvb12 which lacks detailed phenotypic characterization in *Drosophila*. ESCRT-0 recruits ESCRT-I on the endosome from cytosol through direct physical interaction. On the other side of the ESCRT-I subunit, Vps28 interacts with Vps36 of ESCRT-II. ESCRT-I and II induce and stabilize membrane buds that allow the biogenesis of MVB (Boura et al, 2012). ESCRT-II is also heterotetrameric and is composed of Vps36, Vps25 and Vps22 with a 1:2:1 stoichiometry. One Vps25 molecule binds to Vps36 whereas the other Vps25 binds to Vps22, thus forming a Y-shaped structure. Each of these three ESCRT subunits (0, I, II) can bind to ubiquitinated cargoes (Piper et al., 2014).

Unlike ESCRT-0, I and II, ESCRT-III components do not form any stable cytosolic complex. The core components of ESCRT-III include Vps20, Vps32 (Shrub in *Drosophila*), Vps24 and Vps2 (Babst et al, 2002). Vps20 interacts with ESCRT-II and nucleates the rest of the ESCRT-III core complex. Vps32 undergoes oligomerization, recruits Vps24 and subsequently Vps2 to complete the cycle of ESCRT-III filament assembly (Hanson et al., 2008; Wollert et al., 2009; Radulovic et al., 2018). Detailed genetic and biochemical analysis of ESCRT-III in yeast and mammalian cells suggest CHMP4/SNF7 (Vps32 homolog) is the most abundant and the principal filament-forming component that undergoes activation and polymerization upon binding with various nucleating factors (Vietri et al., 2020). Vps24 and Vps2 regulate the shape of the ESCRT-III subunit by crosslinking the Vps32 filaments and also by regulating the filament length. ESCRT-III assembly is followed by recruitment of deubiquitinase. Deubiquitination step follows dissociation of ESCRT-III components from cargoes. Vps4-Vta1 mechanoenzyme complex mediates the final energy-demanding step of membrane scission.

Multiple auxiliary proteins often assist ESCRT function, resulting in functional redundancy of certain ESCRT components. Bro1 in yeast and Alix and HD-PTP in mammals establish a bypass branch for ESCRT-I and II to feed endosomal cargoes directly to the ESCRT-III complex (Bissig et al., 2014; Hurley, 2015; Tabernero et al., 2018). Additionally, accessory ESCRT proteins and Vps4 complex members such as Ist1, Vps60 and Chmp1 modulate the

function of the ESCRT core components, often through synergistic interaction (Baumers et al., 2019).

ESCRT phenotypes

Depletion of critical ESCRT genes in *Drosophila* causes endosomal accumulation of ubiquitinated cargoes including signaling receptors (Vaccari et al., 2009; Herz et al., 2009; Szymanska et al., 2018). This leads to aberrant activation of signaling pathways such as Notch, EGFR, JAK/STAT etc which affect tissue homeostasis. Loss of ESCRT function causes tissue hyperproliferation, loss of cell polarity and neoplastic transformation in both cell-autonomous and non-autonomous manner (Thompson et al., 2005; Vaccari et al., 2009; Herz et al., 2009). ESCRT mutant cells accumulate NICD in endosomal compartments due to sorting defect. Binding of NECD (Notch extracellular domain) to delta, its membrane-bound ligand leads to endocytosis of the receptor-ligand complex, followed by cleavage of NICD by γ -secretase. The cleaved NICD translocates to the nucleus and triggers activation of downstream transcriptional program (Ables et al., 2011). However, loss of ESCRT promotes ligand-independent Notch activation as well (Hori et al., 2012). ESCRT mutants of *Drosophila* accumulate NICD in endocytic class E compartment due to impaired MVB biogenesis. Trapped NICD may cause ectopic Notch gain-of-function effect. Moreover, ESCRT regulates the expression of Notch downstream target Upd which causes non-autonomous activation of the JAK-STAT pathway, causing tissue hyperproliferation (Vaccari et al., 2009).

Apart from endosomal protein sorting, ESCRT-I and III actively regulate membrane remodelling in several other contexts (Vietri et al., 2019) (Fig 1.15). ESCRT components in concert with microtubule, Septins and Spastin remodel membrane during cytokinetic abscission (Matias et al., 2015). Non-endocytic ESCRT-dependent mechanism mediates pruning of plasma membrane in neurons (Loncle et al., 2015). ESCRT-III in coordination with various accessory proteins aid in nuclear envelope sealing during exit from mitosis (Vietri et al., 2015; Olmos et al., 2015). Additionally, ESCRT promotes repair of the membrane of damaged lysosomes (Radulovic et al., 2018; Skowyra et al., 2018), regulates micrautophagy (Sahu et al., 2011; Mejlvang et al., 2018) and aids in exocytosis of cellular content (Garrus et al., 2001; Martin-Serrano et al., 2003). Hence, the multifunctionality of ESCRT can contribute toward a wide range of effects on cell fate and tissue homeostasis.

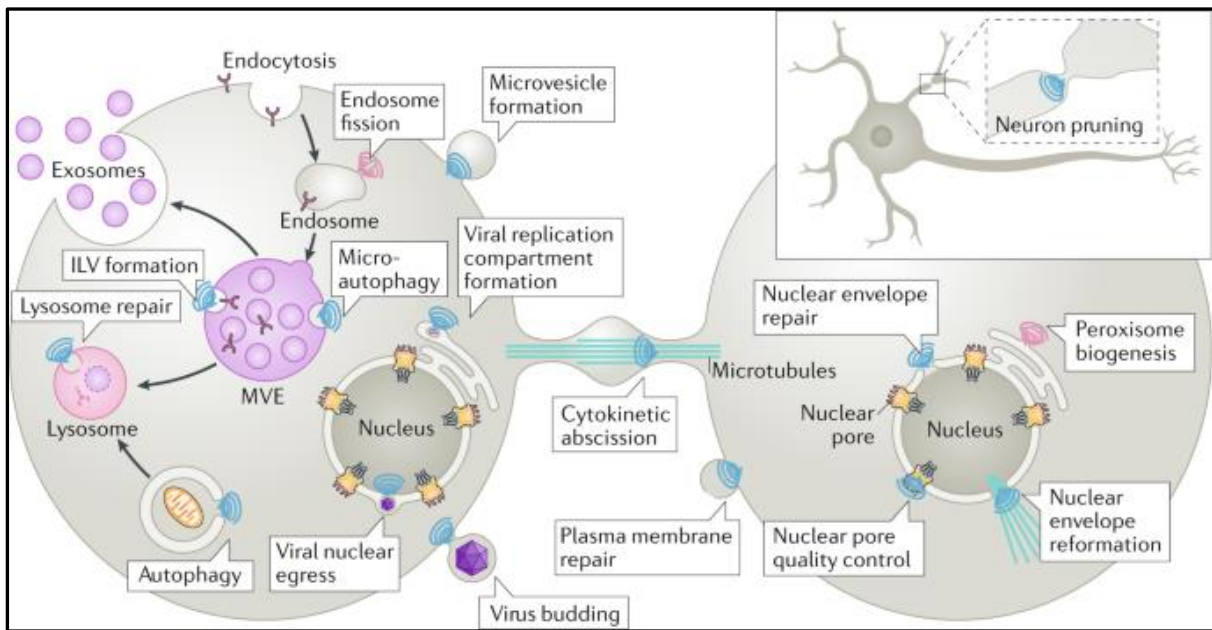


Figure 1.15. ESCRT plays a multifunctional role through membrane remodeling. Blue helices indicate canonical ESCRT-III functions (involving inverted curvature of the associated membrane), whereas pink helices indicate non-canonical functions (scission of positively curved membranes). ILV, intraluminal vesicle; MVE, multivesicular endosomes (Adapted from Vietri et al., *Nat Rev Mol Cell Biol.*, 2021)

In this thesis, we tried to address the active role of ESCRT in blood progenitor homeostasis and present a functional map of all 13 *Drosophila* ESCRT core components in ubiquitinated cargo sorting, signaling activation and blood lineage choice across distinct progenitor subsets.

1.5. Aims of the present study

This thesis aims to address the role of mitochondrial dynamics and endosomal protein sorting in blood cell homeostasis. We have used the *Drosophila* lymph gland as a model to comprehensively analyse progenitor homeostasis *in situ*. The major aims are as follows -

1. Elucidating the role of endosomal ARF1-Asrij axis in *Drosophila* immunity.

(Chapter 2: The endosomal ARF1-Asrij axis modulates cellular and humoral immunity of *Drosophila* to regulate survival upon infection)

2. Validation of Asrij mutant lymph gland proteome that serves as a resource for new regulators of hematopoiesis.

(Chapter 3. Asrij lymph gland proteome analysis reveals potential role of mitochondrial and endosomal proteins in Drosophila blood cell homeostasis)

3. Investigating the role of Asrij in mitochondrial dynamics and its possible functional link with progenitor homeostasis and lineage choice.

(Chapter 4. A conserved role for Asrij/OCIAD1 contributes to the differentiation and lineage specification of progenitors through functional interaction with the regulators of mitochondrial dynamics)

4. Elucidating the role of conserved ESCRT machinery in Drosophila blood cell lineage specification.

(Chapter 5. ESCRT components play distinct roles in cargo sorting and lineage-specific differentiation of blood progenitors in the Drosophila lymph gland)

5. Delineating signaling pathways that contribute to the distinct roles of ESCRT components in lineage commitment across different blood progenitor subsets of the Drosophila lymph gland.

(Chapter 6. ESCRT regulates Notch signaling to maintain progenitor homeostasis in the Drosophila lymph gland)

Chapter 2. The endosomal ARF1-Asrij axis modulates cellular and humoral immunity of *Drosophila* to regulate survival upon infection.

2.1 Introduction

Response to immune challenge depends on the coordinated interplay of several signaling cascades at the systemic level. The immune system of *Drosophila* is innate in nature and comprises of two arms: cellular and humoral. The three different types of terminally differentiated blood cells (plasmatocytes, crystal cells and lamellocytes) regulate the cellular arm. Plasmatocytes are the most abundant (90-95%) type of blood cells that destroy pathogens by phagocytosis. Crystal cells (5-10%) produce Pro-Phenol Oxidase (ProPO), an inactive zymogenic precursor to the enzyme Phenol Oxidase (PO) (Tang, 2009). ProPO is proteolytically cleaved by serine proteases to generate PO, which catalyzes the oxidation of phenolic compounds into quinones. Subsequently quinones polymerize to generate melanin. The main purpose of melanin biosynthesis is wound healing. However, the reactive oxygen species (ROS) generated as a by-product of the melanisation reaction provide immunity against pathogens (Liu et al., 2007; Nappi et al., 2009). The third type of blood cells, lamellocytes are rare in larval circulation and are induced upon immune challenge with parasitoid wasp eggs. Lamellocytes are bigger than the other two blood cell types and encapsulate the wasp eggs to destroy them.

Humoral immunity depends on the anti-microbial peptides (AMP) secreted from the fat body and also partly from the hemocytes. AMP biosynthesis depends upon critical immune regulatory pathways such as Toll and Imd pathway. Fungi or Gram-positive bacterial infection activates the Toll pathway. This leads to nuclear translocation of the NF- κ B homolog Dif or Dorsal and consequent production of AMPs such as Drosomycin, Metchnikowin and Defensin. Infection by Gram-negative bacteria results in nuclear translocation of the Rel homology domain protein Relish through the Imd pathway and leads to the production of Diptericin, Attacin, Cecropin and Drosocin (Bulet et al., 1999). Under normal condition, Dorsal is held inactive in the cytoplasm by I κ B homolog Cactus

while Relish contains an I κ B like autoinhibitory domain towards its C-terminal. The Toll pathway is activated within 30 minutes of bacterial or fungal infection (Ip et al., 1993; Lemaitre et al., 1995; Stoven et al., 2000). Upon activation, Cactus is ubiquitinated and degraded, thus allowing Dorsal to move into the nucleus and causing downstream AMP gene transcription.

The fat body is the primary source of AMPs in *Drosophila* (Lemaitre and Hoffmann, 2007). Toll and Imd pathways regulate the systemic response of the fat body (Aggarwal and Silverman, 2008). Hemocytes also produce AMPs during infection or upon induction with specific cues (Dimarcq et al., 1997; Charroux and Royet, 2009). However, the communication between hemocytes and fat body is not fully understood. Earlier studies showed the involvement of hemocytes in the fat body mediated immune response. Plasmacytes play an essential role in AMP production by the fat body upon oral feeding of bacteria. Psidin is required for lysosomal degradation of bacteria in hemocytes while having an essential role in Defensin production in the fat body (Brennan et al., 2007). Spaetzle, produced and secreted by hemocytes, controls AMP expression in the fat body (Shia et al., 2009; Paddibhatla et al., 2010). Upd3 produced in hemocytes leads to JAK/STAT pathway activation in the gut and fat body (Chakrabarti et al., 2016). Mutations that lead to perturbation of any of these signalling pathways can disrupt systemic homeostasis mimicking an infection- induced condition (Khush et al., 2001; Khush et al., 2002; Kambris et al., 2006; Becker et al., 2010).

Hematopoiesis is intricately related to immunity. Both hematopoiesis and immune function demand complex interplay of molecular networks and signaling pathways. Hence, perturbed blood cell homeostasis may reflect its organismal level output as dysregulated immune function. Organelles are critical regulatory hubs of blood cell homeostasis, function and immunity (Kagan, 2012; Gleeson, 2014; Filippi et al., 2019; Tiku et al., 2020). Endosomes serve as scaffolds for critical signaling receptors that regulate blood cell homeostasis and immunity (Sinenko et al., 2011; Shrivage et al., 2013; Reimels et al., 2015; Yu et al., 2021). The ubiquitous trafficking protein ADP Ribosylation Factor 1 (ARF1-GTP) interacts with and

regulates the *Drosophila* hemocyte-specific endosomal protein Asrij to integrate and regulate blood cell homeostasis. This endosomal axis regulates JAK/STAT, Notch, Pvr and Insulin signaling pathways (Kulkarni, Khadilkar et al., 2011; Khadilkar et al., 2014). Though ARF1 expression is ubiquitous, Asrij expression is restricted to hematopoietic system of *Drosophila* (Inamdar, 2003). Depletion of ARF1 or Asrij leads to precocious differentiation of blood cells. As the primary role of *Drosophila* hemocytes is to mount an immune response, we assessed the organismal level impact of endosomal ARF1-Asrij axis through study of immune response in ARF1 and Asrij depleted flies. Studies done in our laboratory showed that loss of ARF1-Asrij axis leads to increased ProPO-dependent melanisation in larvae, Cactus ubiquitination in hemocytes and upregulated expression of various Toll pathway and Imd pathway AMPs. Also, ubiquitous depletion of ARF1 or Asrij reduces survival of adult flies upon bacterial infection. To understand how immune signalling is affected in ARF1 and Asrij mutants, the status of Toll and Imd activation in hemocytes and fat body as well as survival upon infection was analysed as a part of this thesis.

2.2 Materials and methods

2.2.1 Fly stocks and genetics

All fly stocks were maintained at standard rearing conditions (at 25°C in cornmeal agar medium). Respective *UAS* or *Gal4* parent strains or *w1118* (*asrij* null mutant) were used as controls. Tissue-specific *Gal4* line was used to drive the expression of *UAS* responder genes in F1 generation. Following fly lines were used: *w1118*, *arj9/arj9*, *e33cGal4* (Kathryn Anderson, NY, USA), *HmlGal4 UAS-GFP* (Tina Mukherjee, inStem), *UAS-arf1* (Khadilkar et al., 2014), *btl-Gal4* (Arjun Guha, inStem), *UAS asrij RNAi* (VDRC 6633), *UASarf1 RNAi* (VDRC 23082).

2.2.2 *In-vivo* adult phagocytosis assay

20 adult flies of each genotype were injected with Rhodamine ester (TAMRA) -conjugated heat-killed *E. coli* in the abdomen of adult male flies (10 male and 10 female) using ethanol sterilized pins. After 1.5 hours, the flies were bled to collect the hemolymph. The hemocytes were kept for 30 min in sterile Schneider's media for attachment. After 30 min, the cells were gently washed with 1X PBS to remove extracellular bacteria. Hemocytes were fixed using 4% paraformaldehyde for 20 minutes. Hemocytes were identified by expression of GFP driven by *HmlGal4*. Bacterial particles detected in the median z-sections of the hemocyte images acquired were considered for quantification of phagocytic events. Experiments were performed thrice. Images were acquired using Zeiss LSM510 meta confocal microscope.

2.2.3 Immunostaining of the circulating hemocyte and fat body

Larvae were bled in Schneider's media and the hemolymph was plated on a cover-slip bottom dish for attachment for 45 minutes. Hemocytes were fixed in 4% paraformaldehyde for 20 minutes followed by wash with PBS. Cells were then permeabilized with 0.4% NP40 and blocked with 20% goat serum for 1 hour. The samples were incubated with primary antibodies at 4°C overnight. Primary antibodies used were mouse anti-Dorsal (DSHB, USA), mouse anti-Relish (DSHB, USA), Mouse anti-Cactus (DSHB, USA), Rabbit anti-Ubiquitin (Abcam, UK),. Secondary antibody staining was then performed using Alexa-488 conjugated anti-mouse IgG and Alexa-568 tagged anti-rabbit IgG antibodies (Life Technologies, Thermo Fisher Scientific, USA). Hemocytes were incubated with DAPI to mark the nuclei. Images were acquired in LSM510 Meta Confocal microscope.

Larvae or adult flies were dissected in 1X PBS to isolate the fat bodies. The fat body samples were fixed in 4% paraformaldehyde for 20 minutes followed by wash with PBS, permeabilized with 0.1% Triton-X 100 and blocked with 20% normal goat serum for 1 hour. The samples were then incubated with primary antibodies at 4 °C overnight. Secondary antibody staining was then performed as mentioned before. The fat body samples were

mounted in DAPI-glycerol medium. Images were taken in Zeiss LSM510 Meta and LSM880 confocal Microscope. Autofluorescence was taken care of by optimizing the confocal microscope settings using no primary antibody control.

2.2.4 Infection and survival assay

Adult flies of appropriate genotype were starved for 2 hr before infection; then transferred into vials containing filter paper hydrated with 5% sucrose solution mixed with concentrated Ampicillin resistant Gram-negative bacteria (*E. coli*) ($A_{600} = 1$; concentrated to contain ~ 10 CFU/ml) or Gram-positive bacteria (*B. subtilis*) ($A_{600} = 5-10$) on cornmeal food. For survival assay, flies were challenged with bacteria by oral feeding. Adult flies were starved for 48 hours and then transferred to fresh corn-meal food vials containing fresh filter paper disks inoculated with bacterial cultures. The percentage of survivors was then calculated for each experiment and plotted as a survival curve. N = 100 flies for each genotype.

2.2.5 Statistical analysis

All the data sets were included for analysis. There was no randomization done. Single factor ANOVA has been used for statistical analysis. P-values are as indicated in the graphs.

2.3 Results

2.3.1 Depletion of endosomal proteins ARF1 or Asrij does not affect phagocytosis in hemocytes.

Plasmatocytes play a key role in the phagocytosis of pathogens in circulation. Depletion of either ARF1 or Asrij results in increased plasmatocyte numbers (Kulkarni, Khadilkar et al., 2011; Khadilkar et al., 2014). Previous work showed reduced uptake of India ink in hemocytes upon loss of Asrij or ARF1. We assessed the *in vivo* phagocytic efficiency of the adult hemocytes in Asrij or ARF1 depleted condition by using Rhodamine-conjugated *E. coli*.

We observed no significant change in phagocytosis by adult hemocytes upon hemocyte-specific knockdown of *asrij* (*HmlGal4 UAS GFP; UAS arj RNAi*) or *arf1* (*HmlGal4 UAS GFP; UAS arf1 RNAi*) (Fig 2.1). Hence, endosomal ARF1-Asrij axis does not regulate the phagocytic function of hemocytes.

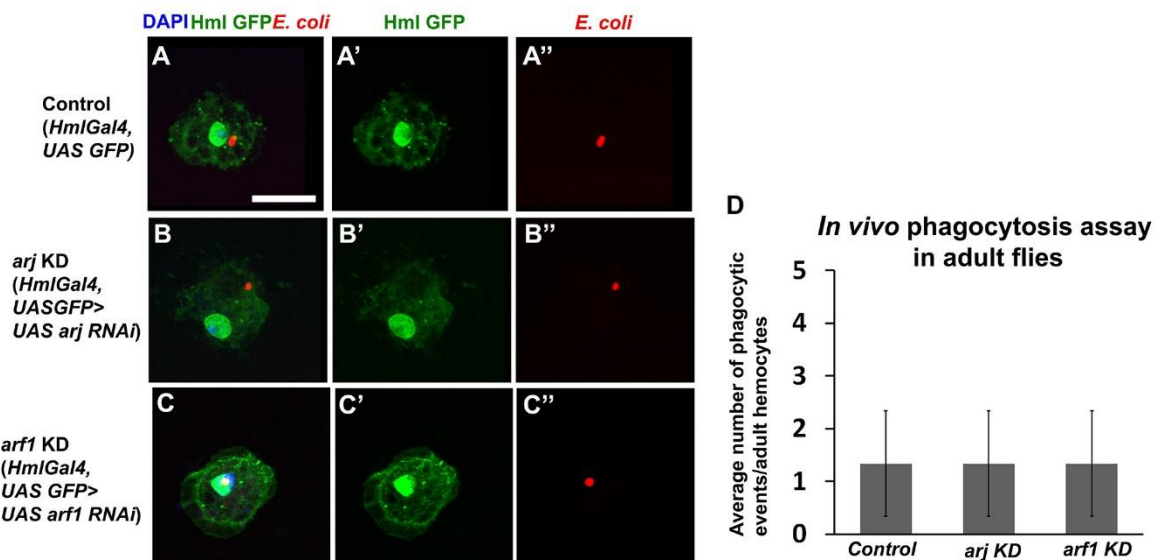


Figure 2.1 In vivo phagocytic uptake assay. Immunofluorescence confocal images of GFP expressing control (A-A''), *arf1* KD (B-B'') and *arf1* KD (C-C'') adult hemocytes with phagocytosed Rhodamine-stained *E. coli*. Scale bar: 10 μ m. (D) Bar graph showing quantification of average phagocytic events per hemocytes. 12 cells successfully undergoing phagocytosis were quantified per genotype. Error bar represents standard error of mean (SEM).

2.3.2 The ARF1-Asrij axis suppresses AMP production through the Toll pathway by stabilizing Cactus.

Previous work from the lab showed inhibitory role of ARF1 in the Toll pathway. Loss of ARF1 leads to increase in the expression of Drosomycin and Metchnikowin. Asrij also differentially affects Toll pathway target genes. *Asrij* null flies show increased expression of Drosomycin and Metchnikowin and reduced level of Defensin. Further, depletion of ARF1 or Asrij leads to increased co-localization of Cactus with Ubiquitin in the circulating hemocytes, suggesting upregulated ubiquitination of Cactus. As the fat bodies serve as the major source of AMPs,

we tested if Toll pathway activation occurs in the fat body as well upon depletion of *Asrij* or ARF1. We observed increased co-localization of Cactus and Ubiquitin in the *asrij* null larval fat body cells (22.5%) as compared to the *w1118* control (3%) (Fig 2.2 A-D), Also, *arf1* null fat bodies showed increased level of both Cactus and ubiquitin (Fig 2.2 E-F) suggesting accumulation of Cactus in ubiquitinated form. *HmlGal4* mediated *arf1* knockdown larval fat body cells showed increased co-localization of Cactus and Ubiquitin (7.5%) as compared to *HmlGal4 UAS GFP* control (0.4%) (Fig 2.2 G-J). Also, expression of both Cactus and Ubiquitin increased in *arf1* KD fat bodies (Fig 2.2 K-L). These data show increased targeting of Cactus for degradation in larval fat bodies upon *Asrij* or ARF1 depletion. Effect on Toll pathway activation in the fat body upon hemocyte-specific depletion of *Asrij* or ARF1 indicates cell non-autonomous systemic regulation of AMP biosynthesis. Also, our data show crosstalk of hemocytes with fat body to regulate Toll pathway activation.

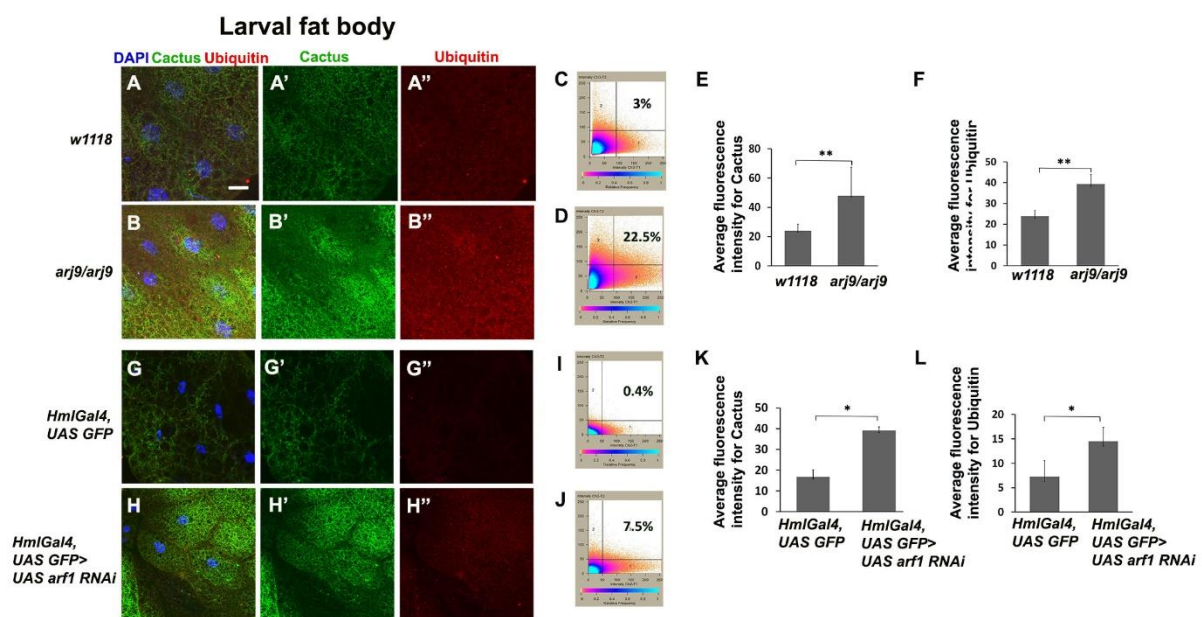


Figure 2.2 Cactus ubiquitination in *asrij* null and *arf1* KD larval fat body. Confocal images show Cactus and ubiquitin staining in larval fat body of control (*w1118*) (A-A'') and *asrij* null (*arj9/arj9*) (B-B'') flies. Scale bar: 10 μ m. Colocalization plots represent colocalization percentage between Cactus and Ubiquitin in *w1118* and *arj9/arj9* (C, D). Cactus and ubiquitin intensities are represented by bar diagram (E, F). Immunofluorescence confocal imaging was performed in control (*HmlGal4 UAS GFP*) and *arf1* KD (*HmlGal4 UAS GFP; UAS arf1 RNAi*) larval fat bodies (G-G'', H-H''). Colocalization plots reflect colocalization between Cactus and Ubiquitin (I, J). Bar diagrams show quantification of Cactus and Ubiquitin

intensities in control and *arf1* KD fat bodies. (K, L). N=10 larvae for each genotype. Error bars in all the bar diagrams represent SEM. * and ** represent P-value<0.05 and <0.01, respectively.

We performed similar analyses in adult fat bodies of *arf* null and *arf1* KD flies. Cactus showed increased co-localization with Ubiquitin in *arf9/arf9* fat bodies as compared to control (Fig 2.3 A-D). Cactus and Ubiquitin level also increased significantly in *arf9/arf9* adult fat bodies (Fig 2.3 E-F). However, we observed no significant increase in co-localization (Fig 2.3 G-J) or individual protein expression for Cactus and Ubiquitin (Fig 2.3 K-L) in fat bodies of *arf1* KD adults. These data suggest that Cactus degradation and subsequent immune activation process in adult flies could be less dependent on ARF1 as compared to Asrij.

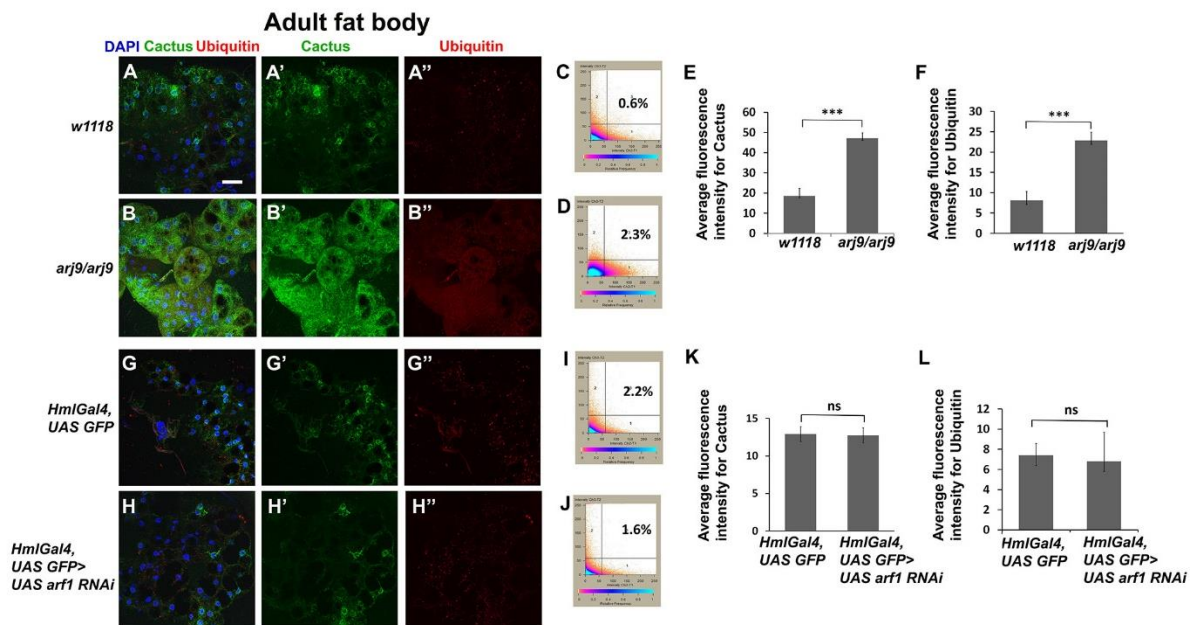


Figure 2.3 Cactus ubiquitination in *asrij* null and *arf1* KD adult fly fat body. Confocal images show Cactus and Ubiquitin staining in adult fat body of control (*w1118*) (A-A'') and *asrij* null (*arf9/arf9*) (B-B'') flies. Scale bar: 10 μ m. Colocalization plots represent colocalization percentage between Cactus and Ubiquitin in *w1118* and *arf9/arf9* (C, D). Bar diagrams show quantification of Cactus and ubiquitin intensities (E, F). Confocal imaging was performed in control (*HmlGal4 UAS GFP*) and *arf1* KD (*HmlGal4 UAS GFP; UAS arf1 RNAi*) adult fat bodies (G-G'', H-H''). Colocalization plots reflect colocalization between Cactus and Ubiquitin (I, J). Bar diagrams show quantification of Cactus and Ubiquitin intensities in control and *arf1* KD

fat bodies. (K, L). N=10 larvae for each genotype. Error bars in all the bar diagrams represent SEM. *** represents P-value<0.001; ns indicates statistically non-significant difference.

Cactus degradation should lead to increased translocation of the Toll pathway effectors Dorsal/Dif to the nucleus. Since Dorsal translocation is essential for AMP production, we stained *asrij* null and ARF1 knockdown hemocytes for Dorsal. We observed increased translocation of Dorsal to the nucleus of *asrij* null (Fig 2.4 A-C) as well as *arf1* KD (Fig 2.4 D-F) hemocytes as compared to the respective controls. Thus, increased Toll activation in *arf9/arf9* or *arf1* KD hemocytes could be a consequence of nuclear translocation of Dorsal.

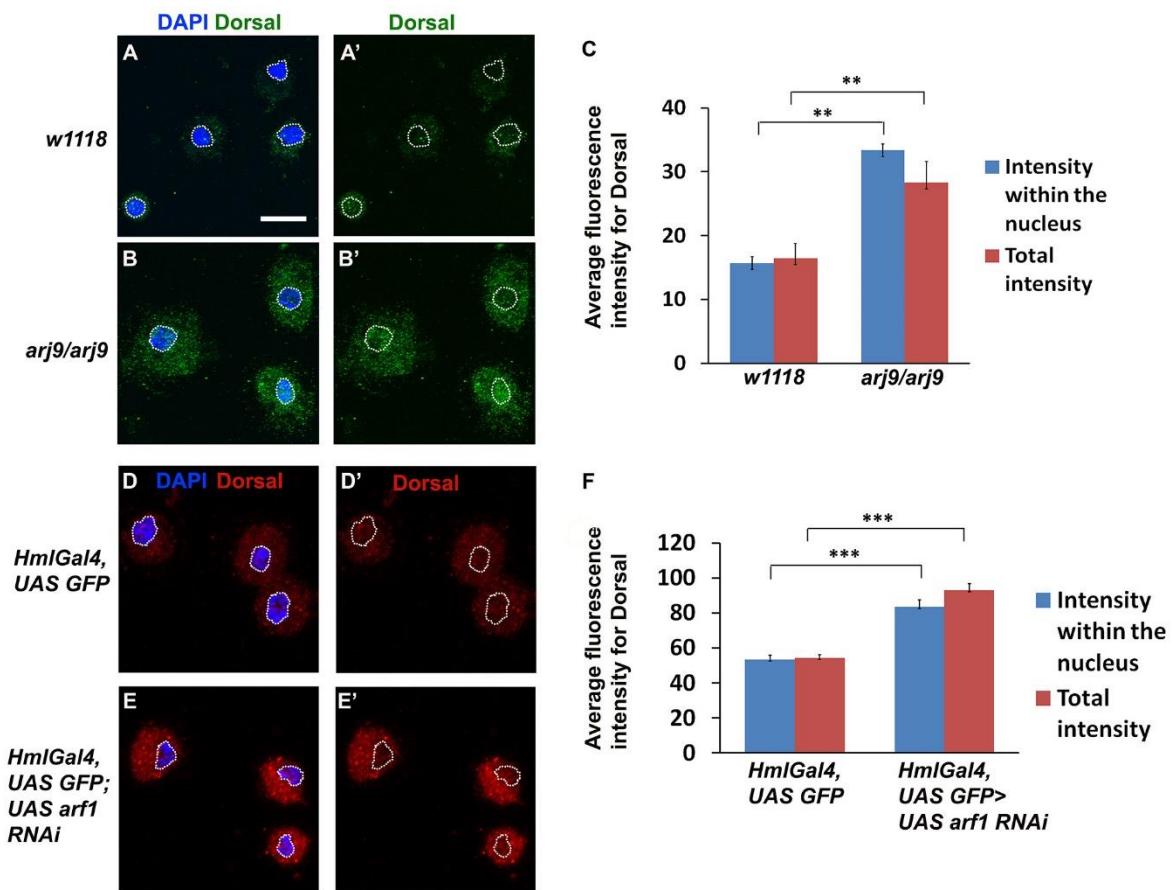


Figure 2.4 Toll pathway activation through Dorsal nuclear translocation in *asrij* null and *arf1* KD hemocytes. Confocal images of Dorsal staining in *w1118* (A-A') and *arf9/arf9* (B-B') hemocytes. Dotted area marks the nucleus. Scale bar: 10 μ m. Bar diagrams show quantification of Dorsal intensity in whole cell and in the nuclei (C). Dorsal staining in control (*HmlGal4 UAS GFP*) and *arf1* KD (*HmlGal4 UAS GFP; UAS arf1 RNAi*) hemocytes are shown in panel (D-D', E-E'). Bar diagrams represent quantification of Dorsal intensity in whole cell and

in the nuclei of *control* and *arf1* KD hemocytes. n=30 cells for each genotype. Error bars in all graphs represent SEM. ** and *** represent P-value<0.01 and <0.001, respectively.

2.3.3 ARF1 and Asrij inhibit AMP biosynthesis through the Imd pathway in hemocytes.

Infection with Gram-negative bacteria activates AMP gene expression through nuclear localisation of Relish. Relish staining has not been reported in hemocytes and we could not detect any specific signal by immunostaining. However fat bodies from infected wild type flies show nuclear Relish (Minakhina et al., 2006). Since systemic signals as well as cross talk between the hemocytes and fat body bring about immune regulation, we assayed for Relish nuclear localization in the fat body cell of *asrij* null and ARF1 depleted (*HmlGal4; UAS arf1 RNAi*) larvae. *Asrij* null fat bodies showed no apparent change in nuclear Relish level as compared to the parental control (Fig 2.5 A-C) whereas fat bodies of ARF1 KD larvae showed increased level of nuclear Relish, indicating Imd pathway activation (Fig 2.5 D-F). These data are in concordance with the previously reported Imd AMP levels seen in ARF1 depleted and *asrij* null flies. Therefore, ARF1 and *Asrij* have non-overlapping roles in regulating Imd pathway AMP expression in the fat body.

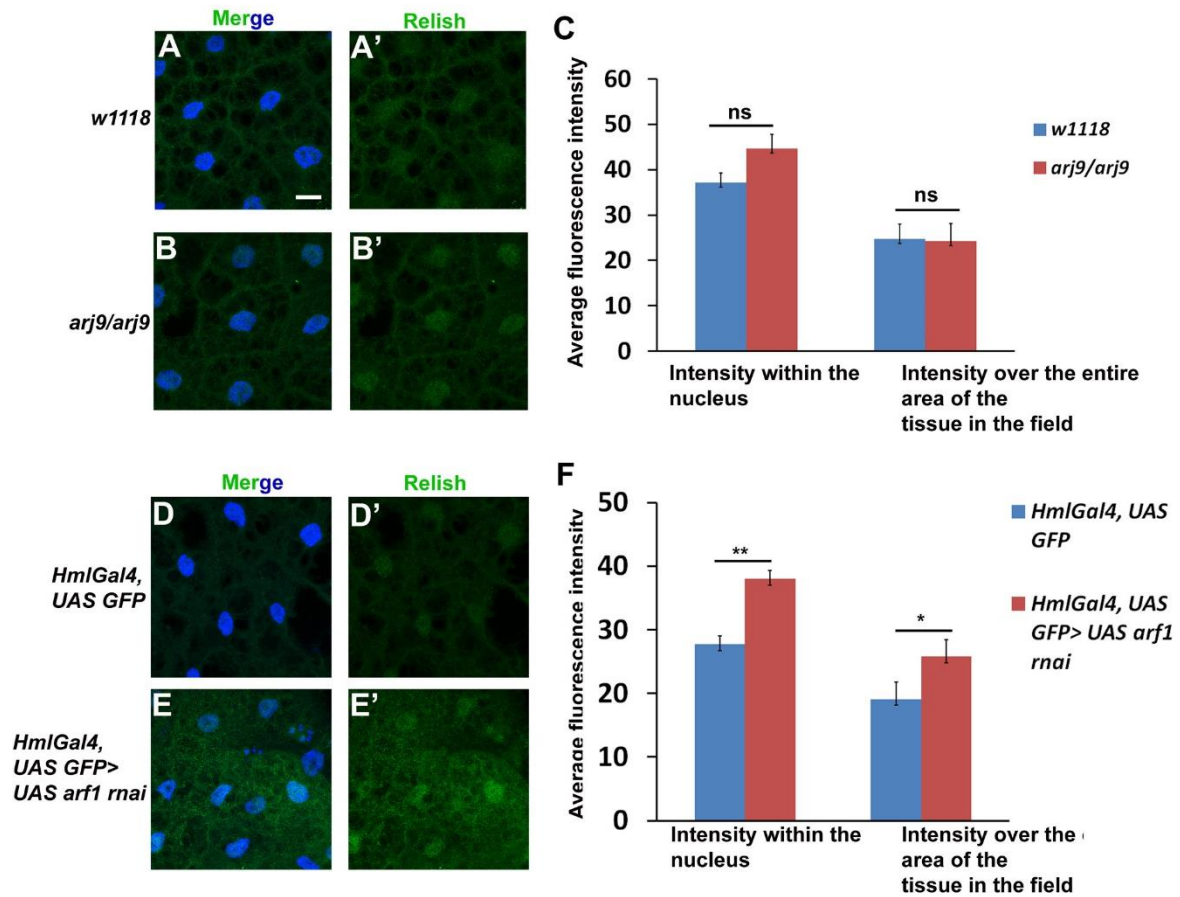


Figure 2.5 Imd pathway activation through Relish nuclear translocation in *asrij* null and *arf1* KD larval fat bodies. Confocal images of Relish staining in *w1118* (A-A') and *arj9/arj9* (B-B') fat body. DAPI marks the nucleus. Scale bar: 10 μ m. Bar diagrams show quantification of Relish intensity in nuclei as well as whole field of view of the fat body (C). Relish staining in control (*HmlGal4 UAS GFP*) and *arf1* KD (*HmlGal4 UAS GFP; UAS arf1 RNAi*) are shown in panel (D-D', E-E'). Bar diagrams represent quantification of Relish intensity in nuclei and whole field of view of the fat body of *control* and *arf1* KD larvae. N=10 for each genotype. Error bars in all graphs represent SEM. * and ** represent P-value<0.05 and <0.01, respectively. ns indicates statistically non-significant difference.

2.3.4 *Asrij* and ARF1 depletion reduces survival of flies upon acute bacterial infection.

While both *Asrij* and ARF1 similarly regulate the Toll pathway, differential regulation of the Imd pathway suggests a complex mechanism of AMP production. Previously it was shown that *B. subtilis* infection causes a rapid decrease in survival of *asrij* null or *arf1* KD (*e33C>arf1 RNAi*) flies. *Asrij* is expressed in *Drosophila* hemocytes, trachea and pole cells (Inamdar, 2003) whereas ARF1 is ubiquitous. To understand if the reduction of survival in *asrij* null flies

upon infection was solely due to hemocyte or due to reduction of overall tolerance of the flies, we depleted *Asrij* specifically in the hemocytes (using *HmlGal4*) and the trachea (using *btlGal4*). Hemocyte specific knockdown of *Asrij* does not affect survival of flies in normal condition. However, survival of adults is reduced in *asrij* KD flies as compared to control upon infection with Gram-positive bacteria *Bacillus subtilis* (Fig 2.6 A) or Gram-negative bacteria *Escherichia coli* (Fig 2.6 B). Trachea-specific knockdown of *Asrij* does not affect survival upon infection with *B. subtilis* (Fig 2C) or *E. coli* (Fig 2D). This suggests hemocyte-specific function of *Asrij* as the key regulator of survival post-infection.

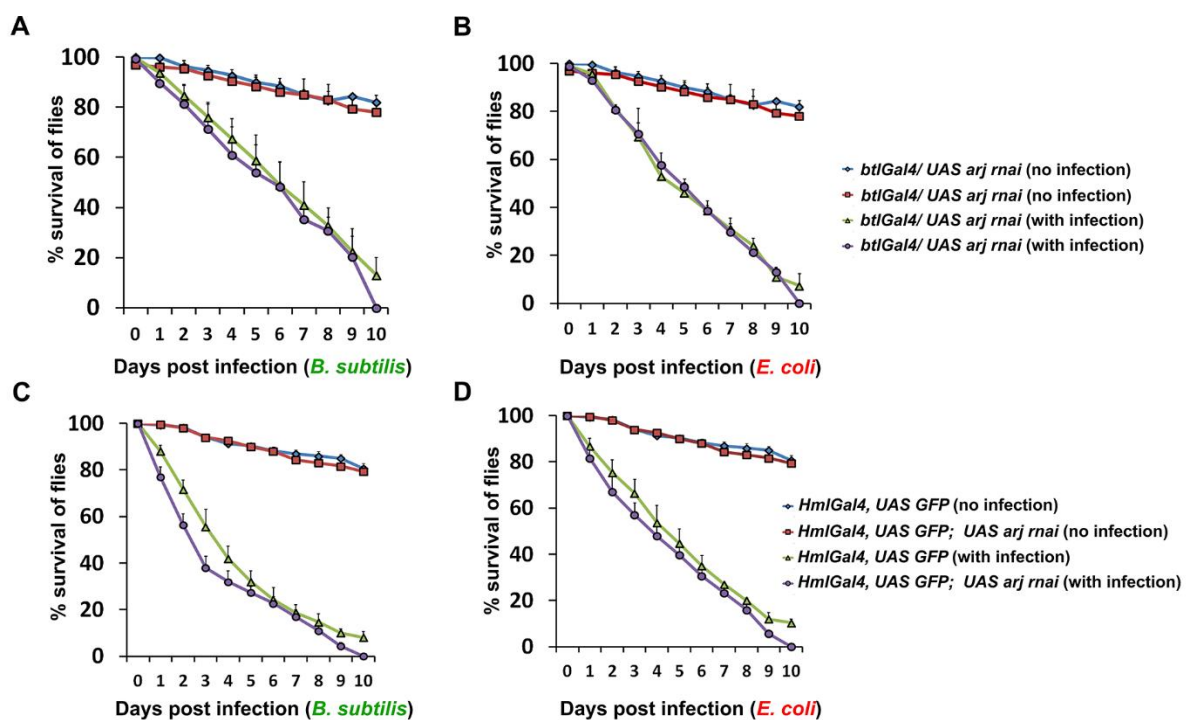


Figure 2.6 Survival of flies upon blood and trachea-specific depletion of *Asrij*. Survival curves of control (*HmlGal4 UAS GFP*) and hemocyte-specific *asrij* KD (*HmlGal4 UAS GFP; UAS arj RNAi*) upon infection with Gram-positive *Bacillus subtilis* and Gram-negative *Escherichia coli* represent the rate of decrease in survival over a period of 10 days (A, B). Similar curves show survival of control (*btlGal4*) and trachea-specific *asrij* KD (*btlGal4>UAS arj RNAi*) flies upon *B. subtilis* and *E. coli* infection (C, D). Error bars represent the SEM.

Flies depleted of ARF1 in the hemocytes have reduced survival upon infection with *B. subtilis* (Fig 2.7 A) or *E. coli* (Fig 2.7 B). ARF1 depletion in the trachea reduced survival of flies with or without infection, suggesting a critical trachea-specific role of ARF1 in survival even

before infection (Fig 2.7 C, D). Hence, Asrij and ARF1 function in hemocytes is essential for mounting an effective immune response. Also, ARF1 depletion in the trachea may contribute to reduced survival upon infection.

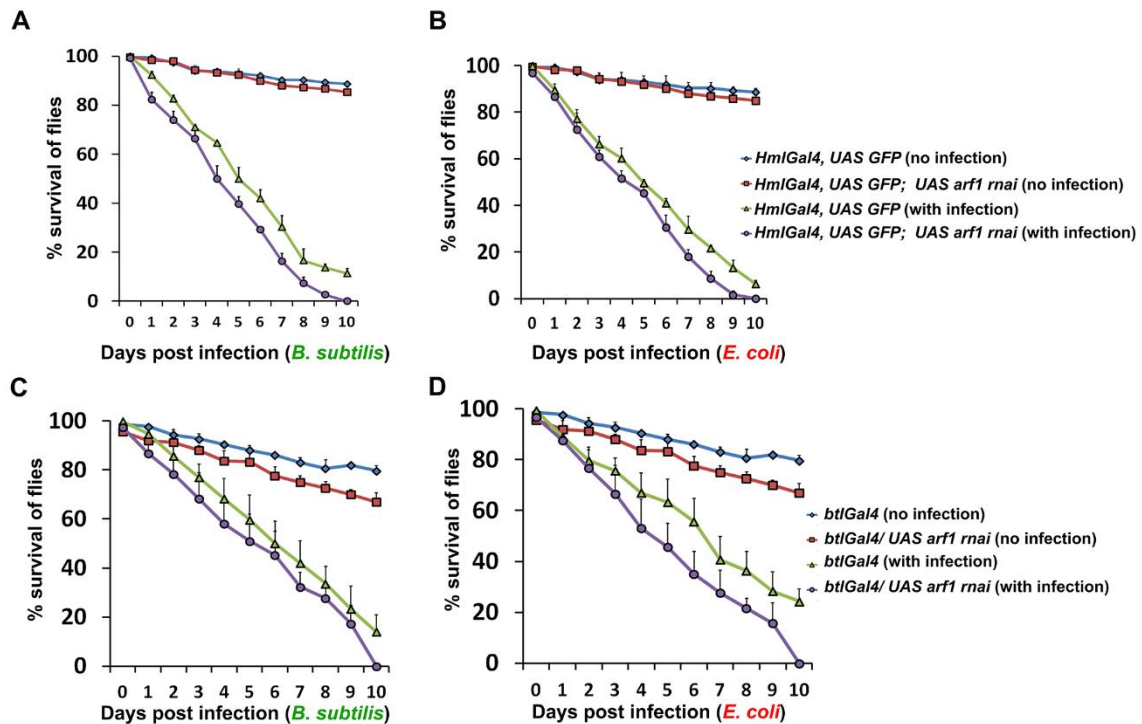


Figure 2.7 Survival of flies upon blood and trachea-specific depletion of ARF1. Survival curves of control (*HmlGal4 UAS GFP*) and hemocyte-specific *arf1* KD (*HmlGal4 UAS GFP; UAS arf1 RNAi*) upon infection with Gram-positive *Bacillus subtilis* and Gram-negative *Escherichia coli* represent the rate of decrease in survival over a period of 10 days (A, B). Similar curves show survival of control (*btlGal4*) and trachea-specific *arf1* KD (*btlGal4>UAS arf1 RNAi*) flies upon *B. subtilis* and *E. coli* infection (C, D). Error bars represent the SEM.

2.4 Discussion

We show differential roles for endosomal proteins ARF1 and Asrij in cellular and humoral immunity. ARF1 regulates Clathrin coat assembly and endocytosis and plays a critical role in membrane bending and scission (D'Souza-Schorey and Chavrier et al., 2006; Beck et al., 2011). However, we found that ARF1, like Asrij, is dispensable for phagocytic uptake. Hence,

other mechanisms may contribute to reduced survival of Asrij or ARF1 depleted flies upon immune challenge.

Endosomes act as critical regulatory platforms for multiple immunity pathways (Husebye et al., 2010; Devergne et al., 2007; Lund et al., 2010; Gleeson, 2014). For example, Toll pathway activation depends on the endosomal proteins Mop and Hrs (Huang et al., 2010). Previous work showed possible involvement of Asrij and ARF1 in endosomal cargo trafficking and sorting (Kulkarni, Khadilkar et al., 2011; Khadilkar et al., 2014). Our mechanistic analyses showed increased Cactus ubiquitination in hemocytes and fat bodies upon depletion of these two proteins. Hence, the endosomal ARF1-Asrij axis may systemically regulate degradation of Cactus, which in turn promotes the nuclear translocation of Toll effector, Dorsal. Our study shows cell-autonomous (Hemocyte) as well as non-autonomous (fat body) effects of the endosomal ARF1-Asrij axis on the Toll pathway.

ADP Ribosylation Factor-1 (ARF1) depletion inhibits GPI-anchored protein and fluid-phase endocytosis. In *Drosophila* S2R+ cells that are functionally similar to hemocytes, ARF1 depletion downregulates pinocytic uptake (Gupta et al., 2009). However, ARF1 does not affect Clathrin-dependent receptor-mediated endocytosis (Kumari and Mayor, *Nat. Cell Biol.*, 2008). Phagocytic uptake of bacteria by hemocytes require receptors such as NimC1 and Eater (Melcarne et al., 2019). Hence, it is quite possible that receptor-mediated uptake of bacteria in hemocytes remain unaffected upon ARF1 depletion. While ARF1 is reported to play an active role in the recruitment of critical molecular complex such AP-1 that promote phagocytosis (Braun et al., 2007), it is still unclear why ARF1 does not affect *in vivo* phagocytic uptake of bacteria in adult hemocytes. Phagocytic ability of hemocytes decline with age (Horn et al., 2014). We are not sure whether a lack of phenotype in ARF1-deficient adult hemocytes is due to decline in phagocytic efficiency of control flies itself. This aspect merits detailed mechanistic exploration.

In addition, we found that hemocyte-specific depletion of ARF1 causes a marked increase in nuclear localization of Relish in the fat body cells whereas *asrij null* flies showed no such phenotype. Hence, ARF1 seems to play a stronger role in Imd pathway while Asrij could fine-tune this effect. Mass spectrometric analysis of purified protein complexes indicates interaction of ARF1 with Imd components (Guruharsha et al., 2011) (*Drosophila* Protein Interaction Mapping Project, <https://interfly.med.harvard.edu>). A more detailed interactome study of Asrij and ARF1 could elucidate further mechanisms of endosomal control of immune pathways. Our study on the role of Asrij and ARF1 in the immune pathways suggests more pronounced effect of ARF1 than Asrij in *Drosophila* immunity. This could be due to a broader expression profile of ARF1. Asrij, having a tissue-restricted expression, could modulate ARF1 function to allow balanced functioning of immune regulatory pathways.

Loss of Asrij or ARF1 upregulates Toll and Imd signaling, thus promoting anti-microbial peptide generation. This could create a sustained inflammatory response in flies. Hence, upon bacterial infection, the mutant flies could possibly eliminate the bacteria but die out of uncontrolled immune activation. Elucidation of immune response in *asrij* knockout mouse model may provide an idea whether Asrij depletion indeed causes strong inflammatory response that may exacerbate further upon immune challenge.

In summary, we show essential but differential roles of Asrij and ARF1 in *Drosophila* immunity. Also, blood cell-specific function of these proteins is necessary for survival upon immune challenge. Many immune response pathways rely heavily on endosomal activity (Gleeson, 2014). Endosomal routes mediate TLR trafficking across different sub-cellular destinations (Petes et al., 2017). Also, Rab-GTPases play a critical role in trafficking of several immune regulatory molecules and receptors that regulate human innate immunity (Prashar et al., 2017). Endosomal proteins have been implicated in several immune disorders. In humans, Amphiphysin mutation which inhibits Clathrin coated vesicle formation leads to autoimmune disorders like Paraneoplastic stiff-person syndrome (De Camilli et al., 1993; Coppens et al., 2006). Synaptotagmin, involved in vesicle docking and fusion to the plasma

membrane acts as an antigenic protein and its mutation leads to an autoimmune disorder called Lambert-Eaton myasthenic syndrome (Takamori et al., 2000). Mutations in endosomal molecules like Rab27A, β subunit of AP3 and SNARE also lead to immune diseases like Griscelli and Hermansky-Pudlak syndrome (Menasche et al., 2003; Stow et al., 2006). Asrij has been associated with inflammatory conditions such as arthritis, thyroiditis, endothelitis and tonsillitis (<http://www.malacards.org/card/tonsillitis?search=OCIAD1>) and myelodysplastic syndromes (Sinha et al., 2019) that often involve dysregulated inflammatory pathway activation. ARF1 is involved in granule translocation in mast cells and IgE mediated anaphylactic response (Nishida et al., 2011). Our study shows the critical role of conserved tissue-restricted regulator of hematopoiesis, Asrij at the organismal level. Endocytic role of ARF1 and Asrij in vertebrate immunity awaits detailed investigation.

2.5 Acknowledgement

This work is published in:

Khadilkar RJ[†], **Ray A**[†], Chetan DR, RoyChowdhury AS, Magadi SS, Kulkarni V, Inamdar MS., (2017) Differential modulation of the cellular and humoral immune responses in Drosophila is mediated by the endosomal ARF1-Asrij axis. *Scientific Reports*, doi: [10.1038/s41598-017-00118-7](https://doi.org/10.1038/s41598-017-00118-7)

[†]Equal contribution

All figures are published in the above mentioned publication. Text and figures have been used from the original research article following the terms of [Creative Commons Attribution International 4.0 License \(CC BY\)](https://creativecommons.org/licenses/by/4.0/).

(<http://creativecommons.org/licenses/by/4.0/>).

Chapter 3. Asrij mutant lymph gland proteome analysis reveals potential role of mitochondrial and endosomal proteins in *Drosophila* blood cell homeostasis.

3.1 Introduction

Blood cell homeostasis depends on several intracellular and extracellular cues. Signaling pathways and metabolic flux regulate hematopoietic stem and progenitor cell fate. Dynamic organelles such as endosomes act as critical regulatory hubs of signaling by providing scaffolds to various signaling receptors (Scita and DiFiore, 2010). Also, mitochondria regulate energy metabolism as well as various biosynthetic and signaling pathways. Endosomal proteins such as Rab5, Rab11, Rabex5, Atg6 regulate blood cell homeostasis in *Drosophila* (Shravage et al., 2013; Reimels et al., 2015; Yu et al., 2021). Regulators of mitochondrial oxidative phosphorylation, ROS biosynthesis and Calcium signaling regulate hematopoiesis in both *Drosophila* and vertebrates (Owusu-Ansah et al., 2009; Diebold and Chandel, 2017). Asrij, the conserved endosomal regulator of hematopoiesis, interacts with endosomal ARF1-GTP and prevents precocious blood cell differentiation in *Drosophila* (Kulkarni, Khadilkar et al., 2011; Sinha et al., 2013; Khadilkar et al., 2014). Recent reports showed localization of OCIAD1, the human ortholog of Asrij in the mitochondria of human embryonic stem cells (hESC) as well as other cell types (Floyd et al., 2016; Lee et al., 2017; Shetty et al., 2018; Le Vasseur et al., 2021). OCIAD1 depletion in hESCs results in increased early mesodermal progenitor formation, indicating increased differentiation propensity (Shetty et al., 2018). Blood cell enriched expression of Asrij suggests tissue-restricted regulation of organelle function and blood cell homeostasis (Inamdar, 2003; Khadilkar et al., 2014, Khadilkar, Ray et al., 2017).

As discussed elaborately in Chapter 1, the *Drosophila* lymph gland harbors the entire blood progenitor pool of the larva and allows comprehensive *in situ* analysis of progenitor homeostasis *in vivo*. *asrij* null (*arj9/arj9*) mutant lymph glands represent a model of hematopoietic differentiation and loss of stemness. Loss of Asrij leads to endosomal

entrapment of Notch intracellular domain (NICD) and upregulation of Notch signaling, leading to precocious differentiation to crystal cells (Kulkarni, Khadilkar et al., 2011). Also, *asrij* null lymph glands undergo hyperproliferation of blood cells in the posterior lobes (Kulkarni, Khadilkar et al., 2011). On the other hand, *Asrij* overexpression promotes stemness and reduces differentiation (Sinha et al., 2013). Hence, perturbing *Asrij* levels either way alters differentiation potential and hence provides valuable tools to study context-dependent regulation of stemness and differentiation.

A proteomic analysis of *Asrij* perturbed lymph glands was performed previously in our lab to understand tissue-restricted mechanisms for conserved regulation of hematopoiesis (Sinha et al., 2019). The proteome identified 2133 proteins of which 1238 were unique to this study. Perturbation of *Asrij* levels led to differential expression of 619 proteins of which 27% have been implicated in various pathological conditions in humans. A detailed gene ontology and pathway enrichment analysis yielded hits such as organelle-associated proteins that are involved in vesicle mediated transport, organelle biogenesis, metabolic regulation and signal transduction (Fig 3.1).

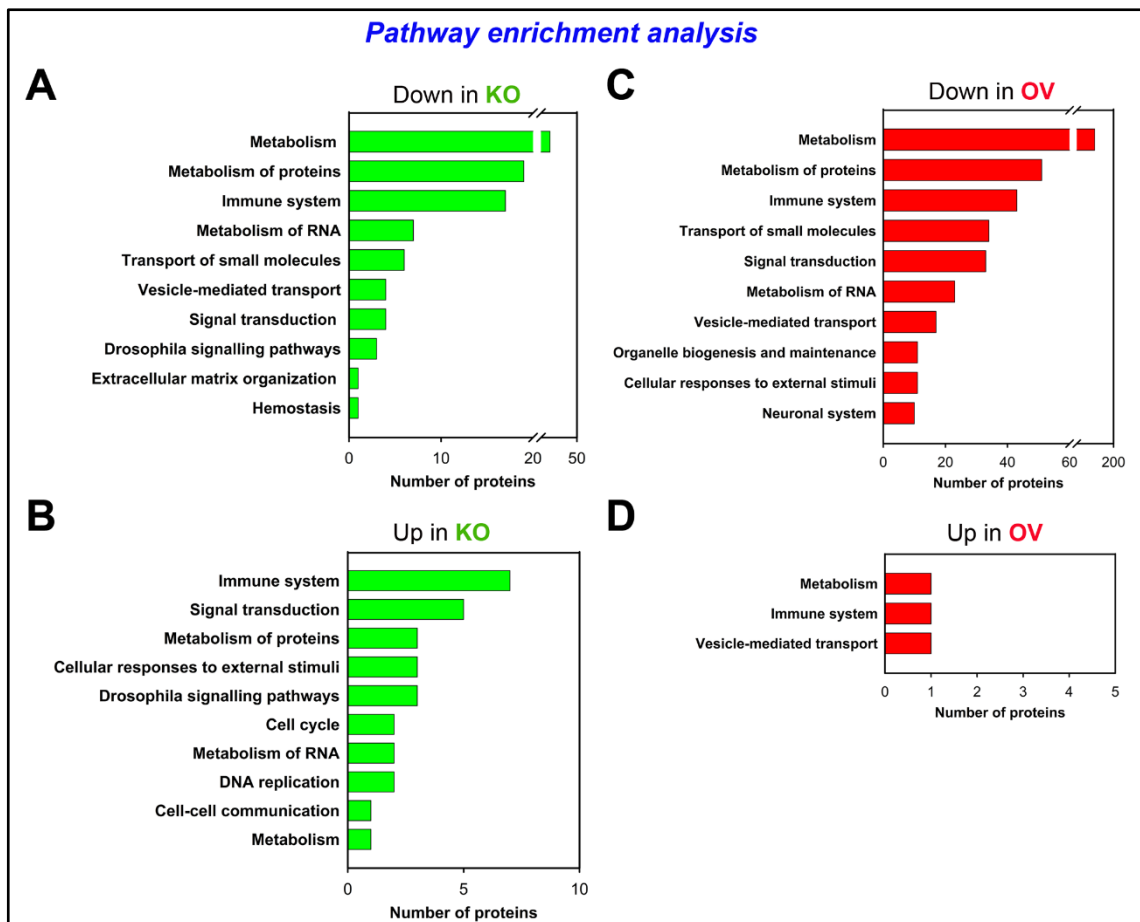


Figure 3.1 Pathway enrichment analysis of Asrij lymph gland proteome. (A-D) Pathway enrichment analysis of the differentially expressed proteins performed using g-profiler classification (Biological Pathways: Reactome). The x-axis shows the number of proteins in each category (Sinha et al., *Molecular and Cellular Proteomics*, 2019).

Previous studies on Asrij showed its active contribution to oxidative phosphorylation and endocytic trafficking (Kulkarni, Khadilkar et al., 2011; Khadilkar et al., 2014; Shetty et al., 2018). Proteome analysis revealed Asrij as an upstream regulator of several endosomal and mitochondrial proteins, consistent with previous findings. In this chapter, we discuss the validation of the Asrij lymph gland proteome and its importance as a resource for the potentially conserved regulators of hematopoiesis.

3.2 Materials and methods

3.2.1 Fly stocks

Canton-S was used as wild type (WT) control for Asrij lymph gland proteome validation. *w1118* was used as background control for *arj9/arj9* (asrij knockout: KO) whereas *e33CGal4* (K. Anderson, Memorial Sloan Kettering Center) was used as parental control for *asrij* overexpression (OV). *UAS arj* stock was used for overexpressing Asrij.

3.2.2 Immunostaining-based analysis

Third instar larvae were dissected in PBS to prepare lymph gland samples as described before (Khadilkar et al., 2014). Samples were fixed with 4% paraformaldehyde (PF) for 20 minutes at room temperature (25°C), permeabilized with 0.3% PTX (Triton X-100 in PBS) and incubated in 20% goat serum before primary antibody addition. Antibodies used for proteome validation were rabbit anti-ARF1 (Khadilkar et al., 2014), rabbit anti-Rab7 and rabbit anti-Rab11 (Marcos Gonzalez-Gaitan, University of Geneva), mouse anti-COXIV (Abcam, UK), mouse anti-NDUFS3 (Abcam, UK), mouse anti-SDHB (Abcam, UK), mouse anti-ATP5A (Abcam, UK). Antibodies used for mitochondria related experiments were mouse anti-COXIV (Abcam, UK), anti-P1 (Istvan Ando, BRC Hungary), mouse anti-ProPO, rabbit anti-dsRed (Takara, Japan), chick anti-GFP (Abcam, UK).

Secondary antibodies used were conjugated to Alexa-Fluor 488, 568 or 633 (Life Technologies, Thermo Fisher Scientific, USA). Lymph glands were mounted on coverslips in DAPI-glycerol media. Images were acquired using Zeiss LSM880 confocal microscope.

3.2.3 Quantification

Fluorescence intensity of lymph gland lobes was quantified using Fiji software. Primary, secondary, and tertiary pair of lymph gland lobes were analyzed for protein expression across different genotypes. The mean fluorescence intensity was estimated for the maximum intensity projection of region of interest as well as the background from the same

image using Fiji. The actual intensity was calculated by subtracting background intensity from ROI intensity to minimize any error due to autofluorescence from the mounting media. Statistical significance was estimated using two factor ANOVA (LG lobe and genotype being the two factors taken into consideration) followed by a post-hoc analysis in STATISTICA v5.0.

3.3 Results

3.3.1 Validation of candidates shows 73% match with the *Drosophila* lymph gland proteome.

Previously performed comparative proteomic analysis involved isolation of protein from 1500 lymph glands of each sample-wild type (WT, strain: Canton-S), *asrij* KO (*arj9/arj9*) and *asrij* OV (*e33CGal4>UAS arj*) (Sinha et al., 2019). Owing to the challenges of performing the same experiment in biological replicates, we validated the proteome in two ways:

a) by comparing changes in specific protein expression with information available in published reports (Kulkarni, Khadilkar et al., 2011; Sinha et al., 2013; Khadilkar et al., 2014) and

b) by analyzing protein expression of candidate genes by immunostaining of lymph glands.

Asrij depletion does not affect ARF1 protein level in circulatory hemocytes (Khadilkar et al., 2014). However, proteome data showed reduced expression of ARF1 in KO and unchanged in OV (Fig 3.2A). The inconsistency between the published report and the proteome data could be attributed to difference in cell populations (circulatory and lymph gland hemocytes) as the cell population in lymph gland is more heterogeneous as compared to that in circulation.

Asrij positively regulates activation of STAT92e and Garz without affecting their level (Sinha et al., 2013; Khadilkar et al., 2014). Pvr acts upstream of *Asrij* and hence is expected to be

unaffected by *Asrij* (Khadilkar et al., 2014). In agreement with this, we found no change in *Garz*, *Stat92e* and *Pvr* level in both KO and OV lymph gland proteome (Fig 3.2A). As plasmacyte and crystal cell differentiation increases upon *Asrij* depletion, we expected an increase in the expression of respective markers, such as *Eater* (for plasmacytes), *Pxn* and *PPO1* (for crystal cells). Even though we observed increased *PPO1* level in KO proteome-thus matching our expectation, we found decreased expression of *eater* and *Pxn*. Other known regulators of blood cell homeostasis (*Npc2a*, *Larp*, *Msk*) and lymph gland hematopoiesis (*sgl*) remained unaffected in KO or OV proteome. Thus, expression 5/7 proteins in KO and 7/7 proteins in OV matched with previously published data.

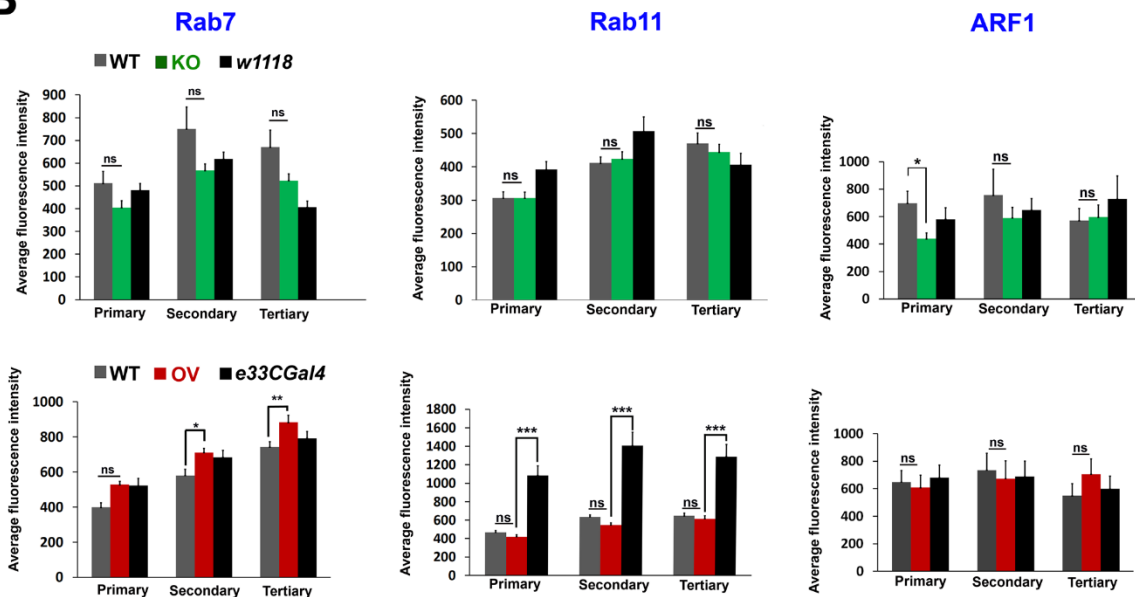
Next, we analyzed protein expression of representative candidates by immunofluorescence microscopy. Based on pathway enrichment analysis and previous reports on *Asrij*, we selected proteins belonging to the categories of transport of small molecules, vesicular transport, and metabolism for experimental validation. *Asrij* localizes to endosomes and plays a critical role in endocytic protein transport (Kulkarni, Khadilkar et al., 2011; Khadilkar et al., 2014). Endosomal and mitochondrial hits that were selected for validation are ubiquitously functional. As expected, we observed uniform expression for majority of the candidate proteins across different compartments. Also, some of the endosomal proteins showed prominent punctate distribution suggesting endosomal pattern whereas mitochondrial proteins showed pattern reflecting mitochondrial network (Fig 3.3, 3.5).

We selected 3 endosomal hits (*Rab7*, *Rab11* and *ARF1*) for validation of the proteome owing to their critical role in endocytic trafficking and also functional link with *Asrij*. Immunostaining-based validation showed reduced *ARF1* level in the primary lobes of KO lymph glands (Fig 3.2B, Fig 3.3C). However, *Rab7* and *Rab11* levels were unaffected in KO lymph glands (Fig 3.2B, Fig 3.3 A-B). Conversely, *Rab7* level was significantly high upon *Asrij* overexpression, whereas *ARF1* and *Rab11* were unchanged. This analysis showed that expression levels were in agreement with proteome alterations for all three endosomal proteins, thus validating the data (Fig 3.2C).

A

Known regulators identified	KO LGs		OV LGs	
	Predicted	Proteome	Predicted	Proteome
I. Lymph gland blood cell homeostasis				
a) Maintenance				
ADP-ribosylation factor 1 (ARF1, FBgn0010348)	Unchanged	Low	Unchanged	Unchanged
STAT92e (STAT92e, FBgn0016917)	Unchanged	Unchanged	Unchanged	Unchanged
Gartenzweg (Garz, FBgn0264560)	Unchanged	Unchanged	Unchanged	Unchanged
PDGF- and VEGF-receptor related (Pvr, FBgn0032006)	Unchanged	Unchanged	Unchanged	Unchanged
b) Differentiation				
Eater (Eater, FBgn0243514)	High	Low	Unchanged	Unchanged
Peroxidasin (Pxn, FBgn0011828)	High	Low	Unchanged	Unchanged
c) Others				
Niemann-Pick type C 2a (Npc2a, FBgn0031381)	Not known	Unchanged	Not known	Unchanged
La related protein (Larp, FBgn0261618)	Not known	Unchanged	Not known	Unchanged
Moleskin (Msk, FBgn0026252)	Not known	Unchanged	Not known	Unchanged
II. Lymph gland development				
Sugarless (sgl, FBgn0261445)	Not known	Unchanged	Not known	Unchanged

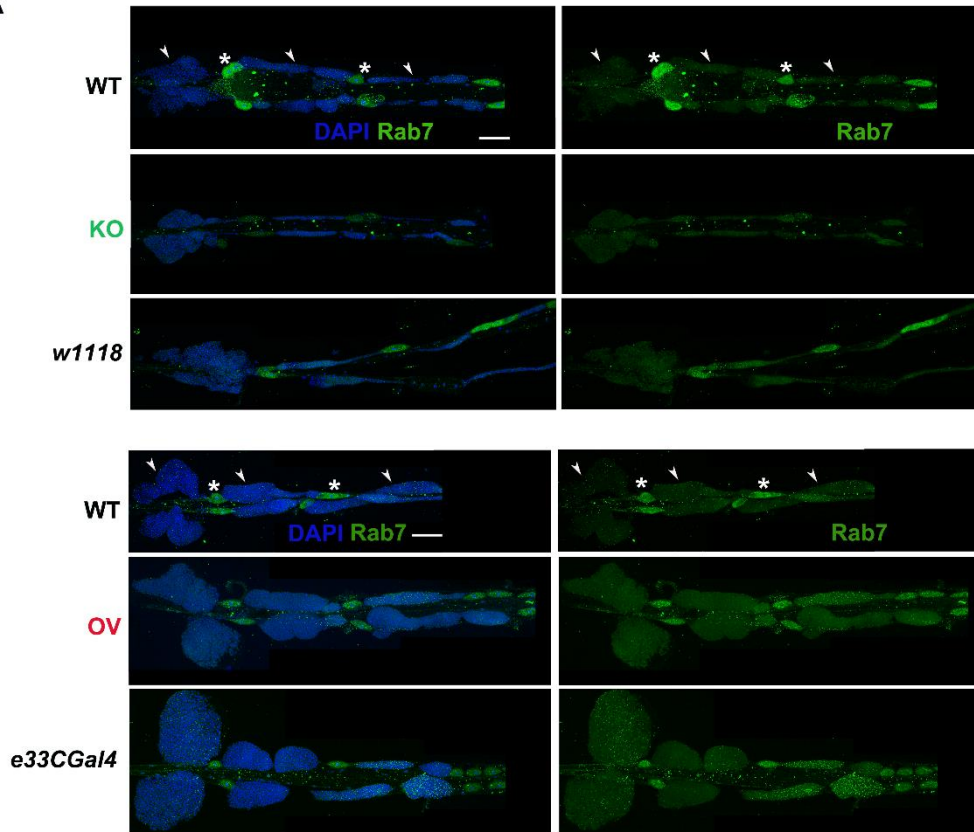
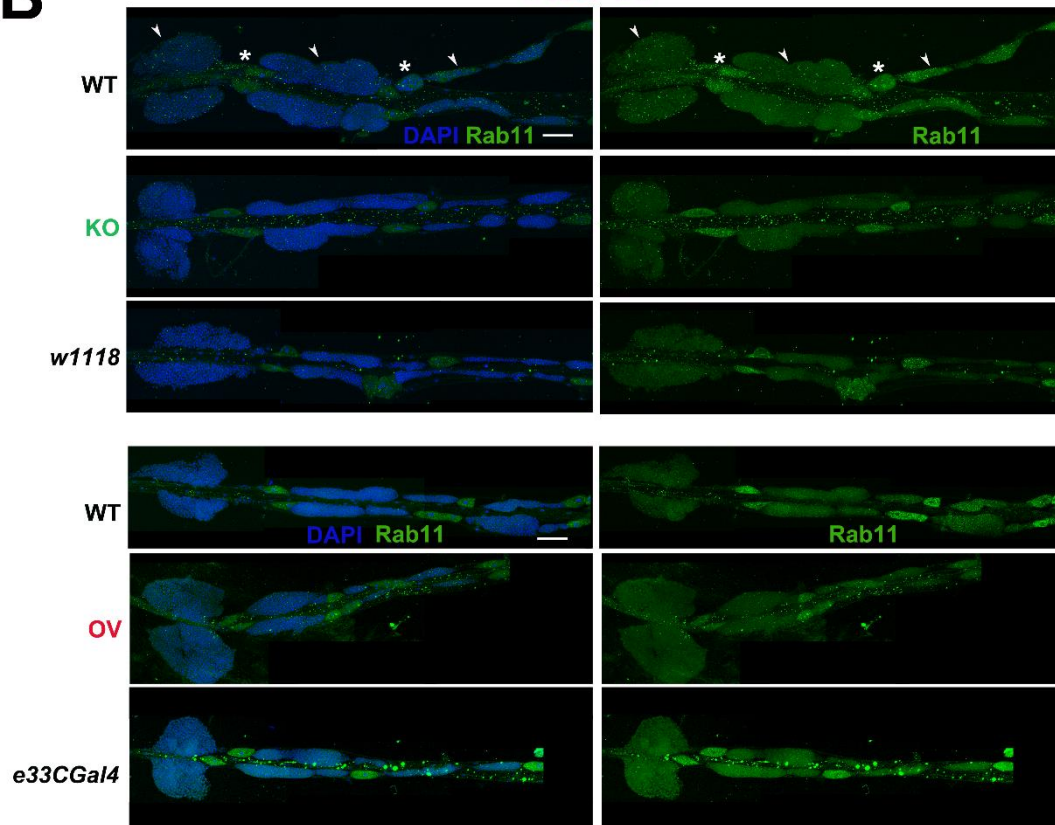
B



C

Endosomal proteins	KO LGs		OV LGs	
	Proteome	Validation	Proteome	Validation
Rab7 (Rab7, FBgn0015795)	Unchanged	Unchanged	High	High
Rab11 (Rab11, FBgn0015790)	Unchanged	Unchanged	Unchanged	Unchanged
ADP-ribosylation factor 1 (ARF1, FBgn0010348)	Low	Low	Unchanged	Unchanged

Figure 3.2 Validation of lymph gland proteome for endosomal candidates Rab7, Rab11 and ARF1. Table represents comparison of proteome data with predicted change of expression of known hematopoietic regulators (A). Bar graphs show average fluorescence intensity of Rab7, Rab11 and ARF1 immunofluorescence signal across primary, secondary and tertiary lymph gland lobes of WT (Canton-S), control (*w1118* and *e33CGal4*), *asrij* KO (*arj9/arj9*) and *arj* OV (*e33C>UAS arj*) larvae. Genotypes are indicated by specific color codes (B). Table shows a comparison between proteome analysis data and validation results (C). Error bars in all graphs represent the standard error of mean (SEM). *, ** and *** represent P-value <0.05, <0.01 and <0.001, respectively. ns indicates statistically non-significant difference.

A**Rab7****B****Rab11**

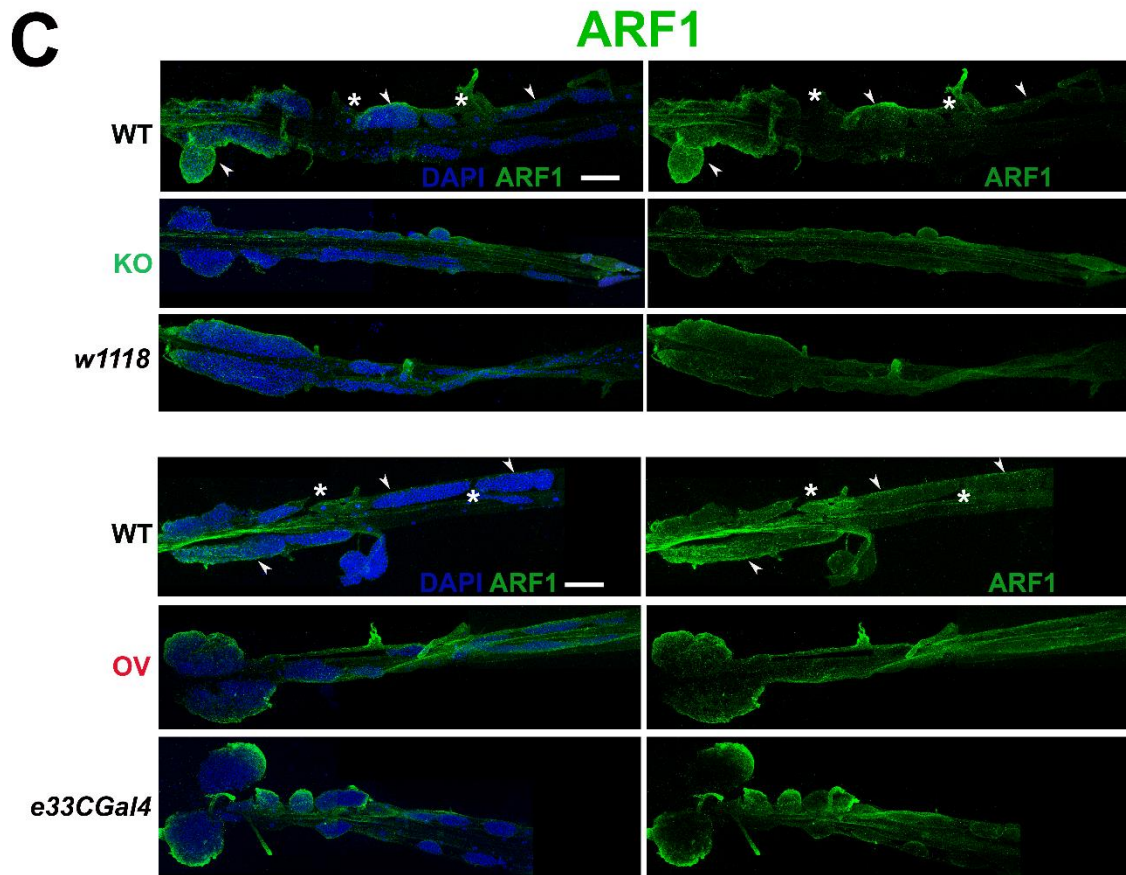


Figure 3.3 Immunofluorescence based validation of endosomal candidates identified from the lymph gland proteome. Third instar lymph gland whole mounts showing expression of endosomal proteins (A) Rab7, (B) Rab11 and (C) ARF1 in different genotypes as indicated (N>7 per genotype). Nuclei were stained with DAPI (blue). Arrowheads and asterisks in the lymph glands mark the lobes and the pericardial cells, respectively. Scale bar: 100 μ m.

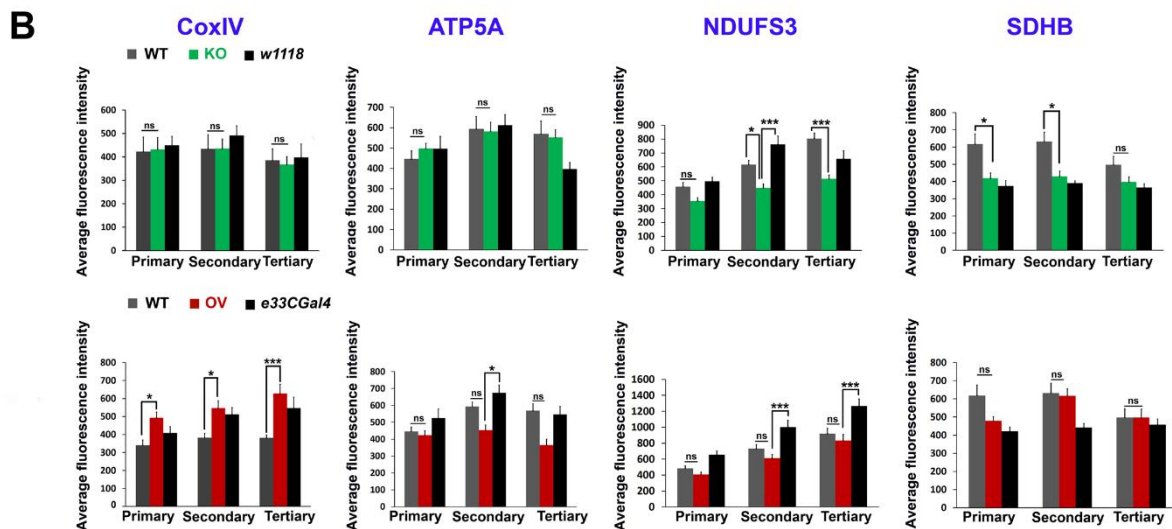
Asrij/OCIAD1 negatively regulates mitochondrial electron transport chain (ETC) Complex-I activity and interacts with its components (Shetty et al., 2018). Since energy metabolism, TCA cycle, respiratory electron transport, Complex-I biogenesis were major perturbed categories (Fig 3.4A), we tested the expression of 4 mitochondrial proteins (COXIV, ATP5A, NDUFS3 and SDHB) that either interacts with OCIAD1 in hESC or may be functionally linked to Asrij/OCIAD1. Proteome analysis indicates unchanged level of these proteins in KO and significantly upregulated level in OV. Immunostaining of KO lymph glands with the respective antibodies showed unchanged level of COXIV and ATP5A (Fig 3.4B, C; Fig 3.5A, C)

but significantly decreased level of NDUFS3 and SDHB in KO lymph glands as compared to WT (Fig 3.4B, C; Fig 3.5B, D). The OV lymph glands showed significantly increased COXIV, unchanged ATP5A, NDUFS3 and SDHB levels, as compared to WT. Hence, change in the level of 2/4 proteins in KO and 1/4 proteins in OV matched with the proteome data (Fig 3.4C).

In summary, we found that 9/13 proteins in KO and 10/13 in OV validated the proteome analysis. These data indicate that our comparative proteome analysis is reliable and can be used as a resource for further studies.

A Biological Pathways (Reactome)

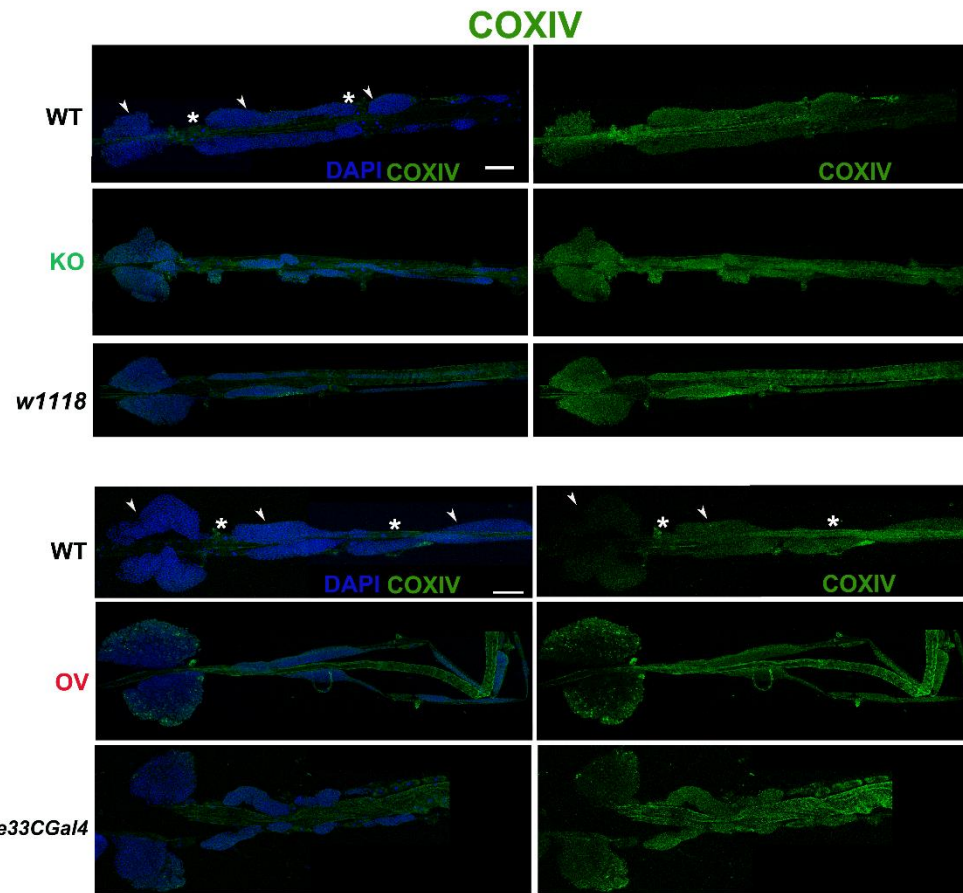
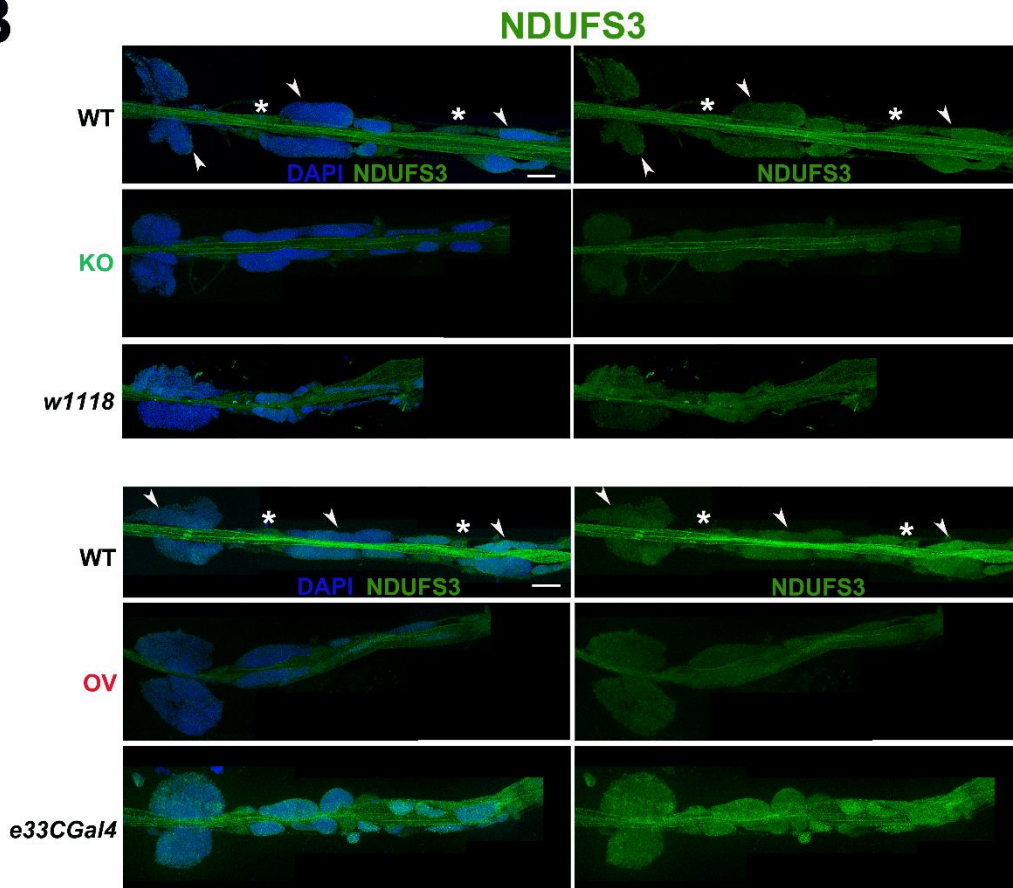
Term (ID)	No. of proteins	Corrected p-value	
<i>Metabolism</i>			
The citric acid (TCA) cycle and respiratory electron transport	R-DME-1428517	63	2.67e-41
Respiratory electron transport, ATP synthesis by chemiosmotic coup ...	R-DME-163200	45	2.56e-31
Respiratory electron transport	R-DME-611105	34	4.14e-22
Complex I biogenesis	R-DME-6799198	22	4.66e-13
Formation of ATP by chemiosmotic coupling	R-DME-163210	11	1.06e-08
Pyruvate metabolism and Citric Acid (TCA) cycle	R-DME-71406	18	1.95e-08
Interconversion of 2-oxoglutarate and 2-hydroxyglutarate	R-DME-880009	1	1.00e+00
Citric acid cycle (TCA cycle)	R-DME-71403	13	4.03e-06
Pyruvate metabolism	R-DME-70268	5	5.52e-01
Regulation of pyruvate dehydrogenase (PDH) complex	R-DME-204174	5	4.32e-02



C

Mitochondrial proteins	KO LGs		OV LGs	
	Proteome	Validation	Proteome	Validation
Cytochrome oxidase IV (CoxIV, FBgn0032833)	Unchanged	Unchanged	High	High
Adenosine Triphosphate 5A (ATP5A, FBgn0011211)	Unchanged	Unchanged	High	Unchanged
NADH: Ubiquinone Oxidoreductase Core Subunit S3 (NDUFS3, FBgn0266582)	Unchanged	Low	High	Unchanged
Succinate dehydrogenase B (SDHB, FBgn0014028)	Unchanged	Low	High	Unchanged

Figure 3.4 Validation of lymph gland proteome for mitochondrial candidates COXIV, ATP5A, NDUFS3 and SDHB. Bar graphs show average fluorescence intensity of COXIV, ATP5A, NDUFS3 and SDHB immunofluorescence signal across primary, secondary and tertiary lymph gland lobes of WT (Canton-S), control (*w1118* and *e33CGal4*), *arj* KO (*arj9/arj9*) and *arj* OV (*e33C>UAS arj*) larvae. Genotypes are indicated by specific color codes (A). Table shows comparison between proteome analysis data and validation results (B). Error bars in all graphs represent SEM. * and *** represent P-value<0.05 and <0.001, respectively. ns indicates statistically non-significant difference.

A**B**

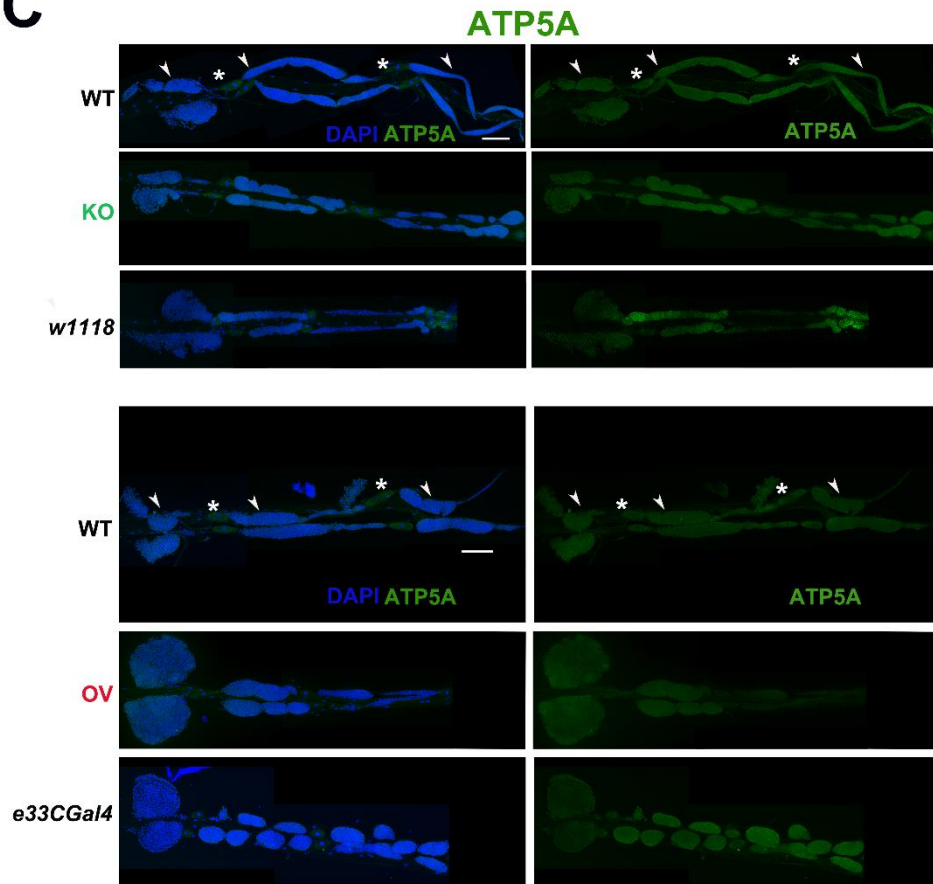
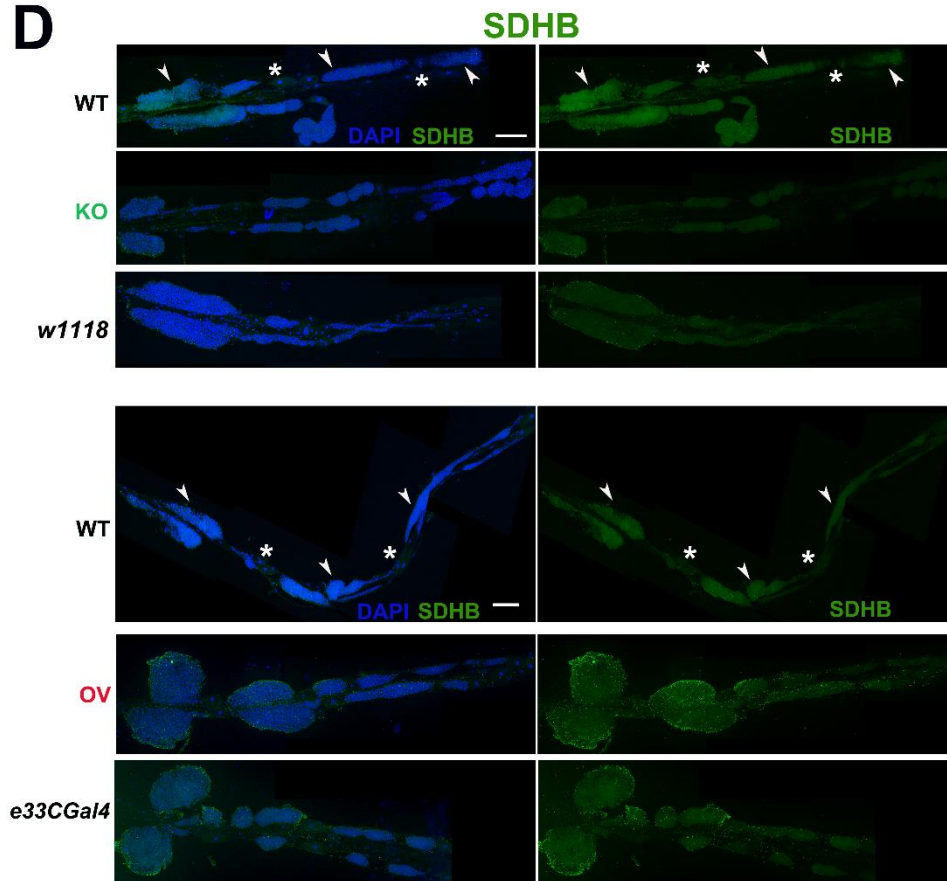
C**D**

Figure 3.5 Immunofluorescence based validation of mitochondrial candidates identified from the lymph gland proteome. Third instar lymph whole mounts showing expression of mitochondrial proteins (A) COXIV, (B) NDUFS3, (C) ATP5A and (D) SDHB in different genotypes as indicated (N>7 per genotype). Nuclei were stained with DAPI (blue). Arrowheads and asterisks in the lymph glands mark the lobes and the pericardial cells, respectively. Scale bar: 100 μ m.

3.4 Discussion

Proteomic analysis of *Asrij* perturbed lymph gland identified mechanisms that may potentially contribute to hematopoiesis. The proteome covers 15.3% of the total fly proteome (Flybase annotation release 6.25) and highlights the critical role of the “endocytic matrix” (Scita and DiFiore, 2010) in modulating several subcellular pathways that contribute to blood cell homeostasis. *Asrij* significantly affects the lymph gland proteome and emerges as a tissue-specific conserved regulator of various critical cellular processes in the hematopoietic system.

Validation of the proteome makes it a reliable resource to explore the mechanisms with hitherto unknown role in hematopoiesis. The comparative proteomic analysis highlights metabolic regulators and various organelle associated proteins as potential regulators of hematopoiesis. Earlier work from our lab showed an active role of *Asrij* homolog OCIAD1 in regulating oxidative phosphorylation in hESCs through a physical interaction with mitochondrial ETC components (Shetty et al., 2018). Here we show that the expression of mitochondrial ETC proteins such as NDUFS3, SDHB and COXIV in the lymph gland is sensitive to *Asrij* level. The proteome identifies mitochondrial dynamics regulator Drp1 and various endocytic proteins as candidates with potential role in blood cell homeostasis. As *Asrij*/OCIAD1 acts as a conserved regulator of stemness, signaling and blood cell homeostasis, similar proteomic analysis in KO vertebrate models or pathological samples would unravel critical molecular network that may govern hematopoietic stem and progenitor cell fate.

3.5 Acknowledgement

This work is published in:

Sinha S, **Ray A**, Abhilash L, Kumar M, Sreenivasamurthy SK, Keshava Prasad TS, Inamdar MS., (2019) Proteomics of Asrij Perturbation in *Drosophila* Lymph Glands for Identification of New Regulators of Hematopoiesis. ***Molecular and Cellular Proteomics***, doi: [10.1074/mcp.RA119.001299](https://doi.org/10.1074/mcp.RA119.001299)

All figures are published in the above mentioned publication. Text and figures have been used from the original research article following the terms of [Creative Commons Attribution License \(CC BY\)](https://creativecommons.org/licenses/by/4.0/).

[\(http://creativecommons.org/licenses/by/4.0/\)](http://creativecommons.org/licenses/by/4.0/)

The lymph gland proteome was generated by Dr. Saloni Sinha. The validation of the Asrij mutant lymph gland proteome based on prediction from published reports was jointly performed with Dr. Saloni Sinha.

Chapter 4. A conserved role for Asrij/OCIAD1 in progenitor differentiation and lineage specification through functional interaction with mitochondrial dynamics regulators.

4.1 Introduction

Dynamicity of the mitochondrial network governs mitochondrial function and cell fate specification (Bejarano-Garcia et al., 2016; Anso et al., 2017; Zhang et al, 2018). Balanced mitochondrial fission and fusion maintain mitochondrial quality control through segregation of damaged mitochondria or exchange of components, electrochemical gradients, and metabolites (Twig et al, 2008; van der Blik et al., 2013; Liu et al, 2020). Mitochondrial morphology and dynamics may vary across cell states, lineages, and tissues (Seo et al., 2018).

Mitochondrial membrane remodelling proteins actively control mitochondrial dynamics to shape the mitochondrial network through regulation of fission, fusion, biogenesis and degradation. Dynamin related protein 1 (Drp1) is a GTPase that acts as the key mediator of fission and segregation of the mitochondrial network whereas Mitofusins (Mfn1/2) are the main membrane bound GTPases that promote mitochondrial outer membrane fusion (Seo et al., 2018). Many signaling pathways including calcium, ROS, and Notch signaling, which are essential for cell fate decisions depend on the fission-fusion machinery. Drp1 can act in a positive feedback loop with Notch signaling in triple negative breast cancer cells (Chen et al., 2018). Inhibition of Mitofusin2 can upregulate Notch signaling through Calcineurin A in mouse embryonic stem cells (Kasahara et al., 2013).

Recent reports highlight the importance of balanced Drp1 or Mitofusin activity in determining HSC fate decisions such as lineage-biased differentiation potential (Luchsinger et al., 2016; Hinge et al., 2020). Drp1 maintains HSC regenerative potential by establishing divisional memory and regulates myeloid lineage reconstitution (Hinge et al, 2020). Also, Mfn2 maintains HSCs with extensive lymphoid potential through inhibition of excessive

calcium-dependent NFAT (Nuclear Factor of Activated T-cells) signaling, probably by tethering mitochondria to the endoplasmic reticulum (Luchsinger et al, 2016). Despite reports suggesting functional links between mitochondrial dynamics regulators and HSC fate, the mechanism by which they regulate lineage-biased signaling and differentiation is not fully elucidated.

Depletion of OCIAD1 leads to elongation and hyperfusion of mitochondria in hESC (Shetty et al, 2018; Praveen et al., 2020). Although OCIAD1 controls mitochondrial morphology in hESCs, its genetic interaction with the canonical mitochondrial dynamics regulatory machinery remains unexplored, especially *in vivo*. As discussed in the introduction (Chapter 1), the *Drosophila* lymph gland serves as an excellent *in vivo* model for a comprehensive *in situ* analysis of blood progenitor homeostasis. Hence, we investigated whether *Asrij* regulates mitochondrial dynamics to progenitor maintenance and cell fate decisions in the lymph gland.

4.2 Materials and methods

4.2.1 Fly stocks

Canton-S was used as wild type strain. *w1118* was used as background control for *arj9/arj9* whereas *e33CGal4* (K. Anderson, Memorial Sloan Kettering Center) was used as parental control for *asrij* knockdown and overexpression. For blood progenitor-specific knockdown, *domeGal4 UAS 2xEGFP/FM7a* or *domeGal4/FM7b* (Utpal Banerjee, UCLA) was used as driver and parental control. Other stocks used are as follows: *UAS asrij RNAi* (VDRC 6633), *UAS arj*, *UAS mito-GFP* (BDSC 8442), *UAS Drp1 RNAi* (BDSC 44155), *UAS Marf RNAi* (BDSC 31157), *UAS Drp1* (BDSC 51647), *UAS Marf* (BDSC 67157), *NRE-GFP/CyO* (BDSC 30727), *UAS mCD8 RFP* (BDSC 27399).

4.2.2 Immunostaining-based analysis

Third instar larvae were dissected in PBS to prepare lymph gland samples as described before (Khadilkar et al., 2014). Samples were fixed with 4% paraformaldehyde (PF) for 20 minutes at room temperature (25°C), permeabilized with 0.3% PTX (Triton X-100 in PBS) and incubated in 20% goat serum before primary antibody addition. Primary antibodies used were mouse anti-COXIV (Abcam, UK), mouse anti-P1 (Istvan Ando, BRC Hungary), mouse anti-ProPO, rabbit anti-dsRed (Takara, Japan), chick anti-GFP (Abcam, UK).

For hemocyte immunostaining, larvae were bled to extract hemolymph into warm Schneider's serum-free media (Thermo Fisher Scientific, USA). Hemocytes were placed on coverslips to allow attachment for 10 minutes, then fixed with 4% PF and permeabilized with 0.4% NP40, blocked with 20% goat serum and incubated in primary antibody.

Secondary antibodies used were conjugated to Alexa-Fluor 488, 568 or 633 (Life Technologies, Thermo Fisher Scientific, USA). Phalloidin conjugated to Alexa 568 or 633 (Life Technologies, Thermo Fisher Scientific, USA) was used to visualise lamellocytes. Lymph glands were mounted on coverslips in DAPI-glycerol media. Images were acquired using Zeiss LSM510 Meta or LSM880 confocal microscope in either normal confocal mode or airy scan mode.

4.2.3 Mitotracker staining

Hemocytes, attached to coverslips, were incubated with Mitotracker Deep Red (Thermo Fisher Scientific, USA) diluted to 200 nM in serum-free Schneider's media for 20 minutes at room temperature in the dark. Mitotracker was then washed off with serum-free Schneider's media and hemocytes fixed in 4% PF. Images were acquired in Zeiss LSM510 Meta microscope at 633 nm excitation.

4.2.4 Live imaging of mitochondria

Mito-GFP expressing hemocytes from larval hemolymph were left to attach onto coverslips in serum-free Schneider's media for 10 minutes at 25°C (Standard experimental temperature). The hemocytes were imaged on Zeiss LSM880 confocal microscope with temperature maintained at 25°C with 5% CO₂. Images were captured every 10 seconds. Auto-focus module was used to adjust focal plane variation during imaging.

4.2.5 Quantification

4.2.5.1 Mitochondria quantification

Co-localization was analysed using Zen software co-localization tool. Various parameters of mitochondrial network such as branch length, number of branches, number of junctions, and mitochondrial footprint in hemocytes and lymph gland progenitors were quantified using MiNA plugin of Fiji software following protocol described previously (Valente et al., 2017). Imaris (Bitplane) software was used to make 3D reconstructions of mitochondrial surfaces and quantify the number of surfaces and average volume per surface as a readout of mitochondrial aggregation in hemocytes.

Dynamics of mitochondrial network was estimated by quantifying the variance of different parameters over time as previously described (Hinge et al., 2020).

4.2.5.2 Quantification of hemocytes in the lymph gland

Progenitor and plasmacyte fraction in each lymph gland lobe was quantified using Imaris. Briefly, the number of spots (DAPI positive nuclei with >2 µm diameter) close to the reconstructed dome>2xEGFP (for prohemocytes) or P1 (for plasmacytes) surface, by a set threshold distance (1 µm for prohemocytes and 2 µm for plasmacytes), was quantified and divided by total number of nuclei. The number of crystal cells and number of cells with high NRE-GFP expression in each lobe was quantified manually and its fraction was calculated in each lobe by dividing with the number of nuclei. Lamellocytes were identified

based on large or elongated morphology as revealed by Phalloidin staining. All images within a given figure panel were adjusted equally for brightness and contrast using Adobe Photoshop CS5 extended. Graphs for all figure panels were prepared using GraphPad Prism version 8. Biorender was used to draw cells in the schematic in Figure 4.20.

4.2.6 Statistical analyses

Each larva was considered as a biological replicate. Data from each lymph gland lobe was individually considered for quantitation in all graphs. One-way ANOVA or Student's t-test was performed for statistical analysis of data. For datasets with unequal variance across groups, non-parametric tests such as Kruskal Wallis test or Mann-Whitney test was performed.

4.3 Results

4.3.1 Mitochondrial morphology reflects larval blood progenitor heterogeneity in *Drosophila*

The Asrij lymph gland proteome suggests regulation of blood cell homeostasis at the organelle level. Previous reports have shown a possible functional link of Asrij with mitochondrial dynamics (Shetty et al., 2018). Proteomic analysis of Asrij perturbed lymph glands highlighted the potential role of mitochondrial dynamics regulators such as Drp1 in hematopoiesis (Sinha et al., 2019). Mitochondria are reported to affect progenitor maintenance in the larval lymph gland primary or anterior lobes but mitochondrial morphology and dynamics have not been investigated in blood progenitors. A recent study from our laboratory showed that the larval blood progenitor pool is heterogeneous and arranged linearly, with younger progenitors in the posterior lobes (Rodrigues et al., 2021). Hence, I undertook a comprehensive analysis of mitochondrial morphology (see methods section 4.2.5.2) in the *dome*⁺ lymph gland progenitors of primary, secondary, and tertiary lobes, using the *domeGal4* driver and the mitoGFP reporter (*domeGal4*^{+/+}; UAS mito-GFP^{+/+}; *+/+*). This showed that while primary and secondary lobe progenitors have similar

mitochondrial morphology, tertiary lobes have relatively shorter mitochondria. Other parameters such as mitochondrial footprint, number of branches and junctions remained unchanged across progenitor subsets (Fig 4.1). This is in agreement with the anterior-posterior developmental and functional heterogeneity of progenitors reported earlier (Rodrigues et al., 2021) and indicates that younger progenitors have less mature mitochondria.

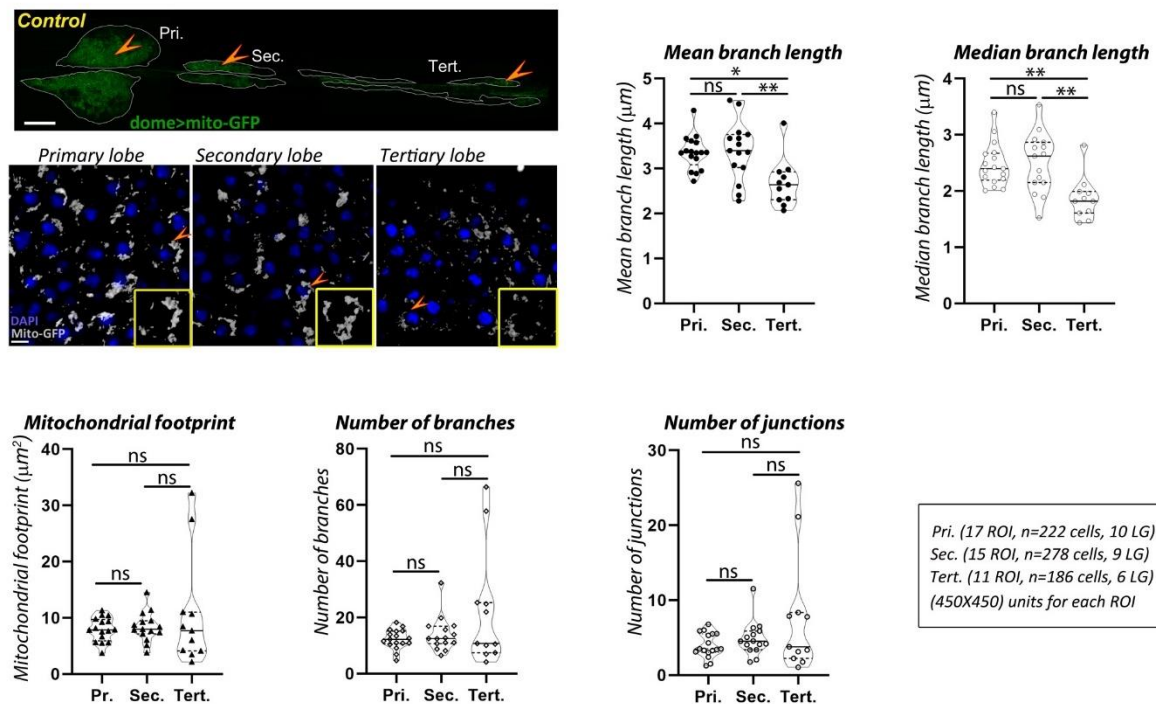


Figure 4.1 Mitochondrial morphology across blood progenitors of the *Drosophila* lymph gland reflects heterogeneity. Mitochondria in lymph gland progenitors (pro-hemocytes) of the primary, secondary and tertiary lobes are marked by *dome>mito-GFP* in wild type/control (*domeGal4/+; UAS mito-GFP/+;+/+*) lymph gland. Arrowheads indicate the *dome>mito-GFP* positive progenitors across different lobes that are shown magnified in the lower panel (Pri.: Primary, Sec.: Secondary, Tert.: Tertiary). Images represent single confocal section of 0.5 μm for easy visualisation of mitochondria. Violin plots show quantification of mitochondrial mean and median branch length, footprint, number of branches and number of junctions across primary, secondary, and tertiary lobes. Scale bar: 100 μm in the upper panel and 5 μm in the lower panel. Number of cells and lymph glands (LG) analysed are mentioned below the image panel. Kruskal Wallis test was performed to determine statistical significance. *P<0.05, **P<0.01, ns: non-significant.

4.3.2 Asrij regulates mitochondrial morphology in *Drosophila* blood progenitors and hemocytes

Several reports show mitochondrial localization of OCIAD1, the human ortholog of Asrij and its interaction with various components of the electron transport chain (ETC) and mitochondrial dynamics machinery (Floyd et al., 2016; Lee et al., 2017; Shetty et al., 2018; Antonicka et al., 2020). OCIAD1 regulates ETC Complex I activity in mitochondria as well as the mitochondrial network architecture (Shetty et al., 2018). Owing to a conserved role in stem cell maintenance and hematopoiesis, we hypothesized that Asrij may similarly regulate mitochondrial features in *Drosophila*.

Immunolocalization analysis for Asrij in *domeGal4/+; UAS mito-GFP/+* lymph glands showed mitochondrial localization of Asrij in progenitors (Fig 4.2A). Further using the mitochondrial marker COXIV as well as by staining with Mitotracker in Canton(S) hemocytes, we showed that Asrij also localizes to mitochondria in circulating hemocytes (Fig 4.2B).

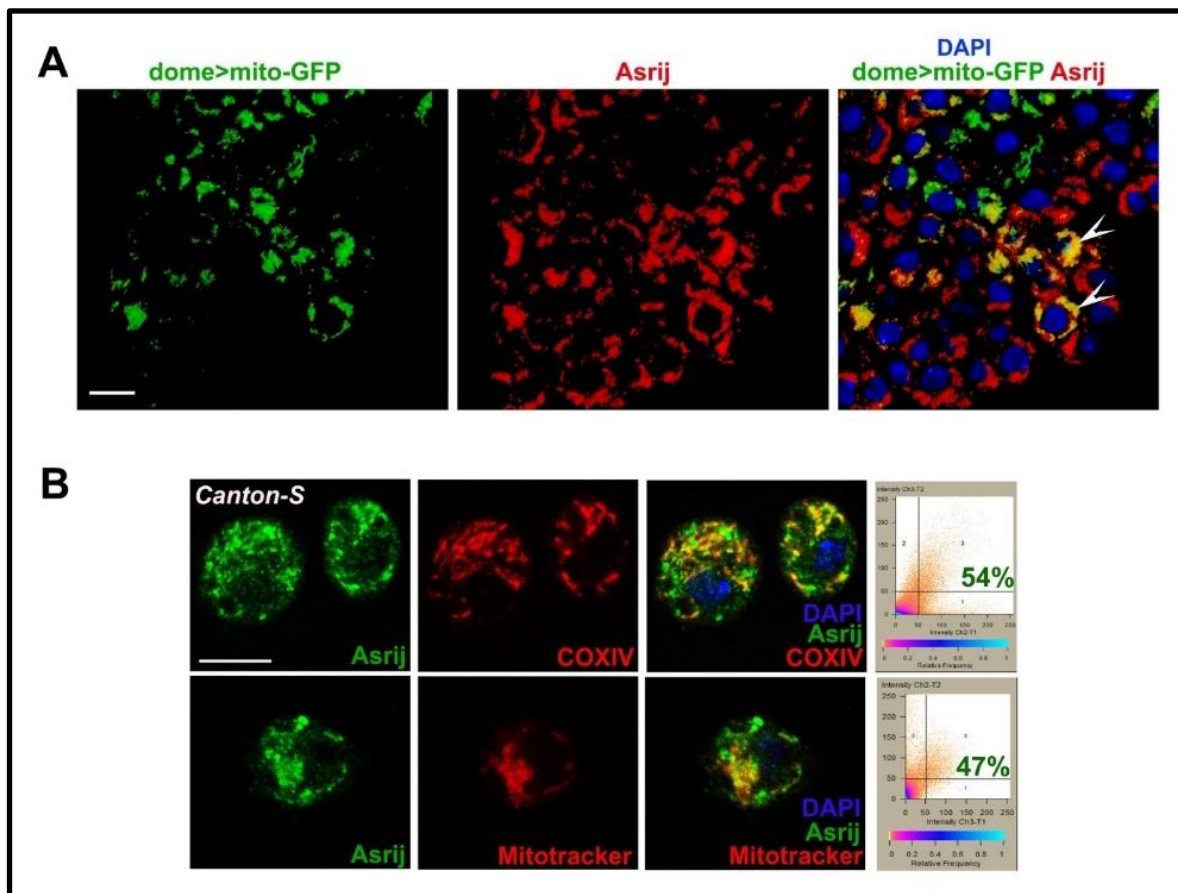


Figure 4.2 Asrij localizes to mitochondria of the *Drosophila* lymph gland progenitors and circulatory hemocytes. (A-B) Asrij (far-red pseudo-colored to red) colocalization with mitochondrial marker mito-GFP (green) in blood progenitors of the lymph gland (*domeGal4/+; UAS mito-GFP/+;+/+*) (A). Image represents single 0.5 μm confocal slice to show colocalization. Arrowheads mark the site of colocalization. DAPI marks the nuclei. Scale bar: 5 μm . (B) Asrij (green) colocalization with mitochondrial markers (red) COXIV or Mitotracker as indicated in wild type (Canton-S) hemocytes in circulation. Colocalization plots are as indicated for 0.3 μm optical section. Scale bar: 10 μm .

Depletion of OCIAD1 in hESCs was shown to increase mitochondrial branch length, footprint, and branch number, indicating a shift of dynamics towards enhanced mitochondrial biogenesis and fusion (Shetty et al., 2018). *Asrij* knockdown (*domeGal4/+; UAS mito-GFP/+; UAS arj RNAi/+*) in lymph gland progenitors resulted in elongated mitochondria (interpreted through increase in mean and median branch length) (Fig 4.3). In addition, mitochondrial footprint, and number of mitochondrial junctions per cell were

increased in primary lobe progenitors, indicating a shift of mitochondrial dynamics towards reduced fission or enhanced fusion. Hence, we conclude that *Asrij* regulates mitochondrial dynamics in anterior progenitors. However, there was a mild effect on secondary lobes (reduced mitochondrial footprint and junctions) and no significant effect on tertiary lobes. This indicates heterogeneity in *dome*⁺ progenitor response from anterior to posterior and also suggests that mitochondria in younger progenitors are less sensitive to perturbations.

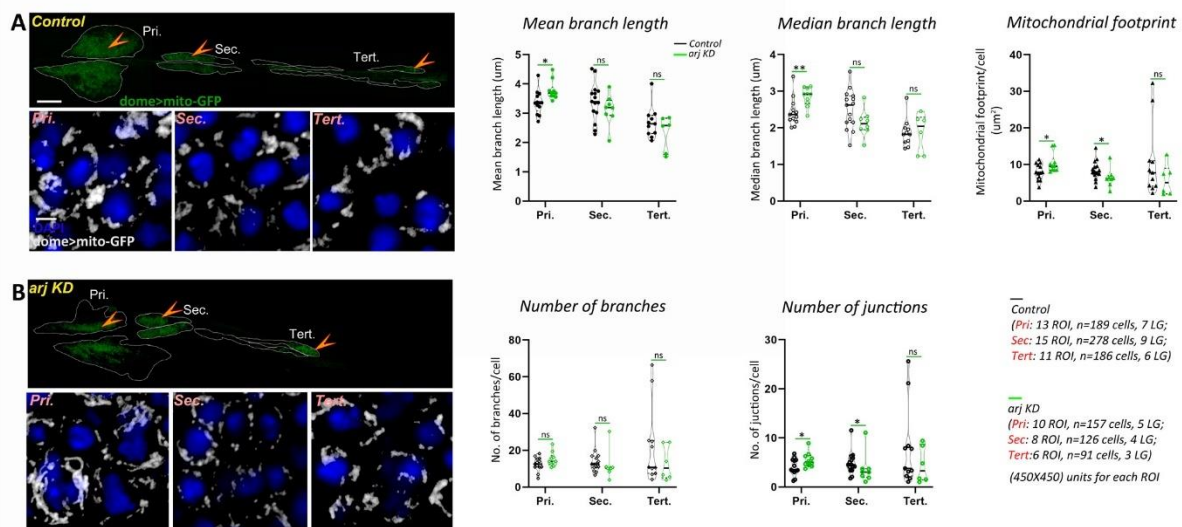


Figure 4.3 *Asrij* regulates mitochondrial morphology in blood progenitors of the *Drosophila* lymph gland. (A-B) Mitochondria in lymph gland progenitors (pro-hemocytes) of the primary, secondary and tertiary lobes are marked by *dome*[>]*mito*-GFP in control (*domeGal4*^{+/+}; *UAS mito-GFP*^{+/+/+}) (A) and *arj* KD (*domeGal4*^{+/+}; *UAS mito-GFP*^{+/+}; *UAS arj RNAi*^{+/+}) (B) lymph glands. Arrowheads indicate the *dome*[>]*mito*-GFP positive progenitors across different lobes that are shown magnified in the lower panel (Pri.: Primary, Sec.: Secondary, Tert.: Tertiary). Images represent single confocal section of 0.5 µm for easy visualisation of mitochondria. Violin plots show quantification of mitochondrial mean and median branch length, footprint, number of branches and number of junctions across primary, secondary, and tertiary lobes. Scale bar: 100 µm in the upper panel and 5 µm in the lower panel. Number of cells and lymph glands (LG) analysed are mentioned below the image panel. Kruskal Wallis test was performed to determine statistical significance. *P<0.05, **P<0.01, ns: non-significant.

Analysis of mitochondrial network using COXIV staining showed higher aggregation of mitochondria (interpreted through mean mitochondrial volume per 3D reconstructed

surface) in the prospective medullary zone of *asrij* null (*arj9/arj9*) lymph gland as compared to control (*w1118*) (Fig 4.4). This further validates the role of *Asrij* in regulating mitochondrial morphology of the blood progenitors and shows that *Asrij* depletion causes hyperfusion of mitochondria in blood progenitors.

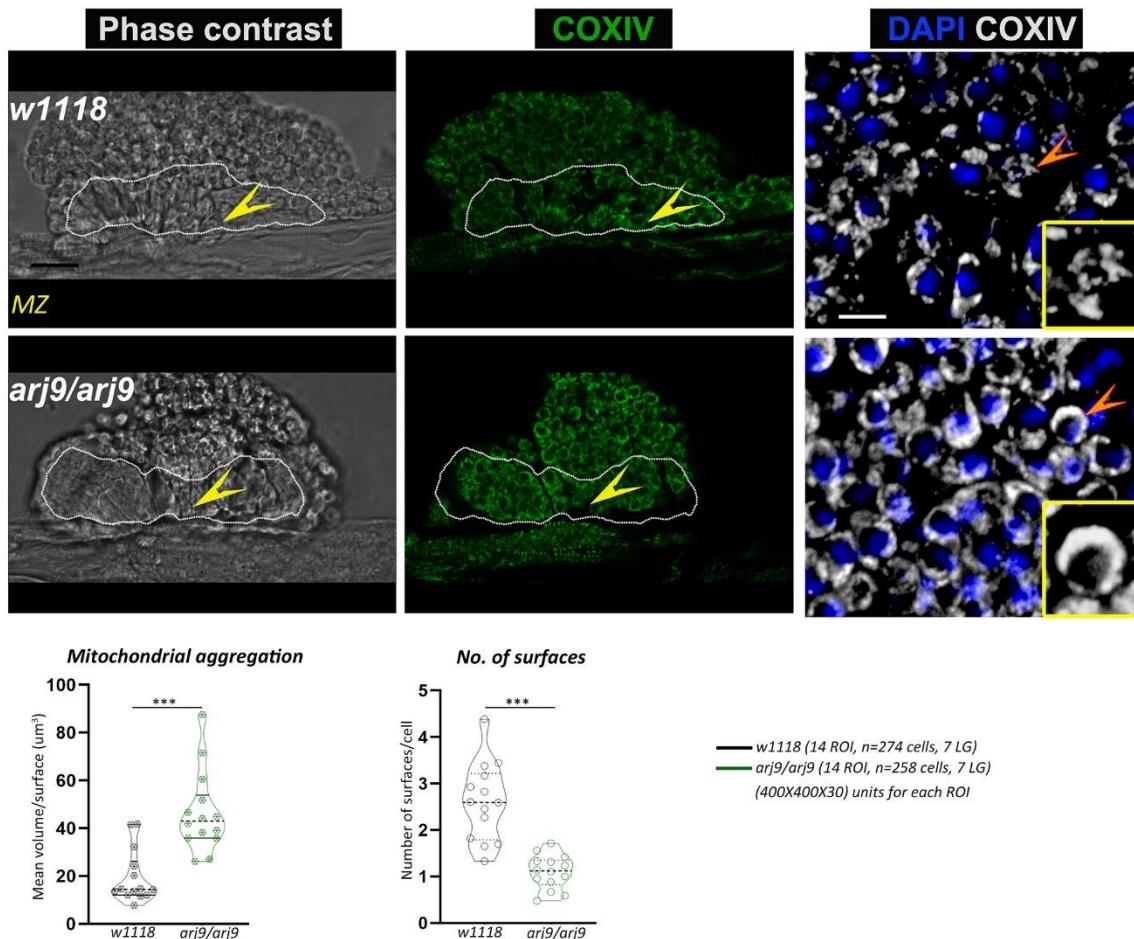
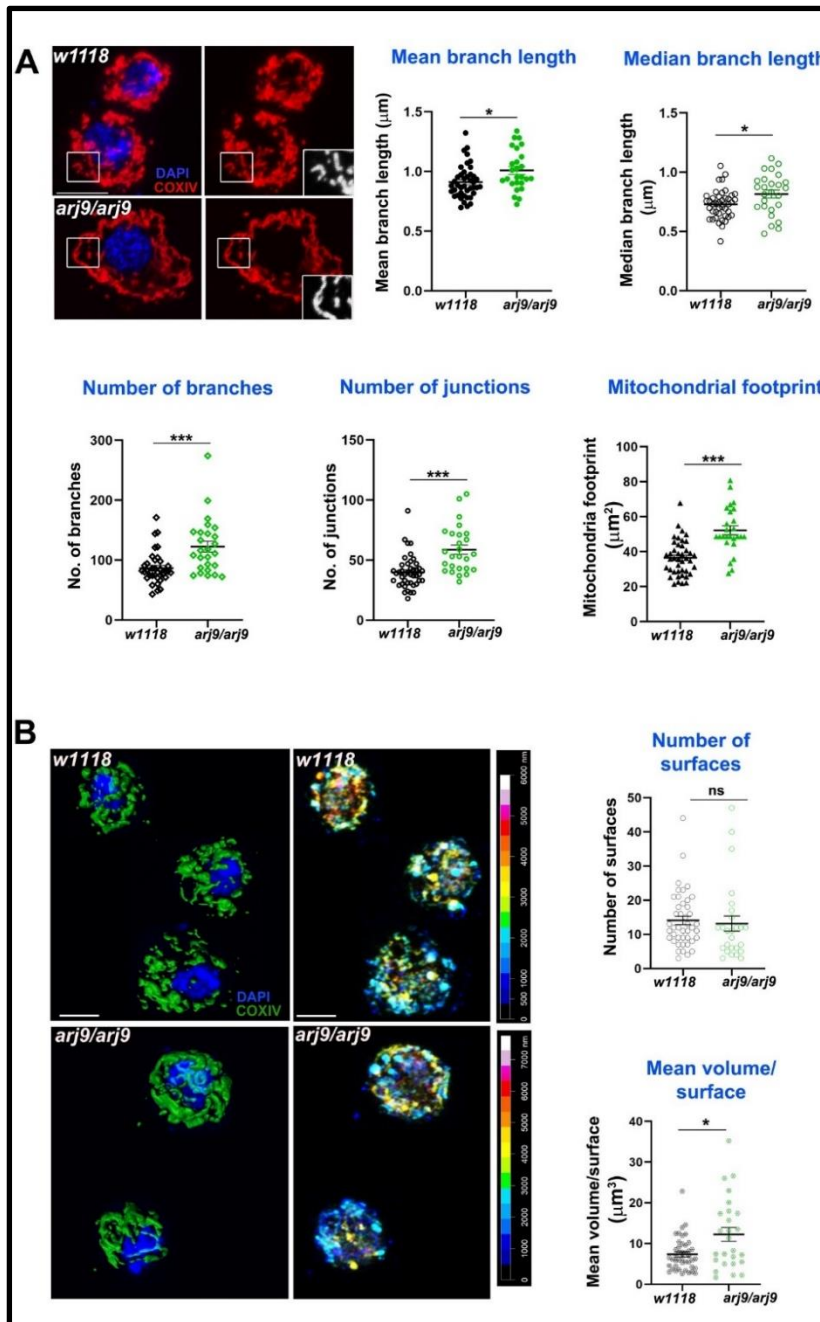


Figure 4.4 *Asrij* regulates mitochondrial aggregation in the lymph gland progenitors. Primary lobes of lymph gland stained with mitochondrial marker COXIV (far-red pseudo-colored to green) in control (*w1118*) and *asrij* null (*arj9/arj9*) genotype. Arrowheads mark the regions in the medullary zone (MZ) [with compact cellular arrangement (visible in phase contrast)] that have been imaged at higher magnification. Insets (grayscale) show magnified view of arrowhead marked region. Images represent single confocal section of $0.5 \mu\text{m}$ for prominent visualisation of mitochondria. Violin plots show quantification of mitochondrial aggregation, number of 3D reconstructed COXIV surfaces and mean mitochondrial volume per cell. Scale bar: $5 \mu\text{m}$. Number of cells and lymph glands (LG) analysed are mentioned in the image panel of (B) and (C). Unpaired t-test was performed to determine statistical significance. *** $P < 0.01$, ns: non-significant.

We also examined the mitochondrial network in *Drosophila* circulating hemocytes as these are single cells amenable to high-resolution imaging. Immunostaining for COXIV showed that *asrij* null mutant (*arj9/arj9*) hemocytes had higher mitochondrial branch length, footprint (content), number of branches and number of junctions as compared to control (*w1118*) (Fig 4.5A). This indicates elongation of mitochondria, poor fission or hyperfusion and increase in mitochondrial content upon loss of *Asrij* in hemocytes. Additionally, we observed an increase in mitochondrial aggregation (as interpreted from increase in mean volume per surface) without a significant decrease in the number of mitochondrial clusters in *arj9/arj9* hemocytes (Fig 4.5B).

Figure 4.5. *Asrij* regulates mitochondrial morphology in *Drosophila* circulatory hemocytes.

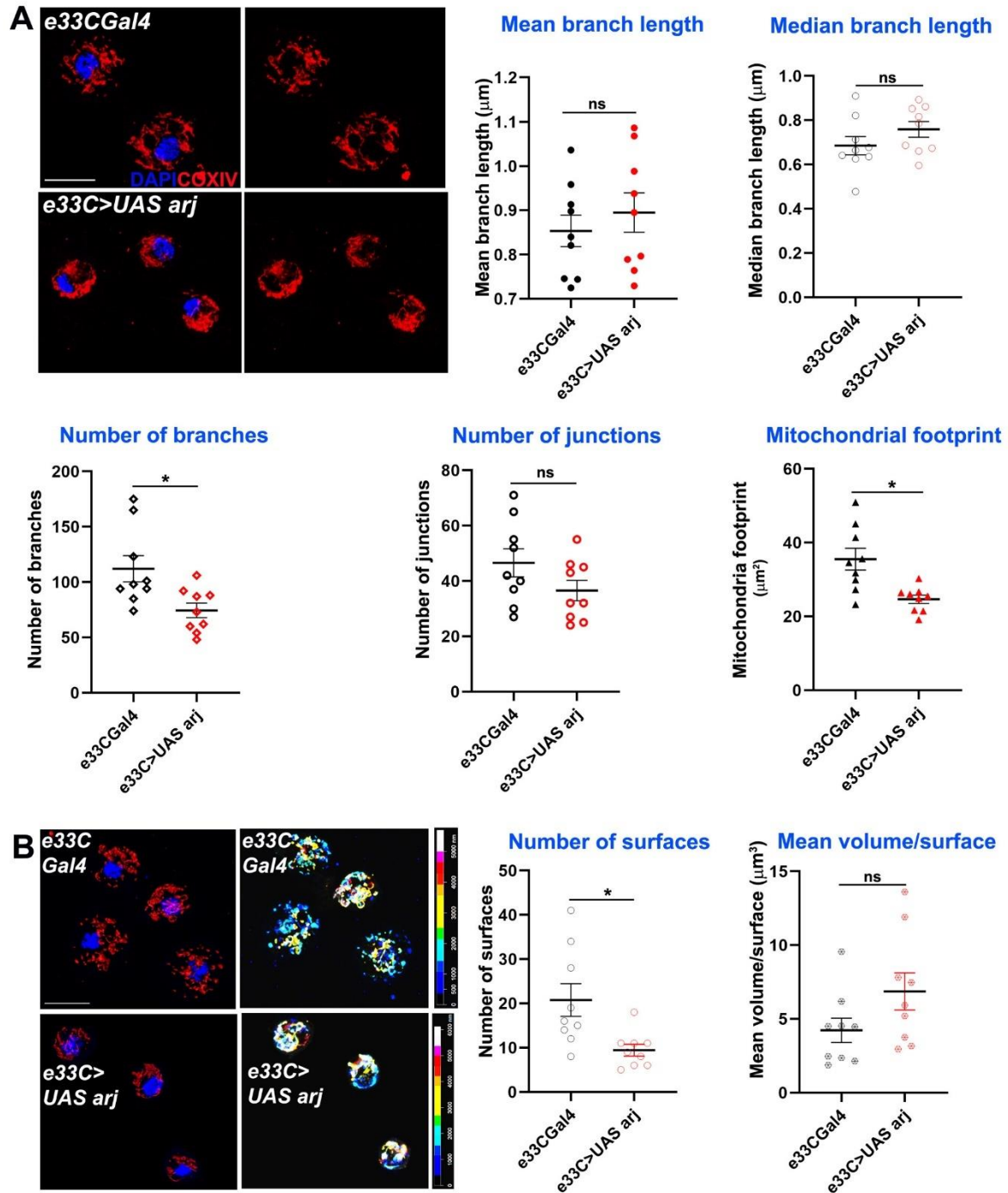


(A) Mitochondria stained by COXIV in control (*w1118*) and *asrij* null (*arj9/arj9*) circulatory hemocytes. Insets (greyscale) show magnified view of boxed region. Scatter plots show quantification of mitochondrial mean branch length, median branch length, number of branches, number of junctions and mitochondria footprint in *w1118* ($n=43$ cells) and *arj9/arj9* ($n=26$ cells) circulatory hemocytes. (B) Maximum intensity projection images reconstructed in three dimensions (left) and depth color-coded projections (right) for COXIV staining in *w1118* and *arj9/arj9* hemocytes.

Three-dimensional surface reconstruction was used to determine the number of surfaces and mean volume per surface in each cell, shown in the scatter plot. Scale bar: 10 μm . Error bars represent SEM. Mann-Whitney two-tailed t-test was used to determine statistical significance. * $P < 0.05$, *** $P < 0.001$, ns: statistically non-significant difference.

OCIAD1 overexpression leads to reduction of the mitochondrial footprint and branch length in hESCs (Shetty et al., 2018). While most mitochondrial network parameters (mean and

median branch length, number of junctions and mitochondrial aggregation) remained unchanged upon overexpression of *Asrij* in hemocytes (*e33cGal4/UAS asrij*) there was a significant reduction in the number of mitochondria (branches and surfaces) and the mitochondrial footprint (Fig 4.6). This suggests that regulatory mechanisms operating to control mitochondrial dynamics in *Drosophila* hemocytes are *Asrij*-dependent. Taken together, our data show functional conservation of *Asrij* in controlling mitochondrial morphology and network architecture.



staining three-dimensional surface reconstruction was used to determine the number of surfaces and mean volume per surface in each cell. Scale bars in all panels: 10 μm . Error bars represent SEM. One-way ANOVA was used to determine statistical significance. * $P < 0.05$, ns: statistically non-significant difference.

4.3.3 Anterior progenitors are more sensitive to perturbation of the mitochondrial fission-fusion machinery.

Drp1 and Marf are well conserved key regulators of mitochondrial dynamics. Hence, we checked whether depleting Drp1 or Marf from dome+ve progenitor subsets (*domeGal4/+; UAS mito-GFP/+; +/+*) may affect mitochondrial architecture similar to *asrij* depletion. In anterior lymph gland lobes mitochondrial branch length increased on Drp1 knockdown (*domeGal4/+; UAS mito-GFP/+; UAS Drp1 RNAi/+*) indicating mitochondrial fission was inhibited (Fig 4.7A-B). Conversely *Marf* KD (*domeGal4/+; UAS mito-GFP/+; UAS Marf RNAi/+*) caused mitochondrial fragmentation (reduced mitochondrial branch length) along with reduced mitochondrial content (mitochondrial footprint, number of branches and junctions) indicating reduced fusion (Fig 4.7A, C). Thus, as expected Drp1 and Marf affect mitochondrial dynamics of blood progenitors. However, there was no significant change in mitochondrial morphology in posterior lobes upon Drp1 depletion (Fig 4.7B). *Marf* knockdown reduced mitochondrial branch length in secondary lobe progenitors as compared to control whereas tertiary lobe remained unaffected (Fig 4.7C). This suggests that posterior progenitors are less sensitive to perturbation in the mitochondrial fission-fusion machinery.

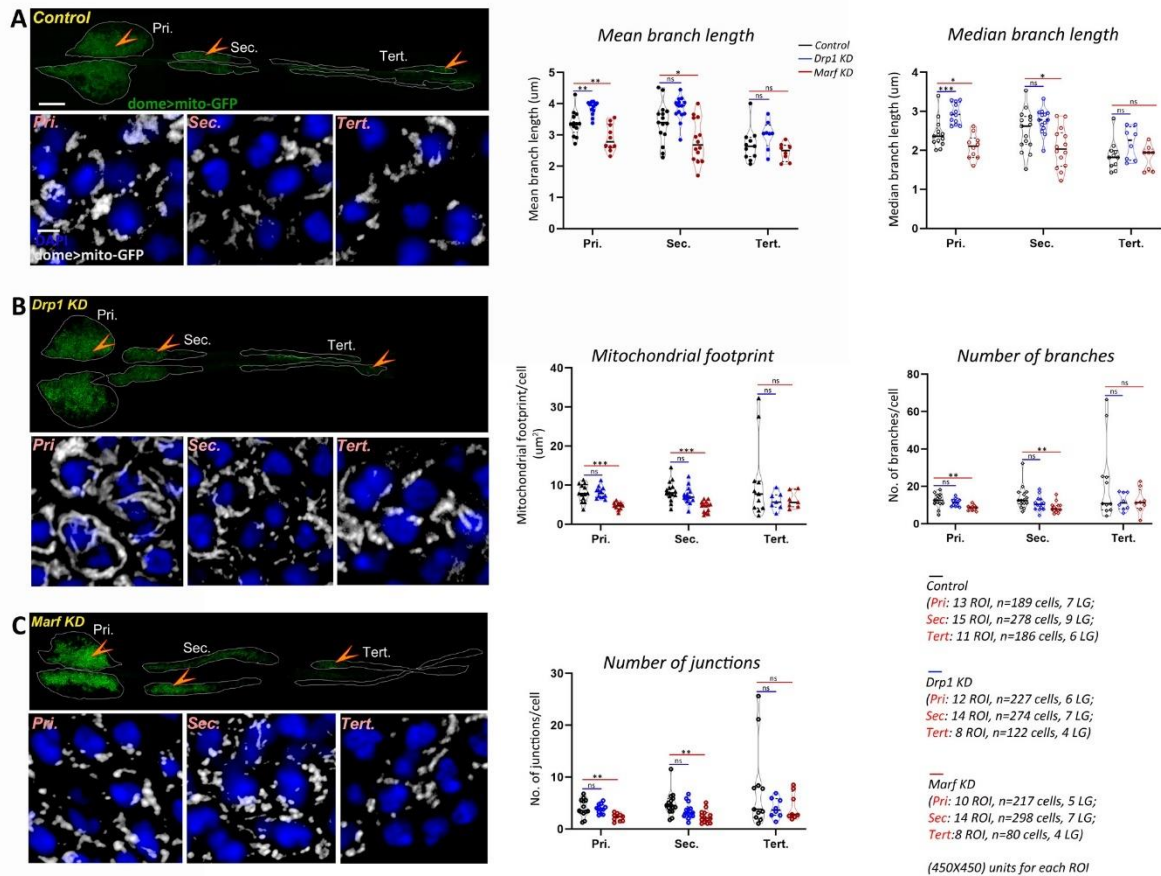


Figure 4.7 Asrij, Drp1 and Marf regulate mitochondrial morphology in blood progenitors of the *Drosophila* lymph gland. (A-C) Mitochondria in lymph gland progenitors (prohemocytes) of the primary, secondary and tertiary lobes are marked by *dome>mito-GFP* in control (*domeGal4/+; UAS mito-GFP/+;+/+*) (A), *Drp1* KD (*domeGal4/+; UAS mito-GFP/+;UAS Drp1 RNAi/+*) (B) and *Marf* KD (*domeGal4/+; UAS mito-GFP/+;UAS Marf RNAi/+*) (C) lymph glands. Arrowheads indicate the *dome>mito-GFP* positive progenitors across different lobes that are shown magnified in the lower panel (Pri.: Primary, Sec.: Secondary, Tert.: Tertiary). Images represent single confocal section of 0.5 µm for easy visualisation of mitochondria. Violin plots show quantification of mitochondrial mean and median branch length, footprint, number of branches and number of junctions across primary, secondary, and tertiary lobes. Scale bar: 100 µm in the upper panel and 5 µm in the lower panel. Number of cells and lymph glands (LG) analysed are mentioned below the image panel. Kruskal Wallis test was performed to determine statistical significance. *P<0.05, **P<0.01, ***P<0.001, ns: non-significant.

4.3.4 Asrij/OCIAD1 depletion reduces mitochondrial network dynamics.

Mitochondrial dynamics is essential for the exchange and distribution of metabolites across the network to different parts of the cell and depends on morphology, number, and

branching (Detmer and Chan, 2007). Change of mitochondrial network parameters upon *Asrij* modulation suggests a possible impact on mitochondrial dynamics. Live imaging analysis of mito-GFP expressing hemocytes from control (*e33C>UAS mitoGFP*) and *Asrij* depleted (Knockdown: KD) (*e33C>UAS mitoGFP>UAS arj RNAi*) larvae showed lower temporal variation in branch number and junction number with unchanged dynamics of the mitochondrial footprint in KD hemocytes (Fig 4.8). This suggests a possible reduction of mitochondrial fission-fusion events in KD hemocytes and might explain the shift of equilibrium towards elongated mitochondria. Mitochondrial footprint dynamics are unaltered suggesting that mitochondrial biogenesis and degradation may be unaffected, which merits further investigation.

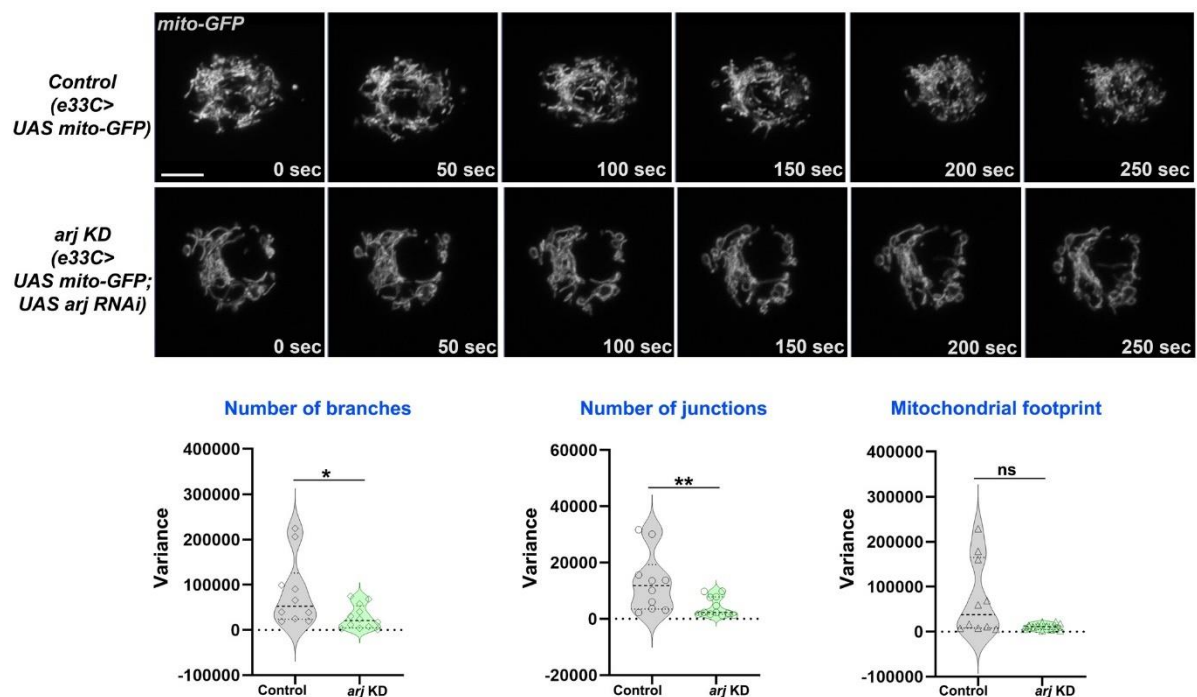


Figure 4.8 *Asrij* depletion reduces mitochondrial network dynamics in hemocytes. Time-lapse live imaging of control (*e33CGal4>UAS mito-GFP*) and *asrij* KD (*e33CGal4>UAS mito-GFP; UAS arj RNAi*) circulatory hemocytes expressing mitochondria-targeted GFP. Violin plots show quantification of variance in number of branches, number of junctions and mitochondrial footprint in control (n=10 cells) and *arj* KD (n=12 cells) hemocytes. Scale bar: 5 μ m. Error bars represent SEM. Mann-Whitney two-tailed t-test was used to determine statistical significance. *P<0.05, **P<0.01, ns: statistically non-significant difference.

Similar analysis was performed in pluripotent human embryonic stem cells (hESCs) that were depleted of OCIAD1 [heterozygous KO (Het-KO): Shetty et al., 2018]. While the dynamics of branch number and footprint were unchanged, mitochondrial junctions in Het-KO hESCs showed reduced dynamics (Fig 4.9A). This indicates reduced temporal variation of mitochondrial fission-fusion events upon OCIAD1 depletion in hESCs. As reported earlier, OCIAD1 overexpression in hESCs led to reduction in branch length and mitochondrial footprint (Shetty et al., 2018). Time-lapse image analysis of OCIAD1 overexpressing hESCs showed significantly reduced temporal variation of mitochondrial junction number as compared to control, whereas mitochondrial branch number and footprint dynamics were similar (Fig 4.9B). Thus, OCIAD1 depletion and overexpression, both impact mitochondrial dynamics. In summary, modulation of mitochondrial dynamics by Asrij/OCIAD1 is a mechanism that operates in diverse systems such as *Drosophila* blood progenitors and human embryonic stem cells.

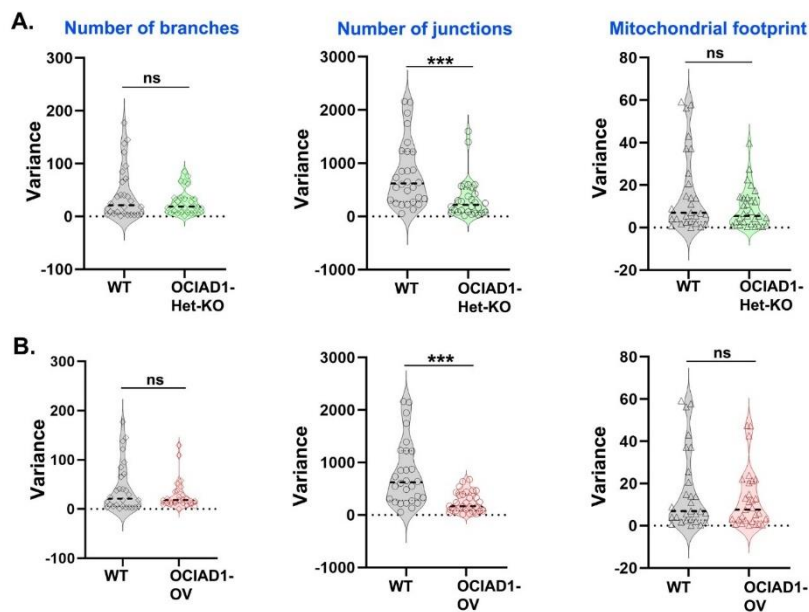


Figure 4.9. OCIAD1 depletion reduces mitochondrial network dynamics in hESC. (A) Time-lapse live imaging of mitotracker stained WT (BJNhem20) (n=30 cells) and OCIAD1-Het-KO (CRISPR-39) (n=30 cells) live hESCs. Violin plots show quantification of variance in number of branches, number of junctions and mitochondrial footprint. (B) Similar quantifications are represented for WT (BJNhem20) (n=30 cells) and OCIAD1-OV (n=30 cells) live hESCs. Original data were used from Shetty et al., *Stem Cell Reports*, 2018 and was analysed by Kajal Kamat. Scale bar: 5 μ m. Error bars represent SEM. Mann-Whitney two-tailed t-test was used to determine statistical significance. *P<0.05, **P<0.01, ***P <0.001, ns: statistically non-significant difference.

4.3.5 Inhibition of mitochondrial fission prevents crystal cell differentiation.

Asrij is essential for lymph gland progenitor maintenance and we find that Asrij depletion alters mitochondrial dynamics. This suggests a possible role for mitochondrial dynamics in progenitor differentiation. Regulated mitochondrial fission and fusion are critical to control mitochondrial dynamics. However, the role of canonical fission and fusion regulators such as Drp1 and Mitofusin in stem cell maintenance and lineage choice is not completely understood.

Drp1 drives mitochondrial dynamics by promoting fission and has a role in regulating myeloid reconstitution potential of HSCs (Hinge et al., 2020). However, the role of mitochondrial fission in hematopoietic lineage choice remains largely underexplored. Hence, we examined the effects of depletion of Drp1 from lymph gland progenitors. RNAi-mediated knockdown (KD) in *domeless*⁺ progenitors (*domeGal4 UAS 2xEGFP;; UAS Drp1 RNAi*) led to reduction in crystal cell (ProPO⁺) differentiation in primary lobes (Fig 4.10A).

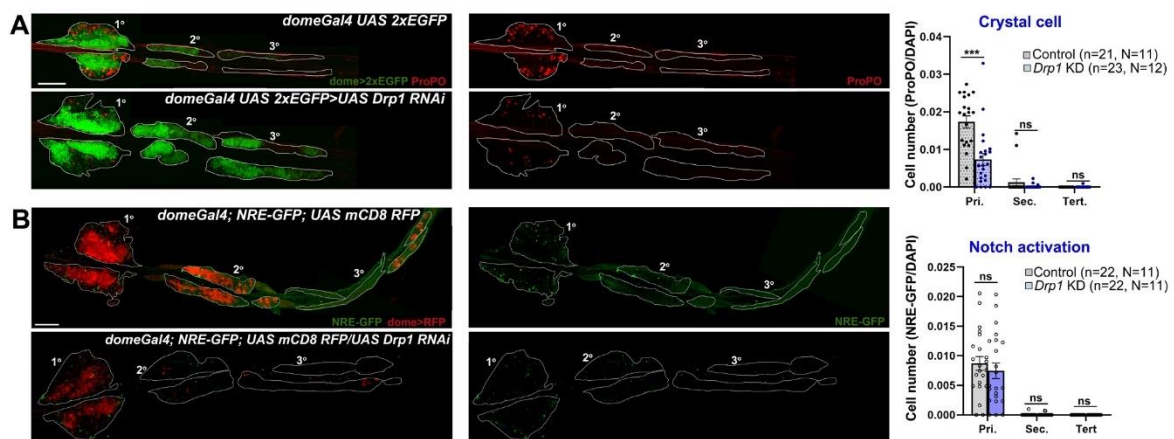


Figure 4.10 Drp1 depletion inhibits crystal cell differentiation in the *Drosophila* lymph gland. (A) Whole mount lymph gland showing expression of crystal cell marker ProPO in primary, secondary and tertiary lobes of control (*domeGal4 UAS 2xEGFP*) and *Drp1* KD (*domeGal4 UAS 2xEGFP>UAS Drp1 RNAi*) larvae. GFP marks the expression of prohemocyte marker Domeless. Bar diagram shows quantification of mean crystal cell fraction in primary, secondary, and tertiary lobes of indicated genotypes. (B) NRE-GFP (Notch responsive element-GFP) reports activation of Notch signaling in control (*domeGal4/+; NRE-GFP/+; UAS mCD8 RFP/+*) and *Drp1* KD (*domeGal4/+; NRE-GFP/+; UAS mCD8RFP/UAS Drp1 RNAi*) lymph

gland primary, secondary and tertiary lobes. RFP marks the expression of prohemocyte marker *Domeless*. Bar diagram shows quantification of mean NRE-GFP positive (high) cell fraction in primary, secondary, and tertiary lobes of indicated genotypes. n represents number of individual lymph gland lobes analysed, and N represents number of larvae for each genotype. Scale bar: 100 μ m. Error bars represent SEM. Multiple t-test was performed to determine statistical significance. ***P<0.001, ns: statistically non-significant difference.

Previous reports show Notch signaling activation is a key mechanism that triggers crystal cell differentiation in the lymph gland while inhibiting differentiation to plasmatocytes or lamellocytes (Duvic et al, 2002; Lebestky et al., 2003; Small et al., 2014; Cho et al., 2020; Blanco-Obregon et al., 2020). However, whether mitochondrial dynamics actively regulate Notch signaling in the lymph gland remains unexplored. We used NRE-GFP (Notch responsive element) reporter to assess the extent of Notch activation upon *Drp1* depletion. NRE-GFP (Notch responsive element-GFP) is a widely used reporter for Notch signaling activation. Notch-dependent activation of transcription through NRE promotes GFP transcription. Thus, increased GFP expression marks enhanced activation of Notch signaling. Progenitor-specific knockdown of *Drp1* (*domeGal4/+; NRE-GFP/+; UAS mCD8 RFP/UAS Drp1 RNAi*) did not affect Notch activation significantly, though there was a downward trend (Fig 4.10B). This suggests that reduced differentiation to ProPO⁺ crystal cells in *Drp1* KD lymph gland primary lobes may be influenced by other mechanisms downstream of mitochondrial fission in addition to activation of Notch signaling.

Drp1 knockdown had no significant effect on progenitor maintenance, plasmatocyte or lamellocyte differentiation in the lymph gland (Fig 4.11A-E). Our data suggest that *Drp1* selectively regulates crystal cell differentiation (Fig 4.12).

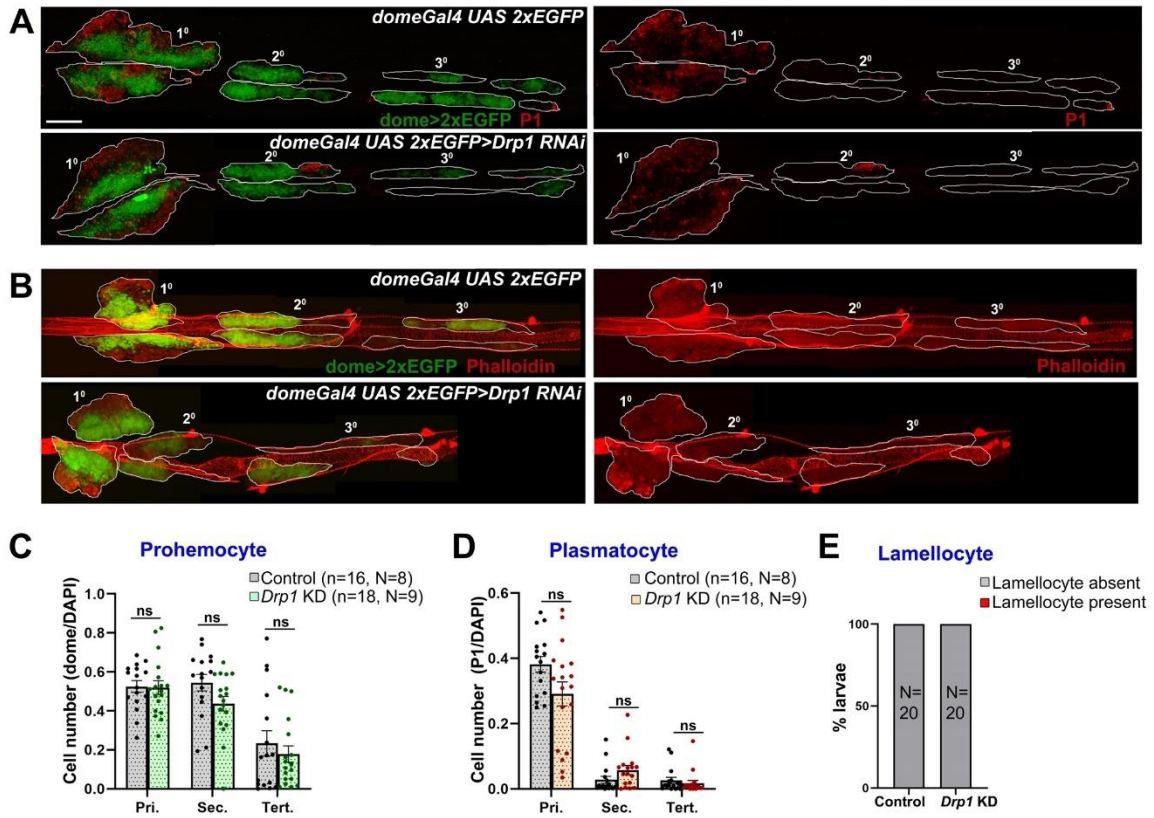


Figure 4.11 Drp1 does not regulate differentiation to plasmatocytes or lamellocytes in the *Drosophila* lymph gland. (A-B) Whole mount lymph gland showing plasmatocytes marker P1 expression in primary, secondary, and tertiary lobes (A). Phalloidin staining shows lamellocytes (B) in control (*domeGal4 UAS 2xEGFP*) and Drp1 KD (*domeGal4 UAS 2xEGFP>UAS Drp1 RNAi*) lymph gland lobes. dome>2xEGFP marks prohemocytes. (C-E) Bar diagrams show quantification of mean dome>2xEGFP positive prohemocyte fraction (C), P1 positive plasmatocyte fraction (D) and percentage of lymph glands with lamellocyte differentiation (E) in control and upon Drp1 KD. n represents number of individual lymph gland lobes analysed, and N represents number of larvae for each genotype. Scale bar: 100 μ m. Error bars represent SEM. Multiple t-test was performed to determine statistical significance. ns: statistically non-significant difference.

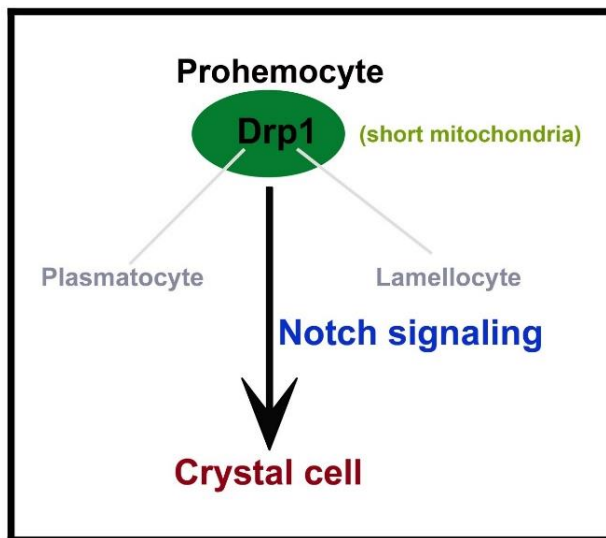


Figure 4.12 Inhibition of Drp1-dependent mitochondrial fission in blood progenitors selectively inhibits crystal cell differentiation.

4.3.6 Reduced mitochondrial fusion promotes Notch signaling and crystal cell differentiation.

Mitofusins drive mitochondrial dynamics by promoting mitochondrial fusion. Mfn2 regulates maintenance of HSCs with lymphoid potential in mouse through regulation of calcium signaling (Luchsinger et al., 2016). However, its role in myeloid lineage specification is not fully understood. Knockdown of *Drosophila* Mfn homolog Marf (*domeGal4 UAS 2xEGFP;; UAS Marf RNAi*) led to dramatic increase in crystal cell differentiation in primary lobes (Fig 4.13A). Both Drp1 and Marf play critical but opposite roles in non-canonical Notch signaling activation and various developmental processes such as neuroblast and synaptic development in *Drosophila* (Lee et al, 2013; Sandoval et al, 2014). In concordance with previous reports, we find that *Marf* KD (*domeGal4/+; NRE-GFP/+; UAS mCD8 RFP/UAS Marf RNAi*) led to an increase in Notch activation in primary and secondary lobes (Fig 4.13B) whereas tertiary lobes remained unaffected. This explains increased crystal cell differentiation in *Marf* KD lymph gland primary lobes. Absence of crystal cells in the tertiary lobes suggests additional regulatory mechanisms and is in agreement with the idea that posterior lobes resist differentiation (Rodrigues et al., 2021).

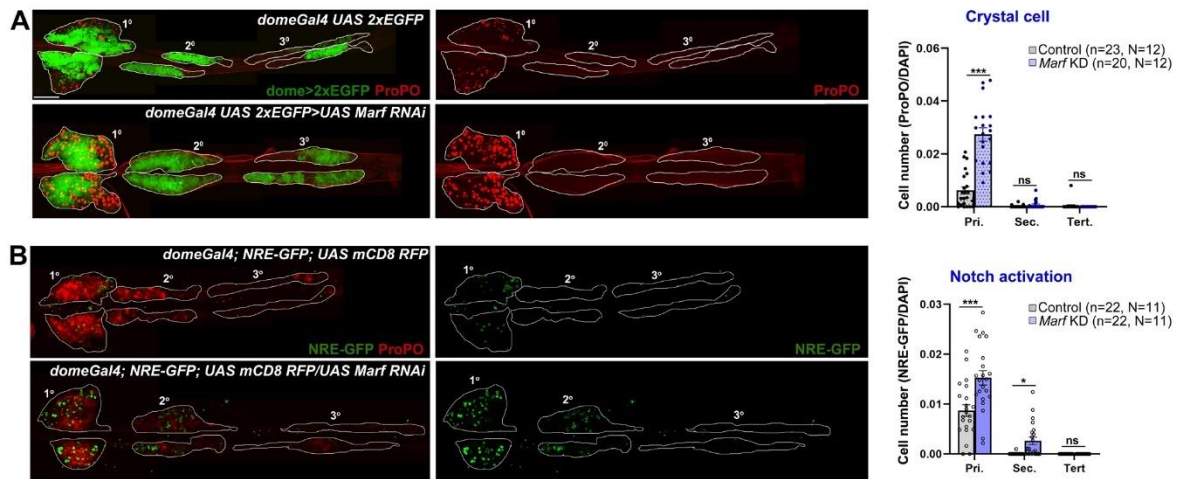


Figure 4.13 Marf regulates crystal cell differentiation and Notch signaling in the *Drosophila* lymph gland. (A) Whole mount lymph gland showing expression of crystal cell marker ProPO in primary, secondary and tertiary lobes of control (*domeGal4 UAS 2xEGFP*) and *Marf* KD (*domeGal4 UAS 2xEGFP>UAS Marf RNAi*) larvae. GFP marks the expression of prohemocyte marker Domeless. Bar diagram shows quantification of mean crystal cell fraction in primary, secondary, and tertiary lobes of indicated genotypes. (B) NRE-GFP reports activation of Notch signaling in control (*domeGal4/+; NRE-GFP/+; UAS mCD8 RFP/+*) and *Marf* KD (*domeGal4/+; NRE-GFP/+; UAS mCD8RFP/UAS Marf RNAi*) lymph gland primary, secondary and tertiary lobes. RFP marks the expression of prohemocyte marker Domeless. Bar diagram shows quantification of mean NRE-GFP positive (high) cell fraction in primary, secondary, and tertiary lobes of indicated genotypes. n represents number of individual lymph gland lobes analysed, and N represents number of larvae for each genotype. Scale bar: 100 μ m. Error bars represent SEM. Multiple t-test was performed to determine statistical significance. * $P < 0.05$, *** $P < 0.001$, ns: statistically non-significant difference.

Marf knockdown did not affect the primary and secondary lobe progenitors. However, surprisingly, the *dome*⁺ progenitor fraction increased in tertiary lobes (Fig 4.14A, C). This could be due to increased proliferation of posterior progenitors that have inherently reduced differentiation potential. Plasmatocyte differentiation remained unchanged in primary and tertiary lobes, increasing mildly in secondary lobes (Fig 4.14A, D). Occasionally there was a small increase (1 out of 20 larvae analysed) in lamellocyte differentiation (Fig 4.14A, E). This indicates that *Marf* activity prevents *dome*⁺ progenitor expansion in the posterior lobes and primarily prevents precocious crystal cell differentiation (Fig 4.15).

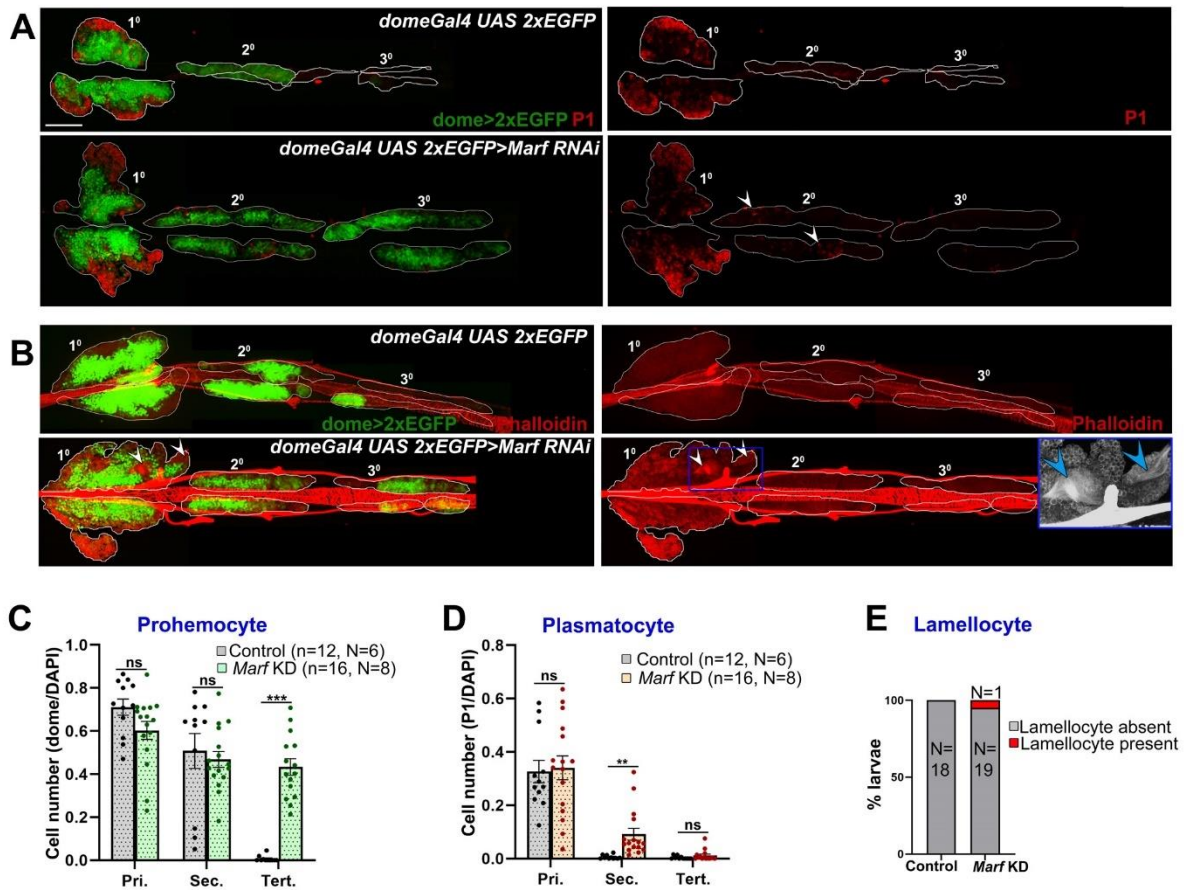


Figure 4.14 Marf does not affect differentiation to plasmatocytes or lamellocytes in the *Drosophila* lymph gland. (A-B) Whole mount lymph gland showing plasmatocytes marker P1 expression in primary, secondary, and tertiary lobes (A). Phalloidin staining shows lamellocytes (B) in control (*domeGal4 UAS 2xEGFP*) and *Marf* KD (*domeGal4 UAS 2xEGFP>UAS Marf RNAi*) lymph gland lobes. *dome>2xEGFP* marks prohemocytes. Arrowheads mark plasmatocytes (A) and lamellocytes (B) in *Marf* KD lymph gland. Insets show magnified view of lamellocytes in arrowhead marked region. (C-E) Bar diagrams show quantification of mean *dome>2xEGFP* positive prohemocyte fraction (C), P1 positive plasmatocyte fraction (D) and percentage of lymph glands with lamellocyte differentiation (E) in control and upon *Marf* KD. n represents number of individual lymph gland lobes analysed, and N represents number of larvae for each genotype. Scale bar: 100 μm. Error bars represent SEM. Multiple t-test was performed to determine statistical significance. **P<0.01, ***P<0.001, ns: statistically non-significant difference.

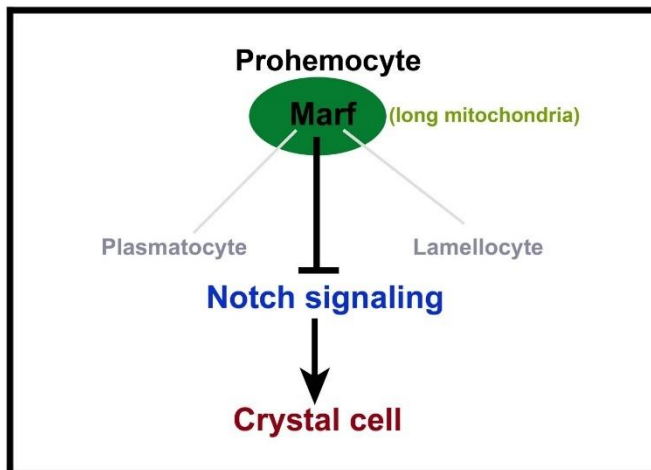


Figure 4.15 Inhibition of Marf-dependent mitochondrial fusion in blood progenitors selectively promotes crystal cell differentiation.

As depletion of Drp1 affects crystal cell differentiation in primary lobes, we next checked if overexpressing Drp1 had any effect. Progenitor-specific overexpression of Drp1 did not affect crystal cell differentiation (Fig 4.16A, B). However, Marf overexpression increased crystal cell differentiation in primary lobes. Posterior lobes remained unaffected (Fig 4.16A, C). This indicates differences in progenitor sensitivity to Marf levels. Taken together, our analyses show that canonical mitochondrial dynamics regulators such as Drp1 and Marf actively modulate Notch activation to dictate crystal cell differentiation in the *Drosophila* lymph gland.

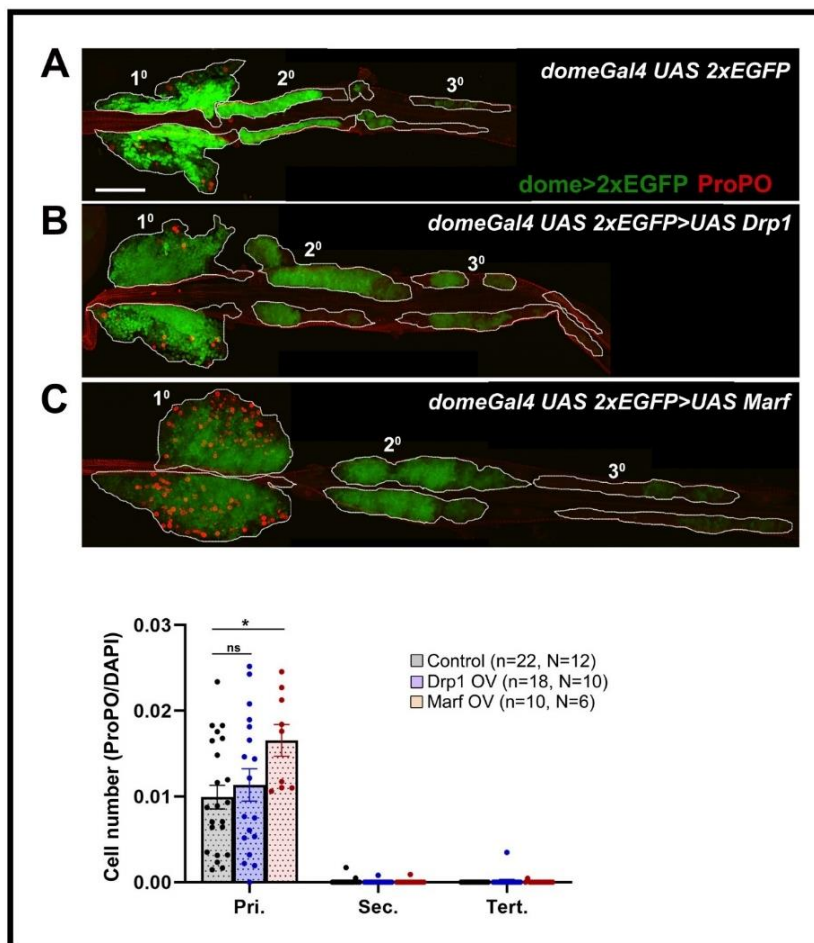


Figure 4.16
Overexpression of Drp1 and Marf differentially affect crystal cell differentiation in the *Drosophila* lymph gland.
 (A-C) ProPO staining marks crystal cells in control (*domeGal4 UAS 2xEGFP*) (A), Drp1 OV (*domeGal4 UAS 2xEGFP>UAS Drp1*) (B) and Marf OV (*domeGal4 UAS 2xEGFP>UAS Marf*) (C) whole mount of lymph gland primary, secondary and tertiary lobes. GFP marks the expression of prohemocyte marker Domeless. n represents number of individual

lymph gland lobes analysed, and N represents number of larvae for each genotype. Scale bar: 100 μ m. Error bars represent SEM. Kruskal Wallis test was performed to determine statistical significance. * $P < 0.05$, ns: statistically non-significant difference.

4.3.7 *Asrij* integrates mitochondrial dynamics with crystal cell differentiation.

Loss of *Asrij* leads to enhanced activation of Notch signaling with a concomitant increase in crystal cell differentiation (Fig 4.17A, B) (Kulkarni, Khadilkar et al., 2011; Khadilkar et al., 2014). Since *Asrij* also regulates mitochondrial dynamics, we next asked whether *Asrij* genetically interacts with the canonical regulators of mitochondrial dynamics. Elongated mitochondria in *asrij* KD progenitors could be a result of impaired fission or enhanced fusion events and hence are expected to be rescued by promoting fission (Drp1 overexpression) or inhibiting fusion (Marf depletion).

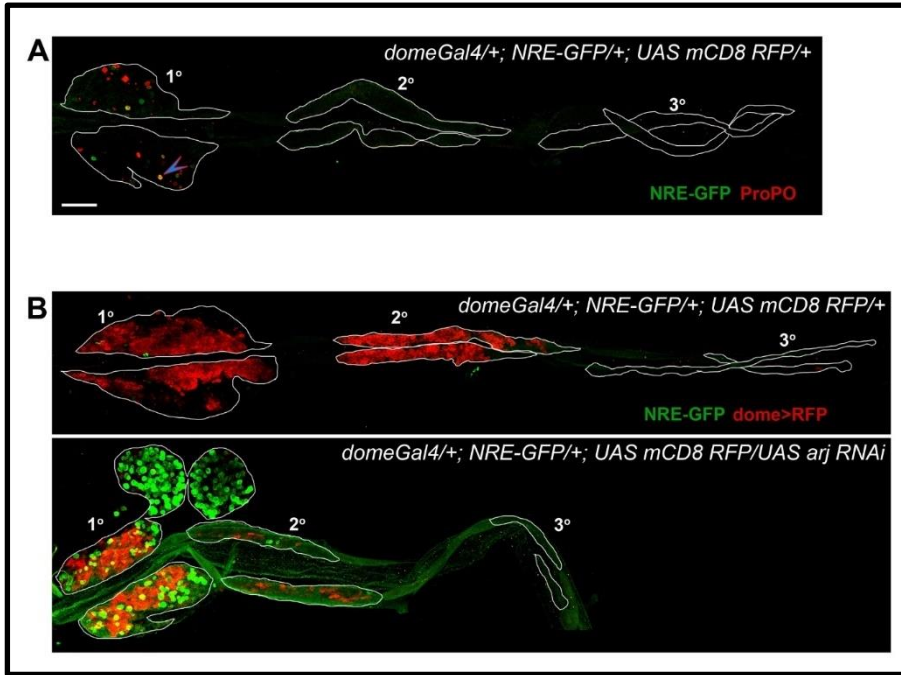


Figure 4.17. NRE-GFP expression increases upon *asrij* knockdown. (A) Notch responsive element-GFP (NRE-GFP) positive cells are present in primary lobes (1°) and the expression overlaps with ProPO as marked by arrowhead. Scale bar: 100 μ m. (B) NRE-GFP reporter positive cells mark

Notch activation in control (*domeGal4/+; NRE-GFP/+; UAS mCD8 RFP/+*) and *asrij* knockdown (*domeGal4/+; NRE-GFP/+; UAS mCD8 RFP/UAS arj RNAi*) lymph glands. Progenitors are marked by *dome>RFP*.

Progenitor-specific Drp1 overexpression (OV) using *domeGal4* driver could not efficiently restore normal mitochondrial architecture in *Asrij* depleted progenitors (*arj KD Drp1 OV: domeGal4/+; UAS mito-GFP/+; UAS Drp1/UAS arj RNAi*) (Fig 4.18A-D, G). However, *Marf* knockdown (*Marf KD*), which caused fragmentation of mitochondria rescued *asrij* KD phenotype in progenitors (*arj KD Marf KD: domeGal4/+; UAS mito-GFP/+; UAS Marf RNAi/UAS arj RNAi*) (Fig 4.18A-B, E-G). This suggests that elongation of mitochondria in *asrij* KD condition is an outcome of enhanced fusion rather than impaired fission.

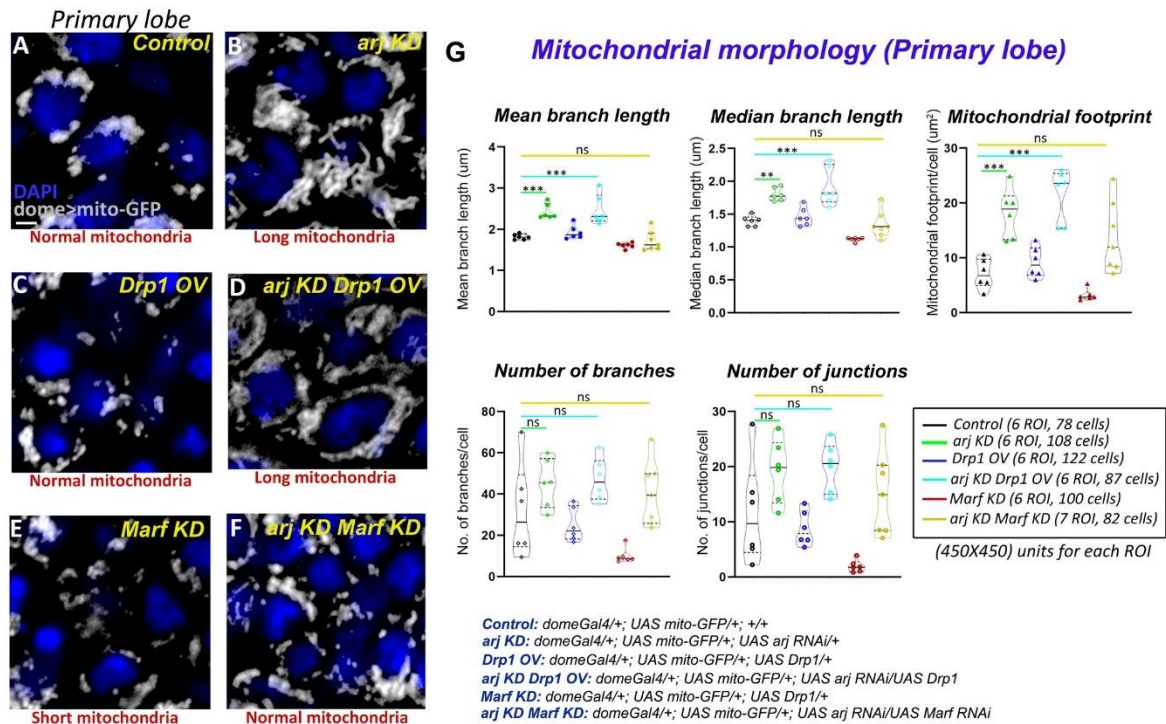


Figure 4.18 Inhibition of *Marf*-dependent mitochondrial fusion rescues mitochondrial elongation phenotype of *Asrij* in the lymph gland progenitors. (A-F) Mitochondrial morphology (*dome>mito-GFP* expression) in the primary lobe progenitors is shown in greyscale for *control* (A), *arj KD* (B), *Drp1 OV* (C), *arj KD Drp1 OV* (D), *Marf KD* (E) and *arj KD Marf KD* (F) lymph gland. The phenotypes of mitochondrial morphology are mentioned below each lymph gland image. The detailed genotypes are mentioned below the graph panel. Single confocal slice of 0.5 µm is represented for easy visualization of mitochondrial network. Scale bar: 5 µm. (G) Mitochondrial morphology analysis is shown for the abovementioned genotypes using violin plots. One-way ANOVA was performed to determine the statistical significance. ** $P < 0.01$, *** $P < 0.001$, ns: non-significant.

We also analysed the extent of crystal cell differentiation in the lymph glands of these genotypes. Increased *Drp1* (OV) or reduced *Marf* (KD) in progenitors in the *asrij* depleted background (*arj KD*) showed a synergistic effect on the crystal cell phenotype. Both *arj KD Drp1 OV* and *arj KD Marf KD* lymph gland primary lobes showed a greater increase in crystal cells compared to single mutants *arj KD*, *Drp1 OV* or *Marf KD* (Fig 4.19A-G). There was no significant increase in crystal cell differentiation in posterior lobes except in the secondary lobes of *arj KD Marf KD* compared to control or *arj KD*. As *Drp1* overexpression could not rescue mitochondrial elongation caused by loss of *Asrij*, it may function upstream of *Asrij* to regulate mitochondrial phenotype. However increased crystal cell differentiation upon *Drp1*

overexpression, which is enhanced in the *asrij* mutant background, suggests a direct effect on crystal cell differentiation. On the other hand, *Marf* acts downstream of *Asrij* in blood progenitors to regulate mitochondrial dynamics and crystal cell differentiation (Fig 4.20). Deciphering how these regulators of mitochondrial architecture control lineage-specific progenitor differentiation requires further investigation.

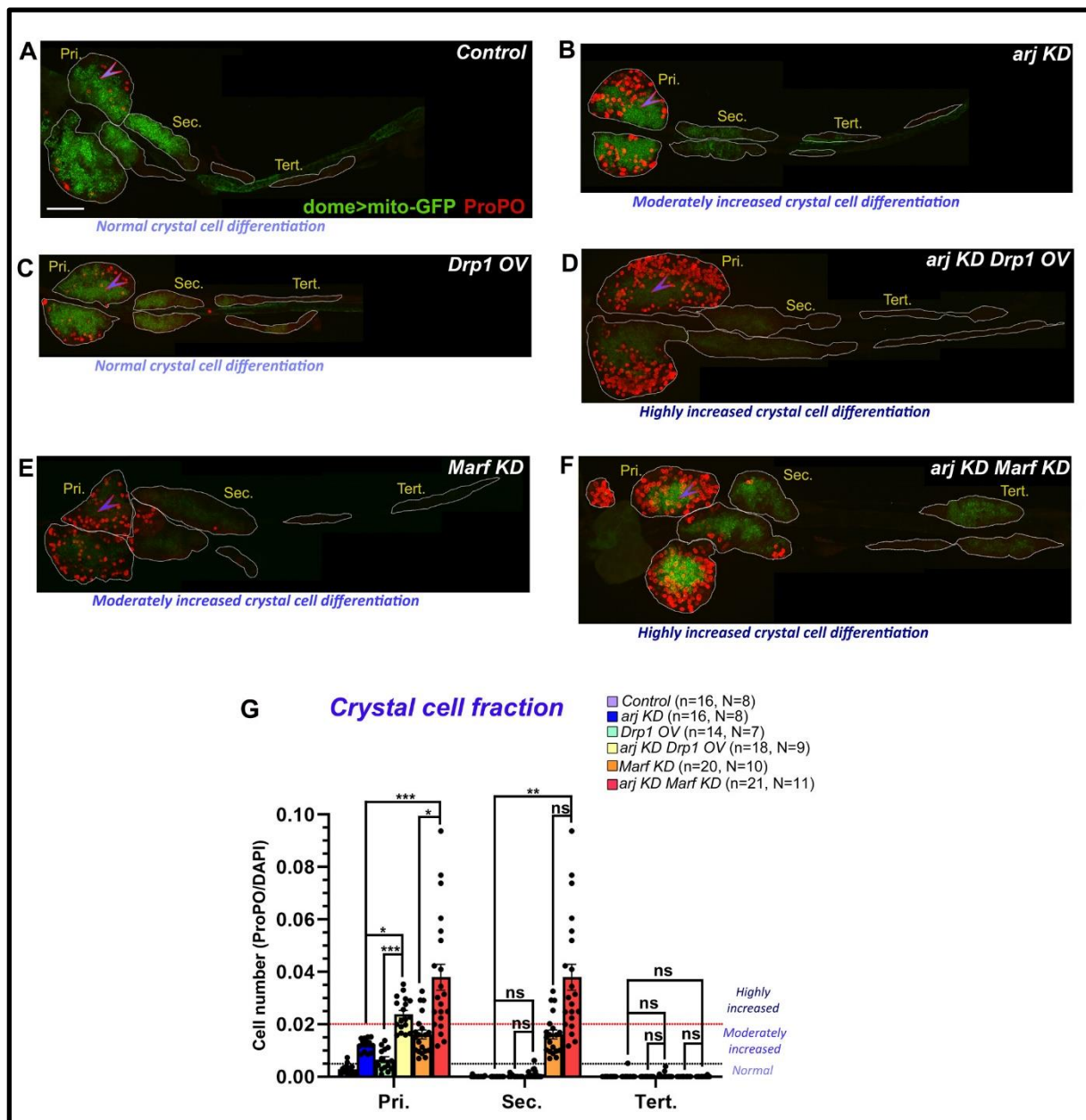


Figure 4.19 Progenitor-specific genetic interaction of *asrij* with *Drp1* and *Marf* controls crystal cell differentiation in lymph gland. (A-F) Whole mount lymph gland showing ProPO expression (far-red pseudo-colored to red) to mark crystal cells in primary (Pri.), secondary (Sec.) and tertiary (Tert.) lobes of control (A), *arj KD* (B), *Drp1 OV* (C), *arj KD Drp1 OV* (D), *Marf KD* (E) and *arj KD Marf KD* (F) larvae. The phenotypes of crystal cell differentiation are

mentioned below each lymph gland image. Arrowheads mark the region which is shown in magnified view in Figure 4.18. Scale bar: 100 μ m. (G) Bar diagrams show quantification of ProPO positive cell fraction in different lobes of the same genotypes. Error bars represent SEM. The values have been classified as normal (0-0.005), moderately increased (0.005-0.02) and highly increased (>0.02). n represents number of individual lymph gland lobes analysed, and N represents number of larvae for each genotype. Kruskal-Wallis test was performed for analysis of crystal cell fraction. *P<0.05, **P<0.01, ***P<0.001, ns: non-significant.

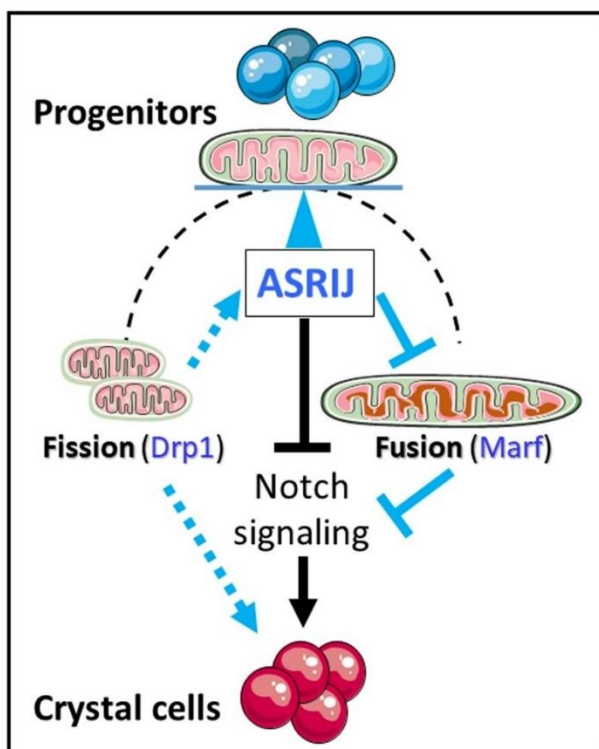


Figure 4.20 Schematic representation of the effect of mitochondrial morphology and dynamics on blood cell differentiation. Asrij is a hub that maintains the balance (blue arrowhead) between mitochondrial fission and fusion to regulate progenitor maintenance and crystal cell differentiation. Arrows indicate activation. T symbol indicates inhibition. Black color indicates previously known interactions; blue color indicates effects reported in this study.

Similar results were observed using the pan-hemocyte driver *e33CGal4*. *Drp1* overexpression or *Marf* KD in *asrij* null hemocytes (*arj9/arj9; e33CGal4/UAS Drp1* and *arj9/arj9; e33CGal4/UAS Marf RNAi*) rescued normal mitochondrial architecture (branch length and aggregation), comparable to control (*w1118*) (Fig 4.21A-G). However, although *Marf* KD rescued increased mitochondrial footprint (content) in *asrij* null hemocytes, *Drp1* overexpression could not. This suggests inefficient clearance of mitochondria even after *Drp1* overexpression. Also, it reaffirms our claim that elongation of mitochondria on *Asrij* depletion is mostly due to enhanced mitochondrial fusion rather than decreased fission.

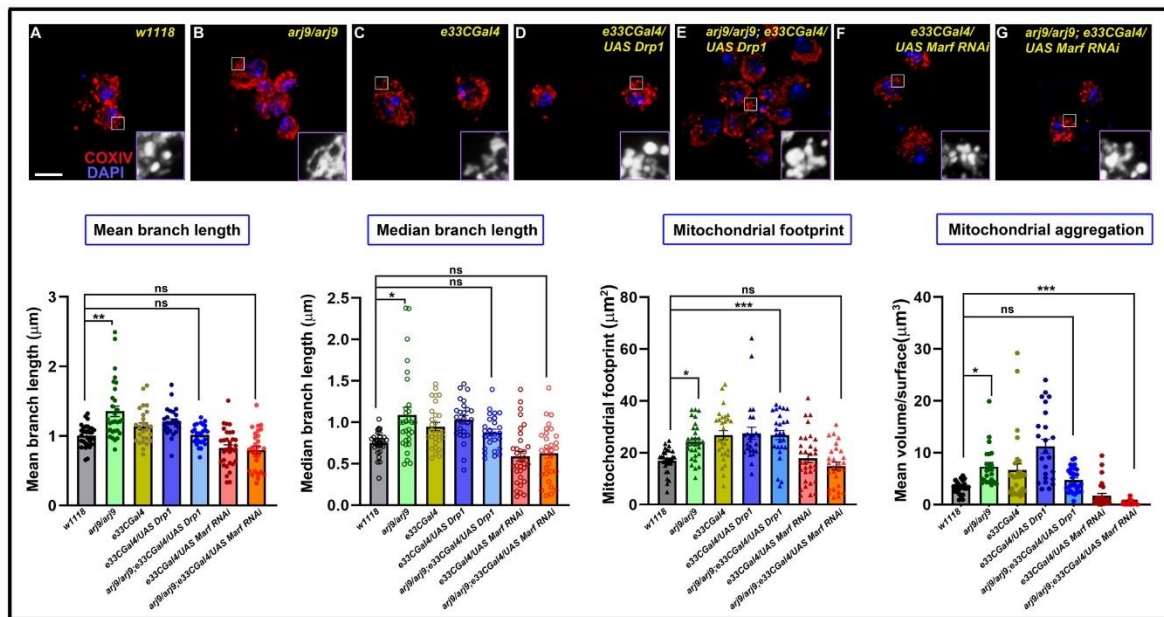


Figure 4.21 Genetic interaction of *asrij* with Drp1 and Marf controls mitochondrial network architecture in circulatory hemocytes. (A-G) COXIV staining in control (w1118) (n=30 cells) (A), *asrij* KO (*arj9/arj9*) (n=30 cells) (B), *e33CGal4* (n=26 cells) (C), Drp1 OV (*e33CGal4/UAS Drp1*) (n=25 cells) (D), *asrij* KO Drp1 OV (*arj9/arj9; e33CGal4/UAS Drp1*) (n=26 cells) (E), *Marf* KD (*e33CGal4/UAS Marf RNAi*) (n=32 cells) (F), (F) and *asrij* KO *Marf* KD (*arj9/arj9; e33CGal4/UAS Marf RNAi*) (n=30 cells) (G) circulatory hemocytes. Insets show magnified view of boxed region. Bar graphs show quantification of mitochondrial mean branch length, median branch length, mitochondrial footprint, and mitochondrial aggregation (mean volume/surface) in the same genotypes. Scale bar: 10 µm. Error bars represent SEM. Kruskal Wallis test was used to determine statistical significance. *P<0.05, **P<0.01 and ***P<0.001. ns: statistically non-significant difference.

Crystal cell differentiation in the primary lobe increased in a synergistic manner upon Drp1 OV or Marf KD in *asrij* null lymph gland (Fig 4.22A-G). Hence, Drp1 overexpression and Marf depletion affect crystal cell differentiation in similar way upon loss of *Asrij*. This suggests *Asrij* depletion makes cells more susceptible to the effect of increasing fission or reducing fusion implying greater sensitivity to mitochondrial dynamics. Hence, distinct functional networks connecting *Asrij* to the fission-fusion machinery may maintain normal mitochondrial dynamics and optimum differentiation of crystal cells.

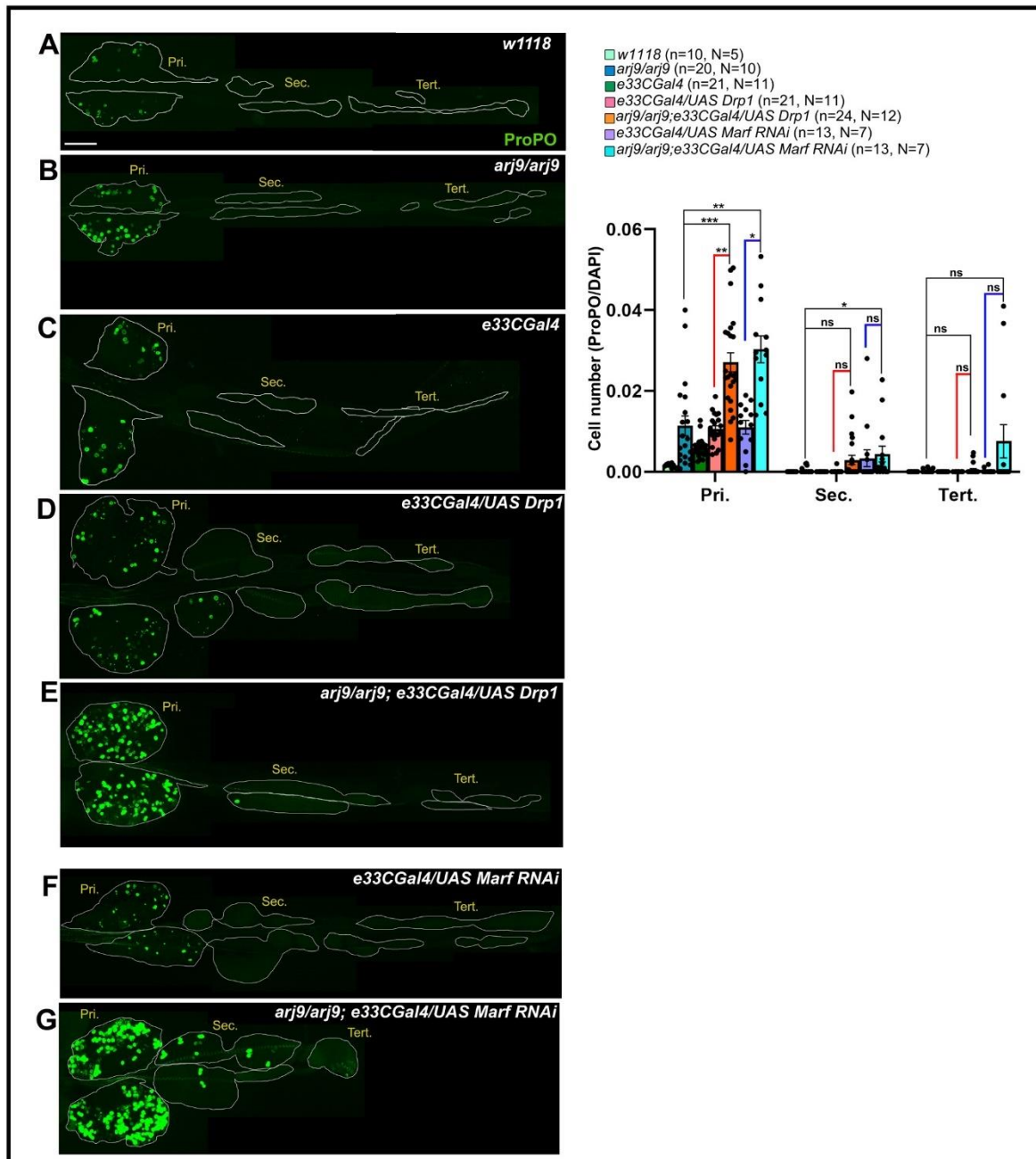


Figure 4.22 Pan-hemocyte-specific genetic interaction of *asrij* with *Drp1* and *Marf* controls crystal cell differentiation in lymph gland. (A-E) Whole mount lymph gland showing ProPO expression to mark crystal cells in primary (Pri.), secondary (Sec.) and tertiary (Tert.) lobes of control (*w1118*) (A), *asrij* KO (*arj9/arj9*) (B), parental Gal4 control (*e33CGal4*) (C), *Drp1* OV (*e33CGal4/UAS Drp1*) (D), *asrij* KO *Drp1* OV (*arj9/arj9; e33CGal4/UAS Drp1*) (E), *Marf* KD (*e33CGal4/UAS Marf RNAi*) (F) and *asrij* KO *Marf* KD (*arj9/arj9; e33CGal4/UAS Marf RNAi*) (G) larvae. (F) Bar graph shows quantification of mean crystal cell fraction in lymph gland lobes of indicated genotypes. Error bars indicate standard error of mean. n represents number of individual lymph gland lobes analysed, and N represents number of larvae for each genotype. Scale bar: 100 μ m. Error bars represent SEM. Kruskal Wallis test was

performed to determine statistical significance. * $P < 0.05$, ** $P < 0.01$ and *** $P < 0.001$; ns: statistically non-significant difference.

4.4 Discussion

The Asrij lymph gland proteome revealed that the expression of Drp1 was affected suggesting potential role of mitochondrial dynamics regulators in hematopoiesis. Given the lack of information about mitochondrial morphology in *Drosophila* hematopoietic progenitors we first undertook a detailed mapping in these cells. To fully exploit the power of the lymph gland model we chose to analyse the progenitor population in all lobes of the lymph gland as these represent temporally distinct stages of progenitor maturation and differing propensity for differentiation. We found differences in mitochondrial morphology between more mature anterior progenitors and younger posterior progenitors. Further, analysis of the effect of modulating mitochondrial fission-fusion regulators as well as Asrij also showed different responses in progenitor subsets. Our results are in agreement with the idea that posterior progenitors differ from anterior ones in their identity and function. Our detailed studies position the *Drosophila* lymph gland as a relevant and accessible *in vivo* model to study mitochondrial regulation of progenitor heterogeneity that is not currently possible in vertebrate models.

Mitochondrial morphology is inextricably related to its function including oxidative phosphorylation (Wai and Langer, 2016). Therefore, mitochondrial dynamics could serve as a potential therapeutic target for several diseases with mitochondrial dysfunction (Whitley et al., 2019; Brandner et al., 2019). While the role of Drp1 and Mfn2 in mitochondrial dynamics is well established, their ability to regulate hematopoiesis in vertebrates has been reported only recently (Luchsinger et al., 2016; Hinge et al., 2020). Misexpression of DNMI1 and Mfn1/2 may underlie several human hematological malignancies including acute myeloid leukemia (AML), chronic myeloid leukemia (CML), chronic lymphocytic leukemia (CLL) and myelodysplastic syndromes (<http://servers.binf.ku.dk/bloodspot>; <https://cancer.sanger.ac.uk/cosmic>). However, these

ubiquitous regulators of mitochondrial dynamics are not suitable therapeutic targets. Therefore, identification of tissue-restricted regulators of mitochondrial dynamics that are not essential for viability, is important.

Using cross-species comparison and *in vivo* analysis, we show a conserved role for Asrij/OCIAD1 in regulating cell fate through functional interaction with mitochondrial dynamics regulators. Asrij-dependent mitochondrial dynamics is a potential mechanism to regulate Notch signaling and myeloid specification.

We show that fission and fusion regulators Drp1 and Marf act through distinct networks to effect differentiation. Though Drp1 and Mfn2 play critical roles in mouse hematopoiesis, their role in lineage-specific signaling activation is unclear. Using the *Drosophila* lymph gland as an *in vivo* model of hematopoiesis, we find critical roles for canonical mitochondrial dynamics regulators such as Drp1 and Marf (dMfn) in blood cell differentiation. Drp1 and Marf play opposite roles in Notch activation for progenitor differentiation to crystal cells. Marf inhibits Notch activation and crystal cell differentiation whereas Drp1 may promote it. Hence, antagonistic roles of Drp1 and Marf in mitochondrial dynamics may mediate balanced activation of Notch signaling and lineage-specific differentiation of lymph gland progenitors.

Drp1 feeds back to activate Notch signaling in triple negative breast cancer cells which in turn can upregulate Drp1-dependent mitochondrial fission (Chen et al., 2018). On the other hand, we find that Marf KD promotes Notch activation. Hence, mitochondrial morphology/dynamics and Notch signaling can regulate each other. Further, Notch activation should result in fragmented mitochondria. Though Notch is activated on Asrij depletion (Kulkarni, Khadilkar et al., 2011), mitochondria are elongated and this phenotype is rescued by Marf KD, indicating that Asrij acts upstream to enhance Notch activation, which is in agreement with our earlier report. However additional regulatory mechanisms may also be in play. Nevertheless, we show that a functional network of Asrij with canonical

mitochondrial dynamics regulators (Drp1 and Marf) synergistically regulates crystal cell differentiation, a lineage downstream to Notch signaling. Mfn2 and DNM1L (Drp1) are reported as components of a proximity interaction network of OCIAD1, thus supporting further our claim of a direct functional interaction of Asrij with these canonical regulators of mitochondrial dynamics (Antonicka et al., 2020) (<https://thebiogrid.org/120280/summary/homo-sapiens/ociad1.html>). Hence, Asrij-dependent Notch signaling may possibly lie downstream of the Asrij-dependent mitochondrial dynamics.

ROS primes progenitors towards unbiased differentiation (Owusu-Ansah et al., 2009). Even though ROS levels are susceptible to change with shift in mitochondrial dynamics (Bhandari et al., 2015; Senos Demarco and Jones, 2019), our results show that the impact of Drp1 or Marf depletion is limited to Notch pathway activation and crystal cell differentiation. This suggests additional mechanisms that may make plasmacyte and lamellocyte differentiation less sensitive to inhibition of mitochondrial fission or fusion.

It is quite possible that Asrij and Marf may have similar roles in some other aspects of mitochondrial function that regulate Notch activation. Probably that is why the combined knockdown of Asrij and Marf, although rescues mitochondrial morphology, cannot rescue increased crystal cell differentiation but rather enhances it synergistically. Previous studies have reported physical interaction of OCIAD1 with regulators of calcium signaling that depends on ER-mitochondria interaction (Floyd et al., 2016). This raises the possibility that other inter-organelle mechanisms may also be involved.

Mechanisms that control posterior progenitor fate are only recently being understood (Krzemien et al., 2010; Rodrigues et al., 2021). Our results show progenitor-specific Marf depletion causes mild increase in plasmacyte differentiation in secondary lobes suggesting mitochondrial fragmentation as a possible mechanism to trigger differentiation in posterior subsets of progenitors. Also, tertiary lobe progenitor population increases upon Marf

depletion. This could be a basis for screens to identify reversal of such phenotypes and lead to novel position-specific regulators of progenitors.

Mitochondrial metabolism and dynamics are inter-dependent (Wai and Langer et al., 2016). We show a conserved role for Asrij in both mitochondrial morphology, dynamics, and function. Hence, Asrij/OCIAD1 may be a key conserved regulator that coordinates different facets of mitochondrial activity, to dictate cell fate decisions. We observed increased mitochondrial content in Asrij depleted hemocytes. This could be due to impaired mitophagy that is often seen upon reduced fission or hyperfusion of the mitochondrial network (Twig et al., 2008). Although Marf depletion can reduce the mitochondrial content in Asrij depleted cells, Drp1 overexpression fails to do so suggesting that Drp1 cannot sufficiently promote mitochondria clearance, possibly through mitophagy, in Asrij depleted condition. Whether loss of Asrij causes elongation of mitochondria through inactivation of Drp1 can be addressed by analysis of Drp1 post-translational modifications and GTPase activity through *in vivo* and *in vitro* assays. Rescue of phenotype in *asrij* mutant progenitors and blood cells by Mitofusin knockdown suggests that the elongation of mitochondria may primarily happen through increased mitochondrial fusion. However, further in-depth analysis would be useful to find out all possible mechanisms through which Asrij may impact mitochondrial dynamics.

Recent reports show a potential role of mitophagy in maintaining hematopoietic progenitors or stimulating hematopoiesis in vertebrates (Jin et al., 2018; Girotra et al., 2020). Inter-organelle communications in signaling homeostasis and downstream cell fate specification could allow for complex spatial and temporal regulation. While canonical Notch signalling leads to crystal cell differentiation, non-canonical activation of Notch pathway due to stalling in endosomes of Asrij mutants (Kulkarni, Khadilkar et al., 2011) may also contribute to the synergistic effects on phenotype. Asrij/OCIAD1 acts as a transmembrane scaffolding protein that regulates assembly and activation of critical signaling components and molecular complexes across organelles (Sinha et al., 2013; Le Vasseur et al, 2021). Hence, Asrij may potentially act as mediator of inter-organelle communication that may influence blood cell homeostasis.

Notch activation increases in secondary lobes upon Marf depletion suggesting that progenitors are primed, but not fully committed towards differentiation. **This may also reflect their immature developmental stage and functional heterogeneity.** Other mechanisms may operate to inhibit crystal cell differentiation (ProPO⁺) downstream to Notch activation in secondary lobes of Marf depleted lymph glands. Further, progenitor fraction in tertiary lobes increases upon Marf depletion indicating a possible increase in progenitor proliferation. On the other hand, Drp1 depletion does not affect blood cell homeostasis in posterior lobes. Hence, Marf-dependent mitochondrial dynamics could be a position-dependent mechanism to regulate posterior progenitors. Further, it raises the possibility that a subset of dome⁺ progenitors are biased towards crystal cell differentiation and that progenitors may differ in lineage potential. Importantly, this effect is position-dependent as dome⁺ posterior progenitors **in secondary lobes, even after undergoing mitochondrial fragmentation due to Marf depletion, fail to differentiate, unlike primary lobe progenitors.** It also implies that the posterior identity of progenitors is maintained even on perturbing mitochondrial morphology, as they continue to be refractile to differentiation. Asrij depletion may unlock lineage differentiation potential to assist progenitor differentiation in posterior lobes.

Even though we show the effect of progenitor-specific knockdown of *asrij*, *Drp1* and *Marf* on blood cell differentiation, any non-autonomous impact cannot be ruled out. Blood cell differentiation in such cases could be due to differentiation of the KD progenitor itself or due to signals originating from the KD progenitors that promote differentiation or trans-differentiation of intermediate progenitors or differentiated hemocytes. Our results show genetic interaction between *Asrij* and *Drp1*/*Marf* within the same pool of cells - either circulatory hemocytes or lymph gland progenitors. So, it is quite possible that the functional synergy to regulate crystal cell differentiation could be due to genetic interaction in the same cell. However, effect on crystal cell differentiation could be cell non-autonomous as well, which can be tested by mitotic mutant clone analysis.

Our data support an interplay of the blood cell enriched protein Asrij with mitochondrial dynamics regulators Drp1 and Marf in lineage-specific differentiation. Given the ubiquitous requirement for Drp1 and Marf and the pan-hemocyte expression of Asrij, it is quite unexpected to see such lineage-specific effects. These insights validate our use of *Drosophila* genetics and the *in vivo* lymph gland hematopoiesis model to uncover such complex and unique interactions. Further they reveal Asrij as a critical regulatory node connecting mitochondrial dynamics, Notch signaling and crystal cell differentiation. Our findings suggest that the functional output of mitochondrial dynamics may be beyond simply the mitochondrial network architecture and depends on other unidentified factors linked to the dynamicity of this network. Modulating mitochondrial dynamics *in vitro* can serve as a way to promote or inhibit lineage-specific differentiation for therapeutic purposes. In summary, Asrij-regulated mitochondrial dynamics emerge as a potential conserved mechanism to maintain blood cell homeostasis.

4.5 Acknowledgement

This work is published in:

Ray A, Kamat K, Inamdar MS., (2021) A conserved role for Asrij/OCIAD1 in progenitor differentiation and lineage specification through functional interaction with the regulators of mitochondrial dynamics. *Frontiers in Cell and Developmental Biology*. doi: 10.3389/fcell.2021.643444.

All figures except figure 4.4 are published in the above mentioned publication. Text and figures have been used from the original research article following the terms of Creative Commons Attribution License (CC BY).

[\(http://creativecommons.org/licenses/by/4.0/\)](http://creativecommons.org/licenses/by/4.0/)

Analysis of mitochondrial dynamics in hESC was performed by Kajal Kamat using data available from Shetty et al., *Stem Cell Reports*, 2018.

Chapter 5. ESCRT components play distinct role in cargo sorting and lineage-specific differentiation of blood progenitors in the *Drosophila* lymph gland.

5.1 Introduction

Blood progenitor homeostasis and lineage-specific differentiation involve a complex interplay of signaling pathways. Endocytic compartments act as critical regulatory stations for various intracellular and extracellular cues (Scita and di Fiore, 2010). Protein trafficking and turnover through the endolysosomal route fine-tunes signal transduction. Several proteins actively participating in different facets of endocytic trafficking have been implicated in developmental signaling and cellular homeostasis. Atg6-dependent endocytosis and autophagy regulates blood cell homeostasis in *Drosophila* (Shravage et al., 2013). Rabex5 regulates blood cell proliferation and differentiation through ubiquitination-dependent relocalization of Ras in endosomes (Reimels and Pleger et al., 2015). Rab5 and Rab11 also regulate blood cell proliferation and differentiation through modulation of JNK signaling in the *Drosophila* lymph gland (Yu et al., 2021).

Endosomal protein sorting plays a critical role in endocytic degradation of cargoes and signaling homeostasis. Asrij, the blood cell-enriched conserved endosomal regulator of hematopoiesis, interacts with ADP Ribosylation Factor 1 (ARF1-GTP) to maintain stemness of blood progenitors in the *Drosophila* lymph gland (Kulkarni, Khadilkar et al., 2011). Loss of Asrij promotes activation of Notch signaling in the lymph gland, thus leading to precocious differentiation to crystal cells (Kulkarni, Khadilkar et al., 2011). Depletion of Asrij causes entrapment of Notch intracellular domain (NICD) in the sorting endosomes mimicking sorting defect. Also, improper endosomal sorting caused by downregulation of WASH complex can inhibit differentiation of hematopoietic stem cells (HSC) in mouse bone marrow (Xia et al., 2014). These reports suggest a potential role of endosomal protein sorting in blood cell homeostasis.

Conserved Endosomal Sorting Complex Required for Transport actively controls the sorting of ubiquitinated cargoes for lysosomal degradation. This heteromultimeric complex consists of four subunits (ESCRT-0, I, II and III) that are sequentially recruited on the endomembrane bound ubiquitinated cargoes, allowing them to be sequestered in the intraluminal vesicles (ILV) of the multivesicular bodies (MVB). 13 components constitute the *Drosophila* ESCRT (Vaccari et al., 2009; Alfred and Vaccari, 2016). ESCRT-0 (Hrs, Stam) binds to the ubiquitinated cargoes through ubiquitin-interacting motif. Subsequently, it recruits ESCRT-I (Vps28, Tsg101, Vps37A, Vps37B) and ESCRT-II (Vps25, Vps22 and Vps36), which act as bridging complex to assemble ESCRT-III (Vps32, Vps24, Vps20, Vps2). ESCRT-III dependent membrane remodelling lies at the heart of endosomal protein sorting that requires inward invagination of the endosomal membrane to allow formation of ILVs containing the sequestered cargoes (Radulovic et al., 2018). Detailed genetic and biochemical analysis of ESCRT-III in yeast and mammalian cells suggest CHMP4/SNF7 (Vps32 homolog) as the principal filament-forming component that undergoes activation and polymerization upon binding with various nucleating factors (Vietri et al., 2020). The final step of endosomal protein sorting involves disassembly of ESCRT subunits and scission of the membrane neck of the intraluminal vesicles that is mediated by the Vps4-Vta1 mechanoenzyme complex. Vps20 of ESCRT-III acts as a nucleator for the most abundant ESCRT-III component Vps32 and cooperatively functions with Vps4 AAA-ATPase to regulate depolymerization of ESCRT-III after successful cargo sorting. Vps24 and Vps2 regulate the shape of the ESCRT-III subunit by crosslinking the Vps32 filaments and also by regulating the filament length.

Accessory proteins can often assist ESCRT function, resulting in functional redundancy of certain ESCRT components. For example, Bro1 in yeast and Alix and HD-PTP in mammals can act as substitute bridging factors for ESCRT-II (Bissig et al., 2014; Tabernero et al., 2018). Also, auxiliary ESCRT proteins and Vps4 complex members such as Ist1, Vps60 and Chmp1 can regulate ESCRT core component function, often through synergistic interaction (Baumers et al., 2019). Loss of function mutation for critical ESCRT genes in metazoan system like *Drosophila* causes endosomal accumulation of ubiquitinated cargoes including signaling receptors (Vaccari et al., 2009; Herz et al., 2009; Szymanska et al., 2018). This leads to aberrant activation of signaling pathways such as Notch, EGFR, JAK/STAT etc that alter

tissue homeostasis. Depletion of ESCRT components causes tissue hyperproliferation, loss of cell polarity and neoplastic transformation in both cell -autonomous and non-autonomous manner (Thompson et al., 2005; Vaccari et al., 2009; Herz et al., 2009).

Though phenotypic diversity is uncommon in yeast, fly ESCRT components may play differential role in cargo sorting, MVB biogenesis, signaling activation and cell fate choice (Vaccari et al., 2009; Herz et al., 2009; Tognon et al., 2014). ESCRT-0 components Hrs and Stam are dispensable for regulating Notch signaling activation, epithelial tissue proliferation or apicobasal polarity while other ESCRT subunits play essential roles for the same (Tognon et al, 2014). Also, intra-subunit phenotypic diversity is reported in ESCRT-II where Vps36, Vps22 and Vps25 differentially control neoplastic overgrowth, apoptotic resistance and Notch signaling activation (Herz et al., 2009). This indicates that despite playing a ubiquitous role in endosomal protein sorting, ESCRT may assume functional pleiotropy through modulation of individual component activity in a context-dependent manner.

As endosomal protein sorting may potentially regulate blood cell homeostasis, we tested the role of ESCRT machinery in progenitor homeostasis and lineage-specific differentiation *in vivo* using *Drosophila* lymph gland as a model. In this chapter, we provide the functional map of all 13 *Drosophila* ESCRT components indicating ubiquitinated cargo sorting and blood lineage choice across distinct progenitor subsets.

5.2 Materials and methods

5.2.1 Fly stocks

Drosophila melanogaster stocks were maintained as described previously (Kulkarni, Khadilkar *et al.*, 2011). Canton-S was used as the wildtype reference strain. *w1118* was used as the genetic background control for *arj9/arj9* (*asrij* null). E33CGal4 (K. Anderson, Memorial Sloan Kettering Center) was used as the parental control for *Asrij* overexpression (*e33CGal4/UAS arj*). For progenitor-specific knockdown of ESCRT genes, *domeGal4*

UAS2xEGFP/FM7a and *domeGal4/FM7b* (Utpal Banerjee, UCLA) were used as driver as well as parental control. *UAS-dsRNA* (RNAi) transgenic lines were used for the knockdown of Hrs (BDSC 33900), Stam (VDRC 22497), Vps28 (VDRC 31894), Tsg101 (BDSC 38306), Vps37A (BDSC 38304), Vps37B (BDSC 60416), Vps36 (BDSC 38286), Vps22 (BDSC 38289), Vps25 (VDRC 108105, BDSC 26286), Vps2 (BDSC 38995), Vps20 (Spyros Artavanis-Tsakonas, Harvard Medical School), Vps24 (BDSC 38281) and Vps32 (VDRC 106823). Other stocks used were *UAS mCD8 RFP* (BDSC 27399), *UAS FLP* (BDSC 4540), *shrb^{G5} FRT42D/CyO GFP* (BDSC 39635), *FRT42D Ubi-GFP/CyO* (BDSC 5626).

5.2.2 Fly Genetics

To obtain flies with prohemocyte-specific knockdown of target genes, 10 male flies of homozygous RNAi line were crossed with 20 virgin female flies of *domeGal4 UAS 2xEGFP/FM7a* genotype. F1 progenies were collected based on GFP expression. *domeGal4 UAS GFP/FM7a* was used as the parental control for all analyses.

For experiments using *domeGal4/FM7b* driver, virgin females were crossed with *UAS mCD8 RFP* males. RFP positive female progenies were crossed with homozygous RNAi lines. RFP positive F1 progenies were used for experiments and *domeGal4;; UAS mCD8 RFP* flies were used as parental control.

Progenitor-specific mosaic mitotic clones were generated using *domeGal4* driven recombination. *domeGal4; FRT42D Ubi-GFP; UAS mCD8 RFP* flies were used as control. Genotype of the mitotic clones: i) *domeGal4; shrb^{G5} FRT42D/FRT42D Ubi-GFP; UAS FLP/UAS mCD8 RFP*, ii) *domeGal4; Vps25^{A3} FRT42D/FRT42D Ubi-GFP; UAS FLP/UAS mCD8 RFP*

5.2.3 Immunofluorescence Microscopy

Drosophila third instar larval lymph glands were dissected in PBS following the protocol described in Rodrigues et al, *Bio-protocol*, 2021. Only the dorsal half of the cuticle and the

brain lobes were kept intact, and the rest of the tissues were removed. After dissection, the samples were immediately fixed with 4% paraformaldehyde made in PBS for 20 minutes followed by three gentle PBS washes. Samples were permeabilised using 0.3% Triton X-100. For blocking, normal goat serum diluted to 20% in PBS was used. The samples were incubated overnight with the primary antibody dilutions. Primary antibodies used were guinea pig anti-Hrs (Benny Shilo, Weizmann Institute), rabbit anti-dVps28 (Helmut Kramer, UT Southwestern Medical Center), rabbit anti-Shrub (Fen B. Gao, University of Massachusetts), mouse anti-P1 (Istvan Ando, BRC Schezed), mouse anti-ProPO, rabbit anti-dsRed (Takara, Japan), FK2 (Enzo Life Sciences, USA). For secondary antibody staining, Alexa Fluor labelled anti-mouse, anti-rabbit, and anti-guinea pig antibodies (Life Technologies, Thermo Fisher Scientific, USA) were used. Phalloidin conjugated to Alexa 568 or 633 (Life Technologies, Thermo Fisher Scientific, USA) was used to visualize lamellocytes. DAPI glycerol was used to mount the lymph gland samples on the coverslip. Images were acquired on Zeiss LSM880 Laser Confocal Microscope.

5.2.4 *In situ* hybridisation

RNA *in situ* hybridisation was performed to check the expression of the ESCRT components against which antibodies are not available. The genes of interest (*Stam*, *Vps22*, *Vps25*, *Vps24*) were PCR amplified from genomic DNA using the primers tabulated below:

Primers were designed with T7 promoter sequence incorporated in the reverse primer. Amplicon was cleaned up using Nucleospin PCR clean-up kit (Macherey-Nagel, Germany) and 200ng-1µg DNA was used as template for *in vitro* transcription. DIG-labelling mix (Roche, Switzerland) was used to generate DIG labelled RNA probe. Length of the probes are 644 bp (*Stam*), 503 bp (*Vps25*), 500 bp (*Vps22*) and 325 bp (*Vps24*). *In situ* hybridisation was performed using protocol as described in Benmimoun *et al.*, 2015. The list of primers used are as following:

Gene name	Primer sequence
Stam	Forward 5' TTGTCAGTCCGATCTGTCC 3'
	Reverse 5' CCTGCTAATACGACTCACTATAGGGTTGACCCAGATAGCCACC 3'
Vps22	Forward 5' ACGTGATTTAGGTGACACTATAGTAGGCCTGGGAGCCATACAG 3'
	Reverse 5' CCGTTAATACGACTCACTATAGGGTGCCAAAAATGCTCAATTTC 3'
Vps25	Forward 5' CCCCAATTTAGGTGACACTATAGCGAAGAAACCAGACAGCAGC 3'
	Reverse 5' GTAATACGACTCACTATAGGGAAGAAGCTTAACGCCGTGGCTG 3'
Vps24	Forward 5' GAGCCTGGTGCCTATCC 3'
	Reverse 5' GGCTTTAATACGACTCACTATAGGGTGCATCTCTTGCAGTTCCTC 3'

5.2.5 RT qPCR

Approximately 2-2.5 µg RNA was isolated from 100 lymph glands using Qiagen RNeasy kit (Qiagen, Germany). 20ng cDNA was used for each qPCR reaction of *Stam*, *Vps25*, *Vps24* and *Rp49*. All SYBR green based experiments were performed in triplicates. Relative fold change was normalised over *Rp49*. Primer sequences are as following:

Gene name	Primers
STAM	Forward 5' ACTGAAAATGCGCCAAGTGC 3'
	Reverse 5' CGGCAACAGTCTTGCTAGTC 3'
Vps25	Forward 5' CCCTTCTTTACTACTACAGCC 3'
	Reverse 5' CTGGTCCCCAATGCTGAGAG 3'
Vps24	Forward 5' AAGAGCAGGTGCAGGAGTGG 3'

	<p>Reverse</p> <p>5' CAAGAATGACGCAGGTGTCG 3'</p>
Rp49	<p>Forward</p> <p>5' CCGCTTCAAGGGACAGTATC 3'</p>
	<p>Reverse</p> <p>5' ACA ATC TCC TTG CGC TTC TTG 3'</p>

5.2.6 Quantification

Fluorescence intensity across lymph gland lobes was quantified using Fiji (ImageJ) to estimate any difference in protein expression. Number of ubiquitin aggregates in each lobe was quantified manually and then normalized over DAPI-positive nuclei count to obtain the fraction of cells accumulating ubiquitinated cargoes in each lobe. Progenitor and plasmacyte fraction in each lymph gland lobe was quantified using Imaris (Bitplane) as described in Chapter 3 (Section 3.2.5.3). Briefly, the number of spots (DAPI positive nuclei with >2 μm diameter) close to the reconstructed dome >2xEGFP (for prohemocytes) or P1 (for plasmacytes) surface, by a set threshold distance (1 μm for prohemocytes and 2 μm for plasmacytes), was quantified and divided by total number of nuclei. The number of crystal cells in each lobe was quantified manually and its fraction was calculated in each lobe by dividing with the number of nuclei. Lamellocytes were identified based on large or elongated morphology as revealed by Phalloidin staining. Percentage of larvae showing lamellocyte differentiation was quantified and represented. All images within a given figure panel were adjusted equally for brightness and contrast using Adobe Photoshop CS5 extended.

5.2.7 Statistical analyses

Each larva was considered as a biological replicate. Data from each lymph gland lobe was individually considered for quantitation in all graphs. One-way ANOVA was performed for statistical analysis of data. For datasets with unequal variance across groups, non-parametric tests such as Kruskal Wallis test was performed.

5.3 Results

5.3.1 ESCRT components are uniformly expressed across the lymph gland.

We performed immunofluorescence (IF) microscopy and RNA *in-situ* hybridisation (ISH) to check the expression of ESCRT components in the lymph gland. We chose 8 components [2 from each subunit (ESCRT-0: Hrs, Stam; ESCRT-I: Vps28, Tsg101; ESCRT-II: Vps25, Vps22; ESCRT-III: Vps32, Vps24)] as representative to analyse the expression of ESCRT across the lymph gland as these are well known regulators of signaling homeostasis and tissue development in *Drosophila* (Vaccari and Bilder, 2005; Vaccari et al., 2008; Vaccari et al., 2009; Herz et al., 2009). Immunostaining-based analysis revealed uniform expression of Hrs, Vps28, Tsg101 and Vps32 across different lobes of wild type *Canton-S* lymph glands (Fig 5.1A-E). We also found transcript-level expression of Stam, Vps25, Vps22 and Vps24 across all lobes of the lymph gland by *in situ* hybridisation (Fig 5.1F-I). Moreover, using *dome>2xEGFP* as a marker of blood progenitors, we found that the expression of Hrs, Vps28, Tsg101 and Vps32 was comparable across cortical and medullary zones of the primary lobe, indicating ESCRT expression in both undifferentiated and differentiated cell population (Fig 5.1J-N). These data suggests that ESCRT genes are expressed in all cell populations of the lymph gland.

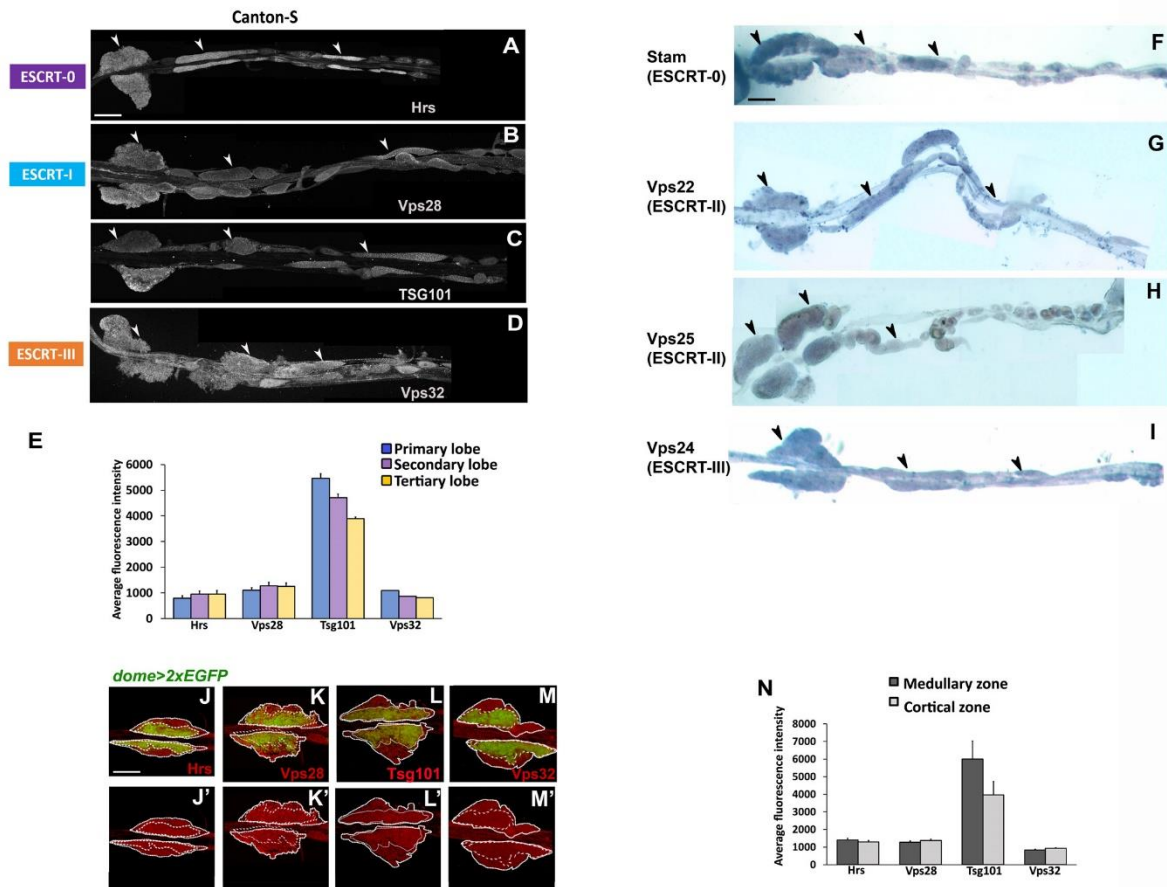
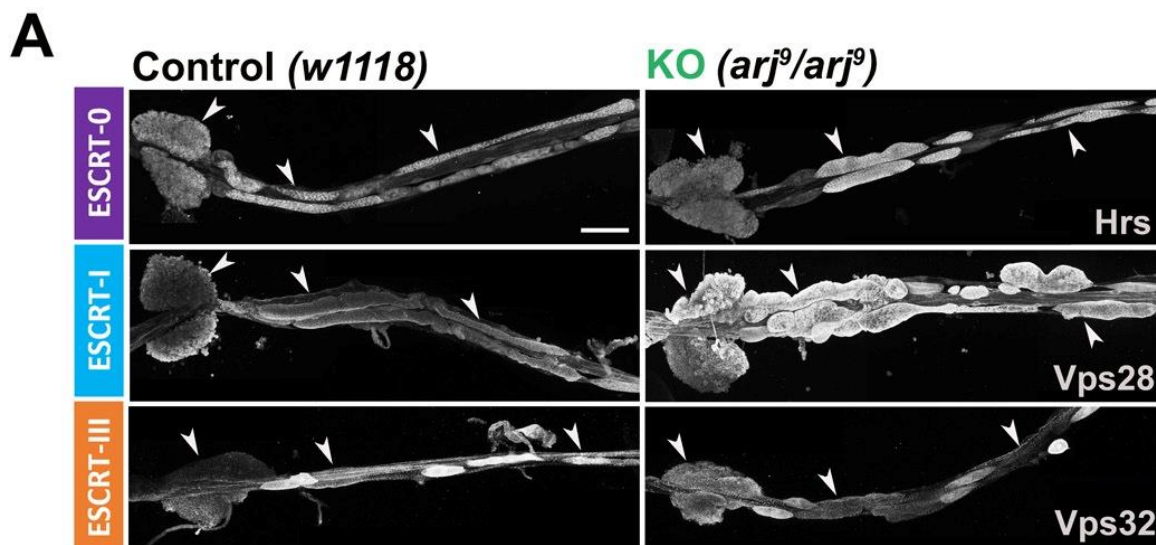


Figure 5.1 ESCRT is uniformly expressed in the lymph gland. (A-E) ESCRT components Hrs (ESCRT-0) (A), Vps28 and Tsg101 (ESCRT-I) (B, C) and Vps32 (ESCRT-III) (D) are uniformly expressed across different lobes of the lymph gland. Arrowheads mark the primary, secondary and tertiary lobes. (E) Bar diagram shows quantification of mean fluorescence intensity for immunostaining of ESCRT components across three lobes. (F-I) RNA *in situ* hybridisation shows expression of ESCRT components Stam (ESCRT-0) (F), Vps22 and Vps25 (ESCRT-II) (G, H) and Vps24 (ESCRT-III) (I) at transcript level across different lobes. Arrowheads mark the different lobes. (J-M) *dome>2xEGFP*+ve region marks prohemocytes in the medullary zone demarcated by dotted line in the primary lobe. Immunostaining for Hrs (J, J'), Vps28 (K, K'), Tsg101 (L, L') and Vps32 (M, M') shows uniform expression. (N) Bar diagrams show quantification and comparison of mean fluorescence intensity of a given component in *dome>2xEGFP*+ve medullary zone and *dome>2xEGFP*-ve cortical zone. Scale bar: 100 μ m. N>5 larvae with each individual lobes analysed. Error bars in the graph represent SEM. One-way ANOVA was performed to determine the statistical significance.

5.3.2 Conserved endosomal regulator of hematopoiesis, *Asrij* regulates ESCRT expression in the lymph gland.

Depletion of conserved regulator of hematopoiesis, *Asrij* leads to NICD accumulation in Hrs⁺ sorting endosomes of hemocytes, thus mimicking endosomal sorting defect (Kulkarni, Khadilkar et al, 2011; Khadilkar et al, 2014). To understand any possible tissue-restricted regulation of ESCRT, we checked the protein level expression of three ESCRT proteins by immunostaining in *Asrij* perturbed lymph glands. We observed no change in the expression of Hrs (ESCRT-0) and Vps32 (ESCRT-III) upon loss of *Asrij* (Fig 5.2A, C). However, the expression of Vps28 (ESCRT-I) increased throughout the lymph gland. Pan-hemocytic overexpression of *Asrij* using *e33CGal4* did not affect Hrs expression (Fig 5.2B, C). However, Vps28 expression significantly decreased and Vps32 expression increased throughout the lymph gland. Dependence of ESCRT expression on *Asrij* reflects potential role of ESCRT in blood cell homeostasis and also its tissue-restricted regulation (Fig 5.2D).



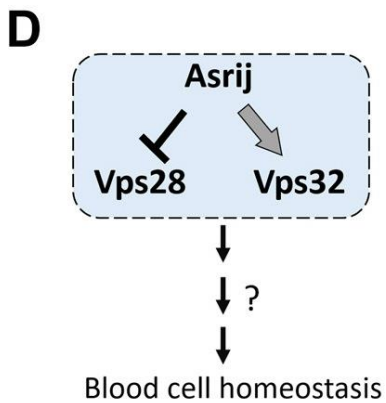
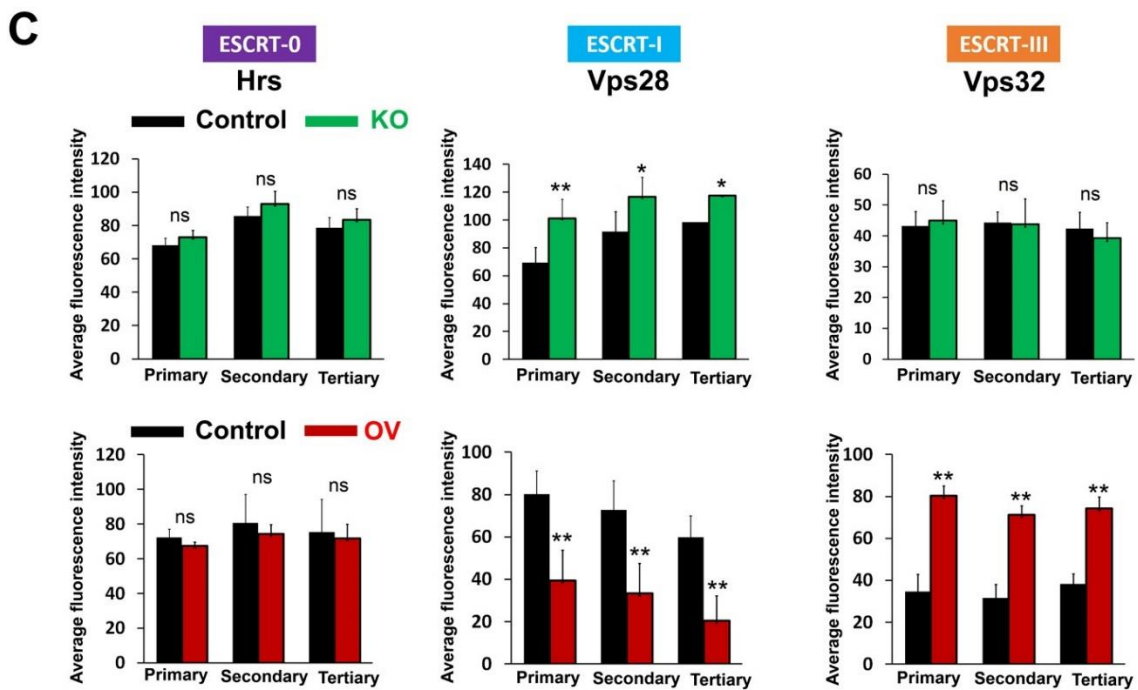
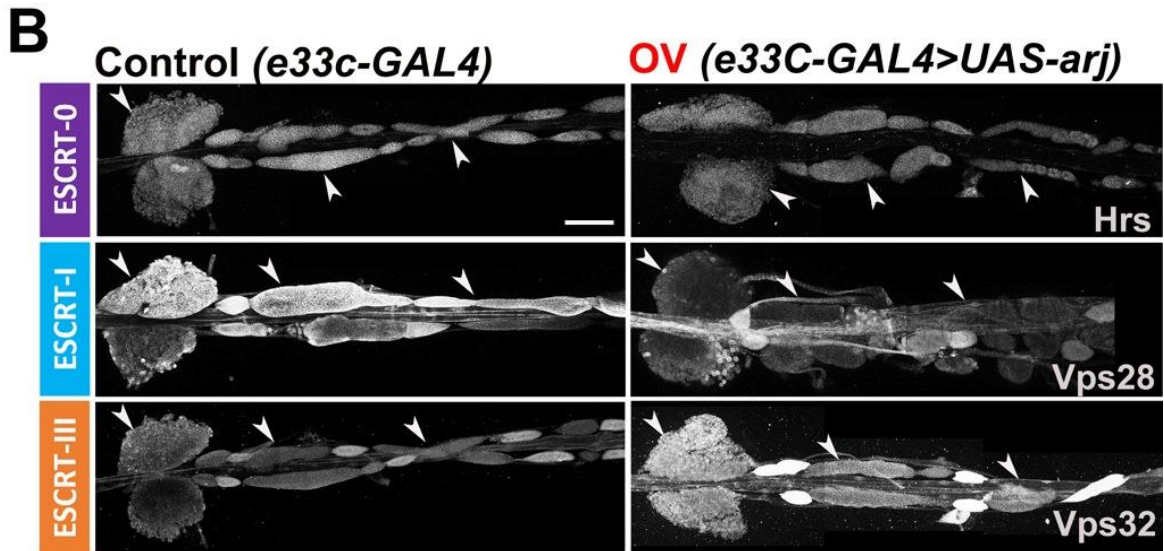


Figure 5.2 Asrij regulates ESCRT expression in the lymph gland. (A) Whole-mount lymph gland showing immunostaining of Hrs (ESCRT-0), Vps28 (ESCRT-I) and Vps32 (ESCRT-III) in control (*w1118*) and *asrij* null (KO: *arj9/arj9*) genetic background. (B) Same staining is shown in parental control (*e33CGal4*) and *Asrij* overexpressing (OV: *e33CGal4/UAS arj*) lymph glands. Arrowheads mark the primary, secondary and tertiary lobes of the lymph glands. Scale bar: 100 μ m. (C) Bar diagrams represent quantification of the mean fluorescence intensity for Hrs, Vps28 and Vps32 staining in control, KO and OV lymph glands across primary, secondary and tertiary lobes. N>7 larvae for each genotype. (D) Schematic shows *Asrij*-dependent regulation of ESCRT expression (Vps28 and Vps32) and suggests a potential role of ESCRT in blood cell homeostasis. Arrow indicates upregulation whereas T-sign indicates downregulation. Statistical significance was determined using one-way ANOVA. Error bars represent SEM. *P-value <0.05, **P<0.01. ns indicates non-significant difference.

5.3.3 ESCRT components regulate ubiquitinated cargo sorting in the lymph gland in a distinct manner.

We used an RNAi-based approach to elucidate the blood progenitor-specific role of ESCRT. *domeGal4* drives gene knockdown specifically in all the lymph gland progenitor subsets. We first validated the knockdown of ESCRT genes in the lymph gland using IF, RT-qPCR and ISH (8 components as described in section 5.3.1) (Fig 5.3).

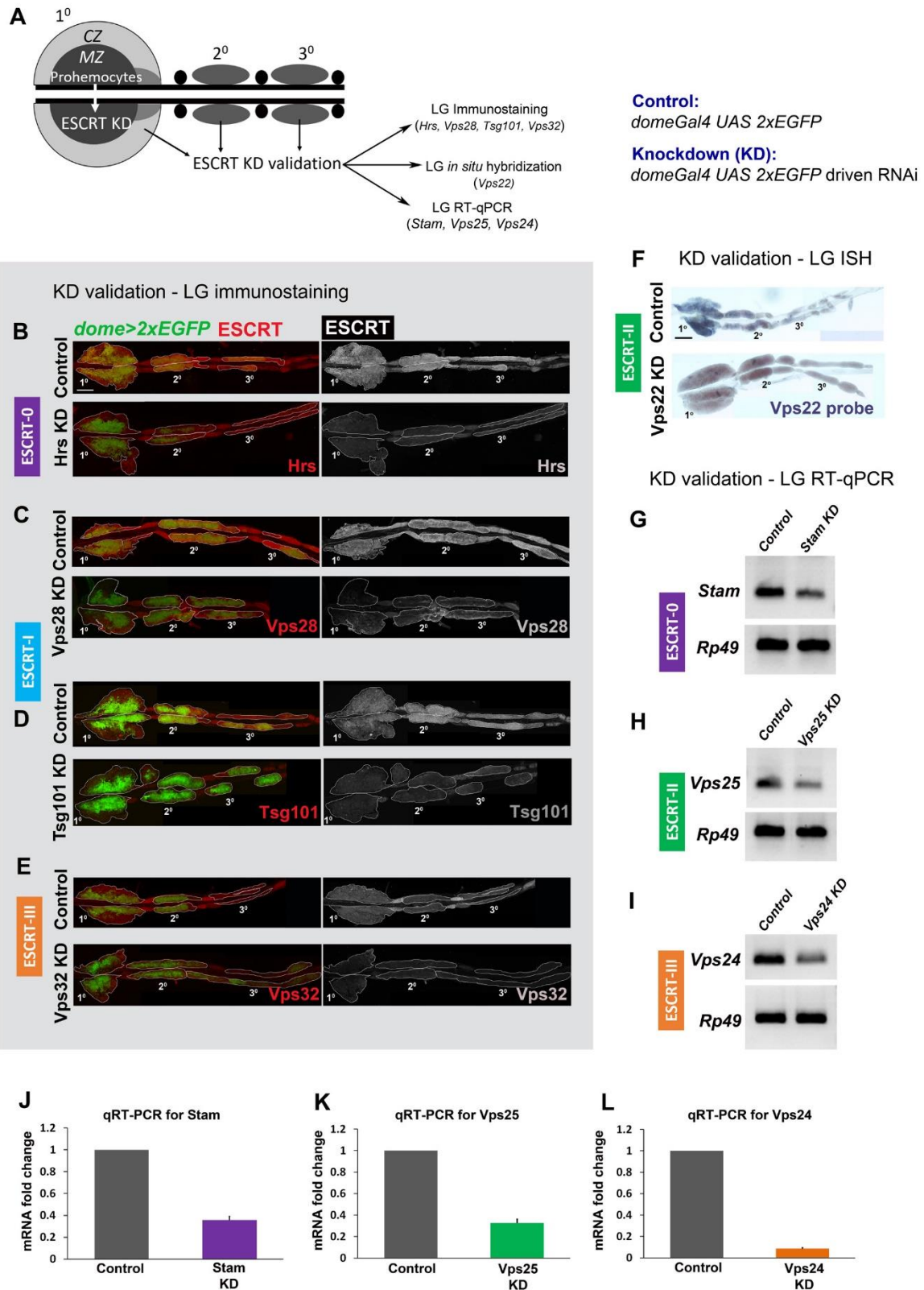


Figure 5.3 Validation for knockdown of ESCRT genes in the lymph gland. (A-E) Validation of *domeGal4*-driven knockdown of ESCRT components was performed using immunofluorescence microscopy, *in situ* hybridisation and RT-qPCR (A). Immunostaining

using respective antibodies shows knockdown of ESCRT component Hrs (ESCRT-0) (B), Vps28 and Tsg101 (ESCRT-I) (C, D) and Vps32 (ESCRT-III) (E). RNA *in situ* hybridisation shows knockdown of Vps22 (ESCRT-II) (F). RT-qPCR from lymph gland validates knockdown of Stam (ESCRT-0), Vps25 (ESCRT-II) and Vps24 (ESCRT-III) (G-L). Scale bar: 100 μ m. N>5 larvae for IF and N=10 larvae for ISH-based validation. RT-qPCR was performed in triplicates using RNA isolated from 100 lymph glands for each genotype. Error bars represent SEM.

To generically assess the role of ESCRT in endosomal protein sorting in the lymph gland, we performed domeGal4-mediated knockdown of all 13 *Drosophila* ESCRT components individually and tested for accumulation of conjugated ubiquitin that reflects sorting defect. As expected, ESCRT depletion in progenitors led to the accumulation of ubiquitinated cargoes. However, while some components were indispensable for ubiquitinated cargo trafficking, some components were dispensable (Fig 5.4). Loss of 5 components [Vps28 and Tsg101 (ESCRT-I); Vps32, Vps20 and Vps2 (ESCRT-III)] resulted in accumulation of ubiquitinated cargoes in the anterior/primary lobe. Majority of the ESCRT components regulating ubiquitinated cargo status belonged to the terminally acting subunit of ESCRT-III. Loss of other 8 components did not affect the status of ubiquitinated cargo (Fig 5.4).

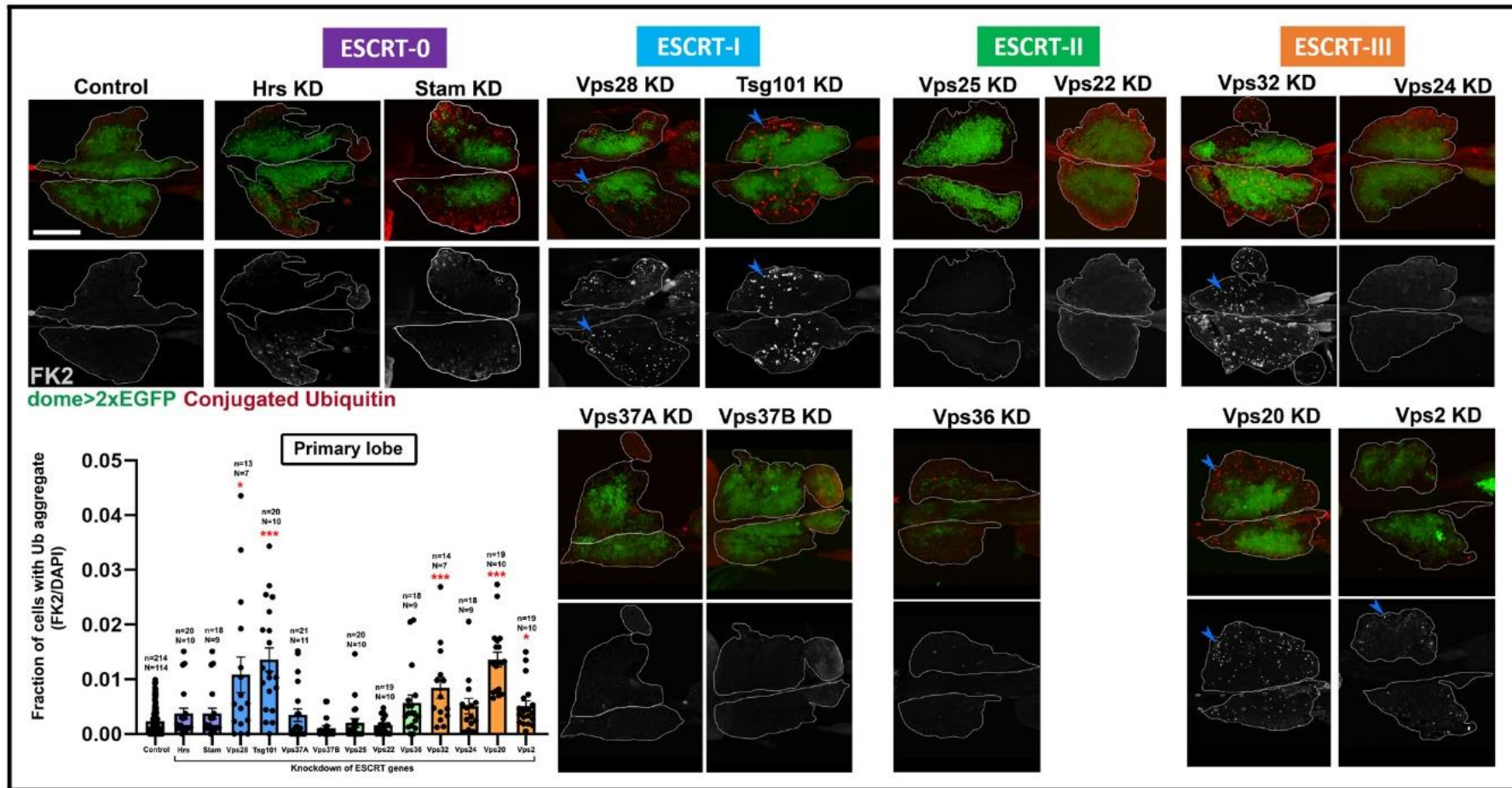


Figure 5.4 ESCRT components regulate ubiquitinated cargo sorting in the lymph gland primary lobe. Whole-mount larval lymph gland showing immunostaining for conjugated ubiquitin in the primary lobe upon knockdown of all 13 components of *Drosophila* ESCRT. Green and red mark progenitors (*dome*>2xEGFP) and conjugated ubiquitin respectively in the upper panel. Ubiquitin staining is shown in grayscale in the lower panel. Accumulation of ubiquitin aggregates is marked by arrowhead. Scale bar: 100 μ m. Bar diagram shows quantification of the fraction of cells accumulating ubiquitin aggregates in the primary lobe. n indicates the number of individual lobes analysed and N indicates the number of larvae analysed. Kruskal Wallis test was performed to determine the statistical significance. *P<0.05, ***P<0.001.

For a comprehensive analysis of ESCRT function in progenitor homeostasis, we additionally analysed the role of ESCRT in the posterior lobes as well. Knockdown of 4 ESCRT components [Vps28 and Vps37A (ESCRT-I); Vps22 (ESCRT-II) and Vps20 (ESCRT-III)] resulted in ubiquitinated cargo accumulation in the secondary lobe whereas 3 components (Vps37A, Vps22 and Vps20) affected the same in the tertiary lobe (Fig 5.5). This suggests reduced sensitivity of progenitor subsets from anterior to posterior. Active role in ubiquitinated cargo sorting in the blood progenitors indicates potential role of ESCRT in progenitor homeostasis.

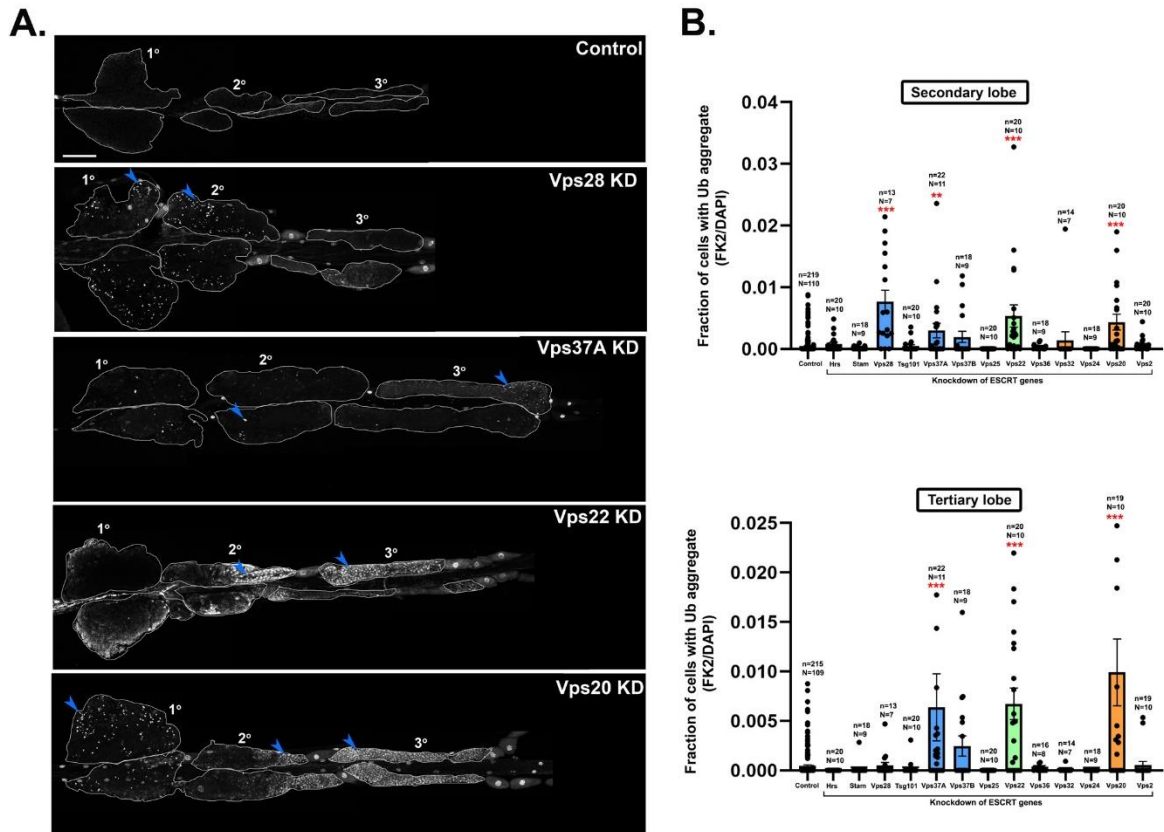


Figure 5.5 ESCRT components differentially regulate ubiquitinated cargo sorting across the lymph gland. (A) Whole-mount larval lymph gland showing conjugated ubiquitin accumulation (in grayscale) in the posterior lobes as marked by blue arrowhead upon progenitor-specific knockdown of ESCRT components Vps28 and Vps37A (ESCRT-I), Vps22 (ESCRT-II) and Vps20 (ESCRT-III). Scale bar: 100 μ m. (B) Bar diagram shows quantification of the fraction of cells accumulating ubiquitin aggregates in secondary and tertiary lobes upon knockdown of all 13 ESCRT components. n indicates the number of individual lobes analysed and N indicates the number of larvae analysed. Kruskal Wallis test was performed to determine the statistical significance. **P<0.01, ***P<0.001.

5.3.4 ESCRT components play distinct roles in progenitor maintenance and lineage-specific differentiation in the lymph gland.

As ESCRT components regulate ubiquitinated cargo sorting in the blood progenitors, they might potentially regulate progenitor homeostasis. Knockdown of 5 components [Vps28 and Tsg101 (ESCRT-I); Vps25, Vps36 (ESCRT-II) and Vps32 (ESCRT-III)] resulted in loss of progenitors in the primary lobe, interpreted through reduction in dome⁺ progenitor fraction (Fig 5.6). Knockdown of 4 ESCRT components [Vps28 (ESCRT-I); Vps22 and Vps36 (ESCRT-II)

and Vps32 (ESCRT-III)] upregulated plasmacyte (P1⁺) differentiation in the primary lobe. Plasmacyte differentiation increased concomitantly with reduction in progenitor fraction in the primary lobe upon knockdown of Vps28, Vps36 and Vps32 (Fig 5.6).

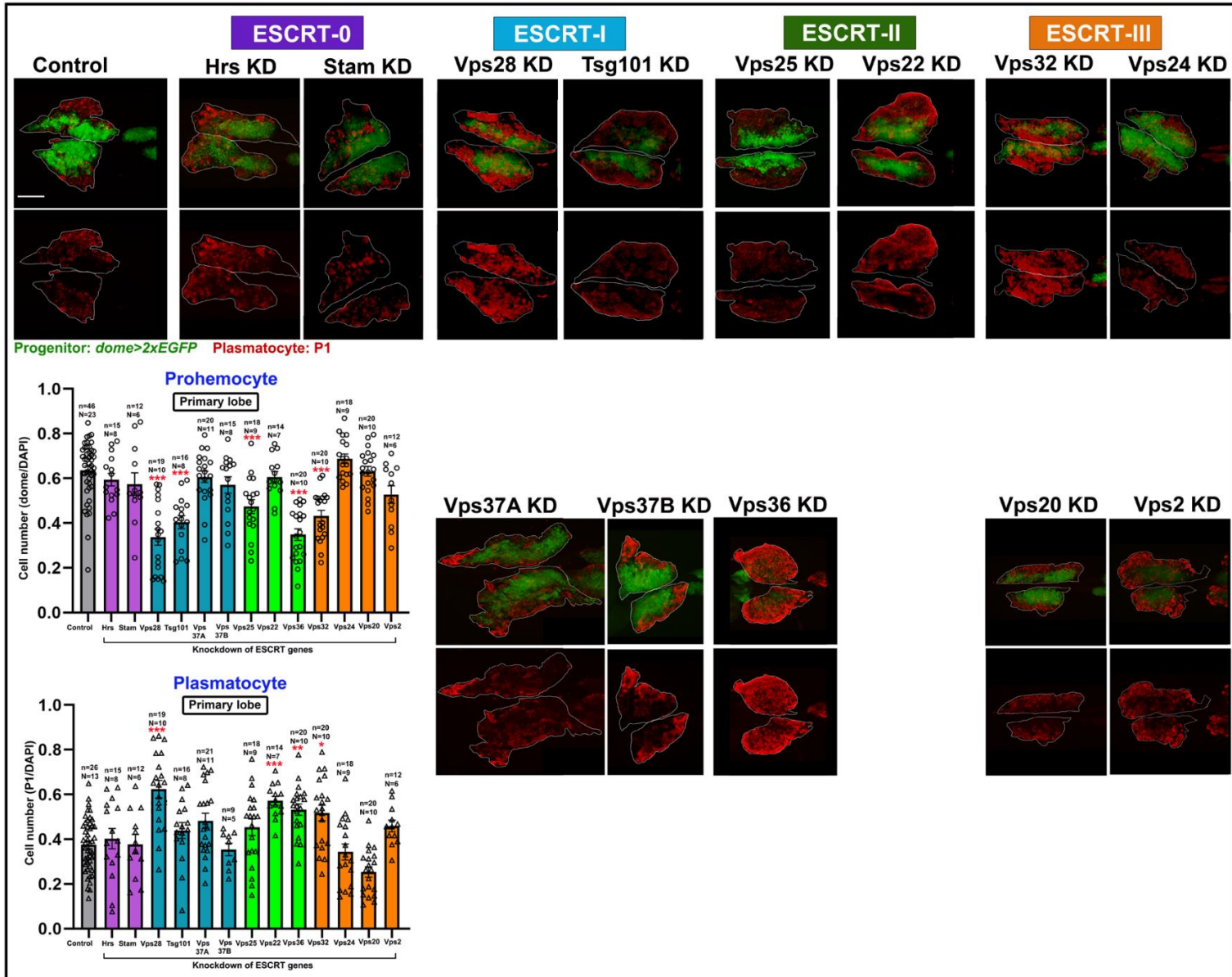


Figure 5.6 ESCRT components regulate progenitor maintenance and plasmatocyte differentiation in the lymph gland primary lobe. Whole-mount larval lymph gland showing dome^{>2}EGFP⁺ve progenitors and P1⁺ve plasmatocytes (red) in primary lobes upon progenitor-specific knockdown of all 13 ESCRT components. Scale bar: 100 μm. Bar diagram shows quantification of the fraction of progenitors and plasmatocytes in the primary lobe upon knockdown of 13 ESCRT components. n indicates the number of individual lobes analysed and N indicates the number of larvae analysed. Kruskal Wallis test was performed to determine the statistical significance. *P<0.05, **P<0.01, ***P<0.001.

Analysis of progenitor and plasmatocyte fraction in the posterior lobes showed loss of progenitors in the secondary lobe upon knockdown of 7 components [Stam (ESCRT-0); Vps28, Tsg101, Vps37A (ESCRT-I); Vps36 (ESCRT-II); Vps32, Vps2 (ESCRT-III)] (Fig 5.7A, B). Vps28, Tsg101, Vps36 and Vps32 affected progenitor fraction in both primary and secondary lobe. Knockdown of only Vps36 and Vps2 led to decrease in progenitor fraction in the tertiary lobe (Fig 5.7 A, B). This supports the refractile nature of dome⁺ progenitors in the tertiary lobe. Plasmatocyte differentiation increased in the secondary lobe upon knockdown of 6 components [Hrs (ESCRT-0); Vps28 and Vps37A (ESCRT-I); Vps36 (ESCRT-II); Vps32 and Vps2 (ESCRT-III)] (Fig 5.7 A, C). Vps28, Vps37A, Vps36, Vps32 and Vps2 depletion caused an increase in plasmatocyte differentiation concomitant with reduction in progenitor fraction in the secondary lobe. Knockdown of only one components [Vps28 (ESCRT-I)] increased plasmatocyte differentiation in the tertiary lobe (Fig 5.7A, C).

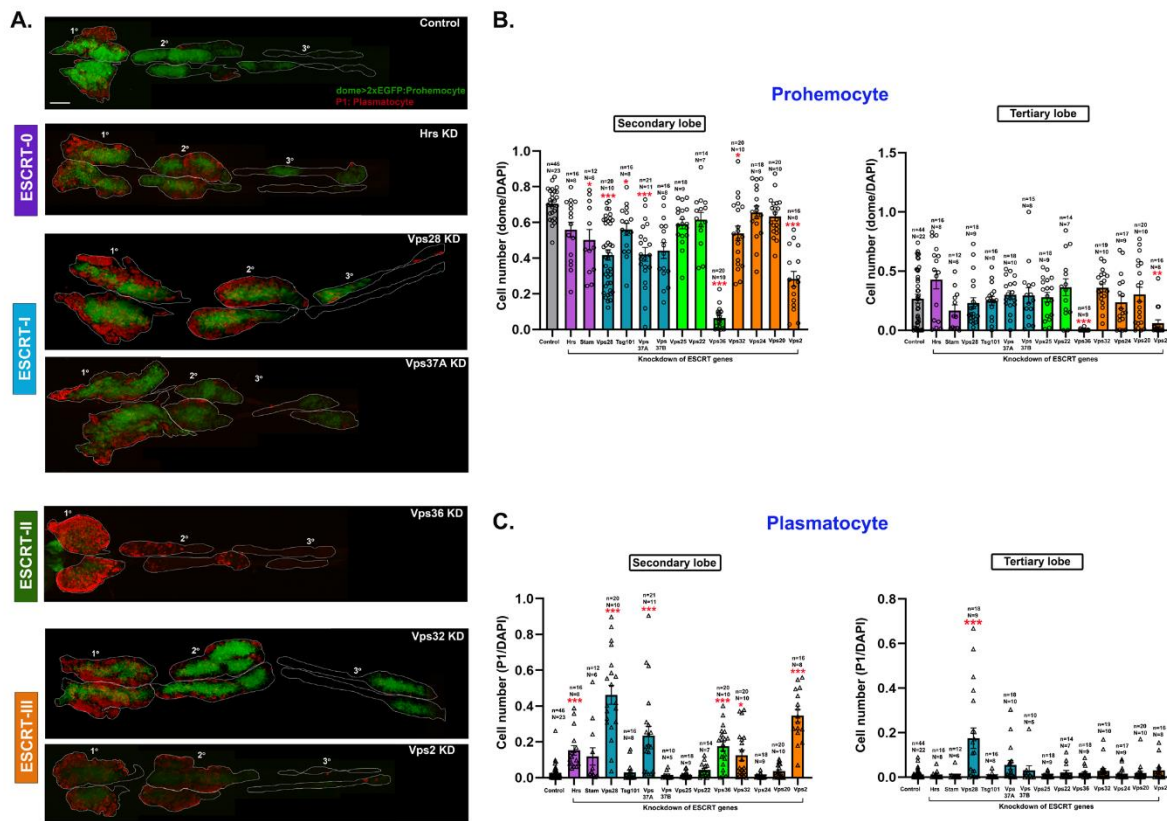


Figure 5.7 ESCRT components differentially regulate plasmatocyte differentiation across the lymph gland. (A) Whole-mount larval lymph gland showing P1 staining (red) to mark plasmatocytes in the posterior lobes upon progenitor-specific knockdown of ESCRT components Hrs (ESCRT-0), Vps28 and Vps37A (ESCRT-I), Vps36 (ESCRT-II), Vps32 and Vps2 (ESCRT-III). Scale bar: 100 μ m. (B-C) Bar diagram shows quantification of dome>2xEGFP+ve progenitor fraction (B) and plasmatocyte fraction (C) in secondary and tertiary lobes upon knockdown of 13 ESCRT components. n indicates the number of individual lobes analysed and N indicates the number of larvae analysed. Kruskal Wallis test was performed to determine the statistical significance. *P<0.05, **P<0.01, ***P<0.001.

ESCRT depletion predisposed progenitors to crystal cell differentiation in a robust manner. Knockdown of 12 components [Hrs, Stam (ESCRT-0); Vps28, Tsg101, Vps37A, Vps37B (ESCRT-I); Vps22, Vps36 (ESCRT-II) and Vps32, Vps24, Vps20, Vps2 (ESCRT-III)] resulted in increased crystal cell (ProPO⁺) differentiation in the primary lobe (Fig 5.8). However, knockdown of only 4 components [Hrs (ESCRT-0), Vps28 (ESCRT-I), Vps36 (ESCRT-II) and Vps2 (ESCRT-III)] led to crystal cell differentiation in the secondary lobe (Fig 5.9A, B). Also, knockdown of only 2 components [Vps28 (ESCRT-I) and Vps36 (ESCRT-II)] resulted in crystal cell differentiation in the tertiary lobe (Fig 5.9A, B).

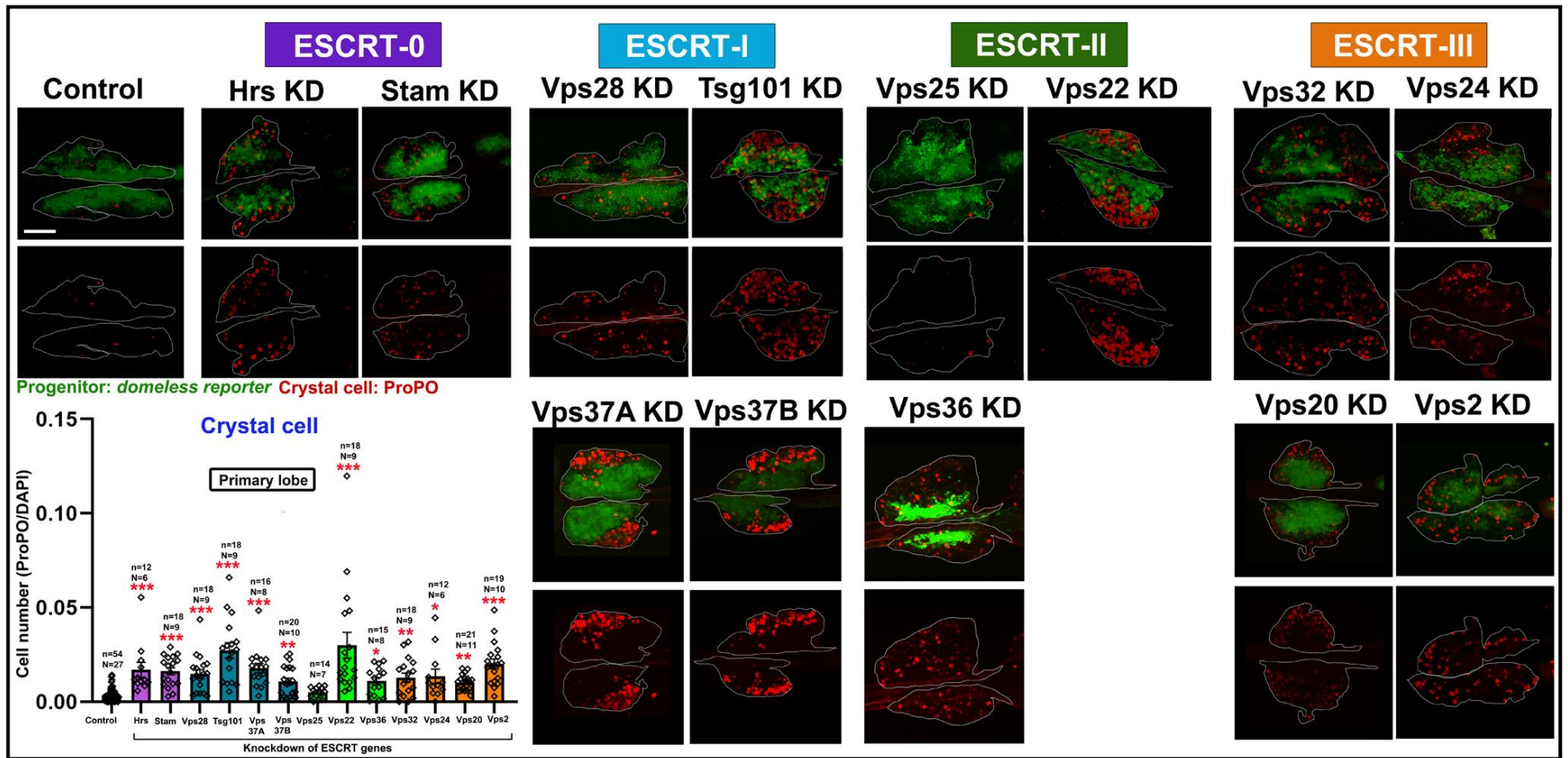


Figure 5.8 ESCRT components differentially regulate crystal cell differentiation in the lymph gland primary lobe. Whole-mount larval lymph gland showing dome+ve progenitors and ProPO+ve crystal cells (red) in primary lobes upon progenitor-specific knockdown of all 13 ESCRT components. Scale bar: 100 μ m. Bar diagram shows quantification of the fraction of crystal cells in the primary lobe upon knockdown of 13 ESCRT components. n indicates the number of individual lobes analysed and N indicates the number of larvae analysed. Kruskal Wallis test was performed to determine the statistical significance. *P<0.05, **P<0.01, ***P<0.001.

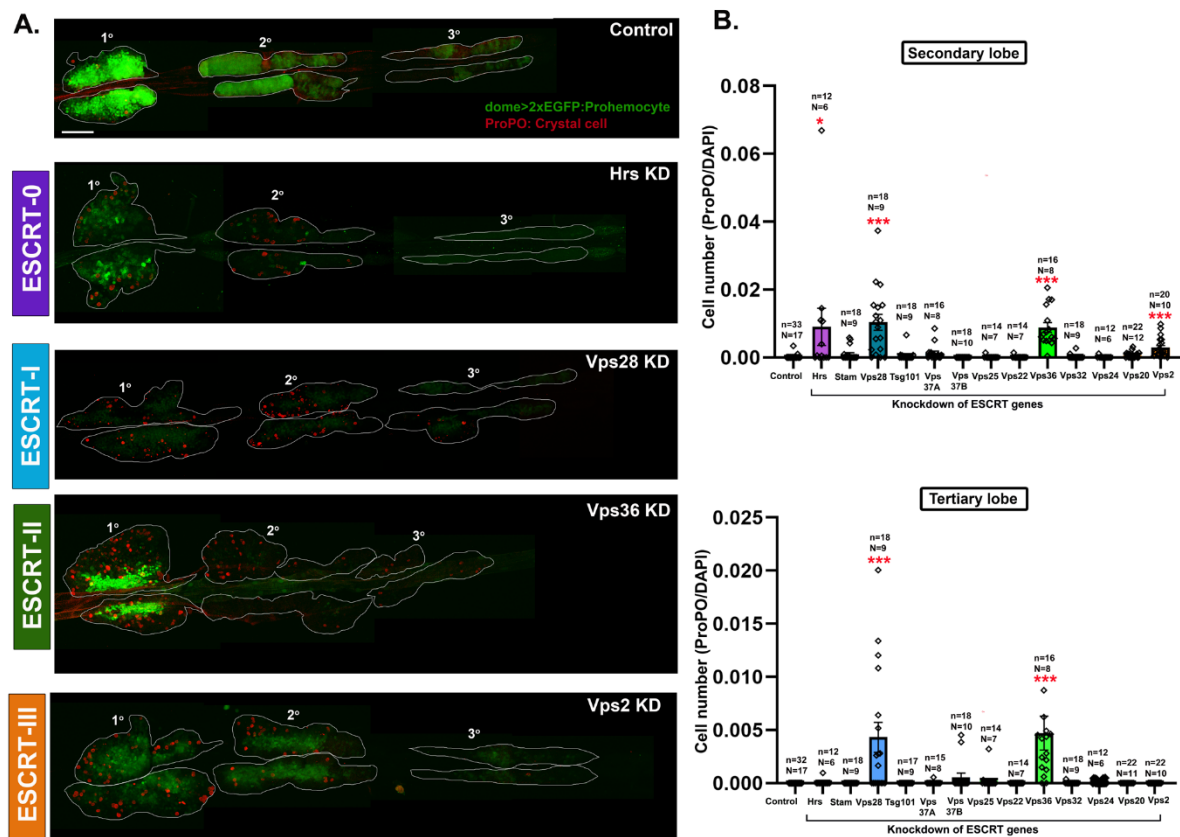


Figure 5.9 ESCRT components regulate crystal cell differentiation across the lymph gland. (A) Whole-mount larval lymph gland showing ProPO staining (red) to mark crystal cells in the posterior lobes upon progenitor-specific knockdown of ESCRT components Hrs (ESCRT-0), Vps28 (ESCRT-I), Vps36 (ESCRT-II) and Vps2 (ESCRT-III). Scale bar: 100 μ m. (B) Bar diagram shows quantification of crystal cell fraction in secondary and tertiary lobes upon knockdown of 13 ESCRT components. n indicates the number of individual lobes analysed and N indicates the number of larvae analysed. Kruskal Wallis test was performed to determine the statistical significance. *P<0.05, ***P<0.001.

Lamellocytes are rarely present in larva without any wasp infestation. However, progenitor-specific knockdown of 5 ESCRT components [Tsg101 and Vps37A (ESCRT-I); Vps36 (ESCRT-II); Vps32 and Vps2 (ESCRT-III)] induced lamellocyte differentiation in the primary lobe, as visualized by Phalloidin (F-actin) staining, even without any immune challenge (Fig 5.10). Only 2 components (Vps36 and Vps2) caused lamellocyte differentiation in the secondary lobe when knocked down and only Vps36 knockdown triggered lamellocyte differentiation in the tertiary lobe (Fig 5.11A, B).

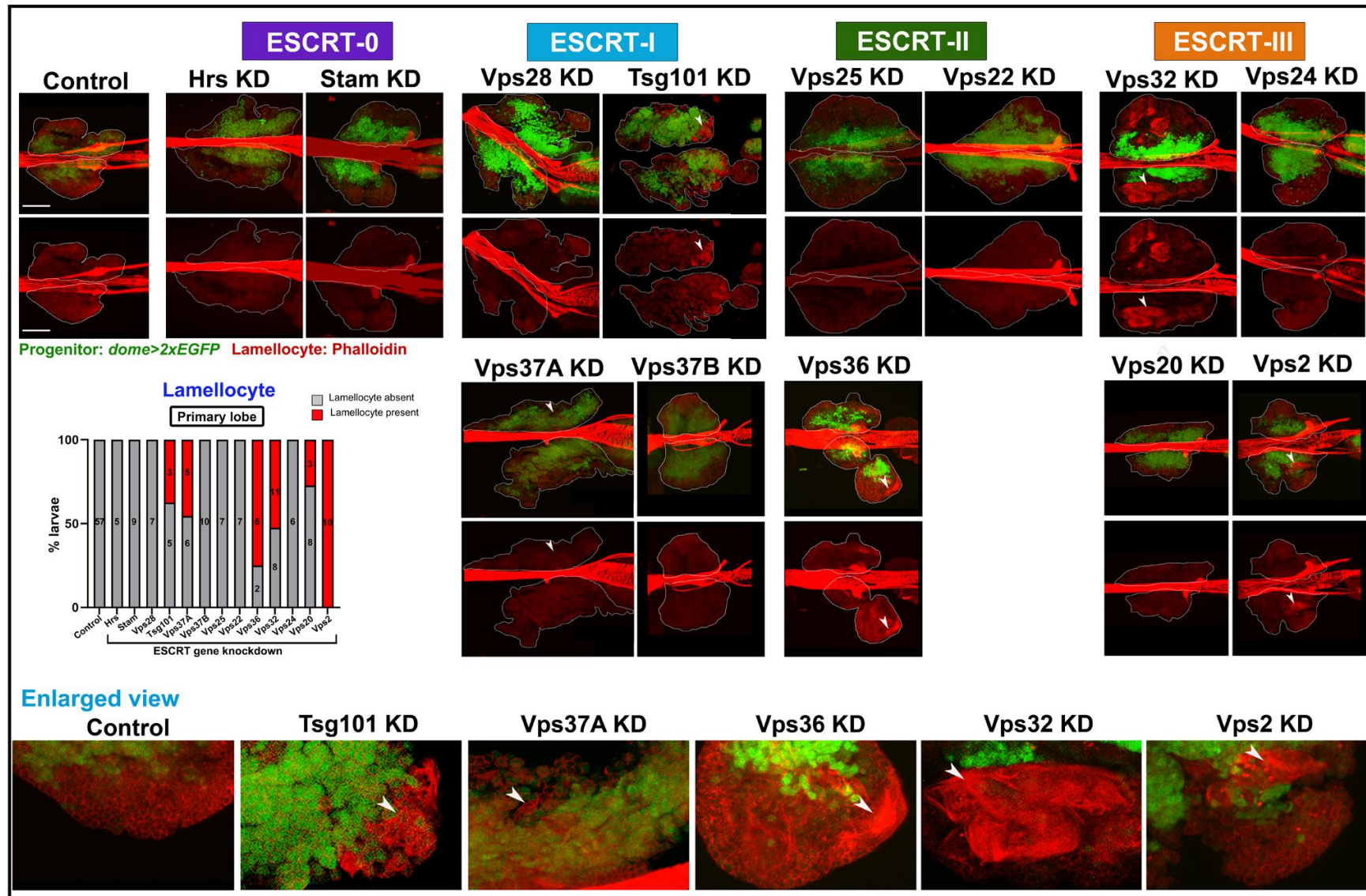


Figure 5.10 ESCRT components regulate lamellocyte differentiation in the lymph gland primary lobe. Whole-mount larval lymph gland showing Phalloidin staining (red) to visualise elongated morphology of lamellocytes in primary lobes upon progenitor-specific knockdown of all 13 ESCRT components. Arrowheads mark the region magnified in the lower panel. The lowermost image panel shows enlarged view of Phalloidin staining with lamellocytes marked by arrowhead in control and progenitor-specific knockdown of Tsg101 and Vps37A (ESCRT-I), Vps36 (ESCRT-II), Vps32 and Vps2 (ESCRT-III). Scale bar: 100 μ m. Bar diagram shows quantification of the percentage of lymph glands showing lamellocyte differentiation in the primary lobe, even without immune challenge. Values in the bar indicate the number of larvae analysed for presence or absence of lamellocytes.

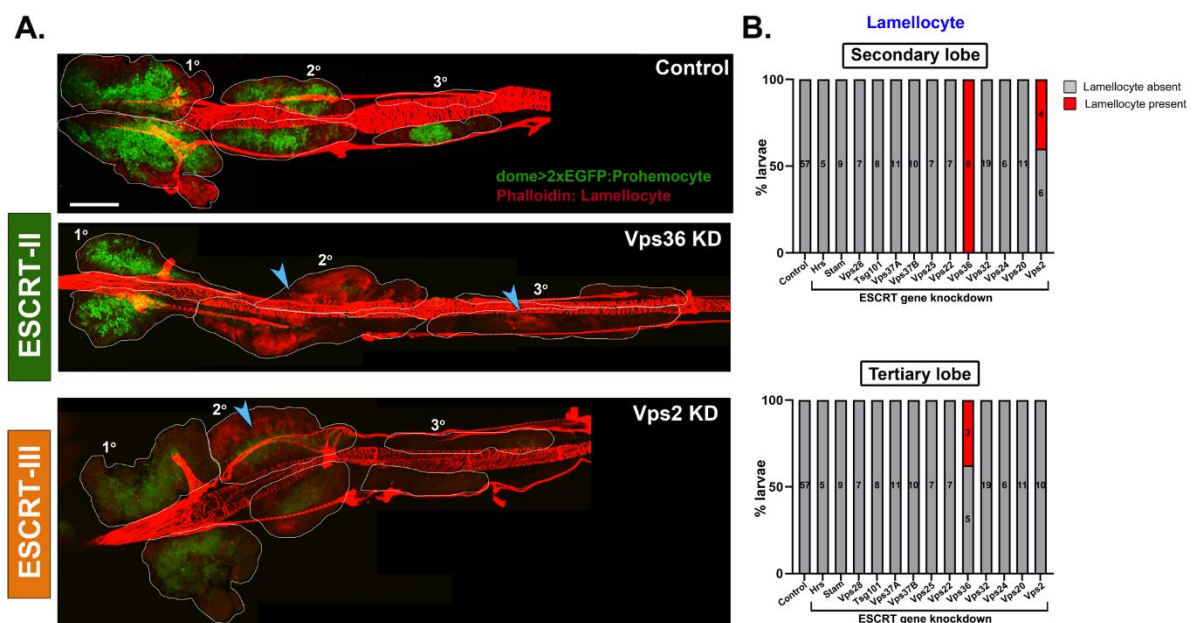


Figure 5.11 ESCRT components differentially regulate lamellocyte differentiation across the lymph gland. (A) Whole-mount larval lymph gland showing Phalloidin staining (red) to visualise lamellocytes marked by arrowhead in the posterior lobes upon progenitor-specific knockdown of ESCRT components Vps36 (ESCRT-II) and Vps2 (ESCRT-III). Scale bar: 100 μ m. (B) Quantification of the percentage of lymph glands showing lamellocyte differentiation in the secondary and tertiary lobes even without immune challenge. Values in the bar indicate number of larvae analysed for presence or absence of lamellocytes.

Our extensive analysis of blood cell differentiation profile for different ESCRT component depletion across all progenitor subsets of the lymph gland yields a functional map that reflects distinct role of ESCRT components in lineage choice (Fig 5.12A). Such phenotypic diversity of co-expressing ESCRT components indicates post-transcriptional control of

individual ESCRT function. Also, in corroboration with the previous claim of refractile nature of posterior progenitors (Rodrigues et al., 2021), the map reflects reduced progenitor sensitivity from anterior to posterior lobes of the lymph gland. Posterior lobe progenitors do not differentiate to lamellocytes even upon immune challenge with wasp (Rodrigues et al., 2021). However, depletion of Vps36 and Vps2 could trigger lamellocyte differentiation in these refractile progenitor pools. ESCRT most strongly influenced crystal cell differentiation out of the three blood cell lineages. The map sets up the basis to probe further the role of ESCRT in regulating lineage-specific signaling activation.

Additionally, we performed a correlation analysis of the ubiquitin accumulation and blood cell differentiation phenotypes upon ESCRT knockdown (Fig 5.12B). A Venn diagram-based correlation map shows that only 5 out of the 12 components that affected crystal cell differentiation in the primary lobe caused ubiquitin accumulation. This suggests of two possibilities:

- 1) The ubiquitination status of the accumulated cargo may not be an important regulator of cell fate.
- 2) The effect of different ESCRT components on endosomal sorting may be cargo-specific and may follow different dynamics of ubiquitination and deubiquitination.
- 3) Functions other than the endosomal protein sorting may also contribute to crystal cell differentiation upon depletion of certain ESCRT components.

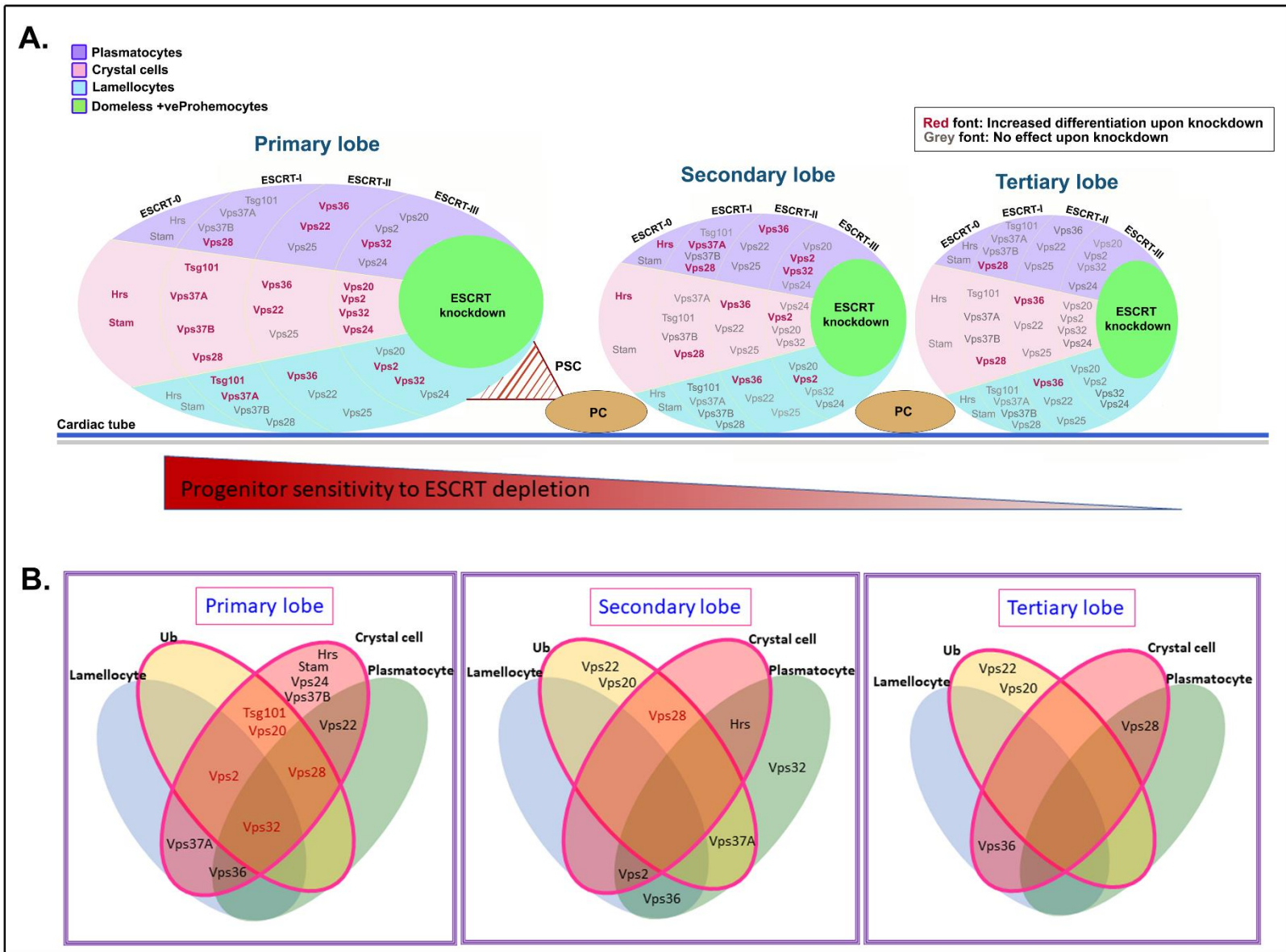


Figure 5.12 A functional map of ESCRT components in cargo sorting and lineage-specific differentiation in the *Drosophila* lymph gland. (A) Schematic shows a cartoon representation of lymph gland lobes from anterior to posterior (left to right). Green region in each lobe represents the progenitor pool where RNAi-mediated knockdown for different ESCRT genes (13 genes from ESCRT-0, I, II and III) has been driven. The different blood cell types are shown in three different colors: violet (plasmatocytes), pink (crystal cells) and blue (lamellocytes). If knockdown of any given ESCRT component upregulates differentiation to a particular lineage, the name of that component is written in red font in the respective color-coded zone. Components that are dispensable for specification of a given blood cell type are written in gray font in respective color-coded region. The heatmap represents sensitivity of the progenitor subsets across the lymph gland upon depletion of ESCRT. (B) Venn diagram shows correlation of ubiquitin accumulation and blood cell differentiation phenotypes for all 13 ESCRT components. Red bordered circles mark phenotypes of crystal cell differentiation and ubiquitin accumulation.

Our analyses indicate complex regulation of the ubiquitous ESCRT machinery to fine-tune lineage specification process. The role of various components in lineage-specific signaling activation and any possible link between ubiquitination of cargoes and progenitor differentiation merit further investigation.

5.3.5 ESCRT cell-autonomously regulates ubiquitinated cargo sorting in blood progenitor.

As shown in section 5.3.2, progenitor-specific downregulation of ESCRT expression leads to the accumulation of ubiquitinated cargoes. However, majority of the ubiquitin aggregates accumulated in dome⁻ region, suggesting a possible cell non-autonomous effect. However, a cell-autonomous function of ESCRT can also trigger such pattern of ubiquitin accumulation if the progenitor cells lose domeless marker expression upon ubiquitin accumulation (Fig 5.13). To test this hypothesis, we used mitotic recombinant clones of a representative ESCRT gene Vps32 (shrub). We generated a progenitor-specific homozygous clone for Vps32 loss of function mutation in the lymph gland. Staining for conjugated ubiquitin revealed accumulation of ubiquitin aggregates in the homozygous mutant patch of the tissue (GFP-ve) indicating a cell-autonomous role of Vps32 in cargo sorting in blood progenitors (Fig 5.14A, B). Hence, temporally regulated cell-autonomous function of ESCRT in the progenitors may contribute to accumulation of ubiquitin in the dome⁻ region of the lymph

gland. This validates our working model and suggests that despite a decrease in domeless expression in the mutant or knockdown cells, the ubiquitin aggregations may persist.

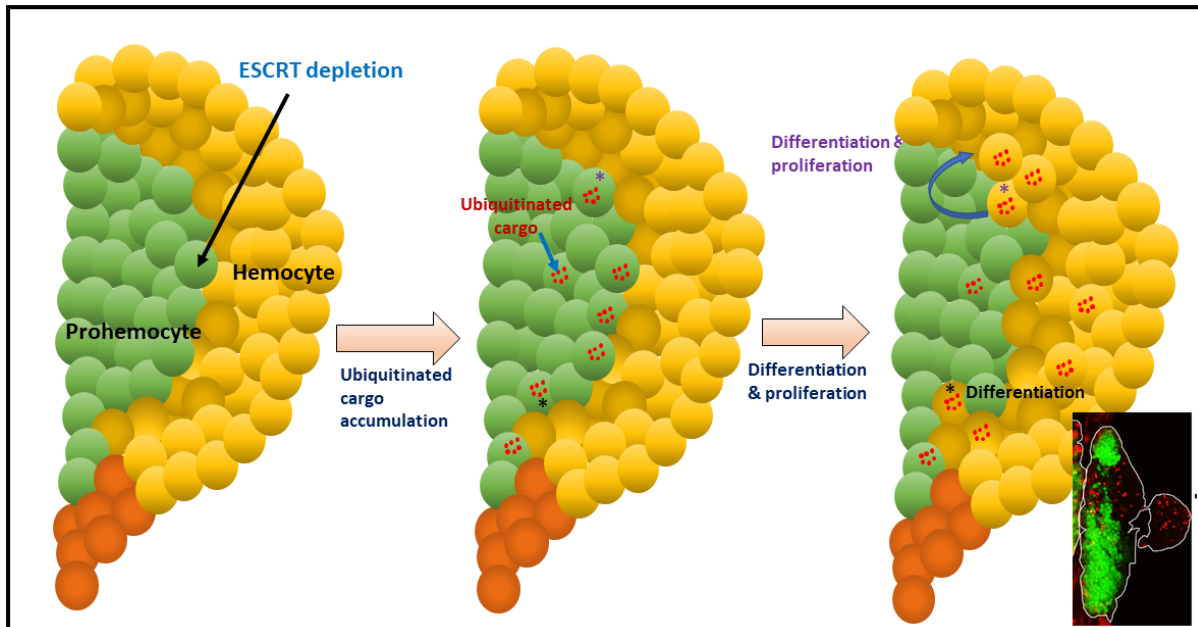


Figure 5.13 Hypothetical model for cell-autonomous function of ESCRT in the lymph gland progenitors. The schematic explains an apparently ectopic cargo accumulation phenotype of ESCRT knockdown in lymph gland progenitors (inset shows representative image for ubiquitin accumulation in Vps32 knockdown primary lobe). Knockdown of ESCRT in the progenitors may result in accumulation of ubiquitinated cargoes in a cell-autonomous manner, eventually leading to loss of progenitor marker, differentiation and proliferation, but still not clearing off the cargo accumulation defect. This may cause cargo accumulation in dome-ve non-progenitor cell population despite knockdown in dome+ve population.

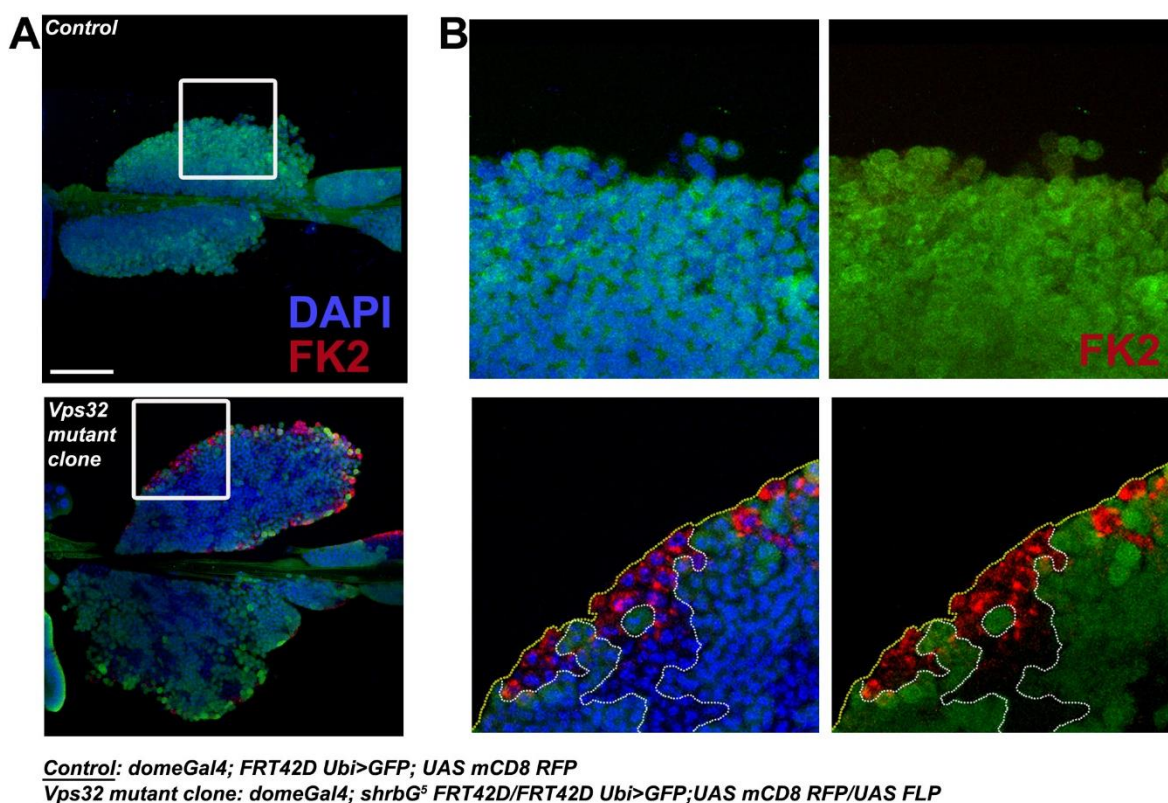


Figure 5.14 ESCRT cell-autonomously regulates ubiquitinated cargo sorting in the lymph gland progenitors. Immunostaining for conjugated ubiquitin (red) in progenitor-specific mutant clone of representative ESCRT component *Vps32/shrub* shows cell-autonomous accumulation of ubiquitinated cargoes in GFP-ve homozygous mutant cell population (marked by dotted white line; yellow line marks tissue boundary). Panels towards the right side represent insets of the boxed area with a magnified view. Scale bar:100 μm .

5.3.6 ESCRT regulates blood cell differentiation in cell non-autonomous manner as well.

We analysed blood cell differentiation in blood progenitor-specific mitotic clone of ESCRT. *Vps32* knockdown results in increased crystal cell differentiation and triggers lamellocyte differentiation as described in section 5.3.3. ProPO staining showed both wild type and mutant origin of crystal cells as revealed by overlap with GFP expression in the mutant tissue (Fig 5.15A). As crystal cells are usually present in the lymph gland in a few numbers, it does not convincingly indicate whether ESCRT regulates increased differentiation in a cell-autonomous manner. However, lamellocytes are absent in the control lymph gland (Fig 5.15B). Phalloidin staining in the *Vps32* mutant clone showed GFP+ve elongated or coalescing cells, mimicking lamellocyte morphology (Fig 5.15B). This suggests non-

autonomous regulation of lamellocyte differentiation by ESCRT. Hence, ESCRT may regulate blood cell differentiation in both cell-autonomous and non-autonomous manner.

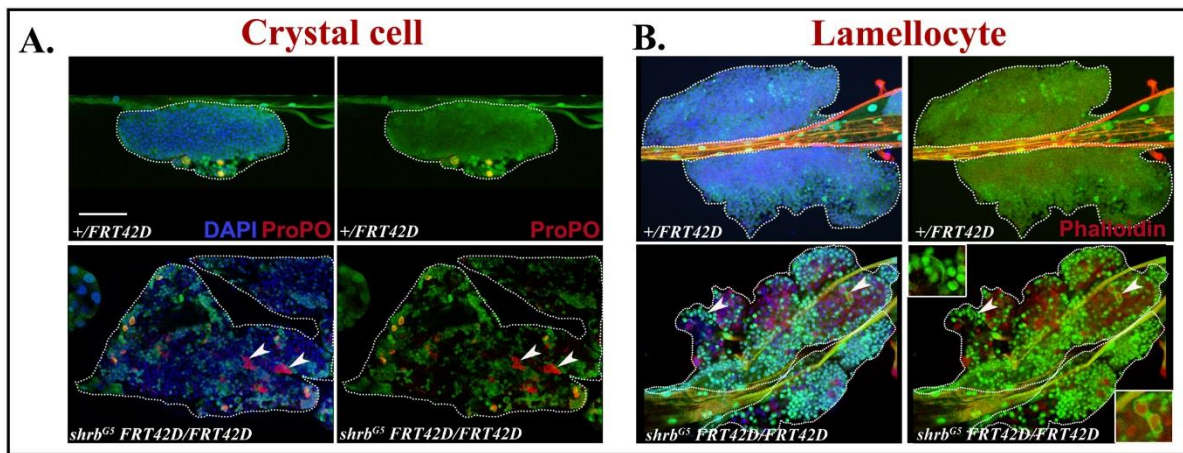


Figure 5.15 ESCRT may regulate progenitor differentiation in both cell-autonomous and cell non-autonomous manner. (A) Primary lobe of control (*domeGal4/+; neoFRT42D/+; UAS mCD8 RFP/+*) and *Vps32* mutant clone (*domeGal4/+; shrb^{G5} neoFRT42D/neoFRT42D; UAS mCD8 RFP/UAS FLP*) showing ProPO staining (red) to mark crystal cells. Arrowheads mark the crystal cells which are GFP-ve and reflect cell-autonomous origin from homozygous mutant progenitors. (B) Phalloidin staining in the same genotypes shows GFP+ve elongated and coalescing cells marked by arrowheads (insets) in the mutant clone, indicating cell non-autonomous origin. Scale bar: 100 μ m.

5.3.7 *Vps25* is dispensable for lineage-specification of the blood progenitors in the lymph gland

To our surprise, *Vps25* knockdown did not affect the status of ubiquitination, progenitor maintenance or differentiation to any particular blood cell lineage despite its expression in the lymph gland. We verified this result using other RNAi line for *Vps25* (BDSC 26286) (Fig 5.16). Additionally, we generated lymph gland progenitor-specific mitotic clone of *Vps25* loss of function mutation (*Vps25^{A3}*). We observed no accumulation of ubiquitin aggregates (Fig 5.17A) or any change in the status of the progenitor (Fig 5.17B), plasmacyte (Fig 5.17C), crystal cell (Fig 5.17D) and lamellocyte differentiation (Fig 5.17E). However, the mutant lymph glands showed enlargement of the primary lobe, suggesting possible increase in blood cell proliferation upon loss of *Vps25* [results on lobe size and the status of

proliferation marker are discussed in the next chapter (Chapter 6)]. Also, phalloidin staining revealed appearance of binucleate, large cells and also very small cells occasionally, along with increase in F-actin content in some patches of the tissue, mostly in a cell autonomous manner (visible in GFP negative area of the tissue) (Fig 5.17E). Hence, Vps25 possibly inhibits uncontrolled cell proliferation and may contribute to critical steps of cell division that may dictate cell shape, number and also polarity. These mechanistic aspects demand further investigation in future to understand the differential function of ESCRT components.

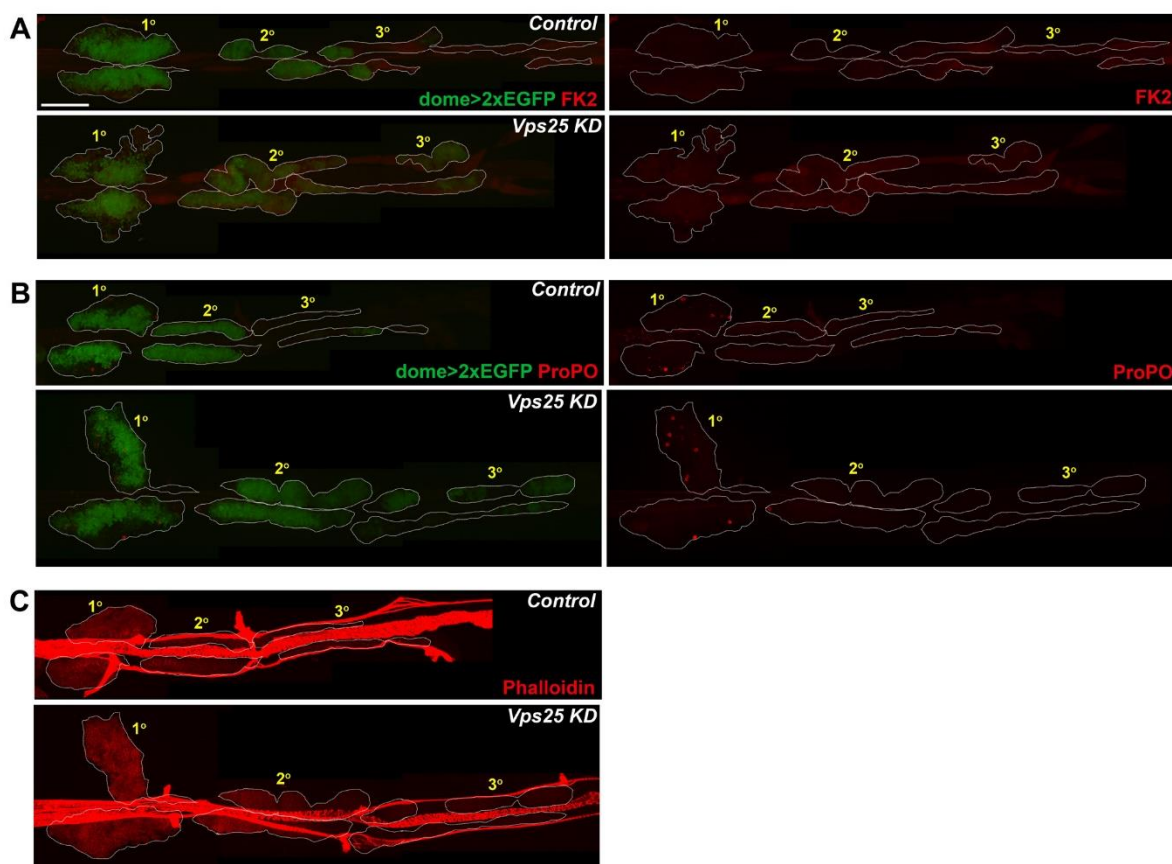
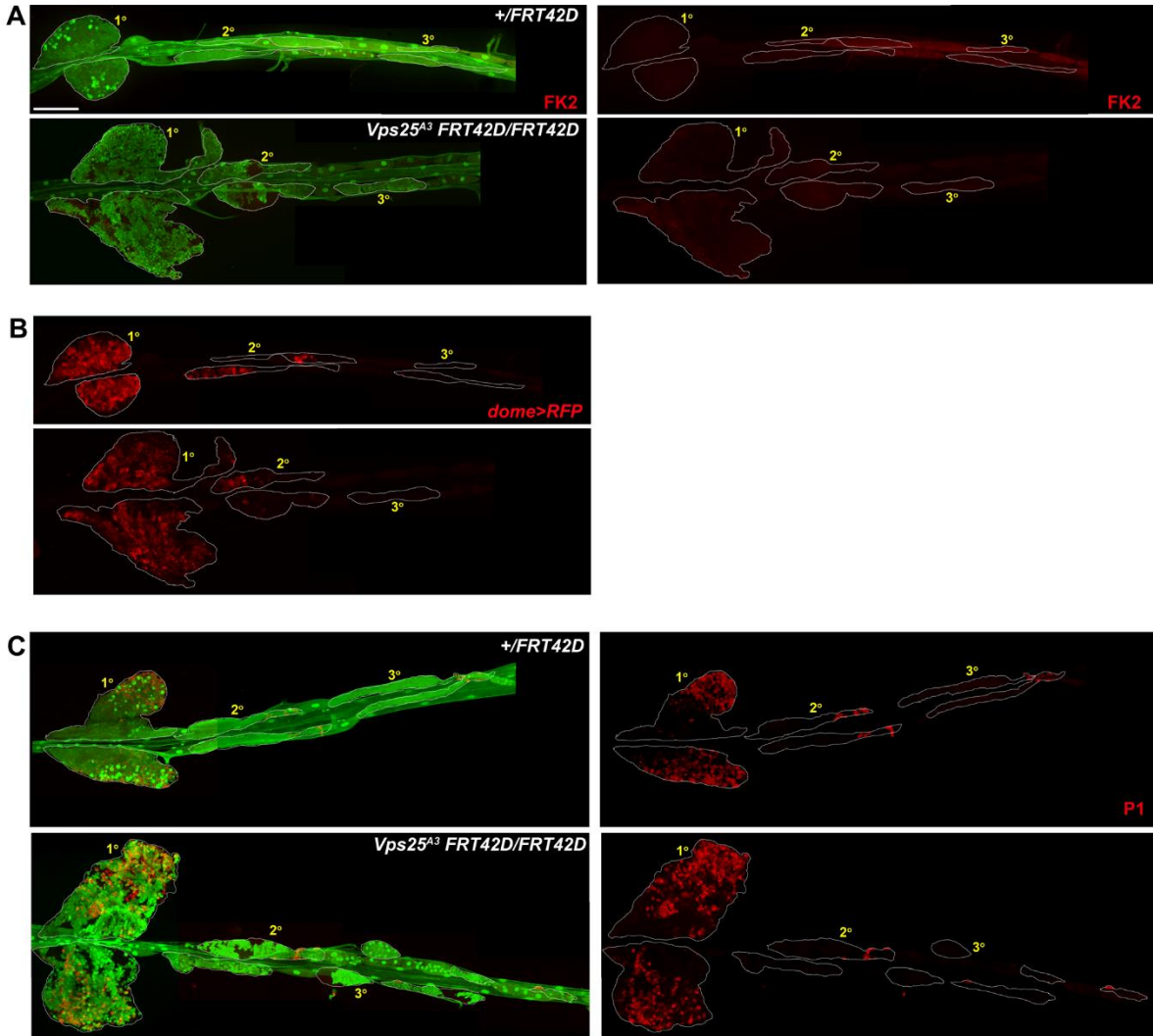


Figure 5.16. Vps25 knockdown in the blood progenitor does not affect ubiquitination or blood cell differentiation. (A) Whole mount lymph gland showing staining for conjugated ubiquitin in control (*domeGal4 UAS 2xEGFP*) and Vps25 knockdown (*domeGal4 UAS 2xEGFP;; UAS Vps25 RNAi*) lymph gland. *dome>2xEGFP* expression marks the progenitors. (B) ProPO staining marks crystal cells in the same genotypes. (C) Phalloidin staining was used to visualize lamellocytes based on their elongated morphology. Scale bar: 100 μm.



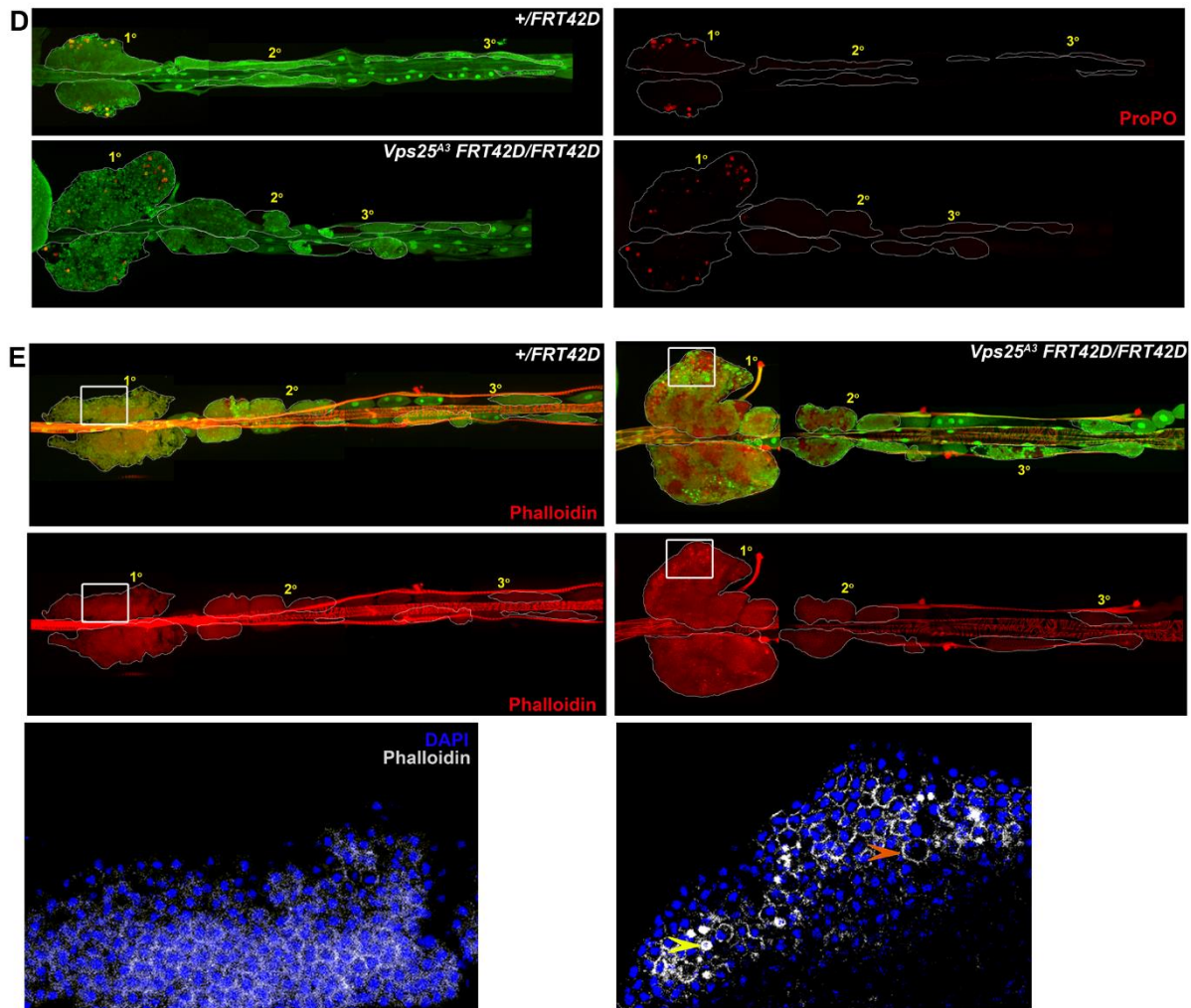


Figure 5.17. Vps25 homozygous mutant clone does not affect ubiquitination and blood cell differentiation in the lymph gland. (A) Whole mount lymph gland showing staining for conjugated ubiquitin in control (*domeGal4; FRT42D Ubi>GFP; UAS mCD8 RFP*) and Vps25 mutant clone (*domeGal4/+; Vps25^{A3}FRT42D/FRT42D Ubi>GFP; UAS mCD8 RFP/UAS FLP*) lymph gland. GFP expression marks the wild type twin-spot while GFP negative region marks the homozygous mutant clone. (B) *dome>RFP* marks the progenitor in the same genotype, (C) P1 marks plasmatocytes, and (D) ProPO marks crystal cells. (E) Phalloidin staining was used to visualize lamellocytes based on their elongated morphology. Bottom-most panel shows enlarged view of the boxed region from control and mutant lymph glands. Phalloidin staining is shown in grayscale. DAPI marks the nuclei. The orange arrowhead marks a big binucleate cell while the yellow arrowhead marks a very small cell with high F-actin expression. Scale bar: 100 μm.

5.4 Discussion

Our study shows the active role of the conserved regulator of endosomal protein sorting, ESCRT in hematopoietic homeostasis using *Drosophila* as an *in vivo* model. The detailed functional map of all 13 ESCRT components in lymph gland hematopoiesis highlights distinct role of individual components in lineage-specific differentiation of the progenitors. The map also elucidates the specific steps of endosomal protein sorting that could play the most crucial role in signaling activation in the blood progenitors. BloodSpot Leukemia MILE study shows misexpression of ESCRT in various hematological disorders including acute myeloid leukemia and myelodysplastic syndrome (<https://servers.binf.ku.dk/bloodspot/>).

Consistent with previous studies, our data shows that ESCRT-I and ESCRT-III play the most critical role in progenitor differentiation. The robust contribution of ESCRT-III toward the specification of all three blood lineages may be consequent to its critical role in the final step of membrane scission that can control the endosomal sorting of a wide range of signaling receptors. Also, ESCRT-I appears as an indispensable functional subunit in the blood progenitors, similar to ESCRT-III. Apart from endosomal protein sorting, other membrane remodelling functions of ESCRT-I and III could also impact signaling pathways and lineage choice. Recent reports highlight the universal role of ESCRT-III, often in concert with ESCRT-I, in various ESCRT-dependent membrane remodelling processes such as nuclear envelope reformation, lysosomal membrane repair, cytokinetic abscission, macroautophagy and exocytosis (Vietri et al., 2020). These additional functions may also contribute to the phenotypic diversity of ESCRT in lineage choice.

A previous report shows that Hrs and Stam, although regulate Notch trafficking, do not regulate Notch pathway activation and downstream phenotypes such as cell polarity and proliferation in epithelial tissue, suggesting a context-dependent role of ESCRT-0 to regulate signaling and cell fate (Tognon et al., 2014). Though Hrs and Stam depletion promoted crystal cell differentiation in the lymph gland, it hardly affected plasmacyte and lamellocyte differentiation. ESCRT-II component Vps25 knockdown did not affect the status of ubiquitinated cargo or any of the blood cell lineages suggesting bypass mechanisms to

regulate endosomal protein sorting. ALIX and HD-PTP mediate ESCRT-III assembly in yeast and mammalian cells, bypassing the need of ESCRT-II (Bissig et al., 2014; Taberner et al., 2018). Also, ALIX and its yeast homolog Bro1 can recognize non-ubiquitinated cargoes and sort them independent of ESCRT-0 (Pashkova et al., 2013). The existence of such bypass routes and post-translational regulatory mechanisms in blood progenitors is not yet explored and might explain functional redundancy of certain ESCRT components in lineage specification.

Progenitor subsets differentially respond to depletion of ESCRT components supporting previous reports on progenitor heterogeneity across the lymph gland (Rodrigues et al., 2021; Ray et al., 2021). Though components from all ESCRT subunits regulate plasmacyte and crystal cell differentiation, only ESCRT-II and ESCRT-III affected differentiation of lamellocytes in secondary and tertiary lobes. Vps36 and Vps2 depletion triggered lamellocyte differentiation in the secondary lobe which is refractile to immune challenge. Also, Vps28 and Vps36 emerge as regulator of blood cell differentiation in the tertiary lobe. Limited regulators of ubiquitinated cargo sorting and lineage choice may explain a post-translational organelle level control of differentiation in the refractile progenitors. This provides new candidates for screening modulators of blood regeneration *in vitro* as well as *in vivo*.

Ubiquitination may impact the fate of endosomal cargoes in several ways. Monoubiquitination can promote cargo endocytosis and lysosomal degradation (Mukai et al., 2012; Swatek and Komander, 2016). NICD is an endomembrane associated cargo that acts as the key signaling component for Notch signaling. Several E3 ubiquitin ligases and deubiquitinases of Notch have been implicated so far in the activation of Notch pathway (Moretti et al., 2013). The E3 ubiquitin ligase Deltex positively regulate Notch pathway in a ligand-independent manner (Diederich et al., 1994). Also, Deltex acts in synergy with ESCRT-III component Vps32 in the *Drosophila* wing disc to fine-tune Notch signaling (Hori et al., 2011). On the other hand, Notch-specific deubiquitinase eIF3f1 acts downstream to Deltex and promote γ -secretase-dependent cleavage of NICD from endosome surface, thus

upregulating Notch pathway (Moretti et al., 2010). Though depletion of 7 components [Hrs and Stam (ESCRT-0); Vps37A and Vps37B (ESCRT-I); Vps22 and Vps36 (ESCRT-II); Vps24 (ESCRT-III)] can affect differentiation of at least one of the blood cell lineages in the primary lobe, they do not affect the status of ubiquitinated cargo. This brings up the question whether the status of cargo ubiquitination contributes to the activation of signaling pathways downstream to ESCRT. Existence of possible genetic interaction between ESCRT and regulators of ubiquitination in the blood progenitors merits further investigation.

Loss of function mutation in ESCRT genes result in cell-autonomous cargo accumulation in *Drosophila* epithelial tissues (Vaccari et al, 2009; Herz et al, 2009). However, cell non-autonomous role of ESCRT in cell proliferation as well as neoplastic transformation suggests altered intercellular communication and aberrant signaling activation in the neighboring cell population (Vaccari and Bilder, 2005; Vaccari et al, 2009; Herz et al, 2009). In concordance with the previous reports, we observed cell-autonomous role of ESCRT in regulating ubiquitinated cargo sorting in the progenitors. However, analysis of crystal cell and lamellocyte differentiation suggests non-autonomous role of ESCRT as well in lineage-specification. This may be attributed to signals emanating from the mutant cell population that dictate cell fate choice in the surrounding population. Mutant cells may accumulate signaling ligands that could potentially affect the neighboring cells. Also, ESCRT-dependent exosomal secretion in lymph gland is previously unexplored. ESCRT-dependent mechanisms may potentially contribute to cell non-autonomous regulation of cell fate by the progenitors and invites detailed elucidation.

Asrij regulates the expression of Vps28 (ESCRT-I) and Vps32 (ESCRT-III) at the post-transcriptional level. This indicates tissue-specific regulation of the housekeeping function of ESCRT. Tissue-restricted conserved regulators such as Asrij may contribute toward the context-dependent role of ubiquitous machinery like ESCRT. In the previous chapter (Chapter 3), we have discussed the importance of Asrij lymph gland proteome to build a functional endocytic network that can regulate blood cell homeostasis. Elucidating the

functional link of Asrij to ESCRT can improve our understanding of targeting a generic mechanism to treat tissue-specific anomalies such as hematological disorders.

5.5 Acknowledgement

This work is published in:

Ray A, Rai Y, Inamdar MS., (2021) Charting ESCRT function reveals distinct and non-compensatory roles in blood progenitor maintenance and lineage choice in *Drosophila*. *bioRxiv*. doi: [10.1101/2021.11.29.470366](https://doi.org/10.1101/2021.11.29.470366)

(under peer review process)

Text and figures have been used following the terms of [Creative Commons Attribution License \(CC BY\)](https://creativecommons.org/licenses/by/4.0/).

[\(http://creativecommons.org/licenses/by/4.0/\)](http://creativecommons.org/licenses/by/4.0/)

Chapter 6. ESCRT regulates Notch signaling to maintain progenitor homeostasis in the *Drosophila* lymph gland.

6.1 Introduction

Endosomal protein sorting maintains signaling homeostasis through control of protein turnover. It involves a complex endocytic network of molecular interactions that fine tune downstream signaling relays. Previous reports highlight the role of the conserved ESCRT machinery in signaling receptor trafficking and turnover (Horner et al., 2018). Loss of ESCRT genes upregulates receptor-dependent signaling pathways such as JAK/STAT, Notch, JNK, EGFR etc (Woodfield et al, 2013; Wenzel et al, 2018). Depletion of ESCRT components results in endosomal accumulation of signaling receptors such as Notch and EGFR, leading to deregulated signaling activation, tissue hyperproliferation and neoplastic overgrowth (Vaccari et al, 2009; Herz et al, 2009; Tognon et al, 2014).

Notch receptor has an extracellular ligand-interacting domain and an intracellular signaling domain. During ligand-mediated activation of Notch signaling, γ -secretase cleaves the Notch intracellular domain (NICD), which translocates to the nucleus to initiate target gene transcription. Cleavage of NICD may take place on the plasma membrane or endosome surface. Nuclear translocation of NICD dissociates the corepressor from suppressor of hairless (*Su(H)*). This allows the formation of a complex stabilized by transcriptional coactivator Mastermind (*Mam*) that activates target gene transcription. However, even in the absence of transcriptional activation, Notch signaling may occur through protein-protein interaction in the cytosol, a mechanism commonly known as non-canonical Notch signaling (Sanalkumar et al., 2010; D'Souza et al, 2010; Ables et al., 2011). Thus, both canonical and non-canonical mode of Notch activation directly depends on the availability of NICD.

Post-translational modification such as ubiquitination can affect the activation status of Notch signaling. NICD-specific E3 ubiquitin ligases and deubiquitinases modulate Notch signaling in *Drosophila* through control of NICD degradation or activation (Moretti and Brou,

2013). E3 ubiquitin ligase Deltex acts as a positive regulator of Notch signaling by binding to the ankyrin repeats on NICD and monoubiquitinating it, thus displacing Su(H) that translocates to the nucleus to activate Notch pathway (Matsuno et al, 1995; Hori et al., 2011). Other ubiquitin ligases such as Mindbomb, Neuralized, d-cbl and Archipelago regulate Notch activation by controlling ubiquitination of Notch ligand Delta (Lai et al., 2001; Itoh et al., 2003; Wang et al., 2010). Deltex acts as a bridging factor between Notch and deubiquitinase eIF3f1 (Moretti et al., 2010). eIF3f1 acts as a positive regulator of Notch activation as eIF3f1-dependent deubiquitination of Notch is necessary for γ -secretase-dependent cleavage of NICD from the endosome surface (Moretti et al., 2010). Deltex acts in synergy with ESCRT-III component Vps32/Shrub to regulate Notch degradation and ligand-independent Notch activation in wing disc epithelial cells (Hori et al, 2011). Antagonistic role of Deltex and ESCRT indicates a functional link between endosomal cargo ubiquitination and cargo sorting.

Lineage-specific differentiation of progenitors requires activation of specific signaling pathway (Banerjee et al., 2019). For example, activation of EGFR signaling in the blood progenitor promotes differentiation to lamellocytes (Sinenko et al, 2011). Endocytic regulators of EGFR signaling control plasmatocyte proliferation (Kim et al., 2017). On the other hand, Notch signaling promotes crystal cell differentiation (Duvic et al, 2002; Lebestky et al., 2003). Notch signaling regulates binary fate specification toward plasmatocytes or crystal cells in distal progenitors of the lymph gland (Blanco-Obregon et al., 2020). Also, downregulation of Notch signaling is essential for lamellocyte differentiation (Small et al., 2014).

Our results from Chapter 5 showed that depletion of ESCRT has a profound impact on crystal cell differentiation. This suggests a potential role of ESCRT in Notch signaling activation, which may possibly lie downstream of the cargo sorting defect. In this chapter, we analysed the role of ESCRT in Notch signaling activation, NICD trafficking and any possible genetic interaction with the regulators of Notch ubiquitination in blood progenitors across the lymph gland.

6.2 Materials and methods

6.2.1 Fly stocks

Drosophila melanogaster stocks were maintained as described previously (Kulkarni, Khadilkar *et al.*, 2011). For progenitor-specific knockdown (KD) of ESCRT genes, *domeGal4 UAS2xEGFP/FM7a* and *domeGal4/FM7b* (Utpal Banerjee, UCLA) were used as driver as well as parental control. *UAS-dsRNA* (RNAi) transgenic lines were used for the knockdown of Hrs (BDSC 33900), Stam (VDRC 22497), Vps28 (VDRC 31894), Tsg101 (BDSC 38306), Vps22 (BDSC 38289), Vps25 (VDRC 108105), Vps24 (BDSC 38281) and Vps32 (VDRC 106823). Other stocks used were *UAS mCD8 RFP* (BDSC 27399), NRE-GFP/CyO (BDSC 30727), *UAS dx RNAi* (BDSC 44455), *UAS eIF3f1 RNAi* (BDSC 33980).

6.2.2 Fly Genetics

To obtain flies with prohemocyte-specific knockdown of target genes, 10 male flies of homozygous RNAi line were crossed with 20 virgin female flies of *domeGal4 UAS 2xEGFP/FM7a* genotype. F1 progenies were collected based on GFP expression. *domeGal4 UAS GFP/FM7a* was used as the parental control for all analyses.

For experiments using *domeGal4/FM7b* driver, virgin females were crossed with UAS mCD8 RFP males. RFP positive female progenies were crossed with NRE-GFP male flies in F1 generation. GFP, RFP double positive flies were crossed with homozygous RNAi lines. GFP, RFP double positive F2 progenies were used for experiments and *domeGal4/+; NRE-GFP/+; UAS mCD8 RFP/+* larvae were used as parental control.

For genetic interaction studies, following fly genotypes were generated-

- 1) *domeGal4/+; UAS Vps32 RNAi/NRE-GFP; UAS Dx RNAi/UAS mCD8 RFP*
- 2) *domeGal4/+; UAS Vps32 RNAi/NRE-GFP; UAS eIF3f1 RNAi/UAS mCD8 RFP*

6.2.3 Immunofluorescence Microscopy

Drosophila third instar larval lymph glands were dissected in PBS following the protocol described in Rodrigues et al, *Bio-protocol*, 2021. Only the dorsal half of the cuticle and the brain lobes were kept intact, and the rest of the unnecessary tissues were removed. After dissection, the samples were immediately fixed with 4% paraformaldehyde made in PBS for 20 minutes followed by three gentle PBS washes. Samples were permeabilised using 0.3% Triton X-100. For blocking, normal goat serum diluted to 20% in PBS was used. The samples were incubated overnight with the primary antibody dilutions. Primary antibodies used were mouse anti-P1 (Istvan Ando, BRC Schezed), mouse anti-ProPO, chick anti-GFP (Abcam, UK), rabbit anti-dsRed (Takara, Japan), anti-NICD (DSHB, USA), rabbit anti-phospho Histone H3 (Merck Millipore, USA). For secondary antibody staining, Alexa Fluor labelled anti-mouse, anti-rabbit, and anti-chick antibodies conjugated to Alexa Fluor 488, 568 and 633 (Life Technologies, Thermo Fisher Scientific, USA) were used. DAPI glycerol was used to mount the lymph gland samples on the coverslip. Images were acquired on Zeiss LSM880 Laser Confocal Microscope.

6.2.4 Proximity ligation assay

PLA was performed using the protocol recommended by DuoLink PLA Fluorescence Protocol (https://www.sigmaaldrich.com/IN/en/technical-documents/protocol/protein-biology/protein-and-nucleic-acid-interactions/duolink-fluorescence-user-manual?gclid=CjwKCAjwz_WGBhA1EiwAUAXlcT4JO0snQFg4YKoa85rywFz2PdNxUq62drROiV_Vqx44L8n8xMBWeiBoCQeAQAvD_BwE#DuolinkPLAFluorescenceProtocol). Rabbit plus and mouse minus probes were used along with orange DuoLink PLA kit (Merck, USA).

6.2.5 Quantification

Number of cells with high NRE-GFP expression was quantified manually in each lobe. For quantifying NICD accumulation, cells with intracellular NICD accumulation (not commonly seen in control lymph glands) were counted in each lobe. To determine the fraction of cells undergoing Notch activation or crystal cell differentiation, the number of cells expressing high level of NRE-GFP or ProPO was normalized over DAPI positive nuclei count (described already in section 5.2.6). Number of PLA dots per 100 μm^2 area of the progenitor subsets across primary, secondary and tertiary lobes of the lymph gland was manually counted. Mitotic potential was determined by estimating the number of nuclei with high H3P expression (above a set threshold value). Lymph glands were binned in three categories based on the primary lobe margin: regular, irregular/disintegrated, tumorous bulge and percentage of lymph gland under each category was estimated. All images within a given figure panel were adjusted equally for brightness and contrast using Adobe Photoshop CS5 extended. GraphPad Prism 8 and MS Excel were used to prepare the graphs. Biorender was used to prepare the model in Fig 6.9.

6.2.6 Statistical analyses

Each larva was considered as a biological replicate. Data from each lymph gland lobe was individually considered for quantitation in all graphs. One-way ANOVA was used for statistical analysis of data.

6.3 Results

6.3.1 ESCRT components inhibit Notch signaling in a distinct manner across lymph gland progenitors.

Our previous results show that ESCRT most strongly affects crystal cell lineage choice. Loss of ESCRT results in increased crystal cell differentiation suggesting upregulation of Notch signaling pathway. We chose 8 ESCRT components with two from each subunit [Hrs, Stam (ESCRT-0); Vps28, Tsg101 (ESCRT-I); Vps25, Vps22 (ESCRT-II); Vps32, Vps24 (ESCRT-III)] for

analysis as these components are well known for their role in endocytic trafficking of NICD and activation of Notch pathway (Vaccari et al., 2009; Tognon et al., 2014). Moreover, they show differential phenotype in lineage-specific differentiation, which would allow us to study differential effects on signaling. We used NRE-GFP reporter as described in section 3.3.6. to assess the role of ESCRT in Notch signaling in the lymph gland progenitors. Except Vps25, progenitor-specific knockdown of all components [Hrs, Stam (ESCRT-0); Vps28, Tsg101 (ESCRT-I); Vps22 (ESCRT-II); Vps32, Vps24 (ESCRT-III)] resulted in upregulation of Notch signaling as interpreted by an increase in the number of NRE-GFP positive cells in the primary lobe (Fig 6.1). This is in concordance with the crystal cell differentiation phenotype as all of the ESCRT components except Vps25 cause increased crystal cell differentiation in the primary lobe upon knockdown. Our result also indicates that these 7 ESCRT subunits are indispensable for regulation of Notch signaling in the blood cell progenitors.

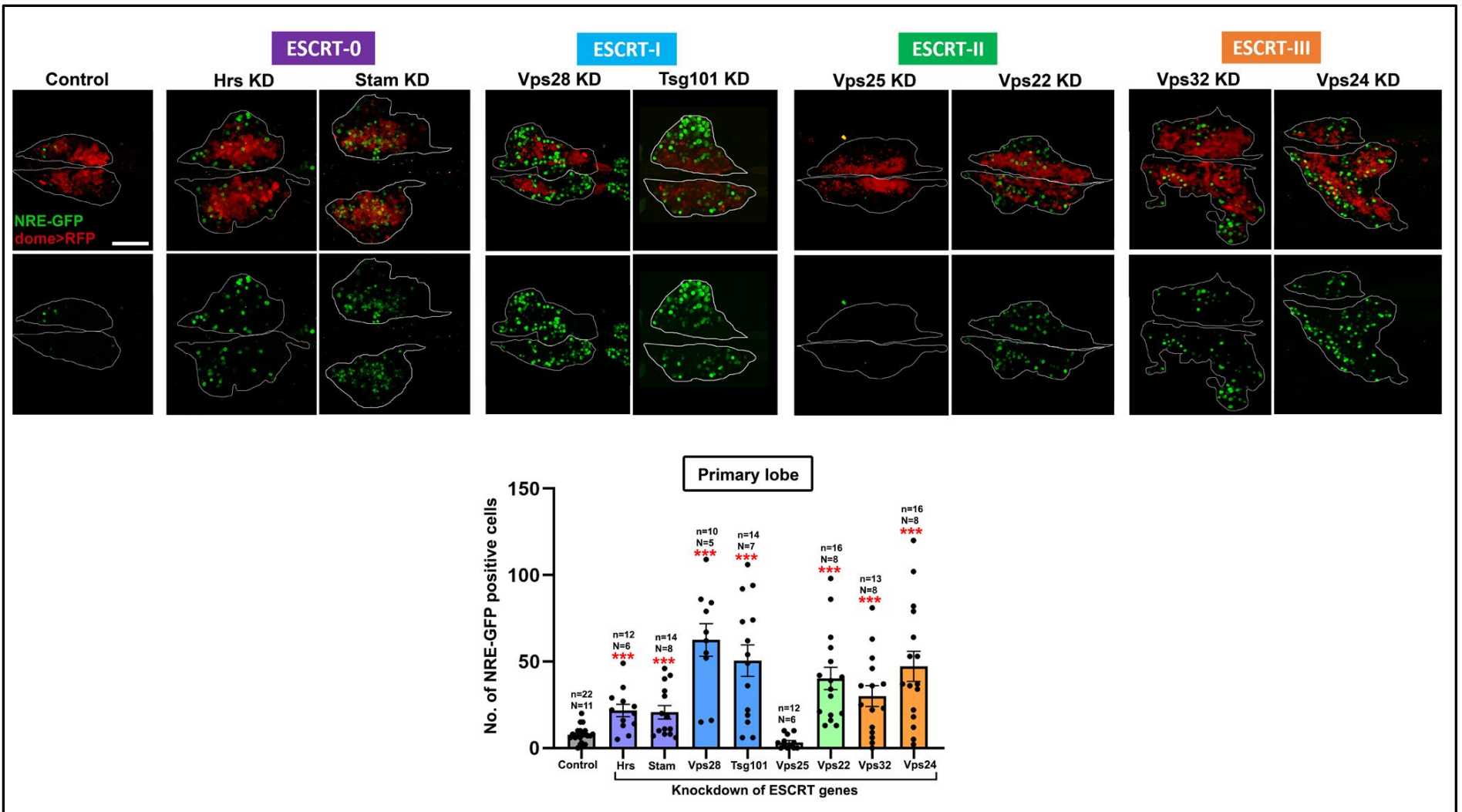


Figure 6.1 ESCRT components regulate Notch signaling in the lymph gland primary lobe. Whole-mount larval lymph gland showing NRE-GFP+ve (Notch reporter) cells (green) and dome+ve progenitors (red) in primary lobes upon progenitor-specific knockdown of all 8 ESCRT components [Hrs, Stam (ESCRT-0); Vps28, Tsg101 (ESCRT-I); Vps25, Vps22 (ESCRT-II); Vps32, Vps24 (ESCRT-III)]. Scale bar: 100 μ m. Bar diagram shows quantification of the number of NRE-GFP positive cells in the primary lobe upon knockdown of 8 ESCRT components. n indicates the number of individual lobes analysed and N indicates the number of larvae analysed. Error bars represent SEM. One-way ANOVA was performed to determine the statistical significance. ***P<0.001.

Knockdown of 3 out of the 8 ESCRT components [Hrs, Stam (ESCRT-0) and Vps28 (ESCRT-I)] resulted in increased Notch signaling activation in the secondary lobe (Fig 5.2A, B). As shown in chapter 5, Hrs and Vps28 knockdown cause crystal cell differentiation in the secondary lobe, which corroborates Notch activation in the secondary lobe. Stam knockdown, though activates Notch signaling in the secondary lobe does not increase crystal cell differentiation, suggesting additional mechanisms downstream to Notch activation that inhibit crystal cell differentiation upon Stam depletion. Only Hrs and Stam knockdown resulted in Notch activation in the tertiary lobe (Fig 6.2A, B). In either case, tertiary lobe progenitors fail to differentiate, indicating their immature nature. Also, Vps28 depletion, though does not significantly activate Notch pathway in the tertiary lobe, can promote crystal cell differentiation, suggesting suppression of Notch signaling after the progenitors differentiate. However, we do see increased Notch activation in Vps28 KD tertiary lobes on a few occasions. Hence, the phenotype of crystal cell differentiation in the tertiary lobe could be due to complex temporal regulation.

Our result shows the active role of ESCRT components in regulating Notch signaling in the blood progenitor that may contribute to crystal cell differentiation and also differential response of the progenitor subsets to depletion of ESCRT.

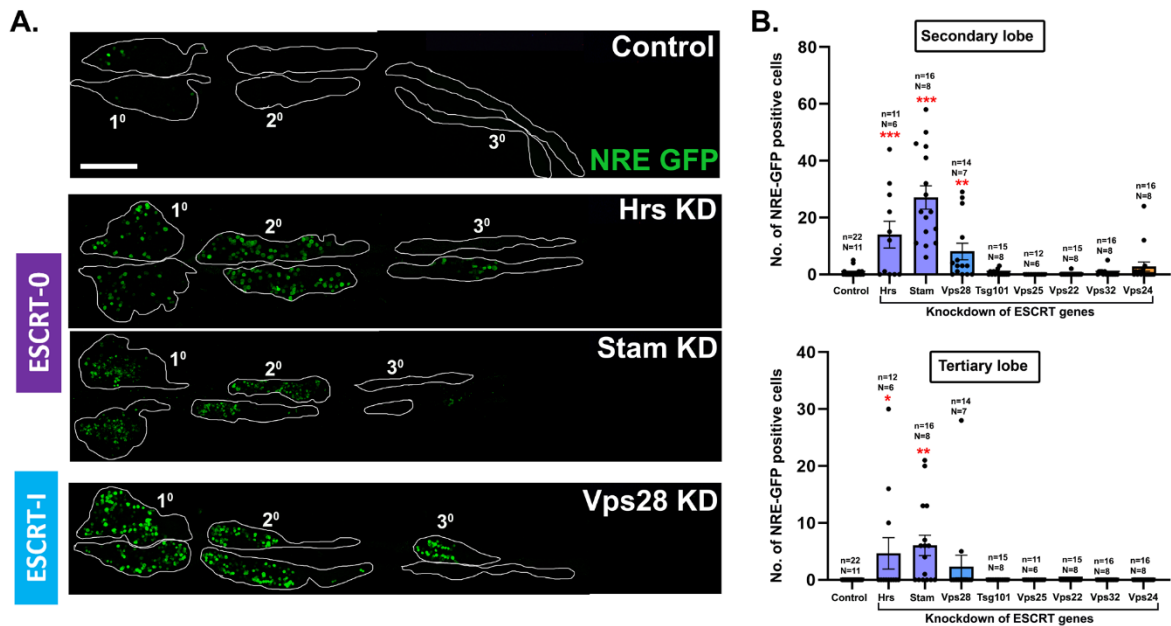


Figure 6.2 ESCRT regulates Notch activation across the lymph gland. (A) Whole-mount larval lymph gland showing NRE-GFP staining to mark Notch activation in the posterior lobes upon progenitor-specific knockdown of ESCRT components Hrs, Stam (ESCRT-0) and Vps28 (ESCRT-I). Scale bar: 100 μ m. (B) Bar diagrams show quantification of the number of NRE-GFP positive cells in secondary and tertiary lobes upon knockdown of 8 ESCRT components [Hrs, Stam (ESCRT-0); Vps28, Tsg101 (ESCRT-I); Vps25, Vps22 (ESCRT-II); Vps32, Vps24 (ESCRT-III)]. n indicates the number of individual lobes analysed and N indicates the number of larvae analysed. Error bars represent SEM. One-way ANOVA was performed to determine the statistical significance. * $P < 0.05$, ** $P < 0.01$, *** $P < 0.001$.

6.3.2 Depletion of ESCRT components in the blood progenitor causes accumulation of NICD.

NICD acts as the principal signaling component to activate canonical and non-canonical mode of Notch pathway. We tested whether ESCRT depletion in lymph gland progenitors causes accumulation of NICD, which may lead to aberrant activation of Notch signaling. Progenitor-specific knockdown of all ESCRT components except of Vps25 resulted in increase in the number of cells accumulating NICD in the primary lobe (Fig 6.3A-B). This suggests a role for majority of the ESCRT components in NICD trafficking which may affect Notch signaling. Absence of any phenotype due to Vps25 knockdown indicates existence of bypass mechanisms to regulate cargo trafficking and lineage-specific signaling activation in

the blood progenitors. We have not quantitatively analysed whether NICD level in the nucleus is high in ESCRT depleted progenitors. However, NICD-dependent Notch activation can happen through its nuclear translocation or through non-canonical mode that involves interaction with other signaling components in the cytosol. Activation of NRE-GFP reporter in ESCRT KD progenitors suggests that the signaling is activated through nuclear translocation of NICD [(Su(H)-dependent activation of GFP transcription)].

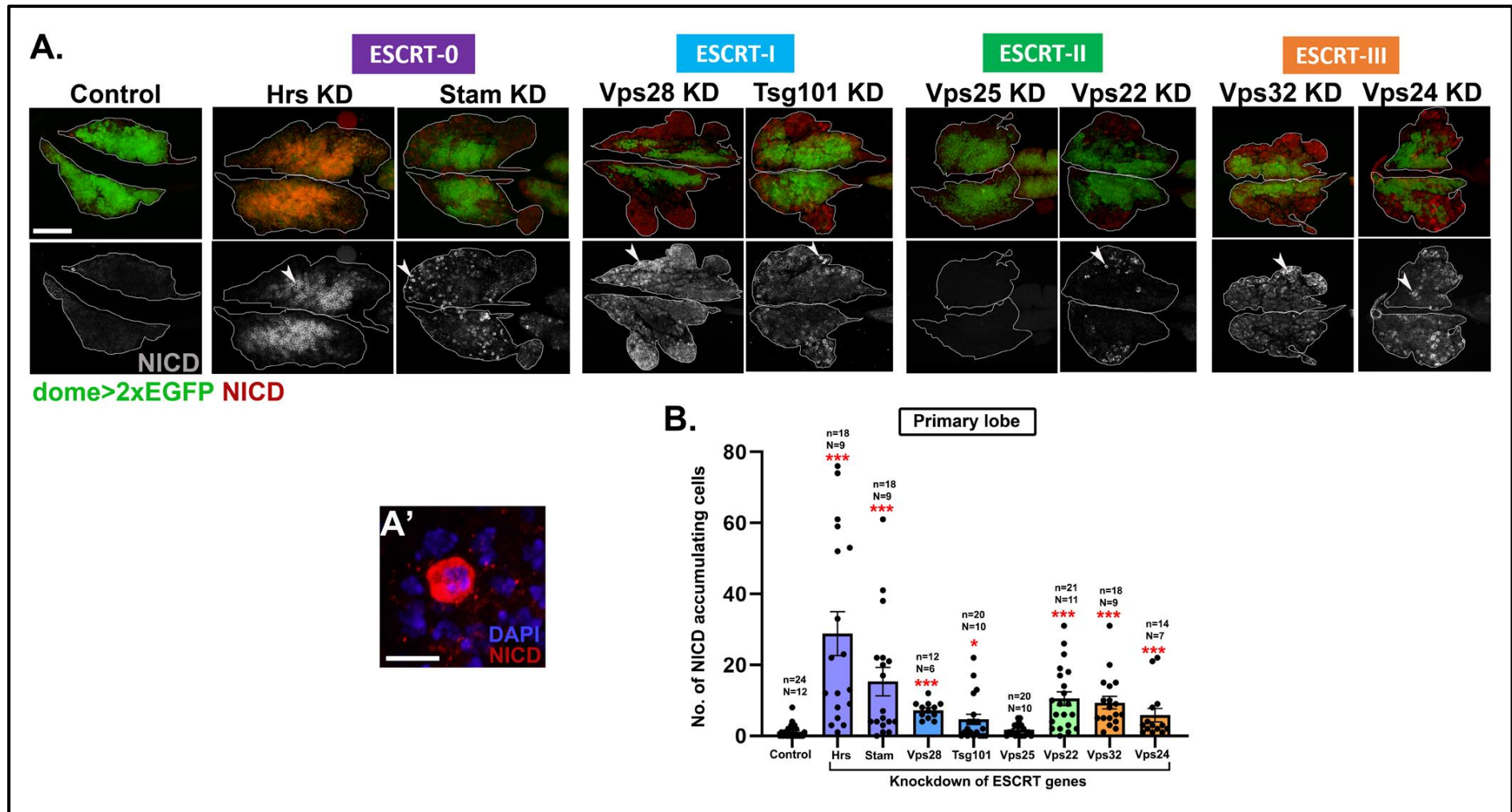


Figure 6.3 Progenitor-specific depletion of ESCRT causes NICD accumulation in the lymph gland primary lobe. (A) Whole-mount larval lymph gland showing NICD expression (shown in red in the upper panel and in grayscale in the lower panel) in primary lobes upon progenitor-specific knockdown of 8 ESCRT components [Hrs, Stam (ESCRT-0); Vps28, Tsg101 (ESCRT-I); Vps25, Vps22 (ESCRT-II); Vps32, Vps24 (ESCRT-III)]. Progenitors are marked by *dome>2xEGFP* (green). Scale bar: 100 μm . (A') An enlarged view of a lymph gland hemocyte accumulating NICD is shown. Number of such NICD accumulating cells were quantified. Scale bar: 10 μm . (B) Bar diagram shows quantification of the number of NICD accumulating cells in the primary lobe upon knockdown of the same 8 ESCRT components. n indicates the number of individual lobes analysed and N indicates the number of larvae analysed. Error bars represent SEM. One-way ANOVA was performed to determine the statistical significance. *** $P < 0.001$.

Knockdown of 3 components [Hrs, Stam (ESCRT-0) and Vps28 (ESCRT-I)] led to an increase in the number of NICD accumulating cells in the secondary lobe (Fig 6.4A, B). However, only Hrs and Stam knockdown resulted in NICD accumulation in the tertiary lobe. This is in concordance with the phenotype of Notch activation upon Hrs, Stam and Vps28 knockdown in the posterior lobes. Our results show that NICD accumulation and Notch signaling activation correlate perfectly with crystal cell differentiation upon ESCRT knockdown. Hence, endocytic sorting defect due to ESCRT depletion may result in aberrant signaling activation, leading to lineage-specific differentiation.

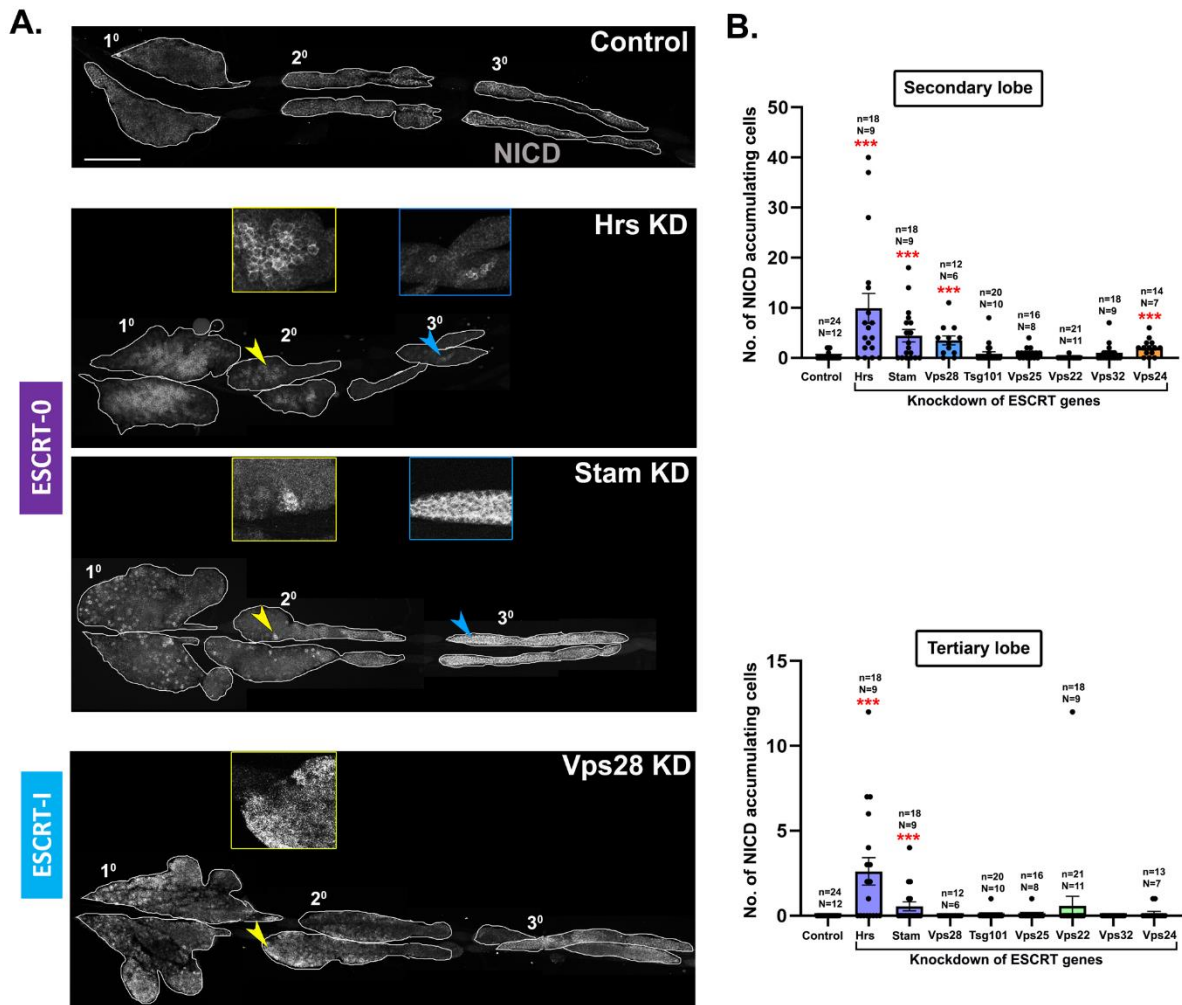


Figure 6.4 Progenitor-specific knockdown of ESCRT components causes NICD accumulation across the lymph gland. (A) Whole-mount larval lymph gland showing NICD staining in grayscale in the posterior lobes upon progenitor-specific knockdown of ESCRT components Hrs, Stam (ESCRT-0) and Vps28 (ESCRT-I). NICD accumulation in secondary (yellow arrowhead) and tertiary lobes (blue arrowhead) are shown in the insets. Scale bar: 100 μ m. (B) Bar diagram shows quantification of the number of cells accumulating NICD in secondary and tertiary lobes upon knockdown of 8 ESCRT components [Hrs, Stam (ESCRT-0); Vps28, Tsg101 (ESCRT-I); Vps25, Vps22 (ESCRT-II); Vps32, Vps24 (ESCRT-III)]. n indicates the number of individual lobes analysed and N indicates the number of larvae analysed. Error bars represent SEM. One-way ANOVA was performed to determine the statistical significance. * $P < 0.05$, *** $P < 0.001$.

6.3.3 ESCRT components co-localize with NICD in lymph gland progenitors.

Blood progenitor subsets across different lobes of the lymph gland respond differentially upon depletion of various ESCRT components despite their uniform expression. Hence, we investigated whether co-expressing ESCRT components differentially interact with endosomal cargoes in these different progenitor subpopulations. We chose two representative components, Vps28 and Vps32 that differentially regulate progenitor homeostasis in the lymph gland- while Vps28 knockdown results in cargo accumulation and signaling activation in anterior as well as posterior subsets of progenitors, Vps32 depletion primarily affects anterior progenitor homeostasis. Immunostaining-based analysis showed colocalization of Vps28 and Vps32 with NICD across all progenitor subsets (Fig 6.5A, B). Next, we performed proximity ligation assay to test any differential physical interaction across lobes. PLA of NICD with Vps28 showed positive signal across progenitors of all three lobes, indicating direct physical interaction in a uniform manner (Fig 6.5C). Such uniform interaction may explain phenotypes of Vps28 depletion seen across all the lobes. However, the signal was negligible for PLA between Vps32 and NICD, indicating no direct physical interaction between Vps32 and NICD (Fig 6.5D). Hence, we could not conclude any variation in Vps32-NICD interaction across progenitor subsets from the PLA result. Our results suggest that NICD may not be actively sorted by Vps32 in posterior lobes. Hence, there could be additional regulators that bring about differential sorting by ESCRT components across progenitor subsets.

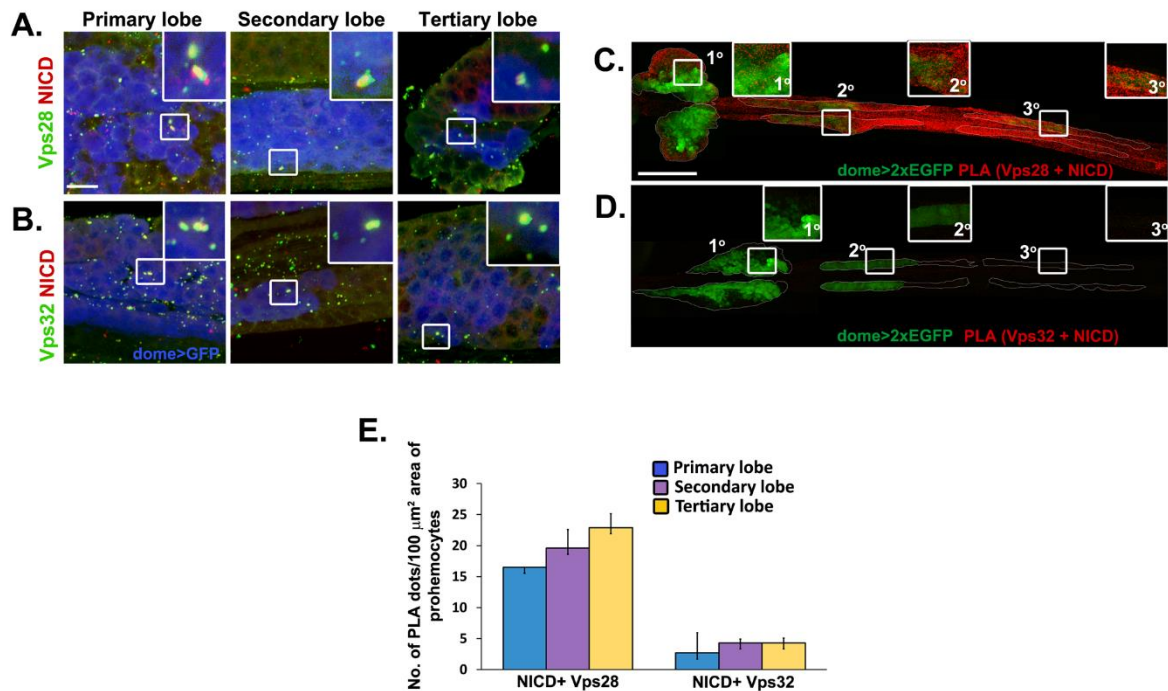


Figure 6.5 ESCRT components colocalize and interact with NICD across all progenitor subsets of the lymph gland. (A-B) Immunostaining for NICD (red) and ESCRT components Vps28 (A) and Vps32 (B) (green) showing colocalization in dome+ve progenitors (blue) across primary, secondary and tertiary lobes of the lymph gland. Scale bar: 10 μm. (C-D) PLA dots (red) mark the interaction of NICD with Vps28 (C) and Vps32 (D) across three lobes of the lymph gland. Progenitors are marked by dome>2xEGFP. Insets show a magnified view of the progenitors from primary, secondary and tertiary lobes. Scale bar: 200 μm. (E) Bar diagram shows quantification of the number of PLA dots per 100 μm² area of the progenitors. N=5 larvae. Error bars represent SEM. One-way ANOVA was performed to determine the statistical significance.

6.3.4 ESCRT regulates Notch activation in blood progenitors independent of Deltex and eIF3f1.

Notch activation and crystal cell differentiation phenotypes of ESCRT knockdown lymph gland only partly match with ubiquitinated cargo accumulation. This suggests ESCRT-dependent activation of Notch signaling may not depend on the known regulators of Notch ubiquitination. As mentioned earlier, several ubiquitin ligases and deubiquitinases regulate the activation of Notch pathway (Moretti et al., 2010). Ubiquitin ligases such as Mindbomb, Neuralized, d-cbl, and Archipelago regulate Notch signaling by regulating the ubiquitination

of Notch-specific ligand Delta (Lai et al., 2001; Itoh et al., 2003; Wang et al., 2010). As both Deltex and eIF3f1 positively regulate Notch signaling in other *Drosophila* tissues by directly regulating the ubiquitination or deubiquitination of Notch (Matsuno et al., 1995; Moretti et al., 2010; Hori et al., 2011), we probed into any possible genetic interaction between ESCRT and Deltex or eIF3f1 in blood progenitors, which may regulate Notch signaling. Vps32 knockdown in the progenitors upregulates Notch signaling and crystal cell differentiation. However, progenitor-specific knockdown of Deltex (Fig 6.6A, B) or eIF3f1 (Fig 6.6C, D) failed to rescue the phenotype of Vps32 knockdown. Our result indicates that Notch activation downstream of ESCRT is independent of Deltex or eIF3f1. This might explain why depletion of some ESCRT components, despite showing no significant accumulation of cargo in ubiquitinated state can promote Notch signaling and crystal cell differentiation.

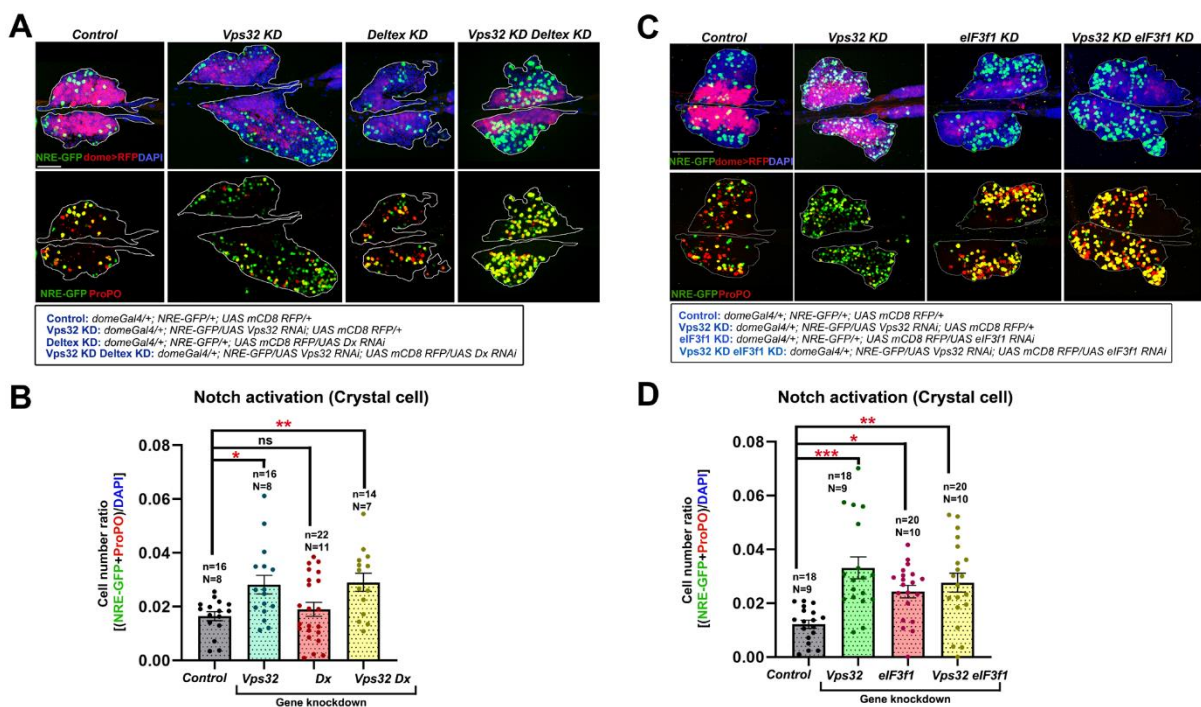


Figure 6.6 ESCRT does not genetically interact with Deltex and eIF3f1 to regulate Notch signaling in the lymph gland progenitor. (A-B) Lymph gland primary lobes showing NRE-GFP and ProPO staining in control, Vps32 KD, Deltex KD and Vps32 KD Deltex KD lymph glands (A). Progenitors are marked by dome>RFP. Detailed genotypes are mentioned in the box below the image panel. Scale bar: 100 μ m. (B) Bar graph shows quantification of the fraction of cells undergoing Notch activation or crystal cell differentiation in the same genotypes. (C-D) NRE-GFP and ProPO staining mark Notch activation and crystal cell differentiation, respectively in the primary lobe of control, Vps32 KD, eIF3f1 KD and Vps32 KD eIF3f1 KD

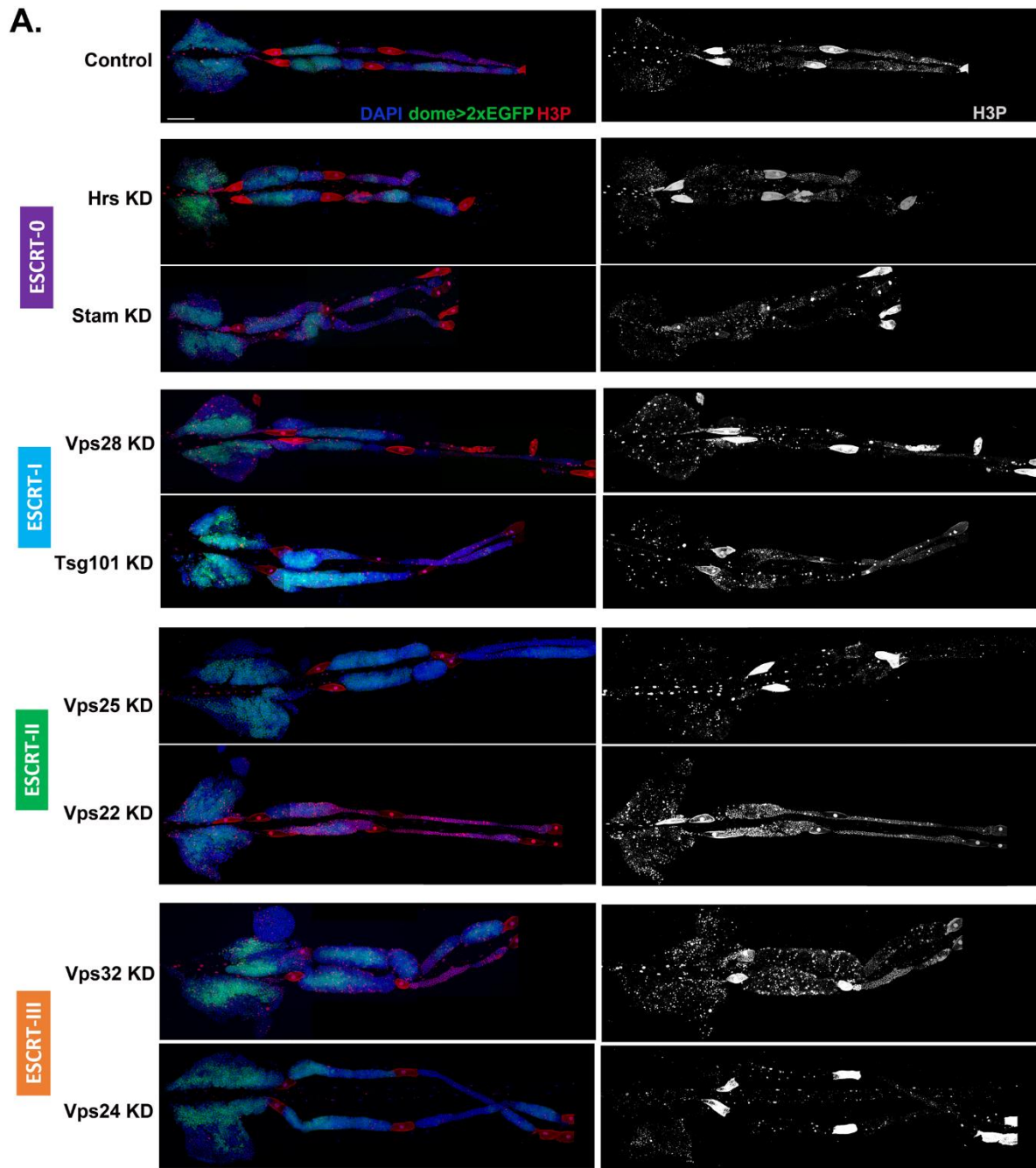
lymph gland (C). Detailed genotypes are mentioned below the image panel. (D) Bar diagram shows quantification of NRE-GFP and ProPO positive cell fraction. Error bars represent SEM. One-way ANOVA was performed to determine the statistical significance. * $P < 0.05$, ** $P < 0.01$, *** $P < 0.001$, ns: statistically non-significant difference.

6.3.5 ESCRT components play distinct roles in regulating mitotic potential across different progenitor subsets of the lymph gland.

Altered cell proliferation can contribute to perturbed tissue homeostasis. Our analysis of blood cell differentiation is based on estimation of the cell fraction, which could be an outcome of not only progenitor differentiation but also proliferation of individual blood cell type. ESCRT genes act as tumor suppressors in epithelial tissues by inhibiting Notch-dependent hyperplastic and neoplastic overgrowth (Hariharan and Bilder, 2006; Vaccari and Bilder, 2009; Horner et al., 2018). We tested whether downregulation of ESCRT expression can impact proliferation of the blood cells. Progenitor-specific knockdown of 3 ESCRT components [Vps28 (ESCRT-I), Vps22 (ESCRT-II) and Vps32 (ESCRT-III)] led to an increase in the number of nuclei with high mitotic potential in the primary lobe as revealed by high level of phosphorylated Histone H3 (Fig 6.7A, B). Vps32 knockdown also caused an increase in the size of the primary lobe as interpreted by the number of nuclei (Fig 6.7A, C). However, Vps28 and Vps22 knockdown did not affect the overall size of the primary lobe. This suggests that cells may not have actively divided in the Vps28 and Vps22 depleted primary lobes in spite of increase in the mitotic potential. Though Tsg101 and Vps25 knockdown did not increase the number of H3P high nuclei in the primary lobe, the overall size of the primary lobe increased. This suggests possible early developmental stage-specific effect on cell proliferation due to knockdown.

Knockdown of two components [Vps22 (ESCRT-II) and Vps32 (ESCRT-III)] resulted in increase in the mitotic potential in the secondary lobe (Fig 6.7A, B). Depletion of 6 components [Hrs, Stam (ESCRT-0); Vps28, Tsg101 (ESCRT-I); Vps22 (ESCRT-II) and Vps32 (ESCRT-III)] however resulted in increase in cell number in the secondary lobe (Fig 6.7A, C). This again reflects temporal regulation of mitotic potential and cell proliferation upon knockdown of various ESCRT components. On the other hand, Vps24 knockdown reduced mitotic potential in the

secondary lobe though the overall size of the secondary lobe remained unaffected (Fig 6.7A-C). This indicates positive regulation of mitotic potential by Vps24. Knockdown of none of the ESCRT genes increased mitotic potential in the tertiary lobe. Rather, proliferative potential decreased in the tertiary lobe upon knockdown of 4 components [Vps28, Tsg101 (ESCRT-I); Vps25 (ESCRT-II) and Vps24 (ESCRT-III)] (Fig 6.7A, B). However, tertiary lobe size increased upon knockdown of 6 components [Hrs, (ESCRT-0); Vps28 and Tsg101 (ESCRT-I); Vps22 (ESCRT-II); Vps32 and Vps24 (ESCRT-III)] (Fig 6.7A, C). This indicates hyperproliferation followed by downregulation of mitotic potential. In summary, depletion of ESCRT components promote proliferation but in a temporally regulated manner.



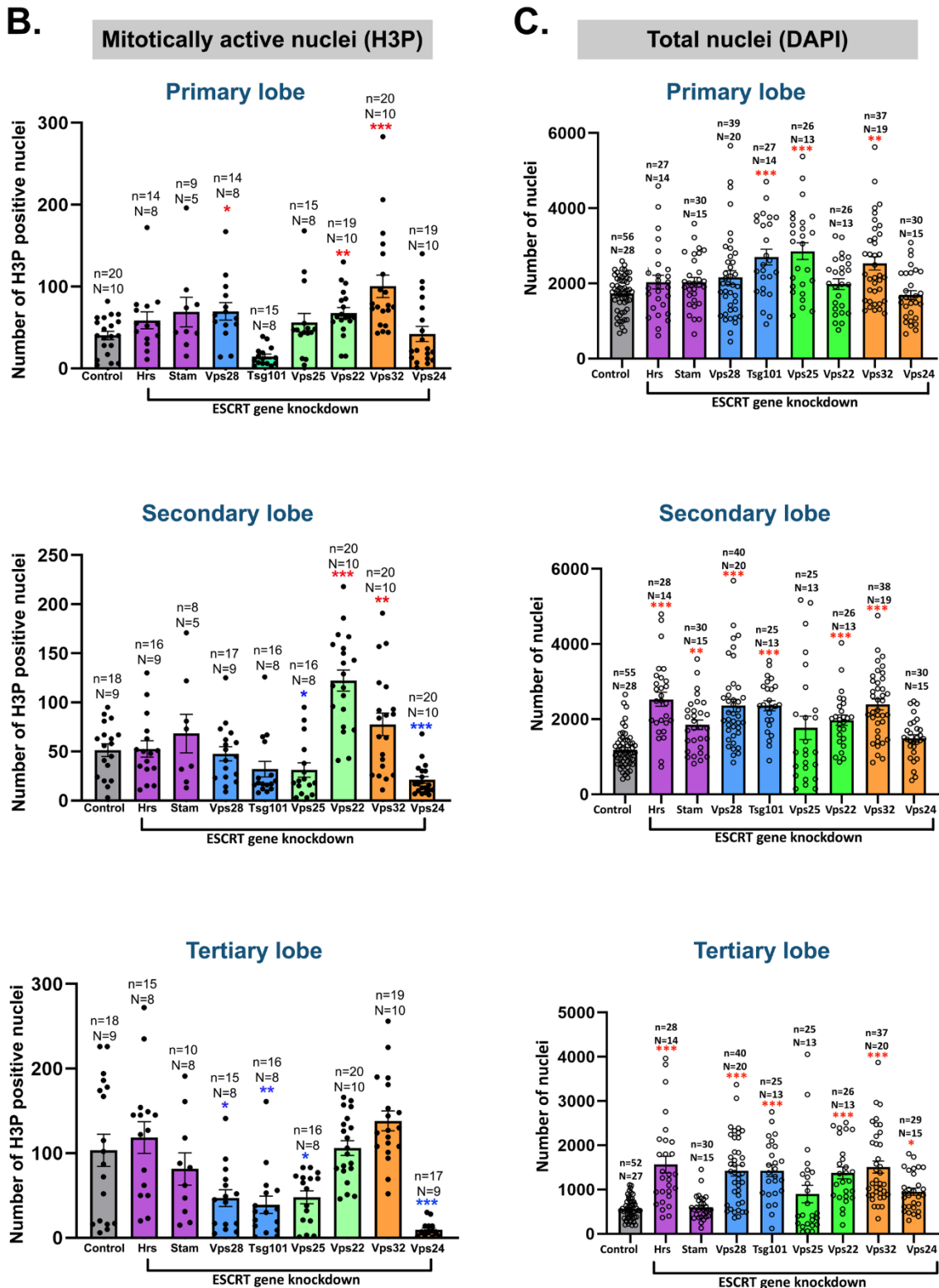


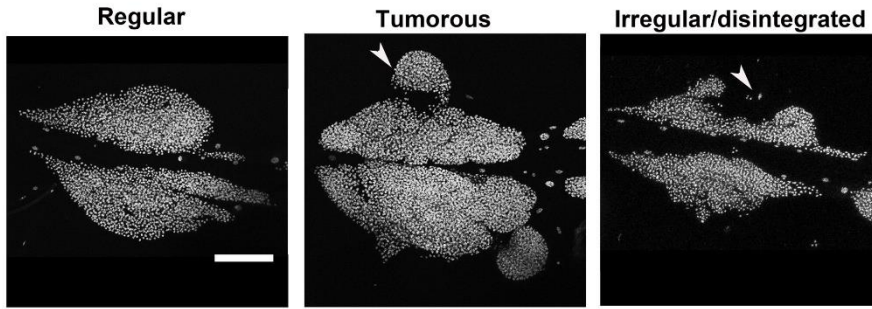
Figure 6.7 ESCRT components differentially regulate mitotic potential across the lymph gland. (A) Whole-mount larval lymph gland showing immunostaining for phosphorylated Histone H3 to mark mitotically active nuclei (red in the left image panel and grayscale in the right image panel) upon progenitor-specific knockdown of 8 ESCRT components [Hrs, Stam

(ESCRT-0); Vps28, Tsg101 (ESCRT-I); Vps25, Vps22 (ESCRT-II); Vps32, Vps24 (ESCRT-III)]. Scale bar: 100 μ m. (B) Bar diagram shows quantification of the number of H3P positive (high H3P) nuclei in primary, secondary and tertiary lobes of the same genotypes. (C) The total number of nuclei in each lobe has also been quantified for each lobe in the same genotypes. n indicates the number of individual lobes analysed and N indicates the number of larvae analysed. Error bars represent SEM. One-way ANOVA was performed to determine the statistical significance. *P<0.05, **P<0.01, ***P<0.001.

Increased differentiation or proliferation can cause disintegration of the primary lobe or appearance of tumorous bulge resembling neoplastic overgrowth. To assess the change in morphology of the lymph gland lobes upon depletion of ESCRT components, we categorized lymph glands in three groups based on the appearance of lobe margin: regular, irregular/disintegrated, and tumorous bulge. While the majority of the control lymph gland primary lobes showed a regular boundary, knockdown of 6 ESCRT components [Hrs (ESCRT-0); Vps28, Tsg101 (ESCRT-I); Vps25, Vps22 (ESCRT-II) and Vps32 (ESCRT-III)] resulted in tumorous outgrowth in the primary lobe (Fig 6.8A, B). Also, Hrs and Vps28 knockdown resulted in a significant increase in primary lobe disintegration as revealed by the irregular boundary. Vps28 and Vps32 knockdown resulted in significant increase in tumorous overgrowth in the secondary and tertiary lobe.

Our analyses show that altered mitotic potential and cellular proliferation due to ESCRT depletion can contribute to altered blood cell homeostasis.

A.



B.

Boundary shape

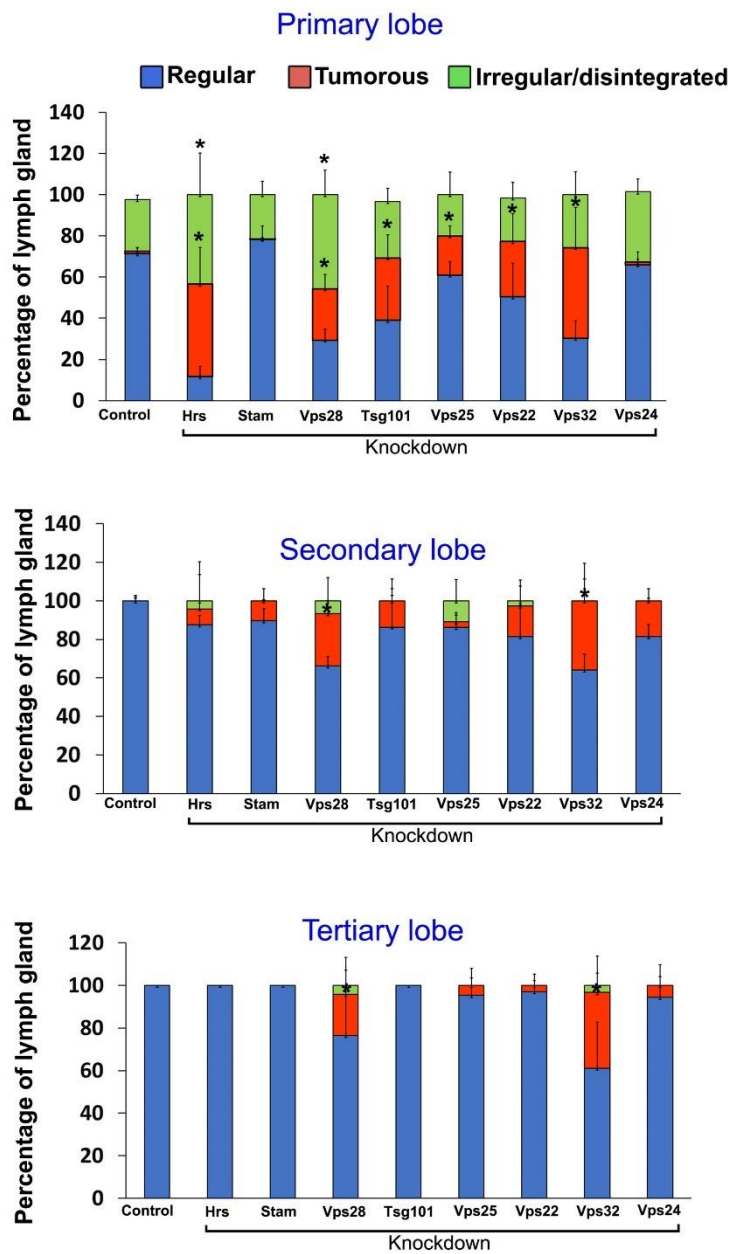


Figure 6.8 Depletion of ESCRT components affects the morphology of the lymph gland lobes. (A) Representative primary lobe images of the lymph gland showing regular boundary, irregular/disintegrated boundary and tumorous bulge. Scale bar: 100 μm . (B) Quantification of the percentage of larvae showing aforementioned morphology of the primary, secondary and tertiary lobes for knockdown of 8 ESCRT genes [Hrs, Stam (ESCRT-0); Vps28, Tsg101 (ESCRT-I); Vps25, Vps22 (ESCRT-II); Vps32, Vps24 (ESCRT-III)]. $N > 30$ for each genotype. Error bars represent SEM. One-way ANOVA was performed to determine the statistical significance. $*P < 0.05$.

6.4 Discussion

Our study shows the distinct role of individual components of ESCRT in Notch signaling in blood progenitors. We show that regulation of Notch signaling in lymph gland progenitors relies heavily on the ESCRT machinery. This establishes the critical role of endosomal protein sorting in signaling regulation to maintain blood progenitor homeostasis. Curiously, Vps25 that has a well-established role in controlling Notch signalling in the eye and wing discs, has no role in blood progenitors, indicating that tissue-specific regulators may provide context-dependent ESCRT function for signaling regulation.

A review of recent research highlights context-dependent modulation of conserved and generic endocytic network to maintain signaling and tissue homeostasis (Sigismund et al, 2021). As discussed previously, ESCRT involves several accessory proteins that set up bypass routes for endosomal protein sorting (Vietri et al., 2020). Though none of the previous studies indicate any Vps25-independent mechanism of Notch trafficking and signaling activation, our analyses of Vps25 knockdown lymph gland using multiple RNAi lines as well as mutant clones indicates its functional redundancy in blood lineage-specific signaling activation (shown in the previous chapter (Chapter 5, section 5.3.7). However, Vps25 depletion affects the size of the lymph gland indicating its potential role in controlling cell proliferation that may depend on other signaling mechanisms.

ESCRT components differentially affect NICD trafficking, Notch activation and crystal cell differentiation across progenitor subsets. Though the majority of the ESCRT components affect the primary lobe, only a few could impact the posterior subsets of progenitors. Such differential sensitivity reflects heterogeneity of progenitor subsets. The posterior pools of progenitors appear refractile, as expected from our previous reports (Rodrigues et al., 2021; Ray et al., 2021) (Fig 6.9). Moreover, transcriptional heterogeneity has been reported within progenitor subsets (Cho et al., 2021). Though ESCRTs are expressed uniformly in all LG cells, phenotypes across the spatially and developmentally distinct progenitor subsets differ. This suggests a role for post-transcriptional regulatory mechanisms operating at the organellar level in effecting ESCRT function.

Though Deltex and eIF3f1 positively regulate Notch signaling, they appear dispensable for Notch activation in the progenitors downstream of ESCRT knockdown. This suggests a context-dependent role of the Notch ubiquitination regulators (Fig 6.9). Other E3 ubiquitin ligases and deubiquitinases may possibly compensate for Deltex or eIF3f1 depletion and remain to be unravelled. As ESCRT mediates even ligand-independent mode of Notch signaling in epithelial tissues (Hori et al., 2012), it would be interesting to investigate whether ESCRT-dependent Notch signaling activation in the blood progenitors relies on ligands such as Serrate. Also, progenitor maintenance and differentiation to plasmacytes and lamellocytes depends on other signaling pathways such as JAK/STAT, EGFR, Hedgehog etc., which can be regulated at the endosomal level. The role of ESCRT in progenitor-specific activation of such signaling pathways merits further investigation.

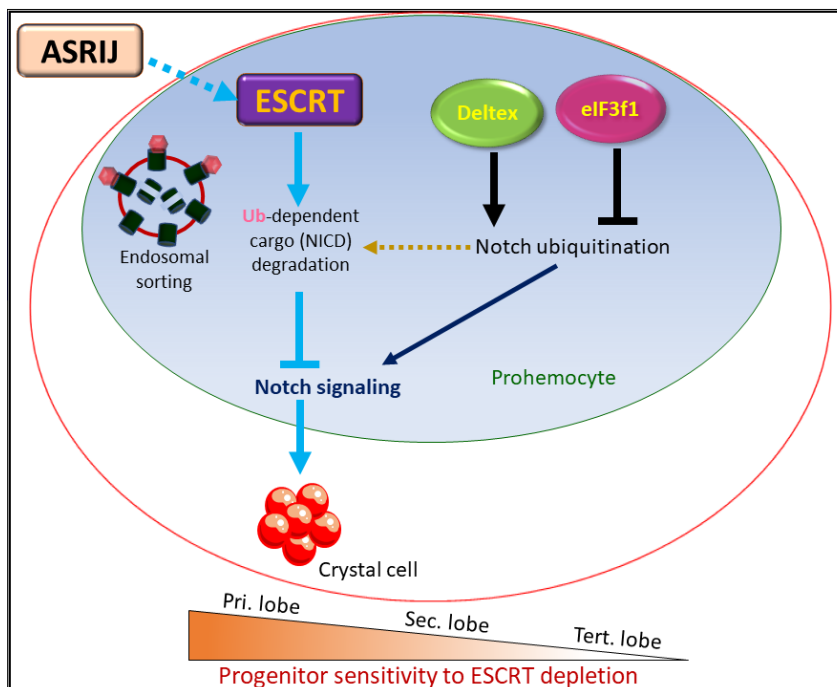


Figure 6.9. Model showing ESCRT-dependent regulation of cargo trafficking and Notch signaling across lymph gland progenitor subsets. ESCRT mediates endosomal sorting of ubiquitinated cargoes such as NICD in the blood progenitors (prohemocytes) and inhibits uncontrolled activation of Notch signaling and crystal cell differentiation. However,

Notch ubiquitin ligase Deltex and deubiquitinase eIF3f1 do not affect ESCRT-dependent Notch activation. Response to ESCRT depletion varies across progenitor subsets, with the anterior progenitors showing the highest sensitivity in terms of signaling activation and lineage-specific differentiation. Also, tissue-enriched conserved regulator of hematopoiesis, Asrij regulates ESCRT expression, suggesting context-dependent modulation of generic endocytic machinery.

Both progenitor differentiation and proliferation can influence blood cell homeostasis in the lymph gland. ESCRT depletion not only activates lineage-specific signaling activation but also promote blood cell proliferation. Cell type-specific increase in proliferation and enlargement of lymph gland lobes can affect the proportion of different hemocytes. Further studies on the genetic interaction of ESCRT with components of mitogenic signaling machinery could elucidate whether suppressing excessive mitosis may restore hematopoietic normalcy.

Our analysis of signaling pathways may explain phenotypic diversity of ESCRT in lineage-specific differentiation across different progenitor subpopulations. Components of ESCRT machinery despite playing a generic role in endosomal protein sorting may show distinct roles in lineage choice through differential regulation of signaling pathways. As discussed in

Chapter 5, Asrij, the endosomal regulator of hematopoiesis, can modulate expression of various ESCRT components. Such conserved regulators may mediate local fine-tuning of ESCRT function (Fig 6.9). A recent report shows the dependence of ESCRT-III on Lgd (lethal giant discs)/CC2D1 for full activity in intraluminal vesicle formation while sorting proteins (Baeumers et al., 2020). Also, post-translational modifications may contribute to distinct functions of ESCRT components (Tsunematsu et al., 2010). Such subtle regulatory mechanisms may explain why co-expressing ESCRT components contribute to distinct lineages. Also, additional functions of ESCRT involving organellar membrane remodelling may impart phenotypic diversity (discussed elaborately in chapter 5). ESCRT components emerge as potential candidates to screen for lineage-specific modulators of signaling in blood progenitors. Further understanding of context-specific function of ESCRT may improve our understanding of lineage-specific regeneration of tissue, including blood.

6.5 Acknowledgement

This work is published in:

Ray A, Rai Y, Inamdar MS., (2021) Charting ESCRT function reveals distinct and non-compensatory roles in blood progenitor maintenance and lineage choice in *Drosophila*. ***bioRxiv***. doi: [10.1101/2021.11.29.470366](https://doi.org/10.1101/2021.11.29.470366)

(under peer review process)

Text and figures have been used following the terms of [Creative Commons Attribution License \(CC BY\)](https://creativecommons.org/licenses/by/4.0/).

[\(http://creativecommons.org/licenses/by/4.0/\)](http://creativecommons.org/licenses/by/4.0/)

Chapter 7. Discussion

In this thesis, we attempted to elucidate the role of mitochondrial dynamics regulators and components of the ESCRT machinery in blood progenitor homeostasis. We used the *Drosophila* lymph gland as an *in vivo* model to show that organelles such as mitochondria and endosomes, which act as sub-cellular signal regulatory stations, control lineage-specific differentiation of blood progenitors. We show that though mitochondrial dynamics and endosomal protein sorting play generic roles in maintaining cellular homeostasis, their contribution toward lineage specification is context-dependent and could be modulated by post-transcriptional and post-translational regulatory mechanisms. Also, tissue-enriched conserved regulators of cell fate such as Asrij, regulate the expression of key organellar proteins to fine-tune hematopoietic development.

7.1 Asrij mutant lymph gland proteome serves as a valuable resource for organellar hits with potentially conserved roles in hematopoiesis.

Owing to the critical and conserved role of Asrij in hematopoiesis, we aimed to understand the molecular network downstream of Asrij that may potentially impact progenitor homeostasis. As detailed in the introduction, the larval lymph gland harbors the entire blood progenitor population. Hence, it serves as a useful model for a comprehensive analysis of progenitor homeostasis. Our proteomic analysis of Asrij KO and OV lymph glands provides a resource of candidate proteins with potential roles in blood cell homeostasis (Sinha et al., 2019). Abundance of organelle associated proteins in the candidates list highlights the role of Asrij in post-transcriptional control of signaling for blood cell homeostasis. The major outcomes are discussed in detail in the following sections.

7.2 The Asrij-dependent endocytic axis contributes to immune signaling activation in *Drosophila*.

Earlier reports showed a conserved role for Asrij in maintaining stemness of blood progenitors (Kulkarni, Khadilkar et al., 2011) as well as pluripotent stem cells (mESC) (Sinha

et al., 2013). However, the organismal level requirement of Asrij was underexplored. As hematopoiesis is intricately linked to immune function, analysis of the immune response upon depletion of Asrij could reveal the importance of context-dependent regulation of signaling in the overall physiology of the organism. Asrij regulates endocytic trafficking of Notch intracellular domain (NICD) in hemocytes (Kulkarni, Khadilkar et al., 2011). One possibility could be an active role for Asrij in ubiquitinated cargo transport and sorting process. Also, Asrij regulates the expression of several components of the proteasome and COP9 signalosome machinery that directly contribute to cytosolic protein degradation (Sinha et al., 2019). Our immunofluorescence-based analysis shows upregulation of Cactus ubiquitination that may facilitate its degradation leading to nuclear translocation of Dorsal for the activation of Toll signaling and downstream AMP gene expression (Khadilkar, Ray et al., 2017; Chapter 2 of this thesis). This suggests that Asrij regulates protein ubiquitination and turnover of critical immune signaling components. Additionally, Asrij regulates ProPO expression, thereby contributing to cell-mediated immunity by facilitating ROS generation and melanin biosynthesis. Further, Asrij perturbed lymph gland proteome analysis shows immunity as a significantly affected process (Sinha et al., 2019). Our analyses suggest that Asrij has cell autonomous as well as non-autonomous roles in regulating systemic immune response upon acute bacterial infection. Hence, the conserved Asrij-dependent endosomal axis regulates blood cell homeostasis and immunity.

7.3 Endosomes emerge as potential regulatory hubs for signaling during hematopoiesis.

Previous immunolocalization-based analyses across *Drosophila* and mouse models showed partial localization of Asrij to endosomal compartments of blood cells (Kulkarni, Khadilkar et al., 2011). Also, loss of Asrij inhibits endosomal trafficking of cargoes such as NICD (Kulkarni, Khadilkar et al., 2011; Khadilkar et al., 2014). The Asrij lymph gland proteome provides a repertoire of “endocytic matrix” components that may potentially regulate blood progenitor homeostasis (Sinha et al., 2019; Thesis Chapter 3). A significant number of vesicular transport proteins were enriched in the Asrij perturbed lymph gland proteome. The proteome revealed endosomal candidates Rab7, Rab11, ARF1 etc., which take part in crucial steps of endocytic trafficking such as vesicle biogenesis, fusion, cargo transport and sorting.

The functional link of hematopoiesis with various endosomal proteins may unravel new context-dependent regulatory mechanisms of progenitor homeostasis.

7.4 Asrij significantly impacts regulators of metabolism.

Metabolic flux acts as a critical rate-limiting factor to dictate HSC and progenitor differentiation (Ito et al., 2019). Mitochondrial respiration generates energy metabolites and ROS, both of which contribute to the differentiation of stem cells including HSCs (Papa et al., 2019). A recent report highlights the importance of metabolic status, in addition to marker expression and position of the cell in the tissue, in governing individual lymph gland cell fate (Girard et al., 2021, bioRxiv preprint). Asrij lymph gland proteome analysis reveals metabolism-associated proteins as major hits (Sinha et al., 2019). The human ortholog of Asrij, OCIAD1 localizes to mitochondria and inhibits the activity of mitochondrial Complex I to affect oxygen consumption and energy metabolism in human embryonic stem cells (hESC) (Shetty et al., 2018). Validation of the lymph gland proteome shows that Asrij regulates the expression of NDUFS3, SDHB and COXIV, all of which are well known for their contribution toward metabolic switch from glycolysis to oxidative phosphorylation (Sinha et al., 2019). Hence, Asrij may regulate hematopoiesis through organellar control of metabolism.

7.5 Critical regulators of mitochondrial dynamics play an indispensable role in Notch signaling-dependent differentiation of *Drosophila* blood progenitors.

OCIAD1 regulates mitochondrial morphology in hESC (Shetty et al., 2018). Mitochondrial dynamics maintain the architecture of the mitochondrial network through balanced fission and fusion of mitochondria. Though OCIAD1 potentially regulates mitochondrial dynamics, its *in vivo* relevance remained unexplored. Proteomic analysis of Asrij perturbed lymph glands showed Drp1 as an affected candidate (Sinha et al., 2019). In this thesis, we sought to address the role of Asrij in controlling mitochondrial dynamics *in vivo* through a cross-species comparison.

Mitochondrial dynamics regulators dictate lineage-biased differentiation of progenitors.

We found that depletion of Drp1 or Mitofusin (Marf) from progenitors selectively promotes crystal cell differentiation in the lymph gland (Ray et al., 2021; Chapter 4). This could be attributed to selective activation of signaling pathways such as Notch while suppressing other signaling pathways or predisposing factors that govern plasmatocyte and lamellocyte differentiation. Our analysis suggests that mitochondrial dynamics regulators could potentially affect myeloid biased differentiation or signaling activation. However, the mechanisms underlying lineage commitment may not solely depend on mitochondrial fission and fusion as these mitochondrial architects additionally regulate inter-organellar crosstalk and peroxisome biogenesis. Previous reports have already shown that both Drp1 and Mitofusin may potentially regulate lineage-biased fate of HSC in mice. Drp1 regulates HSC regenerative potential and myeloid reconstitution through a number of biosynthetic pathways (Hinge et al., 2020). Also, Mitofusin regulates the maintenance of HSCs with extensive lymphoid potential through Calcium-dependent NFAT signaling (Luchsinger et al., 2016). Hence, our findings corroborate the role of Drp1 and Mitofusin in lineage-biased differentiation of HSC and blood progenitors. As Drp1 and Marf-dependent signaling activation may be a direct or indirect effect of mitochondrial membrane remodelling, identifying the key steps of signal modulation downstream of mitochondrial dynamics would be useful to improve lineage-specific differentiation of the HSC and blood progenitor.

Mitochondrial dynamics contributes to cellular metabolism, which may in turn dictate cell fate.

Mitochondrial dynamics not only act as a marker of cellular metabolic state but also as a governing factor for metabolic and signaling function of mitochondria, both of which affect HSC and blood progenitor fate (Wai and Langer, 2016; Diebold and Chandel, 2016; Luis et al., 2020). Perturbed expression of mitochondrial dynamics regulators affects the metabolic profile of various tissues and organs in vertebrates (Wai and Langer, 2016). Genetic ablation of Opa1 results in altered insulin secretion and glucose homeostasis systemically (Zhang et al., 2011). Mfn2 regulates metabolic signaling in mouse skeletal muscle (Sebastian et al.,

2012). Also, deletion of Mfn2 from the liver results in increased glucose production and impaired insulin signaling (Sebastian et al., 2012). Skeletal muscle-specific transgenic overexpression of Drp1 downregulates protein translation, upregulates Fgf21, activates mitochondrial unfolded protein response and impairs basal metabolism of skeletal muscle (Touvier et al., 2015). Loss of Drp1 impairs several biosynthetic pathways in mouse HSCs (Hinge et al., 2020). Hence, Asrij-dependent mitochondrial dynamics in the lymph gland progenitors may potentially contribute to altered expression and activity of metabolism associated proteins, including components of the electron transport chain (ETC), as found in the lymph gland proteome.

7.6 Asrij/OCIAD1 acts as a conserved modulator of mitochondrial dynamics.

OCIAD1 physically interacts with several proteins associated with the ETC and acts as a scaffold in the supramolecular Prohibitin assemblies on the inner mitochondrial membrane (IMM) (Floyd et al., 2016; Shetty et al., 2018; Le Vasseur et al., 2021). OCIAD1 also interacts with multiple regulators of mitochondrial dynamics and ER-mitochondria communication (Floyd et al., 2016; Antonicka et al., 2020; <https://thebiogrid.org/120280/summary/homo-sapiens/ociad1.html>). While Asrij regulates mitochondrial dynamics in blood progenitors and hemocytes in *Drosophila*, OCIAD1 regulates mitochondrial dynamics in hESCs in a similar way (Ray et al., 2021; Thesis Chapter 4). Our *in vivo* analysis of genetic interaction shows that Asrij acts upstream of Marf and regulates crystal cell differentiation in a synergistic manner. Hence, Asrij plays a conserved role in progenitor differentiation and lineage specification through functional interaction with the ubiquitous key regulators of mitochondrial dynamics.

7.7 Redundancy, multifunctionality and post-translational regulatory mechanisms may underlie the distinct role of ESCRT components in progenitor homeostasis and lineage choice.

We show that conserved ESCRT machinery components regulate hematopoiesis in *Drosophila* lymph gland. An active role of ESCRT machinery in hematopoiesis indicates

endosomal protein sorting as a critical step, orchestrating signaling pathways in the blood progenitors. Though ESCRT components are ubiquitous, we observed that their role towards lineage choice is distinct and varies across blood progenitor subsets. The differential contribution of different ESCRT components toward a given lineage specification may be attributed to several factors such as- 1) existence of bypass routes for endosomal protein sorting, involving additional auxiliary components, 2) post-translational modifications that may render some ESCRT components inactive towards sorting of specific signaling receptors, 3) multifunctionality of a few components in other membrane remodelling processes such as cytokinetic abscission, exosome biogenesis, nuclear envelope sealing, lysosomal membrane repair, macroautophagy, mitochondria and peroxisome biogenesis, etc.

Differentiation to each blood cell type demands activation of specific transcription factors and signaling pathways. Many of these signaling pathways are regulated by ESCRT. Though depletion of most of the ESCRT components upregulate Notch signaling and crystal cell differentiation, only a few ESCRT components regulate lamellocyte differentiation that depends on the activation of EGFR signaling and downregulation of JAK/STAT and Notch signaling (Sinenko et al., 2011; Morin-Poulard et al., 2013; Small et al., 2014). Differential activation of various endosomal signaling pathways by a given ESCRT component may depend on its cargo-specific sorting function. How the ESCRT subunits and individual components differentially regulate the sorting of a specific cargo and segregate signals in different biological contexts remains unclear and demand further investigation in the future.

Though ESCRT-0 components contribute to plasmacyte and crystal cell differentiation, they are dispensable for lamellocyte differentiation (Fig 7.1). Hrs depletion causes increased plasmacyte differentiation, Notch signaling activation and crystal cell differentiation in the secondary lobe. However, Stam knockdown does not affect plasmacyte or crystal cell differentiation in the secondary lobe. This reflects intra-subunit phenotypic diversity within ESCRT-0. Also, none of the ESCRT-0 components affects lamellocyte differentiation. Earlier reports have shown that post-translational modification such as monoubiquitination may

render ESCRT-0 inactive (Hoeller et al., 2006). Also, auxiliary ESCRT component Alix can recognize endosomal cargoes and sort them independent of ESCRT-0 and ESCRT-I, but in an ESCRT-III dependent manner (Dores et al., 2016; Gahloth et al., 2017). The phenotypes of ESCRT-0 depletion in the lymph gland suggests existence of similar bypass mechanisms (Fig 7.1). Also, analysis for a double KD or double KO for Hrs and Stam may explain if they complement each other's role in the specific context of blood progenitor differentiation.

To our surprise, depletion or mutation of Vps25, a critical component of ESCRT-II subunit did not affect differentiation to any of the blood cell lineages, despite its expression in the lymph gland. Also, Vps25 knockdown, though causes enlargement of the primary lobe, does not affect the mitotic potential, suggesting its developmental stage-specific role that may be temporally regulated. Though Vps25 is a critical player in endosomal protein sorting pathway, the absence of phenotype in terms of lineage-specific differentiation indicates alternate routes for signaling regulation in the blood progenitor. Earlier genetic analysis of ESCRT function has shown that Bro1 in yeast, and Alix and HD-PTP in mammals act as alternate bridging factors to ESCRT-II to mediate endosomal protein sorting (Bissig et al., 2014; Taberero et al., 2018). Also, phenotypic diversity within the ESCRT-II subunit has been previously reported in *Drosophila* eye imaginal disc epithelium (Herz et al., 2009). Though the interaction of Vps36 and Vps22 with ESCRT-III depends on Vps25, we see very strong phenotype of blood cell differentiation across lobes upon depletion of Vps36. Also, Vps22 depletion promotes plasmacyte and crystal cell differentiation in the primary lobe. Hence, Vps36 and Vps22 may act through additional adaptors that act in parallel with Vps25 (Fig 7.1). Also, Vps36 potentially participates in functions other than endosomal protein sorting which may make it indispensable for lineage choice across progenitor subsets.

Majority of the ESCRT components regulating progenitor differentiation belong to ESCRT-I and ESCRT-III that participate in intraluminal vesicle budding and scission, respectively (Fig 7.1). This could be attributed to the critical role of ESCRT-I and ESCRT-III in membrane remodelling, which acts as a vital step of endosomal sorting and several other processes. As mentioned earlier, several reports have highlighted the phenotypic diversity of ESCRT

mutation. ESCRT components differentially contribute to intraluminal vesicle formation in *Drosophila* epithelial tissues (Vaccari et al., 2009). What remains an intriguing question is the mechanisms that regulate the differential role of ESCRT components in lineage choice. However, growing evidence converges to the mechanisms of rapid dynamics of ESCRT component exchange, context-dependent compositional variation and malleable geometric transition of the complexes as the primary contributing factors to such distinct outcomes in different biological situations (Pavlin and Hurley, 2020).

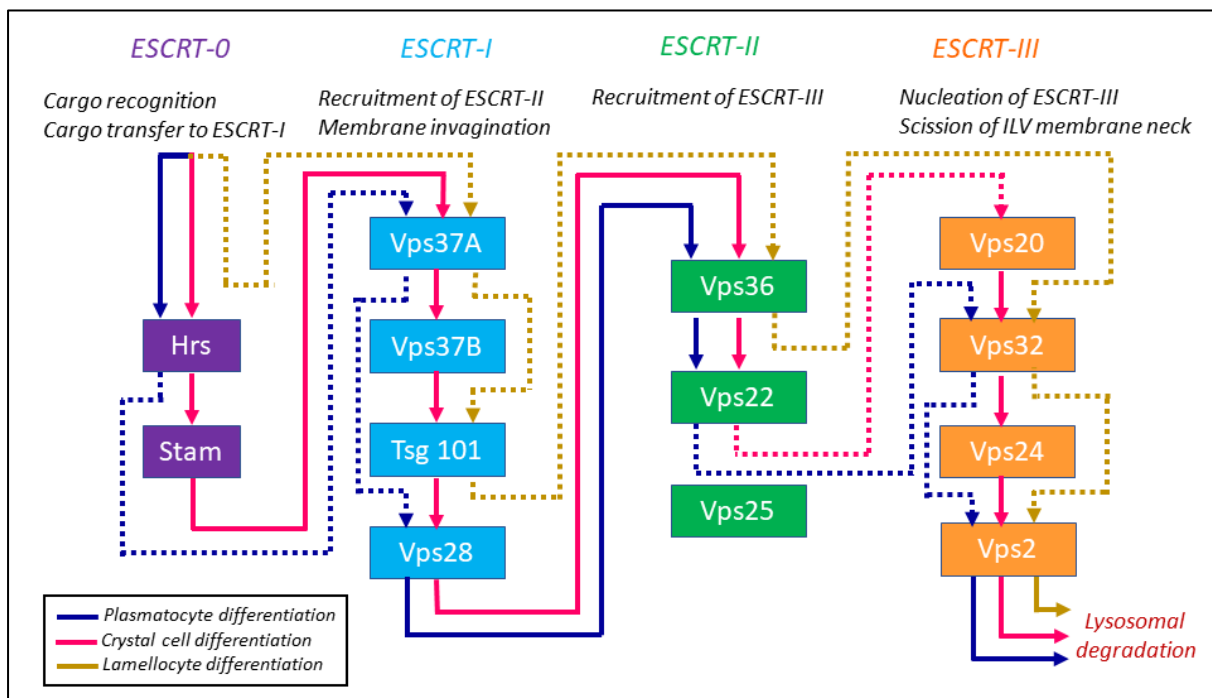


Figure 7.1. ESCRT components play a distinct role in lineage choice. Analysis of the role of 13 *Drosophila* ESCRT core components in lineage-specific differentiation of progenitors reflect the existence of several bypass routes (dotted lines). The predicted routes for cargo sorting and degradation during the differentiation of the three *Drosophila* blood cell lineages are shown using three different color-coded arrow sets (Blue lines: Route for regulating plasmatocyte differentiation; pink for crystal cell differentiation; brown for lamellocyte differentiation). While shunt routes may impart functional redundancy to certain ESCRT components, the phenotypic outcome may depend on non-ESCRT role of the components as well.

7.8 Organelle level contribution to inherent developmental and functional heterogeneity of the blood progenitor subsets in the lymph gland lobes.

Posterior progenitor subsets of the lymph gland rarely differentiate to lamellocytes upon severe wasp infestation (Rodrigues et al., 2021). These progenitor subpopulations are functionally hardwired to maintain stemness throughout the larval stage as they possibly act as a reserve pool dedicated to various developmental roles. However, our findings show that critical organellar components could play a pivotal role to unlock the differentiation cues in such refractile progenitor populations.

The compartmentalized progenitor subsets of the lymph gland are transcriptionally heterogeneous, assume differential proliferative potential and respond in a non-uniform manner upon immune challenge (Rodrigues et al., 2021). Also, earlier phenotypic analysis of *asrij* mutant lymph gland showed differential proliferative response of primary and posterior lobe hemocytes (Kulkarni, Khadilkar et al., 2011). Our analyses of mitochondrial morphology across different subsets reveals that the mitochondria in tertiary lobe progenitors are mostly fragmented, unlike primary and secondary lobes. As fragmented appearance of mitochondria generally correlates with a higher degree of stemness, this may reflect a more immature nature of tertiary lobe progenitors as expected. We find that progenitor response upon depletion of *Asrij*, *Drp1* or *Marf* varies across different lobes of the lymph gland. Though progenitor-specific downregulation of *Marf* leads to fragmentation of mitochondria and activation of Notch signaling in the secondary lobe progenitors, it fails to cause differentiation to ProPO⁺ crystal cells. Also, tertiary lobe progenitors do not undergo Notch activation or blood cell differentiation upon knockdown of *Asrij*, *Drp1* or *Marf*. This indicates developmentally immature and refractile nature of the posterior pool of progenitors. Also, additional regulatory mechanisms may operate downstream of Notch signaling in the posterior pool of blood progenitors to inhibit differentiation.

Vps36 depletion triggers lamellocyte differentiation across all progenitor subsets of the lymph gland, in the absence of any immune challenge. Also, depletion of ESCRT-III

component Vps2 triggers lamellocyte differentiation in both primary and secondary lobes. This indicates that not all but very specific molecular events associated with endosomal protein sorting could play a critical role in posterior progenitor differentiation to lamellocytes. This knowledge can be exploited to screen for key regulators of progenitor homeostasis and may help design strategies to improve the regenerative potential of blood stem cells and progenitors both *in vitro* and *in vivo*.

It is quite fascinating how ESCRT components, despite their uniform expression across the lymph gland yield distinct phenotypes across these developmentally distinct progenitor pools. The absence of strong phenotypes, despite uniform expression indicates possible redundancy and the existence of additional and likely more stringent signaling checkpoints in the posterior progenitors. Further genetic and proteomic analyses may unravel the regulatory mechanisms of spatial and developmental heterogeneity of progenitors.

Lineage tracing-based experiments have previously demonstrated different ontogeny of the anterior and posterior progenitors. While the posterior pools of cells are derived from Ubx+ anlage, the anterior lobes have a different origin (Lo et al., 2002). Moreover, the posterior lobes express higher level of certain extracellular matrix organising proteins like Dlp that may potentially contribute to differential signaling activation upon acute immune challenge (Rodrigues et al., 2021). This supports the finding that the progenitor subpopulations, arranged linearly along the anteroposterior axis, differ in their origin as well as gene expression profile. *We propose that endosomes and mitochondria contribute actively to this inherent progenitor heterogeneity resulting in differential sensitivity to genetic alteration or immune stimuli.* It would be interesting to see how the mitochondrial dynamics or endosomal sorting efficiency changes across such progenitor subsets upon immune challenge or mechanical stress. Also, through downregulation of genes such as Marf, Vps36 or Vps2, a sensitized milieu to test various paradigms for the effect on blood cell differentiation across progenitor subpopulations is now available. This should help model various pathological situations arising due to organelle defects or dysregulation.

7.9 Organelle membrane remodelling is critical for the modulation of developmental signaling.

Membrane remodelling plays a crucial role in signal homeostasis through variation of its composition and architecture. Maintenance of membrane integrity and membrane-associated molecular interactions dictate organelle function and cell physiology. The bilamellar limiting membranes of various sub-cellular organelles act as the site of signal generation, integration, and attenuation by harboring a plethora of molecular players that establish an intricate cell signaling network. Hence, membrane architect proteins could greatly influence the dynamicity of organellar crosstalk and the downstream signaling cascade.

Work from our laboratory and that of others shows that mitochondrial membrane-associated GTPases regulate various signaling pathways such as Notch signaling and calcium-dependent NFAT to maintain HSC and progenitor homeostasis across model systems (Luchsinger et al., 2016; Hinge et al., 2020; Thesis Chapter 4). Asrij/OCIAD1 harbors putative transmembrane helices in the N-terminal conserved OCIA domain, which is required for its organellar localization (Sinha et al., 2013; Khadilkar et al., 2014) (Figure 7.2). OCIAD1 interacts with several IMM proteins including components of oxidative phosphorylation, mitochondrial dynamics, ER-mitochondrial calcium signaling, etc (Floyd et al., 2016; Shetty et al., 2018; Antonicka et al., 2020). Also, loss of Asrij leads to elongation of mitochondria which suggests change in the dynamics of mitochondrial membrane remodelling. Additionally, our genetic interaction analysis indicates that Asrij acts through Mitofusin to regulate mitochondrial morphology. The future plan in this regard involves detailed mechanistic analysis of Asrij-dependent regulation of organellar membrane dynamics.

As inter-compartmental communications in the endocytic route primarily occur at the organellar interface, endosomal membrane topology significantly impacts critical molecular interactions. Though endosomal cargo sorting involves distinct steps of post-translational modification and molecular recognition, this process primarily acts through energy-

dependent modulation of the membrane curvature. As discussed elaborately in section 7.7, ESCRT components regulate a number of sub-cellular events, all of which require membrane budding, severing or sealing. Hence, mechanical control of organellar membrane stability is critical for signal homeostasis. However, the nature, site and time of action for membrane remodelling proteins including ESCRT components would possibly dictate their role in signaling regulation and tissue development.

7.10 Asrij may potentially mediate inter-organellar crosstalk.

Mitophagy maintains hematopoietic progenitors or stimulates hematopoiesis in vertebrates (Jin et al., 2018; Girotra et al., 2020). Inter-organellar communications allow complex spatiotemporal regulation of signaling and cell fate specification. Loss of *Asrij* leads to elongation of mitochondria and increase in mitochondrial content that reflects impaired mitochondrial degradation and possible perturbation in the mitophagy flux. While canonical Notch signalling leads to crystal cell differentiation, non-canonical activation due to endosomal NICD entrapment (Kulkarni, Khadilkar et al., 2011) may also contribute to the *asrij* mutant phenotype. Apart from its role in mitochondria, *Asrij* could also act as a scaffolding protein to assemble critical signaling complexes on the endosomal surface (Sinha et al., 2013; Motiwala et al., 2021). BioGRID analysis shows physical interaction of OCIAD1 with a number of proteins including Vps33B, Vps13A, Vps13D, VDAC, PARK13, Rab5c, Fis1 etc, all of which functionally bridge mitochondria to the endocytic route through inter-organellar crosstalk (Hein et al., 2015; Botham et al., 2018; Antonicka et al., 2020). Moreover, Mitofusin and Drp1, which are potential physical interactors of *Asrij*, regulate ER-mitochondria crosstalk and calcium signaling (Marchi et al., 2014). Hence, *Asrij* may potentially act as a mediator of inter-organellar communication to influence blood cell homeostasis. *Asrij*-dependent mitochondrial dynamics can regulate Notch signaling in an ESCRT-independent manner as well through its mitochondria-associated functional axis and merits further investigation. On the other hand, *Asrij* positively regulates expression of critical ESCRT components such as Vps32 which could also impact Notch activation through regulation of NICD endocytic degradation. Any possibility of *Asrij*-mitochondrial dynamics-

ESCRT axis in Notch signaling regulation during steady state hematopoiesis demands further mechanistic elucidation through genetics-based approach. Live tracking of Asrij across organellar compartments or identification of molecular signatures that segregate Asrij pool in different organellar compartments may clarify how Asrij regulates multiple organelle function. The role of mitochondria-endosome communication in the context of progenitor homeostasis merits further investigation (Fig 7.2).

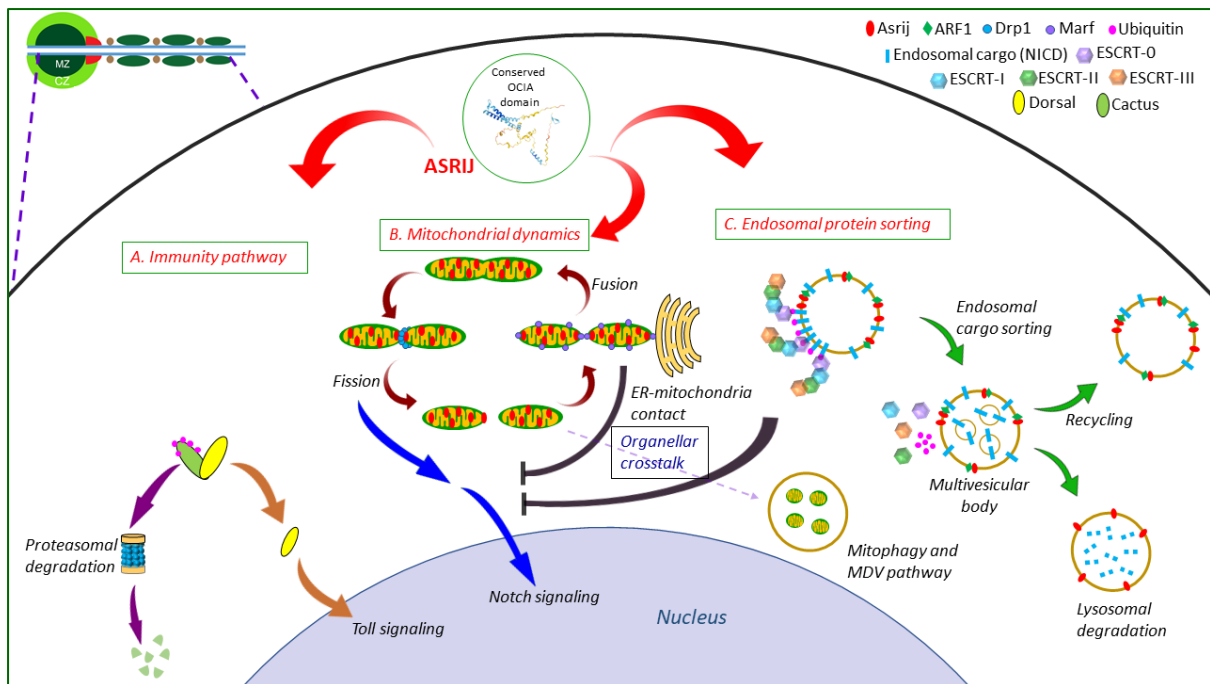


Figure 7.2. Asrij integrates critical organellar circuitries to maintain blood progenitor homeostasis in the *Drosophila* lymph gland. (A) Asrij regulates ubiquitination and degradation of cytosolic protein Cactus and promotes nuclear translocation of Dorsal to activate immune signaling pathways such as Toll signaling. This could be through the regulatory role of Asrij in protein ubiquitination. (B) Asrij regulates mitochondrial dynamics primarily through a Mitofusin-dependent route. Mitochondrial dynamics regulators contribute to the activation of Notch signaling, which triggers lineage-specific differentiation of the blood progenitor. (C) While Asrij interacts with ARF1 and may potentially regulate endosomal sorting of Notch intracellular domain (NICD), the conserved ESCRT machinery constitutes a complex functional network with distinct role of individual components in signaling activation and lineage choice. ESCRT acts downstream of Asrij to regulate endosomal degradation of NICD and downregulates Notch pathway. Dual organellar localization of Asrij suggests its potential role in inter-organellar crosstalk through mechanisms such as ER-mitochondria contact, mitophagy and MDV (mitochondria-derived vesicle) pathway.

7.11 Misexpression of mitochondrial dynamics regulators and ESCRT components may result in hematological disorders.

Perturbed expression of the regulators of mitochondrial dynamics may underlie several pathophysiological conditions across tissue types and organs in humans, indicating their generic role. Drp1 loss of function or dominant negative mutation causes prenatal and postnatal microcephaly, which occasionally could be fatal (Waterham et al., 2007; Sheffer et al., 2016). Also, Drp1-dependent mitochondrial fragmentation plays an active role in the pathogenesis of acute kidney injury and diabetic nephropathy (Zhan et al., 2013). Mfn2 mutation leads to Charcot-Marie-Tooth type 2A autosomal dominant hereditary disorder which is characterized by axonal neuropathy and neurodegeneration (Zuchner et al., 2004). Germline knockout of Mfn1 or Mfn2 in mice causes embryonic lethality, indicating the essential role of these genes in development (Chen et al., 2003). Conditional knockout of Mfn2 causes Purkinje cell degeneration leading to defective postnatal development of the cerebellum (Chen et al., 2007).

Hematological disorders may also be associated with the misexpression of mitochondrial dynamics regulators. BloodSpot Leukemia MILE database shows upregulation or downregulation of DNM1L (Drp1) and Mitofusin (Mfn1 and Mfn2) expression in conditions such as Acute Myeloid Leukemia (AML) and Acute Lymphocytic Leukemia (ALL) (<https://servers.binf.ku.dk/bloodspot/>). Additionally, Drp1 and Mitofusin mutations are reported in diseased samples of hematopoietic and lymphoid tissues (<https://cancer.sanger.ac.uk/cosmic>). A recent report shows that Drp1-dependent mitochondrial fission promotes *in vitro* human thrombopoiesis and inhibition of mitochondrial fission inhibits megakaryocyte maturation *in vitro* (Poirault-Chassac et al., 2021).

ESCRT genes are misexpressed under conditions of hematological aberrations such as acute lymphoblastic leukemia (ALL), acute myeloid leukemia (AML), Myelodysplastic syndromes etc (<https://servers.binf.ku.dk/bloodspot/>). However, the role of endosomal protein sorting and ESCRT machinery in vertebrate hematopoiesis remain largely unexplored. Unlike the

vertebrate hematopoietic system, *Drosophila* has only myeloid lineage of blood cells with limited diversity. Also, the hematopoietic microenvironment may differ due to fundamental differences in invertebrate and vertebrate development. Despite mechanistic similarity in the process of blood cell formation, some obvious differences of the *Drosophila* hematopoietic model system necessitate similar analyses in vertebrates. Deciphering the role of ESCRT in vertebrate hematopoiesis may pave the way for novel therapeutic modalities to treat hematological disorders.

Hence, the role of both mitochondrial dynamics and endosomal protein sorting machinery in hematopoiesis holds relevance from a clinical perspective. Also, blood cell enriched regulator of mitochondrial dynamics and ESCRT expression, Asrij can be tested further as a possible target to develop therapeutic strategies.

7.12 Concluding remarks

In this thesis, we highlight the existence and importance of context-dependent regulation of generic organellar functions in maintaining blood progenitor homeostasis and lineage choice. Using the *Drosophila* lymph gland as the model for a comprehensive analysis of blood progenitor homeostasis, we identified the mitochondrial dynamics regulators and endosomal protein sorting machinery (ESCRT) as active regulators of homeostasis. Though uniformly expressed, the individual components of ESCRT play distinct role in lineage-biased differentiation of the blood progenitors. As the intricate network of critical organellar proteins continues to unravel, elucidating the role of individual functional branches in blood progenitor homeostasis may potentially find an application in regenerative therapy.

Asrij emerges as a tissue-specific regulator of mitochondrial and endosomal proteins including components of mitochondrial dynamics and endosomal sorting machinery in the *Drosophila* hematopoietic organ, the lymph gland. Asrij and its vertebrate homolog OCIAD1 regulate the expression and activity of critical organellar proteins and molecular complexes. Identification of such tissue-enriched conserved regulators of signaling and hematopoiesis would facilitate the designing of targeted therapy for various hematological disorders.

References:

- A**BLES, J. L., BREUNIG, J. J., EISCH, A. J. & RAKIC, P. 2011. Not(ch) just development: Notch signalling in the adult brain. *Nat Rev Neurosci*, 12, 269-83.
- ADOLFSSON, J., MANSSON, R., BUZA-VIDAS, N., HULTQUIST, A., LIUBA, K., JENSEN, C. T., BRYDER, D., YANG, L., BORGE, O. J., THOREN, L. A., ANDERSON, K., SITNICKA, E., SASAKI, Y., SIGVARDSSON, M. & JACOBSEN, S. E. 2005. Identification of Flt3+ lymphomyeloid stem cells lacking erythro-megakaryocytic potential a revised road map for adult blood lineage commitment. *Cell*, 121, 295-306.
- AGGARWAL, K. & SILVERMAN, N. 2008. Positive and negative regulation of the *Drosophila* immune response. *BMB Rep*, 41, 267-77.
- ALFONSO, T. B. & JONES, B. W. 2002. *gcm2* promotes glial cell differentiation and is required with glial cells missing for macrophage development in *Drosophila*. *Dev Biol*, 248, 369-83.
- ALFRED, V. & VACCARI, T. 2016. When membranes need an ESCRT: endosomal sorting and membrane remodelling in health and disease. *Swiss Med Wkly*, 146, w14347.
- ANAND, R., WAI, T., BAKER, M. J., KLADT, N., SCHAUSS, A. C., RUGARLI, E. & LANGER, T. 2014. The i-AAA protease YME1L and OMA1 cleave OPA1 to balance mitochondrial fusion and fission. *J Cell Biol*, 204, 919-29.
- ANSO, E., WEINBERG, S. E., DIEBOLD, L. P., THOMPSON, B. J., MALINGE, S., SCHUMACKER, P. T., LIU, X., ZHANG, Y., SHAO, Z., STEADMAN, M., MARSH, K. M., XU, J., CRISPINO, J. D. & CHANDEL, N. S. 2017. The mitochondrial respiratory chain is essential for haematopoietic stem cell function. *Nat Cell Biol*, 19, 614-625.
- ANTONICKA, H., LIN, Z. Y., JANER, A., AALTONEN, M. J., WERAARPACHAI, W., GINGRAS, A. C. & SHOUBRIDGE, E. A. 2020. A High-Density Human Mitochondrial Proximity Interaction Network. *Cell Metab*, 32, 479-497 e9.
- AVET-ROCHEX, A., BOYER, K., POLESSELLO, C., GOBERT, V., OSMAN, D., ROCH, F., AUGE, B., ZANET, J., HAENLIN, M. & WALTZER, L. 2010. An in vivo RNA interference screen identifies gene networks controlling *Drosophila melanogaster* blood cell homeostasis. *BMC Dev Biol*, 10, 65.
- B**ABST, M., KATZMANN, D. J., SNYDER, W. B., WENDLAND, B. & EMR, S. D. 2002. Endosome-associated complex, ESCRT-II, recruits transport machinery for protein sorting at the multivesicular body. *Dev Cell*, 3, 283-9.
- BAEUMERS, M., RUHNAU, K., BREUER, T., PANNEN, H., GOERLICH, B., KNIEBEL, A., HAENSCH, S., WEIDTKAMP-PETERS, S., SCHMITT, L. & KLEIN, T. 2020. Lethal (2) giant discs (Lgd)/CC2D1 is required for the full activity of the ESCRT machinery. *BMC Biol*, 18, 200.
- BALDEOSINGH, R., GAO, H., WU, X. & FOSSETT, N. 2018. Hedgehog signaling from the Posterior Signaling Center maintains U-shaped expression and a prohemocyte population in *Drosophila*. *Dev Biol*, 441, 132-145.
- BANERJEE, U., GIRARD, J. R., GOINS, L. M. & SPRATFORD, C. M. 2019. *Drosophila* as a Genetic Model for Hematopoiesis. *Genetics*, 211, 367-417.

- BANKAITIS, V. A., JOHNSON, L. M. & EMR, S. D. 1986. Isolation of yeast mutants defective in protein targeting to the vacuole. *Proc Natl Acad Sci U S A*, 83, 9075-9.
- BAUMERS, M., KLOSE, S., BRUSER, C., HAAG, C., HANSCH, S., PANNEN, H., WEIDTKAMP-PETERS, S., FELDBRUGGE, M. & KLEIN, T. 2019. The auxiliary ESCRT complexes provide robustness to cold in poikilothermic organisms. *Biol Open*, 8.
- BECK, R., PRINZ, S., DIESTELKOTTER-BACHERT, P., ROHLING, S., ADOLF, F., HOEHNER, K., WELSCH, S., RONCHI, P., BRUGGER, B., BRIGGS, J. A. & WIELAND, F. 2011. Coatamer and dimeric ADP ribosylation factor 1 promote distinct steps in membrane scission. *J Cell Biol*, 194, 765-77.
- BECKER, K. L., SNIDER, R. & NYLEN, E. S. 2010. Procalcitonin in sepsis and systemic inflammation: a harmful biomarker and a therapeutic target. *Br J Pharmacol*, 159, 253-64.
- BEJARANO-GARCIA, J. A., MILLAN-UCLES, A., ROSADO, I. V., SANCHEZ-ABARCA, L. I., CABALLERO-VELAZQUEZ, T., DURAN-GALVAN, M. J., PEREZ-SIMON, J. A. & PIRUAT, J. I. 2016. Sensitivity of hematopoietic stem cells to mitochondrial dysfunction by SdhD gene deletion. *Cell Death Dis*, 7, e2516.
- BENMIMOUN, B., POLESELLO, C., HAENLIN, M. & WALTZER, L. 2015. The EBF transcription factor Collier directly promotes Drosophila blood cell progenitor maintenance independently of the niche. *Proc Natl Acad Sci U S A*, 112, 9052-7.
- BERNARDONI, R., VIVANCOS, V. & GIANGRANDE, A. 1997. glide/gcm is expressed and required in the scavenger cell lineage. *Dev Biol*, 191, 118-30.
- BHANDARI, P., SONG, M. & DORN, G. W., 2ND 2015. Dissociation of mitochondrial from sarcoplasmic reticular stress in Drosophila cardiomyopathy induced by molecularly distinct mitochondrial fusion defects. *J Mol Cell Cardiol*, 80, 71-80.
- BILODEAU, P. S., URBANOWSKI, J. L., WINISTORFER, S. C. & PIPER, R. C. 2002. The Vps27p Hse1p complex binds ubiquitin and mediates endosomal protein sorting. *Nat Cell Biol*, 4, 534-9.
- BISSIG, C. & GRUENBERG, J. 2014. ALIX and the multivesicular endosome: ALIX in Wonderland. *Trends Cell Biol*, 24, 19-25.
- BLANCO-OBREGON, D., KATZ, M. J., DURRIEU, L., GANDARA, L. & WAPPNER, P. 2020. Context-specific functions of Notch in Drosophila blood cell progenitors. *Dev Biol*, 462, 101-115.
- BOTHAM, A., COYAUD, E., NIRMALANANDHAN, V. S., GRONDA, M., HURREN, R., MACLEAN, N., ST-GERMAIN, J., MIRALI, S., LAURENT, E., RAUGHT, B. & SCHIMMER, A. 2019. Global Interactome Mapping of Mitochondrial Intermembrane Space Proteases Identifies a Novel Function for HTRA2. *Proteomics*, 19, e1900139.
- BOURA, E., ROZYCKI, B., CHUNG, H. S., HERRICK, D. Z., CANAGARAJAH, B., CAFISO, D. S., EATON, W. A., HUMMER, G. & HURLEY, J. H. 2012. Solution structure of the ESCRT-I and -II supercomplex: implications for membrane budding and scission. *Structure*, 20, 874-86.
- BRANDNER, A., DE VECCHIS, D., BAADEN, M., COHEN, M. M. & TALY, A. 2019. Physics-based oligomeric models of the yeast mitofusin Fzo1 at the molecular scale in the context of membrane docking. *Mitochondrion*, 49, 234-244.
- BRAUN, V., DESCHAMPS, C., RAPOSO, G., BENAROCH, P., BENMERAH, A., CHAVRIER, P. & NIEDERGANG, F. 2007. AP-1 and ARF1 control endosomal dynamics at sites of FcR mediated phagocytosis. *Mol Biol Cell*, 18, 4921-31.

- BRENNAN, C. A., DELANEY, J. R., SCHNEIDER, D. S. & ANDERSON, K. V. 2007. Psidin is required in *Drosophila* blood cells for both phagocytic degradation and immune activation of the fat body. *Curr Biol*, 17, 67-72.
- BUCHON, N., SILVERMAN, N. & CHERRY, S. 2014. Immunity in *Drosophila melanogaster*--from microbial recognition to whole-organism physiology. *Nat Rev Immunol*, 14, 796-810.
- BULET, P., HETRU, C., DIMARCO, J. L. & HOFFMANN, D. 1999. Antimicrobial peptides in insects; structure and function. *Dev Comp Immunol*, 23, 329-44.
- C**HAKRABARTI, S., DUDZIC, J. P., LI, X., COLLAS, E. J., BOQUETE, J. P. & LEMAITRE, B. 2016. Remote Control of Intestinal Stem Cell Activity by Haemocytes in *Drosophila*. *PLoS Genet*, 12, e1006089.
- CHARROUX, B. & ROYET, J. 2009. Elimination of plasmatocytes by targeted apoptosis reveals their role in multiple aspects of the *Drosophila* immune response. *Proc Natl Acad Sci U S A*, 106, 9797-802.
- CHEN, H., DETMER, S. A., EWALD, A. J., GRIFFIN, E. E., FRASER, S. E. & CHAN, D. C. 2003. Mitofusins Mfn1 and Mfn2 coordinately regulate mitochondrial fusion and are essential for embryonic development. *J Cell Biol*, 160, 189-200.
- CHEN, H., MCCAFFERY, J. M. & CHAN, D. C. 2007. Mitochondrial fusion protects against neurodegeneration in the cerebellum. *Cell*, 130, 548-62.
- CHEN, L., ZHANG, J., LYU, Z., CHEN, Y., JI, X., CAO, H., JIN, M., ZHU, J., YANG, J., LING, R., XING, J., REN, T. & LYU, Y. 2018. Positive feedback loop between mitochondrial fission and Notch signaling promotes survivin-mediated survival of TNBC cells. *Cell Death Dis*, 9, 1050.
- CHO, B., YOON, S. H., LEE, D., KORANTENG, F., TATTIKOTA, S. G., CHA, N., SHIN, M., DO, H., HU, Y., OH, S. Y., VIPIN MENON, A., MOON, S. J., PERRIMON, N., NAM, J. W. & SHIM, J. 2020. Single-cell transcriptome maps of myeloid blood cell lineages in *Drosophila*. *Nat Commun*, 11, 4483.
- CLEMENTS, W. K. & TRAVER, D. 2013. Signalling pathways that control vertebrate haematopoietic stem cell specification. *Nat Rev Immunol*, 13, 336-48.
- COPPENS, T., VAN DEN BERGH, P., DUPREZ, T. J., JEANJEAN, A., DE RIDDER, F. & SINDIC, C. J. 2006. Paraneoplastic rhombencephalitis and brachial plexopathy in two cases of amphiphysin auto-immunity. *Eur Neurol*, 55, 80-3.
- D**'SOUZA-SCHOREY, C. & CHAVRIER, P. 2006. ARF proteins: roles in membrane traffic and beyond. *Nat Rev Mol Cell Biol*, 7, 347-58.
- D'SOUZA, B., MELOTY-KAPPELLA, L. & WEINMASTER, G. 2010. Canonical and non-canonical Notch ligands. *Curr Top Dev Biol*, 92, 73-129.
- DE ALMEIDA, M. J., LUCHSINGER, L. L., CORRIGAN, D. J., WILLIAMS, L. J. & SNOECK, H. W. 2017. Dye-Independent Methods Reveal Elevated Mitochondrial Mass in Hematopoietic Stem Cells. *Cell Stem Cell*, 21, 725-729 e4.
- DE CAMILLI, P., THOMAS, A., COFIELL, R., FOLLI, F., LICHTER, B., PICCOLO, G., MEINCK, H. M., AUSTONI, M., FASSETTA, G., BOTTAZZO, G., BATES, D., CARLIDGE, N., SOLIMENA, M., KILIMANN, M. W. & ET AL. 1993. The synaptic vesicle-associated protein

- amphiphysin is the 128-kD autoantigen of Stiff-Man syndrome with breast cancer. *J Exp Med*, 178, 2219-23.
- DE PATER, E., KAIMAKIS, P., VINK, C. S., YOKOMIZO, T., YAMADA-INAGAWA, T., VAN DER LINDEN, R., KARTALAEI, P. S., CAMPER, S. A., SPECK, N. & DZIERZAK, E. 2013. Gata2 is required for HSC generation and survival. *J Exp Med*, 210, 2843-50.
- DEVERGNE, O., GHIGLIONE, C. & NOSELLI, S. 2007. The endocytic control of JAK/STAT signalling in *Drosophila*. *J Cell Sci*, 120, 3457-64.
- DEY, N. S., RAMESH, P., CHUGH, M., MANDAL, S. & MANDAL, L. 2016. Dpp dependent Hematopoietic stem cells give rise to Hh dependent blood progenitors in larval lymph gland of *Drosophila*. *Elife*, 5.
- DIEBOLD, L. P. & CHANDEL, N. S. 2016. HSC Fate Is Tethered to Mitochondria. *Cell Stem Cell*, 18, 303-4.
- DIEDERICH, R. J., MATSUNO, K., HING, H. & ARTAVANIS-TSAKONAS, S. 1994. Cytosolic interaction between deltex and Notch ankyrin repeats implicates deltex in the Notch signaling pathway. *Development*, 120, 473-81.
- DIMARCO, J. L., IMLER, J. L., LANOT, R., EZEKOWITZ, R. A., HOFFMANN, J. A., JANEWAY, C. A. & LAGUEUX, M. 1997. Treatment of I(2)mbn *Drosophila* tumorous blood cells with the steroid hormone ecdysone amplifies the inducibility of antimicrobial peptide gene expression. *Insect Biochem Mol Biol*, 27, 877-86.
- DORES, M. R., GRIMSEY, N. J., MENDEZ, F. & TREJO, J. 2016. ALIX Regulates the Ubiquitin-Independent Lysosomal Sorting of the P2Y1 Purinergic Receptor via a YPX3L Motif. *PLoS One*, 11, e0157587.
- DURAND, C., ROBIN, C., BOLLEROT, K., BARON, M. H., OTTERSBUCH, K. & DZIERZAK, E. 2007. Embryonic stromal clones reveal developmental regulators of definitive hematopoietic stem cells. *Proc Natl Acad Sci U S A*, 104, 20838-43.
- DUVIC, B., HOFFMANN, J. A., MEISTER, M. & ROYET, J. 2002. Notch signaling controls lineage specification during *Drosophila* larval hematopoiesis. *Curr Biol*, 12, 1923-7.
- FILIPPI, M. D. & GHAFFARI, S. 2019. Mitochondria in the maintenance of hematopoietic stem cells: new perspectives and opportunities. *Blood*, 133, 1943-1952.**
- FLOYD, B. J., WILKERSON, E. M., VELING, M. T., MINOGUE, C. E., XIA, C., BEEBE, E. T., WROBEL, R. L., CHO, H., KREMER, L. S., ALSTON, C. L., GROMEK, K. A., DOLAN, B. K., ULBRICH, A., STEFELY, J. A., BOHL, S. L., WERNER, K. M., JOCHEM, A., WESTPHALL, M. S., RENSVOLO, J. W., TAYLOR, R. W., PROKISCH, H., KIM, J. P., COON, J. J. & PAGLIARINI, D. J. 2016. Mitochondrial Protein Interaction Mapping Identifies Regulators of Respiratory Chain Function. *Mol Cell*, 63, 621-632.
- FOSSETT, N., HYMAN, K., GAJEWSKI, K., ORKIN, S. H. & SCHULZ, R. A. 2003. Combinatorial interactions of serpent, lozenge, and U-shaped regulate crystal cell lineage commitment during *Drosophila* hematopoiesis. *Proc Natl Acad Sci U S A*, 100, 11451-6.
- FOSSETT, N., TEVOSIAN, S. G., GAJEWSKI, K., ZHANG, Q., ORKIN, S. H. & SCHULZ, R. A. 2001. The Friend of GATA proteins U-shaped, FOG-1, and FOG-2 function as negative regulators of blood, heart, and eye development in *Drosophila*. *Proc Natl Acad Sci U S A*, 98, 7342-7.
- FU, Z., YE, J., DEAN, J. W., BOSTICK, J. W., WEINBERG, S. E., XIONG, L., OLIFF, K. N., CHEN, Z. E., AVRAM, D., CHANDEL, N. S. & ZHOU, L. 2019. Requirement of Mitochondrial

Transcription Factor A in Tissue-Resident Regulatory T Cell Maintenance and Function. *Cell Rep*, 28, 159-171 e4.

- G**AHLOTH, D., HEAVEN, G., JOWITT, T. A., MOULD, A. P., BELLA, J., BALDOCK, C., WOODMAN, P. & TABERNERO, L. 2017. The open architecture of HD-PTP phosphatase provides new insights into the mechanism of regulation of ESCRT function. *Sci Rep*, 7, 9151.
- GAO, C., ZHUANG, X., SHEN, J. & JIANG, L. 2017. Plant ESCRT Complexes: Moving Beyond Endosomal Sorting. *Trends Plant Sci*, 22, 986-998.
- GAO, J., GRAVES, S., KOCH, U., LIU, S., JANKOVIC, V., BUONAMICI, S., EL ANDALOUSSI, A., NIMER, S. D., KEE, B. L., TAICHMAN, R., RADTKE, F. & AIFANTIS, I. 2009. Hedgehog signaling is dispensable for adult hematopoietic stem cell function. *Cell Stem Cell*, 4, 548-58.
- GARRUS, J. E., VON SCHWEDLER, U. K., PORNILLOS, O. W., MORHAM, S. G., ZAVITZ, K. H., WANG, H. E., WETTSTEIN, D. A., STRAY, K. M., COTE, M., RICH, R. L., MYSZKA, D. G. & SUNDQUIST, W. I. 2001. Tsg101 and the vacuolar protein sorting pathway are essential for HIV-1 budding. *Cell*, 107, 55-65.
- GERING, M. & PATIENT, R. 2005. Hedgehog signaling is required for adult blood stem cell formation in zebrafish embryos. *Dev Cell*, 8, 389-400.
- GHAFOURI-FARD, S., NIAZI, V. & TAHERI, M. 2021. Contribution of extracellular vesicles in normal hematopoiesis and hematological malignancies. *Heliyon*, 7, e06030.
- GIRARD, J. R., GOINS, L. M., VUU, D. M., SHARPLEY, M. S., SPRATFORD, C. M., MANTRI, S. R. & BANERJEE, U. 2021. Paths and Pathways that Generate Cell-Type Heterogeneity and Developmental Progression in Hematopoiesis. *bioRxiv*, 2021.02.11.430681.
- GIROTRA, M., NAVEIRAS, O. & VANNINI, N. 2020. Targeting mitochondria to stimulate hematopoiesis. *Aging (Albany NY)*, 12, 1042-1043.
- GLEESON, P. A. 2014. The role of endosomes in innate and adaptive immunity. *Semin Cell Dev Biol*, 31, 64-72.
- GOODE, D. K., OBIER, N., VIJAYABASKAR, M. S., LIE, A. L. M., LILLY, A. J., HANNAH, R., LICHTINGER, M., BATTI, K., FLORKOWSKA, M., PATEL, R., CHALLINOR, M., WALLACE, K., GILMOUR, J., ASSI, S. A., CAUCHY, P., HOOGENKAMP, M., WESTHEAD, D. R., LACAUD, G., KOUSKOFF, V., GOTTGENS, B. & BONIFER, C. 2016. Dynamic Gene Regulatory Networks Drive Hematopoietic Specification and Differentiation. *Dev Cell*, 36, 572-87.
- GROVER, A., SANJUAN-PLA, A., THONGJUEA, S., CARRELHA, J., GIUSTACCHINI, A., GAMBARDELLA, A., MACAULAY, I., MANCINI, E., LUIS, T. C., MEAD, A., JACOBSEN, S. E. & NERLOV, C. 2016. Single-cell RNA sequencing reveals molecular and functional platelet bias of aged haematopoietic stem cells. *Nat Commun*, 7, 11075.
- GUO, G., LUC, S., MARCO, E., LIN, T. W., PENG, C., KERENYI, M. A., BEYAZ, S., KIM, W., XU, J., DAS, P. P., NEFF, T., ZOU, K., YUAN, G. C. & ORKIN, S. H. 2013. Mapping cellular hierarchy by single-cell analysis of the cell surface repertoire. *Cell Stem Cell*, 13, 492-505.
- GUPTA, G. D., SWETHA, M. G., KUMARI, S., LAKSHMINARAYAN, R., DEY, G. & MAYOR, S. 2009. Analysis of endocytic pathways in Drosophila cells reveals a conserved role for GBF1 in internalization via GEECs. *PLoS One*, 4, e6768.

GURUHARSHA, K. G., RUAL, J. F., ZHAI, B., MINTSERIS, J., VAIDYA, P., VAIDYA, N., BEEKMAN, C., WONG, C., RHEE, D. Y., CENAJ, O., MCKILLIP, E., SHAH, S., STAPLETON, M., WAN, K. H., YU, C., PARSA, B., CARLSON, J. W., CHEN, X., KAPADIA, B., VIJAYRAGHAVAN, K., GYGI, S. P., CELNIKER, S. E., OBAR, R. A. & ARTAVANIS-TSAKONAS, S. 2011. A protein complex network of *Drosophila melanogaster*. *Cell*, 147, 690-703.

HAAS, S., HANSSON, J., KLIMMECK, D., LOEFFLER, D., VELTEN, L., UCKELMANN, H., WURZER, S., PRENDERGAST, A. M., SCHNELL, A., HEXEL, K., SANTARELLA-MELLWIG, R., BLASZKIEWICZ, S., KUCK, A., GEIGER, H., MILSOM, M. D., STEINMETZ, L. M., SCHROEDER, T., TRUMPP, A., KRIJGSVELD, J. & ESSERS, M. A. 2015. Inflammation-Induced Emergency Megakaryopoiesis Driven by Hematopoietic Stem Cell-like Megakaryocyte Progenitors. *Cell Stem Cell*, 17, 422-34.

HAAS, S., TRUMPP, A. & MILSOM, M. D. 2018. Causes and Consequences of Hematopoietic Stem Cell Heterogeneity. *Cell Stem Cell*, 22, 627-638.

HANSON, P. I., ROTH, R., LIN, Y. & HEUSER, J. E. 2008. Plasma membrane deformation by circular arrays of ESCRT-III protein filaments. *J Cell Biol*, 180, 389-402.

HARIHARAN, I. K. & BILDER, D. 2006. Regulation of imaginal disc growth by tumor-suppressor genes in *Drosophila*. *Annu Rev Genet*, 40, 335-61.

HEIN, M. Y., HUBNER, N. C., POSER, I., COX, J., NAGARAJ, N., TOYODA, Y., GAK, I. A., WEISSWANGE, I., MANSFELD, J., BUCHHOLZ, F., HYMAN, A. A. & MANN, M. 2015. A human interactome in three quantitative dimensions organized by stoichiometries and abundances. *Cell*, 163, 712-23.

HENG, J., LV, P., ZHANG, Y., CHENG, X., WANG, L., MA, D. & LIU, F. 2020. Rab5c-mediated endocytic trafficking regulates hematopoietic stem and progenitor cell development via Notch and AKT signaling. *PLoS Biol*, 18, e3000696.

HERZ, H. M., WOODFIELD, S. E., CHEN, Z., BOLDUC, C. & BERGMANN, A. 2009. Common and distinct genetic properties of ESCRT-II components in *Drosophila*. *PLoS One*, 4, e4165.

HINGE, A., HE, J., BARTRAM, J., JAVIER, J., XU, J., FJELLMAN, E., SESAKI, H., LI, T., YU, J., WUNDERLICH, M., MULLOY, J., KOFRON, M., SALOMONIS, N., GRIMES, H. L. & FILIPPI, M. D. 2020. Asymmetrically Segregated Mitochondria Provide Cellular Memory of Hematopoietic Stem Cell Replicative History and Drive HSC Attrition. *Cell Stem Cell*, 26, 420-430 e6.

HOELLER, D., CROSETTO, N., BLAGOEV, B., RAIBORG, C., TIKKANEN, R., WAGNER, S., KOWANETZ, K., BREITLING, R., MANN, M., STENMARK, H. & DIKIC, I. 2006. Regulation of ubiquitin-binding proteins by monoubiquitination. *Nat Cell Biol*, 8, 163-9.

HOFFMANN, A. D., PETERSON, M. A., FRIEDLAND-LITTLE, J. M., ANDERSON, S. A. & MOSKOWITZ, I. P. 2009. sonic hedgehog is required in pulmonary endoderm for atrial septation. *Development*, 136, 1761-70.

HORI, K., SEN, A., KIRCHHAUSEN, T. & ARTAVANIS-TSAKONAS, S. 2011. Synergy between the ESCRT-III complex and Deltex defines a ligand-independent Notch signal. *J Cell Biol*, 195, 1005-15.

HORI, K., SEN, A., KIRCHHAUSEN, T. & ARTAVANIS-TSAKONAS, S. 2012. Regulation of ligand-independent Notch signal through intracellular trafficking. *Commun Integr Biol*, 5, 374-6.

- HORN, L., LEIPS, J. & STARZ-GAIANO, M. 2014. Phagocytic ability declines with age in adult *Drosophila* hemocytes. *Aging Cell*, 13, 719-28.
- HORNER, D. S., PASINI, M. E., BELTRAME, M., MASTRODONATO, V., MORELLI, E. & VACCARI, T. 2018. ESCRT genes and regulation of developmental signaling. *Semin Cell Dev Biol*, 74, 29-39.
- HUANG, H. R., CHEN, Z. J., KUNES, S., CHANG, G. D. & MANIATIS, T. 2010. Endocytic pathway is required for *Drosophila* Toll innate immune signaling. *Proc Natl Acad Sci U S A*, 107, 8322-7.
- HUANG, P., GALLOWAY, C. A. & YOON, Y. 2011. Control of mitochondrial morphology through differential interactions of mitochondrial fusion and fission proteins. *PLoS One*, 6, e20655.
- HURLEY, J. H. 2015. ESCRTs are everywhere. *EMBO J*, 34, 2398-407.
- HUSEBYE, H., AUNE, M. H., STENVIK, J., SAMSTAD, E., SKJELDAL, F., HALAAS, O., NILSEN, N. J., STENMARK, H., LATZ, E., LIEN, E., MOLLNES, T. E., BAKKE, O. & ESPEVIK, T. 2010. The Rab11a GTPase controls Toll-like receptor 4-induced activation of interferon regulatory factor-3 on phagosomes. *Immunity*, 33, 583-96.
- I**NAMDAR, M. S. 2003. *Drosophila* asrij is expressed in pole cells, trachea and hemocytes. *Dev Genes Evol*, 213, 134-7.
- IP, Y. T., REACH, M., ENGSTROM, Y., KADALAYIL, L., CAI, H., GONZALEZ-CRESPO, S., TATEI, K. & LEVINE, M. 1993. Dif, a dorsal-related gene that mediates an immune response in *Drosophila*. *Cell*, 75, 753-63.
- ITO, K. 2018. Hematopoietic stem cell fate through metabolic control. *Exp Hematol*, 64, 1-11.
- ITO, K. & BONORA, M. 2019. Metabolism as master of hematopoietic stem cell fate. *Int J Hematol*, 109, 18-27.
- ITO, K., TURCOTTE, R., CUI, J., ZIMMERMAN, S. E., PINHO, S., MIZOGUCHI, T., ARAI, F., RUNNELS, J. M., ALT, C., TERUYA-FELDSTEIN, J., MAR, J. C., SINGH, R., SUDA, T., LIN, C. P. & FRENETTE, P. S. 2016. Self-renewal of a purified Tie2⁺ hematopoietic stem cell population relies on mitochondrial clearance. *Science*, 354, 1156-1160.
- ITOH, M., KIM, C. H., PALARDY, G., ODA, T., JIANG, Y. J., MAUST, D., YEO, S. Y., LORICK, K., WRIGHT, G. J., ARIZA-MCNAUGHTON, L., WEISSMAN, A. M., LEWIS, J., CHANDRASEKHARAPPA, S. C. & CHITNIS, A. B. 2003. Mind bomb is a ubiquitin ligase that is essential for efficient activation of Notch signaling by Delta. *Dev Cell*, 4, 67-82.
- J**IN, G., XU, C., ZHANG, X., LONG, J., REZAEIAN, A. H., LIU, C., FURTH, M. E., KRIDEL, S., PASCHE, B., BIAN, X. W. & LIN, H. K. 2018. Atad3a suppresses Pink1-dependent mitophagy to maintain homeostasis of hematopoietic progenitor cells. *Nat Immunol*, 19, 29-40.
- JING, L. & ZON, L. I. 2011. Zebrafish as a model for normal and malignant hematopoiesis. *Dis Model Mech*, 4, 433-8.
- JULIAN, L. M. & STANFORD, W. L. 2020. Organelle Cooperation in Stem Cell Fate: Lysosomes as Emerging Regulators of Cell Identity. *Front Cell Dev Biol*, 8, 591.

JUNG, S. H., EVANS, C. J., UEMURA, C. & BANERJEE, U. 2005. The *Drosophila* lymph gland as a developmental model of hematopoiesis. *Development*, 132, 2521-33.

- KAGAN**, J. C. 2012. Signaling organelles of the innate immune system. *Cell*, 151, 1168-78.
- KAMBRIS, Z., BRUN, S., JANG, I. H., NAM, H. J., ROMEO, Y., TAKAHASHI, K., LEE, W. J., UEDA, R. & LEMAITRE, B. 2006. *Drosophila* immunity: a large-scale in vivo RNAi screen identifies five serine proteases required for Toll activation. *Curr Biol*, 16, 808-13.
- KASAHARA, A., CIPOLAT, S., CHEN, Y., DORN, G. W., 2ND & SCORRANO, L. 2013. Mitochondrial fusion directs cardiomyocyte differentiation via calcineurin and Notch signaling. *Science*, 342, 734-7.
- KATZMANN, D. J., BABST, M. & EMR, S. D. 2001. Ubiquitin-dependent sorting into the multivesicular body pathway requires the function of a conserved endosomal protein sorting complex, ESCRT-I. *Cell*, 106, 145-55.
- KHADILKAR, R. J., RAY, A., CHETAN, D. R., SINHA, A. R., MAGADI, S. S., KULKARNI, V. & INAMDAR, M. S. 2017. Differential modulation of the cellular and humoral immune responses in *Drosophila* is mediated by the endosomal ARF1-Asrij axis. *Sci Rep*, 7, 118.
- KHADILKAR, R. J., RODRIGUES, D., MOTE, R. D., SINHA, A. R., KULKARNI, V., MAGADI, S. S. & INAMDAR, M. S. 2014. ARF1-GTP regulates Asrij to provide endocytic control of *Drosophila* blood cell homeostasis. *Proc Natl Acad Sci U S A*, 111, 4898-903.
- KHUSH, R. S., CORNWELL, W. D., URAM, J. N. & LEMAITRE, B. 2002. A ubiquitin-proteasome pathway represses the *Drosophila* immune deficiency signaling cascade. *Curr Biol*, 12, 1728-37.
- KHUSH, R. S., LEULIER, F. & LEMAITRE, B. 2001. *Drosophila* immunity: two paths to NF-kappaB. *Trends Immunol*, 22, 260-4.
- KIM, S., NAHM, M., KIM, N., KWON, Y., KIM, J., CHOI, S., CHOI, E. Y., SHIM, J., LEE, C. & LEE, S. 2017. Graf regulates hematopoiesis through GEEC endocytosis of EGFR. *Development*, 144, 4159-4172.
- KINDER, M., WEI, C., SHELAT, S. G., KUNDU, M., ZHAO, L., BLAIR, I. A. & PURE, E. 2010. Hematopoietic stem cell function requires 12/15-lipoxygenase-dependent fatty acid metabolism. *Blood*, 115, 5012-22.
- KOHNKEN, R., PORCU, P. & MISHRA, A. 2017. Overview of the Use of Murine Models in Leukemia and Lymphoma Research. *Front Oncol*, 7, 22.
- KOSCHADE, S. E. & BRANDTS, C. H. 2020. Selective Autophagy in Normal and Malignant Hematopoiesis. *J Mol Biol*, 432, 261-282.
- KOSTELANSKY, M. S., SCHLUTER, C., TAM, Y. Y., LEE, S., GHIRLANDO, R., BEACH, B., CONIBEAR, E. & HURLEY, J. H. 2007. Molecular architecture and functional model of the complete yeast ESCRT-I heterotetramer. *Cell*, 129, 485-98.
- KRISHNAN, M., KUMAR, S., KANGALE, L. J., GHIGO, E. & ABNAVE, P. 2021. The Act of Controlling Adult Stem Cell Dynamics: Insights from Animal Models. *Biomolecules*, 11.
- KRZEMIEN, J., DUBOIS, L., MAKKI, R., MEISTER, M., VINCENT, A. & CROZATIER, M. 2007. Control of blood cell homeostasis in *Drosophila* larvae by the posterior signalling centre. *Nature*, 446, 325-8.
- KRZEMIEN, J., OYALLON, J., CROZATIER, M. & VINCENT, A. 2010. Hematopoietic progenitors and hemocyte lineages in the *Drosophila* lymph gland. *Dev Biol*, 346, 310-9.

- KULKARNI, V., KHADILKAR, R. J., MAGADI, S. S. & INAMDAR, M. S. 2011. Asrij maintains the stem cell niche and controls differentiation during *Drosophila* lymph gland hematopoiesis. *PLoS One*, 6, e27667.
- KUMARI, S. & MAYOR, S. 2008. ARF1 is directly involved in dynamin-independent endocytosis. *Nat Cell Biol*, 10, 30-41.
- LABBE, K., MURLEY, A. & NUNNARI, J. 2014. Determinants and functions of mitochondrial behavior. *Annu Rev Cell Dev Biol*, 30, 357-91.
- LAI, E. C., DEBLANDRE, G. A., KINTNER, C. & RUBIN, G. M. 2001. *Drosophila* neuralized is a ubiquitin ligase that promotes the internalization and degradation of delta. *Dev Cell*, 1, 783-94.
- LANOT, R., ZACHARY, D., HOLDER, F. & MEISTER, M. 2001. Postembryonic hematopoiesis in *Drosophila*. *Dev Biol*, 230, 243-57.
- LAWSON, N. D., VOGEL, A. M. & WEINSTEIN, B. M. 2002. sonic hedgehog and vascular endothelial growth factor act upstream of the Notch pathway during arterial endothelial differentiation. *Dev Cell*, 3, 127-36.
- LE VASSEUR, M., FRIEDMAN, J., JOST, M., XU, J., YAMADA, J., KAMPMANN, M., HORLBECK, M. A., SALEMI, M. R., PHINNEY, B. S., WEISSMAN, J. S. & NUNNARI, J. 2021. Genome-wide CRISPRi screening identifies OCIAD1 as a prohibitin client and regulatory determinant of mitochondrial Complex III assembly in human cells. *Elife*, 10.
- LEBESTKY, T., CHANG, T., HARTENSTEIN, V. & BANERJEE, U. 2000. Specification of *Drosophila* hematopoietic lineage by conserved transcription factors. *Science*, 288, 146-9.
- LEBESTKY, T., JUNG, S. H. & BANERJEE, U. 2003. A Serrate-expressing signaling center controls *Drosophila* hematopoiesis. *Genes Dev*, 17, 348-53.
- LEE, S. Y., KANG, M. G., SHIN, S., KWAK, C., KWON, T., SEO, J. K., KIM, J. S. & RHEE, H. W. 2017. Architecture Mapping of the Inner Mitochondrial Membrane Proteome by Chemical Tools in Live Cells. *J Am Chem Soc*, 139, 3651-3662.
- LEFRANCAIS, E., ORTIZ-MUNOZ, G., CAUDRILLIER, A., MALLAVIA, B., LIU, F., SAYAH, D. M., THORNTON, E. E., HEADLEY, M. B., DAVID, T., COUGHLIN, S. R., KRUMMEL, M. F., LEAVITT, A. D., PASSEGUE, E. & LOONEY, M. R. 2017. The lung is a site of platelet biogenesis and a reservoir for haematopoietic progenitors. *Nature*, 544, 105-109.
- LEMAITRE, B. & HOFFMANN, J. 2007. The host defense of *Drosophila melanogaster*. *Annu Rev Immunol*, 25, 697-743.
- LEMAITRE, B., KROMER-METZGER, E., MICHAUT, L., NICOLAS, E., MEISTER, M., GEORGEL, P., REICHHART, J. M. & HOFFMANN, J. A. 1995. A recessive mutation, immune deficiency (*imd*), defines two distinct control pathways in the *Drosophila* host defense. *Proc Natl Acad Sci U S A*, 92, 9465-9.
- LETOURNEAU, M., LAPRAZ, F., SHARMA, A., VANZO, N., WALTZER, L. & CROZATIER, M. 2016. *Drosophila* hematopoiesis under normal conditions and in response to immune stress. *FEBS Lett*, 590, 4034-4051.
- LISOWSKI, P., KANNAN, P., MLODY, B. & PRIGIONE, A. 2018. Mitochondria and the dynamic control of stem cell homeostasis. *EMBO Rep*, 19.
- LIU, H., JIRAVANICHPAISAL, P., CERENIUS, L., LEE, B. L., SODERHALL, I. & SODERHALL, K. 2007. Phenoloxidase is an important component of the defense against *Aeromonas hydrophila* Infection in a crustacean, *Pacifastacus leniusculus*. *J Biol Chem*, 282, 33593-33598.

- LIU, Y., MEI, Y., HAN, X., KOROBOVA, F. V., PRADO, M. A., YANG, J., PENG, Z., PAULO, J. A., GYGI, S. P., FINLEY, D. & JI, P. 2021. Membrane skeleton modulates erythroid proteome remodeling and organelle clearance. *Blood*, 137, 398-409.
- LIU, Y. J., MCINTYRE, R. L., JANSSENS, G. E. & HOUTKOOOPER, R. H. 2020. Mitochondrial fission and fusion: A dynamic role in aging and potential target for age-related disease. *Mech Ageing Dev*, 186, 111212.
- LO, P. C., SKEATH, J. B., GAJEWSKI, K., SCHULZ, R. A. & FRASCH, M. 2002. Homeotic genes autonomously specify the anteroposterior subdivision of the *Drosophila* dorsal vessel into aorta and heart. *Dev Biol*, 251, 307-19.
- LONCLE, N., AGROMAYOR, M., MARTIN-SERRANO, J. & WILLIAMS, D. W. 2015. An ESCRT module is required for neuron pruning. *Sci Rep*, 5, 8461.
- LORINCZ, P., LAKATOS, Z., VARGA, A., MARUZS, T., SIMON-VECSEI, Z., DARULA, Z., BENKO, P., CSORDAS, G., LIPPAI, M., ANDO, I., HEGEDUS, K., MEDZIHRADSZKY, K. F., TAKATS, S. & JUHASZ, G. 2016. MiniCORVET is a Vps8-containing early endosomal tether in *Drosophila*. *Elife*, 5.
- LUCHSINGER, L. L., DE ALMEIDA, M. J., CORRIGAN, D. J., MUMAU, M. & SNOECK, H. W. 2016. Mitofusin 2 maintains haematopoietic stem cells with extensive lymphoid potential. *Nature*, 529, 528-31.
- LUIS, T. C., LAWSON, H. & KRANC, K. R. 2020. Divide and Rule: Mitochondrial Fission Regulates Quiescence in Hematopoietic Stem Cells. *Cell Stem Cell*, 26, 299-301.
- LUND, V. K., DELOTTO, Y. & DELOTTO, R. 2010. Endocytosis is required for Toll signaling and shaping of the Dorsal/NF-kappaB morphogen gradient during *Drosophila* embryogenesis. *Proc Natl Acad Sci U S A*, 107, 18028-33.
- LUO, F., YU, S. & JIN, L. H. 2020. The Posterior Signaling Center Is an Important Microenvironment for Homeostasis of the *Drosophila* Lymph Gland. *Front Cell Dev Biol*, 8, 382.
- M**AKKI, R., MEISTER, M., PENNETIER, D., UBEDA, J. M., BRAUN, A., DABURON, V., KRZEMIEN, J., BOURBON, H. M., ZHOU, R., VINCENT, A. & CROZATIER, M. 2010. A short receptor downregulates JAK/STAT signalling to control the *Drosophila* cellular immune response. *PLoS Biol*, 8, e1000441.
- MARCHI, S., PATERGNANI, S. & PINTON, P. 2014. The endoplasmic reticulum-mitochondria connection: one touch, multiple functions. *Biochim Biophys Acta*, 1837, 461-9.
- MARTIN-SERRANO, J., ZANG, T. & BIENIASZ, P. D. 2003. Role of ESCRT-I in retroviral budding. *J Virol*, 77, 4794-804.
- MATIAS, N. R., MATHIEU, J. & HUYNH, J. R. 2015. Abscission is regulated by the ESCRT-III protein shrub in *Drosophila* germline stem cells. *PLoS Genet*, 11, e1004653.
- MATSUNO, K., DIEDERICH, R. J., GO, M. J., BLAUMUELLER, C. M. & ARTAVANIS-TSAKONAS, S. 1995. Deltex acts as a positive regulator of Notch signaling through interactions with the Notch ankyrin repeats. *Development*, 121, 2633-44.
- MEJLVANG, J., OLSVIK, H., SVENNING, S., BRUUN, J. A., ABUDU, Y. P., LARSEN, K. B., BRECH, A., HANSEN, T. E., BRENNE, H., HANSEN, T., STENMARK, H. & JOHANSEN, T. 2018. Starvation induces rapid degradation of selective autophagy receptors by endosomal microautophagy. *J Cell Biol*, 217, 3640-3655.
- MELCARNE, C., RAMOND, E., DUDZIC, J., BRETSCHER, A. J., KURUCZ, E., ANDO, I. & LEMAITRE, B. 2019. Two Nimrod receptors, NimC1 and Eater, synergistically

- contribute to bacterial phagocytosis in *Drosophila melanogaster*. *FEBS J*, 286, 2670-2691.
- MENASCHE, G., FELDMANN, J., HOUDUSSE, A., DESAYMARD, C., FISCHER, A., GOUD, B. & DE SAINT BASILE, G. 2003. Biochemical and functional characterization of Rab27a mutations occurring in Griscelli syndrome patients. *Blood*, 101, 2736-42.
- MICHEL, T., REICHHART, J. M., HOFFMANN, J. A. & ROYET, J. 2001. *Drosophila* Toll is activated by Gram-positive bacteria through a circulating peptidoglycan recognition protein. *Nature*, 414, 756-9.
- MILLAR, D. A. & RATCLIFFE, N. A. 1989. The evolution of blood cells: facts and enigmas. *Endeavour*, 13, 72-7.
- MINAKHINA, S. & STEWARD, R. 2006. Nuclear factor-kappa B pathways in *Drosophila*. *Oncogene*, 25, 6749-57.
- MISHRA, P. & CHAN, D. C. 2014. Mitochondrial dynamics and inheritance during cell division, development and disease. *Nat Rev Mol Cell Biol*, 15, 634-46.
- MORETTI, J. & BROU, C. 2013. Ubiquitinations in the notch signaling pathway. *Int J Mol Sci*, 14, 6359-81.
- MORETTI, J., CHASTAGNER, P., GASTALDELLO, S., HEUSS, S. F., DIRAC, A. M., BERNARDS, R., MASUCCI, M. G., ISRAEL, A. & BROU, C. 2010. The translation initiation factor 3f (eIF3f) exhibits a deubiquitinase activity regulating Notch activation. *PLoS Biol*, 8, e1000545.
- MORIN-POULARD, I., VINCENT, A. & CROZATIER, M. 2013. The *Drosophila* JAK-STAT pathway in blood cell formation and immunity. *JAKSTAT*, 2, e25700.
- MOTIWALA, Z., DARNE, P., PRABHUNE, A., INAMDAR, M. S. & KULKARNI, K. 2021. Expression, Purification and Crystallization of Asrij, A Novel Scaffold Transmembrane Protein. *J Membr Biol*, 254, 65-74.
- MUKAI, A., YAMAMOTO-HINO, M., KOMADA, M., OKANO, H. & GOTO, S. 2012. Balanced ubiquitination determines cellular responsiveness to extracellular stimuli. *Cell Mol Life Sci*, 69, 4007-16.
- N**APPI, A., POIRIE, M. & CARTON, Y. 2009. The role of melanization and cytotoxic by-products in the cellular immune responses of *Drosophila* against parasitic wasps. *Adv Parasitol*, 70, 99-121.
- NISHIDA, K., YAMASAKI, S., HASEGAWA, A., IWAMATSU, A., KOSEKI, H. & HIRANO, T. 2011. Gab2, via PI-3K, regulates ARF1 in FcepsilonRI-mediated granule translocation and mast cell degranulation. *J Immunol*, 187, 932-41.
- O**LMOS, Y., HODGSON, L., MANTELL, J., VERKADE, P. & CARLTON, J. G. 2015. ESCRT-III controls nuclear envelope reformation. *Nature*, 522, 236-9.
- OWUSU-ANSAH, E. & BANERJEE, U. 2009. Reactive oxygen species prime *Drosophila* haematopoietic progenitors for differentiation. *Nature*, 461, 537-41.

- P**ADDIBHATLA, I., LEE, M. J., KALAMARZ, M. E., FERRARESE, R. & GOVIND, S. 2010. Role for sumoylation in systemic inflammation and immune homeostasis in *Drosophila* larvae. *PLoS Pathog*, 6, e1001234.
- PAPA, L., DJEDAINI, M. & HOFFMAN, R. 2019. Mitochondrial Role in Stemness and Differentiation of Hematopoietic Stem Cells. *Stem Cells Int*, 2019, 4067162.
- PASHKOVA, N., GAKHAR, L., WINISTORFER, S. C., SUNSHINE, A. B., RICH, M., DUNHAM, M. J., YU, L. & PIPER, R. C. 2013. The yeast Alix homolog Bro1 functions as a ubiquitin receptor for protein sorting into multivesicular endosomes. *Dev Cell*, 25, 520-33.
- PENNETIER, D., OYALLON, J., MORIN-POULARD, I., DEJEAN, S., VINCENT, A. & CROZATIER, M. 2012. Size control of the *Drosophila* hematopoietic niche by bone morphogenetic protein signaling reveals parallels with mammals. *Proc Natl Acad Sci U S A*, 109, 3389-94.
- PETES, C., ODOARDI, N. & GEE, K. 2017. The Toll for Trafficking: Toll-Like Receptor 7 Delivery to the Endosome. *Front Immunol*, 8, 1075.
- PIPER, R. C., DIKIC, I. & LUKACS, G. L. 2014. Ubiquitin-dependent sorting in endocytosis. *Cold Spring Harb Perspect Biol*, 6.
- POIRAULT-CHASSAC, S., NIVET-ANTOINE, V., HOUVERT, A., KAUSKOT, A., LAURET, E., LAIKUEN, R., DUSANTER-FOURT, I. & BARUCH, D. 2021. Mitochondrial dynamics and reactive oxygen species initiate thrombopoiesis from mature megakaryocytes. *Blood Adv*, 5, 1706-1718.
- PRASHAR, A., SCHNETTGER, L., BERNARD, E. M. & GUTIERREZ, M. G. 2017. Rab GTPases in Immunity and Inflammation. *Front Cell Infect Microbiol*, 7, 435.
- PRAVEEN, W., SINHA, S., BATABYAL, R., KAMAT, K. & INAMDAR, M. S. 2020. The OCIAD protein family: comparative developmental biology and stem cell application. *Int J Dev Biol*, 64, 223-235.
- R**ADULOVIC, M. & STENMARK, H. 2018. ESCRTs in membrane sealing. *Biochem Soc Trans*, 46, 773-778.
- RAMOND, E., MEISTER, M. & LEMAITRE, B. 2015. From Embryo to Adult: Hematopoiesis along the *Drosophila* Life Cycle. *Dev Cell*, 33, 367-8.
- RAY, A., KAMAT, K. & INAMDAR, M. S. 2021. A Conserved Role for Asrij/OCIAD1 in Progenitor Differentiation and Lineage Specification Through Functional Interaction With the Regulators of Mitochondrial Dynamics. *Front Cell Dev Biol*, 9, 643444.
- RAY, A., RAI, Y. & INAMDAR, M. S. 2021b. Charting ESCRT function reveals distinct and non-compensatory roles in blood progenitor maintenance and lineage choice in *Drosophila*. *bioRxiv*, 2021.11.29.470366.
- REIMELS, T. A. & PFLEGER, C. M. 2015. *Drosophila* Rabex-5 restricts Notch activity in hematopoietic cells and maintains hematopoietic homeostasis. *J Cell Sci*, 128, 4512-25.
- REMEC PAVLIN, M. & HURLEY, J. H. 2020. The ESCRTs - converging on mechanism. *J Cell Sci*, 133.
- REN, X. & HURLEY, J. H. 2011. Structural basis for endosomal recruitment of ESCRT-I by ESCRT-0 in yeast. *EMBO J*, 30, 2130-9.

- ROBERTSON, A. L., AVAGYAN, S., GANSNER, J. M. & ZON, L. I. 2016. Understanding the regulation of vertebrate hematopoiesis and blood disorders - big lessons from a small fish. *FEBS Lett*, 590, 4016-4033.
- RODRIGUES, D., VIJAYRAGHAVAN, K., WALTZER, L. & INAMDAR, M. S. 2021. Intact *in situ* preparation of *Drosophila melanogaster* lymph gland for comprehensive analysis of larval hematopoiesis. *Bio-protocol* (in press).
- RODRIGUES, D., RENAUD, Y., VIJAYRAGHAVAN, K., WALTZER, L. & INAMDAR, M. S. 2021. Differential activation of JAK-STAT signaling reveals functional compartmentalization in *Drosophila* blood progenitors. *Elife*, 10.
- ROTHMAN, J. H., HOWALD, I. & STEVENS, T. H. 1989. Characterization of genes required for protein sorting and vacuolar function in the yeast *Saccharomyces cerevisiae*. *EMBO J*, 8, 2057-65.
- RYALL, J. G., DELL'ORSO, S., DERFOUL, A., JUAN, A., ZARE, H., FENG, X., CLERMONT, D., KOULNIS, M., GUTIERREZ-CRUZ, G., FULCO, M. & SARTORELLI, V. 2015. The NAD(+)-dependent SIRT1 deacetylase translates a metabolic switch into regulatory epigenetics in skeletal muscle stem cells. *Cell Stem Cell*, 16, 171-83.
- S**AHU, R., KAUSHIK, S., CLEMENT, C. C., CANNIZZO, E. S., SCHARF, B., FOLLENZI, A., POTOLICCHIO, I., NIEVES, E., CUERVO, A. M. & SANTAMBROGIO, L. 2011. Microautophagy of cytosolic proteins by late endosomes. *Dev Cell*, 20, 131-9.
- SANALKUMAR, R., DHANESH, S. B. & JAMES, J. 2010. Non-canonical activation of Notch signaling/target genes in vertebrates. *Cell Mol Life Sci*, 67, 2957-68.
- SANDOVAL, H., YAO, C. K., CHEN, K., JAISWAL, M., DONTI, T., LIN, Y. Q., BAYAT, V., XIONG, B., ZHANG, K., DAVID, G., CHARNG, W. L., YAMAMOTO, S., DURAIN, L., GRAHAM, B. H. & BELLEN, H. J. 2014. Mitochondrial fusion but not fission regulates larval growth and synaptic development through steroid hormone production. *Elife*, 3.
- SCHELL, J. C. & RUTTER, J. 2017. Mitochondria link metabolism and epigenetics in haematopoiesis. *Nat Cell Biol*, 19, 589-591.
- SCHMID, M. R., ANDERL, I., VESALA, L., VANHA-AHO, L. M., DENG, X. J., RAMET, M. & HULTMARK, D. 2014. Control of *Drosophila* blood cell activation via Toll signaling in the fat body. *PLoS One*, 9, e102568.
- SCITA, G. & DI FIORE, P. P. 2010. The endocytic matrix. *Nature*, 463, 464-73.
- SEBASTIAN, D., HERNANDEZ-ALVAREZ, M. I., SEGALES, J., SORIANELLO, E., MUNOZ, J. P., SALA, D., WAGET, A., LIESA, M., PAZ, J. C., GOPALACHARYULU, P., ORESIC, M., PICH, S., BURCELIN, R., PALACIN, M. & ZORZANO, A. 2012. Mitofusin 2 (Mfn2) links mitochondrial and endoplasmic reticulum function with insulin signaling and is essential for normal glucose homeostasis. *Proc Natl Acad Sci U S A*, 109, 5523-8.
- SENOS DEMARCO, R. & JONES, D. L. 2019. Mitochondrial fission regulates germ cell differentiation by suppressing ROS-mediated activation of Epidermal Growth Factor Signaling in the *Drosophila* larval testis. *Sci Rep*, 9, 19695.
- SEO, B. J., YOON, S. H. & DO, J. T. 2018. Mitochondrial Dynamics in Stem Cells and Differentiation. *Int J Mol Sci*, 19.
- SHEFFER, R., DOUIEV, L., EDVARDSON, S., SHAAG, A., TAMIMI, K., SOIFERMAN, D., MEINER, V. & SAADA, A. 2016. Postnatal microcephaly and pain insensitivity due to a de novo

- heterozygous DNMT1L mutation causing impaired mitochondrial fission and function. *Am J Med Genet A*, 170, 1603-7.
- SHETTY, D. K., KALAMKAR, K. P. & INAMDAR, M. S. 2018. OCIAD1 Controls Electron Transport Chain Complex I Activity to Regulate Energy Metabolism in Human Pluripotent Stem Cells. *Stem Cell Reports*, 11, 128-141.
- SHIA, A. K., GLITTENBERG, M., THOMPSON, G., WEBER, A. N., REICHHART, J. M. & LIGOXYGAKIS, P. 2009. Toll-dependent antimicrobial responses in *Drosophila* larval fat body require Spatzle secreted by haemocytes. *J Cell Sci*, 122, 4505-15.
- SHIN, M., CHA, N., KORANTENG, F., CHO, B. & SHIM, J. 2020. Subpopulation of Macrophage-Like Plasmacytes Attenuates Systemic Growth via JAK/STAT in the *Drosophila* Fat Body. *Front Immunol*, 11, 63.
- SHRAVAGE, B. V., HILL, J. H., POWERS, C. M., WU, L. & BAEHRECKE, E. H. 2013. Atg6 is required for multiple vesicle trafficking pathways and hematopoiesis in *Drosophila*. *Development*, 140, 1321-9.
- SIGISMUND, S., LANZETTI, L., SCITA, G. & DI FIORE, P. P. 2021. Endocytosis in the context-dependent regulation of individual and collective cell properties. *Nat Rev Mol Cell Biol*.
- SINENKO, S. A., MANDAL, L., MARTINEZ-AGOSTO, J. A. & BANERJEE, U. 2009. Dual role of wingless signaling in stem-like hematopoietic precursor maintenance in *Drosophila*. *Dev Cell*, 16, 756-63.
- SINENKO, S. A., SHIM, J. & BANERJEE, U. 2011. Oxidative stress in the haematopoietic niche regulates the cellular immune response in *Drosophila*. *EMBO Rep*, 13, 83-9.
- SINHA, A., KHADILKAR, R. J., S, V. K., ROYCHOWDHURY SINHA, A. & INAMDAR, M. S. 2013. Conserved regulation of the Jak/STAT pathway by the endosomal protein asrij maintains stem cell potency. *Cell Rep*, 4, 649-58.
- SINHA, S., DWIVEDI, T. R., YENGHOM, R., BHEEMSETTY, V. A., ABE, T., KIYONARI, H., VIJAYRAGHAVAN, K. & INAMDAR, M. S. 2019a. Asrij/OCIAD1 suppresses CSN5-mediated p53 degradation and maintains mouse hematopoietic stem cell quiescence. *Blood*, 133, 2385-2400.
- SINHA, S., RAY, A., ABHILASH, L., KUMAR, M., SREENIVASAMURTHY, S. K., KESHAVA PRASAD, T. S. & INAMDAR, M. S. 2019b. Proteomics of Asrij Perturbation in *Drosophila* Lymph Glands for Identification of New Regulators of Hematopoiesis. *Mol Cell Proteomics*, 18, 1171-1182.
- SKOWYRA, M. L., SCHLESINGER, P. H., NAISMITH, T. V. & HANSON, P. I. 2018. Triggered recruitment of ESCRT machinery promotes endolysosomal repair. *Science*, 360.
- SMALL, C., RAMROOP, J., OTAZO, M., HUANG, L. H., SALEQUE, S. & GOVIND, S. 2014. An unexpected link between notch signaling and ROS in restricting the differentiation of hematopoietic progenitors in *Drosophila*. *Genetics*, 197, 471-83.
- SORRENTINO, R. P., CARTON, Y. & GOVIND, S. 2002. Cellular immune response to parasite infection in the *Drosophila* lymph gland is developmentally regulated. *Dev Biol*, 243, 65-80.
- SORRENTINO, R. P., TOKUSUMI, T. & SCHULZ, R. A. 2007. The Friend of GATA protein U-shaped functions as a hematopoietic tumor suppressor in *Drosophila*. *Dev Biol*, 311, 311-23.
- STOVEN, S., ANDO, I., KADALAYIL, L., ENGSTROM, Y. & HULTMARK, D. 2000. Activation of the *Drosophila* NF-kappaB factor Relish by rapid endoproteolytic cleavage. *EMBO Rep*, 1, 347-52.

- STOW, J. L., MANDERSON, A. P. & MURRAY, R. Z. 2006. SNAREing immunity: the role of SNAREs in the immune system. *Nat Rev Immunol*, 6, 919-29.
- SWATEK, K. N. & KOMANDER, D. 2016. Ubiquitin modifications. *Cell Res*, 26, 399-422.
- SZYMANSKA, E., BUDICK-HARME LIN, N. & MIACZYNSKA, M. 2018. Endosomal "sort" of signaling control: The role of ESCRT machinery in regulation of receptor-mediated signaling pathways. *Semin Cell Dev Biol*, 74, 11-20.

- T**ABERNERO, L. & WOODMAN, P. 2018. Dissecting the role of His domain protein tyrosine phosphatase/PTPN23 and ESCRTs in sorting activated epidermal growth factor receptor to the multivesicular body. *Biochem Soc Trans*, 46, 1037-1046.
- TAKAMORI, M., KOMAI, K. & IWASA, K. 2000. Antibodies to calcium channel and synaptotagmin in Lambert-Eaton myasthenic syndrome. *Am J Med Sci*, 319, 204-8.
- TAN, K. L., GOH, S. C. & MINAKHINA, S. 2012. Genetic screen for regulators of lymph gland homeostasis and hemocyte maturation in *Drosophila*. *G3 (Bethesda)*, 2, 393-405.
- TANG, H. 2009. Regulation and function of the melanization reaction in *Drosophila*. *Fly (Austin)*, 3, 105-11.
- THOMPSON, B. J., MATHIEU, J., SUNG, H. H., LOESER, E., RORTH, P. & COHEN, S. M. 2005. Tumor suppressor properties of the ESCRT-II complex component Vps25 in *Drosophila*. *Dev Cell*, 9, 711-20.
- TIKU, V., TAN, M. W. & DIKIC, I. 2020. Mitochondrial Functions in Infection and Immunity. *Trends Cell Biol*, 30, 263-275.
- TOGNON, E., WOLLSCHIED, N., CORTESE, K., TACCHETTI, C. & VACCARI, T. 2014. ESCRT-0 is not required for ectopic Notch activation and tumor suppression in *Drosophila*. *PLoS One*, 9, e93987.
- TONDERA, D., SANTEL, A., SCHWARZER, R., DAMES, S., GIESE, K., KLIPPEL, A. & KAUFMANN, J. 2004. Knockdown of MTP18, a novel phosphatidylinositol 3-kinase-dependent protein, affects mitochondrial morphology and induces apoptosis. *J Biol Chem*, 279, 31544-55.
- TOUVIER, T., DE PALMA, C., RIGAMONTI, E., SCAGLIOLA, A., INCERTI, E., MAZELIN, L., THOMAS, J. L., D'ANTONIO, M., POLITI, L., SCHAEFFER, L., CLEMENTI, E. & BRUNELLI, S. 2015. Muscle-specific Drp1 overexpression impairs skeletal muscle growth via translational attenuation. *Cell Death Dis*, 6, e1663.
- TROWBRIDGE, J. J., SCOTT, M. P. & BHATIA, M. 2006. Hedgehog modulates cell cycle regulators in stem cells to control hematopoietic regeneration. *Proc Natl Acad Sci U S A*, 103, 14134-9.
- TSUNEMATSU, T., YAMAUCHI, E., SHIBATA, H., MAKI, M., OHTA, T. & KONISHI, H. 2010. Distinct functions of human MVB12A and MVB12B in the ESCRT-I dependent on their posttranslational modifications. *Biochem Biophys Res Commun*, 399, 232-7.
- TWIG, G., ELORZA, A., MOLINA, A. J., MOHAMED, H., WIKSTROM, J. D., WALZER, G., STILES, L., HAIGH, S. E., KATZ, S., LAS, G., ALROY, J., WU, M., PY, B. F., YUAN, J., DEENEY, J. T., CORKEY, B. E. & SHIRIHAI, O. S. 2008. Fission and selective fusion govern mitochondrial segregation and elimination by autophagy. *EMBO J*, 27, 433-46.
- TYAGI, A., GUPTA, A., DUTTA, A., POTLURI, P. & BATTI, B. 2020. A Review of Diamond-Blackfan Anemia: Current Evidence on Involved Genes and Treatment Modalities. *Cureus*, 12, e10019.

VACCARI, T. & BILDER, D. 2005. The *Drosophila* tumor suppressor *vps25* prevents nonautonomous overproliferation by regulating notch trafficking. *Dev Cell*, 9, 687-98.

VACCARI, T., RUSTEN, T. E., MENUT, L., NEZIS, I. P., BRECH, A., STENMARK, H. & BILDER, D. 2009. Comparative analysis of ESCRT-I, ESCRT-II and ESCRT-III function in *Drosophila* by efficient isolation of ESCRT mutants. *Journal of Cell Science*, 122, 2413-2423.

VALENTE, A. J., MADDALENA, L. A., ROBB, E. L., MORADI, F. & STUART, J. A. 2017. A simple ImageJ macro tool for analyzing mitochondrial network morphology in mammalian cell culture. *Acta Histochem*, 119, 315-326.

VAN DER BLIEK, A. M., SHEN, Q. & KAWAJIRI, S. 2013. Mechanisms of mitochondrial fission and fusion. *Cold Spring Harb Perspect Biol*, 5.

VELTEN, L., HAAS, S. F., RAFFEL, S., BLASZKIEWICZ, S., ISLAM, S., HENNIG, B. P., HIRCHE, C., LUTZ, C., BUSS, E. C., NOWAK, D., BOCH, T., HOFMANN, W. K., HO, A. D., HUBER, W., TRUMPP, A., ESSERS, M. A. & STEINMETZ, L. M. 2017. Human haematopoietic stem cell lineage commitment is a continuous process. *Nat Cell Biol*, 19, 271-281.

VIETRI, M., RADULOVIC, M. & STENMARK, H. 2020. The many functions of ESCRTs. *Nat Rev Mol Cell Biol*, 21, 25-42.

WAI, T. & LANGER, T. 2016. Mitochondrial Dynamics and Metabolic Regulation. *Trends Endocrinol Metab*, 27, 105-117.

WALTZER, L., BATAILLE, L., PEYREFITTE, S. & HAENLIN, M. 2002. Two isoforms of Serpent containing either one or two GATA zinc fingers have different roles in *Drosophila* haematopoiesis. *EMBO J*, 21, 5477-86.

WANG, Y., CHEN, Z. & BERGMANN, A. 2010. Regulation of EGFR and Notch signaling by distinct isoforms of D-cbl during *Drosophila* development. *Dev Biol*, 342, 1-10.

WATANABE, T., CHUMA, S., YAMAMOTO, Y., KURAMOCHI-MIYAGAWA, S., TOTOKI, Y., TOYODA, A., HOKI, Y., FUJIYAMA, A., SHIBATA, T., SADO, T., NOCE, T., NAKANO, T., NAKATSUJI, N., LIN, H. & SASAKI, H. 2011. MITOPLD is a mitochondrial protein essential for nuage formation and piRNA biogenesis in the mouse germline. *Dev Cell*, 20, 364-75.

WATERHAM, H. R., KOSTER, J., VAN ROERMUND, C. W., MOOYER, P. A., WANDERS, R. J. & LEONARD, J. V. 2007. A lethal defect of mitochondrial and peroxisomal fission. *N Engl J Med*, 356, 1736-41.

WENZEL, E. M., SCHULTZ, S. W., SCHINK, K. O., PEDERSEN, N. M., NAHSE, V., CARLSON, A., BRECH, A., STENMARK, H. & RAIBORG, C. 2018. Concerted ESCRT and clathrin recruitment waves define the timing and morphology of intraluminal vesicle formation. *Nat Commun*, 9, 2932.

WHITLEY, B. N., ENGELHART, E. A. & HOPPINS, S. 2019. Mitochondrial dynamics and their potential as a therapeutic target. *Mitochondrion*, 49, 269-283.

WILKINSON, R. N., POUGET, C., GERING, M., RUSSELL, A. J., DAVIES, S. G., KIMELMAN, D. & PATIENT, R. 2009. Hedgehog and Bmp polarize hematopoietic stem cell emergence in the zebrafish dorsal aorta. *Dev Cell*, 16, 909-16.

WILSON, N. K., FOSTER, S. D., WANG, X., KNEZEVIC, K., SCHUTTE, J., KAIMAKIS, P., CHILARSKA, P. M., KINSTON, S., OUWEHAND, W. H., DZIERZAK, E., PIMANDA, J. E., DE BRUIJN, M. F. & GOTTGENS, B. 2010. Combinatorial transcriptional control in blood

- stem/progenitor cells: genome-wide analysis of ten major transcriptional regulators. *Cell Stem Cell*, 7, 532-44.
- WOLLERT, T., WUNDER, C., LIPPINCOTT-SCHWARTZ, J. & HURLEY, J. H. 2009. Membrane scission by the ESCRT-III complex. *Nature*, 458, 172-7.
- WOODFIELD, S. E., GRAVES, H. K., HERNANDEZ, J. A. & BERGMANN, A. 2013. De-regulation of JNK and JAK/STAT signaling in ESCRT-II mutant tissues cooperatively contributes to neoplastic tumorigenesis. *PLoS One*, 8, e56021.
- XIA**, P., WANG, S., HUANG, G., ZHU, P., LI, M., YE, B., DU, Y. & FAN, Z. 2014. WASH is required for the differentiation commitment of hematopoietic stem cells in a c-Myc-dependent manner. *J Exp Med*, 211, 2119-34.
- YAMAMOTO**, K., MIWA, Y., ABE-SUZUKI, S., ABE, S., KIRIMURA, S., ONISHI, I., KITAGAWA, M. & KURATA, M. 2016. Extramedullary hematopoiesis: Elucidating the function of the hematopoietic stem cell niche (Review). *Mol Med Rep*, 13, 587-91.
- YU, S., LUO, F. & JIN, L. H. 2021. Rab5 and Rab11 maintain hematopoietic homeostasis by restricting multiple signaling pathways in *Drosophila*. *Elife*, 10.
- ZHAN**, M., BROOKS, C., LIU, F., SUN, L. & DONG, Z. 2013. Mitochondrial dynamics: regulatory mechanisms and emerging role in renal pathophysiology. *Kidney Int*, 83, 568-81.
- ZHANG, H., MENZIES, K. J. & AUWERX, J. 2018. The role of mitochondria in stem cell fate and aging. *Development*, 145.
- ZHANG, Q., ZHANG, Y., FENG, H., GUO, R., JIN, L., WAN, R., WANG, L., CHEN, C. & LI, S. 2011. High density lipoprotein (HDL) promotes glucose uptake in adipocytes and glycogen synthesis in muscle cells. *PLoS One*, 6, e23556.
- ZHANG, Z., SONG, Y., ZHANG, X., TANG, J., CHEN, J. & CHEN, Y. 2003. Msx1/Bmp4 genetic pathway regulates mammalian alveolar bone formation via induction of Dlx5 and Cbfa1. *Mech Dev*, 120, 1469-79.
- ZHOU, X., CROW, A. L., HARTIALA, J., SPINDLER, T. J., GHAZALPOUR, A., BARSKY, L. W., BENNETT, B. J., PARKS, B. W., ESKIN, E., JAIN, R., EPSTEIN, J. A., LUSIS, A. J., ADAMS, G. B. & ALLAYEE, H. 2015. The Genetic Landscape of Hematopoietic Stem Cell Frequency in Mice. *Stem Cell Reports*, 5, 125-38.

Appendix 1: Details of the Antibodies

Antibodies used for immunofluorescence:

S. No.	Antibody	Host	Source/Company	Catalog no.	Dilution
1.	DmAsrij C-terminal	Rabbit	Home raised (Abexome)	-	1:50
2.	P1	Mouse	Prof. Istvan Ando, BRC Schezed	-	1:30
3.	ProPO	Mouse	Home raised	-	1:20
4.	Vps28	Rabbit	Prof. Helmut Kramer, UT Southwestern Medical Center	-	1:100
5.	Vps32/Shrub	Rabbit	Prof. Fen B. Gao, University of Massachusetts	-	1:100
6.	Tsg101	Mouse	Abcam, UK	ab83	1:25
7.	Hrs	Guineapig	Prof. Benny Shilo, Weizmann Insitute	-	1:100
8.	GFP	Chicken	Abcam, UK	ab13970	1:200
9.	dsRed	Rabbit	Takara, Japan	632496	1:200
10.	Phospho-Histone H3	Rabbit	Merck Millipore, USA	06-570	1:200
11.	FK2 (Mono- and polyubiquitinated protein)	Mouse	Enzo Life Sciences, USA	BML-PW8810-0100	1:200
12.	Ubiquitin	Rabbit	Abcam, UK	ab7780	1:50
13.	Cactus	Mouse	DSHB, USA	3H12s	1:10
14.	Dorsal	Mouse	DSHB, USA	7A4s	1:10
15.	Relish	Mouse	DSHB, USA	21F3	1:25
16.	NICD	Mouse	DSHB, USA	C17.9C6c	1:10

17.	COXIV	Mouse	Abcam, UK	ab33985	1:200
18.	SDHB	Mouse	Abcam, UK	ab14714	1:100
19.	ATP5A	Mouse	Abcam, UK	ab14748	1:100
20.	NDUFS3	Mouse	Abcam, UK	ab14748	1:200
21.	Rab7	Rabbit	Prof. Marcos Gonzalez-Gaitan	-	1:25
22.	Rab11	Rabbit	Prof. Marcos Gonzalez-Gaitan	-	1:25

Appendix 2: Details of the Reagents

S. No.	Reagent	Source/Company	Catalog no.:
1.	RNeasy Mini Kit	Qiagen, Germany	74104
2.	Duolink PLA kit (orange)	Merck, USA	DUO92102
3.	NucleoSpin PCR clean-up kit	Macherey-Nagel, Germany	740609.50
4.	T7 RNA polymerase	Promega, USA	P2075
5.	Transcription Optimized 5X buffer	Promega, USA	P1181
6.	SP6 RNA polymerase	Roche, Switzerland	10210274001
7.	RNasein	Promega, USA	N2111
8.	DIG-labelling mix	Merck, USA	11277073910
9.	Anti-Digoxigenin Alkaline Phosphatase Conjugated	Merck, USA	11093274910
10.	t-RNA from Brewer's yeast	Merck, USA	29349900
11.	NBT/BCIP	Promega, USA	S380C, S381C
12.	Phalloidin 568	Life Technologies, Thermo Fisher Scientific, USA	A12380
13.	Phalloidin 633	Life Technologies, Thermo Fisher Scientific, USA	A22284
14.	Schneider's <i>Drosophila</i> media	Thermo Fisher Scientific, USA	21720024
15.	Mitotracker™ Deep Red FM	Thermo Fisher Scientific, USA	M22426
16.	iQ SYBR® Green Supermix	Biorad	1708882

List of Publications:

1. Khadilkar RJ[†], **Ray A**[†], Chetan DR, RoyChowdhury AS, Magadi SS, Kulkarni V, Inamdar MS., (2017) Differential modulation of the cellular and humoral immune responses in *Drosophila* is mediated by the endosomal ARF1-Asrij axis. *Scientific Reports*, doi: [10.1038/s41598-017-00118-7](https://doi.org/10.1038/s41598-017-00118-7)


[†]Equal contribution

2. Sinha S, **Ray A**, Abhilash L, Kumar M, Sreenivasamurthy SK, Keshava Prasad TS, Inamdar MS., (2019) Proteomics of Asrij Perturbation in *Drosophila* Lymph Glands for Identification of New Regulators of Hematopoiesis. *Molecular and Cellular Proteomics*, doi: [10.1074/mcp.RA119.001299](https://doi.org/10.1074/mcp.RA119.001299)

3. **Ray A**, Kamat K, Inamdar MS., (2021) A conserved role for Asrij/OCIAD1 in progenitor differentiation and lineage specification through functional interaction with the regulators of mitochondrial dynamics. *Frontiers in Cell and Developmental Biology*. doi: [10.3389/fcell.2021.643444](https://doi.org/10.3389/fcell.2021.643444).

4. **Ray A**, Rai Y, Inamdar MS., Charting ESCRT function reveals distinct and non-compensatory roles in blood progenitor maintenance and lineage choice in *Drosophila*. *bioRxiv*. doi: [10.1101/2021.11.29.470366](https://doi.org/10.1101/2021.11.29.470366) (under peer review process)

SCIENTIFIC REPORTS



OPEN

Differential modulation of the cellular and humoral immune responses in *Drosophila* is mediated by the endosomal ARF1-Asrij axis

Rohan J. Khadilkar, Arindam Ray, D. R. Chetan, Arghyashree RoyChowdhury Sinha, Srivathsa S. Magadi, Vani Kulkarni & Maneesha S. Inamdar 

Received: 12 May 2016

Accepted: 10 January 2017

Published online: 08 March 2017

How multicellular organisms maintain immune homeostasis across various organs and cell types is an outstanding question in immune biology and cell signaling. In *Drosophila*, blood cells (hemocytes) respond to local and systemic cues to mount an immune response. While endosomal regulation of *Drosophila* hematopoiesis is reported, the role of endosomal proteins in cellular and humoral immunity is not well-studied. Here we demonstrate a functional role for endosomal proteins in immune homeostasis. We show that the ubiquitous trafficking protein ADP Ribosylation Factor 1 (ARF1) and the hemocyte-specific endosomal regulator Asrij differentially regulate humoral immunity. Asrij and ARF1 play an important role in regulating the cellular immune response by controlling the crystal cell melanization and phenoloxidase activity. ARF1 and Asrij mutants show reduced survival and lifespan upon infection, indicating perturbed immune homeostasis. The ARF1-Asrij axis suppresses the Toll pathway anti-microbial peptides (AMPs) by regulating ubiquitination of the inhibitor Cactus. The Imd pathway is inversely regulated- while ARF1 suppresses AMPs, Asrij is essential for AMP production. Several immune mutants have reduced Asrij expression, suggesting that Asrij co-ordinates with these pathways to regulate the immune response. Our study highlights the role of endosomal proteins in modulating the immune response by maintaining the balance of AMP production. Similar mechanisms can now be tested in mammalian hematopoiesis and immunity.

A cascade of appropriate responses to infection or injury is dynamically regulated to co-ordinate the immune response. However, mechanistic details of how the immune organs and molecules they produce communicate, are poorly understood. In the open circulatory system of *Drosophila*, hemocytes carry out phagocytosis and melanization whereas the humoral immune response is mediated by the fat body and gut. Plasmatocytes, which form a majority of the hemocyte population, phagocytose invading pathogens, crystal cells melanize and restrict pathogens to the affected area and lamellocytes encapsulate and neutralize large objects such as parasites¹. A serine protease cascade in crystal cells activates prophenoloxidase (ProPO), which then catalyzes the conversion of phenols to quinones that then polymerize to form melanin². A Toll pathway-dependent protease inhibitor Serpin27A produced by the fat body is required to limit melanization to crystal cells^{3,4}. Thus mechanisms of transport and uptake are essential to regulate systemic communication and melanization. Larvae and adults deficient in Serpin27A or the ProPO mutant *Black cells* show spontaneous melanization yet are immune compromised⁵.

Humoral immunity is primarily governed by the Toll and Imd (Immune deficiency) pathways, which regulate anti-microbial peptide (AMP) production. Fungi or Gram positive bacteria induce the Toll pathway, which causes activation of the NF-KB factor Dif or Dorsal and production of AMPs such as Drosomycin, Metchnikowin and Defensin. Infection by Gram negative bacteria causes activation of the Rel homology and IkappaB homology domain protein Relish, through the Imd pathway and leads to the production of Diptericin, Attacin, Cecropin and Drosocin⁶. Additionally, immune pathways have also been shown in tissue-specific contexts. The JAK/STAT pathway regulates gut-mediated defense mechanisms by controlling intestinal stem cell proliferation^{7,8} and is also essential for the production of humoral factors like thio-ester proteins and turandot molecules in response

Molecular Biology and Genetics Unit, Jawaharlal Nehru Centre for Advanced Scientific Research, Bangalore, India. Rohan J. Khadilkar and Arindam Ray contributed equally to this work. Correspondence and requests for materials should be addressed to M.S.I. (email: inamdar@jncasr.ac.in)

to septic injury⁹. The receptor tyrosine kinase Pvr also plays an important role in regulating the Imd pathway. *Drosophila* JNK activates the expression of Pvr ligands, Pvf2 and Pvf3 which bind Pvr and lead to the activation of the Pvr/ERK pathway which negatively regulates the JNK and NF- κ B arm of the Imd pathway¹⁰.

AMPs are primarily produced by the fat body, the equivalent of the mammalian liver, and secreted into circulation to reach target tissues¹¹. The systemic response by the fat body is mainly governed by the Toll and Imd pathways¹². An intriguing question is the mode of communication between the hemocyte and fat body-mediated immune response. Few studies have recently shown that the hemocytes contribute towards fat body mediated immune responses. Psidin is a lysosomal protein required for degradation of bacteria in hemocytes and simultaneously required for Defensin production in the fat body¹³ and Spaetzle has been shown to have a paracrine effect on the fat body mediated immune response^{14,15}. Recently, upd3 from hemocytes has been shown to induce Drosomycin production in the gut upon septic injury¹⁶. Normal physiological levels of AMPs are altered in response to infections but can also be affected by genetic mutations, thus perturbing homeostasis similar to an infection-induced condition^{17–20}.

Just as in hematopoiesis, a complex network of molecular interactions is essential to regulate immune function and maintain homeostasis. Hence understanding organismal regulation of these processes is a major challenge. Elucidating mechanisms that can integrate the varying inputs received at the cellular level and orchestrate the outcome will be key to generating tools that allow control of the system. Several recent studies highlight the importance of unique signal generation and regulation in cellular organelles, such as endosomes, in a variety of cell types^{21–27}.

Endosomal regulation is a potent mechanism to integrate and modulate signals in *Drosophila* hematopoiesis^{28,29}. We recently showed that the GTP bound form of the ubiquitous endosomal protein ADP Ribosylation Factor 1 (ARF1-GTP), interacts with and regulates the hemocyte-specific endosomal protein Asrij to integrate and modulate multiple signalling pathways required to maintain blood cell homeostasis, including the JAK/STAT and Notch pathways and Pvr and Insulin signaling^{27,30}. Depletion of ARF1 or Asrij leads to increased circulating and differential hemocyte counts. As the primary role of *Drosophila* hemocytes is to mount an immune response like their mammalian blood cell counterparts, and because both ARF1 and Asrij have conserved functions, we analyzed their requirement in the cellular and humoral immune response of *Drosophila*. We show that crystal cell number in ARF1 and Asrij mutants correlates with the extent of melanization. Further, perturbation of the ARF1-Asrij axis results in aberrant AMP production and compromises the response to bacterial infection. ARF1 and Asrij have similar effects on the Toll pathway but regulate Imd pathway AMPs inversely. Thus, we demonstrate that regulation by endosomal proteins allows differential response to signals to achieve immune homeostasis.

Results

Depletion of ubiquitous (ARF1) or hemocyte-specific (Asrij) endosomal proteins does not affect phagocytosis. Phagocytosis is a cellular immune response brought about by plasmatocytes, a differentiated hemocyte type. Depletion of either ARF1 or Asrij results in increased plasmatocyte numbers^{27,30}. To analyze whether there is any alteration in the phagocytic ability of the mutant hemocytes, we incubated the ARF1 knockdown or *asrij* null mutant larval circulating hemocytes with India ink dye particles³¹. Our analysis shows that phagocytosis is unaltered in both mutant genotypes as compared to controls (Fig. S1A–D). We also assessed the ability of the adult hemocytes to phagocytose rhodamine conjugated *E. coli* in Asrij or ARF1 depleted hemocytes and found that there is no difference in their ability to phagocytose the bacteria as compared to the respective controls (Fig. S1E,F). Thus the ARF1-Asrij axis is not essential for phagocytosis.

Increased crystal cell number upon ARF1 or Asrij depletion correlates with increased melanization and phenoloxidase activity. Crystal cells usually attach to the larval cuticle and mechanical injury or infection triggers melanization, leading to blackening of crystal cells³¹. Asrij and ARF1 were earlier shown to be expressed in crystal cells^{27,30}. We specifically depleted or overexpressed Asrij or ARF1 in the hemocyte population using a hemocyte specific driver *e33cGal4* which is expressed in epidermal tissues but not in immune organs like the fat body and/or the gut³². Larvae depleted of ARF1 using a hemocyte driver (*e33cGAL4*) as well as *asrij* null mutant larvae, have increased crystal cells^{27,30}. To test whether the mutant crystal cells were functional, we subjected them to a melanization assay (see methods). Both mutant genotypes showed increase in melanized cells upon heat activation (about 1.5 fold for ARF1 knockdown and 2 fold for *asrij* mutant), as compared to controls (Figs 1A–G and 2A–G). The depleted phenotypes could be rescued to near control levels by over-expressing the respective protein in larvae using *e33cGal4* (Figs 1E,G and 2F,G). Overexpression of ARF1 or Asrij in wild type animals resulted in reduced crystal cell number as compared to the UAS control corresponding to reduced differentiation seen in these larvae as reported earlier^{27,30} (Figs 1D,E,G and 2D,E,G). Notably, the size and intensity of melanized spots was higher in the *asrij* null mutant compared to controls and Asrij overexpressing larvae (Fig. 2A–G). This suggested increase in crystal cell number may be accompanied by increased function.

To test crystal cell function we assayed for phenoloxidase (PO) activity. Melanin biosynthesis is brought about by PO, which catalyzes the oxidation of phenols to quinones, which subsequently polymerize into melanin. A protease cascade cleaves the inactive zymogen ProPO (PPO) to generate active PO. Both ARF1 knockdown and *asrij* null mutant larvae showed similarly increased PO activity (4 fold above control), which was completely restored by ARF1 overexpression but only partially restored (2 fold above control) upon Asrij over-expression (Figs 1H and 2H). Interestingly, either ARF1 or Asrij over-expression in a wild type background reduced PO activity significantly as compared to the UAS control, as expected from the reduced crystal cell number.

Lamellocytes also have the ability to produce enzymes that can trigger a melanization reaction^{33,34}. We have earlier shown that there is no difference in the lamellocyte counts in the *asrij* null mutant whereas lamellocyte counts are increased upon *PxnGal4* or *e33cGal4* mediated ARF1 knockdown²⁷. We also found that

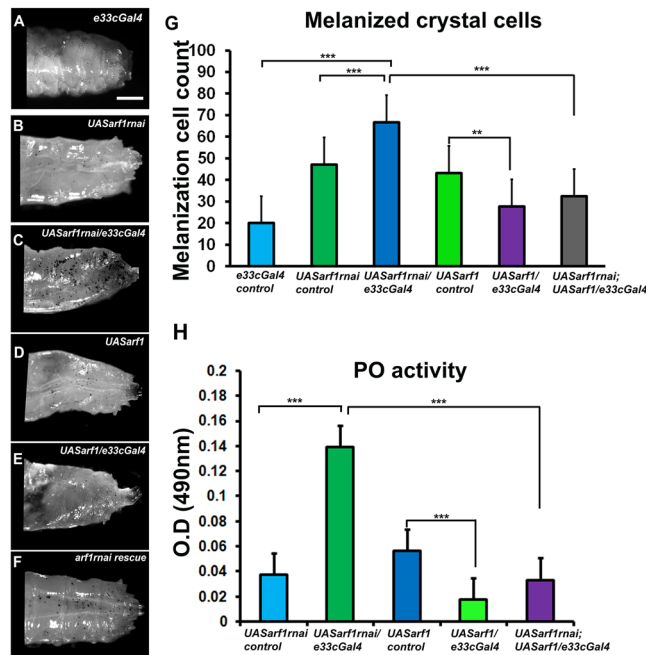


Figure 1. ARF1 regulates crystal cell-mediated melanization and phenoloxidase activity. (A–F) Photomicrographs showing posterior region of third instar larvae of specific genotypes (A) *e33cGal4* (B) *UAS arf1rnai* (C) *UAS arf1rnai/e33cGal4* (D) *UAS arf1* (E) *UAS arf1/e33cGal4* (F) *UAS arf1rnai/UASarf1rnai*; *UAS arf1/e33cGal4* that were heated at 60 °C for 10 min to visualize the melanization response. (G) Melanized crystal cells were quantified and represented graphically. (H) Graph representing phenoloxidase activity in the hemolymph of the indicated genotypes (detected as absorbance at 490 nm) after conversion of L-3, 4-dihydroxyphenylalanine. Scale Bar: (A–F) 100 μ m. Number of larvae analyzed per genotype (n = 10). Error bars show standard error of mean. P-value: ** and *** indicate $P < 0.01$ and $P < 0.001$ respectively.

over-expression of *Asrij* or ARF1 using *e33cGal4* in the pan hemocyte population did not change circulating lamellocyte numbers (L1 positive) (Fig. S2E,F). Hence the increased melanization observed in *asrij* null mutant is exclusively induced by the crystal cell population. However the melanization upon ARF1 knockdown could be due to a contribution of both crystal cells and lamellocytes.

ARF1 and *Asrij* cooperatively regulate expression of Toll pathway AMPs. Activation of the Toll pathway results in production of a repertoire of AMPs mainly, Drosomycin in response to fungal infection and Metchnikowin and Defensin in response to infection by Gram positive bacteria^{35–38}. Under normal conditions these peptides are expressed at very low levels. However, by quantitative polymerase chain reaction-based analysis of reverse transcribed RNA (qRT-PCR) from uninfected adult flies, we found that transcript levels of *drosomycin* and *metchnikowin* are highly upregulated in ARF1 knockdown flies (*e33cGAL4 > UASarf1-RNAi*) (5.5 fold and 3.5 fold respectively) compared to the GAL4 control whereas *defensin* expression is not significantly altered (0.5 fold) (Fig. 3A). These data indicate that ARF1 depletion leads to activation of Toll pathway target genes even in the absence of infection. *Asrij* mediates ARF1 function by interacting with ARF1-GTP during *Drosophila* hematopoiesis. Further ARF1 regulates *Asrij* expression and stability. Hence we also checked the effect of *Asrij* depletion on AMP transcript levels. In the *asrij* null mutant we saw modest increase in *drosomycin* and *metchnikowin* transcript levels as compared to *w1118* control whereas *defensin* expression was slightly reduced (Fig. 3B). These data indicate that *Asrij* depletion also leads to differential activation of Toll pathway target genes. However a significant difference was the substantially greater effect of ARF1 depletion on *drosomycin* and *metchnikowin* transcript levels than that of *Asrij* depletion. This suggests that ARF1 has a wider role in regulating AMPs of the Toll pathway.

We also performed *in vivo* reporter assays to test the activation status of representative Toll pathway AMPs using transgenic flies that would express GFP under the control of an AMP promoter upon infection. Introduction of Drosomycin-GFP or Defensin-GFP reporter in ARF1 knockdown or in *asrij* null or *asrij* knockdown background respectively was assayed after infection with *B. subtilis*. Quantification of the GFP+ flies showed that ARF1 knockdown, resulted in significantly more GFP positive flies for Drosomycin (93% compared to 53% in GAL4 control) and a smaller increase in Defensin-GFP (75% compared to 61% in GAL4 control) (Fig. 3C,D). Similarly *asrij* depletion resulted in greatly increased Drosomycin-GFP expressing flies (76% compared to 14% in control) with a small reduction in Defensin-GFP flies (63% compared to 71% in control) (Fig. 3E,F). There was no expression of the target antimicrobial peptide GFP reporters of the Toll pathway in the absence of *B. subtilis* infection in control as well as mutant/knockdown conditions. Thus our *in vivo* reporter analysis is in agreement with the mRNA expression analysis.

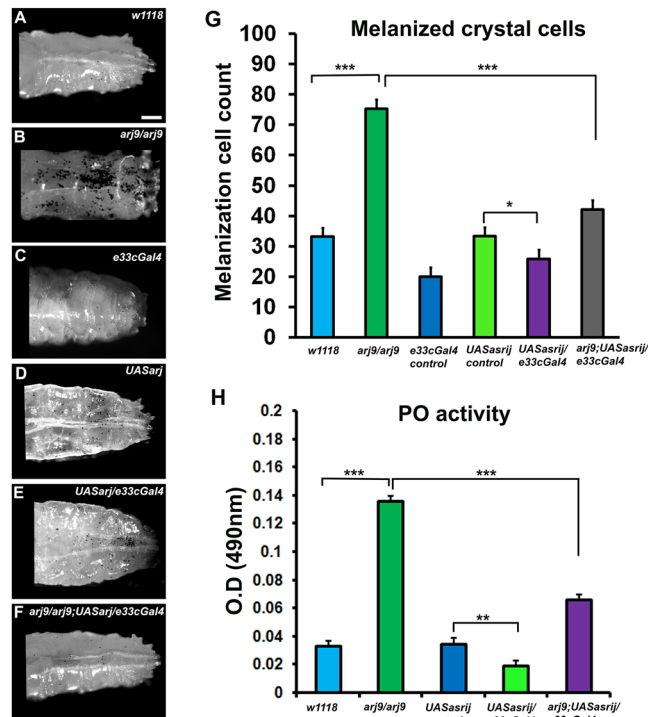


Figure 2. Asrij regulates crystal cell-mediated melanization and phenoloxidase activity. (A–F) Photomicrographs showing posterior region of third instar larvae of specific genotypes (A) *w1118* (B) *arj9/arj9* (C) *e33cGal4* (D) *UAS arj* (E) *UAS arj/e33cGal4* (F) *arj9/arj9; UAS arj/e33cGal4* that were heated at 60 °C for 10 min to visualize the melanization response. (G) Melanized crystal cells were quantified and represented graphically. (H) Graph representing phenoloxidase activity in the hemolymph of the indicated genotypes (detected as absorbance at 490 nm) after conversion of L-3, 4-dihydroxyphenylalanine. Scale Bar: (A–F) 100 μm. Number of larvae analyzed per genotype (n = 10). Error bars show standard error of mean. P-value: *, **, *** indicate P < 0.05, P < 0.01 and P < 0.001 respectively.

The ARF1-Asrij axis suppresses Toll pathway AMP production by stabilizing Cactus. Activation of the Toll pathway leads to nuclear translocation of the transcription factors Dorsal and Dif. In the absence of the Toll ligand Spaetzle, Dorsal and Dif are bound by Cactus, a negative regulator of the Toll pathway, inhibiting their activity and nuclear localization³⁹. Receptor activation leads to phosphorylation of Cactus followed by its ubiquitination and degradation, thus releasing Dorsal/Dif to translocate to the nucleus for target AMP gene activation. Since Toll pathway AMPs were upregulated in both Asrij and ARF1 depleted conditions, we probed the status of ubiquitinated Cactus in these conditions. Depletion of ARF1 or Asrij led to increased co-localization of Cactus with Ubiquitin in the circulating hemocytes as well as the fat bodies (Fig. 3G, Fig. S2). ARF1 depletion increased the co-localization in hemocytes to 44% from 11% in control, whereas *asrij* null hemocytes showed 77% co-localization compared to 8% in control. There was also increased co-localization (22.5%) of Cactus and Ubiquitin in the *asrij* null mutant fat body cells as compared to the *w1118* controls (3%), whereas *HmlGal4* mediated ARF1 knockdown larval fat body cells showed (7.5%) co-localization as compared to its respective controls (0.4%) (Fig. S2A,B). Analysis of the adult fat body cells also showed increased cactus and ubiquitin levels in *asrij* null mutant but not in *HmlGal4* mediated ARF1 knockdown adult fat body cells (Fig. S2C,D). This suggests that Cactus may be increasingly targeted for degradation when the ARF1-Asrij axis is perturbed in the larval stage. However additional mechanisms may operate in the adult fat body that compensate the loss of ARF1.

Cactus degradation should lead to increased translocation of the Toll pathway effectors Dorsal/Dif to the nucleus. Since Dorsal translocation is essential for AMP production, we stained for Dorsal in *asrij* null and ARF1 knockdown hemocytes. There was increased translocation of Dorsal to the nucleus as compared to the control hemocytes (Fig. 3H–M). This indicates increased Toll pathway activity is achieved by promoting nuclear translocation of Dorsal. Thus the ARF1-Asrij axis can maintain homeostatic conditions of Toll signaling by stabilizing Cactus and preventing aberrant AMP production (Fig. 3N).

Differential effect of ARF1 and Asrij on Imd pathway AMPs. Infection with Gram negative bacteria brings about nuclear localization of the NF-κB transcription factor Relish, thus activating its main target AMP, Diptericin^{35, 36, 38}. The other Imd pathway target genes include *attacin A1*, *cecropin A1* and *drosocin*. We analyzed the effect of ARF1 depletion on the transcript levels of Imd pathway targets and found that they were constitutively upregulated in ARF1 knockdown flies. *Attacin*, *drosocin* and *diptericin* transcripts were highly upregulated (~18 fold, ~15 fold and ~22 fold) whereas *cecropin* levels showed modest increase (1.25 fold) as compared to the parental control (Fig. 4A). Upon *in vivo* AMP-GFP reporter analysis after infection with *E. coli*, ARF1

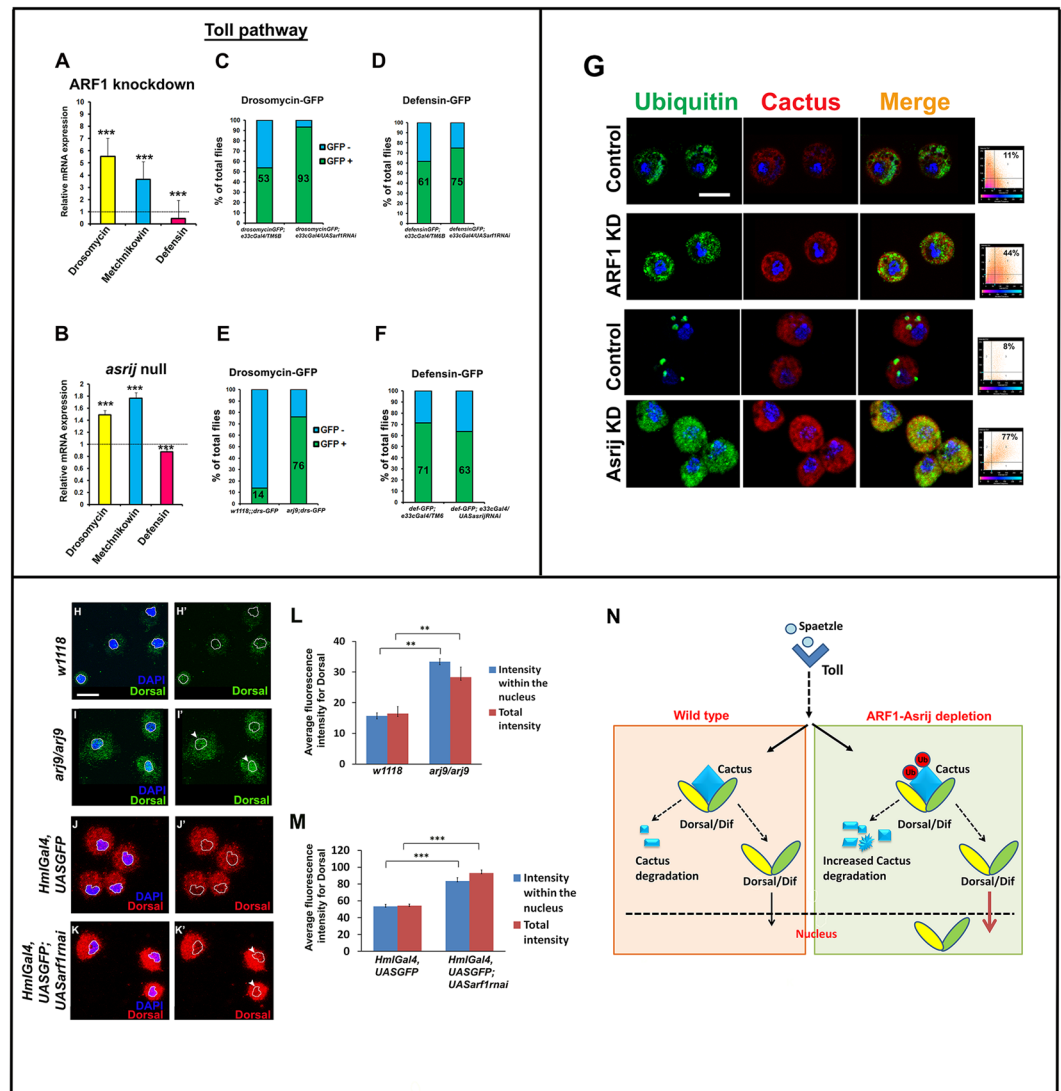


Figure 3. ARF1 and Asrij negatively regulate Toll pathway-mediated immune response. (A,B) Quantification of Toll pathway-governed antimicrobial peptide expression by qRT-PCR analysis shows that *Drosomycin* and *Metchnikowin* are upregulated and *Defensin* is downregulated in *arf1* knockdown (A) and *asrij* null mutant (B) larvae. (C–F) Quantification for the total percentile of flies expressing the Toll pathway reporters - Drosomycin-GFP and Defensin-GFP in flies with *e33cGal4*-mediated *arf1* knockdown (C,D) or *asrij* null (E) or *e33cGal4*-mediated *asrij* knockdown (F) respectively. (G) Images showing increased colocalization of Cactus and Ubiquitin in *arf1* or *asrij* knockdown circulating larval hemocytes as compared to respective controls, also indicated by adjacent co-localization plots. (H) Images showing higher Dorsal specific signal in the entire hemocyte as well as in DAPI stained region (nucleus) for the *asrij* null (*arj9/arj9*) and *arf1* knockdown (*HmlGal4, UASGFP; UAS arj1rnai*) larvae as compared to the respective controls (*w1118* and *HmlGal4, UASGFP*). White dotted line indicates nuclear area under consideration. Arrowheads mark nuclei with higher Dorsal signal (I,J) Quantification of the fluorescence intensity for Dorsal staining in the entire cell as well as in the DAPI stained area of the cell for *asrij* null (I) and *arf1* knockdown hemocytes (n = 10) (J). (K) Model indicating the suggested role of the ARF1-Asrij endocytic axis in regulating the Toll pathway. Error bars indicate standard error of mean. ** indicates P < 0.01 and *** indicates P-value < 0.001. Scale Bar: (G,H) 10 μ m.

knockdown showed a dramatic up-regulation of the percent of GFP positive flies for Attacin, Cecropin, Drosocin and Dipteracin (87.5%, 88.8%, 100% and 84.21% respectively) as compared to Gal4 control (68.75%, 77.7%, 54.5% and 63.6% respectively) (Fig. 4C–F).

In contrast to the effect of ARF1 depletion, *Asrij* null mutants showed no significant change in expression of *dipteracin* transcripts, which is a standard indicator of Imd activation (Fig. 4B). However, while levels of *attacin* and *drosocin* were reduced, *cecropin* transcript levels were marginally affected (1.4 fold) and comparable to ARF1 knockdown flies. *In vivo* AMP-GFP reporter analysis upon *E. coli* infection for the Imd pathway governed AMPs showed no significant change in GFP+ flies for Attacin and Cecropin (72.22%, 80% in knockdown compared to 65%, 78.94% in controls respectively) whereas Drosocin and Dipteracin GFP+ flies were significantly higher

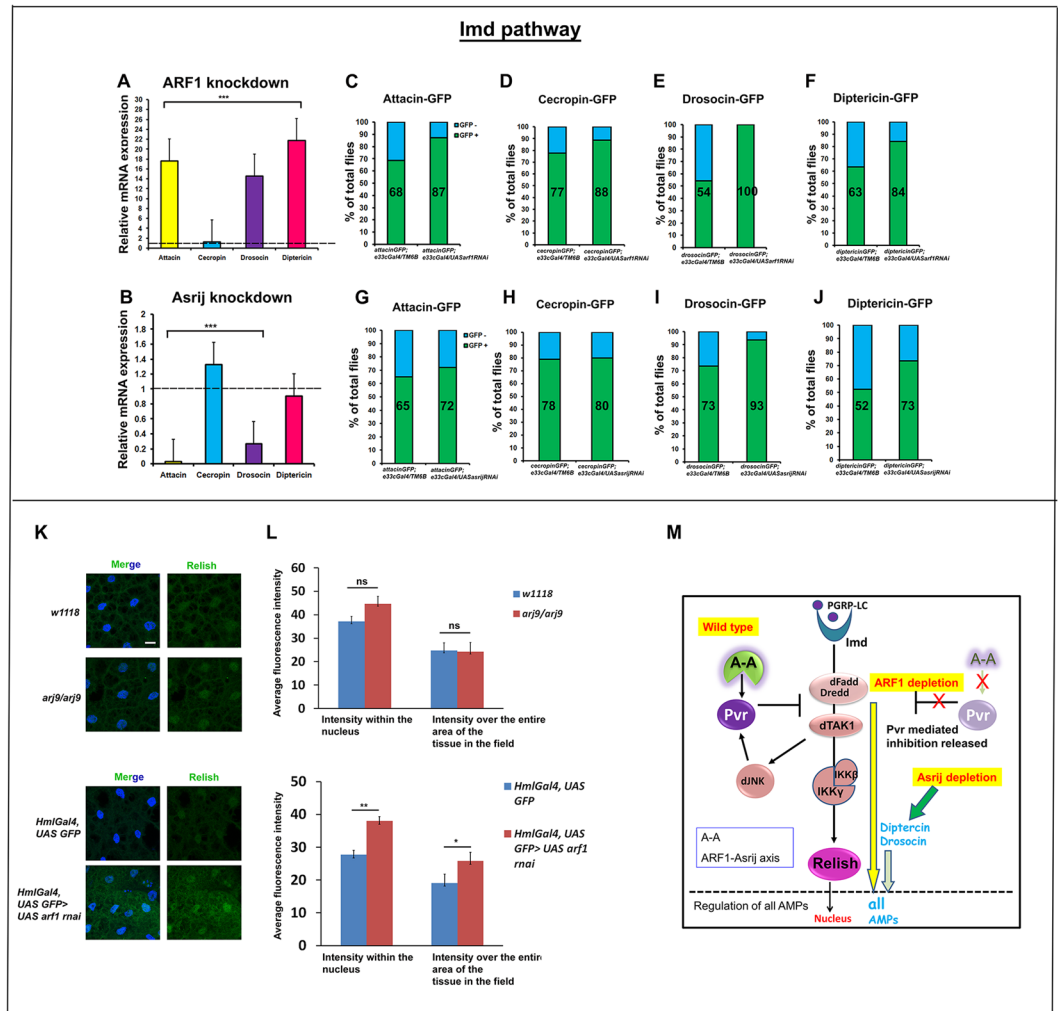


Figure 4. ARF1 and Asrij differentially regulate the Imd pathway. (A,B) Quantification of Imd pathway-governed antimicrobial peptide expression by qRT-PCR analysis shows that *Attacin*, *Drosocin* and *Diptericin* are highly up-regulated whereas *Cecropin* levels are unaffected in *e33cGal4*-mediated ARF1 knockdown flies (A). *Cecropin* levels are upregulated and *Attacin*, *Drosocin*, *Diptericin* levels are down-regulated in *e33cGal4*-mediated Asrij knockdown flies (B). (C–J) Quantification of the total percentile of flies expressing the Imd pathway reporters - Attacin-GFP, Cecropin-GFP, Drosocin-GFP and Diptericin-GFP in flies with *e33cGal4* mediated ARF1 knockdown (C–F) or *asrij* knockdown (G–J) respectively. (K) Images showing unchanged intensity of Relish in the nucleus of *arf9/arf9* larval fat body but increase in the intensity in *arf1* knockdown larval fat body compared to the respective controls. Scale bar 10 μ m. (L) Quantification of Relish intensity over the entire area of the tissue in the field of view as well as in the nucleus (DAPI stained area) in *arf9/arf9* and *arf1* knockdown fat bodies and in the respective controls (n = 10). Error bar represents standard error of mean. ns indicates statistically non-significant difference. * and ** indicates P-value < 0.05 and < 0.01 respectively. (M) Model indicating the suggested role of the ARF1-Asrij endocytic axis in regulating the Imd pathway.

(93.75% and 73.68% in knockdown compared to 73.68% and 52.63% in controls respectively) (Fig. 4G–J). There was no expression of the target antimicrobial peptide GFP reporters of the Imd pathway in the absence of *E. coli* infection in both control or mutant/knockdown conditions. Imd pathway activation results in nuclear localization of Relish and thereby upregulation of AMP genes. Hence, we also looked at Relish localization, as nuclear Relish is indicative of pathway activation. Relish staining has not been reported in hemocytes and we could not detect any specific signal by immunostaining. However fat bodies from infected control flies show nuclear Relish as reported³⁶. Since systemic signals as well as cross talk between the hemocytes and fat body bring about immune regulation, we assayed for Relish nuclear localization in fat bodies of larvae depleted of *asrij* (null) or ARF1 (*HmlGAL4-arf1 RNAi*). *asrij* null fat bodies showed no apparent change in nuclear Relish as compared to the parental control whereas ARF1 depleted fat bodies showed increased nuclear Relish, indicating pathway activation (Fig. 4K,L). This is in agreement with the increase in AMP levels seen in ARF1 depleted flies, whereas *asrij* mutants show no significant change for most AMPs. Thus while ARF1 can regulate all Imd pathway AMPs tested, *Asrij* has a milder differential effect.

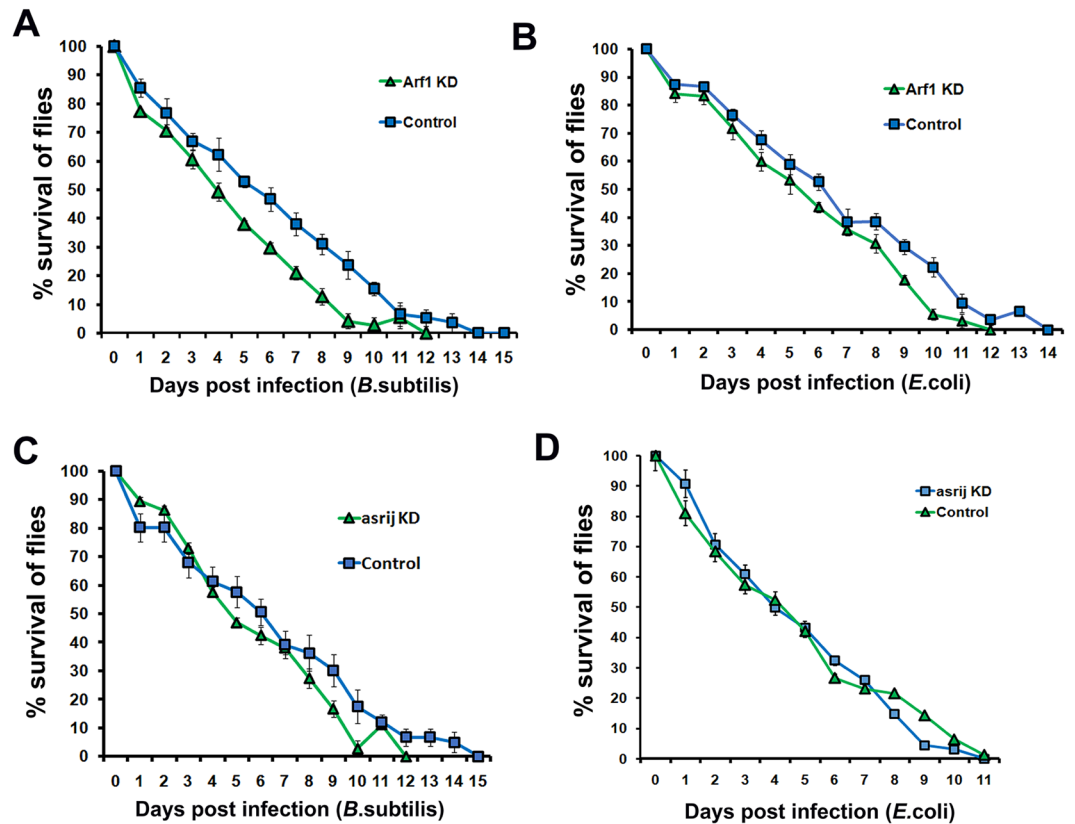


Figure 5. ARF1 and Asrij knockdown flies show compromised survival upon infection. (A–D) Survival curves showing that *e33cGal4*-mediated *ARF1* or *asrij* knockdown flies show a reduced survival ability as compared to its control upon infection with either *B. subtilis* (A,C) or *E. coli* (B,D). At least 100 flies were tested per genotype over at least three independent experiments.

These data show that both ARF1 and Asrij have major non-overlapping roles in regulating Imd pathway AMP expression. ARF1 is a generic negative regulator of the Imd pathway, as its depletion leads to heightened levels of all the target AMPs. While there is only a small change in *dipteracin* or *cecropin* transcript levels upon Asrij depletion, Dipteracin peptide levels are higher indicating Asrij normally checks Dipteracin levels, possibly post-transcriptionally. While Asrij positively regulates *attacin* and *drosocin* transcript expression, the effect on Attacin AMP levels was not significant. However there was a dramatic increase in Drosocin-GFP flies. This indicates that Asrij shows differential/discriminatory effects on AMP production (Fig. 4M). Thus co-ordinated and complementary regulation of Imd targets by the ARF1-Asrij axis is essential to maintain immune homeostasis.

Survival and lifespan of Asrij or ARF1- depleted flies is compromised upon acute bacterial infection.

Impaired AMP production upon infection can lead to reduced survival due to an inability to combat the bacterial infection. Loss-of-function mutations in the Toll and Imd pathway effectors such as Dif and Relish⁴⁰ lead to reduced ability to combat infections. Earlier studies show that Asrij is epistatic to ARF1 and depends on ARF1 for its stability²⁷. While they both similarly regulate the Toll pathway, differential regulation of the Imd pathway suggests complex control on AMP production. Hence we tested the effect of Asrij or ARF1 depletion on the ability of flies to combat infection and survive.

Upon infection with *B. subtilis*, while 80% control flies continued to survive after 48 hrs with a gradual reduction in number over subsequent days, mutant numbers rapidly declined after 48 hrs and the mutant population perished 3–4 days earlier than controls. This resulted in a steep decrease in % survival upon infection as compared to the *Gal4* and *w1118* controls respectively (Fig. 5A,C). Thus the increased production of the Toll pathway AMP Drosomycin in the absence of ARF1 or Asrij does not protect lifespan upon Gram positive bacterial infection.

While *ARF1* depletion results in increased production of all Imd pathway AMPs, *asrij* depletion caused limited and differential activation of Imd pathway AMPs. Upon infection with *E. coli*, flies depleted of ARF1 or Asrij, both showed compromised survival (Fig. 5B,D). All mutant genotypes perished before controls, indicating that increased AMP production does not confer the ability to combat infection.

In order to know if the reduction in survival of the *asrij* null flies upon infection is solely due to defect in the hematopoietic system or due to reduction of overall tolerance of the flies, we depleted Asrij specifically in the hemocytes using Hemolectin-Gal4 (*HmlGal4*) or trachea using breathless-Gal4 (*btlGal4*) where Asrij was also seen to be expressed in the embryo⁴¹. Trachea specific knockdown of Asrij does not reduce the survival significantly as compared to the control upon infection with both *B. subtilis* or *E. coli* (Fig. S3A,B). However, hemocyte specific knockdown of Asrij leads to reduction in survival of the flies (Fig. S3C,D). This indicates that the effect

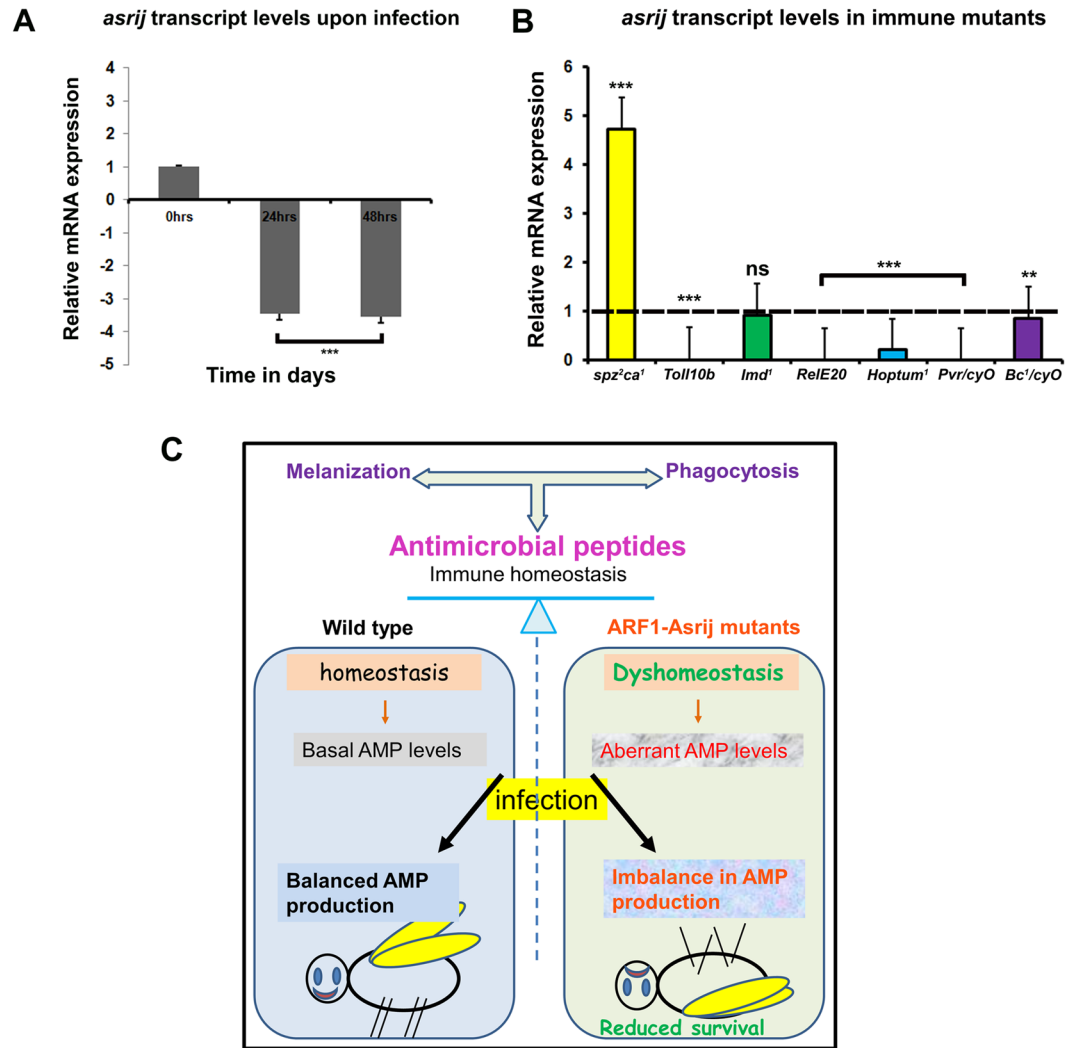


Figure 6. *Asrij* expression is modulated upon infection and in immune mutants. (A,B) qRT-PCR analysis of adult flies showing that *asrij* mRNA levels are down-regulated 24 and 48 hours post infection (A) and that *asrij* transcript levels vary among immune mutants (B). (C) Model illustrating loss of immune homeostasis in ARF1-Asrij depleted conditions leading to compromised survival of the flies.

of loss of *Asrij* on the survival is a consequence of malfunctioning of the hematopoietic system and not due to its absence in other organs like trachea.

Further, we also tested whether ARF1 depletion in the hemocyte compartment specifically or in other organs like trachea has any effect on the survival of the flies post infection. Survival of flies depleted of ARF1 in the trachea (Fig. S3E,F) is reduced with or without infection. Also, the flies depleted of ARF1 in the hemocyte compartment have reduced survival post-infection (Fig. S3G,H). This indicates that while *Asrij* and ARF1 function in the hematopoietic system is essential for regulating the immune response, ARF1 depletion from other organs may deteriorate the overall health of the flies and make them more susceptible to infection. Given its ubiquitous expression, ARF1 may also mediate its effect through other interactors that are involved in responding to infection.

***Asrij* expression is downregulated upon Gram negative bacterial infection.** Immune response in normal animals requires AMP upregulation to combat infection^{6,8,42}. ARF1 and *Asrij* have opposite effects on the *Imd* pathway, suggesting that *Asrij* acts independent of ARF1 in *Imd* pathway regulation. However, increased AMP levels in ARF1 knockdown do not provide additional ability to combat infection. Additionally, *Asrij* is downstream of ARF1 and reduces AMP levels. Therefore *Asrij* expression levels positively correlate with *Imd* pathway target AMP transcript levels. Hence we checked the status of *Asrij* expression upon immune challenge. Wild type flies infected with *E. coli* showed reduced *asrij* transcript levels (Fig. 6A). This indicates that *asrij* levels co-relate with *Imd* pathway activation.

***Asrij* levels are differentially regulated in immune pathway mutants.** *Asrij* levels are downregulated upon bacterial infection and survival is compromised in *Asrij* depleted conditions indicating an important

role for Asrij in mounting an immune response. Since pathway activation and attenuation are both important for maintaining homeostasis, it is likely that Asrij expression is in turn regulated by components of the Toll or Imd pathways as well as other pathways like Jak/Stat and Pvr. To test this we assayed *asrij* transcript levels in a range of immune pathway mutants, which either inactivate or activate the pathway. We found that *asrij* levels are upregulated in Toll pathway mutants like *spz^{tm7}* whereas they are downregulated in Toll pathway gain-of-function mutants like *Toll^{10b}* (Fig. 6B). This is in agreement with increased ubiquitination of cactus, suggesting a requirement for the ARF1-Asrij axis in regulating Toll pathway activity possibly via a feed-forward loop.

Asrij levels are downregulated in Imd pathway mutants like *Rel^{E20}* (Imd effector) suggesting that *asrij* may be a target of *relish*. Also mutants of the other pathways like *Hop^{1um1}* (Jak gain of function) and *Pvr* (*Pvr/Cyo*) show reduced *Asrij* levels (Fig. 6B). There was no significant downregulation of *asrij* levels in *Imd* and *Black cells* mutant. This suggests that *asrij* is differentially regulated by downstream effectors of the Toll and Imd immune pathways. While the Toll pathway suppresses *asrij* expression, Imd pathway promotes *asrij* expression. Taken together with our data that *Asrij* levels are reduced upon *E. coli* infection this suggests that *Asrij* expression may be dependent on Imd pathway activation.

Discussion

A balanced cellular and humoral immune response is essential to achieve and maintain immune homeostasis^{20,43,44}. In *Drosophila*, aberrant hematopoiesis and impaired hemocyte function can both affect the ability to fight infection and maintain immune homeostasis. Endosomal proteins are known to regulate *Drosophila* hematopoiesis^{27,30}. Here, we show an essential function for endosomal proteins in regulating immunity.

Altered hemocyte number and distribution as a result of defective hematopoiesis, can also lead to immune phenotypes like increased melanization or phagocytosis. We illustrate that perturbation of normal levels of endocytic molecules ARF1 or Asrij leads to aberrant hematopoiesis, affecting the circulating hemocyte number^{27,30}. We show that this in turn leads to an impaired cellular immune response. The aberrant hematopoietic phenotypes with pan-hemocyte tissue-specific depletion of ARF1 using *e33cGal4* or *HmlGal4* are comparable to the phenotypes observed in the case of *asrij* null mutant. Hence we have compared Gal4-mediated ARF1 knockdown to *asrij* null mutant in this study.

In addition, we also show that ARF1 and Asrij have a direct role in humoral immunity by regulating AMP gene expression. This is likely to be a contribution from the hemocyte compartment which is primarily affected upon perturbation of Asrij or ARF1. It is well established that hemocytes, apart from acting as the cellular arm of the immune response, also act as sentinels and relay signals to the immune organs that mount the humoral immune response. Hemocytes have been shown to produce ligands like Spaetzle and upd3 that activate immune pathways and induce anti-microbial peptide secretion from the fat body or gut^{16,45}. Asrij or ARF1 could also be affecting the production of such ligand molecules thereby affecting the target immune-activation pathways.

Considering the involvement of Asrij and ARF1 in both the arms of immune response, we propose a model for the role of the ARF1-Asrij axis in maintaining immune homeostasis (Fig. 6C) that can be used for testing additional players in the process.

It is known that ARF1 is involved in clathrin coat assembly and endocytosis^{46,47} and has a critical role in membrane bending and scission⁴². In this context it is also intriguing to note that ARF1, like Asrij, does not seem to have an essential role in phagocytosis. This suggests that hemocytes could be involved in additional mechanisms beyond phagocytosis in order to combat an infection.

Both ARF1 and Asrij control hemocyte proliferation as their individual depletion leads to an increase in the total and differential hemocyte counts. Also, both mutants have higher crystal cell numbers due to over-activation of Notch as a result of endocytic entrapment^{27,30}. This suggests that increased melanization accompanied by increase in phenoloxidase activity upon ARF1 or Asrij depletion is a consequence of aberrant hematopoiesis and not likely due to a cellular requirement in regulating the melanization response. Constitutive activation of the Toll pathway or impaired Jak/Stat or Imd pathway signaling in various mutants also leads to the formation of melanotic masses³⁶. Thus the phenotypes seen on Asrij or ARF1 depletion could either be due to the defective hematopoiesis which directly affects the cellular immune response or leads to a mis-regulation of the immune regulatory pathways.

Regulation of many signaling pathways, including the immune regulatory pathways takes place at the endosomes^{48–51}. For example, endocytic proteins Mop and Hrs co-localize with the Toll receptor at endosomes and function upstream of MyD88 and Pelle, thus indicating that Toll signalling is regulated by endocytosis⁵⁰. Our study shows that loss of function of the ARF1-Asrij axis leads to an upregulation of some AMP targets of the Toll pathway. Upon depletion of ARF1-Asrij endosomal axis we find increased ubiquitination of Cactus, a negative regulator of the Toll pathway, in both hemocytes as well as fat bodies. This suggests non-autonomous regulation of signals by the ARF1-Asrij axis, which is in agreement with our earlier model of signalling through this route (Khadilkar *et al.*²⁷). Thus the endosomal axis may systemically control the sorting and thereby degradation of Cactus, which in turn promotes the nuclear translocation of Toll effector, Dorsal. This could explain the significant increase in Toll pathway reporter expression such as Drosomycin-GFP. Interestingly the effect of ARF1 depletion on the Toll pathway is more pronounced than that of Asrij depletion. This is not surprising as ARF1 is a ubiquitous and essential trafficking molecule that regulates a variety of signals. This suggests that ARF1 is likely to be involved with additional steps of the Toll pathway and may also interact with multiple regulators of AMP expression.

ARF1 and Asrij show complementary effects on IMD pathway target AMPs. While ARF1 suppresses the production of IMD pathway AMPs, Asrij has a discriminatory role. Asrij seems to promote transcription of AttacinA and Drosocin, whereas it represses Cecropin. However in terms of AMP production only Drosocin and Dipterocin are affected, but not to the extent of ARF1. In addition, Relish shows marked nuclear localization in fat body cells of hemocyte-specific *arf1* knockdown larvae whereas there is no significant difference in the

localization in Asrij depleted larval fat bodies. This indicates that ARF1-Asrij axis exerts differential control over the Imd pathway. Thus ARF1 causes strong generic suppression of the Imd pathway while the role of Asrij could be to fine tune this effect. Mass spectrometric analysis of purified protein complexes indicates that ARF1 and Imd interact⁵² (*Drosophila* Protein Interaction Mapping Project, <https://interfly.med.harvard.edu>). Hence it is very likely that ARF1 regulates Imd pathway activation at the endosomes. Whether this interaction involves Asrij or not remains to be tested and will give insight into modes of differential activation of immune pathways.

Our analysis shows that Asrij is the tuner for endosomal regulation of the humoral immune response by ARF1 and provides specialized tissue-specific and finer control over AMP regulation. This is in agreement with earlier data showing that Asrij acts downstream of ARF1²⁷. Since ARF1 is expressed in the fat body²⁷ it could communicate with the hemocyte-specific molecule, Asrij, to mediate immune cross talk.

As we see reduced Asrij expression in Toll and Jak/Stat pathway mutants such as *Rel^{E20}* and *Hop^{Tum1}*, it is likely that these effectors also regulate Asrij, setting up a feedback mechanism to modulate the immune response. We have earlier shown that ARF1-Asrij axis modulates different signalling outputs like Notch by endosomal regulation of NICD (Notch Intracellular Domain) transport and activity and JAK/STAT by endosomal activation of Stat92e. Further, ARF1 along with Asrij regulates Pvr signaling in order to maintain HSCs^{27,30}. ARF1 acts downstream of Pvr²⁷. Surprisingly, Asrij levels are downregulated in the *Pvr* mutant. Hence it is likely that the ARF1-Asrij axis regulates trafficking of the Pvr receptor, which then also regulates Asrij levels thus providing feedback regulation. While active modulation of signal activity and outcome at endosomes could be orchestrated by ARF1 and Asrij, their activities in turn need to be modulated. Our data suggest that targets of Asrij endosomal regulation may in turn regulate Asrij expression at the transcript level. Further, upon Gram positive infection in wild type flies, *asrij* transcript levels decrease with a concomitant increase in suppressed AMPs such as Cecropin. This indicates additional regulatory loops such as that mediated by the IMD pathway effector NFκβ may regulate *asrij* transcription. Using bioinformatics tools, we do see presence of binding sites for NFκβ and Rel family of transcription factors in the upstream regulatory sequence (1 kb upstream) of *asrij* and *arf1*. Hence, we propose feedback regulation of Asrij and ARF1 by the effectors of the Toll and Imd pathway respectively. This is reflected in the regulation of Asrij expression by these pathways. This also implies multiple modes of regulation of *asrij* and *arf1*, which are likely important in its role as a tuner of the generic immune response, thereby allowing it to discriminate between AMPs that were thought to be uniformly regulated, such as those downstream of IMD. Thus our analysis gives insight into additional complex regulation of the *Drosophila* immune response that can now be investigated further.

Asrij and ARF1 being endocytic proteins are likely to interact with a number of molecules that regulate different cell signalling cascades. Due to endosomal localization, molecular interactions may be favored that further translate into signalling output. Hence, it is not surprising that Asrij and ARF1 genetically interact with multiple signalling pathways and can aid crosstalk to regulate important developmental and physiological processes like hematopoiesis or immune response. It is quite likely that Asrij and ARF1 are themselves also part of different feedback loops or feed-forward mechanisms as their levels need to be tightly regulated. We find evidence for this with respect to the Toll, JAK/STAT and Pvr pathway as described earlier. Hence we propose that the Asrij-ARF1 endosomal signalling axis genetically interacts with various signalling components thereby regulating blood cell and immune homeostasis.

AMP transcript level changes upon ARF1 or Asrij depletion also correspond to reporter-AMP levels seen after infection. This suggests that although ARF1 is known to have a role in secretion, mutants do not have an AMP secretion defect. Hence aberrant regulation of immune pathways on perturbation of the ARF1-Asrij axis is most likely due to perturbed endosomal regulation.

ARF1 has a ubiquitous function in the endosomal machinery⁴⁶ and is well-positioned to regulate the interface between metabolism, hematopoiesis and immunity in order to achieve homeostasis. Along with Asrij and other tissue-specific modulators, it can actively modulate the metabolic and immune status in *Drosophila*. In this context, it is interesting to note that Asrij is a target of MEF2⁵³, which is required for the immune-metabolic switch *in vivo*⁵⁴. Thus Asrij could bring tissue specificity to ARF1 action, for example, by modulating insulin signalling in the hematopoietic system.

It is likely that in Asrij or ARF1 mutants, the differentiated hemocytes mount a cellular immune response and perish as in the case of wild type flies where immunosenescence sets in with age and the ability of hemocytes to combat infection declines⁵⁵. Since their hematopoietic stem cell pool is exhausted, they may fail to replenish the blood cell population, thus compromising the ability to combat infections. Alternatively, mechanisms that downregulate the inflammatory responses and prevent sustained activation^{43,56} may be inefficient when the trafficking machinery is perturbed. This could result in constitutive upregulation thus compromising immune homeostasis^{56,57}.

In summary, we show that in addition to its requirement in hematopoiesis, the ARF1-Asrij axis can differentially regulate humoral immunity in *Drosophila*, most likely by virtue of its endosomal function. ARF1 and Asrij bring about differential endocytic modulation of immune pathways and their depletion leads to aberrant pathway activity and an immune imbalance. In humans, loss of function mutations in molecules involved in vesicular machinery like Amphiphysin I in which clathrin coated vesicle formation is affected leads to autoimmune disorders like Paraneoplastic stiff-person syndrome⁵⁸. Synaptotagmin, involved in vesicle docking and fusion to the plasma membrane acts as an antigenic protein and its mutation leads to an autoimmune disorder called Lambert-Eaton myasthenic syndrome⁵⁹. Mutations in endosomal molecules like Rab27A, β subunit of AP3, SNARE also lead to immune diseases like Griscelli and Hermansky-Pudlak syndrome^{60,61}. Mutants of both ARF1 and Asrij are likely to have drastic effects on the immune system. Asrij has been associated with inflammatory conditions such as arthritis, thyroiditis, endothelitis and tonsillitis (<http://www.malacards.org/card/tonsillitis?search=OCIAD1>), whereas the ARF family is associated with a wide variety of diseases. ARF1 has been shown to be involved in mast cell degranulation and IgE mediated anaphylaxis response⁶². Generation and analysis of

vertebrate models for these genes such as knockout and transgenic mice will provide tools to understand their function in human immunity.

Materials and Methods

***Drosophila* Stocks.** All fly stocks were maintained at standard rearing conditions. Respective UAS or Gal4 parent strains or *w1118* (*asrij* null mutant) were used as controls. Tissue specific Gal4 promoter line was used to drive the expression of UAS responder genes. Following fly lines were used: *arf⁹/arf⁹*, *UAS-asrij* (Kulkarni, Khadilkar *et al.*³⁰), *Rel^{E20}*, *Black cells (Bc¹/CyO)*, *Hop^{Tum1}*, *Imd¹* (NCBS stock centre), *Pvr/Cyo* (Pernille Rorth, Denmark), Gal4 driver lines *e33cGAL4* (Kathryn Anderson, NY, USA), *HmlGal4*, *UASGFP* (Tina Mukherjee, inStem), *UAS-arf1* (Khadilkar *et al.*²⁷), *btl-Gal4* (Arjun Guha, inStem), *UASarf1rnai* (VDRC), GFP reporter flies for Toll and Imd pathway (David Ferrandon, France).

Antibodies used. Mouse anti-Dorsal (1:50, 7A4, DSHB), mouse anti-Relish (1:10, 21F3, DSHB), mouse anti-L1 antibody (1:50 gift from Istvan Ando), Mouse anti-Cactus (1:25 3H12, DSHB), Rabbit anti-ubiquitin (1:100 ab7780, Abcam), Rabbit anti-ubiquitin (1:100, ab19247, Abcam).

***In vitro* Larval Phagocytosis assay.** Primary hemocyte cultures were prepared as described earlier⁶³. Briefly, third instar larvae were surface sterilized, and hemolymph was collected by puncturing the integument using dissection forceps into 150 µl of 1X PBS (Phosphate Buffer Saline) in 35-mm coverslip-bottom dishes and incubated with India Ink (HIMEDIA, India) for 10 min followed by 5 washes with PBS. After 1 hour hemocyte preparations were fixed with 2.5% paraformaldehyde for 20 min and imaged. Phagocytosis of India ink particles by primary hemocytes was assessed using Zeiss LSM510 meta.

***In-vivo* adult phagocytosis assay.** 20 adult flies of each genotype were injected with Rhodamine conjugated heat-killed *E. coli* in the abdomen. After 1.5 hours, the flies were bled to collect the hemolymph. The hemocytes were kept for 30 min in sterile Schneider's media for attachment. After 30 min, the cells were gently washed with 1X PBS to remove extracellular bacteria. Hemocytes were fixed using 4% para-formaldehyde for 20 minutes. Hemocytes were identified by expression of GFP driven by *HmlGal4*. Bacterial particles detected in the z-sections of the hemocyte images acquired were considered for quantification of phagocytic events. Experiments were repeated at least three times with biological and technical replicates. Images were acquired using Zeiss LSM510 meta confocal microscope.

Circulating hemocyte and fat body staining. Larvae were bled in Schneider's media and the hemolymph was plated on a cover-slip bottom dish for attachment for 45 minutes. Hemocytes were fixed in 4% para-formaldehyde for 20 minutes followed by wash with PBS. Cells were then permeabilized with 0.4% NP40 and blocked with 20% goat serum for 1 hour. The preps were incubated with primary antibodies at 4 °C overnight. Secondary antibody staining was performed following this and the hemocytes were incubated with DAPI to mark the nuclei. Images were taken in LSM510 Meta Confocal microscope. For hemocyte count, images were taken in Olympus IX81 microscope.

Larvae or adult flies were dissected in 1X PBS to isolate the fat body. The fat body preps were fixed in 4% para-formaldehyde for 20 minutes followed by wash with PBS, permeabilized with 0.1% Triton-X 100 and blocked with 20% normal goat serum for 1 hour. The preps were then incubated with primary antibodies at 4 °C overnight. Secondary antibody staining was then performed using Alexa-488 conjugated anti-mouse IgG and Alexa-568 tagged anti-rabbit IgG antibodies (Life Technologies). The fat body preps were mounted in DAPI. Images were taken in Zeiss LSM510 Meta and LSM880 confocal Microscope. Autofluorescence was taken care of by optimizing the confocal microscope settings using the no primary antibody control.

Crystal cell melanization assay. Crystal cells are characterized by crystalline inclusions that contain the zymogen ProPO and can be visualized due to specific blackening upon heating larvae at 60 °C for 10 min⁶⁴. Third instar wandering stage larvae were heat treated to visualize crystal cells and imaged using SZX12 stereozoom microscope (Olympus). Melanised crystal cell were counted from three posterior abdominal segments of at least 20 larvae per genotype. Error bars represent the standard deviation. P-values were calculated using one way ANOVA.

Prophenol oxidase activity assay. For the measurement of PO activity by dot blots, 5 µl hemolymph was applied to a filter paper pre-soaked with 20 mM L-DOPA (L-3, 4-dihydroxyphenylalanine- Cat. No. D9628, SIGMA) in phosphate buffer pH 6.6, incubated for 20 minutes at 37 °C and heated in a microwave till the paper was dried completely⁶⁵. The melanised black hemolymph spots correlate with PO activity in hemolymph and were imaged under an Olympus SZX12 stereozoom microscope.

For photometric measurement of PO activity, 10 µl hemolymph from each strain was pooled on ice by quickly bleeding 3–5 larvae and withdrawing 6 µl hemolymph. Aliquots of mixed hemolymph were activated at 25 °C for 10 minutes, then 40 µl L-DOPA was added and optical density (OD) measured from 0 to 30 minutes at 490 nm with a VmaxTM Kinetic Microplate Reader (*BIO-RAD*). Activation of PO was measured as the relative change in absorbance (A_{490}). Experiments were repeated at least three times with biological and technical replicates.

RNA extraction and Quantitative Real Time PCR. *Drosophila* larvae or adults were collected in TRIzol (TRIzol[®] Reagent, Cat. No. 15596-026, Invitrogen), homogenized for 30–60 seconds and centrifuged. The supernatant was processed for RNA extraction according to the manufacturer's protocol. RNA was quantified by spectrophotometry and quality was analyzed by agarose gel electrophoresis. Quantitative RT-PCR (qRT-PCR) was performed using SYBR green chemistry in a Rotor Gene 3000 (Corbett Life Science) and analysed with the

accompanying software. Primer sequences used for RT-PCR and qRT-PCR are provided in supplementary information (Supplementary Table S1).

Infection and survival assay. Briefly, prior to infection, adult flies of appropriate genotype were starved for 2 hr, then transferred into vials containing filter paper hydrated with 5% sucrose solution mixed with concentrated Ampicillin resistant *E. coli* ($A_{600} = 1$; concentrated to contain ~ 10 CFU/ml) or Gram positive bacteria (*B. subtilis*) $A_{600} = 5-10$) on cornmeal food. Following incubation at 25 °C for 24 hr, flies were processed for RNA extraction or examined for reporter-GFP expression. For survival assay, flies were challenged with bacteria by oral feeding. Adult flies were starved for 48 hours and then transferred to fresh corn-meal food vials containing fresh filter paper disks inoculated with bacterial cultures. The percentage of survivors was then calculated for each experiment and plotted as a survival curve. ($N = 100$) for each genotype. Reporter-GFP expressing flies were imaged on an SZX12 stereozoom microscope (Olympus) and processed uniformly for brightness/contrast using Adobe Photoshop CS3.

Statistical analysis. For all the survival assays, 100 flies were used and the assays were repeated thrice. For the melanization experiment, crystal cells were counted from three posterior abdominal segments of at least 20 larvae per genotype. Phenoloxidase assay was repeated thrice with biological and technical replicates. For hemocyte and fat body staining, 10 larvae of each genotype were taken. For hemocyte staining, quantification of fluorescence intensity was done for at least 30 cells per genotype. All the data sets were included for analysis. There was no randomization done. Extreme outliers were excluded for the crystal cell count analysis. For lamellocyte count, L1 staining was done thrice with 10 larvae per genotype each time. Student's t-test with unequal variances has been used for statistical analysis. P-values are as indicated in the graphs.

References

- Evans, C., Hartenstein, V. & Banerjee, U. Thicker than blood: conserved mechanisms in Drosophila and vertebrate hematopoiesis. *Developmental Cell* **5**, 673–690 (2003).
- Cerenius, L. & Soderhall, K. The prophenoloxidase-activating system in invertebrates. *Immunol Rev* **198**, 116–126 (2004).
- De Gregorio, E. *et al.* An Immune-Responsive Serpin Regulates the Melanization Cascade in Drosophila. *Developmental Cell* **3**, 581–592 (2002).
- Ligoxygakis, P. A serpin mutant links Toll activation to melanization in the host defence of Drosophila. *The EMBO Journal* **21**, 6330–6337 (2002).
- Braun, A., Hoffmann, J. & Meister, M. Analysis of the Drosophila host defense in domino mutant larvae, which are devoid of hemocytes. *Proceedings of the National Academy of Sciences* **95**, 14337–14342 (1998).
- Bulet, P. Antimicrobial peptides in insects: structure and function. *Developmental & Comparative Immunology* **23**, 329–344 (1999).
- Buchon, N., Broderick, N., Poidevin, M., Pradervand, S. & Lemaitre, B. Drosophila Intestinal Response to Bacterial Infection: Activation of Host Defense and Stem Cell Proliferation. *Cell Host & Microbe* **5**, 200–211 (2009).
- Kounatidis, I. & Ligoxygakis, P. Drosophila as a model system to unravel the layers of innate immunity to infection. *Open Biology* **2**, 120075–120075 (2012).
- Agaisse, H. & Perrimon, N. The roles of JAK/STAT signaling in Drosophila immune responses. *Immunol Rev* **198**, 72–82 (2004).
- Bond, D. & Foley, E. A Quantitative RNAi Screen for JNK Modifiers Identifies Pvr as a Novel Regulator of Drosophila Immune Signaling. *PLoS Pathog* **5**, e1000655 (2009).
- Lemaitre, B. & Hoffmann, J. The Host Defense of Drosophila melanogaster. *Annual Review of Immunology* **25**, 697–743 (2007).
- Aggarwal, K. & Silverman, N. Positive and negative regulation of the Drosophila immune response. *BMB Reports* **41**, 267–277 (2008).
- Brennan, C., Delaney, J., Schneider, D. & Anderson, K. Psidin Is Required in Drosophila Blood Cells for Both Phagocytic Degradation and Immune Activation of the Fat Body. *Current Biology* **17**, 67–72 (2007).
- Shia, A. *et al.* Toll-dependent antimicrobial responses in Drosophila larval fat body require Spatzle secreted by haemocytes. *Journal of Cell Science* **122**, 4505–4515 (2009).
- Paddibhatla, I., Lee, M., Kalamarz, M., Ferrarese, R. & Govind, S. Role for Sumoylation in Systemic Inflammation and Immune Homeostasis in Drosophila Larvae. *PLoS Pathog* **6**, e1001234 (2010).
- Chakrabarti, S. *et al.* Remote Control of Intestinal Stem Cell Activity by Haemocytes in Drosophila. *PLoS Genet* **12**, e1006089 (2016).
- Khush, R., Leulier, F. & Lemaitre, B. Drosophila immunity: two paths to NF- κ B. *Trends in Immunology* **22**, 260–264 (2001).
- Khush, R., Cornwell, W., Uram, J. & Lemaitre, B. A Ubiquitin-Proteasome Pathway Represses the Drosophila Immune Deficiency Signaling Cascade. *Current Biology* **12**, 1728–1737 (2002).
- Kambris, Z. *et al.* Drosophila Immunity: A Large-Scale *In Vivo* RNAi Screen Identifies Five Serine Proteases Required for Toll Activation. *Current Biology* **16**, 808–813 (2006).
- Becker, T. *et al.* FOXO-dependent regulation of innate immune homeostasis. *Nature* **463**, 369–373 (2010).
- Scita, G. & Di Fiore, P. The endocytic matrix. *Nature* **463**, 464–473 (2010).
- Dobrowolski, R. & De Robertis, E. Endocytic control of growth factor signalling: multivesicular bodies as signalling organelles. *Nature Reviews Molecular Cell Biology* doi:10.1038/nrm3244 (2011).
- Sehgal, P., Guo, G., Shah, M., Kumar, V. & Patel, K. Cytokine Signaling: STATS in plasma membrane rafts. *Journal of Biological Chemistry* **277**, 12067–12074 (2002).
- Shah, M. *et al.* Membrane-associated STAT3 and PY-STAT3 in the Cytoplasm. *Journal of Biological Chemistry* **281**, 7302–7308 (2005).
- Sehgal, P. Paradigm shifts in the cell biology of STAT signaling. *Seminars in Cell & Developmental Biology* **19**, 329–340 (2008).
- Sinha, A., Khadilkar, R., S., V., RoyChowdhury Sinha, A. & Inamdar, M. Conserved Regulation of the JAK/STAT Pathway by the Endosomal Protein Asrij Maintains Stem Cell Potency. *Cell Reports* **4**, 649–658 (2013).
- Khadilkar, R. *et al.* ARF1-GTP regulates Asrij to provide endocytic control of Drosophilablood cell homeostasis. *Proceedings of the National Academy of Sciences* **111**, 4898–4903 (2014).
- Korolchuk, V. *et al.* Drosophila Vps35 function is necessary for normal endocytic trafficking and actin cytoskeleton organisation. *Journal of Cell Science* **120**, 4367–4376 (2007).
- Shravage, B., Hill, J., Powers, C., Wu, L. & Baehrecke, E. Atg6 is required for multiple vesicle trafficking pathways and hematopoiesis in Drosophila. *Development* **140**, 1321–1329 (2013).
- Kulkarni, V., Khadilkar, R., Magadi, S. S. & Inamdar, M. Asrij Maintains the Stem Cell Niche and Controls Differentiation during Drosophila Lymph Gland Hematopoiesis. *PLoS ONE* **6**, e27667 (2011).

31. Fujita, H., Ueda, A., Nishida, T. & Otori, T. Uptake of India ink particles and latex beads by corneal fibroblasts. *Cell and Tissue Research* **250** (1987).
32. Matova, N. & Anderson, K. Rel/NF- B double mutants reveal that cellular immunity is central to Drosophila host defense. *Proceedings of the National Academy of Sciences* **103**, 16424–16429 (2006).
33. Nam, Hyuck-Jin *et al.* Involvement of pro-phenoloxidase 3 in lamellocyte-mediated spontaneous melanization in Drosophila. *Mol Cells* **26**, 606–610 (2008).
34. Cerenius, L., Lee, B. & Söderhäll, K. The proPO-system: pros and cons for its role in invertebrate immunity. *Trends in Immunology* **29**, 263–271 (2008).
35. Ferrandon, D., Imler, J., Hetru, C. & Hoffmann, J. The Drosophila systemic immune response: sensing and signalling during bacterial and fungal infections. *Nat Rev Immunol* **7**, 862–874 (2007).
36. Minakhina, S. & Steward, R. Nuclear factor-kappa B pathways in Drosophila. *Oncogene* **25**, 6749–6757 (2006).
37. Valanne, S., Wang, J. & Ramet, M. The Drosophila Toll Signaling Pathway. *The Journal of Immunology* **186**, 649–656 (2011).
38. Wang, L. & Ligoxygakis, P. Pathogen recognition and signalling in the Drosophila innate immune response. *Immunobiology* **211**, 251–261 (2006).
39. Wu, Louisa P. & Kathryn, V. Anderson Regulated nuclear import of Rel proteins in the Drosophila immune response. *Nature* **392**, 93–97 (1998).
40. Hoffmann, J. & Reichhart, J. Drosophila innate immunity: an evolutionary perspective. *Nature Immunology* **3**, 121–126 (2002).
41. Inamdar, Maneesha S. Drosophila asrij is expressed in pole cells, trachea and hemocytes. *Development genes and evolution* **213.3**, 134–137 (2003).
42. Engström, Y. *et al.* κB-like Motifs Regulate the Induction of Immune Genes in Drosophila. *Journal of Molecular Biology* **232**, 327–333 (1993).
43. Ryu, J. *et al.* Innate Immune Homeostasis by the Homeobox Gene Caudal and Commensal-Gut Mutualism in Drosophila. *Science* **319**, 777–782 (2008).
44. Leulier, F. & Royet, J. Maintaining immune homeostasis in fly gut. *Nature Immunology* **10**, 936–938 (2009).
45. Shia, A. *et al.* Toll-dependent antimicrobial responses in Drosophila larval fat body require Spatzle secreted by haemocytes. *Journal of Cell Science* **122**, 4505–4515 (2009).
46. D'Souza-Schorey, C. & Chavrier, P. ARF proteins: roles in membrane traffic and beyond. *Nature Reviews Molecular Cell Biology* **7**, 347–358 (2006).
47. Beck, R. *et al.* Coatamer and dimeric ADP ribosylation factor 1 promote distinct steps in membrane scission. *J Cell Biol* **194**, 765–777 (2011).
48. Husebye, H. *et al.* The Rab11a GTPase Controls Toll-like Receptor 4-Induced Activation of Interferon Regulatory Factor-3 on Phagosomes. *Immunity* **33**, 583–596 (2010).
49. Devergne, O., Ghiglione, C. & Noselli, S. The endocytic control of JAK/STAT signalling in Drosophila. *Journal of Cell Science* **120**, 3457–3464 (2007).
50. Huang, H., Chen, Z., Kunes, S., Chang, G. & Maniatis, T. Endocytic pathway is required for Drosophila Toll innate immune signaling. *Proceedings of the National Academy of Sciences* **107**, 8322–8327 (2010).
51. Lund, V., DeLotto, Y. & DeLotto, R. Endocytosis is required for Toll signaling and shaping of the Dorsal/NF- B morphogen gradient during Drosophila embryogenesis. *Proceedings of the National Academy of Sciences* **107**, 18028–18033 (2010).
52. Guruharsha, K. *et al.* A Protein Complex Network of Drosophila melanogaster. *Cell* **147**, 690–703 (2011).
53. Cunha, P. *et al.* Combinatorial Binding Leads to Diverse Regulatory Responses: Lmd Is a Tissue-Specific Modulator of Mef2 Activity. *PLoS Genetics* **6**, e1001014 (2010).
54. Clark, R. *et al.* MEF2 Is an *In Vivo* Immune-Metabolic Switch. *Cell* **155**, 435–447 (2013).
55. Horn, L., Leips, J. & Starz-Gaiano, M. Phagocytic ability declines with age in adult Drosophila hemocytes. *Aging Cell* **13**, 719–728 (2014).
56. Zaidman-Rémy, A. *et al.* The Drosophila Amidase PGRP-LB Modulates the Immune Response to Bacterial Infection. *Immunity* **24**, 463–473 (2006).
57. Bischoff, V. *et al.* Downregulation of the Drosophila Immune Response by Peptidoglycan-Recognition Proteins SC1 and SC2. *PLoS Pathog* **2**, e14 (2006).
58. De Camilli, P. *et al.* The synaptic vesicle-associated protein amphiphysin is the 128-kD autoantigen of Stiff-Man syndrome with breast cancer. *Journal of Experimental Medicine* **178**, 2219–2223 (1993).
59. Takamori, Shigeo *et al.* Identification of a vesicular glutamate transporter that defines a glutamatergic phenotype in neurons. *Nature* **407**, 189–194 (2000).
60. Menasche, G. *et al.* Biochemical and functional characterization of Rab27a mutations occurring in Griscelli syndrome patients. *Blood* **101**, 2736–2742 (2002).
61. Stow, J., Manderson, A. & Murray, R. SNAREing immunity: the role of SNAREs in the immune system. *Nat Rev Immunol* **6**, 919–929 (2006).
62. Nishida, K. *et al.* Gab2, via PI-3K, Regulates ARF1 in Fc RI-Mediated Granule Translocation and Mast Cell Degranulation. *The Journal of Immunology* **187**, 932–941 (2011).
63. Guha, A. *et al.* shibire mutations reveal distinct dynamin-independent and -dependent endocytic pathways in primary cultures of Drosophila hemocytes. *Journal of Cell Science* **116**, 3373–3386 (2003).
64. Neyen, C. *et al.* The Black cells phenotype is caused by a point mutation in the Drosophila pro-phenoloxidase 1 gene that triggers melanization and hematopoietic defects. *Developmental & Comparative Immunology* **50**, 166–174 (2015).
65. Sorrentino, R. P., Small, C. N. & Govind, S. Quantitative analysis of phenol oxidase activity in insect hemolymph. *BioTechniques* **32**, 815 (2002).

Acknowledgements

This work was funded by a grant to MSI from the Department of Science and Technology, Government of India and by intramural funds from the Jawaharlal Nehru Centre for Advanced Scientific Research.

Author Contributions

R.J.K., A.R., C.D.R., A.R.C.S., S.S.M., V.K. and M.S.I. performed experiments; R.J.K., A.R. and M.S.I. analyzed data and wrote the manuscript; M.S.I. obtained funding and facilities for the work.

Additional Information

Supplementary information accompanies this paper at doi:10.1038/s41598-017-00118-7

Competing Interests: The authors declare that they have no competing interests.

Publisher's note: Springer Nature remains neutral with regard to jurisdictional claims in published maps and institutional affiliations.



This work is licensed under a Creative Commons Attribution 4.0 International License. The images or other third party material in this article are included in the article's Creative Commons license, unless indicated otherwise in the credit line; if the material is not included under the Creative Commons license, users will need to obtain permission from the license holder to reproduce the material. To view a copy of this license, visit <http://creativecommons.org/licenses/by/4.0/>

© The Author(s) 2017

Proteomics of Asrij Perturbation in *Drosophila* Lymph Glands for Identification of New Regulators of Hematopoiesis

Authors

Saloni Sinha, Arindam Ray, Lakshman Abhilash, Manish Kumar, Sreelakshmi K. Sreenivasamurthy, T. S. Keshava Prasad, and Maneesha S. Inamdar

Correspondence

inamdar@jncasr.ac.in

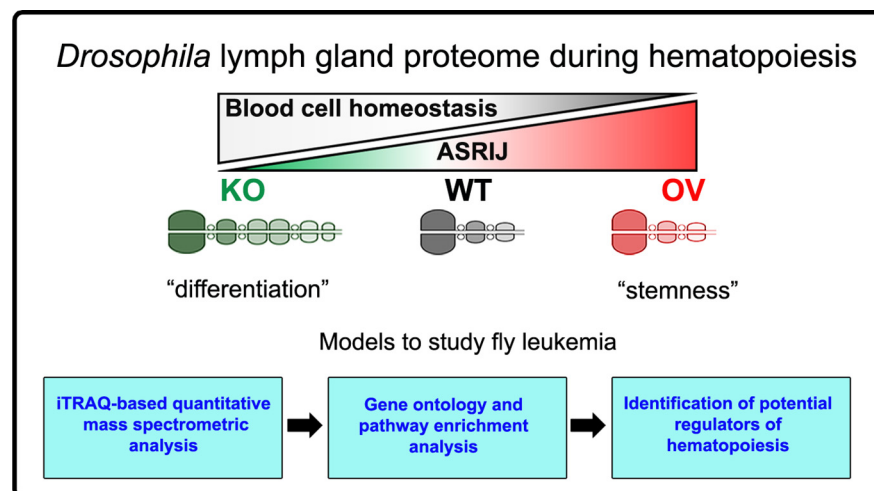
In Brief

Identification of molecules and processes that regulate hematopoiesis using *Drosophila* lymph gland (LG) as a model, is important for widening its scope and applicability as a tool to understand mechanisms regulating blood cell homeostasis. Using Asrij modulation, we compared the LG proteome under conditions that maintain precursors or promote differentiation *in vivo* and identified conserved as well as additional regulators of *Drosophila* hematopoiesis. The LG proteome provides an invaluable resource for studying insect as well as vertebrate blood cell development.

Highlights



- First report on the quantitative proteomic profiling of *Drosophila* lymph glands.
- Comparative proteomic analysis under conditions of perturbed blood cell homeostasis.
- Resource for identifying new regulators of insect and vertebrate hematopoiesis.

Graphical Abstract





Proteomics of Asrij Perturbation in *Drosophila* Lymph Glands for Identification of New Regulators of Hematopoiesis*

Saloni Sinha‡, Arindam Ray‡, Lakshman Abhilash‡, Manish Kumar§¶,  Sreelakshmi K. Sreenivasamurthy§||, T. S. Keshava Prasad§**, and  Maneesha S. Inamdar‡‡§§

Hematopoiesis is the process of differentiation of precursor blood cells into mature blood cells that is controlled by a complex set of molecular interactions. Understanding hematopoiesis is important for the study of hematological disorders. However, a comprehensive understanding of how physiological and genetic mechanisms regulate blood cell precursor maintenance and differentiation is lacking. Owing to simplicity and ease of genetic analysis, the *Drosophila melanogaster* lymph gland (LG) is an excellent model to study hematopoiesis. Here, we quantitatively analyzed the LG proteome under genetic conditions that either maintain precursors or promote their differentiation *in vivo*, by perturbing expression of Asrij, a conserved endosomal regulator of hematopoiesis. Using iTRAQ-based quantitative proteomics, we determined the relative expression levels of proteins in Asrij-knockout and overexpressing LGs from 1500 larval dissections compared with wild type. Our data showed that at least 6.5% of the *Drosophila* proteome is expressed in wild type LGs. Of the 2133 proteins identified, 780 and 208 proteins were common to previously reported cardiac tube and hemolymph proteomes, respectively, resulting in the identification of 1238 proteins exclusive to the LG. Perturbation of Asrij levels led to differential expression of 619 proteins, of which 27% have human homologs implicated in various diseases. Proteins regulating metabolism, immune system, signal transduction and vesicle-mediated transport were significantly enriched. Immunostaining of representative candidates from the enriched categories and previous reports confirmed 73% of our results, indicating the validity of our LG proteome. Our study provides, for the first time, an *in vivo* proteomics resource for identifying novel regulators of hematopoiesis that will

also be applicable to understanding vertebrate blood cell development. *Molecular & Cellular Proteomics* 18: 1171–1182, 2019. DOI: 10.1074/mcp.RA119.001299.

Blood cell development (hematopoiesis) follows well-defined steps that are controlled by a complex set of molecular interactions in both invertebrates and vertebrates. Hematopoietic stem and progenitor cells (HSPCs)¹ in *Drosophila* and vertebrates, give rise to an organized hierarchy of intermediates that eventually generate an array of terminally differentiated cells responsible for maintenance of the blood system (1). Differentiation of vertebrate HSPCs along each lineage is orchestrated by a team of transcription factors and signaling molecules. Owing to the high conservation of signaling pathways and proteins between *Drosophila* and vertebrate hematopoiesis (2), the *Drosophila* larval lymph gland (LG) is a relevant and well-accepted model for studying mechanisms underlying hematopoiesis (3).

The *Drosophila* third instar larval lymph gland (LG) lobes are composed entirely of blood cells and their precursors. They flank the cardiac tube and are interspersed by two pairs of pericardial cells (4). The anterior-most pair of lobes (primary lobes) are the most studied and have three major populations: differentiated blood cells (hemocytes) in the outer cortical zone (CZ), undifferentiated cells (pro-hemocytes) in the inner medullary zone (MZ) and a posterior signaling center (PSC) that functions as a stem cell niche to maintain hematopoiesis. The posterior lobes are poorly characterized but thought to comprise mainly of pro-hemocytes (3, 5). Although the LG tissue is believed to have limited cell lineage diversity, new subpopulations continue to be reported (6), however, the

From the ‡Jawaharlal Nehru Centre for Advanced Scientific Research, Jakkur, Bangalore 560064, India; §Institute of Bioinformatics, International Technology Park, Bangalore 560066, India; ¶Department of Immunology and Infectious Diseases, Harvard T.H. Chan School of Public Health, Boston, MA; ||NIMHANS-IOB Proteomics and Bioinformatics Laboratory, Neurobiology Research Centre, National Institute of Mental Health and Neurosciences, Bangalore 560029, India; **Center for Systems Biology and Molecular Medicine, Yenepoya Research Center, Yenepoya (Deemed to be University), Mangalore-575018, India; ‡‡Institute for Stem Cell Biology and Regenerative Medicine, GKVK, Bellary Road, Bangalore 560065, India

* Author's Choice—Final version open access under the terms of the Creative Commons CC-BY license.

Received January 23, 2019, and in revised form, March 7, 2019

Published, MCP Papers in Press, March 28, 2019, DOI 10.1074/mcp.RA119.001299

proteins expressed in these cells remain largely unknown. Further, systemic perturbations also affect blood stem cell maintenance and aberrant systemic signals can disrupt blood cell homeostasis (7, 8). Therefore, mapping the endogenous LG proteome is important to understand the hematopoietic niche, progenitor populations and blood stem cell maintenance, especially given its significance to vertebrate hematopoiesis. Although a proteomic investigation of the *Drosophila* LG is promising and likely to provide novel insights into the mechanisms governing blood cell homeostasis, it presents its own unique challenges. The microscopically small size coupled with the lack of automated dissection techniques have been major roadblocks that have prevented application of proteomics to the LG tissue.

In this study, we probed the *Drosophila* LG proteome under conditions that maintain stemness or promote differentiation *in vivo*, to identify potential regulators with hitherto unknown function in hematopoiesis. Earlier studies have established the role of Asrij as an important regulator of *Drosophila* hematopoiesis and immunity (7, 9, 10). Deficiency of Asrij leads to a situation mimicking fly leukemia characterized by hyperproliferation and increased differentiation of pro-hemocytes (10). Using the sensitized background of genetically modified *asrij* null mutant (knockout, KO) or overexpressing (OV) LGs, we report, for the first time, the peptide and protein compendium of the *Drosophila* larval LG, under conditions of normal as well as perturbed blood cell homeostasis. Our study provides a timely addition to the limited repertoire of LG proteins and informs about cellular processes and pathways critical for maintenance of blood cell homeostasis.

EXPERIMENTAL PROCEDURES

Fly Stocks—*Drosophila melanogaster* stocks were maintained as described before (10). *Canton-S* was used as the wild type reference strain. Based on the experimental design, *w1118* or appropriate GAL4 (*e33CGAL4/TM6tb* from K. Anderson) controls were also used. Other fly stocks used were *arf⁹/arf⁹* (Asrij knockout, KO) (10) and *UAS-Dmasrij* (7).

Experimental Design and Statistical Rationale—In this study, we aimed to perform a proteomic characterization of the *Drosophila melanogaster* lymph gland (LG). Owing to the limited amount of tissue available per LG, we chose to perform proteomic analysis using

pooled samples. Pilot experiments conducted helped standardize the amount of protein that could be isolated from a given number of LGs. *Canton-S* was used as the wild type (WT) strain. To maximize identification of additional regulators of hematopoiesis, we probed the *in vivo* LG proteome under conditions that maintain blood cell progenitors or promote their differentiation, by modulating levels of Asrij (overexpression (OV) and knockout (KO)), an important regulator of *Drosophila* hematopoiesis (7, 10). Although technically demanding and challenging, we performed 1500 LG dissections from third instar *Drosophila* larvae for each genotype (WT, KO and OV) to obtain ~300 μ g of protein for performing iTRAQ-based quantitative proteomic analysis. Because of the small size of the LG and the immensely time-consuming process of dissection and isolation, doing biological replicates at the time at which these experiments were performed was not feasible. The lack of automated LG dissection protocols and the unique nature of the sample itself present unique and major challenges to collecting enough protein for the study. To overcome these roadblocks that have prevented application of proteomics to this sample, we chose to analyze hits obtained, by immunostaining, to validate our findings from the LG proteome.

Peptides generated by trypsin digestion from WT, KO and OV LGs were labeled with iTRAQ 4-plex reagents, as per manufacturer's protocol, yielding 114, 115, and 116 reporter ions, respectively. To increase coverage, iTRAQ-labeled peptides pooled from each genotype were split into 13 distinct fractions prior to LC-MS/MS analysis. Raw MS/MS data was processed using search engines Sequest and Mascot (version 2.4.1) in the Proteome Discoverer version 2.0 suite (Thermo Fisher Scientific) and results were exported as Microsoft Excel files (supplemental Tables S1 and S2) for further analysis. Peptide abundance values represented by iTRAQ reporter ion intensities were used to perform a Chi-square test to compare if the fold change of each peptide belonging to any two genotypes differs statistically from 1:1. We performed two tests for each peptide, *vis-à-vis*, (1) KO *versus* WT and (2) OV *versus* WT. Because of the large number of hypotheses being tested, we adjusted the *p* values of these tests using Benjamini-Hochberg (11) correction such that the net false discovery rate (FDR) is set at 1%. The relative expression of proteins was calculated based on the relative abundance for the corresponding unique peptides. For downstream analyses such as Gene Ontology and pathway enrichment, differentially abundant proteins were used, selection criteria for which included an adjusted *p* value <0.01 and fold change of <0.6 [based on Asrij (FBpp0305129) values] and >1.4. Although the lower limit of <0.6 was statistically derived, the upper limit of >1.4 was derived arbitrarily only to maintain symmetry in picking relevant regulated targets. Although experimental methods confirm the complete absence of Asrij in KO LGs (10), we obtained a KO/WT peptide abundance ratio of 0.59. This is most likely because of the iTRAQ-based quantitation approach adopted for our proteomics study, which is known to have issues with reporting reliable relative protein abundance estimates (12, 13). All the analyses described here were performed using custom scripts in R.

***Drosophila melanogaster* Lymph Gland (LG) Isolation for Proteomics Analysis**—Wandering third instar larvae were immobilized by cooling, pinned ventral side up and a longitudinal excision was made. Viscera and excess parts of the body wall were removed; leaving a thin strip of body wall to which the dorsal vessel remained attached. The LG having the primary, secondary and tertiary lobes intact was collected in phosphate buffer saline (PBS) containing protease inhibitor mixture (Sigma) and phenylmethanesulfonyl fluoride (Sigma) in order to prevent proteases from degrading the tissue. Dissected LGs were stored at -80°C . 1500 LGs of desired genotype were lysed in 0.5% SDS, homogenized by sonication and centrifuged at 13,000 rpm for 10 min at 4°C followed by protein estimation of the supernatants using bicinchoninic acid (BCA) assay (Thermo Fisher Scien-

¹ The abbreviations used are: HSPC, hematopoietic stem and progenitor cell; ARF1, adenosine diphosphate (ADP)-ribosylation factor 1; ATP5A, adenosine triphosphate (ATP) synthase subunit alpha; BCA, bicinchoninic acid; BSA, bovine serum albumin; CoxIV, cytochrome oxidase subunit IV; DAPI, 4',6-diamidino-2-phenylindole; Drp1, dynamin related protein 1; FDR, false discovery rate; GO, gene ontology; hESC, human embryonic stem cell; iTRAQ, isobaric tags for relative and absolute quantitation; KO, knockout; Larp, la related protein; LG, lymph gland; MassIVE, mass spectrometry interactive virtual environment; Msk, moleskin; NCBI, national center for biotechnology information; NDUFS3, NADH ubiquinone oxidoreductase core subunit S3; Npc2a, niemann-pick type C 2a; OV, overexpressing; PBS, phosphate buffer saline; PE, pathway enrichment; PSM, peptide-spectrum match; Rab, ras related GTP binding protein; SDHB, succinate dehydrogenase subunit B; SDS-PAGE, sodium dodecyl sulfate-polyacrylamide gel electrophoresis; TCA cycle, tricarboxylic acid cycle.

tific) for normalization on gel. Equivalent amounts of protein quantified spectrophotometrically from each sample was reduced and alkylated and then subjected to trypsin (Sequencing Grade Modified Trypsin, Promega) digestion in an enzyme to substrate ratio of 1:20 (w/w) at 37 °C for 16 h.

Mass Spectrometry Methodology—The pooled LGs were given to the proteomics mass spectrometry department of the Institute of Bioinformatics (IOB), Bangalore, for sample processing according to standard procedure. Peptides generated by trypsin digestion from WT, KO and OV LGs were labeled with iTRAQ 4-plex reagents (Applied Biosystems) as per manufacturer's protocol, yielding 114, 115, and 116 reporter ions, respectively. These iTRAQ-labeled peptides were eventually pooled, reconstituted in SCX solvent A (10 mM potassium phosphate, 20% acetonitrile, pH 2.8) and subjected to strong cation exchange chromatography on a polysulfoethyl A column (200 × 2.1 mm; 5 μm; 200 Å PolyLC, Columbia) using Agilent's 1200 series HPLC system. Fractionation of peptides was carried out by a linear gradient of solvent B (350 mM KCl in solvent A) for 70 min at a flow rate of 200 μl per minute. The fractions thus collected, were dried in a Speedvac, reconstituted in 10 μl of 0.1% TFA and cleaned using C₁₈ stage tips prior to LC-MS/MS analysis.

Tandem mass spectrometric analysis of the iTRAQ-labeled peptides was carried out using LTQ-Orbitrap Velos mass spectrometer (Thermo Fisher Scientific) interfaced with Easy nanoLC II (Thermo Fisher Scientific). The nanospray ionization source of the mass spectrometer was fitted with a 10 μm emitter tip (New Objective) and maintained at 2000 V ion spray voltage. Peptide samples were loaded onto an enrichment column (2 cm × 75 μm, Magic AQ C18 material 5 μm particle size, 100 Å pore size) in 0.1% formic acid, 5% acetonitrile for 15 min and peptide separation was carried out on analytical column (10 cm × 75 μm, Magic AQ C18 material 5 μm particle size, 100 Å pore size) using a linear gradient of 7–35% solvent B (90% acetonitrile in 0.1% formic acid) for 60 min at a constant flow rate of 350 nL/minute. Data was acquired using Xcalibur 2.1 (Thermo Fisher Scientific) in a data-dependent manner in the *m/z* range of 350 to 1800 at a mass resolution of 60,000 at 400 *m/z* at the MS level and 15,000 at 400 *m/z* at MS/MS level by targeting the top 20 abundant ions for fragmentation using higher energy collisional dissociation at 39% normalized collision energy. The dynamic exclusion option was enabled during data acquisition with exclusion duration of 60 s. Lock mass option was enabled for real time calibration using polycyclodimethylsiloxane (*m/z*, 415.12) ions.

Database Search Parameters and Acceptance Criteria for Identifications—Raw MS/MS spectra files were searched against *Drosophila melanogaster* RefSeq protein database (release 70; 30,513 entries) appended with the known contaminants using SEQUEST and MASCOT (version 2.4.1) search engines in the Proteome Discoverer version 2.0 suite (Thermo Scientific, Germany). A precursor ion mass range of 600–5000 Da and a signal-to-noise ratio of 1.5 was used for the searches. Enzyme specificity was set to trypsin, allowing for a maximum of one missed cleavage. Variable (oxidation of methionine and phosphorylation of serine, threonine and tyrosine) and fixed (carbamidomethylation of cysteine; iTRAQ-labeling at N terminus of the peptide and lysine) modifications were selected. Mass tolerance was set to 15 ppm and 0.1 Da for precursor and fragment ions, respectively. Peptide lists were filtered to remove known contaminants such as BSA and human keratin proteins. To maximize the coverage of identifications, 1% FDR cut-off was used at PSM level for all the identifications as calculated by percolator algorithm using decoy search approach. Data analysis was performed using custom scripts in R.

Mass Spectrometry Data Analysis—Intensities of iTRAQ values from the MS/MS spectra were used to calculate peptide abundances using the 'peptide and protein quantifier' in Proteome Discoverer

version 2.0 suite (Thermo Fisher Scientific). Peptide abundance scores were exported as Microsoft Excel file (supplemental Table S1) from the software to perform quantitative comparisons. FDR confidence for each protein was estimated and PSMs that did not qualify the 1% FDR were excluded from the analysis. Additionally, peptides shared between protein isoforms were excluded for quantitative estimation and only the unique peptides, identified across all LG genotypes, were used for the relative quantitation and statistical analyses, as described in Experimental Design and Statistical Rationale. Proteins that are discussed in the manuscript were manually inspected for the MS/MS spectra quality of the respective peptides.

In Silico Analysis—A web-based toolset g:Profiler was used for performing Gene Ontology (GO), pathway enrichment (PE) analysis and for identifying proteins with human homologs implicated in various diseases (<https://biit.cs.ut.ee/gprofiler/>) (14). Venn diagrams were made using the online tool Venny 2.1 (<http://bioinfogp.cnb.csic.es/tools/venny/>).

LG Immunostaining, Imaging and Analysis—To validate findings from the LG proteome, immunostaining was performed for selected proteins identified with multiple (at least 4) peptides with high confidence (supplemental Table S1). All the proteins selected for validation by LG immunostaining showed a good MS/MS spectra quality. Immunostaining analysis was performed for LGs isolated from KO and OV with appropriate controls (*Canton-S*, as the wild type control; *w1118*, as *asrij* mutation was made in this genetic background; and *e33CGal4*, as the parental control for OV) as described before (10). Images were captured with a Zeiss LSM880 confocal microscope. Primary antibodies used were against Rab7 (rabbit) and Rab11 (rabbit) (both from MarcosGonzalez Gaitan, University of Geneva); ARF1 (rabbit) (7); ATP5A (mouse), SDHB (mouse), CoxIV (mouse) and NDUFS3 (mouse) (all from Abcam). Secondary antibody was coupled to Alexa-Fluor 488 or 568 or 633 (all from Life Technologies). Estimation of area and fluorescence intensity of LG lobes was performed using Fiji (Image J) software for the primary, secondary and tertiary pair of LG lobes to analyze differences in protein expression across different genotypes. Statistical significance was estimated using two factor ANOVA (LG lobe and genotype being the two factors taken into consideration) followed by a post-hoc analysis in STATISTICA v5.0.

RESULTS

Mass Spectrometric Mapping of the *Drosophila melanogaster* Lymph Gland Proteome—Understanding the detailed molecular processes underlying *Drosophila* lymph gland (LG) hematopoiesis remains a challenge, despite the increasing attention it has received over the past few years. A proteomic analysis of the *Drosophila* LGs would reveal important additional clues and generate a resource for deeper understanding of hematopoiesis. However, the entire LG tissue is only about ~1.5–2 mm in length, relatively transparent and made up of about ~1000–1500 cells (15). This, coupled with a lack of technological developments, makes large scale microdissection of enough numbers of LGs for proteomic analysis extremely challenging. Owing to sampling issues, analysis thus far has been primarily genetic or performed using cultured S2 cells that represent embryonic hemocytes.

The *Drosophila* LG is heterogeneous and contains developmentally distinct zones (MZ, CZ, PSC) (Fig. 1A). Nevertheless, as compared with vertebrate bone marrow or *in vitro* cultured hematopoietic cells, it offers a relatively pure population of *in vivo* blood cells with limited cell lineage diversity.

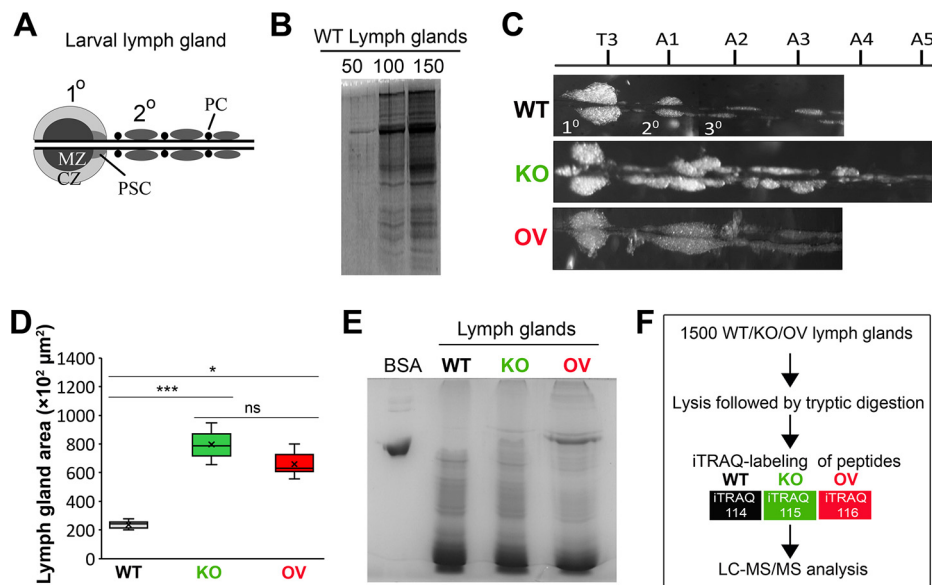


FIG. 1. Experimental design for mapping the proteome of *Drosophila melanogaster* lymph glands. *A*, Schematic representation of a wild type (WT) lymph gland (LG). Primary (1°) and posterior (2°) LG lobes flank the cardiac tube and are interspersed by pericardial cells (PC). CZ: cortical zone; MZ: medullary zone; PSC: posterior signaling center. *B*, Protein quality verification by SDS-PAGE and Coomassie blue staining of lysates obtained from 50, 100 and 150 WT LGs. *C*, Representative images of WT, *Asrij* knockout (KO) and *Asrij* overexpressing (OV) LGs. Thoracic (T) and abdominal (A) segment numbers are indicated. Primary lobe is anterior to T3. *D*, Graph showing LG area across different genotypes ($n = 10$). *E*, Protein quality verification by SDS-PAGE and Coomassie blue staining of lysates obtained from 1500 WT, KO and OV LGs. BSA was used as positive control. *F*, Schematic representation of the protocol followed for comparative proteomic analysis of *Asrij* modified *Drosophila* LGs.

As cells are harvested from the natural context *i.e.* the *Drosophila* larva, this provides the added advantage of minimal artifact generation. Thus, we reasoned that although technically demanding and time consuming, manual dissection was imperative for direct sampling of LGs to obtain a reasonably good proteomic characterization of the *Drosophila* LGs. A detailed protocol for the isolation and collection of LG samples for proteomic analysis is described (see Experimental procedures).

The first and the most critical step toward deciphering the proteome of *Drosophila* LGs was performing large scale dissections for sample collection. As the amount of protein obtained from one LG is insufficient owing to its small size, it was necessary to pool LG samples for proteomic analysis. At the time at which this experiment was performed, logistical constraints compelled us to opt for a strategy wherein large-scale pooling of LG samples from a long-term inbred strain of *Drosophila* seemed feasible. We thought this to be appropriate for two reasons, *vis-a-vis*, (1) because of the inbred nature of our stocks, low among individual variation is less likely to yield erroneous expression values from the experiment (which could otherwise be dealt with by having multiple biological replicates), and as a consequence, (2) inference regarding expression levels of proteins could be made with greater confidence as the values are more likely to represent the population level expression value. For deciding upon the number of LG samples to be pooled, we standardized and evaluated the amount of protein that could be extracted from

a given number of LGs. Protein concentrations of lysates prepared from 50, 100, and 150 wild type (WT, *Canton-S*) LGs were estimated and the corresponding protein profiles were examined using SDS-PAGE followed by Coomassie Blue staining (Fig. 1*B*). Our results suggested that $\sim 30 \mu\text{g}$ protein could be isolated by dissecting 150 WT LGs and hence we estimated that dissecting 1500 LGs should yield enough protein ($\sim 300 \mu\text{g}$) for performing a successful proteomics experiment.

To increase the prospect of identifying novel regulators of hematopoiesis, we chose to inspect the proteome of *asrij* null mutant (“knockout,” KO) and overexpressing (OV) LGs, which mostly represent the differentiated and undifferentiated blood cell states, respectively (7, 10, 16). Compared with control, KO LGs show premature differentiation, resulting in increased numbers of plasmatocytes and crystal cells (10), whereas OV LGs do not show aberrant differentiation and can maintain blood cell homeostasis (16). Although there is no gross difference in morphology at the embryonic, first and second instar stages, by the third instar stage, KO LGs develop increased number of posterior lobes, which are asymmetric and extend up to abdominal segments A4 or A5 along with a disrupted pericardial cell arrangement (10) (Fig. 1*C*). When quantified, both KO and OV LGs show significantly increased area as compared with WT (Fig. 1*D*), owing to the increased sizes of the secondary and tertiary lobes (supplemental Fig. S1A–S1C). Based on these characteristics of the *asrij* mutants, we reasoned that performing a comparative analysis of

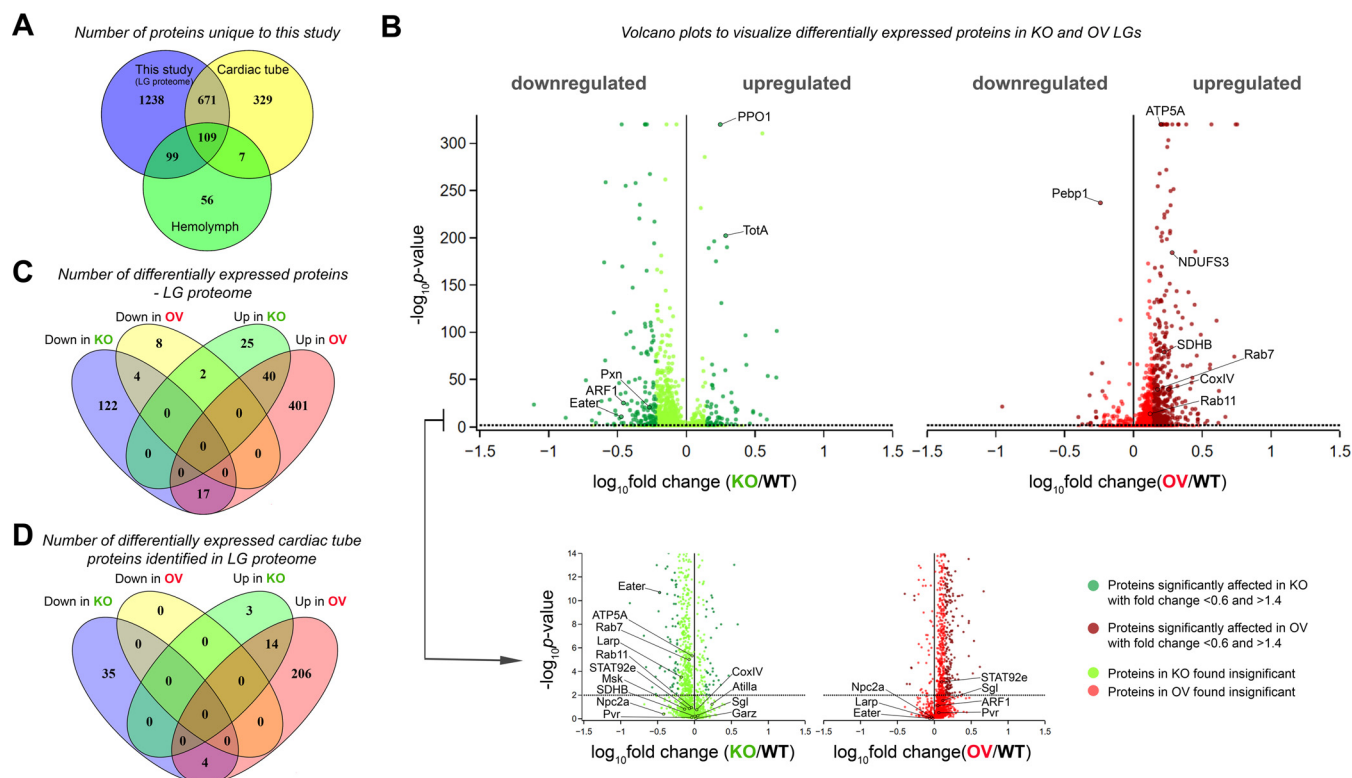


FIG. 2. Proteomic analysis of *Drosophila melanogaster* lymph glands. *A*, Venn diagram representing the distribution of proteins in WT LG samples identified in our study and previously reported studies (17, 18). *B*, Representation of all identified proteins in KO and OV LGs by volcano plot. Dotted black line represents the p value cut-off used. Darker shade of color in each of the volcano plots represents the proteins whose expression is significantly affected. *C*, Venn diagram representing number of upregulated and downregulated differentially expressed (DE) proteins in KO and OV LGs. *D*, Venn diagram representing number of cardiac tube proteins DE in KO and OV LGs.

LGs harvested and pooled, from each of the three different genotypes- WT, KO and OV (inbred *Drosophila* strains), might make it easier to find the major proteome changes accompanying hematopoiesis. Hence, 1500 LGs from staged wandering third instar *Drosophila* larvae were manually dissected, pooled and total protein was extracted (see Experimental Procedures). The lysates obtained included proteins from the primary lobes, posterior lobes, two pairs of pericardial cells and the cardiac tube (Fig. 1E). Subsequently, the peptides isolated from WT, KO and OV LGs were differentially labeled with iTRAQ 4-plex reagents, subjected to quantitative mass spectrometry and analyzed for the effect of *Asrij* deletion or overexpression for each pooled sample (see Experimental Procedures, Fig. 1F).

Overview of the *Drosophila melanogaster* Lymph Gland Proteome—Searches of the mass spectrometry derived data against the *Drosophila melanogaster* RefSeq protein database (release 70) using Proteome Discoverer software (version 2.0) identified 2133 LG proteins, supported by more than 9900 peptides with a total of 23140 peptide spectral matches (PSMs) (supplemental Table S2). This indicates that at least 6.5% of the *Drosophila* proteome is expressed in the third instar *Drosophila* larval LG. To assess the tissue specificity of our LG proteome, we compared our dataset to the already

reported proteomic profiles of the cardiac tube (17) and hemolymph (18). Of the 2133 proteins identified, 780 have been previously reported to express in the adult fly cardiac cells (17) and 208 in larval hemolymph (18) (see Fig. 2A and supplemental Table S3). Although no proteomic study of pericardial cells has been reported till date, an *in vivo* functional analysis study reported 80 genes to be expressed in pericardial nephrocytes (19). No common proteins were found upon comparison of the data sets, probably owing to the underrepresentation of pericardial cells (4–6 cells/LG). This indicates that a bulk of the 1238 proteins are newly identified and have not been reported earlier in the LG (Fig. 2A). Most of these identified proteins are likely to be expressed exclusively in the LG lobes.

Several proteins with well-defined roles in the regulation of *Drosophila* blood cell homeostasis were identified in our proteome. Known regulators of blood cell survival, proliferation and differentiation such as Eater (FBgn0243514), ADP-ribosylation factor 1 (ARF1, FBgn0010348), signal transducer and activator of transcription protein at 92E (STAT92e, FBgn0016917), gartenzweg (Garz, FBgn0264560), PDGF- and VEGF-receptor related (Pvr, FBgn0032006), Niemann-Pick type C 2a (Npc2a, FBgn0031381), La related protein (Larp, FBgn0261618), Moleskin (Msk, FBgn0026252), Proph-

enoloxidase 1 (PPO1, FBgn0283437), Atilla (FBgn0032422) and Peroxidase (Pxn, FBgn0011828) were identified. Additionally, proteins involved in regulation of immunity [Turandot A (TotA, FBgn0028396), Phosphatidylethanolamine Binding Protein 1 (Pebp1, FBgn0038973)] and LG development (Sugarless (Sgl, FBgn0261445)) were also identified (Fig. 2B, [supplemental Table S2](#)), thus validating our approach. Taken together, comparison with existing proteome datasets of cardiac tube cells and hemolymph and identification of known regulators of LG hematopoiesis and development, demonstrates that our approach has successfully yielded a LG-enriched proteome.

Identification of the *Drosophila* Lymph Gland Proteome Responsive to *Asrij*—To identify proteins showing differential expression, we compared the abundance ratios of peptides detected in *Asrij* modulated conditions, across all three LG genotypes (WT, KO and OV). Although KO LGs show complete absence of transcript and protein expression of *asrij* (10), the proteomic analysis showed a KO/WT ratio of 0.59 for *Asrij*. This quantitation was based on the one unique peptide (FBpp0305129) identified against *Asrij*. This is likely because of the interference of mixed MS/MS events from isobaric peptides that occur during precursor selection and can lead to underestimation of quantitative differences (12, 13). Based on statistical analyses and the peptide abundance ratio of *Asrij* in KO/WT, proteins with a fold change <0.6 or >1.4 and an adjusted p value <0.01 , were identified as differentially expressed (see Experimental Procedures and [supplemental Table S4](#)). For visual representation of these differentially expressed proteins, volcano plots were generated (Fig. 2B). Expression of 619 proteins significantly changed as compared with WT and changes observed in the proteome profile were mostly synergistic with *Asrij* levels. As compared with WT, KO showed reduced expression of 143 out of 210 proteins, whereas 458 out of 472 proteins were overexpressed in *Asrij* OV (Fig. 2C). Of these, 17 proteins were proportionately regulated by *Asrij*, *i.e.* down in KO and up in OV, whereas 2 proteins showed opposite changes in abundance when compared with *Asrij* levels (Fig. 2C). Thus, the LG proteome is sensitive to *Asrij* levels. Interestingly, of the 780 cardiac tube proteins identified in the LG proteome, 262 were significantly affected (56 in KO (39 downregulated and 17 upregulated) and 224 in OV (all upregulated)), suggesting that *Asrij* may be involved in playing a role in remodeling the cardiac tube tissue to facilitate stromal interactions on *Drosophila* hematopoietic development (Fig. 2D, [supplemental Table S5](#)). Among the 619 differentially expressed proteins, human homologs of 166 proteins were found to be implicated in various diseases such as “abnormality of metabolism/homeostasis” (HP:0001939, $p = 8.3E-05$), “respiratory insufficiency” (HP:0002093, $p = 0.0387$), and “abnormality of the mitochondrion” (HP:0003287, $p = 1.67E-08$), among others ([supplemental Table S6](#)). The novel proteins identified from our study can now be targeted to generate *Drosophila* models

for a wide variety of hematopoietic as well as metabolic disorders.

Functional Annotation Enrichment Analysis—To define how the *Asrij*-regulated proteome affects hematopoiesis, Gene Ontology (GO) analysis of the 619 differentially expressed proteins was performed using tools available from g:Profiler (14) to categorize proteins according to their biological function, cellular component and molecular function (Fig. 3). The biological processes mediated by *Asrij* mainly included “metabolic processes” (GO: 0008152), “cellular processes” (GO: 0009987), “multicellular organismal process” (GO: 0032501), among others (Fig. 3A). Enrichment of “metabolic processes” is not surprising given the already established role of metabolism in regulation of stem cell fate (20) and the ability of *Asrij* to regulate energy metabolism in human pluripotent stem cells (21). Further, “cell communication” (GO: 0007154) and “cell cycle” (GO: 0007049) were the major sub-categories enriched in “cellular processes.” The cellular components involved encompassed “cell” (GO: 0005623), “cell part” (GO: 0044464), “organelle” (GO: 0043226), “organelle part” (GO: 0044422), “extracellular region” (GO: 0005576), etc. (Fig. 3B). Molecular functions enriched for *Asrij* were primarily related to “binding” (GO: 0005488), “catalytic activity” (GO: 0003824), “structural molecular activity” (GO: 0005198), etc. (Fig. 3C).

Pathway enrichment (PE) analysis of the 210 (143 downregulated, 67 upregulated) and 472 (14 downregulated, 458 upregulated) proteins perturbed in KO and OV LGs, respectively, performed using g:Profiler (Biological Pathways: Reactome) (14) revealed a significant enrichment of protein clusters involved in regulation of metabolism (R-DME-1430728), immune system (R-DME-168256), transport of small molecules (R-DME-382551), vesicle-mediated transport (R-DME-5653656) and signal transduction (R-DME-162582), among others (Fig. 4A–4D). As *Asrij* plays an important role in regulating diverse cellular processes such as mitochondrial oxidative phosphorylation (21), immunity (9) and endocytosis (7, 10), enrichment of the above-mentioned pathways in the *Asrij* perturbed (KO and OV) LG proteomes is expected and consistent with known functions of *Asrij* (7, 9, 10, 21).

Validation of Candidates Identified from the *Drosophila* Lymph Gland Proteome—As it was not practical to perform biological replicates owing to the unique challenges associated with sample collection, we validated the proteome in two ways: (1) by comparing changes in protein levels assessed by the proteome to that expected, based on the known function and mechanism of action of *Asrij*, as per reports from the literature (7, 10, 16), and (2) by analyzing protein expression of representative candidates by immunostaining LGs. To understand the effect of *asrij* dosage on perturbed expression of the candidate proteins, validation by immunostaining was performed using the WT (*Canton-S*) control and the relevant genetic background controls for KO (*w1118*) and OV (*e33cGAL4*) (see Experimental procedures).

Gene ontology analysis

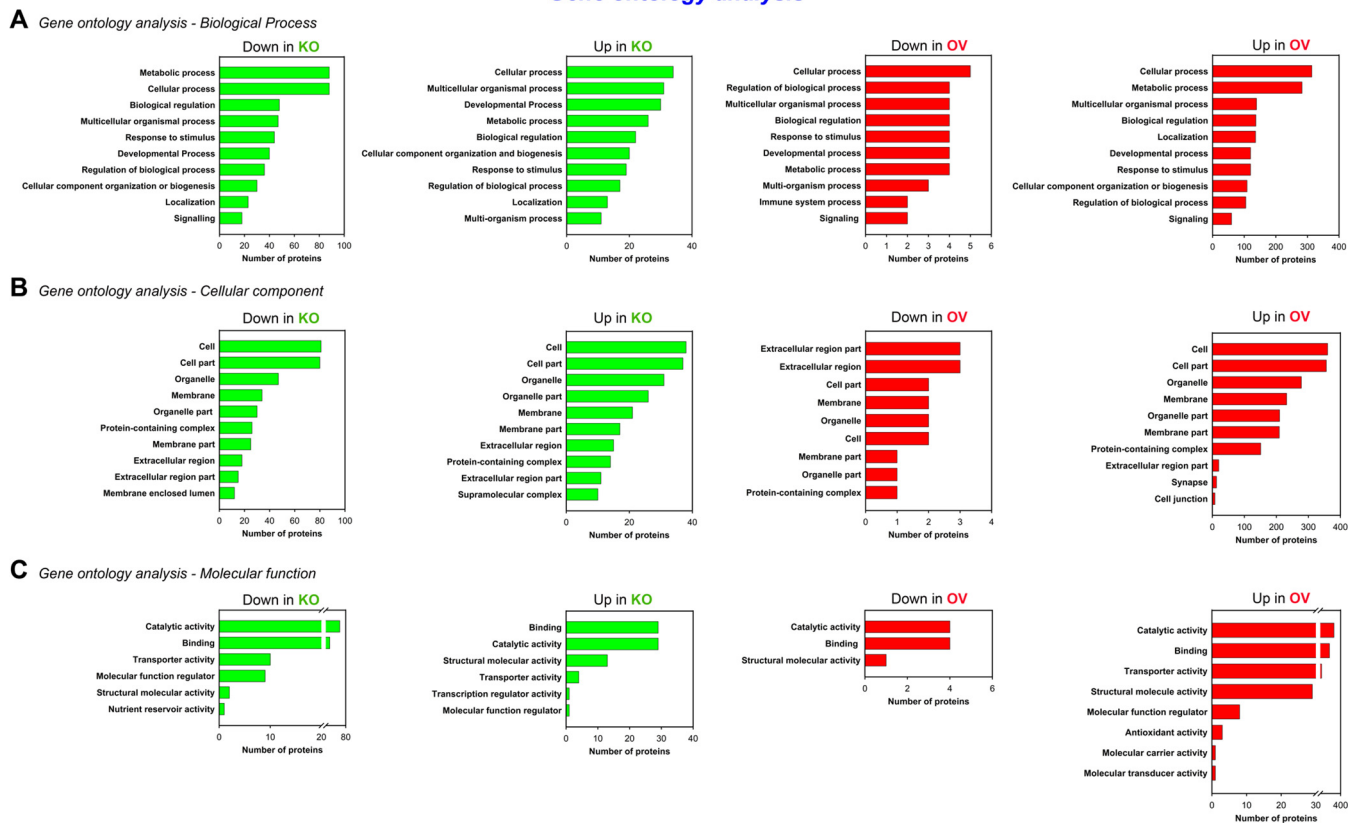


FIG. 3. **Functional enrichment analysis.** Bar plots representing Gene Ontology analysis of the differentially expressed proteins based on (A) biological process, (B) cellular component and (C) molecular function, done using the g:Profiler classification. The x axis shows the number of proteins in each category.

Pathway enrichment analysis

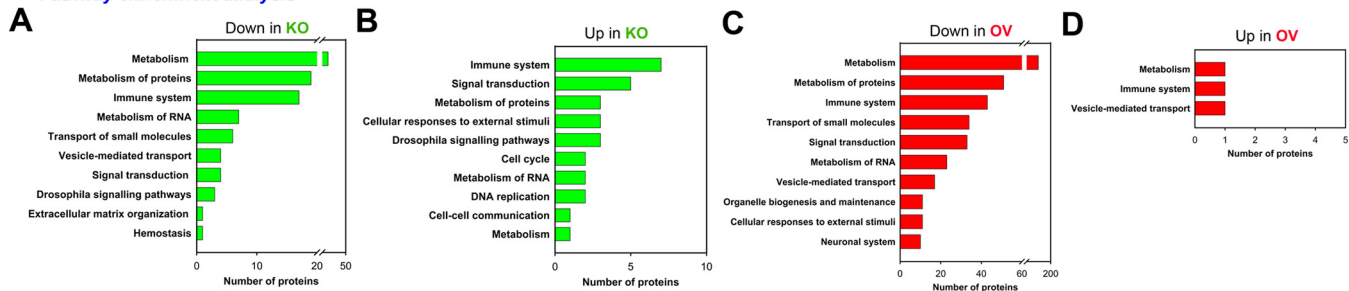


FIG. 4. **Pathway enrichment analysis.** A–D, Pathway enrichment analysis of the differentially expressed proteins performed using the g:Profiler (Biological Pathways: Reactome) classification. The x axis shows the number of proteins in each category.

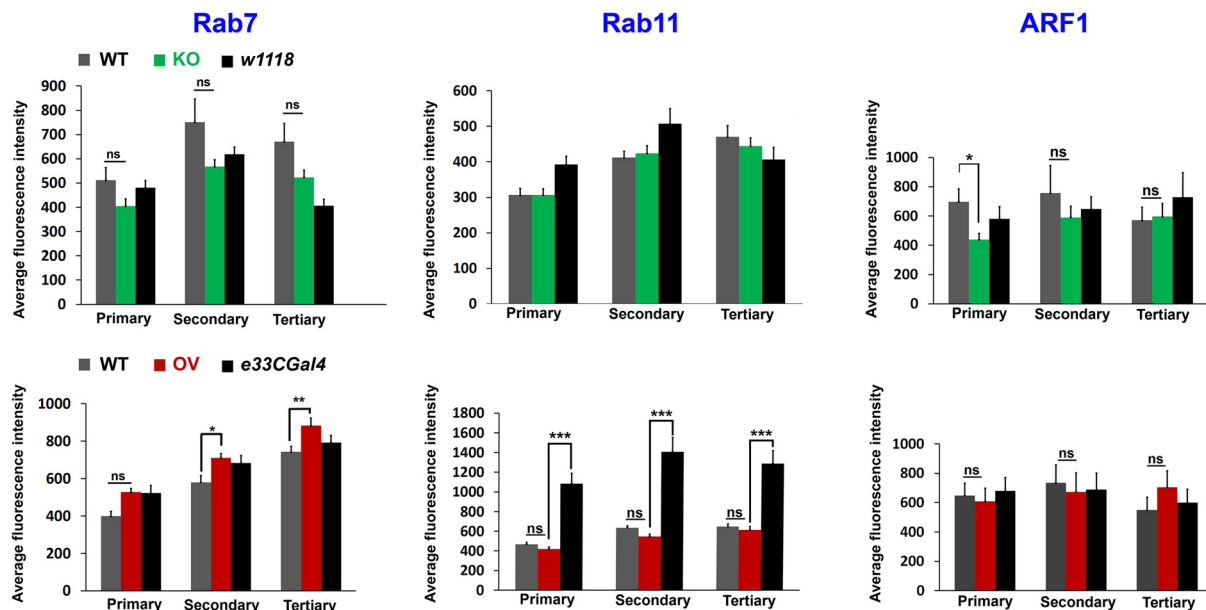
Asrij depletion does not affect ARF1 levels in circulatory hemocytes (7), however, the LG proteome showed ARF1 as reduced in KO and unchanged in OV (Fig. 5A). Validation by immunostaining (see below) showed that this was indeed the case, wherein we observed significantly reduced levels of ARF1 in the primary lobes of KO LGs (Fig. 5B, C and supplemental Fig. S2). The inconsistency between the predicted (unchanged expression, based on circulatory hemocyte data) and the obtained/validated (low expression, based on LG proteome) expression of ARF1 in LG is likely because of the different cell populations being compared. Unlike circulatory

hemocytes, which comprise differentiated blood cells in majority, the LG is a more heterogeneous population that includes progenitors, differentiated blood cells and niche cells. Like ARF1, levels of Garz and STAT92e are not expected to change, based on previous reports that show Asrij affects their activation, but not total levels (7, 16). The same holds true for Pvr, which was shown to act upstream of Asrij (7), hence not expected to change in levels. In agreement with this, the proteome data shows that Garz, Stat92e and Pvr levels are unchanged in both KO and OV LGs (Fig. 5A). As Asrij KO LGs have increased differentiation to plasmato-

A

Known regulators identified	KO LGs		OV LGs	
	Predicted	Proteome	Predicted	Proteome
I. Lymph gland blood cell homeostasis				
a) Maintenance				
ADP-ribosylation factor 1 (ARF1, FBgn0010348)	Unchanged	Low	Unchanged	Unchanged
STAT92e (STAT92e, FBgn0016917)	Unchanged	Unchanged	Unchanged	Unchanged
Gartenzweg (Garz, FBgn0264560)	Unchanged	Unchanged	Unchanged	Unchanged
PDGF- and VEGF-receptor related (Pvr, FBgn0032006)	Unchanged	Unchanged	Unchanged	Unchanged
b) Differentiation				
Eater (Eater, FBgn0243514)	High	Low	Unchanged	Unchanged
Peroxidasin (Pxn, FBgn0011828)	High	Low	Unchanged	Unchanged
Prophenoloxidase 1 (PPO1, FBgn0283437)	High	High	Unchanged	Unchanged
c) Others				
Niemann-Pick type C 2a (Npc2a, FBgn0031381)	Not known	Unchanged	Not known	Unchanged
La related protein (Larp, FBgn0261618)	Not known	Unchanged	Not known	Unchanged
Moleskin (Msk, FBgn0026252)	Not known	Unchanged	Not known	Unchanged
II. Lymph gland development				
Sugarless (sgl, FBgn0261445)	Not known	Unchanged	Not known	Unchanged

B



C

Endosomal proteins	KO LGs		OV LGs	
	Proteome	Validation	Proteome	Validation
Rab7 (Rab7, FBgn0015795)	Unchanged	Unchanged	High	High
Rab11 (Rab11, FBgn0015790)	Unchanged	Unchanged	Unchanged	Unchanged
ADP-ribosylation factor 1 (ARF1, FBgn0010348)	Low	Low	Unchanged	Unchanged

cytes and crystal cells, their respective markers, Eater (for plasmatocytes), Pxn and PPO1 (for crystal cells) could be expected at high levels in the KO proteome and likely unchanged in the OV LGs. Although KO LGs showed significantly increased PPO1 expression, matching our expectation, both Eater and Pxn levels were low in the KO proteome, though unchanged in OV (Fig. 5A). The relation of *Asrij* to other identified regulators of blood cell homeostasis (*Npc2a*, *Larp*, *Msk*) and LG hematopoiesis (*sgl*) is not known (Fig. 5A). Thus, the change in level of 5/7 proteins in KO and 7/7 proteins in OV LG proteome matched with that expected/reported.

To further strengthen the applicability of the LG proteome, we analyzed protein expression of representative candidates by immunostaining. Based on results obtained from PE analysis (Fig. 4A–4D) and the reported role of *Asrij* (7, 10, 21), we selected proteins belonging to the categories transport of small molecules (R-DME-382551), vesicle-mediated transport (R-DME-5653656) and metabolism (R-DME-1430728) for experimental validation. Given the proven role of *Asrij* in the endosomal trafficking pathway (7), we validated levels of proteins involved in mediating vesicle-mediated transport and transport of small molecules (*Rab7*, *Rab11* and *ARF1*) by immunostaining LGs with the respective antibodies. The proteome data indicated *Rab7* and *Rab11* levels are not affected in KO LG, whereas the known *Asrij* interactor, *ARF1* (7), is significantly low. Conversely, *Rab7* levels are significantly high upon *Asrij* overexpression, whereas *ARF1* and *Rab11* are unchanged. Validation of these data by immunofluorescence-based analysis (Fig. 5B and supplemental Fig. S2A–S2C), showed that protein levels for all three endosomal molecules were as per the proteome analysis (Fig. 5C).

In human embryonic stem cells, *Asrij*/*OCIAD1* regulates mitochondrial energy metabolism and interacts with components of the electron transport chain (21). Because energy metabolism (sub-categories: TCA cycle (R-DME-1428517), respiratory electron transport (R-DME-611105), complex I biogenesis (R-DME-6799198)) was a major perturbed category (Fig. 6A), we tested expression of mitochondrial molecules such as *COXIV*, *ATP5A*, *NDUFS3* and *SDHB*, whose levels were unchanged in KO and significantly upregulated in OV, as per the LG proteome. Immunostaining of KO and control LGs with the respective antibodies showed that although *COXIV* and *ATP5A* levels were unchanged, *NDUFS3* and *SDHB* levels were significantly downregulated in KO LGs as compared with *Canton-S* (Fig. 6B and supplemental Fig. S3A–S3D). The OV LGs showed significantly increased *COXIV* levels, unchanged *ATP5A*, *NDUFS3* and *SDHB* levels, as

compared with *Canton-S* (Fig. 6B and supplemental Fig. S3A–S3D). Based on results obtained from LG immunostaining, change in level of 2/4 proteins in KO and 1/4 proteins in OV agreed with the proteome data (Fig. 6C).

Thus, combining these two approaches, we find that levels of 9/13 proteins in KO and 10/13 in OV shown by the proteome are valid, giving high confidence to our analysis. These data indicate that our comparative proteome analysis is quite reliable and can be used as a resource for further studies.

DISCUSSION

Studying hematopoiesis in *Drosophila* is far simpler than in vertebrates owing to the limited gene redundancy and few blood cell lineages. Although this makes analysis of gene function relatively easier in *Drosophila*, understanding how proteins and their signaling networks regulate hematopoiesis remains challenging. Proteomic analysis using genetically modified *Drosophila* LGs allowed us to identify potential regulators of hematopoiesis, which are relevant *in vivo* and whose active regulatory role would otherwise be masked. Here, for the first time, we present a detailed view of the *Drosophila* LG proteome under conditions that maintain blood cell precursors or trigger their aberrant differentiation using *Asrij* overexpressing and *asrij* null LGs, respectively, as models. In this analysis, we could identify at least 15.3% of the total protein-coding genes annotated in the latest release of FlyBase (annotation release 6.25). Also, identification of most of the proteins reported earlier in the cardiac tube and hemolymph, in our study, supports the LG proteome.

Changes in expression levels of most of the known regulators of blood cell survival, proliferation and differentiation, upon *Asrij* modulation, agree with earlier reports. For example, whereas the KO LG proteome showed a significant increase in PPO1 expression, no change was observed in *Atilia* expression in KO/OV LGs, which is expected and agrees with previously published data (9, 10). However, the increased expression of *TotA*, a downstream effector of the JAK/STAT pathway, observed in the KO LG proteome is surprising as *Asrij* depletion results in decreased activation of *STAT92e* (16). These findings coupled with the *in vivo* immunofluorescence based validation of candidate proteins boost confidence in the LG proteome. Validation of the LG proteome data involved comparing the expression of candidate proteins in KO and OV LGs to the WT control (*Canton-S*) and the relevant strain background controls (*w1118*, *e33CGAL4*) to accurately identify the effect of dosage of *asrij* on candidate protein expression. Inclusion of *Canton-S* as a control was necessary to test the quality and reliability of the LG proteome, as this

FIG. 5. Validation of endosomal hits *Rab7*, *Rab11* and *ARF1* obtained from the LG proteome. A, Comparison of predicted and proteome-obtained expression levels of known regulators of *Drosophila* LG blood cell homeostasis and development. B, Graphs showing average fluorescence intensity levels of *Rab7*, *Rab11* and *ARF1* across primary, secondary and tertiary LG lobes. Genotypes are as indicated. Error bars represent standard error of mean and 'ns' indicates statistically non-significant difference. * $p < 0.05$, ** $p < 0.01$. C, Comparison of proteome-obtained and experimentally validated expression levels of LG *Rab7*, *Rab11*, and *ARF1*.

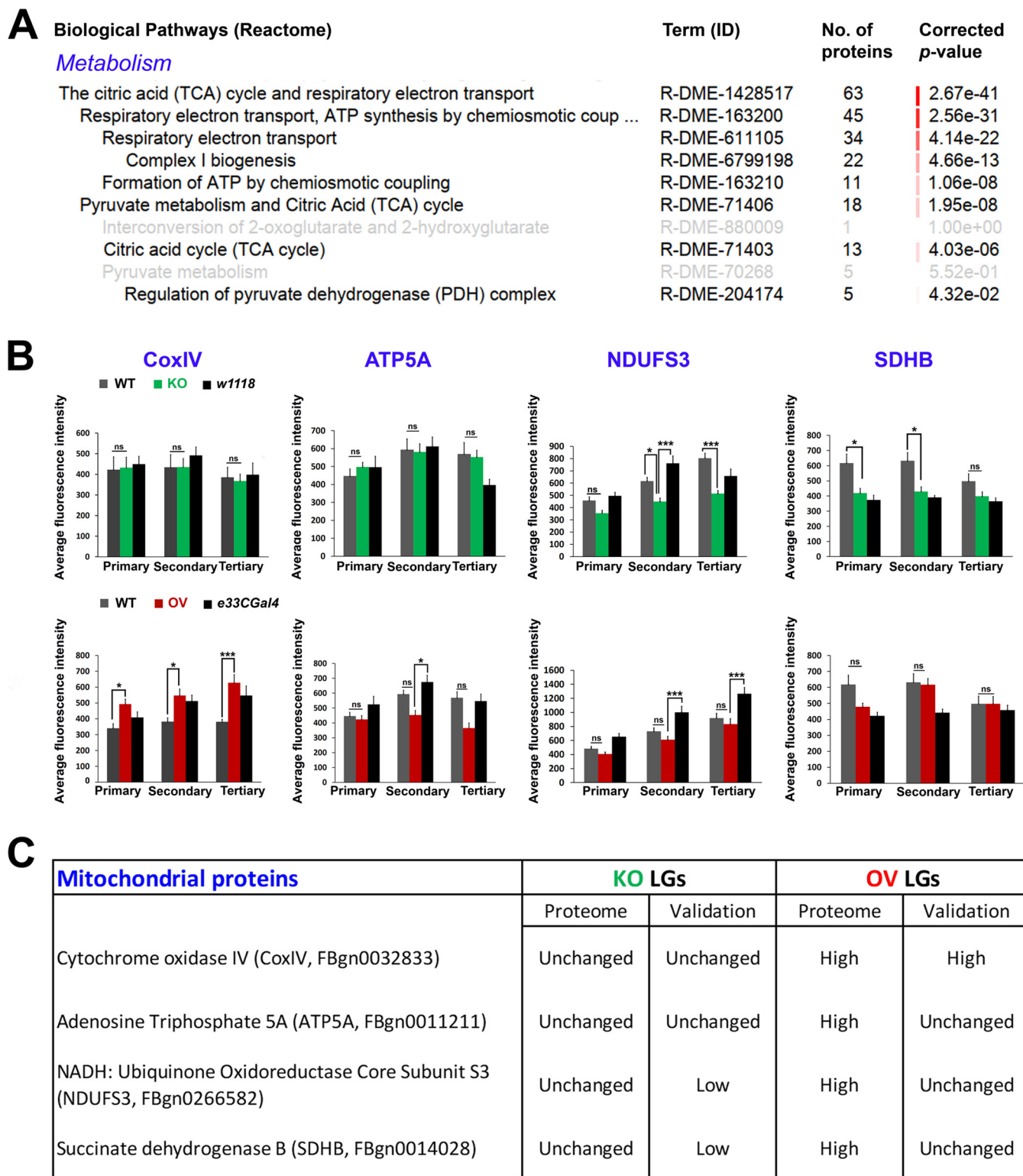


FIG. 6. Validation of mitochondrial hits CoxIV, ATP5A, NDUFS3 and SDHB obtained from the LG proteome. A, Sub-categories significantly enriched under the category “metabolism” in Asrij OV LGs. B, Graphs showing average fluorescence intensity levels of CoxIV, ATP5A, NDUFS3 and SDHB across primary, secondary and tertiary LG lobes. Genotypes are as indicated ($n > 7$ per genotype). Error bars represent standard error of mean and “ns” indicates statistically non-significant difference. * $p < 0.05$, ** $p < 0.01$ and *** $p < 0.001$. C, Comparison of proteome-obtained and experimentally validated expression levels of LG CoxIV, ATP5A, NDUFS3 and SDHB.

was the only control used during mass spectrometry. As various parameters differ between a wild type and a strain background control, which can be attributed to differential genetic constitution and activity (22, 23), it was also important to consider *w1118* and *e33CGAL4* as experimental controls. Our findings show that a majority of endosomal and mitochondrial hits agree with the LG proteome data (5/7 in KO and 4/7 in OV), further increasing its reliability and applicability.

Our data support the idea that endosomal proteins can effectively modulate the net output of various other cellular processes such as oxidative phosphorylation and metabolism; and highlights the ability of the “endosomal matrix” (24) to modulate a wide range of targets in a context-specific manner. Moreover, identification of other molecules involved in mediating vesicle-mediated transport and endocytosis from the LG proteome, warrants further investigation of these pathways in maintaining blood cell homeostasis. Thus, *Asrij* can promote specific signaling outcomes from multiple signals that intersect to maintain blood cell homeostasis.

Among biological processes, the largest impact of *Asrij* perturbation in LGs was on proteins involved in metabolism. In vertebrates, although hematopoietic stem cells (HSCs) derive energy primarily from glycolysis, differentiated blood cells utilize oxidative phosphorylation (25). Also, the metabolic state plays an important role in determining HSC fate (25). Deregulation of the metabolic machinery in HSCs has been reported to result in leukemia (26, 27). Recently we showed that depletion of *OCIAD1*, the human ortholog of *Asrij*, causes enhancement of electron transport chain complex-I activity leading to increased differentiation of human embryonic stem cells to early mesodermal progenitors, which are the precursors of HSCs (21). We propose that *Asrij* might be involved in regulating important metabolic functions including regulation of oxidative phosphorylation machinery during hematopoiesis. Interestingly, our *in vivo* validation shows that although LG *COXIV*, *NDUFS3* and *SDHB* levels are sensitive to *Asrij* levels, *ATP5A* is not. The difference in *ATP5A* levels observed in the LG proteome could also be because of significant contribution from the cardiac tube, which is energy dependent, based on the mitochondrial electron transport chain. The role of these molecules in hematopoiesis can now be tested in insect models like *Drosophila* and vertebrate models like mouse.

Perturbing *Asrij* levels affects mitochondrial morphology in hESCs (21). Interestingly, the LG proteome reveals that a key regulator of mitochondrial dynamics, Dynamin related protein 1 (*Drp1*, FBpp0077424), is significantly perturbed, in direct proportion to *Asrij* levels. The role of mitochondrial dynamics in hematopoiesis is a relatively underexplored subject. Recent reports suggest an essential role for regulators of mitochondrial dynamics in lymphoid lineage specification (28) and HSC self-renewal (29). It would be interesting to test how components regulating mitochondrial dynamics affect maintenance and differentiation of blood progenitors to various lineages in *Drosophila* as well as vertebrates.

In addition to the cardiac tube proteins, several proteins involved in muscle development were affected in *Asrij* mutant LGs. For example, proteins such as dystroglycan (FBpp0297348), an important structural constituent of muscle; and activity-regulated cytoskeleton associated protein 1 (*Arc1*, FBpp0086687) were significantly downregulated in KO, whereas, tropomyosin 2 (FBpp0291171), upheld (FBpp0073682) and myosin alkali light chain 1 (FBpp0088688) were significantly upregulated in OV LGs. The possible function of the above-mentioned proteins in regulation of LG hematopoiesis is intriguing. Alternatively, the LG could generate systemic signals that regulate cardiac muscle gene expression.

Perturbation of the hemocyte-specific protein *Asrij* triggers substantial remodelling of the LG proteome that could serve as a resource to unravel protein networks and circuitry that control human hematopoiesis. Further, *Asrij/OCIAD1* in humans is associated with several carcinomas and imparts resistance to radiotherapy and chemotherapeutic drugs such as paclitaxel (30). An extensive study on various aspects of the LG proteome in invertebrate as well as vertebrate models may aid in unraveling new candidates, possibly with a pivotal role in regulating human hematopoiesis.

Acknowledgments—We thank the JNCASR Confocal Microscopy Facility for providing access to instrumentation.

DATA AVAILABILITY

The raw mass spectrometry data has been submitted to the ProteomeXchange Consortium (<http://proteomecentral.proteomexchange.org>) via the PRIDE (<https://www.ebi.ac.uk/pride/archive/>) (31) partner repository with the dataset identifier PXD010753. The data has also been submitted to MassIVE (<https://massive.ucsd.edu/>) and is available under the accession MSV000079315 or for direct download through <ftp://MSV000079315@massive.ucsd.edu>.

* This work was funded by grants to M.S.I from the Wellcome Trust, UK (094879/A/10/Z), the Department of Biotechnology, Govt. of India, the Science and Engineering Research Board, the Department of Science and Technology, Govt. of India and the Jawaharlal Nehru Centre for Advanced Scientific Research (JNCASR), Bangalore.

§ This article contains supplemental Figures and Tables.

§§ To whom correspondence should be addressed. Tel: 080-2208-2818; Fax: 080-2208-2766; E-mail: inamdar@jncasr.ac.in.

Author contributions: S.S., A.R., S.K.S., and T.S.K.P. performed research; S.S., A.R., L.A., and M.K. analyzed data; S.S., A.R., L.A., and M.S.I. wrote the paper; T.S.K.P. and M.S.I. contributed new reagents/analytic tools; M.S.I. designed research.

REFERENCES

- Orkin, S. H., and Zon, L. I. (2008) Hematopoiesis: an evolving paradigm for stem cell biology. *Cell* **132**, 631–644
- Evans, C. J., Hartenstein, V., and Banerjee, U. (2003) Thicker than blood: conserved mechanisms in *Drosophila* and vertebrate hematopoiesis. *Dev. Cell* **5**, 673–690
- Jung, S. H., Evans, C. J., Uemura, C., and Banerjee, U. (2005) The *Drosophila* lymph gland as a developmental model of hematopoiesis. *Development* **132**, 2521–2533

4. Das, D., Aradhya, R., Ashoka, D., and Inamdar, M. (2008) Macromolecular uptake in *Drosophila* pericardial cells requires rudhira function. *Exp. Cell Res.* **314**, 1804–1810
5. Krzemien, J., Oyallon, J., Crozatier, M., and Vincent, A. (2010) Hematopoietic progenitors and hemocyte lineages in the *Drosophila* lymph gland. *Dev. Biol.* **346**, 310–319
6. Shim, J., Gururaja-Rao, S., and Banerjee, U. (2013) Nutritional regulation of stem and progenitor cells in *Drosophila*. *Development* **140**, 4647–4656
7. Khadiilkar, R. J., Rodrigues, D., Mote, R. D., Sinha, A. R., Kulkarni, V., Magadi, S. S., and Inamdar, M. S. (2014) ARF1-GTP regulates Asrij to provide endocytic control of *Drosophila* blood cell homeostasis. *Proc. Natl. Acad. Sci. U.S.A.* **111**, 4898–4903
8. Shim, J., Mukherjee, T., and Banerjee, U. (2012) Direct sensing of systemic and nutritional signals by haematopoietic progenitors in *Drosophila*. *Nat. Cell Biol.* **14**, 394–400
9. Khadiilkar, R. J., Ray, A., Chetan, D. R., Sinha, A. R., Magadi, S. S., Kulkarni, V., and Inamdar, M. S. (2017) Differential modulation of the cellular and humoral immune responses in *Drosophila* is mediated by the endosomal ARF1-Asrij axis. *Sci. Rep.* **7**, 118
10. Kulkarni, V., Khadiilkar, R. J., Magadi, S. S., and Inamdar, M. S. (2011) Asrij maintains the stem cell niche and controls differentiation during *Drosophila* lymph gland hematopoiesis. *PLoS ONE* **6**, e27667
11. Benjamini, Y., and Hochberg, Y. (1995) Controlling the false discovery rate: a practical and powerful approach to multiple testing. *J. Royal Statistical Soc.* **57**, 289–300
12. Ow, S. Y., Salim, M., Noirel, J., Evans, C., Rehman, I., and Wright, P. C. (2009) iTRAQ underestimation in simple and complex mixtures: “the good, the bad and the ugly.” *J. Proteome Res.* **8**, 5347–5355
13. Karp, N. A., Huber, W., Sadowski, P. G., Charles, P. D., Hester, S. V., and Lilley, K. S. (2010) Addressing accuracy and precision issues in iTRAQ quantitation. *Mol. Cell. Proteomics* **9**, 1885–1897
14. Reimand, J., Kull, M., Peterson, H., Hansen, J., and Vilo, J. (2007) g:Profiler—a web-based toolset for functional profiling of gene lists from large-scale experiments. *Nucleic Acids Res.* **35**, W193–W200
15. Lanot, R., Zachary, D., Holder, F., and Meister, M. (2001) Postembryonic hematopoiesis in *Drosophila*. *Dev. Biol.* **230**, 243–257
16. Sinha, A., Khadiilkar, R. J., Roychowdhury, S. V. K., Sinha, A., and Inamdar, M. S. (2013) Conserved regulation of the Jak/STAT pathway by the endosomal protein asrij maintains stem cell potency. *Cell Rep.* **4**, 649–658
17. Cammarato, A., Ahrens, C. H., Alayari, N. N., Qeli, E., Rucker, J., Reedy, M. C., Zmasek, C. M., Gucek, M., Cole, R. N., Van Eyk, J. E., Bodmer, R., O’Rourke, B., Bernstein, S. I., and Foster, D. B. (2011) A mighty small heart: the cardiac proteome of adult *Drosophila melanogaster*. *PLoS ONE* **6**, e18497
18. Handke, B., Poernbacher, I., Goetze, S., Ahrens, C. H., Omasits, U., Marty, F., Simigdala, N., Meyer, I., Wollscheid, B., Brunner, E., Hafen, E., and Lehner, C. F. (2013) The hemolymph proteome of fed and starved *Drosophila* larvae. *PLoS ONE* **8**, e67208
19. Zhang, F., Zhao, Y., and Han, Z. (2013) An in vivo functional analysis system for renal gene discovery in *Drosophila* pericardial nephrocytes. *J. Am. Soc. Nephrol.* **24**, 191–197
20. Burgess, R. J., Agathocleous, M., and Morrison, S. J. (2014) Metabolic regulation of stem cell function. *J. Intern. Med.* **276**, 12–24
21. Shetty, D. K., Kalamkar, K. P., and Inamdar, M. S. (2018) OCIAD1 controls electron transport chain complex I activity to regulate energy metabolism in human pluripotent stem cells. *Stem Cell Reports* **11**, 128–141
22. Tortoriello, G., Rhodes, B. P., Takacs, S. M., Stuart, J. M., Basnet, A., Raboune, S., Widlanski, T. S., Doherty, P., Harkany, T., and Bradshaw, H. B. (2013) Targeted lipidomics in *Drosophila melanogaster* identifies novel 2-monoacylglycerols and N-acyl amides. *PLoS ONE* **8**, e67865
23. Qiu, S., Xiao, C., and Meldrum Robertson, R. (2017) Different age-dependent performance in *Drosophila* wild-type Canton-S and the white mutant w¹¹¹⁸ flies. *Comp. Biochem. Physiol. A.* **206**, 17–23
24. Sigismund, S., Confalonieri, S., Ciliberto, A., Polo, S., Scita, G., and Di Fiore, P. P. (2012) Endocytosis and signaling: cell logistics shape the eukaryotic cell plan. *Physiol. Rev.* **92**, 273–366
25. Ito, K. (2016) Metabolism and the control of cell fate decisions and stem cell renewal. *Annu. Rev. Cell Dev. Biol.* **32**, 399–409
26. Parsons, D. W., Jones, S., Zhang, X., Lin, J. C., Leary, R. J., Angenendt, P., Mankoo, P., Carter, H., Siu, I. M., Gallia, G. L., Olivari, A., McLendon, R., Rasheed, B. A., Keir, S., Nikolskaya, T., Nikolsky, Y., Busam, D. A., Tekleab, H., Diaz, L. A. Jr, Hartigan, J., Smith, D. R., Strausberg, R. L., Marie, S. K., Shinjo, S. M., Yan, H., Riggins, G. J., Bigner, D. D., Karchin, R., Papadopoulos, N., Parmigiani, G., Vogelstein, B., Velculescu, V. E., and Kinzler, K. W. (2008) An integrated genomic analysis of human glioblastoma multiforme. *Science* **321**, 1807–1812
27. Mardis, E. R., Ding, L., Dooling, D. J., Larson, D. E., McLellan, M. D., Chen, K., Koboldt, D. C., Fulton, R. S., Delehaunty, K. D., McGrath, S. D., Fulton, L. A., Locke, D. P., Magrini, V. J., Abbott, R. M., Vickery, T. L., Reed, J. S., Robinson, J. S., Wylie, T., Smith, S. M., Carmichael, L., Eldred, J. M., Harris, C. C., Walker, J., Peck, J. B., Du, F., Dukes, A. F., Sanderson, G. E., Brummett, A. M., Clark, E., McMichael, J. F., Meyer, R. J., Schindler, J. K., Pohl, C. S., Wallis, J. W., Shi, X., Lin, L., Schmidt, H., Tang, Y., Haipek, C., Wiechert, M. E., Ivy, J. V., Kalicki, J., Elliott, G., Ries, R. E., Payton, J. E., Westervelt, P., Tomasson, M. H., Watson, M. A., Baty, J., Heath, S., Shannon, W. D., Nagarajan, R., Link, D. C., Walter, M. J., Graubert, T. A., DiPersio, J. F., Wilson, R. K., and Ley, T. J. (2009) Recurring mutations found by sequencing an acute myeloid leukemia genome. *N. Engl. J. Med.* **361**, 1058–1066
28. Luchsinger, L. L., de Almeida, M. J., Corrigan, D. J., Mumau, M., and Snoeck, H. W. (2016) Mitofusin 2 maintains haematopoietic stem cells with extensive lymphoid potential. *Nature* **529**, 528–531
29. Hinge, A. S., He, J., Mose, E., Javier, J., Bartram, J., Fjellman, E., Sesaki, H., Leighton Grimes, H., Salomonis, N., and Filippi, M. (2017) Mitochondrial morphology controls hematopoietic stem cell self-renewal and confers them divisional memory. *Blood*. **130**, 633
30. Sengupta, S., Michener, C. M., Escobar, P., Belinson, J., and Ganapathi, R. (2008) Ovarian cancer immuno-reactive antigen domain containing 1 (OCIAD1), a key player in ovarian cancer cell adhesion. *Gynecol. Oncol.* **109**, 226–233
31. Vizcaino, J. A., Csordas, A., Del-Toro, N., Dianes, J. A., Griss, J., Lavidas, I., Mayer, G., Perez-Riverol, Y., Reisinger, F., Ternent, T., Xu, Q. W., Wang, R., and Hermjakob, H. (2016) 2016 update of the PRIDE database and its related tools. *Nucleic Acids Res.* **44**, D447–D456



A Conserved Role for Asrij/OCIAD1 in Progenitor Differentiation and Lineage Specification Through Functional Interaction With the Regulators of Mitochondrial Dynamics

OPEN ACCESS

Arindam Ray, Kajal Kamat and Maneesha S. Inamdar*

Edited by:

Richa Rikhy,
Indian Institute of Science Education
and Research, Pune, India

Reviewed by:

Jiwon Shim,
Hanyang University, South Korea
Manish Jaiswal,
Centre for Interdisciplinary Sciences,
Tata Institute of Fundamental
Research, India

*Correspondence:

Maneesha S. Inamdar
inamdar@jncasr.ac.in

Specialty section:

This article was submitted to
Stem Cell Research,
a section of the journal
*Frontiers in Cell and Developmental
Biology*

Received: 18 December 2020

Accepted: 14 June 2021

Published: 06 July 2021

Citation:

Ray A, Kamat K and Inamdar MS
(2021) A Conserved Role
for Asrij/OCIAD1 in Progenitor
Differentiation and Lineage
Specification Through Functional
Interaction With the Regulators
of Mitochondrial Dynamics.
Front. Cell Dev. Biol. 9:643444.
doi: 10.3389/fcell.2021.643444

Molecular Biology and Genetics Unit, Jawaharlal Nehru Centre for Advanced Scientific Research, Bengaluru, India

Mitochondria are highly dynamic organelles whose activity is an important determinant of blood stem and progenitor cell state. Mitochondrial morphology is maintained by continuous fission and fusion and affects stem cell proliferation, differentiation, and aging. However, the mechanism by which mitochondrial morphology and dynamics regulate cell differentiation and lineage choice remains incompletely understood. Asrij/OCIAD1 is a conserved protein that governs mitochondrial morphology, energy metabolism and human embryonic stem cell (hESC) differentiation. To investigate the *in vivo* relevance of these properties, we compared hESC phenotypes with those of *Drosophila* hematopoiesis, where Asrij is shown to regulate blood progenitor maintenance by conserved mechanisms. In concordance with hESC studies, we found that *Drosophila* Asrij also localizes to mitochondria of larval blood cells and its depletion from progenitors results in elongated mitochondria. Live imaging of *asrij* knockdown hemocytes and of OCIAD1 knockout hESCs showed reduced mitochondrial dynamics. Since key regulators of mitochondrial dynamics actively regulate mitochondrial morphology, we hypothesized that mitochondrial fission and fusion may control progenitor maintenance or differentiation in an Asrij-dependent manner. Knockdown of the fission regulator Drp1 in *Drosophila* lymph gland progenitors specifically suppressed crystal cell differentiation whereas depletion of the fusion regulator Marf (*Drosophila* Mitofusin) increased the same with concomitant upregulation of Notch signaling. These phenotypes were stronger in anterior progenitors and were exacerbated by Asrij depletion. Asrij is known to suppress Notch signaling and crystal cell differentiation. Our analysis reveals that synergistic interactions of Asrij with Drp1 and Marf have distinct impacts on lymph gland progenitor mitochondrial dynamics and crystal cell differentiation. Taken together, using invertebrate and mammalian model

systems we demonstrate a conserved role for Asrij/OCIAD1 in linking mitochondrial dynamics and progenitor differentiation. Our study sets the stage for deciphering how regulators of mitochondrial dynamics may contribute to functional heterogeneity and lineage choice in vertebrate blood progenitors.

Keywords: mitochondrial dynamics, blood progenitor differentiation, blood lineage choice, progenitor heterogeneity, Asrij, Notch signaling, *Drosophila* lymph gland, human embryonic stem cells (hESC)

INTRODUCTION

In addition to their well-established role in energy metabolism, recent studies show that mitochondria act as a critical regulatory hub of signaling and contribute to stem and progenitor survival and cell fate decisions in pluripotent embryonic stem cells (ESCs) or multipotent hematopoietic stem cells (HSCs) (Bejarano-Garcia et al., 2016; Anso et al., 2017; Zhang et al., 2018). Dynamicity of the mitochondrial network governs mitochondrial function and cell fate specification (Liesa and Shirihai, 2013; Ni et al., 2015; Wai and Langer, 2016; Seo et al., 2018). Balanced mitochondrial fission and fusion maintains mitochondrial quality control through segregation of damaged mitochondria or exchange of components, electrochemical gradients, and metabolites (Twig et al., 2008; van der Bliek et al., 2013; Liu et al., 2020). Mitochondrial morphology and dynamics vary across cell states, lineages, and tissues. Stem and progenitor cells contain fragmented mitochondria with immature cristae, while differentiated cells generally have longer mitochondria with mature ultrastructure (Khacho et al., 2016; Seo et al., 2018). Mitochondria in HSCs also undergo fragmentation upon differentiation to lineage committed progenitors (Luchsinger et al., 2016).

Mitochondrial membrane remodeling proteins actively control mitochondrial dynamics to shape the mitochondrial network through regulation of fission, fusion, biogenesis and degradation. Dynamin related protein 1 (Drp1) is a GTPase that acts as the key mediator of fission and segregation of the mitochondrial network whereas Mitofusins (Mfn1/2) are the main membrane bound GTPases that promote mitochondrial outer membrane fusion (Seo et al., 2018). Other proteins such as Opa1, Fis1, Mid49/51, etc., also regulate various other steps of mitochondrial fission and fusion (Atkins et al., 2016; Wai and Langer, 2016; Tilokani et al., 2018). Many signaling pathways including calcium, ROS, and Notch signaling, which are essential for cell fate decisions depend on the fission-fusion machinery. Drp1 can act in a positive feedback loop with Notch signaling in triple negative breast cancer cells (Chen et al., 2018). Inhibition of Mitofusin2 can upregulate Notch signaling through Calcineurin A in mouse embryonic stem cells (Kasahara et al., 2013). Recent reports highlight the importance of balanced Drp1 or Mitofusin activity in determining HSC fate decisions such as lineage-biased differentiation potential (Luchsinger et al., 2016; Hinge et al., 2020). Drp1 maintains HSC regenerative potential by establishing divisional memory and regulates myeloid lineage reconstitution (Hinge et al., 2020). Also, Mfn2 maintains HSCs with extensive lymphoid potential through inhibition of excessive calcium-dependent

NFAT (Nuclear Factor of Activated T-cells) signaling, probably by tethering mitochondria to the endoplasmic reticulum (Luchsinger et al., 2016). Drp1 and Mfn2 may impact various developmental processes in different ways, due to their opposite roles in mitochondrial dynamics (Sandoval et al., 2014). Such correlation of mitochondrial shape to cell fate suggests a possible role of mitochondrial network architecture during hematopoiesis. Despite reports suggesting functional links between mitochondrial dynamics regulators and HSC fate, the mechanism by which they regulate lineage-biased signaling and differentiation is not fully elucidated.

Asrij/OCIAD1 (Ovarian Carcinoma Immunoreactive Antigen Domain containing 1), a conserved regulator of differentiation, localizes to mitochondria in human embryonic stem cells (hESCs) and negatively regulates mitochondrial Complex I activity (Shetty et al., 2018). Depletion of OCIAD1 leads to elongation of mitochondria and increased early mesodermal progenitor formation indicating that OCIAD1 possibly regulates mitochondrial dynamics to influence mitochondrial activity and cellular differentiation (Shetty et al., 2018; Praveen et al., 2020). The *Drosophila* ortholog of OCIAD1, Asrij maintains blood progenitors in the larval hematopoietic organ, the lymph gland. Asrij expression is restricted to the hematopoietic system (Inamdar, 2003). Loss of Asrij causes precocious differentiation to crystal cells, a lineage that is specified by Notch activation (Kulkarni et al., 2011; Khadilkar et al., 2014). Proteomic analysis showed reduced Drp1 levels in *asrij* null lymph glands (Sinha et al., 2019b). Although OCIAD1 controls mitochondrial morphology in hESCs, its genetic interaction with the canonical mitochondrial dynamics regulatory machinery remains unexplored, especially *in vivo*. Hence, we used *Drosophila* larval hematopoiesis as an accessible *in vivo* model to explore whether Asrij regulates mitochondrial dynamics for progenitor maintenance and cell fate decisions.

The *Drosophila* larval lymph gland is a linearly arranged multi-lobed hematopoietic organ that allows analysis of different stages of blood development in a single animal (Rodrigues et al., 2021). This makes it an excellent model to study conserved mechanisms of blood cell homeostasis and function (Jung et al., 2005; Banerjee et al., 2019). The lobes are arranged in pairs along the antero-posterior axis. The anterior-most or primary lobes are well-characterized and demarcated into distinct zones with the peripheral differentiated hemocytes (cortical zone), inner blood progenitors (medullary zone) and a hematopoietic niche (posterior signaling center) (Banerjee et al., 2019). We recently showed that secondary, tertiary, and quaternary lobes, collectively called the posterior lobes, constitute the major part of the progenitors and persist till

the end of the larval life (Rodrigues et al., 2021). Blood progenitor cells in the lymph gland have diverse origins and distinct functions and are identified by expression of *domeless*, *TepIV*, or *E-Cadherin*. Unlike anterior progenitors, posterior progenitors are refractile to immune challenge. Blood progenitor diversity is an essential element of the immune response and leads to functional compartmentalization such that younger posterior blood progenitors are maintained as a reserve pool (Rodrigues et al., 2021).

Hemocytes in *Drosophila* are analogous to the myeloid lineage and are of three types- macrophage-like plasmacytes (identified by expression of *P1*), crystal cells that melanize (identified by *ProPO* (Prophenoloxidase) expression) and large lamellocytes (identified by Phalloidin staining for F-actin) that encapsulate foreign bodies such as parasitoid wasp eggs (Banerjee et al., 2019; Cho et al., 2020; Tattikota et al., 2020). Lineage specification is achieved by controlled activation of distinct signaling pathways to maintain hematopoietic homeostasis.

In this study, we elucidate the role of *Asrij* in mitochondrial dynamics and show that *Asrij* regulates remodeling of the mitochondrial network in concert with canonical mitochondrial dynamics regulators *Drosophila* *Drp1* and *Mfn* (Mitochondria Assembly Regulatory Factor/*Marf*), to regulate Notch signaling and blood cell homeostasis. Moreover, our analyses of mitochondrial dynamics across all the progenitor subsets reflects heterogeneity and developmental diversity of such sub-populations. We establish a functional link of *Asrij* to canonical mitochondrial dynamics regulators in lineage-biased hematopoiesis that will help elucidate the conserved role of this interaction in influencing cell fate decisions.

MATERIALS AND METHODS

Fly Stocks

Canton-S was used as wild type fly strain. *w1118* was used as background control for *arj9/arj9* whereas *e33CGal4* (K. Anderson, Memorial Sloan Kettering Center) was used as parental control for *asrij* knockdown and overexpression. For progenitor-specific knockdown, *domeGal4 UAS 2xEGFP/FM7a* or *domeGal4/FM7b* (Utpal Banerjee, UCLA) was used as driver and parental control. Other stocks used are as follows: *UAS arj RNAi* (VDRC 6633), *UAS arj*, *UAS mito-GFP* (BDSC 8442), *UAS Drp1 RNAi* (BDSC 44155), *UAS Marf RNAi* (BDSC 31157), *UAS Drp1* (BDSC 51647), *UAS Marf* (BDSC 67157), *NRE-GFP/CyO* (BDSC 30727), and *UAS mCD8 RFP* (BDSC 27399).

Immunostaining Analysis

Third instar larvae were dissected in PBS to prepare lymph gland samples as described before (Khadilkar et al., 2014). Samples were fixed with 4% paraformaldehyde (PF) for 20 min at room temperature (25°C), permeabilized with 0.3% PTX (Triton X-100 in PBS) and incubated in 20% goat serum before primary antibody addition. Antibodies used were mouse anti-COX IV (Abcam, United Kingdom), rabbit anti-*Asrij* (Kulkarni et al., 2011), mouse anti-P1 (Istvan Ando, BRC

Hungary), mouse anti-*ProPO*, rabbit anti-*dsRed* (Takara, Japan), and chick anti-GFP (Abcam, United Kingdom).

For hemocyte immunostaining, larvae were bled to extract hemolymph into warm Schneider's serum-free media (Thermo Fisher Scientific, Waltham, MA, United States). Hemocytes were placed on coverslips to allow attachment for 10 min, then fixed with 4% PF and permeabilized with 0.4% NP40, blocked with 20% goat serum and incubated in primary antibody.

Secondary antibodies used were conjugated to Alexa-Fluor 488, 568, or 633 (Life Technologies, Carlsbad, CA, United States). Phalloidin conjugated to Alexa 568 or 633 (Life Technologies, Carlsbad, CA, United States) was used to visualize lamellocytes. Lymph glands were mounted on coverslips in DAPI-glycerol media. Images were acquired using Zeiss LSM510 Meta or LSM880 confocal microscope in either normal confocal mode or airy scan mode.

MitoTracker Staining

Hemocytes, attached to coverslips, were incubated with Mitotracker Deep Red (Thermo Fisher Scientific, Waltham, MA, United States) diluted to 200 nM in serum-free Schneider's media for 20 min at room temperature in the dark. Mitotracker was then washed off with serum-free Schneider's media and hemocytes fixed in 4% PF. Images were acquired in Zeiss LSM510 Meta microscope at 633 nm excitation.

Live Imaging of Mitochondria

Mito-GFP expressing hemocytes from larval hemolymph were left to attach onto coverslips in serum-free Schneider's media for 10 min at 25°C (Standard experimental temperature). The hemocytes were imaged on Zeiss LSM880 confocal microscope with temperature maintained at 25°C with 5% CO₂. Images were captured every 10 s. Auto-focus module was used to adjust focal plane variation during imaging.

Quantification

Mitochondria Quantification

Co-localization was analyzed using Zen software co-localization tool. Various parameters of mitochondrial network such as branch length, number of branches, number of junctions, and mitochondrial footprint in hemocytes and lymph gland progenitors were quantified using MiNA plugin of Fiji software following protocol described in Valente et al. (2017). Imaris software was used to make 3D reconstruction of mitochondrial surface and quantify number of surfaces and average volume per surface as a readout of aggregation in hemocytes.

Dynamics of mitochondrial network was estimated by quantifying variance of different parameters over time as shown in Hinge et al. (2020). Similar analyses of mitochondrial parameters were performed to assess mitochondrial dynamics in wild type (BJNhem20), OCIAD1 depleted (OCIAD1-Het-KO), and overexpressing (OCIAD1-OV) hESCs (Shetty et al., 2018).

Quantification of Hemocytes in Lymph Gland

Progenitor and plasmacyte fraction in each lymph gland lobe was quantified using Imaris. Briefly, the number of spots (DAPI positive nuclei with > 2 μm diameter) close to the reconstructed

dome >2xEGFP (for prohemocytes) or P1 (for plasmatocytes) surface, by a set threshold distance (1 μm for prohemocytes and 2 μm for plasmatocytes), was quantified and divided by total number of nuclei. Number of crystal cells and number of cells with high NRE-GFP expression in each lobe was quantified manually and its fraction was calculated in each lobe by dividing with the number of nuclei. Lamellocytes were identified based on large or elongated morphology as revealed by Phalloidin staining. All images within a given figure panel were adjusted equally for brightness and contrast using Adobe Photoshop CS5 extended. Graphs for all figure panels were prepared using GraphPad Prism version 8. BioRender was used to draw cells in the schematic in **Figure 5**.

Each larva was considered as a biological replicate. Data from each lymph gland lobe was individually considered for quantitation in all graphs. One-way ANOVA or Student's *t*-test was performed for statistical analysis of data. For datasets with unequal variance across groups, non-parametric tests such as Kruskal Wallis test or Mann-Whitney test was performed.

RESULTS

Mitochondrial Morphology Reflects Larval Blood Progenitor Heterogeneity in *Drosophila*

Mitochondria are reported to affect progenitor maintenance in the larval lymph gland primary or anterior lobe but mitochondrial morphology and dynamics have not been investigated in blood progenitors. We recently showed that the larval blood progenitor pool is heterogeneous and arranged linearly, with younger progenitors in the posterior lobes (Rodrigues et al., 2021). A comprehensive analysis of mitochondrial morphology (see methods) in the dome + lymph gland progenitors of primary, secondary, and tertiary lobes, using the *domeGal4* driver and the mitoGFP reporter (*domeGal4/+; UAS mito-GFP/+; +/+*) showed that while primary and secondary lobe progenitors have similar mitochondrial morphology, tertiary lobes have relatively shorter mitochondria. Other parameters such as mitochondrial footprint, number of branches and junctions remained unchanged across progenitor subsets (**Figures 1A,E**). This is in agreement with the anterior-posterior developmental and functional heterogeneity of progenitors reported earlier (Rodrigues et al., 2021) and indicates that younger progenitors have less mature mitochondria.

Asrij Regulates Mitochondrial Morphology in *Drosophila* Blood Progenitors and Hemocytes

Several reports show mitochondrial localization of OCIAD1, the human ortholog of Asrij and its interaction with various components of the electron transport chain (ETC) and mitochondrial dynamics machinery (Floyd et al., 2016; Lee et al., 2017; Shetty et al., 2018; Antonicka et al., 2020). OCIAD1 regulates ETC Complex I activity in mitochondria as well as the

mitochondrial network architecture (Shetty et al., 2018). Owing to a conserved role in stem cell maintenance and hematopoiesis, we hypothesized that Asrij may similarly regulate mitochondrial features in *Drosophila*.

Immunolocalization analysis for Asrij in *domeGal4/+; UAS mito-GFP/+* lymph glands showed mitochondrial localization of Asrij in progenitors (**Supplementary Figure 1A**). Further using the mitochondrial marker COXIV as well as by staining with Mitotracker in Canton(S) hemocytes, we showed that Asrij also localizes to mitochondria in circulating hemocytes (**Supplementary Figure 1B**).

Depletion of OCIAD1 in hESCs was shown to increase mitochondrial branch length, footprint, and branch number, indicating a shift of dynamics toward enhanced mitochondrial biogenesis and fusion (Shetty et al., 2018). *Asrij* knockdown (*domeGal4/+; UAS mito-GFP/+; UAS arj RNAi/+*) in lymph gland progenitors resulted in elongated mitochondria (interpreted through increase in mean and median branch length) (**Figures 1A,B,E**). In addition, mitochondrial footprint, and number of mitochondrial junctions per cell were increased in primary lobe progenitors, indicating a shift of mitochondrial dynamics toward reduced fission or enhanced fusion. Hence, we conclude that Asrij regulates mitochondrial dynamics in anterior progenitors. However, there was a mild effect on secondary lobes (reduced mitochondrial footprint and junctions) and no significant effect on tertiary lobes. This indicates heterogeneity in dome + progenitor response from anterior to posterior and also suggests that mitochondria in younger progenitors are less sensitive to perturbations (**Figures 1A,B,E**).

We also examined the mitochondrial network in *Drosophila* circulating hemocytes as these are single cells amenable to high-resolution imaging. Immunostaining for COXIV showed that *asrij* null mutant (*arj9/arj9*) hemocytes had higher mitochondrial branch length, footprint (content), number of branches, and number of junctions as compared to control (*w1118*) (**Supplementary Figure 1C**). This indicates elongation of mitochondria, poor fission or hyperfusion and increase in mitochondrial content upon loss of Asrij in hemocytes. Additionally, we observed increase in mitochondrial aggregation (as interpreted from increase in mean volume per surface) without significant decrease in the number of mitochondrial clusters in *arj9/arj9* hemocytes (**Supplementary Figure 1D**).

OCIAD1 overexpression leads to reduction of the mitochondrial footprint and branch length in hESCs (Shetty et al., 2018). While most mitochondrial network parameters (mean and median branch length, number of junctions and mitochondrial aggregation) remained unchanged upon overexpression of Asrij in hemocytes (*e33cGal4/UAS asrij*) there was a significant reduction in number of mitochondria (branches and surfaces) and the mitochondrial footprint (**Supplementary Figures 2A,B**). This suggests that regulatory mechanisms operating to control mitochondrial dynamics in *Drosophila* hemocytes are Asrij-dependent. Taken together, our data show functional conservation of Asrij in controlling mitochondrial morphology and network architecture.

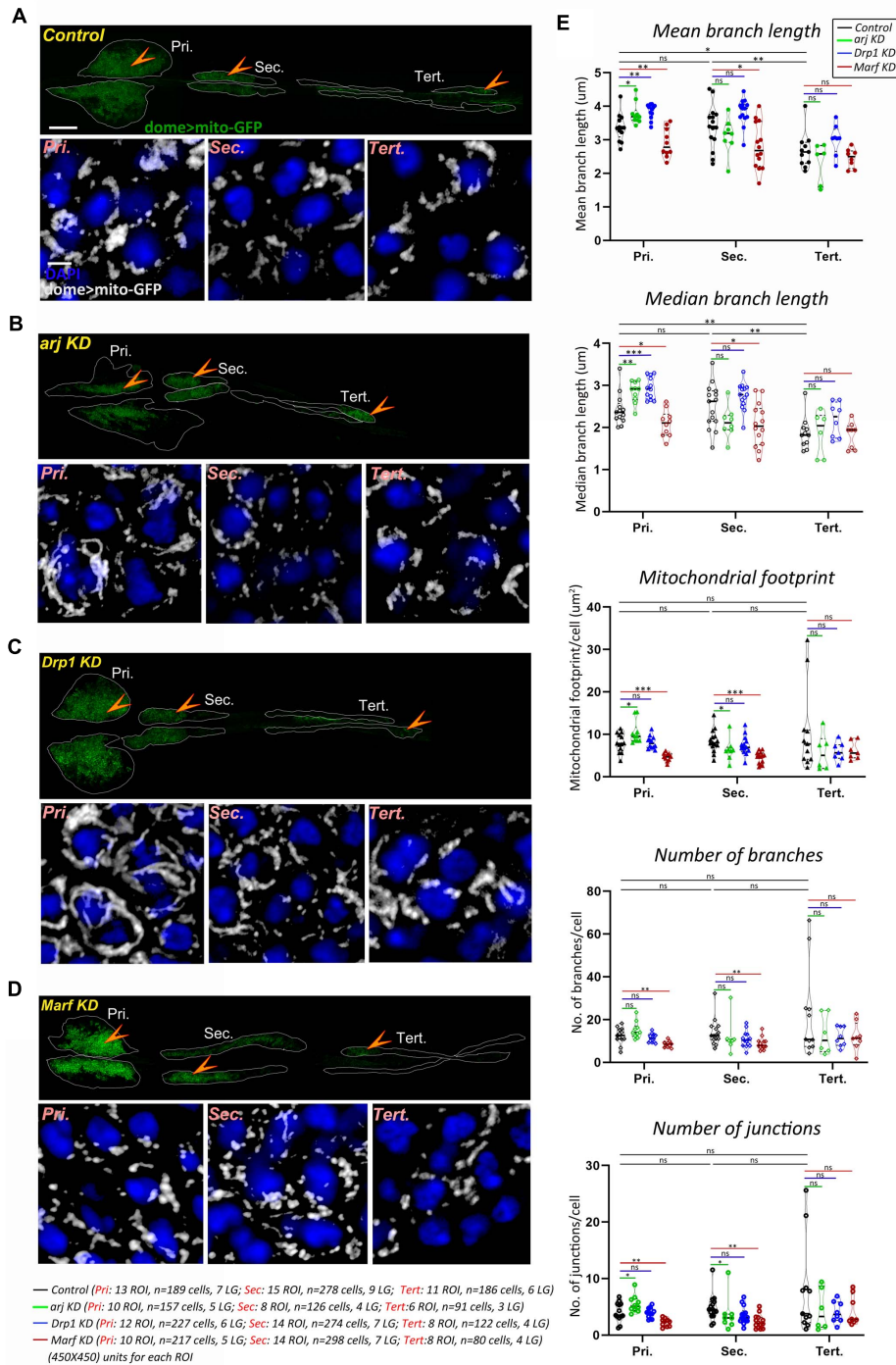


FIGURE 1 | Asrij, Drp1, and Marf regulate mitochondrial morphology in blood progenitors of *Drosophila* lymph gland. **(A–D)** Mitochondria in lymph gland progenitors (pro-hemocytes) of the primary, secondary, and tertiary lobes are marked by *dome > mito-GFP* in control (*domeGal4/+ ; UAS mito-GFP/+ ; +/+*) **(A)**, *arj KD* (*domeGal4/+ ; UAS mito-GFP/+ ; UAS arj RNAi/+*) **(B)**, *Drp1 KD* (*domeGal4/+ ; UAS mito-GFP/+ ; UAS Drp1 RNAi/+*) **(C)**, and *Marf KD* (*domeGal4/+ ; UAS mito-GFP/+ ; UAS Marf RNAi/+*) **(D)** lymph glands. Arrowheads indicate the *dome > mito-GFP* positive progenitors across different lobes that are shown magnified in the lower panel (Pri.: Primary, Sec.: Secondary, and Tert.: Tertiary). Images represent single confocal section of 0.5 μm for easy visualization of mitochondria. **(E)** Violin plots show quantification of mitochondrial mean and median branch length, footprint, number of branches and number of junctions across primary, secondary, and tertiary lobes. Scale bar: 100 μm for upper LG panel and 5 μm for lower magnified view panel. Kruskal Wallis test was performed to determine statistical significance. * $P < 0.05$, ** $P < 0.01$, *** $P < 0.001$, ns: non-significant.

Anterior Progenitors Are More Sensitive to Perturbation of the Mitochondrial Fission-Fusion Machinery

Drp1 and Marf are well conserved key regulators of mitochondrial dynamics. Hence, we checked whether depleting Drp1 or Marf from dome + ve progenitor subsets (*domeGal4/+; UAS mito-GFP/+; +/+*) may affect mitochondrial architecture similar to *asrij* depletion. In anterior lymph gland lobes, mitochondrial branch length increased on Drp1 knockdown (*domeGal4/+; UAS mito-GFP/+; UAS Drp1 RNAi/+*) indicating mitochondrial fission was inhibited (Figures 1A,C,E). Conversely *Marf* KD (*domeGal4/+; UAS mito-GFP/+; UAS Marf RNAi/+*) caused mitochondrial fragmentation (reduced mitochondrial branch length) along with reduced mitochondrial content (mitochondrial footprint, number of branches and junctions) indicating reduced fusion (Figures 1A,D,E). Thus, as expected, Drp1 and Marf affect mitochondrial dynamics of blood progenitors. However, there was no significant change in mitochondrial morphology in posterior lobes upon Drp1 depletion (Figures 1A,C,E). *Marf* knockdown reduced mitochondrial branch length in secondary lobe progenitors as compared to control whereas tertiary lobe remained unaffected (Figures 1A,D,E). This suggests that posterior progenitors are less sensitive to perturbation in the mitochondrial fission-fusion machinery.

Asrij/OCIAD1 Depletion Reduces Mitochondrial Network Dynamics

Mitochondrial dynamics is essential for exchange and distribution of metabolites across the network to different parts of the cell and depends on morphology, number, and branching (Detmer and Chan, 2007). Change of mitochondrial network parameters upon *Asrij* modulation suggests a possible impact on mitochondrial dynamics. Live imaging analysis of mito-GFP expressing hemocytes from control (*e33C > UAS mito-GFP*) and *Asrij* depleted (Knockdown: KD) (*e33C > UAS mito-GFP > UAS arj RNAi*) larvae showed lower temporal variation in branch number and junction number with unchanged dynamics of the mitochondrial footprint in KD hemocytes (Figure 2A; Supplementary Video 1). This suggests a possible reduction of mitochondrial fission-fusion events in KD hemocytes and might explain the shift of equilibrium toward elongated mitochondria. Mitochondrial footprint dynamics are unaltered suggesting that mitochondrial biogenesis and degradation may be unaffected, which merits further investigation.

We performed similar analyses in pluripotent human embryonic stem cells (hESCs) that were depleted of OCIAD1 [heterozygous KO (Het-KO); Shetty et al. (2018)]. While the dynamics of branch number and footprint were unchanged, mitochondrial junctions in Het-KO hESCs showed reduced dynamics (Figure 2B). This indicates reduced temporal variation of mitochondrial fission-fusion events upon OCIAD1 depletion in hESCs. As reported earlier, OCIAD1 overexpression in hESCs led to reduction in branch length and mitochondrial footprint (Shetty et al., 2018). Time-lapse image analysis of OCIAD1 overexpressing hESCs showed significantly reduced

temporal variation of mitochondrial junction number as compared to control, whereas mitochondrial branch number and footprint dynamics were similar (Supplementary Figure 3). Thus, OCIAD1 depletion and overexpression, both impact mitochondrial dynamics. In summary, modulation of mitochondrial dynamics by *Asrij*/OCIAD1 is a mechanism that operates in diverse systems such as *Drosophila* blood progenitors and human embryonic stem cells.

Inhibition of Mitochondrial Fission Prevents Crystal Cell Differentiation

Asrij is essential for lymph gland progenitor maintenance and we find that *Asrij* depletion alters mitochondrial dynamics. This suggests a possible role for mitochondrial dynamics in progenitor differentiation. Regulated mitochondrial fission and fusion are critical to control mitochondrial dynamics. However, the role of canonical fission and fusion regulators such as Drp1 and Mitofusin in stem cell maintenance and lineage choice is not completely understood.

Drp1 drives mitochondrial dynamics by promoting fission and has a role in regulating myeloid reconstitution potential of HSCs (Hinge et al., 2020). However, the role of mitochondrial fission in hematopoietic lineage choice remains largely underexplored. Hence, we examined the effects of depletion of Drp1 from lymph gland progenitors. RNAi-mediated knockdown (KD) in *domeless*⁺ progenitors (*domeGal4 UAS 2xEGFP;; UAS Drp1 RNAi*) led to reduction in crystal cell (ProPO⁺) differentiation in primary lobes (Figure 3A).

Previous reports show Notch signaling activation is a key mechanism that triggers crystal cell differentiation in the lymph gland while inhibiting differentiation to plasmacytes or lamellocytes (Duvic et al., 2002; Lebestky et al., 2003; Small et al., 2014; Blanco-Obregon et al., 2020; Cho et al., 2020). However, whether mitochondrial dynamics actively regulate Notch signaling in the lymph gland remains unexplored. We used NRE-GFP (Notch responsive element) reporter to assess the extent of Notch activation upon Drp1 depletion. NRE-GFP (Notch responsive element-GFP) is a widely used reporter for Notch signaling activation. Notch-dependent activation of transcription through NRE promotes GFP transcription. Thus, increased GFP expression marks enhanced activation of Notch signaling. NRE-GFP positive cells are fewer in number in control (*domeGal4/+; NRE-GFP/+; UAS mCD8 RFP/+*) lymph glands and its expression does not overlap with Dome-positive area or medullary zone (MZ) (Supplementary Figure 4A). Also, it overlaps with the standard crystal cell marker ProPO, indicating active Notch signaling in such cells (Supplementary Figure 4A arrowhead). Progenitor-specific knockdown of *Drp1* (*domeGal4/+; NRE-GFP/+; UAS mCD8 RFP/UAS Drp1 RNAi*) did not affect Notch activation significantly, though there was a downward trend (Figure 3B). This suggests that reduced differentiation to ProPO⁺ crystal cells in *Drp1* KD lymph gland primary lobes may be influenced by other mechanisms downstream of mitochondrial fission in addition to activation of Notch signaling.

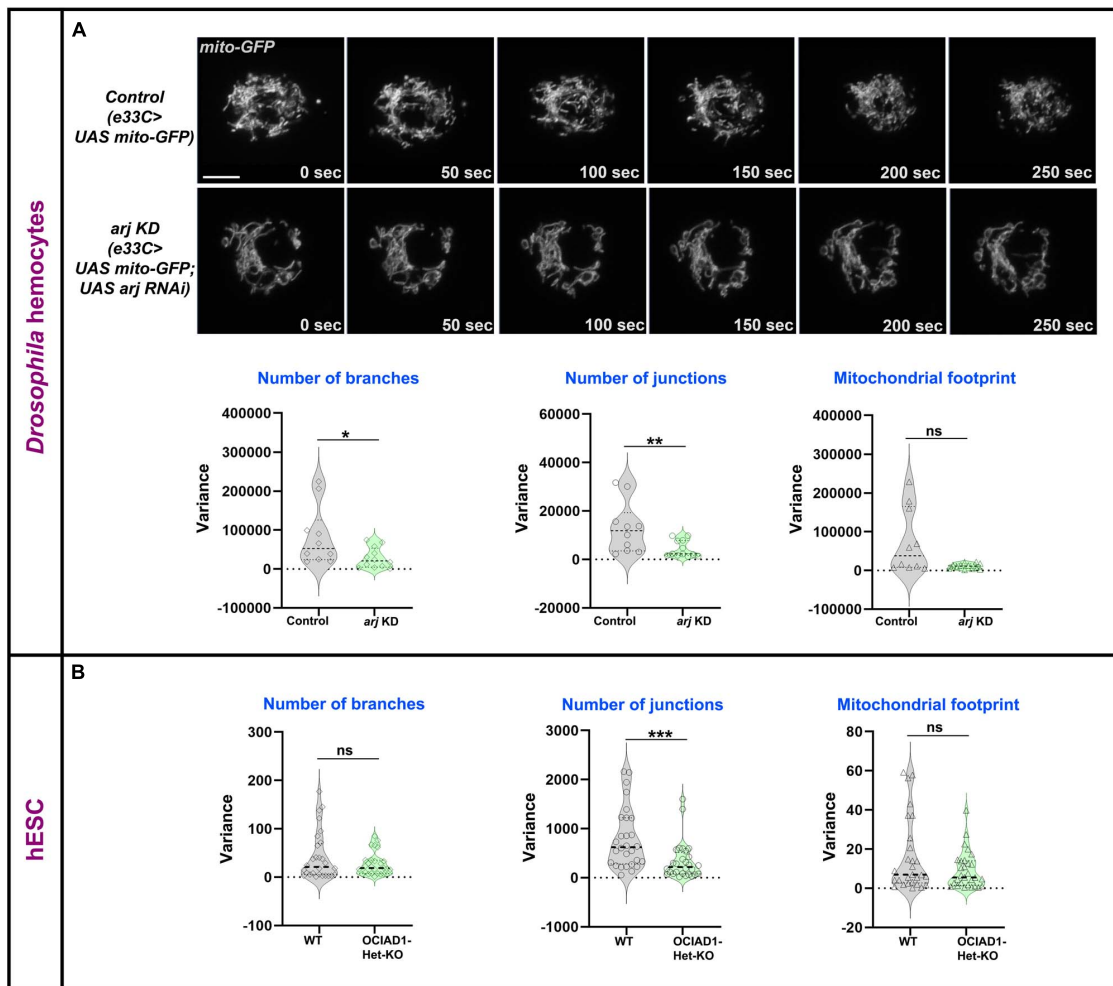


FIGURE 2 | Asrij/OCIAD1 depletion reduces mitochondrial network dynamics. **(A)** Time lapse live imaging of control (*e33CGal > UAS mito-GFP*) and *asrij* KD (*e33CGal4 > UAS mito-GFP; UAS arj RNAi*) circulatory hemocytes expressing mitochondria targeted GFP. Violin plots show quantification of variance in number of branches, number of junctions and mitochondrial footprint in control (*n* = 10 cells) and *arj* KD (*n* = 12 cells) hemocytes. **(B)** Similar quantifications are represented for Mitotracker stained WT (BJNh20) (*n* = 30 cells) and OCIAD1-Het-KO (CRISPR-39) (*n* = 30 cells) live hESCs. Original data were used from Shetty et al. (2018) for analysis. Scale bar: 5 μ m. Error bars represent SEM. Mann-Whitney two-tailed *t*-test was used to determine statistical significance. **P* < 0.05, ***P* < 0.01, ****P* < 0.001, ns: statistically non-significant difference.

Drp1 knockdown had no significant effect on progenitor maintenance, plasmacyte or lamellocyte differentiation in the lymph gland (**Supplementary Figures 5A,B; Figures 3C-E**). As depletion of Drp1 affects crystal cell differentiation in primary lobes, we next checked if overexpressing Drp1 had any effect. Progenitor-specific overexpression of Drp1 did not affect crystal cell differentiation (**Supplementary Figures 6A,B**). Our data suggest that Drp1 selectively regulates crystal cell differentiation (**Figure 3F**).

Reduced Mitochondrial Fusion Promotes Notch Signaling and Crystal Cell Differentiation

Mitofusins drive mitochondrial dynamics by promoting mitochondrial fusion. Mfn2 regulates maintenance of HSCs

with lymphoid potential in mouse through regulation of calcium signaling (Luchsinger et al., 2016). However, its role in myeloid lineage specification is not fully understood. Knockdown of *Drosophila* Mfn homolog Marf (*domeGal4 UAS 2xEGFP; UAS Marf RNAi*) led to dramatic increase in crystal cell differentiation in primary lobes (**Figure 4A**). Both Drp1 and Marf play critical but opposite roles in non-canonical Notch signaling activation and various developmental processes such as neuroblast and synaptic development in *Drosophila* (Lee et al., 2013; Sandoval et al., 2014). In concordance with previous reports, we find that *Marf* KD (*domeGal4/+; NRE-GFP/+; UAS mCD8 RFP/UAS Marf RNAi*) led to increase in Notch activation in primary and secondary lobes (**Figure 4B**) whereas tertiary lobes remained unaffected. This explains increased crystal cell differentiation in *Marf* KD lymph gland primary lobes. Absence of crystal cells in the tertiary lobes suggests additional regulatory mechanisms

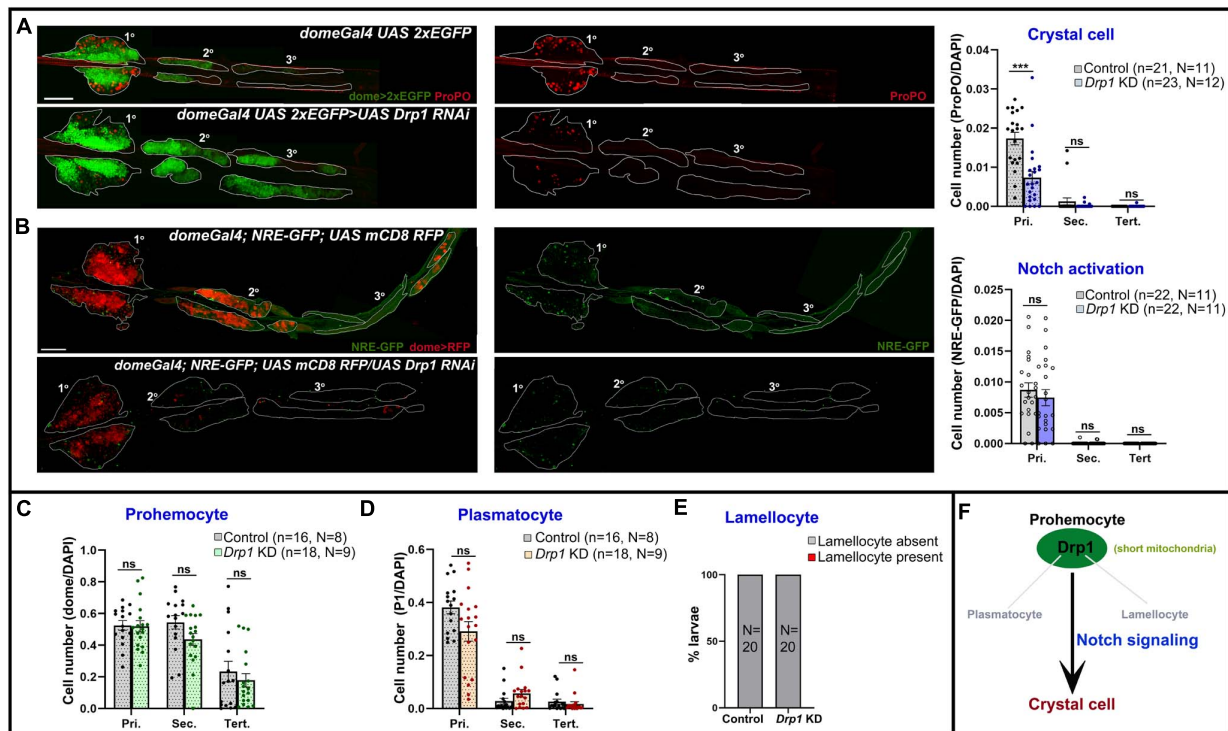


FIGURE 3 | Drp1 regulates blood cell homeostasis in *Drosophila* lymph gland. **(A)** Whole mount lymph gland showing expression of crystal cell marker ProPO in primary, secondary, and tertiary lobes of control (*domeGal4 UAS 2xEGFP*) and *Drp1* KD (*domeGal4 UAS 2xEGFP > UAS Drp1 RNAi*) larvae. GFP marks the expression of prohemocyte marker Domeless. Bar diagram shows quantification of mean crystal cell fraction in primary, secondary, and tertiary lobes of indicated genotypes. **(B)** NRE-GFP (Notch responsive element-GFP) reports activation of Notch signaling in control (*domeGal4/+; NRE-GFP/+; UAS mCD8 RFP/+*) and *Drp1* KD (*domeGal4/+; NRE-GFP/+; UAS mCD8 RFP/UAS Drp1 RNAi*) lymph gland primary, secondary, and tertiary lobes. RFP marks the expression of prohemocyte marker Domeless. Bar diagram shows quantification of mean NRE-GFP positive (high) cell fraction in primary, secondary, and tertiary lobes of indicated genotypes. **(C–E)** Bar diagrams show quantification of mean dome > 2xEGFP positive prohemocyte fraction **(C)**, P1 positive plasmatocyte fraction **(D)** and percentage of lymph glands with lamellocyte differentiation **(E)** in control and upon *Drp1* KD. **(F)** Schematic summarizes effect of Drp1 on various hemocyte lineages and Notch signaling. n represents number of individual lymph gland lobes analyzed, and N represents number of larvae for each genotype. Scale bar: 100 μ m. Error bars represent SEM. Multiple *t*-test was performed to determine statistical significance. ****P* < 0.001, ns: statistically non-significant difference.

and is in agreement with the idea that posterior lobes resist differentiation (Rodrigues et al., 2021).

Marf knockdown did not affect the primary and secondary lobe progenitors. However, surprisingly, the dome⁺ progenitor fraction increased in tertiary lobes (Supplementary Figure 5C; Figure 4C). This could be due to increased proliferation of posterior progenitors that have inherently reduced differentiation potential. Plasmatocyte differentiation remained unchanged in primary and tertiary lobes, increasing mildly in secondary lobes (Supplementary Figure 5C; Figure 4D). Occasionally there was a small increase (1 out of 20 larvae analyzed) in lamellocyte differentiation (Supplementary Figure 5D; Figure 4E). This indicates that *Marf* activity prevents dome⁺ progenitor expansion in the posterior lobes and primarily prevents precocious crystal cell differentiation (Figure 4F). *Marf* overexpression increased crystal cell differentiation in primary lobes. However, posterior lobes were unaffected (Supplementary Figures 6A,C). This indicates differences in progenitor sensitivity to *Marf* levels.

Taken together our analyses show that canonical mitochondrial dynamics regulators such as Drp1 and *Marf*

actively modulate Notch activation to dictate crystal cell differentiation in the *Drosophila* lymph gland.

Asrij Integrates Mitochondrial Dynamics With Crystal Cell Differentiation

Loss of *Asrij* leads to enhanced activation of Notch signaling with a concomitant increase in crystal cell differentiation (Supplementary Figure 4B) (Kulkarni et al., 2011; Khadilkar et al., 2014). Since *Asrij* also regulates mitochondrial dynamics, we next asked whether *Asrij* genetically interacts with the canonical regulators of mitochondrial dynamics. Elongated mitochondria in *asrij* KD progenitors could be a result of impaired fission or enhanced fusion events and hence are expected to be rescued by promoting fission (*Drp1* overexpression) or inhibiting fusion (*Marf* depletion).

Progenitor-specific *Drp1* overexpression (OV) using *domeGal4* driver could not efficiently restore normal mitochondrial architecture in *Asrij* depleted progenitors (*arj* KD *Drp1* OV: *domeGal4/+; UAS mito-GFP/+; UAS Drp1/UAS arj RNAi*) (Figures 5A–D insets and Figure 5G). However,

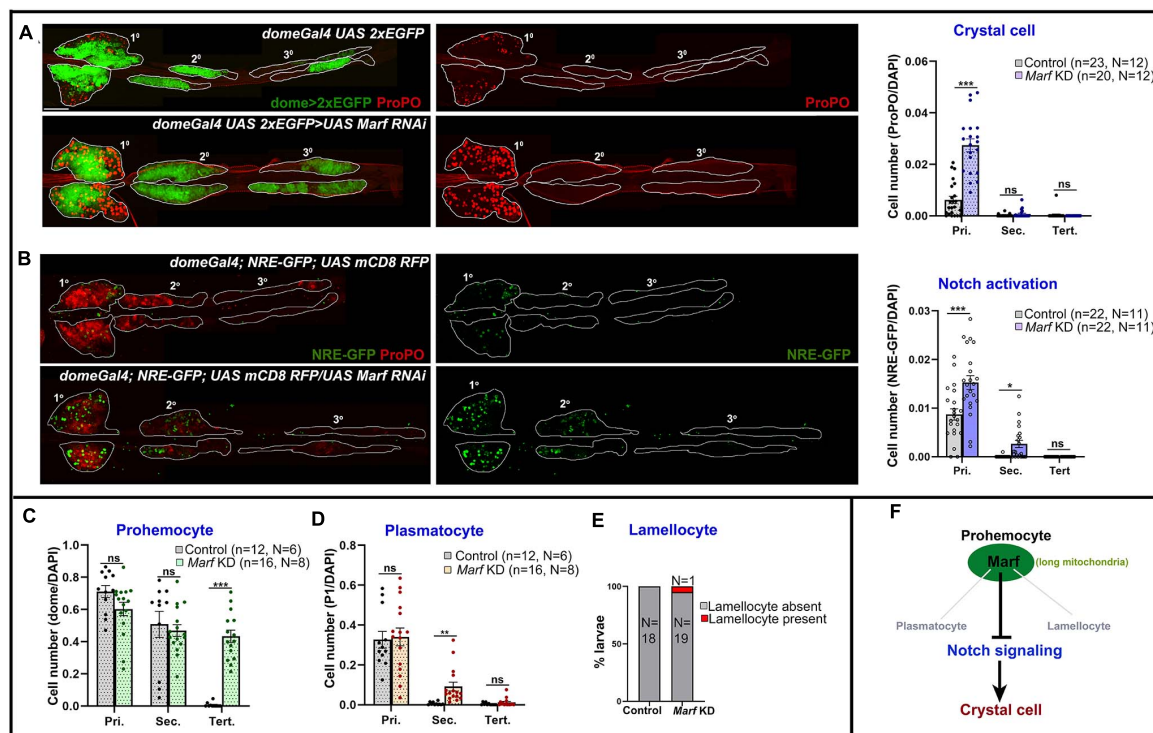


FIGURE 4 | Marf regulates blood cell homeostasis and Notch signaling in *Drosophila* lymph gland. **(A)** Whole mount lymph gland showing expression of crystal cell marker ProPO in primary, secondary, and tertiary lobes of control (*domeGal4 UAS 2xEGFP*) and *Marf* KD (*domeGal4 UAS 2xEGFP > UAS Marf RNAi*) larvae. GFP marks the expression of prohemocyte marker Domeless. Bar diagram shows quantification of mean crystal cell fraction in primary, secondary, and tertiary lobes of indicated genotypes. **(B)** NRE-GFP reports activation of Notch signaling in control (*domeGal4/+; NRE-GFP/+; UAS mCD8 RFP/+*) and *Marf* KD (*domeGal4/+; NRE-GFP/+; UAS mCD8 RFP/UAS Marf RNAi*) lymph gland primary, secondary, and tertiary lobes. RFP marks the expression of prohemocyte marker Domeless. Bar diagram shows quantification of mean NRE-GFP positive (high) cell fraction in primary, secondary, and tertiary lobes of indicated genotypes. **(C–E)** Bar diagrams show quantification of mean dome > 2xEGFP positive prohemocyte fraction **(C)**, P1 positive plasmatocyte fraction **(D)**, and percentage of lymph glands with lamellocyte differentiation **(E)** in control and upon *Marf* KD. **(F)** Schematic summarizes effect of Marf on various hemocyte lineages and Notch signaling. n represents number of individual lymph gland lobes analyzed, and N represents number of larvae for each genotype. Scale bar: 100 μ m. Error bars represent SEM. Multiple *t*-test was performed to determine statistical significance. **P* < 0.05, ***P* < 0.01, ****P* < 0.001, ns: statistically non-significant difference.

Marf knockdown (*Marf* KD), which caused fragmentation of mitochondria rescued *asrij* KD phenotype in progenitors (*arj* KD *Marf* KD: *domeGal4/+; UAS mito-GFP/+; UAS Marf RNAi/UAS arj RNAi*) (Figures 5A,B,E,F insets and Figure 5G). This suggests that elongation of mitochondria in *asrij* KD condition is an outcome of enhanced fusion rather than impaired fission.

We also analyzed the extent of crystal cell differentiation in the lymph glands of these genotypes. Increased Drp1 (OV) or reduced *Marf* (KD) in progenitors in the *asrij* depleted background (*arj* KD) showed a synergistic effect on the crystal cell phenotype. Both *arj* KD *Drp1* OV and *arj* KD *Marf* KD lymph gland primary lobes showed a greater increase in crystal cells compared to single mutants *arj* KD, *Drp1* OV or *Marf* KD (Figures 5A–F,H). There was no significant increase in crystal cell differentiation in posterior lobes except in the secondary lobes of *arj* KD *Marf* KD compared to control or *arj* KD. As *Drp1* overexpression could not rescue mitochondrial elongation caused by loss of *Asrij*, it may function upstream of *Asrij* to regulate mitochondrial phenotype. However, increased crystal cell differentiation upon *Drp* overexpression, which is enhanced

in the *asrij* mutant background, suggests a direct effect on crystal cell differentiation. On the other hand, *Marf* acts downstream of *Asrij* in blood progenitors to regulate mitochondrial dynamics and crystal cell differentiation (Figure 5I). Deciphering how these regulators of mitochondrial architecture control lineage-specific progenitor differentiation requires further investigation.

Similar results were observed using the pan-hemocyte driver *e33CGal4*. *Drp1* overexpression or *Marf* KD in *asrij* null hemocytes (*arj9/arj9; e33CGal4/UAS Drp1* and *arj9/arj9; e33CGal4/UAS Marf RNAi*) rescued normal mitochondrial architecture (branch length and aggregation), comparable to control (*w1118*) (Supplementary Figure 7). However, although *Marf* KD rescued increased mitochondrial footprint (content) in *asrij* null hemocytes, *Drp1* overexpression could not. This suggests inefficient clearance of mitochondria even after *Drp1* overexpression. Also, it reaffirms our claim that elongation of mitochondria on *Asrij* depletion is mostly due to enhanced mitochondrial fusion rather than decreased fission. Crystal cell differentiation in the primary lobe increased in a synergistic manner upon *Drp1* OV or *Marf* KD in *asrij* null lymph gland (Supplementary Figure 8). Hence,

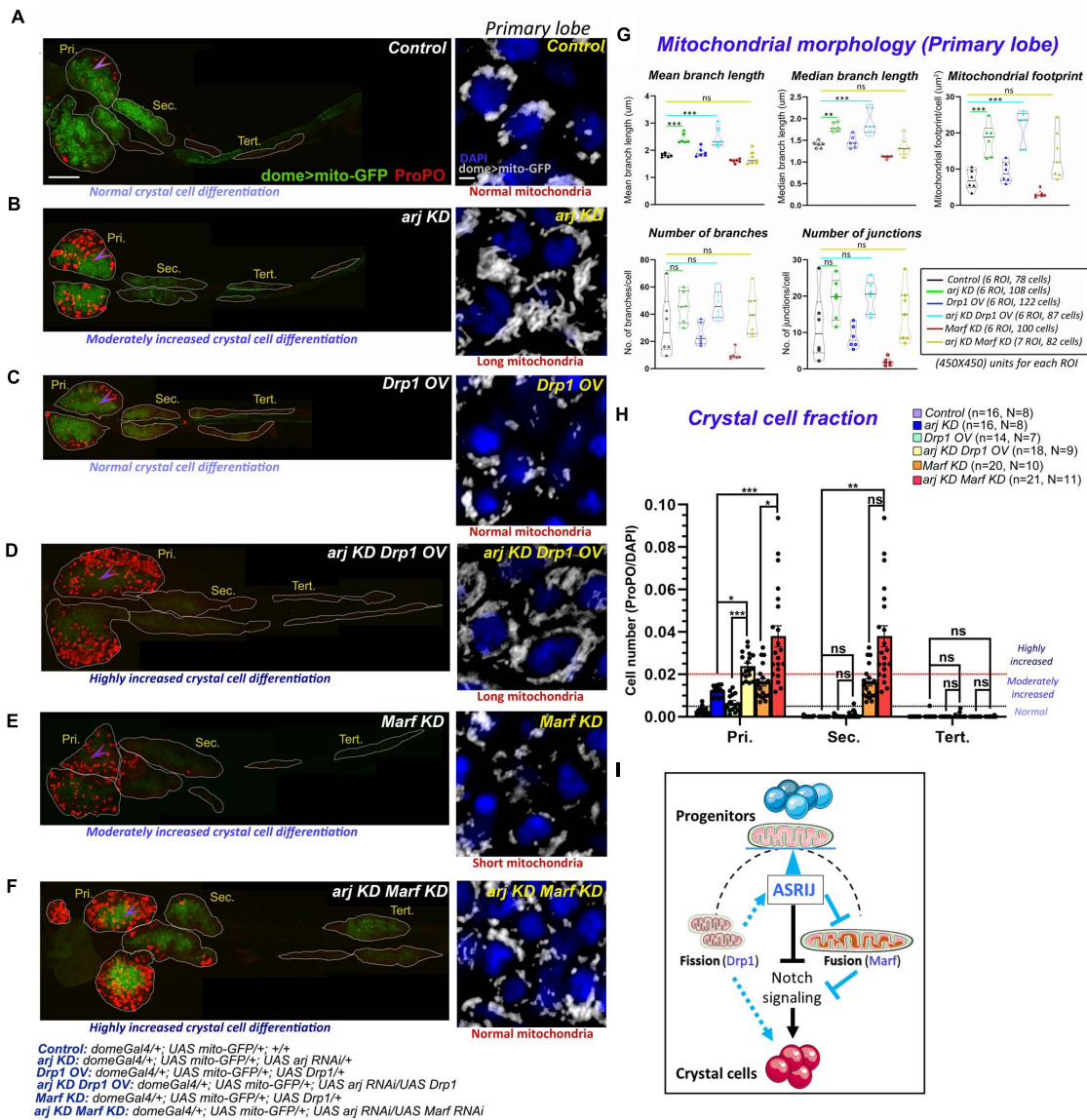


FIGURE 5 | Progenitor-specific genetic interaction of *asrij* with *Drp1* and *Marf* controls crystal cell differentiation in the lymph gland. **(A–F)** Whole mount lymph gland showing ProPO expression (far red pseudo-colored to red) to mark crystal cells in primary (Pri.), secondary (Sec.), and tertiary (Tert.) lobes of *control* **(A)**, *arj KD* **(B)**, *Drp1 OV* **(C)**, *arj KD Drp1 OV* **(D)**, *Marf KD* **(E)**, and *arj KD Marf KD* **(F)** larvae. The phenotypes of crystal cell differentiation are mentioned below each lymph gland image. The detailed genotypes are mentioned below the images panel for lymph gland. Scale bar: 100 µm. Mitochondrial morphology (*dome > mito-GFP* expression) in the primary lobe progenitors (marked by arrowhead) is shown adjacent to the lymph gland images of the respective genotypes in gray scale. The phenotype of mitochondria morphology is mentioned below each image. Single confocal slice of 0.5 µm is represented for easy visualization of mitochondrial network. Scale bar: 5 µm. **(G,H)** Mitochondrial morphology analysis is shown for the abovementioned genotypes **(G)**. Bar diagrams show quantification of ProPO positive cell fraction in different lobes of the same genotypes **(H)**. Error bars represent SEM. The values have been classified as normal (0–0.005), moderately increased (0.005–0.02) and highly increased (>0.02). n represents number of individual lymph gland lobes analyzed, and N represents number of larvae for each genotype. One-way ANOVA was performed to determine statistical significance for *mito-GFP* quantitation while Kruskal-Wallis test was performed for analysis of crystal cell fraction. **P* < 0.05, ***P* < 0.01, ****P* < 0.001, ns: non-significant. **(I)** Schematic representation of the effect of mitochondrial morphology and dynamics on blood cell differentiation. *Asrij* is a hub that maintains the balance (blue arrowhead) between mitochondrial fission and fusion to regulate progenitor maintenance and crystal cell differentiation. Arrows indicate activation. T symbol indicates inhibition. Black color indicates previously known interactions; blue color indicates effects reported in this study.

Drp1 overexpression and *Marf* depletion affect crystal cell differentiation in similar way upon loss of *Asrij*. This suggests *Asrij* depletion makes cells more susceptible to the effect of increasing fission or reducing fusion implying greater sensitivity

to mitochondrial dynamics. Hence, distinct functional networks connecting *Asrij* to the fission-fusion machinery may maintain normal mitochondrial dynamics and optimum differentiation of crystal cells.

DISCUSSION

Mitochondria play an indispensable role in cell fate choice both in healthy tissue and in diseased conditions (Zhang et al., 2018). Mitochondrial dysfunction underlies several cytopathological conditions including neurological disorders and cancers (Annesley and Fisher, 2019). Perturbed mitochondrial function in stem cells may affect their proliferation or differentiation (Seo et al., 2018). Recently genetic models have been used to validate the role of mitochondria in hematopoietic stem cell maintenance and differentiation (Diebold and Chandel, 2016; Filippi and Ghaffari, 2019). Here we combine analysis of an invertebrate *in vivo* model with an *in vitro* human stem cell model to understand the role of mitochondrial dynamics and its regulators in lineage specification.

Given the lack of information about mitochondrial morphology in *Drosophila* hematopoietic progenitors, we first undertook a detailed mapping in these cells. To fully exploit the power of the lymph gland model, we chose to analyze the progenitor population in all lobes of the lymph gland as these represent temporally distinct stages of progenitor maturation and differing propensity for differentiation. We found differences in mitochondrial morphology between more mature anterior progenitors and younger posterior progenitors. Further, analysis of the effect of modulating mitochondrial fission-fusion regulators as well as Asrij also showed different responses in progenitor subsets. Our results are in agreement with the idea that posterior progenitors differ from anterior ones in their identity and function. The physiological relevance of this appears to be context dependent – for example, Asrij-dependent mitochondrial phenotypes affect progenitor fate choice in the lymph gland but may have additional roles in differentiated hemocytes that merit further investigation. Our detailed studies position the *Drosophila* lymph gland as a relevant and accessible *in vivo* model to study mitochondrial regulation of progenitor heterogeneity that is not currently possible in vertebrate models. It would be interesting to see whether expression or activity of OCIAD1 within vertebrate stem cell pools can contribute to heterogeneity and fate choice through regulation of mitochondrial function.

Mitochondrial morphology is inextricably related to its function including oxidative phosphorylation (Wai and Langer, 2016). Therefore, mitochondrial dynamics could serve as a potential therapeutic target for several diseases with mitochondrial dysfunction (Brandner et al., 2019; Whitley et al., 2019). While the role of Drp1 and Mfn2 in mitochondrial dynamics is well established, their ability to regulate hematopoiesis in vertebrates has been reported only recently (Luchsinger et al., 2016; Hinge et al., 2020). Misexpression of DNMI1 and Mfn1/2 may underlie several human hematological malignancies including acute myeloid leukemia (AML), chronic myeloid leukemia (CML), chronic lymphocytic leukemia (CLL) and myelodysplastic syndromes^{1,2}. However, these ubiquitous regulators of mitochondrial dynamics

are not suitable therapeutic targets. Therefore, identification of tissue-restricted regulators of mitochondrial dynamics that are not essential for viability, is important.

Asrij, a pan-hematopoietic protein regulates hematopoiesis (Inamdar, 2003; Kulkarni et al., 2011), yet complete loss of Asrij does not cause lethality in *Drosophila* (Kulkarni et al., 2011) or in mouse (Sinha et al., 2019a). Hence, *asrij* null (*arj9/arj9*) flies serve as an excellent *in vivo* model for leukemia and hematopoietic anomalies. OCIAD1 has been implicated in several pathological conditions including ovarian carcinoma, myelodysplastic syndromes, and mitochondrial disorders (Praveen et al., 2020). Here using cross-species comparison and *in vivo* analysis, we show a conserved role for Asrij/OCIAD1 in regulating cell fate through mitochondrial dynamics. Asrij has an indispensable role in specifying myeloid biased fate of blood progenitors (Kulkarni et al., 2011; Sinha et al., 2019a). Asrij-dependent mitochondrial dynamics is a potential mechanism to regulate myeloid specification. Further we identify Asrij as a common modulator of mitochondrial fission and fusion that controls Notch signaling for crystal cell differentiation.

Asrij depletion causes elongation of mitochondria that could be rescued by suppressing mitochondrial fusion. OCIAD1 inhibits Complex I activity and oxygen consumption to suppress excessive early mesodermal progenitor formation from hESCs (Shetty et al., 2018). Hence, change in mitochondrial dynamics upon depletion or overexpression of OCIAD1 could possibly underpin its impact on respiration and downstream metabolic or signaling pathways.

We show that fission and fusion regulators Drp1 and Marf act through distinct networks to effect differentiation. Though Drp1 and Mfn2 play critical roles in mouse hematopoiesis, their role in lineage-specific signaling activation is unclear. Using the *Drosophila* lymph gland as an *in vivo* model of hematopoiesis, we find critical roles for canonical mitochondrial dynamics regulators such as Drp1 and Marf (dMfn) in blood cell differentiation. Drp1 and Marf play opposite roles in Notch activation for progenitor differentiation to crystal cells. Marf inhibits Notch activation and crystal cell differentiation whereas Drp1 may promote it. This is in concordance with previous reports showing opposing effects of Drp1 and Marf on developmental processes such as neuroblast and synaptic development in *Drosophila* larva (Mitra et al., 2012; Lee et al., 2013; Sandoval et al., 2014). Moreover, it supports a previously reported positive role of Drp1 in Notch activation in *Drosophila* germline and neural stem cells (Mitra et al., 2012; Lee et al., 2013). Hence, antagonistic roles of Drp1 and Marf in mitochondrial dynamics may mediate balanced activation of Notch signaling and lineage-specific differentiation of lymph gland progenitors.

Drp1 feeds back to activate Notch signaling in triple negative breast cancer cells which in turn can upregulate Drp1-dependent mitochondrial fission (Chen et al., 2018). On the other hand, we find that Marf KD promotes Notch activation. Hence, mitochondrial morphology/dynamics and Notch signaling can regulate each other. Further, Notch activation should result in fragmented mitochondria. Though Notch is activated on Asrij depletion (Kulkarni et al., 2011), mitochondria are elongated and this phenotype is rescued

¹<http://servers.binf.ku.dk/bloodspot>

²<https://cancer.sanger.ac.uk/cosmic>

by Marf KD, indicating that Asrij acts upstream to enhance Notch activation, which is in agreement with our earlier report. However, additional regulatory mechanisms may also be in play. Nevertheless, we show that a functional network of Asrij with canonical mitochondrial dynamics regulators (Drp1 and Marf) synergistically regulates crystal cell differentiation, a lineage downstream to Notch signaling. Mfn2 and DNML1 (Drp1) are reported as components of a proximity interaction network of OCIAD1, thus supporting further our claim of a direct functional interaction of Asrij with these canonical regulators of mitochondrial dynamics (Antonicka et al., 2020)³. Hence, Asrij-dependent Notch signaling may possibly lie downstream of the Asrij-dependent mitochondrial dynamics.

Despite extensive studies on the role of mitochondria in vertebrate hematopoiesis, their role in regulating lymph gland lineage choice remains elusive. ROS prime progenitors for differentiation to all hemocyte lineages (Owusu-Ansah and Banerjee, 2009). Even though ROS levels are susceptible to change with shift in mitochondrial dynamics (Bhandari et al., 2015; Senos Demarco and Jones, 2019), our results show that the impact of Drp1 or Marf depletion is limited to Notch pathway activation and crystal cell differentiation. This suggests additional mechanisms that may make plasmatocyte and lamellocyte differentiation sensitive to inhibition of mitochondrial fission or fusion.

It is quite possible that Asrij and Marf may have similar roles in some other aspects of mitochondrial function that regulate Notch activation. Probably that is why the combined knockdown of Asrij and Marf, although rescues mitochondrial morphology, cannot rescue increased crystal cell differentiation but rather enhances it synergistically. Previous studies have reported physical interaction of OCIAD1 with regulators of calcium signaling that depends on ER-mitochondria interaction (Floyd et al., 2016). This raises the possibility that other inter-organelle mechanisms may also be involved.

Posterior subsets of lymph gland progenitors resist differentiation upon infection as they are younger and developmentally less mature as compared to primary lobe progenitors. However, mechanisms that control posterior progenitor fate are only recently being understood (Krzemien et al., 2010; Rodrigues et al., 2021). Our results show progenitor-specific Marf depletion causes mild increase in plasmatocyte differentiation in secondary lobes suggesting mitochondrial fragmentation as a possible mechanism to trigger differentiation in posterior subsets of progenitors. Also, tertiary lobe progenitor population increases upon Marf depletion. This could be a basis for screens to identify reversal of such phenotypes and lead to novel position-specific regulators of progenitors.

Mitochondrial metabolism and dynamics are inter-dependent (Wai and Langer, 2016). We show a conserved role for Asrij in both mitochondrial morphology, dynamics, and function. Hence, Asrij/OCIAD1 may be a key conserved regulator that coordinates different facets of mitochondrial activity, to dictate cell fate decisions. We observed increased mitochondrial

content in Asrij depleted hemocytes. This could be due to impaired mitophagy that is often seen upon reduced fission or hyperfusion of the mitochondrial network (Twig et al., 2008). Although Marf depletion can reduce the mitochondrial content in Asrij depleted cells, Drp1 overexpression fails to do so suggesting that Drp1 cannot sufficiently promote mitochondria clearance, possibly through mitophagy, in Asrij depleted condition. This also indicates that mitochondrial fusion rather than fission has a pivotal role in Asrij-dependent blood cell homeostasis.

Both mitophagy and mitochondria-derived vesicle biogenesis control mitochondria quality. These pathways establish a functional link between mitochondria and endocytic compartments. Recent reports show a potential role of mitophagy in maintaining hematopoietic progenitors or stimulating hematopoiesis in vertebrates (Jin et al., 2018; Girotra et al., 2020). Such inter-organelle communications in signaling homeostasis and downstream cell fate specification could allow for complex spatial and temporal regulation. While canonical Notch signaling leads to crystal cell differentiation, non-canonical activation of Notch pathway due to stalling in endosomes of Asrij mutants (Kulkarni et al., 2011) may also contribute to the synergistic effects on phenotype. Asrij/OCIAD1 acts as a transmembrane scaffolding protein that regulates assembly and activation of critical signaling components and molecular complexes across organelles (Sinha et al., 2013; Le Vasseur et al., 2021). A recent report shows that OCIAD1 is a client of Prohibitin supramolecular complex that acts as a scaffold for the assembly of mitochondrial electron transport chain Complex III in HEK293T and U2OS cells (Le Vasseur et al., 2021). Hence, Asrij may potentially act as mediator of inter-organelle communication that may influence blood cell homeostasis.

Notch activation increases in secondary lobes upon Marf depletion suggesting that progenitors are primed, but not fully committed toward differentiation. This may also reflect their immature developmental stage and functional heterogeneity. Other mechanisms may operate to inhibit crystal cell differentiation (ProPO⁺) downstream to Notch activation in secondary lobes of Marf depleted lymph glands. Further, progenitor fraction in tertiary lobes increases upon Marf depletion indicating possible increase in progenitor proliferation. On the other hand, Drp1 depletion does not affect blood cell homeostasis in posterior lobes. Hence, Marf-dependent mitochondrial dynamics could be a position-dependent mechanism to regulate posterior progenitors. Further, it raises the possibility that a subset of dome + progenitors are biased toward crystal cell differentiation and that progenitors may differ in lineage potential. Importantly, this effect is position-dependent as dome + posterior progenitors in secondary lobes, even after undergoing mitochondrial fragmentation due to Marf depletion, fail to differentiate, unlike primary lobe progenitors. It also implies that the posterior identity of progenitors is maintained even on perturbing mitochondrial morphology, as they continue to be refractile to differentiation. Asrij depletion may unlock lineage differentiation potential to assist progenitor differentiation in posterior lobes.

³<https://thebiogrid.org/120280/summary/homo-sapiens/ociad1.html>

Even though we show the effect of progenitor-specific knockdown of *asrij*, *Drp1* and *Marf* on blood cell differentiation, any non-autonomous impact cannot be ruled out. Blood cell differentiation in such cases could be due to differentiation of the KD progenitor itself or due to signals originating from the KD progenitors that promote differentiation or trans-differentiation of intermediate progenitors or differentiated hemocytes. Our results show genetic interaction between *Asrij* and *Drp1*/*Marf* within the same pool of cells - either circulatory hemocytes or lymph gland progenitors. So, it is quite possible that the functional synergy to regulate crystal cell differentiation could be due to genetic interaction in the same cell. However, effect on crystal cell differentiation could be cell non-autonomous as well, which can be tested by mitotic mutant clone analysis.

Our data support an interplay of the blood cell enriched protein *Asrij* with mitochondrial dynamics regulators *Drp1* and *Marf* in lineage-specific differentiation. Given the ubiquitous requirement for *Drp1* and *Marf* and the pan-hemocyte expression of *Asrij*, it is quite unexpected to see such lineage specific effects. These insights validate our use of *Drosophila* genetics and the *in vivo* lymph gland hematopoiesis model to uncover such complex and unique interactions. Further they reveal *Asrij* as a critical regulatory node connecting mitochondrial dynamics, Notch signaling and crystal cell differentiation. Our findings suggest that the functional output of mitochondrial dynamics may be beyond simply the mitochondrial network architecture and depends on other unidentified factors linked to the dynamicity of this network. Modulating mitochondrial dynamics *in vitro* can serve as a way to promote or inhibit lineage-specific differentiation for therapeutic purposes. In summary, *Asrij*-regulated mitochondrial dynamics emerge as a potential conserved mechanism to maintain blood cell homeostasis.

DATA AVAILABILITY STATEMENT

The original contributions presented in the study are included in the article/**Supplementary Materials**, further inquiries can be directed to the corresponding author/s.

AUTHOR CONTRIBUTIONS

AR performed the experiments. MI contributed reagents and materials. All authors designed research, analyzed the data, wrote

REFERENCES

- Annesley, S. A., and Fisher, P. R. (2019). Mitochondria in health and disease. *Cells* 8:680. doi: 10.3390/cells8070680
- Anso, E., Weinberg, S. E., Diebold, L. P., Thompson, B. J., Malinge, S., Schumacker, P. T., et al. (2017). The mitochondrial respiratory chain is essential for haematopoietic stem cell function. *Nat. Cell Biol.* 19, 614–625. doi: 10.1038/ncb3529

the manuscript, contributed to the article, and approved the submitted version.

FUNDING

This work was funded by grants to MI from SERB (Grant no. EMR/2016/000641) and JC Bose fellowship (Grant no. JCB/2019/000020), Department of Science and Technology, Government of India; Department of Biotechnology (Grant no. BT/PR23947/MED/31/372/2017), Government of India, and Jawaharlal Nehru Centre for Advanced Scientific Research (JNCASR), Bangalore.

ACKNOWLEDGMENTS

We thank JNCASR confocal facility and NCBS Fly Facility for access.

SUPPLEMENTARY MATERIAL

The Supplementary Material for this article can be found online at: <https://www.frontiersin.org/articles/10.3389/fcell.2021.643444/full#supplementary-material>

Supplementary Figure 1 | (related to **Figure 1**) *Asrij* regulates mitochondrial morphology in *Drosophila* circulatory hemocytes.

Supplementary Figure 2 | (related to **Figure 1** and **Supplementary Figure 1**) *Asrij* overexpression affects mitochondrial network architecture in hemocytes.

Supplementary Figure 3 | (related to **Figure 2**) OCIAD1 overexpression affects mitochondrial dynamics in hESCs.

Supplementary Figure 4 | (related to **Figures 3–5**) NRE-GFP expression increases upon *asrij* knockdown.

Supplementary Figure 5 | (related to **Figures 3, 4**) *Drp1* and *Marf* regulate blood cell homeostasis in *Drosophila* lymph gland.

Supplementary Figure 6 | (related to **Figures 3, 4**) Overexpression of *Drp1* and *Marf* differentially affect crystal cell differentiation in *Drosophila* lymph gland.

Supplementary Figure 7 | (related to **Figure 5**) Genetic interaction of *asrij* with *Drp1* and *Marf* controls mitochondrial network architecture in circulatory hemocytes.

Supplementary Figure 8 | (related to **Figure 5**) Pan-hemocyte-specific genetic interaction of *asrij* with *Drp1* and *Marf* controls crystal cell differentiation in lymph gland.

Supplementary Video 1 | (related to **Figure 2**) *Asrij* regulates mitochondrial dynamics in hemocytes.

Antonicka, H., Lin, Z. Y., Janer, A., Aaltonen, M. J., Weraarpachai, W., Gingras, A. C., et al. (2020). A high-density human mitochondrial proximity interaction network. *Cell Metab.* 32, 479–497.e9. doi: 10.1016/j.cmet.2020.07.017

Atkins, K., Dasgupta, A., Chen, K. H., Mewburn, J., and Archer, S. L. (2016). The role of *Drp1* adaptor proteins MiD49 and MiD51 in mitochondrial fission: implications for human disease. *Clin. Sci. (Lond.)* 130, 1861–1874. doi: 10.1042/CS20160030

- Banerjee, U., Girard, J. R., Goins, L. M., and Spratford, C. M. (2019). *Drosophila* as a genetic model for hematopoiesis. *Genetics* 211, 367–417. doi: 10.1534/genetics.118.300223
- Bejarano-Garcia, J. A., Millan-Ucles, A., Rosado, I. V., Sanchez-Abarca, L. I., Caballero-Velazquez, T., Duran-Galvan, M. J., et al. (2016). Sensitivity of hematopoietic stem cells to mitochondrial dysfunction by SdhD gene deletion. *Cell Death Dis.* 7:e2516. doi: 10.1038/cddis.2016.411
- Bhandari, P., Song, M., and Dorn, G. W. II (2015). Dissociation of mitochondrial from sarcoplasmic reticular stress in *Drosophila* cardiomyopathy induced by molecularly distinct mitochondrial fusion defects. *J. Mol. Cell Cardiol.* 80, 71–80. doi: 10.1016/j.yjmcc.2014.12.018
- Blanco-Oregon, D., Katz, M. J., Durrieu, L., Gandara, L., and Wappner, P. (2020). Context-specific functions of Notch in *Drosophila* blood cell progenitors. *Dev. Biol.* 462, 101–115. doi: 10.1016/j.ydbio.2020.03.018
- Brandner, A., De Vecchis, D., Baaden, M., Cohen, M. M., and Taly, A. (2019). Physics-based oligomeric models of the yeast mitofusin Fzo1 at the molecular scale in the context of membrane docking. *Mitochondrion* 49, 234–244. doi: 10.1016/j.mito.2019.06.010
- Chen, L., Zhang, J., Lyu, Z., Chen, Y., Ji, X., Cao, H., et al. (2018). Positive feedback loop between mitochondrial fission and Notch signaling promotes survivin-mediated survival of TNBC cells. *Cell Death Dis.* 9:1050. doi: 10.1038/s41419-018-1083-y
- Cho, B., Yoon, S.-H., Lee, D., Koranteng, F., Tattikota, S. G., Cha, N., et al. (2020). Single-cell transcriptome maps of myeloid blood cell lineages in *Drosophila*. *BioRxiv* [Preprint]. doi: 10.1101/2020.01.15.908350
- Diebold, L. P., and Chandel, N. S. (2016). HSC fate is tethered to mitochondria. *Cell Stem Cell* 18, 303–304. doi: 10.1016/j.stem.2016.02.007
- Detmer, S. A., and Chan, D. C. (2007). Functions and dysfunctions of mitochondrial dynamics. *Nat. Rev. Mol. Cell Biol.* 8, 870–879. doi: 10.1038/nrm2275
- Duvic, B., Hoffmann, J. A., Meister, M., and Royet, J. (2002). Notch signaling controls lineage specification during *Drosophila* larval hematopoiesis. *Curr. Biol.* 12, 1923–1927. doi: 10.1016/s0960-9822(02)01297-6
- Filippi, M.-D., and Ghaffari, S. (2019). Mitochondria in the maintenance of hematopoietic stem cells: new perspectives and opportunities. *Blood* 133, 1943–1952. doi: 10.1182/blood-2018-10-808873
- Floyd, B. J., Wilkerson, E. M., Veling, M. T., Minogue, C. E., Xia, C., Beebe, E. T., et al. (2016). Mitochondrial protein interaction mapping identifies regulators of respiratory chain function. *Mol. Cell* 63, 621–632. doi: 10.1016/j.molcel.2016.06.033
- Girotra, M., Naveiras, O., and Vannini, N. (2020). Targeting mitochondria to stimulate hematopoiesis. *Aging* 12, 1042–1043. doi: 10.18632/aging.102807
- Hinge, A., He, J., Bartram, J., Javier, J., Xu, J., Fjellman, E., et al. (2020). Asymmetrically segregated mitochondria provide cellular memory of hematopoietic stem cell replicative history and drive HSC attrition. *Cell Stem Cell* 26, 420–430.e6. doi: 10.1016/j.stem.2020.01.016
- Inamdar, M. S. (2003). *Drosophila asrij* is expressed in pole cells, trachea and hemocytes. *Dev. Genes Evol.* 213, 134–137. doi: 10.1007/s00427-003-0305-0
- Jin, G., Xu, C., Zhang, X., Long, J., Rezaeian, A. H., Liu, C., et al. (2018). Atad3a suppresses Pink1-dependent mitophagy to maintain homeostasis of hematopoietic progenitor cells. *Nat. Immunol.* 19, 29–40. doi: 10.1038/s41590-017-0002-1
- Jung, S. H., Evans, C. J., Uemura, C., and Banerjee, U. (2005). The *Drosophila* lymph gland as a developmental model of hematopoiesis. *Development* 132, 2521–2533. doi: 10.1242/dev.01837
- Kasahara, A., Cipolat, S., Chen, Y., Dorn, G. W. II, and Scorrano, L. (2013). Mitochondrial fusion directs cardiomyocyte differentiation via calcineurin and Notch signaling. *Science* 342, 734–737. doi: 10.1126/science.1241359
- Khacho, M., Clark, A., Svoboda, D. S., Azzi, J., MacLaurin, J. G., Meghaizel, C., et al. (2016). Mitochondrial dynamics impacts stem cell identity and fate decisions by regulating a nuclear transcriptional program. *Cell Stem Cell* 19, 232–247. doi: 10.1016/j.stem.2016.04.015
- Khadilkar, R. J., Rodrigues, D., Mote, R. D., Sinha, A. R., Kulkarni, V., Magadi, S. S., et al. (2014). ARF1-GTP regulates Asrij to provide endocytic control of *Drosophila* blood cell homeostasis. *Proc. Natl. Acad. Sci. U.S.A.* 111, 4898–4903. doi: 10.1073/pnas.1303559111
- Krzemien, J., Oyallon, J., Crozatier, M., and Vincent, A. (2010). Hematopoietic progenitors and hemocyte lineages in the *Drosophila* lymph gland. *Dev. Biol.* 346, 310–319. doi: 10.1016/j.ydbio.2010.08.003
- Kulkarni, V., Khadilkar, R. J., Magadi, S. S., and Inamdar, M. S. (2011). Asrij maintains the stem cell niche and controls differentiation during *Drosophila* lymph gland hematopoiesis. *PLoS One* 6:e27667. doi: 10.1371/journal.pone.0027667
- Le Vasseur, M., Friedman, J., Jost, M., Xu, J., Yamada, J., Kampmann, M., et al. (2021). Genome-wide CRISPRi screening identifies OCIAD1 as a prohibitin client and regulatory determinant of mitochondrial Complex III assembly in human cells. *eLife* 10:e67624. doi: 10.7554/eLife.67624
- Lebestky, T., Jung, S. H., and Banerjee, U. (2003). A serrate-expressing signaling center controls *Drosophila* hematopoiesis. *Genes Dev.* 17, 348–353. doi: 10.1101/gad.1052803
- Lee, K. S., Wu, Z., Song, Y., Mitra, S. S., Feroze, A. H., Cheshier, S. H., et al. (2013). Roles of PINK1, mTORC2, and mitochondria in preserving brain tumor-forming stem cells in a noncanonical Notch signaling pathway. *Genes Dev.* 27, 2642–2647. doi: 10.1101/gad.225169.113
- Lee, S. Y., Kang, M. G., Shin, S., Kwak, C., Kwon, T., Seo, J. K., et al. (2017). Architecture mapping of the inner mitochondrial membrane proteome by chemical tools in live cells. *J. Am. Chem. Soc.* 139, 3651–3662. doi: 10.1021/jacs.6b10418
- Liesa, M., and Shirihi, O. S. (2013). Mitochondrial dynamics in the regulation of nutrient utilization and energy expenditure. *Cell Metab.* 17, 491–506. doi: 10.1016/j.cmet.2013.03.002
- Liu, Y. J., McIntyre, R. L., Janssens, G. E., and Houtkooper, R. H. (2020). Mitochondrial fission and fusion: a dynamic role in aging and potential target for age-related disease. *Mech. Ageing Dev.* 186:11212. doi: 10.1016/j.mad.2020.11212
- Luchsinger, L. L., de Almeida, M. J., Corrigan, D. J., Mumau, M., and Snoecker, H. W. (2016). Mitofusin 2 maintains haematopoietic stem cells with extensive lymphoid potential. *Nature* 529, 528–531. doi: 10.1038/nature16500
- Mitra, K., Rikhy, R., Lilly, M., and Lippincott-Schwartz, J. (2012). DRP1-dependent mitochondrial fission initiates follicle cell differentiation during *Drosophila* oogenesis. *J. Cell Biol.* 197, 487–497. doi: 10.1083/jcb.201110058
- Ni, H. M., Williams, J. A., and Ding, W. X. (2015). Mitochondrial dynamics and mitochondrial quality control. *Redox Biol.* 4, 6–13. doi: 10.1016/j.redox.2014.11.006
- Owusu-Ansah, E., and Banerjee, U. (2009). Reactive oxygen species prime *Drosophila* haematopoietic progenitors for differentiation. *Nature* 461, 537–541. doi: 10.1038/nature08313
- Praveen, W., Sinha, S., Batabyal, R., Kamat, K., and Inamdar, M. S. (2020). The OCIAD protein family: comparative developmental biology and stem cell application. *Int. J. Dev. Biol.* 64, 223–235. doi: 10.1387/ijdb.190038mi
- Rodrigues, D., Renaud, Y., VijayRaghavan, K., Waltzer, L., and Inamdar, M. S. (2021). Differential activation of JAK-STAT signaling reveals functional compartmentalization in *Drosophila* blood progenitors. *eLife* 10:e61409. doi: 10.7554/eLife.61409
- Sandoval, H., Yao, C. K., Chen, K., Jaiswal, M., Donti, T., Lin, Y. Q., et al. (2014). Mitochondrial fusion but not fission regulates larval growth and synaptic development through steroid hormone production. *eLife* 3:e03558. doi: 10.7554/eLife.03558
- Senos Demarco, R., and Jones, D. L. (2019). Mitochondrial fission regulates germ cell differentiation by suppressing ROS-mediated activation of epidermal growth factor signaling in the *Drosophila* larval testis. *Sci. Rep.* 9:19695. doi: 10.1038/s41598-019-55728-0
- Seo, B. J., Yoon, S. H., and Do, J. T. (2018). Mitochondrial dynamics in stem cells and differentiation. *Int. J. Mol. Sci.* 19, 3893. doi: 10.3390/ijms19123893
- Shetty, D. K., Kalamkar, K. P., and Inamdar, M. S. (2018). OCIAD1 controls electron transport chain complex I Activity to regulate energy metabolism in human pluripotent stem cells. *Stem Cell Rep.* 11, 128–141. doi: 10.1016/j.stemcr.2018.05.015

- Sinha, A., Khadilkar, R. J., S, V. K., Roychowdhury Sinha, A., and Inamdar, M. S. (2013). Conserved regulation of the Jak/STAT pathway by the endosomal protein asrij maintains stem cell potency. *Cell Rep.* 4, 649–658. doi: 10.1016/j.celrep.2013.07.029
- Sinha, S., Dwivedi, T. R., Yengkhom, R., Bheemsetty, V. A., Abe, T., Kiyonari, H., et al. (2019a). Asrij/OCIAD1 suppresses CSN5-mediated p53 degradation and maintains mouse hematopoietic stem cell quiescence. *Blood* 133, 2385–2400. doi: 10.1182/blood.2019000530
- Sinha, S., Ray, A., Abhilash, L., Kumar, M., Sreenivasamurthy, S. K., Keshava Prasad, T. S., et al. (2019b). Proteomics of asrij perturbation in *Drosophila* lymph glands for identification of new regulators of hematopoiesis. *Mol. Cell Proteomics* 18, 1171–1182. doi: 10.1074/mcp.RA119.001299
- Small, C., Ramroop, J., Otazo, M., Huang, L. H., Saleque, S., and Govind, S. (2014). An unexpected link between notch signaling and ROS in restricting the differentiation of hematopoietic progenitors in *Drosophila*. *Genetics* 197, 471–483. doi: 10.1534/genetics.113.159210
- Tattikota, S. G., Cho, B., Liu, Y., Hu, Y., Barrera, V., Steinbaugh, M. J., et al. (2020). A single-cell survey of *Drosophila* blood. *eLife* 9:e54818. doi: 10.7554/eLife.54818
- Tilokani, L., Nagashima, S., Paupe, V., and Prudent, J. (2018). Mitochondrial dynamics: overview of molecular mechanisms. *Essays Biochem.* 62, 341–360. doi: 10.1042/EBC20170104
- Twig, G., Elorza, A., Molina, A. J., Mohamed, H., Wikstrom, J. D., Walzer, G., et al. (2008). Fission and selective fusion govern mitochondrial segregation and elimination by autophagy. *EMBO J.* 27, 433–446. doi: 10.1038/sj.emboj.7601963
- Valente, A. J., Maddalena, L. A., Robb, E. L., Moradi, F., and Stuart, J. A. (2017). A simple imageJ macro tool for analyzing mitochondrial network morphology in mammalian cell culture. *Acta Histochem.* 119, 315–326. doi: 10.1016/j.acthis.2017.03.001
- van der Blik, A. M., Shen, Q., and Kawajiri, S. (2013). Mechanisms of mitochondrial fission and fusion. *Cold Spring Harb. Perspect. Biol.* 5:a011072. doi: 10.1101/cshperspect.a011072
- Wai, T., and Langer, T. (2016). Mitochondrial dynamics and metabolic regulation. *Trends Endocrinol. Metab.* 27, 105–117. doi: 10.1016/j.tem.2015.12.001
- Whitley, B. N., Engelhart, E. A., and Hoppins, S. (2019). Mitochondrial dynamics and their potential as a therapeutic target. *Mitochondrion* 49, 269–283. doi: 10.1016/j.mito.2019.06.002
- Zhang, H., Menzies, K. J., and Auwerx, J. (2018). The role of mitochondria in stem cell fate and aging. *Development* 145:dev143420.

Conflict of Interest: The authors declare that the research was conducted in the absence of any commercial or financial relationships that could be construed as a potential conflict of interest.

Copyright © 2021 Ray, Kamat and Inamdar. This is an open-access article distributed under the terms of the Creative Commons Attribution License (CC BY). The use, distribution or reproduction in other forums is permitted, provided the original author(s) and the copyright owner(s) are credited and that the original publication in this journal is cited, in accordance with accepted academic practice. No use, distribution or reproduction is permitted which does not comply with these terms.

1 **Charting ESCRT function reveals distinct and non-compensatory roles in blood progenitor**
2 **maintenance and lineage choice in *Drosophila***

3

4 Arindam Ray, Yashashwinee Rai, Maneesha S Inamdar

5 Molecular Biology and Genetics Unit, Jawaharlal Nehru Centre for Advanced Scientific Research,
6 Jakkur, Bangalore-560064, India

7

8 **Abstract**

9 Tissue heterogeneity permits diverse biological outputs in response to systemic signals but requires
10 context-dependent spatiotemporal regulation of a limited number of signaling circuits. In addition to
11 their stereotypical roles of transport and cargo sorting, endocytic networks provide rapid, adaptable,
12 and often reversible means of signaling. Aberrant function of the Endosomal Sorting Complex
13 Required for Transport (ESCRT) components results in ubiquitinated cargo accumulation, uncontrolled
14 signaling and neoplastic transformation. However, context-specific effects of ESCRT on developmental
15 decisions are not resolved. By a comprehensive spatiotemporal profiling of ESCRT in *Drosophila*
16 hematopoiesis *in vivo*, here we show that pleiotropic ESCRT components have distinct effects on blood
17 progenitor maintenance, lineage choice and response to immune challenge. Of all 13 core ESCRT
18 components tested, only Vps28 and Vp36 were required in all progenitors, whereas others maintained
19 spatiotemporally defined progenitor subsets. ESCRT depletion also sensitized posterior progenitors
20 that normally resist differentiation, to respond to immunogenic cues. Depletion of the critical Notch
21 signaling regulator Vps25 did not promote progenitor differentiation at steady state but made
22 younger progenitors highly sensitive to wasp infestation, resulting in robust lamellocyte
23 differentiation. We identify key heterotypic roles for ESCRT in controlling Notch activation and thereby
24 progenitor proliferation and differentiation. Further, we show that ESCRT ability to regulate Notch
25 activation depends on progenitor age and position along the anterior-posterior axis. The phenotypic
26 range and disparity in signaling upon depletion of components provides insight into how ESCRT may
27 tailor developmental diversity. These mechanisms for subtle control of cell phenotype may be
28 applicable in multiple contexts.

29

30 **Keywords**

31 Blood cell homeostasis, Endosomal protein sorting, ESCRT, Progenitor homeostasis, Lineage choice,
32 Ubiquitination, NICD, Notch signaling, Crystal Cell, Progenitor heterogeneity, Lamellocytes

33 **Significance**

34 The Endosomal Sorting Complex Required for Transport (ESCRT) machinery sorts ubiquitinated cargo
35 for degradation or recycling. Aberrant ESCRT function is associated with many blood disorders. We
36 did a comprehensive functional analysis of all 13 core ESCRT components in maintenance and
37 differentiation of *Drosophila* larval blood progenitors. We show that ESCRT have diverse and non-
38 compensatory functions in blood progenitors. ESCRT depletion from progenitors affects ubiquitination
39 status cell autonomously and independent of progenitor maintenance. ESCRT function is more critical
40 to maintain older progenitors and to prevent Notch-dependent crystal cell differentiation. Further,
41 ESCRT depletion sensitizes refractile younger progenitors for lamellocyte differentiation. Our *in situ*
42 developmental map of ESCRT function reveals critical checkpoints for cell fate choice and new
43 paradigms for generating progenitor heterogeneity.

44 **Introduction**

45 Tissue patterning requires spatiotemporally controlled cell proliferation, progenitor specification and
46 lineage differentiation. While a limited number of signaling circuits impact these complex cell
47 properties, their context-dependent regulation elicits multiple diverse biological outputs. Endocytic
48 trafficking can maintain, attenuate or amplify signaling to regulate inter or intracellular
49 communication [1]. In addition to their stereotypical roles of transport and cargo sorting, endocytic
50 networks can regulate the behaviour of individual cells as well as groups or collectives, thereby
51 significantly impacting tissue homeostasis.

52 Protein trafficking and turnover through the endolysosomal route allows rapid post-translational
53 adjustment of signal transduction efficiency. The conserved Endosomal Sorting Complex Required for
54 Transport (ESCRT) actively controls the sorting of ubiquitinated cargoes for lysosomal degradation.
55 This hetero-multimeric complex consists of four subunits (ESCRT-0, I, II and III) that are sequentially
56 recruited onto endomembrane-bound ubiquitinated cargoes, allowing them to be sequestered in the
57 intraluminal vesicles (ILV) of the multivesicular bodies (MVB). The initial steps of recognition and
58 binding of ubiquitinated cargoes, converge into the subsequent crucial steps of membrane
59 remodelling during ILV formation. ESCRT components act in a co-operative manner, following defined
60 molecular stoichiometry, to successfully sequester cargoes for degradation. Hence, phenotypic
61 diversity of ESCRT mutants is rare in unicellular organisms like budding yeast. However, dysfunction
62 of metazoan ESCRT components can manifest as distinct and diverse cellular and histological
63 phenotypes such as defective MVB biogenesis and incorrect cell fate choice, tissue hyperproliferation,
64 apoptotic resistance, etc due to aberrant activation of signaling pathways such as Notch, EGFR and
65 JAK/STAT that alter tissue homeostasis[2-5].

66 Blood progenitors are exposed to a plethora of signals and need to respond to a rapidly changing
67 environment for stem- and progenitor cell maintenance and controlled differentiation. Previous
68 genetic screens and knockout-based functional analyses in both *Drosophila* and mouse models
69 showed a role of ESCRT in maturation of specific blood cell types in erythroid and lymphoid lineages
70 and a possible functional link of ESCRT to blood cell homeostasis [6-8]. Several key endosomal proteins
71 such as Rabex5, Atg6, Rab5 and Rab11 actively control endocytic trafficking and are implicated in
72 developmental signaling and blood cell homeostasis [9-13]. The blood cell-enriched conserved
73 endosomal regulator of hematopoiesis, Asrij interacts with ADP Ribosylation Factor 1 (ARF1-GTP),
74 regulates the endocytic proteome and maintains stemness of blood progenitors in the *Drosophila*
75 lymph gland [14]. Loss of Asrij promotes activation of Notch signaling in hematopoiesis, thereby
76 leading to precocious differentiation to crystal cells [14]. Also, *asrij* mutant hemocytes accumulate

77 Notch intracellular domain (NICD) in the sorting endosomes, mimicking an endosomal sorting defect.
78 Mouse Asrij also maintains hematopoietic stem cell quiescence [15]. This suggests conserved
79 mechanisms of endosomal protein sorting in blood cell homeostasis that merit further investigation.

80 The *Drosophila* larval lymph gland serves as a simple yet powerful model to study conserved
81 mechanisms of hematopoiesis *in situ*. Using this *in vivo* model, we investigated the role of ESCRT
82 components in spatiotemporal control of blood progenitor homeostasis and myelopoiesis. Blood
83 progenitors reside in the multi-lobed lymph gland that flanks the cardiac tube in segments T3 and A1.
84 The primary lobe of the lymph gland comprises of three distinct zones enriched in progenitors,
85 differentiated blood cells (plasmacytes, crystal cells and lamellocytes) and the hematopoietic niche.
86 Blood progenitors of *Drosophila* are linearly arranged in anterior (primary) and posterior lobes
87 (secondary, tertiary and often quaternary) of the lymph gland and are characterized by the expression
88 of several markers such as Domeless, TepIV and DE-Cadherin. The lymph gland develops in an anterior
89 to posterior sequence, with younger progenitors in the posterior lobes [16]. Previous studies showed
90 that the progenitor population is heterogeneous in gene expression, mitochondrial morphology and
91 dynamics, signaling, differentiation potential and immune function [16, 17]. Posterior progenitors are
92 refractile to immune challenge due to immature mitochondrial morphology and differential activation
93 of JAK/STAT and Notch signaling [16, 17]. The lymph gland harbors the entire blood progenitor
94 population of *Drosophila*, and hence allows complete sampling and a comprehensive study of
95 progenitor homeostasis.

96 The *Drosophila* ESCRT is comprised of 13 core components [2, 18]. ESCRT-0 (Hrs, Stam) binds to the
97 ubiquitinated cargoes through a ubiquitin-interacting motif. It then recruits ESCRT-I (Vps28, Tsg101,
98 Vps37A, Vps37B) and ESCRT-II (Vps25, Vps22 and Vps36), which act as a bridging complex to assemble
99 ESCRT-III (Vps32, Vps24, Vps20, Vps2). ESCRT-I-dependent membrane inward budding (negative
100 curvature) and ESCRT-III-dependent membrane scission lie at the heart of endosomal protein sorting,
101 resulting in the formation of intraluminal vesicles (ILV) containing the sequestered cargo [19]. Vps32
102 is the principal filament-forming component that undergoes activation and polymerization upon
103 binding with various nucleating factors and integrates previous steps of endosomal sorting [5]. The
104 final step involves disassembly of ESCRT subunits and scission of the membrane neck of the
105 intraluminal vesicles, which is mediated by the Vps4-Vta1 mechanoenzyme complex.

106 Here, we provide a functional map of the role of all 13 *Drosophila* core ESCRT components in
107 ubiquitinated cargo sorting and blood cell lineage choice across distinct progenitor subsets. We show
108 that though ESCRT components are expressed in all cells of the lymph gland (LG), their roles in
109 controlling lineage-specific differentiation and immune response of blood progenitors are distinct and

110 position-dependent. We also find that ESCRT dysfunction primarily affects Notch activation-
111 dependent crystal cell differentiation. Our study supports heterogeneity of blood progenitors and
112 highlights the role of ESCRT in spatiotemporal segregation of signaling.

113

114

115 **Materials and methods**

116 **Fly stocks and genetics**

117 *Drosophila melanogaster* stocks were maintained at 25°C as described previously [14]. The details of
118 fly stocks, genetics and control genotypes used are in supplementary methods.

119

120 **Immunostaining analysis**

121 *Drosophila* third instar larval lymph glands were dissected in PBS as described before and
122 immunostained for microscopic analysis [20]. The detailed protocol and reagents used are in
123 supplementary methods.

124

125 **Wasp parasitism assay**

126 Wasp infestation was performed following standardised protocol as described in Rodrigues et al.,
127 2021a [16]. Details are mentioned in supplementary methods.

128

129 **Quantification and statistical analysis**

130 Blood cell differentiation was quantified as described in Ray et al., 2021 [17]. The details of
131 quantification of various parameters and statistical analysis are mentioned in supplementary
132 methods.

133

134

135

136 **Results**

137 **Divergent requirement for ESCRT components in ubiquitinated cargo sorting in the *Drosophila***
138 **lymph gland.**

139 To explore whether ESCRT function may determine blood progenitor identity or potential, we
140 depleted each of the 13 core ESCRT components individually in the lymph gland by RNAi mediated
141 knockdown (KD) in domeless (*dome*) expressing blood progenitors (*domeGal4>UAS ESCRT RNAi*). As
142 ESCRT plays an active role in ubiquitinated cargo sorting, the accumulation of ubiquitinated cargoes
143 serves as a hallmark of dysfunctional ESCRT machinery and impaired endosomal protein sorting. A
144 comprehensive analysis of conjugated ubiquitination (Ub) status (see methods) in the primary,
145 secondary and tertiary lobes by immunostaining the complete lymph gland showed a range of effects
146 with the phenotype varying among ESCRT components within a given ESCRT complex and between
147 complexes.

148 Control LG showed low or no Ub in primary, secondary, and tertiary lobes (Fig 1A, B). A similar trend
149 was seen on depletion of ESCRT-0 components Hrs or Stam, with an occasional increase in Ub in
150 primary lobes, which was not significant (Figure 1A, B). In contrast ESCRT-I, -II and -III depletion had
151 effects on all lobes, though not all components affected the Ub status. Among ESCRT-I components
152 (Vps28, Tsg101, Vps37A, Vps37B), depletion of Vps28 or Tsg101 very significantly increased Ub in the
153 primary lobe, Vps28 and Vps37A affected the secondary lobe and Vps37A showed an increase in Ub
154 in the tertiary lobe. Vps37B depletion had a mild non-significant effect on the Ub status of the LG
155 (Figure 1A, B). ESCRT-II components Vps25, Vps22 and Vps36 had no effect on the primary lobe.
156 However, Vps22 depletion caused a dramatic increase in Ub in the secondary and tertiary lobes, where
157 Vps25 and Vps36 depletion had no effect. Finally, depletion of ESCRT-III components (Vps32, Vps20
158 and Vps2) caused a significant increase in Ub in the primary lobes whereas secondary and tertiary
159 lobes were sensitive only to Vps20 depletion.

160 In summary, our data indicates non-uniform response of progenitors to perturbation of the cargo
161 sorting machinery, depending on the ESCRT component that is depleted as well as the target
162 progenitor population (Figure 1B schematic). Of the 13 core ESCRT components, 7 caused increased
163 Ub in the LG when depleted. Interestingly, the effects were not uniform amongst progenitor subsets
164 - 5 affected Ub status in the primary lobes, 4 in the secondary lobes and 3 in the tertiary lobes. This is
165 in agreement with the anterior-posterior developmental and functional heterogeneity of progenitors
166 reported earlier [16] and suggests that younger progenitors have a reduced requirement for ESCRT
167 function. Thus, our analysis provides a spatiotemporal correlation of Ub status to ESCRT depletion in

168 LG progenitor subsets. We next tested whether this correlation reflects the response of progenitors
169 to maintenance and differentiation cues.

170

171 **ESCRT components play distinct roles in lymph gland progenitor maintenance.**

172 As ESCRT components regulate ubiquitinated cargo sorting in the blood progenitors, they might
173 potentially regulate progenitor homeostasis. Hence, we checked whether depleting the 13 ESCRT
174 components individually from *dome*⁺ progenitor subsets (marked by GFP expression)
175 (*domeGal4>2XEGFP/+; UAS ESCRT-RNAi/+; +/+*) may affect progenitor status similar to the effect on
176 Ub accumulation. As in the case of Ub status, a comprehensive analysis of progenitor fraction (see
177 methods) in the primary, secondary, and tertiary lobes of the lymph gland showed a range of effects
178 with the phenotype varying among ESCRT components within a complex and between complexes
179 (Figure 2A, B). Assessment of mitotically active nuclei and cell counts showed that ESCRT affects
180 proliferation of blood progenitors (Fig S1A-C; see supplementary results).

181 In controls, anterior lymph gland lobe progenitors are restricted to the inner medullary zone (MZ)
182 while the posterior lobes are composed almost entirely of progenitors [16]. ESCRT-0 (Hrs, Stam)
183 knockdown did not show any significant change in progenitor status indicating non-essential roles for
184 these in progenitor maintenance (Fig 2A, B). Depletion of ESCRT-I components Vps28 and Tsg101
185 caused reduction in progenitor fraction in the primary lobes whereas secondary lobe progenitors were
186 reduced by depletion of Vps28, Vps37A or Vps37B but not of Tsg101. Interestingly, ESCRT-I
187 components had no effect on tertiary lobe progenitors. Among ESCRT-II components, Vps25 had an
188 effect on proliferation causing an absolute increase in primary lobe cell numbers with a concomitant
189 decrease in progenitor fraction (Fig 2A, B; S1A, C; S6; Supplementary results). Vps22 also did not affect
190 LG progenitor fraction. In contrast, Vps36 drastically reduced progenitor fraction in all LG lobes, with
191 phenotype severity increasing from anterior to posterior. ESCRT-III had very restricted effects on
192 progenitors with Vps32 KD causing a reduction only in anterior progenitors, Vps2 KD reduced both
193 anterior and posterior progenitors and Vps24 and Vps20 had no effect (Fig. 2A-C).

194 Since increased Ub accumulation indicates dysfunctional cargo sorting and this is likely a cause of
195 progenitor loss, we compared Ub status on ESCRT KD with progenitor maintenance. Superimposition
196 of the phenotype chart for each of these (Fig 6B, C) showed that there was no absolute correlation
197 between increased Ub and reduced progenitor numbers in older (primary lobe) or younger (posterior
198 lobes) progenitors. While knockdown of some ESCRT components [(Vps28, Tsg101 (ESCRT-I), Vps32
199 and Vps2 (ESCRT-III)] caused increased Ub and reduced progenitors in the primary lobe, others

200 [(Vps25, Vps36 (ESCRT-II)) showed no change in Ub but progenitor numbers were reduced. Similarly,
201 knockdown of Vps20 (ESCRT-III) had increased Ub but no effect on progenitors. Hence in addition to
202 Ub cargo sorting, ESCRT components Vps25 and Vps36 have a critical independent role in progenitor
203 maintenance. Notably, there was no correlation at all between Ub increase and progenitor reduction
204 in the youngest progenitors (tertiary lobe). This suggests that notwithstanding defects in cargo sorting,
205 posterior progenitors remain less sensitive to perturbation, indicating that they are maintained by
206 other robust mechanisms.

207

208 **Older progenitors are more prone to plasmatocyte differentiation upon ESCRT depletion**

209 Plasmatocytes, marked by P1 expression, make up about 95% of the differentiated hemocyte
210 population. In the LG, they are restricted to the cortical zone of the primary lobe, with occasional P1
211 positive cells seen in posterior lobes. Reduced progenitor numbers are expected to be accompanied
212 by an increase in the plasmatocyte population due to differentiation. Enumeration of P1 positive cells
213 in the ESCRT KD LG (*domeGal4 UAS 2XEGFP > UAS ESCRT RNAi*) showed an expected increase in the
214 plasmatocyte fraction of the primary lobe for Vps28, Tsg101, Vps36 and Vps32, where the progenitor
215 fraction was mostly reduced (Fig 2A, C) However, Vps25 depletion had no apparent effect on
216 differentiation. This could be due to the failure of progenitors to terminally differentiate into
217 plasmatocytes or due to non-autonomous overproliferation of the intermediate population.
218 Additionally, Vps22 KD also showed increased plasmatocyte numbers though there was no significant
219 effect on the progenitor fraction, suggesting possible non-autonomous overproliferation or
220 exhaustion of the intermediate population. The remaining ESCRT components had no effect on
221 primary lobe plasmatocytes. Interestingly, KD of ESCRT-0 component Hrs and ESCRT-III component
222 Vps32, that had no effect on progenitors, caused an increase in plasmatocyte numbers only in the
223 secondary lobes. This indicates that though there is no effect as assessed by progenitor marker
224 analysis, Hrs or Vps32 depletion has sensitized the tissue to respond to proliferation and
225 differentiation cues. Along similar lines, Vps36 and Vps2 depletion drastically reduced the secondary
226 progenitor fraction and increased plasmatocyte differentiation. Except for Vps28, ESCRT KD did not
227 induce plasmatocytes in the tertiary lobes, even when progenitors were lost (e.g. Vps36 KD and Vps2
228 KD).

229

230

231 **ESCRT components are most effective in suppressing the crystal cell lineage.**

232 Crystal cells make up only about 5% of the differentiated hemocyte pool. Under steady state
233 conditions each primary lobe harbors approximately 0-10 crystal cells, while they are generally absent
234 from posterior lobes, even upon immune challenge [16]. As seen earlier, 8 of the 13 core ESCRT
235 components affect progenitor numbers in one or more lobes (Fig 3A, B). Further these effects are
236 position-dependent. Hence, we next analysed crystal cell status by checking expression of ProPO in
237 the ESCRT depleted LGs.

238 Knockdown of 12 out of 13 ESCRTs increased crystal cell differentiation in the primary lobes. Vps25
239 depletion in the progenitors had no effect on crystal cell differentiation. Secondary lobes were
240 sensitive to depletion of Hrs, Vps28, Vps36 and Vps2 showing increased crystal cell numbers in all
241 cases. Tertiary lobes showed increase in crystal cell numbers only on Vps28 or Vps36 depletion. This
242 suggested that cargo sorting is critical to regulate crystal cell differentiation. Perturbation in the ESCRT
243 machinery results in activation of signaling pathways that promote crystal cells. Since Notch pathway
244 activation is a key requirement of crystal cell differentiation and Notch is a well-known target of
245 ESCRT-mediated cargo sorting [3, 21-23], we next checked for the status of Notch pathway activation
246 upon ESCRT depletion.

247

248 **ESCRT depletion in blood progenitors ectopically activates Notch signaling.**

249 Increased crystal cell differentiation upon depletion of some ESCRT components suggests that they
250 normally suppress Notch pathway activation. We focused our study on analysis of 8 ESCRT
251 components [Hrs, Stam (ESCRT-0); Vps28, Tsg101 (ESCRT-I); Vps25, Vps22 (ESCRT-II); Vps32, Vps24
252 (ESCRT-III)] as these are well known for their role in NICD trafficking and Notch pathway activation [2,
253 4]. These components showed uniform expression across different lobes and developmental zones of
254 the lymph gland, as assessed by immunofluorescence (IF) or RNA *in situ* hybridisation in wild type
255 lymph gland (Fig S2). *DomeGal4* driven knockdown of the ESCRT components was validated using
256 immunofluorescence analysis where antibodies were available or by *in situ* hybridisation and RT-qPCR
257 for analysing transcript levels (Fig S3). The Notch response element driving GFP (NRE-GFP) is a useful
258 reporter to assess activation of Notch signaling. Upon KD in the lymph gland progenitors, except
259 Vps25, all components tested [Hrs, Stam (ESCRT-0); Vps28, Tsg101 (ESCRT-I); Vps22 (ESCRT-II); Vps32,
260 Vps24 (ESCRT-III)] caused upregulation of Notch signaling as interpreted by an increase in NRE-GFP
261 positive cells in the primary lobe (Fig 4A). This is in concordance with the crystal cell differentiation
262 phenotype as all of the ESCRT components except Vps25 cause increased crystal cell differentiation in

263 the primary lobe upon knockdown. Our result also indicates that these 7 ESCRT components are
264 indispensable for regulation of Notch signaling in the blood cell progenitors possibly with non-
265 compensatory roles.

266 Knockdown of 3 out of the 8 ESCRT components [Hrs, Stam (ESCRT-0) and Vps28 (ESCRT-I)] resulted
267 in increased Notch signaling activation in the secondary lobe (Fig 4A, S4A). Of these only Hrs and Vps28
268 knockdown resulted in increased crystal cell differentiation in the secondary lobe (Fig 3), suggesting
269 additional mechanisms downstream of Notch activation prevent crystal cell differentiation in the
270 absence of Stam. Interestingly, in the tertiary lobe, both Hrs or Stam knockdown resulted in Notch
271 activation (Fig4A, S4A) though neither resulted in crystal cell differentiation (Fig 3). In either case,
272 tertiary lobe progenitors fail to differentiate, indicating their immature nature (Fig4A, S4A). Also,
273 though Vps28 depletion does not significantly activate Notch signaling in the tertiary lobe it can
274 promote crystal cell differentiation, suggesting a possible mechanism to downregulate Notch signaling
275 likely after progenitors differentiate. However, we do see occasional increase in Notch activation in
276 Vps28 KD tertiary lobes. Hence, crystal cell differentiation in the tertiary lobe could be under complex
277 temporal regulation. Our analysis demonstrates the active role of ESCRT components in regulating
278 Notch signaling, which may contribute to crystal cell differentiation and also differential response of
279 the progenitor subsets.

280 NICD cleavage and transport to the nucleus to activate target gene transcription is key to effecting
281 canonical and non-canonical modes of Notch signaling. Accumulation of NICD may lead to aberrant
282 activation of Notch signaling. Progenitor-specific knockdown of all tested ESCRT components, except
283 Vps25, resulted in increase in the number of cells accumulating NICD in the primary lobe (Fig 4B). This
284 suggests a role for a majority of the ESCRT components in NICD trafficking, which may affect Notch
285 signaling. The absence of any phenotype due to Vps25 knockdown suggests compensatory
286 mechanisms may regulate cargo trafficking and lineage-specific signaling activation, which is sufficient
287 to maintain progenitors at steady state.

288 Knockdown of 4 components [Hrs, Stam (ESCRT-0), Vps28 (ESCRT-I) and Vps24 (ESCRT-III)] led to an
289 increase in the number of NICD accumulating cells in the secondary lobe (Fig 4B, S4A). However, only
290 Hrs and Stam knockdown resulted in NICD accumulation in the tertiary lobe. This is in concordance
291 with the phenotype of Notch activation upon Hrs, Stam and Vps28 knockdown in the posterior lobes.
292 Our results show that NICD accumulation and Notch pathway activation correlate perfectly with
293 crystal cell differentiation upon ESCRT knockdown. Notch signaling is known to be sensitive to
294 endocytic sorting defects due to ESCRT in other contexts [24]. Similar effects may result in ectopic
295 activation and promoting crystal cell differentiation. Despite a differential effect on NICD trafficking

296 and Notch activation across progenitor subsets, immunolocalization and proximity ligation assay
297 indicated uniform interaction of ESCRT with NICD (Fig S4B, C; see supplementary results). Also, Notch
298 activation triggered by ESCRT depletion in blood progenitors may be independent of the status of
299 Notch ubiquitination (Fig S4D, E; see supplementary results). Hence the role of ESCRT in Notch
300 signaling may lie downstream of subtle post-translational regulatory mechanisms.

301

302 **ESCRT depletion sensitizes progenitors for lamellocyte differentiation.**

303 Lamellocytes are rarely present in the larva without any wasp infestation. However, progenitor-
304 specific knockdown of 6 ESCRT components [Tsg101 and Vps37A (ESCRT-I); Vps36 (ESCRT-II); Vps32,
305 Vps20 and Vps2 (ESCRT-III)] induced lamellocyte differentiation in the primary lobe, as visualized by
306 Phalloidin (F-actin) staining, even without any immune challenge (Fig 5A-C). Only 2 components
307 (Vps36 and Vps2) caused lamellocyte differentiation in the secondary lobe when knocked down and
308 only Vps36 knockdown triggered lamellocyte differentiation in the tertiary lobe (Fig 5A, B). This
309 indicates that the majority of the ESCRT components are not involved in suppressing lamellocyte
310 differentiation in the refractile posterior progenitors at steady state. However, it is likely that KD
311 progenitors may be more sensitive to immunogenic cues as compared to normal, unperturbed
312 progenitors.

313 Wild type larvae are generally able to mount a sufficiently robust immune response against wasp
314 infestation, that aids their survival and eclosion. Systemic signals are generated upon wasp infestation
315 and are received by the lymph gland progenitors [25], possibly through a complex extracellular matrix
316 [16]. This results in lamellocyte differentiation in the primary lobe followed by disintegration and
317 release of lamellocytes into circulation. Secondary and tertiary lobes are refractile to wasp infestation
318 and do not form lamellocytes even upon immune challenge. Hence, we chose to test the response to
319 wasp infestation in- a) ESCRT KD that had no effect on lamellocyte formation (Vps25 KD) and b) ESCRT
320 KD that caused lamellocyte differentiation only in the primary lobe (Vps32 KD). Knockdown of both
321 Vps25 and Vps32 triggered lamellocyte differentiation across all progenitor subsets upon immune
322 challenge with wasp (Fig 5C). This shows that Vps25 and Vps32 play essential roles in preventing all
323 posterior progenitors from lamellocyte differentiation in response to a natural immune challenge.
324 Further, loss of ESCRT sensitizes progenitors to systemic cues by unlocking differentiation programs.

325 Our detailed analyses of blood progenitor differentiation upon knockdown of the 13 core ESCRT
326 components yielded a functional map that reflects distinct lineage-specific roles of ESCRT in blood cell
327 homeostasis and reduced sensitivity of younger progenitors to endocytic perturbation (Fig 6 A, B).

328 **ESCRT regulates cargo sorting in a cell-autonomous manner in blood progenitors.**

329 Progenitor-specific downregulation of ESCRT expression leads to accumulation of ubiquitinated
330 cargoes. However, a majority of the ubiquitin aggregates were found to accumulate in non-progenitor
331 (domeless⁻) cells, suggesting a possible cell non-autonomous effect. To test whether this could be due
332 to ubiquitin accumulation in progenitors prior to their differentiation (cells lose domeless marker
333 expression), we generated homozygous mutant mitotic recombinant clones for a representative
334 ESCRT gene *Vps32* (*shrub*), in progenitors. *Vps32* is a terminally acting ESCRT that affects ubiquitinated
335 cargo sorting and its depletion affects all blood cell lineages (Fig. 6). Hence it serves as a good model
336 to assess cell autonomous function of ESCRT. Staining for conjugated ubiquitin revealed accumulation
337 of ubiquitin aggregates in the homozygous mutant patch of the tissue (GFP⁻) indicating *Vps32* has a
338 cell autonomous role in cargo sorting in blood progenitors (Fig 7A). Hence, it is likely that ubiquitin
339 seen in dome⁻ cells (Fig. 1) accumulated when the cells were still expressing domeless. This suggests
340 that despite a decrease in dome expression in the knockdown cells, ubiquitin aggregates may persist
341 during differentiation, likely due to dysfunctional cargo sorting in a cell-autonomous manner.

342

343 **ESCRT affects progenitor differentiation in a cell non-autonomous manner.**

344 We analysed differentiation in progenitor-specific mitotic clones of ESCRT. *Vps32* knockdown results
345 in increased crystal cell differentiation and triggers lamellocyte differentiation, as described earlier
346 (Fig 3, 5-6). ProPO staining showed both wild type and mutant origin of crystal cells as revealed by
347 overlap with GFP expression in the mutant tissue (Fig 7B). As crystal cells are usually present in the
348 lymph gland in low numbers, it is difficult to interpret cell-autonomous origin of crystal cells from
349 mutant progenitors. However, lamellocytes are completely absent in the control lymph gland at
350 steady state (Fig 7C). Phalloidin staining in the *Vps32* mutant clone showed GFP⁺ elongated or
351 coalescing cells, indicating the presence of lamellocytes and possibly their precursors (Fig 7C). This
352 suggests non-autonomous regulation of lamellocyte differentiation by ESCRT. Hence, ESCRT may
353 regulate progenitor differentiation in both a cell-autonomous as well as non-cell-autonomous
354 manner.

355 *Vps25* knockdown did not affect the status of ubiquitination, progenitor maintenance or
356 differentiation to any particular blood cell lineage despite its expression in the lymph gland. To further
357 verify this, we generated lymph gland progenitor-specific homozygous mitotic clones of *Vps25* loss of
358 function mutation (*Vps25*^{A3}). There was no accumulation of ubiquitin aggregates (Fig S5A) or any
359 change in the status of the progenitor (Fig S5B), plasmacyte (Fig S5C), crystal cell (Fig S5D) and

360 lamellocyte differentiation (Fig S5E). However, the mutant lymph glands showed enlargement of the
361 primary lobe, suggesting possible increase in blood cell proliferation upon loss of Vps25, due to non-
362 autonomous effects. Also, phalloidin staining revealed appearance of binucleate, large cells and also
363 very small cells occasionally, along with increase in F-actin content in some patches of the tissue,
364 mostly in a cell autonomous manner (visible in GFP negative area of the tissue) (Fig S5E). Hence, Vps25
365 possibly inhibits uncontrolled cell proliferation and may contribute to critical steps of cell division that
366 may dictate cell shape, number and polarity.

367

368

369 **Discussion**

370 Cargo sorting by the ESCRT machinery is a ubiquitous requirement. We asked whether ESCRTs play a
371 decisive role in progenitor maintenance and lineage choice during development. For this we chose the
372 well-conserved *Drosophila* hematopoietic system as a model. It is a simple, accessible and genetically
373 tractable developmental model with limited cell types, whose development is regulated by conserved
374 signaling networks.

375 Our study shows the active role of endosomal protein sorting in hematopoietic homeostasis *in vivo*.
376 The detailed functional map of all 13 ESCRT core components in lymph gland hematopoiesis highlights
377 distinct regulatory roles of individual components in lineage-specific progenitor differentiation. The
378 functional chart reveals the most crucial steps of endosomal protein sorting in blood progenitor fate
379 choice. ESCRT-I remodels the endosomal membrane through budding and ESCRT-III carries out
380 scission, to allow cargo sorting. Loss of ESCRT-I or ESCRT-III components result in progenitor
381 differentiation to all blood cell lineages. Moreover, Vps28 knockdown significantly affects crystal cell
382 differentiation in all lymph gland lobes and Vps2 depletion induces posterior progenitor
383 differentiation to lamellocytes. Hence, membrane budding and scission during endosomal protein
384 sorting appear to affect a wide range of signaling pathways across distinct progenitor subsets. Recent
385 reports highlight the universal role of ESCRT-III, often in concert with ESCRT-I, in various ESCRT-
386 dependent membrane remodelling processes such as nuclear envelope reformation, lysosomal
387 membrane repair, cytokinetic abscission, macroautophagy and exocytosis [5]. Whether such
388 moonlighting functions of ESCRT-I and ESCRT-III impact signaling that determines lineage specification
389 merits further investigation.

390 Curiously, we observed drastic functional diversity of ESCRT-II components in progenitor fate
391 specification. While Vps36 depletion affected all lineages across progenitor subsets, Vps25 depletion

392 did not affect differentiation. Loss of Vps25 caused hyperproliferation in blood cells and failed to
393 activate signaling pathways such as Notch, which are necessary for progenitor differentiation. Though
394 Vps25 is a critical player in endosomal protein sorting in epithelial tissues [23, 26], its redundancy in
395 lineage-specific differentiation suggests alternate routes for endosomal protein sorting in blood
396 progenitors or a temporally regulated, developmental stage-specific role that has not yet been
397 identified. Notably, though Vps25 is dispensable for steady state hematopoiesis, its depletion
398 sensitizes all progenitors to differentiate upon immune challenge. This supports the possibility that
399 the diverse roles of ESCRT may contribute to differential regulation of steady state and stress
400 hematopoiesis.

401 Our study shows the distinct role of individual components of ESCRT in Notch signaling in blood
402 progenitors. Expectedly, regulation of Notch signaling in lymph gland progenitors relies heavily on the
403 ESCRT machinery. Our previous reports highlight the potential functional link of endosomal protein
404 sorting with blood progenitor homeostasis [14, 27]. Though Hrs and Stam depletion promoted crystal
405 cell differentiation in the lymph gland, it hardly affected plasmacyte and lamellocyte differentiation.
406 In epithelial tissue, though Hrs and Stam regulate Notch trafficking, they do not regulate Notch
407 pathway activation and downstream phenotypes such as cell polarity and proliferation [4]. Similar
408 mechanisms specific to hematopoietic tissue are not yet explored. It is notable that ALIX and its yeast
409 homolog Bro1 can recognize non-ubiquitinated cargoes and sort them independent of ESCRT-0 [28].
410 Also, Bro1, ALIX and HD-PTP act as alternate bridging factors to ESCRT-II to mediate endosomal protein
411 sorting in yeast and mammalian cells [29, 30]. Even post-translational regulatory mechanisms may
412 render ESCRT components inactive [31]. The non-compensatory roles of only a limited number of
413 ESCRT components, in spite of uniform expression across the lymph gland, supports the idea that
414 endosomal protein sorting possibly acts through multiple analogous components and parallel routes,
415 with only a few indispensable, critical regulatory nodes.

416 ESCRT may potentially regulate EGFR cargo transport, sorting and signaling activation that governs
417 plasmacyte proliferation and lamellocyte differentiation. Also, JAK/STAT and Hedgehog signaling
418 can be regulated at the level of endosomal sorting in the blood progenitor. We speculate that lineage-
419 specific signaling activation could be achieved through modulation of individual ESCRT component
420 expression and function at the post-transcriptional or post-translational level. Though Deltex and
421 eIF3f1 positively regulate Notch signaling in epithelial tissues [32-34], they appear dispensable for
422 controlling Notch activation in blood progenitors upon ESCRT knockdown. While other E3 ubiquitin
423 ligases and deubiquitinases may possibly complement for Deltex or eIF3f1 depletion, signaling
424 activation may not always depend on the status of ubiquitination. For example, Vps36 depletion elicits
425 a strong phenotype of differentiation without causing ubiquitinated cargo accumulation. Further

426 genetic interaction-based studies with other regulators of Notch signaling may reveal ESCRT-
427 dependent mechanisms of Notch activation.

428 Lymph gland progenitor subsets are functionally heterogeneous and show reduced sensitivity to
429 differentiation cues from anterior to posterior [16, 17]. Posterior progenitors resist differentiation
430 upon immune challenge suggesting that they have additional signal regulatory checkpoints. What
431 remains largely underexplored is the mechanism through which progenitor subsets differentially
432 respond to systemic cues. One possibility is that younger progenitors have inherently low levels of
433 ubiquitination and protein turnover and hence show mild effects on ESCRT depletion. Depletion of
434 Vps36 and Vps2 can trigger lamellocyte differentiation in refractile progenitors even without any
435 immune challenge, indicating that they actively prevent differentiation. Also, while Hrs knockdown
436 activates Notch signaling and crystal cell differentiation in posterior progenitors, Stam knockdown fails
437 to trigger terminal differentiation to crystal cells despite Notch activation. This indicates existence of
438 multiple checkpoints and highlights the complexity of mechanisms that progenitors may employ to
439 maintain their identity. Elucidating expression and function at the single cell level may aid in an
440 improved understanding of ESCRT-dependent lineage specification across these distinct progenitor
441 subsets. Such candidates can be screened further for efficient modulation of vertebrate blood
442 regeneration *in vitro* as well as *in vivo*.

443 Loss of function mutation in ESCRT genes result in cell-autonomous cargo accumulation in *Drosophila*
444 epithelial tissues [2, 3]. However, the cell non-autonomous role of ESCRT in cell proliferation as well
445 as neoplastic transformation, suggests altered intercellular communication and aberrant signaling
446 activation in the neighboring cell population [2, 3, 23]. In concordance with the previous reports, we
447 observed a cell-autonomous role of ESCRT in regulating ubiquitinated cargo sorting in the blood
448 progenitors. However, analysis of lamellocyte differentiation suggests that ESCRT may regulate
449 lineage-specification non-autonomously. Both progenitor differentiation and proliferation can
450 influence blood cell homeostasis in the lymph gland. ESCRT depletion not only activates lineage-
451 specific signaling pathways but also promotes blood cell proliferation. Cell type-specific increase in
452 proliferation and enlargement of lymph gland lobes can affect the proportion of different types of
453 hemocytes. Elucidating the interplay between ESCRT components and the mitogenic signaling
454 machinery could reveal whether downregulation of mitotic potential may restore steady state
455 hematopoiesis.

456 BloodSpot Leukemia MILE and COSMIC databases show aberrant expression of ESCRT genes in
457 hematopoietic and lymphoid tissues in acute lymphoblastic leukemia (ALL), acute myeloid leukemia
458 (AML), myelodysplastic syndromes, etc (<https://servers.binf.ku.dk/bloodspot/>;

459 <https://cancer.sanger.ac.uk/cosmic>). Our study has application in understanding endosomal
460 regulation of proliferative hematological pathologies. Further, as the role of endosomal protein
461 sorting and the ESCRT machinery in vertebrate hematopoiesis is largely unexplored, it could help
462 identify new regulators of hematopoietic homeostasis and provide novel targets for therapies,
463 especially for improved blood regeneration during autologous transplantation. Further understanding
464 of context-specific functions of ESCRT may improve our understanding of lineage-specific regeneration
465 of tissue, including blood.

466

467

468 **Acknowledgements**

469 This work was funded by grants to M.S.I from SERB and JC Bose fellowship, Department of Science and
470 Technology, Government of India, LSRET grant from Department of Biotechnology and Jawaharlal
471 Nehru Centre for Advanced Scientific Research (JNCASR), Bangalore. We thank JNCASR confocal
472 facility for access and our laboratory members for helpful discussions.

473

474

475 **Author Contributions**

476 A.R. and M.S.I. designed research; A.R. and Y.R. performed experiments; M.S.I. contributed reagents
477 and materials; A.R., Y.R. and M.S.I. analysed the data; AR and MSI wrote the manuscript.

478

479

480 **Competing interest**

481 The authors declare no competing interest.

482

483

484

485 References

- 486 1. Di Fiore, P.P., and von Zastrow, M. (2014). Endocytosis, signaling, and beyond. *Cold Spring*
487 *Harb Perspect Biol* 6.
- 488 2. Vaccari, T., Rusten, T.E., Menut, L., Nezis, I.P., Brech, A., Stenmark, H., and Bilder, D. (2009).
489 Comparative analysis of ESCRT-I, ESCRT-II and ESCRT-III function in *Drosophila* by efficient
490 isolation of ESCRT mutants. *Journal of Cell Science* 122, 2413-2423.
- 491 3. Herz, H.M., Woodfield, S.E., Chen, Z., Bolduc, C., and Bergmann, A. (2009). Common and
492 distinct genetic properties of ESCRT-II components in *Drosophila*. *PLoS One* 4, e4165.
- 493 4. Tognon, E., Wollscheid, N., Cortese, K., Tacchetti, C., and Vaccari, T. (2014). ESCRT-0 is not
494 required for ectopic Notch activation and tumor suppression in *Drosophila*. *PLoS One* 9,
495 e93987.
- 496 5. Vietri, M., Radulovic, M., and Stenmark, H. (2019). The many functions of ESCRTs. *Nat Rev Mol*
497 *Cell Biol*.
- 498 6. Avet-Rochex, A., Boyer, K., Polesello, C., Gobert, V., Osman, D., Roch, F., Auge, B., Zanet, J.,
499 Haenlin, M., and Waltzer, L. (2010). An in vivo RNA interference screen identifies gene
500 networks controlling *Drosophila melanogaster* blood cell homeostasis. *BMC Dev Biol* 10, 65.
- 501 7. Adoro, S., Park, K.H., Bettigole, S.E., Lis, R., Shin, H.R., Seo, H., Kim, J.H., Knobloch, K.P., Shim,
502 J.H., and Glimcher, L.H. (2017). Post-translational control of T cell development by the ESCRT
503 protein CHMP5. *Nat Immunol* 18, 780-790.
- 504 8. Liu, Y., Mei, Y., Han, X., Korobova, F.V., Prado, M.A., Yang, J., Peng, Z., Paulo, J.A., Gygi, S.P.,
505 Finley, D., et al. (2021). Membrane skeleton modulates erythroid proteome remodeling and
506 organelle clearance. *Blood* 137, 398-409.
- 507 9. Shrivage, B.V., Hill, J.H., Powers, C.M., Wu, L., and Baehrecke, E.H. (2013). Atg6 is required for
508 multiple vesicle trafficking pathways and hematopoiesis in *Drosophila*. *Development* 140,
509 1321-1329.
- 510 10. Xia, P., Wang, S., Huang, G., Zhu, P., Li, M., Ye, B., Du, Y., and Fan, Z. (2014). WASH is required
511 for the differentiation commitment of hematopoietic stem cells in a c-Myc-dependent
512 manner. *J Exp Med* 211, 2119-2134.
- 513 11. Reimels, T.A., and Pflieger, C.M. (2015). *Drosophila* Rabex-5 restricts Notch activity in
514 hematopoietic cells and maintains hematopoietic homeostasis. *J Cell Sci* 128, 4512-4525.
- 515 12. Yu, S., Luo, F., and Jin, L.H. (2021). Rab5 and Rab11 maintain hematopoietic homeostasis by
516 restricting multiple signaling pathways in *Drosophila*. *Elife* 10.
- 517 13. Evans, C.J., Olson, J.M., Mondal, B.C., Kandimalla, P., Abbasi, A., Abdusamad, M.M., Acosta,
518 O., Ainsworth, J.A., Akram, H.M., Albert, R.B., et al. (2021). A functional genomics screen
519 identifying blood cell development genes in *Drosophila* by undergraduates participating in a
520 course-based research experience. *G3 (Bethesda)* 11.
- 521 14. Kulkarni, V., Khadilkar, R.J., Magadi, S.S., and Inamdar, M.S. (2011). Asrij maintains the stem
522 cell niche and controls differentiation during *Drosophila* lymph gland hematopoiesis. *PLoS*
523 *One* 6, e27667.
- 524 15. Sinha, S., Dwivedi, T.R., Yengkhom, R., Bheemsetty, V.A., Abe, T., Kiyonari, H., VijayRaghavan,
525 K., and Inamdar, M.S. (2019). Asrij/OCIAD1 suppresses CSN5-mediated p53 degradation and
526 maintains mouse hematopoietic stem cell quiescence. *Blood* 133, 2385-2400.
- 527 16. Rodrigues, D., Renaud, Y., VijayRaghavan, K., Waltzer, L., and Inamdar, M.S. (2021).
528 Differential activation of JAK-STAT signaling reveals functional compartmentalization in
529 *Drosophila* blood progenitors. *Elife* 10.
- 530 17. Ray, A., Kamat, K., and Inamdar, M.S. (2021). A Conserved Role for Asrij/OCIAD1 in Progenitor
531 Differentiation and Lineage Specification Through Functional Interaction With the Regulators
532 of Mitochondrial Dynamics. *Front Cell Dev Biol* 9, 643444.
- 533 18. Alfred, V., and Vaccari, T. (2016). When membranes need an ESCRT: endosomal sorting and
534 membrane remodelling in health and disease. *Swiss Med Wkly* 146, w14347.

- 535 19. Radulovic, M., Schink, K.O., Wenzel, E.M., Nahse, V., Bongiovanni, A., Lafont, F., and Stenmark,
536 H. (2018). ESCRT-mediated lysosome repair precedes lysophagy and promotes cell survival.
537 *EMBO J* 37.
- 538 20. Rodrigues, D., VijayRaghavan, K., Waltzer, L., and Inamdar, M.S. (2021). Intact in situ
539 Preparation of the *Drosophila melanogaster* Lymph Gland for a Comprehensive Analysis of
540 Larval Hematopoiesis. *Bio-protocol* 11, e4204.
- 541 21. Duvic, B., Hoffmann, J.A., Meister, M., and Royet, J. (2002). Notch signaling controls lineage
542 specification during *Drosophila* larval hematopoiesis. *Curr Biol* 12, 1923-1927.
- 543 22. Lebestky, T., Jung, S.H., and Banerjee, U. (2003). A Serrate-expressing signaling center controls
544 *Drosophila* hematopoiesis. *Genes Dev* 17, 348-353.
- 545 23. Vaccari, T., and Bilder, D. (2005). The *Drosophila* tumor suppressor vps25 prevents
546 nonautonomous overproliferation by regulating notch trafficking. *Dev Cell* 9, 687-698.
- 547 24. Palmer, W.H., and Deng, W.M. (2015). Ligand-Independent Mechanisms of Notch Activity.
548 *Trends Cell Biol* 25, 697-707.
- 549 25. Morin-Poulard, I., Vincent, A., and Crozatier, M. (2013). The *Drosophila* JAK-STAT pathway in
550 blood cell formation and immunity. *JAKSTAT* 2, e25700.
- 551 26. Herz, H.M., Chen, Z., Scherr, H., Lackey, M., Bolduc, C., and Bergmann, A. (2006). vps25
552 mosaics display non-autonomous cell survival and overgrowth, and autonomous apoptosis.
553 *Development* 133, 1871-1880.
- 554 27. Khadilkar, R.J., Rodrigues, D., Mote, R.D., Sinha, A.R., Kulkarni, V., Magadi, S.S., and Inamdar,
555 M.S. (2014). ARF1-GTP regulates Asrij to provide endocytic control of *Drosophila* blood cell
556 homeostasis. *Proc Natl Acad Sci U S A* 111, 4898-4903.
- 557 28. Pashkova, N., Gakhar, L., Winistorfer, S.C., Sunshine, A.B., Rich, M., Dunham, M.J., Yu, L., and
558 Piper, R.C. (2013). The yeast Alix homolog Bro1 functions as a ubiquitin receptor for protein
559 sorting into multivesicular endosomes. *Dev Cell* 25, 520-533.
- 560 29. Bissig, C., and Gruenberg, J. (2014). ALIX and the multivesicular endosome: ALIX in
561 Wonderland. *Trends Cell Biol* 24, 19-25.
- 562 30. Taberner, L., and Woodman, P. (2018). Dissecting the role of His domain protein tyrosine
563 phosphatase/PTPN23 and ESCRTs in sorting activated epidermal growth factor receptor to the
564 multivesicular body. *Biochem Soc Trans* 46, 1037-1046.
- 565 31. Tsunematsu, T., Yamauchi, E., Shibata, H., Maki, M., Ohta, T., and Konishi, H. (2010). Distinct
566 functions of human MVB12A and MVB12B in the ESCRT-I dependent on their posttranslational
567 modifications. *Biochem Biophys Res Commun* 399, 232-237.
- 568 32. Matsuno, K., Diederich, R.J., Go, M.J., Blaumueller, C.M., and Artavanis-Tsakonas, S. (1995).
569 Deltex acts as a positive regulator of Notch signaling through interactions with the Notch
570 ankyrin repeats. *Development* 121, 2633-2644.
- 571 33. Moretti, J., Chastagner, P., Gastaldello, S., Heuss, S.F., Dirac, A.M., Bernards, R., Masucci, M.G.,
572 Israel, A., and Brou, C. (2010). The translation initiation factor 3f (eIF3f) exhibits a
573 deubiquitinase activity regulating Notch activation. *PLoS Biol* 8, e1000545.
- 574 34. Hori, K., Sen, A., Kirchhausen, T., and Artavanis-Tsakonas, S. (2012). Regulation of ligand-
575 independent Notch signal through intracellular trafficking. *Commun Integr Biol* 5, 374-376.

576

577

578

579

580

581 **Figures**

582 **Figure 1. ESCRT components regulate ubiquitinated cargo sorting in the lymph gland.**

583 **(A)** Whole-mount larval lymph gland showing accumulation of conjugated ubiquitin (FK2) in the lymph
584 gland upon progenitor-specific (*domeGal4 UAS 2xEGFP* driven) knockdown of 7 *Drosophila* ESCRT
585 components indicated (Vps28, Tsg101, Vps37A, Vps22, Vps32, Vps20, Vps2). Ubiquitin staining is
586 shown in gray scale. Accumulation of ubiquitin aggregates is marked by arrowhead and magnified in
587 insets. Scale bar: 100 μ m. **(B)** Bar diagrams show quantification of the fraction of cells accumulating
588 ubiquitin aggregates in primary, secondary and tertiary lobes upon knockdown of all 13 core ESCRT
589 components. n indicates the number of individual lobes analysed and N indicates the number of larvae
590 analysed. Error bars represent SEM. Kruskal Wallis test was performed to determine the statistical
591 significance. *P<0.05, P**<0.01, ***P<0.001. Summary chart indicating presence (colored box) or
592 absence (white box) of ubiquitin accumulation in the primary, secondary and tertiary lobes upon
593 depletion of the respective ESCRT component (left).

594

595 **Figure 2. ESCRT components regulate progenitor maintenance and plasmacyte differentiation in**
596 **the lymph gland.**

597 **(A)** Whole-mount larval lymph gland showing change in the fraction of *dome*>2xEGFP+ve progenitors
598 (green) or P1+ve plasmacytes (red) in the lymph gland upon progenitor-specific knockdown of 6
599 ESCRT components (Hrs, Vps28, Vps37A, Vps36, Vps32, Vps2). Scale bar: 100 μ m. **(B-C)** Bar diagrams
600 shows quantification of the fraction of progenitors (B) and plasmacytes (C) in primary, secondary
601 and tertiary lobes upon knockdown of all 13 core ESCRT components. n indicates the number of
602 individual lobes analysed and N indicates the number of larvae analysed. Error bars represent SEM.
603 Kruskal Wallis test was performed to determine the statistical significance. *P<0.05, **P<0.01,
604 ***P<0.001. Summary chart indicating presence (colored box) or absence (white box) of phenotypes
605 of progenitor loss (B) or increased plasmacytes differentiation (C) in the primary, secondary and
606 tertiary lobes upon depletion of the respective ESCRT component (left). Also see Fig. 6, Fig.S1.

607

608 **Figure 3. ESCRT components differentially regulate crystal cell differentiation of lymph gland**
609 **progenitors.**

610 **(A)** Whole-mount larval lymph gland showing increase in differentiation of ProPO+ve crystal cells (red)
611 in the lymph gland upon progenitor-specific knockdown of 12 core ESCRT components (All except
612 Vps25). Dome>2xEGFP (green) marks the progenitors across different lobes. Arrowheads mark

613 presence of crystal cells in posterior lobes. Scale bar: 100 μm . **(B)** Bar diagram shows quantification of
614 the fraction of crystal cells in primary, secondary and tertiary lobes upon knockdown of all 13 core
615 ESCRT components. n indicates the number of individual lobes analysed and N indicates the number
616 of larvae analysed. Error bars represent SEM. Kruskal Wallis test was performed to determine the
617 statistical significance. * $P < 0.05$, ** $P < 0.01$, *** $P < 0.001$. Summary chart indicating presence (colored
618 box) or absence (white box) of phenotypes of increased crystal cell differentiation in the primary,
619 secondary and tertiary lobes upon depletion of the respective ESCRT component (left). Also see Fig.
620 6.

621

622 **Figure 4. ESCRT components regulate Notch activation and NICD trafficking in the lymph gland.**

623 **(A)** Whole-mount larval lymph gland showing NRE-GFP+ve (Notch reporter) cells (green) and dome+ve
624 progenitors (red) in primary lobes upon progenitor-specific knockdown of 8 representative ESCRT
625 components indicated [Hrs, Stam (ESCRT-0); Vps28, Tsg101 (ESCRT-I); Vps25, Vps22 (ESCRT-II); Vps32,
626 Vps24 (ESCRT-III)]. Scale bar: 100 μm . Bar diagrams show quantification of the number of NRE-GFP
627 positive cells in primary, secondary and tertiary lobes upon knockdown of the same 8 ESCRT
628 components. **(B)** Whole-mount larval lymph gland showing NICD expression (shown in red in the upper
629 panel and in gray scale in the lower panel) in primary lobes upon progenitor-specific knockdown of
630 the same 8 aforementioned ESCRT components. Progenitors are marked by dome>2xEGFP (green).
631 Scale bar: 100 μm . **(B')** Magnified view showing lymph gland hemocytes with (arrow) or without
632 (arrowhead) NICD accumulation. Scale bar: 10 μm . Bar diagrams show quantification of the number
633 of NICD accumulating cells in primary, secondary and tertiary lobes. n indicates the number of
634 individual lobes analysed and N indicates the number of larvae analysed. Error bars represent SEM.
635 One-way ANOVA was performed to determine the statistical significance. * $P < 0.05$, ** $P < 0.01$,
636 *** $P < 0.001$. See also Fig S4.

637

638 **Figure 5. ESCRT components regulate lamellocyte differentiation in the lymph gland.**

639 **(A)** Whole-mount larval lymph gland showing Phalloidin staining (red) to visualise elongated
640 morphology of lamellocytes upon progenitor-specific knockdown of 5 ESCRT components (Tsg101,
641 Vps37A, Vps36, Vps20, Vps2). Blue arrowheads mark the region from primary, secondary or tertiary
642 lobes, magnified in the insets. The inset panel shows enlarged view of Phalloidin staining with
643 lamellocytes marked by orange arrowhead. Scale bar: 100 μm . **(B)** Bar diagram shows quantification
644 of the percentage of lymph glands showing lamellocyte differentiation in primary, secondary and

645 tertiary lobes upon knockdown of all 13 core ESCRT components, without any immune challenge.
646 Values in the columns indicate the number of larvae analysed for presence or absence of lamellocytes.
647 Summary chart indicating presence (colored box) or absence (white box) of lamellocytes
648 differentiation in the primary, secondary and tertiary lobes upon depletion of the respective ESCRT
649 component (left). **(C)** Whole-mount lymph glands of *Vps25* KD (*domeGal4 UAS 2xEGFP; UAS Vps25*
650 *RNAi;+/+*) and *Vps32* KD (*domeGal4 UAS 2xEGFP; UAS Vps32 RNAi;+/+*) larvae uninfested or 3 days
651 after wasp infestation. Phalloidin staining shows presence of lamellocytes (marked by orange
652 arrowhead in the inset). Schematic representing the phenotype of *Vps25* KD and *Vps32* KD lymph
653 glands with and without wasp infestation. Box marks lamellocyte differentiation in posterior lobes.
654 See also, Fig 6.

655

656 **Figure 6. A spatiotemporal map indicating ESCRT function in cargo sorting, progenitor maintenance**
657 **and lineage-specific differentiation in *Drosophila* larval hematopoiesis.**

658 **(A)** Schematic representation of lymph gland lobes from anterior to posterior (left to right). Green
659 circle (medullary zone) in primary lobe and green dotted lines in posterior lobe indicates the
660 progenitor pool depleted of ESCRT components (13 genes from ESCRT-0, I, II and III). Blood cell types
661 are represented as violet (plasmacytes), pink (crystal cells) and blue (lamellocytes). Red font denotes
662 ESCRT components whose depletion affected a given lineage whereas grey font indicates that there
663 was no discernible change. Red monochrome heatmap indicates position-dependent progenitor
664 sensitivity to depletion of ESCRT. See also Fig S2. **(B)** Comprehensive summary chart of the effects of
665 individual ESCRT depletion on the various aspects of hematopoiesis as indicated. Presence or absence
666 of a phenotype is depicted by colored or white boxes respectively. Red asterisk indicates Notch
667 pathway activation and grey asterisk indicates no change, for components that were tested. **(C)** Venn
668 diagram showing superimposition of phenotypes caused by the knockdown of different ESCRT
669 components from progenitors. The underlined components in the lower panel affect both ubiquitin
670 accumulation and progenitor status as described in the upper panel and (B).

671

672 **Figure 7. ESCRT cell-autonomously regulates ubiquitinated cargo sorting in the lymph gland**
673 **progenitors but may regulate differentiation in non-autonomous manner as well.**

674 **(A)** Whole-mount lymph glands showing immunostaining for conjugated ubiquitin (red) in control
675 (*domeGal4/+; neoFRT42D/+; UAS mCD8 RFP/+*) and progenitor-specific mutant clone of
676 representative ESCRT component *Vps32/shrub* (*domeGal4/+; shrub^{GS} neoFRT42D/neoFRT42D; UAS*

677 *mCD8 RFP/UAS FLP*). Area marked by blue arrowheads are magnified in the insets to show
678 homozygous mitotic clones (GFP-ve patch, demarcated by dotted white line). Orange arrowheads
679 indicate ubiquitin accumulation in the mutant cells. DAPI marks the nuclei. **(B)** Primary lobe of control
680 and *Vps32* mutant clone showing ProPO staining (red) to mark crystal cells. Arrowheads mark the
681 crystal cells which are GFP-ve (homozygous mutant). **(C)** Phalloidin staining in the same genotypes
682 shows GFP+ elongated and coalescing cells marked by arrowheads (insets) in the mutant clone. Scale
683 bar in all image panels: 100 μm .

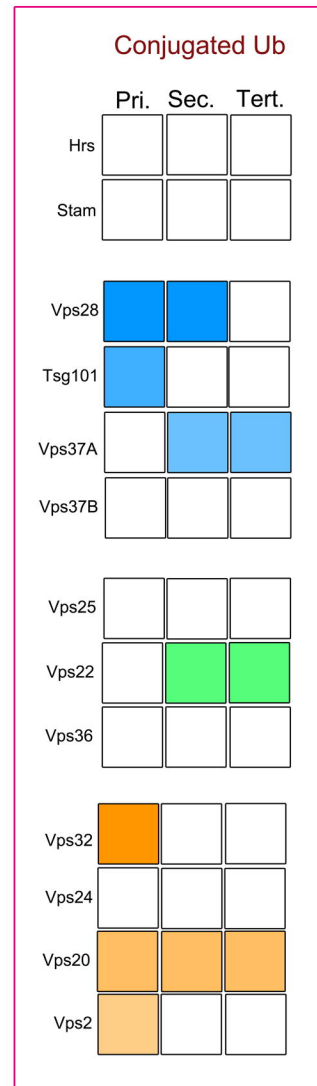
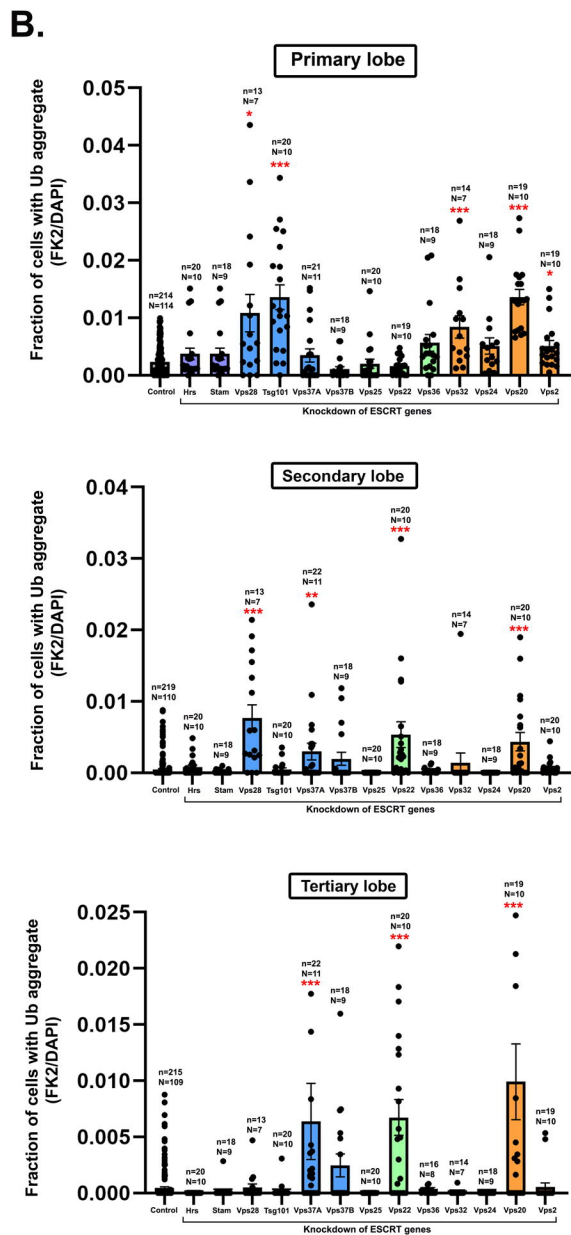
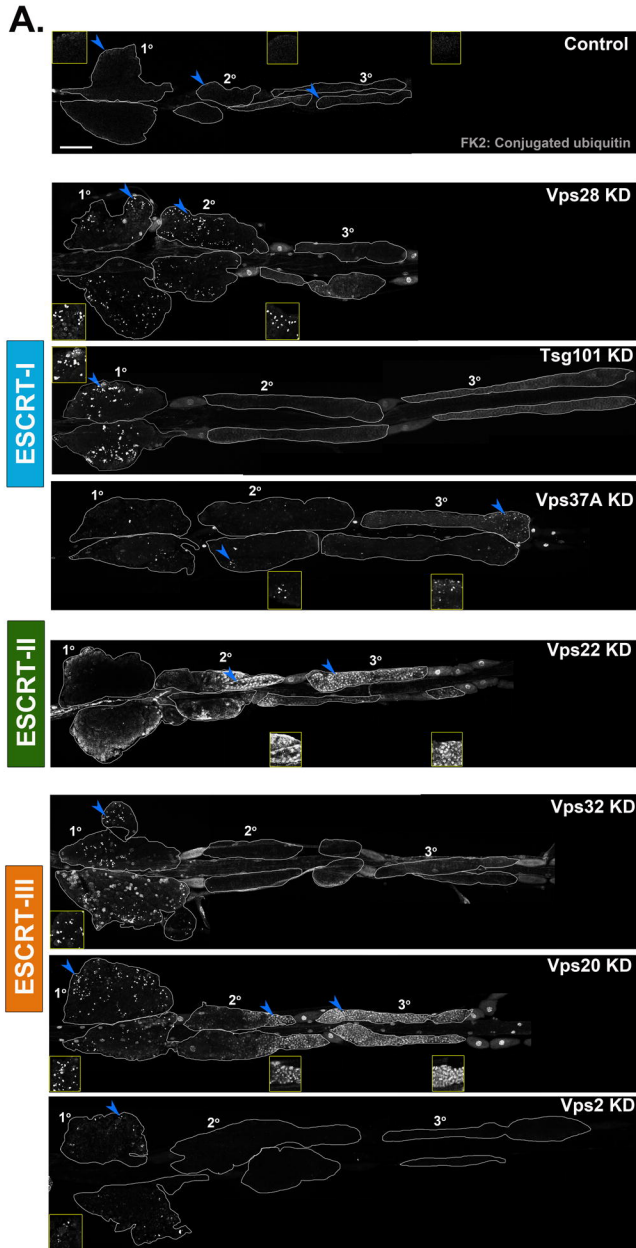


Figure 1

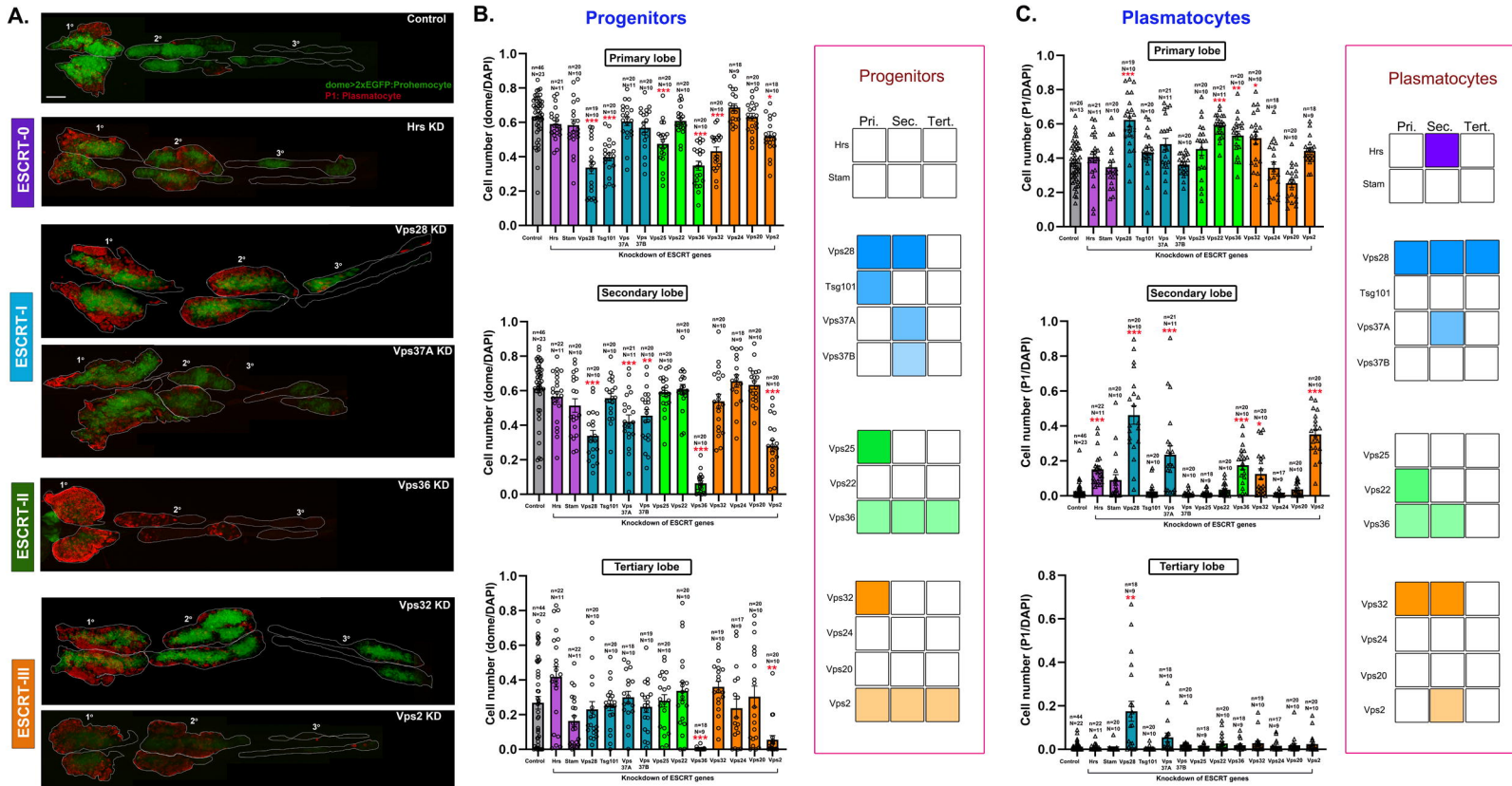
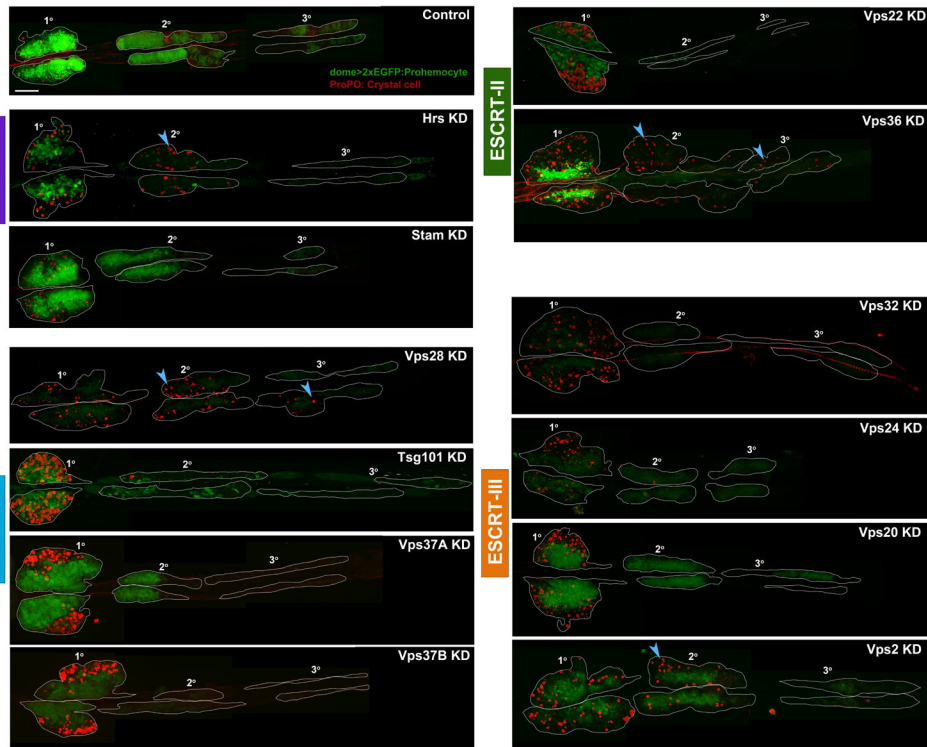


Figure 2

A.



B.

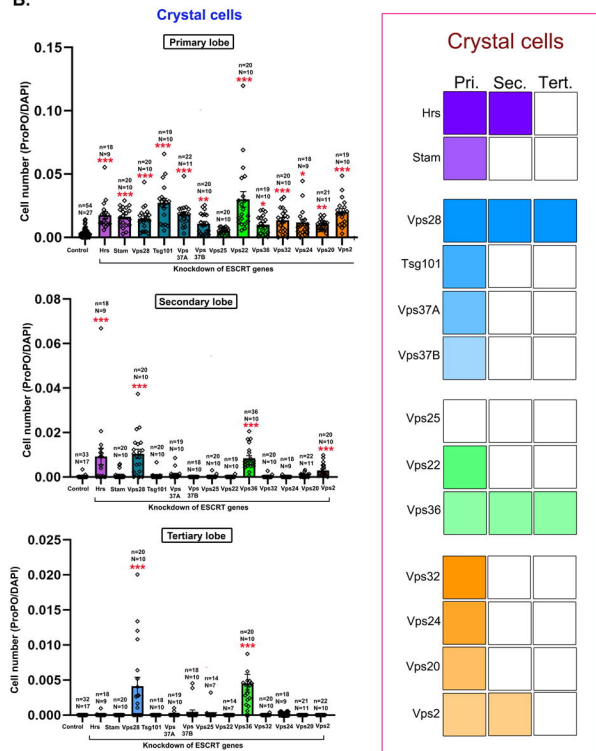


Figure 3

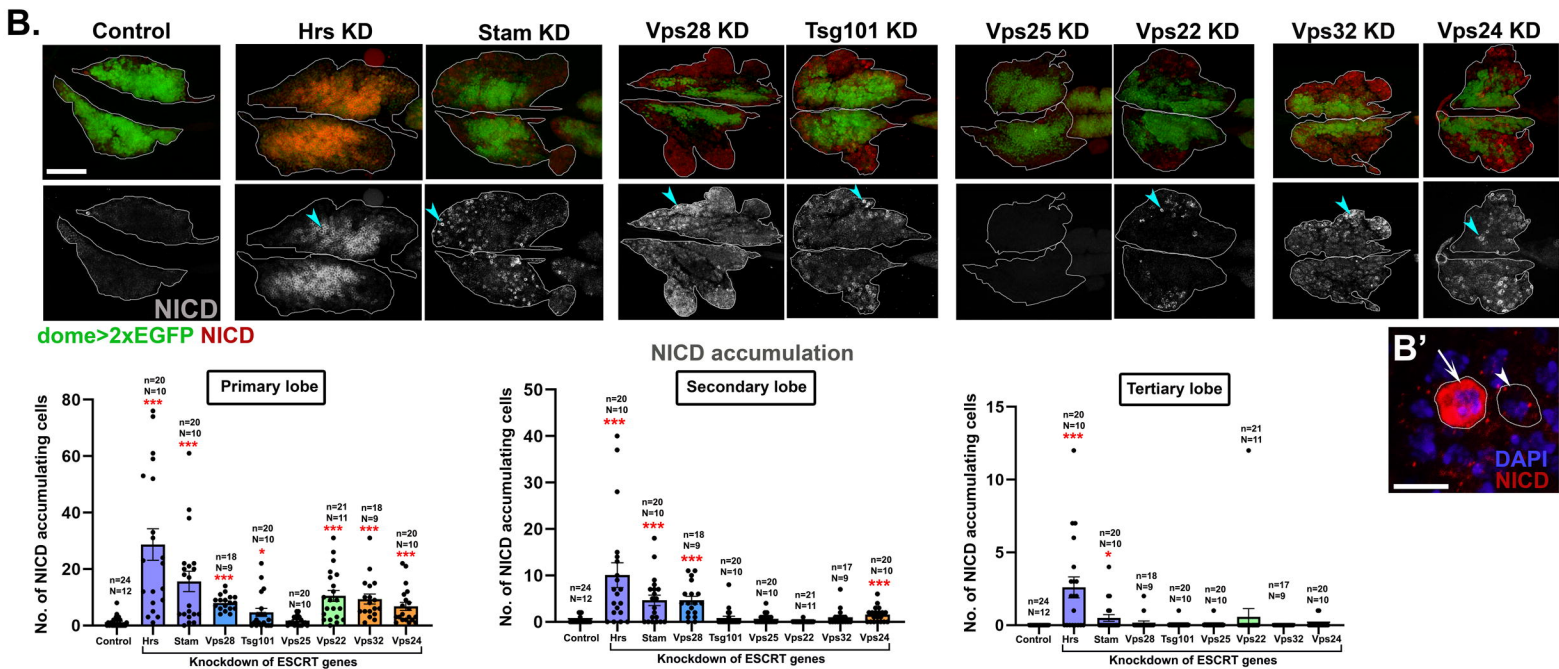
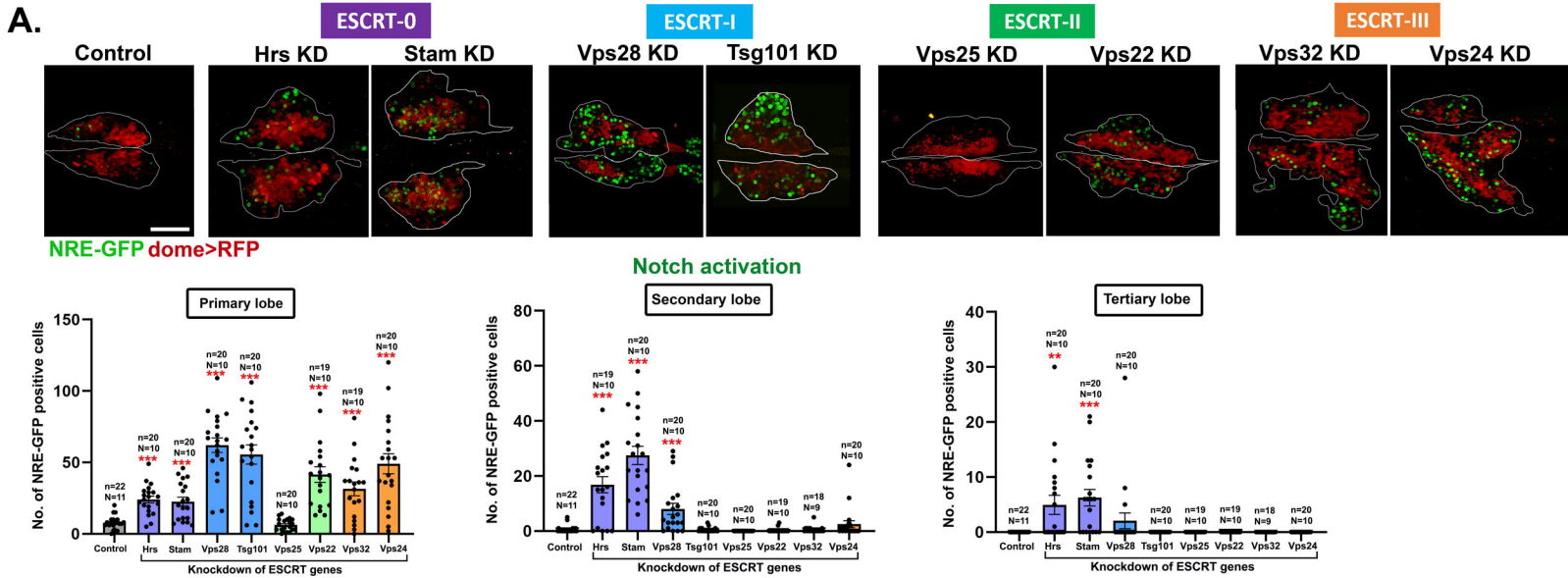
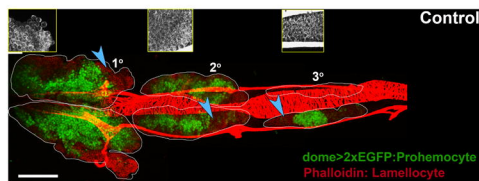
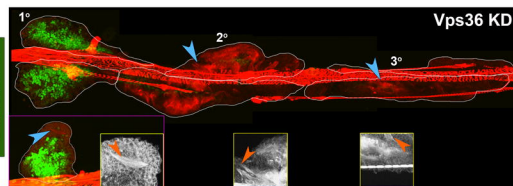


Figure 4

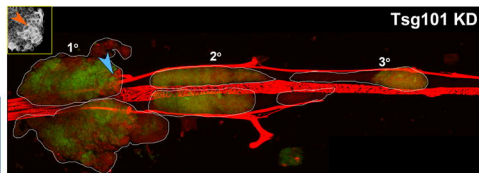
A.



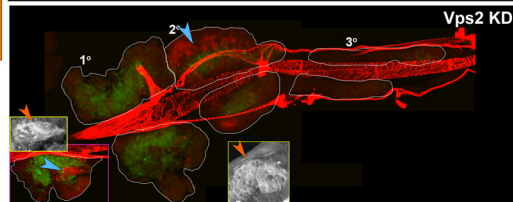
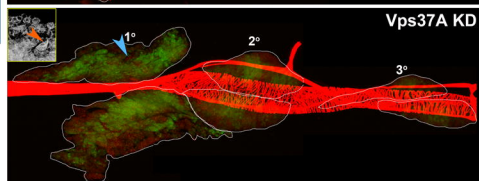
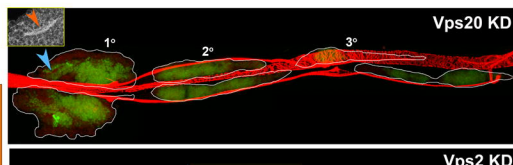
ESCRT-II



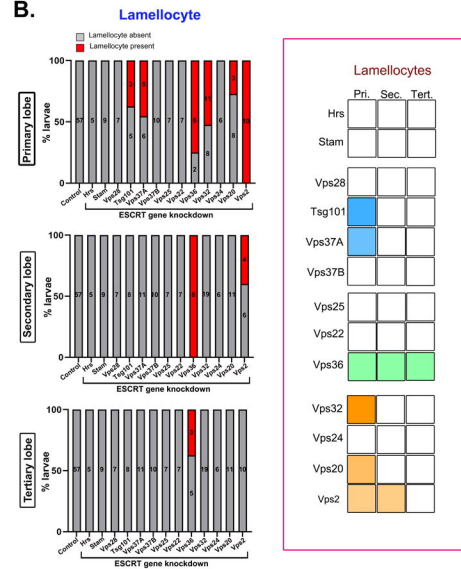
ESCRT-I



ESCRT-III



B.



C.

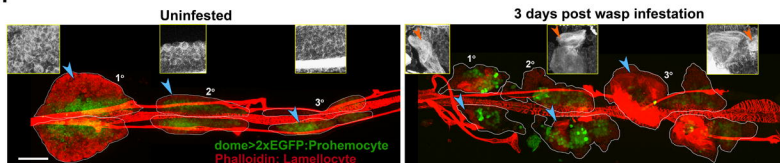
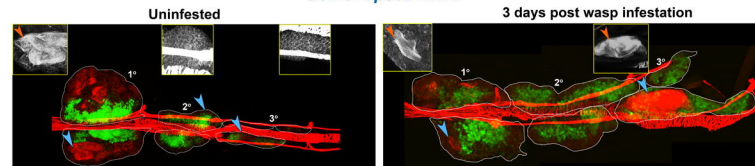
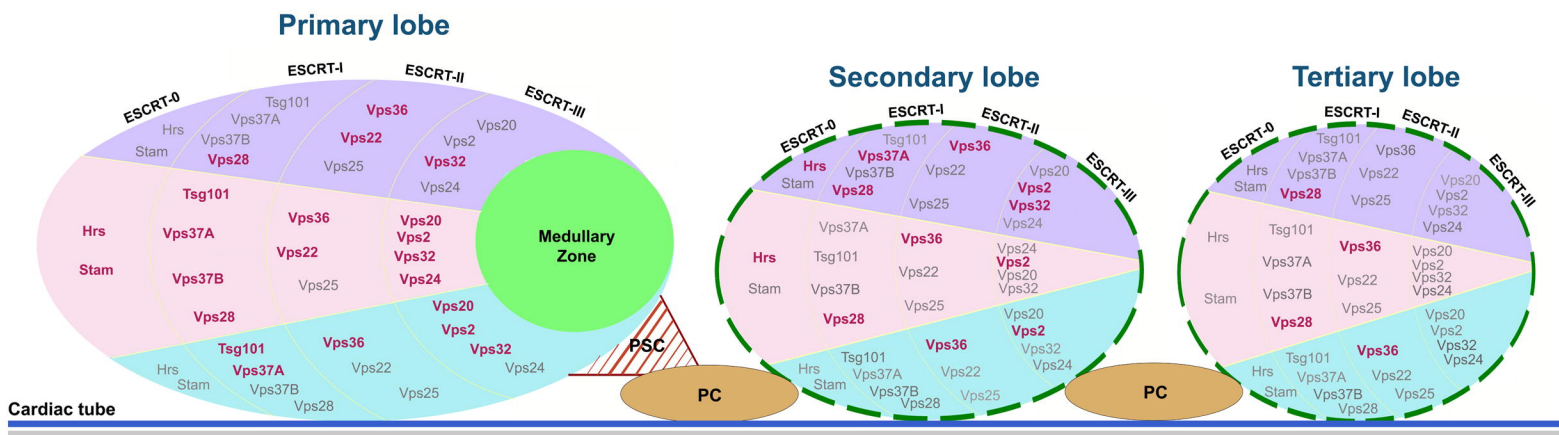
dome>Vps25 RNAi*dome>Vps32 RNAi*

Figure 5

A.

- Plasmatoocytes
- Crystal cells
- Lamellocytes
- Domeless +veProhemocytes

Red font: Increased differentiation upon knockdown
Grey font: No effect upon knockdown



Progenitor sensitivity to ESCRT depletion

B.

	Conjugated Ub			Progenitors			Plasmatoocytes			Crystal cells			Lamellocytes		
	Pri.	Sec.	Tert.	Pri.	Sec.	Tert.	Pri.	Sec.	Tert.	Pri.	Sec.	Tert.	Pri.	Sec.	Tert.
Hrs															
Stam															
Vps28	■	■		■	■		■	■	■	■	■	■			
Tsg101	■	■		■	■		■	■		■	■	■	■		
Vps37A	■	■		■	■		■	■		■	■	■	■		
Vps37B	■	■		■	■		■	■		■	■	■	■		
Vps25					■			■			■				
Vps22					■			■			■				
Vps36					■			■			■				
Vps32	■			■			■			■			■		
Vps24	■			■			■			■			■		
Vps20	■			■			■			■			■		
Vps2	■			■			■			■			■		

C.

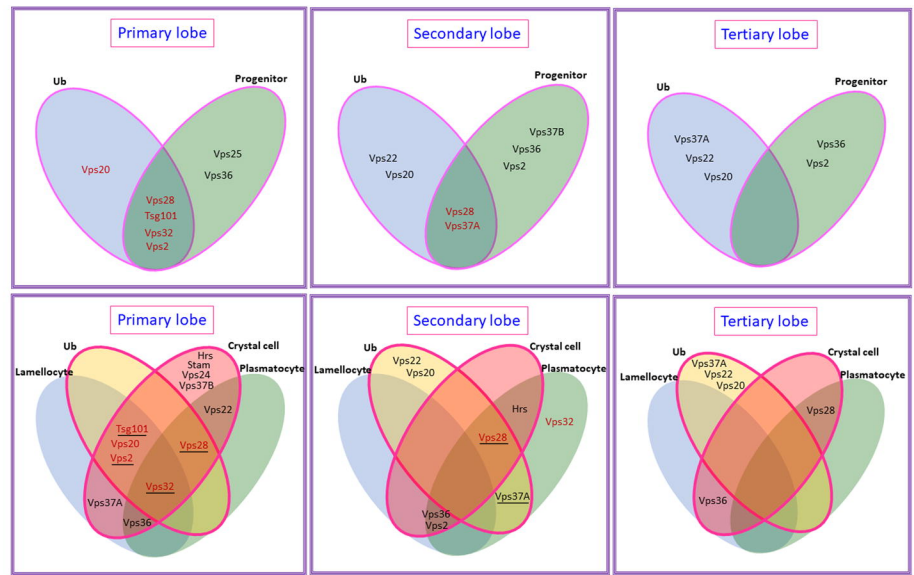


Figure 6

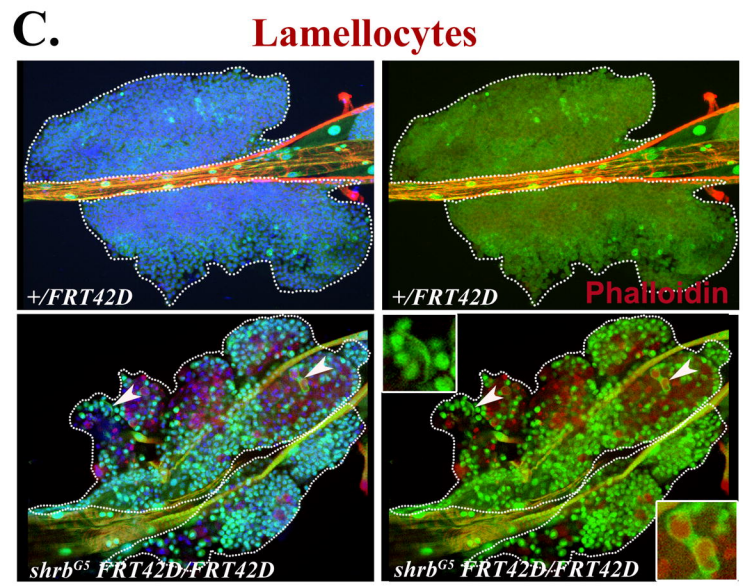
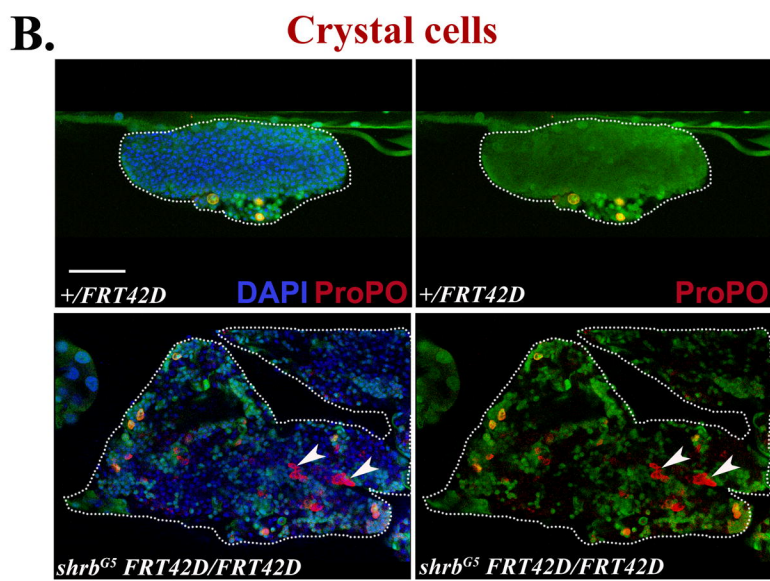
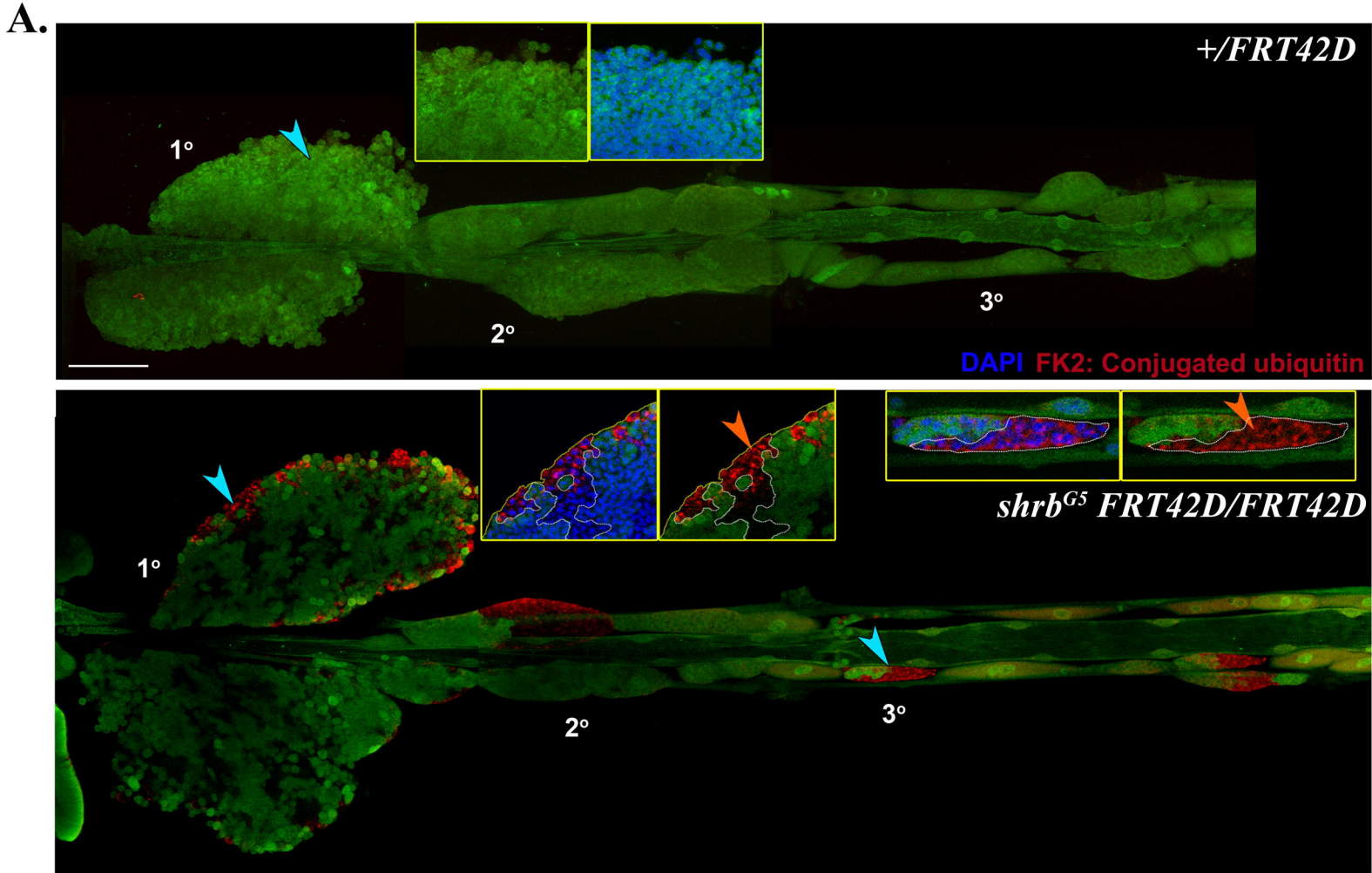


Figure 7